TRANSFERRED ELECTRON OSCILLATORS AT MM WAVE FREQUENCIES AND THEIR CHARACTERISATION USING QUASI-OPTICAL TECHNIQUES

Graham Murray Smith

A Thesis Submitted for the Degree of PhD
at the
University of St Andrews

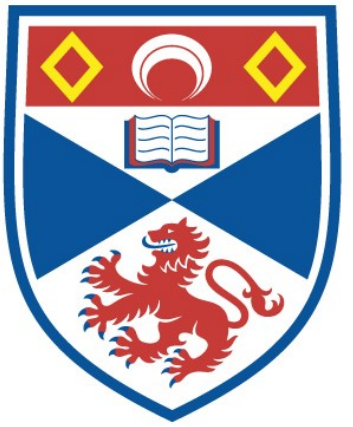

1990

TRANSFERRED ELECTRON OSCILLATORS AT MM WAVE FREQUENCIES AND THEIR CHARACTERISATION USING QUASI-OPTICAL TECHNIQUES

A thesis presented by
Graham. M. Smith, BSc. MSc.
to the
University of St Andrews
in application for the degree of
Doctor of Philosophy
March 1990

DECLARATION

I Graham Smith hereby certify that this thesis has been composed by myself, that it is a record of my own work, and that it has not been accepted in partial or complete fulfilment of any other degree of professional qualification.

This research was carried out in the Physical Sciences Laboratory of St.Salvators College, at the University of St Andrews, under the supervision of Dr.J.C.G.Lesurf.

G.M.SMITH

MAY 1996

I was admitted to the Faculty of Science of the University of St Andrews under Ordinance General No 12 on October 1984 and as a candidate for the degree of Ph.D. on October 1985

G.M.SMITH

MAY 1990

CERTIFICATE

I certify that G.M.Smith has spent nine terms at research work in the Physical Sciences Laboratory of St. Salvators College, in the University of St. Andrews, under my direction and that he has fulfilled the conditions of the Resolution and Regulations appropriate to the Degree of Ph.D.

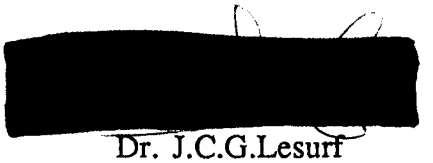

Dr. J.C.G.Lesurf

Research Supervisor

ACKNOWLEDGEMENTS

I wish to especially thank my supervisor Dr. J.C.G.Lesurf for all his help, patience, inspiration and encouragement and for putting up with me for four years. Thanks Jim! I would also like to thank my partner in crime Andy Harvey who is responsible for much of the original design work involved in the optical systems, and has generally livened up the lab with his whacky sense of humour! In this respect I would also like to mention the more recent group acquisitions Malcolm Robertson, Darryl Smith, Mike Leeson and Michael Webb. Michael Webb deserving a special acknowledgement for the design and manufacture of the quasi-optical circulator that was used in the noise bench system.

Almost all of the optics and oscillators described has been constructed in St.Andrews, and a very special thanks must go to the workshop for all the care and effort that went into the manufacture. Many thanks to Ron McGraw, George Radleigh, Bill Brown, Myles Whyte, Bill Smith and Jim Clarke. I also gratefully acknowledge all the help from J.Duff and Nigel Keys from EEV who provided me with sponsorship for one year, and Mike Kelly and Nigel Couch from GEC Hirst who provided devices to evaluate. I would also like to especially thank Sean Neylon ftom M.E.D.L., Mike Kelly from GEC and S.Naqi from M.D.S. for all their support and encouragement for the work on the Noise Bench System.

On a lighter note, many thanks to all those friends with whom I have gone climbing, squashing, footballing and drinking. I would also like to thank all those Postgrads in the Physics Department and in University Hall that have made St.Andrews fun to live in over the last four years. In particular, I would like to mention my two long suffering flatmates Andy Finch and Colin Wilson.

Lastly, I would like to thank and dedicate this thesis to my parents who have provided me with the inspiration and drive to do well.

TO MY PARENTS

ABSTRACT

A study of high frequency millimetre wave oscillators is performed operating at W-band and above, using test bench equipment designed and constructed in St. Andrews. Octave tuneable oscillators have been designed, constructed, and used to characterise developmental Gunn dervices, as well as to provide ideal oscillators for test bench measurement systems. These oscillators have been sold to many millimetre-wave laboratories throughout Britain. The operation, optimisation and characterisation of these oscillators is described in detail, and various non-linear effects are explained and modelled successfully. The wideband tuneability and matching has also allowed evaluation of new developmental Gunn devices to accurately determine the optimum operating frequency range of the devices. This was part of a developmental program by GEC Hirst and MEDL which has now produced state of the art GaAs Gunn oscillators at 94GHz.

Much of the characterisation of the oscillators is performed using novel quasi-optical techniques, which has allowed low loss accurate performance at these very high frequencies. Several quasi-optical techniques are described and the design, manufacture and evaluation of many optical components are given. In particular, the frequency and harmonic content of the oscillators was determined using a Martin-Puplett Interferometer which utilised a frequency counting technique. This enabled easy wideband measurements to be performed with much greater accuracy than traditional cavity wavemeters. In addition, a state of the art noise bench has been designed and constructed for operation at W-band and above, that utilises a novel open resonator to effect a very high Q suppression filter. The system has been shown to make noise measurements at much lower power levels and with greater sensitivity than comparable systems.

CONTENTS

1.0 INTRODUCTION

1.1 MILLIMETRE WAVE APPLICATIONS

Millimetre waves represent that portion of the electromagnetic spectrum that extends from 30 to 300GHz, or in terms of wavelength, from 1mm to 10mm (Fig.1.1). It is a transition region between the microwave and infrared part of the spectrum, in which there has been a growing interest over the past few decades.

In many applications the millimeter wave spectrum has considerable advantages over its more familiar microwave and infrared neighbours. It is still amenable to many of the the electronic techniques used at lower frequencies, as well as some of the optical techniques more commonly used at higher frequencies. The advantages over microwave frequencies mainly accrue from the smaller wavelength, which enables narrower beam angles, smaller antenna size, and greater bandwidth. This having clear implications for line of sight communication and high resolution radar. Also, very importantly, it still maintains a relatively low atmospheric attenuation compared to much higher frequencies [1, 2]. This can be seen in Figs 1.2 and 1.3 where the important atmospheric windows at 30, 94, 140 and 220GHz are clearly visible.

The new generation of battlefield missile systems use the atmospheric window at 95 GHz, as it has low attenuation in smoke, high resolution for identification of targets, and is more insensitive to burning material than infrared systems. Ground hugging long distance missiles such as CRUISE also use mm-wave radar at this frequency. The high atmospheric attenuation at 60 GHz (due to an oxygen molecule resonance) has also been exploited for covert line of sight communication to prevent eavesdropping, such as that now used for communication between military jets flying in formation. Satellite to earth communication systems are starting to move into the millimeter wave frequency band, to make greater use of the bandwidth, and more importantly to find new carrier frequencies. There is also a developmental local line-of-sight television link being planned by British Telecom whch is to operate around 30GHz.

In addition the mm-wave region lies just under the peak of the black body radiation spectrum at room temperature, and this enables accurate topographical imaging using natural radiation for earth resource studies, such as that successfully used for oil exploration, or for military systems. At 3-4K millimetre waves are actually at the peak of the black-body spectrum and experiments are underway to make sensitive measurements of the cosmic background radiation at this frequency.

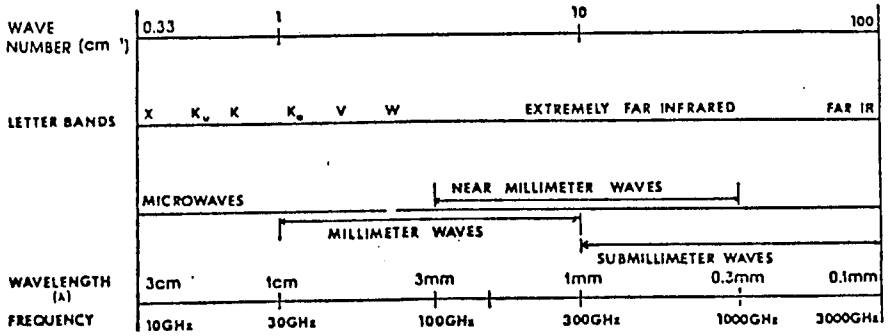

Fig. 1.1 Common terminology for millimeter and submillimeter waves and other frequency ranges.

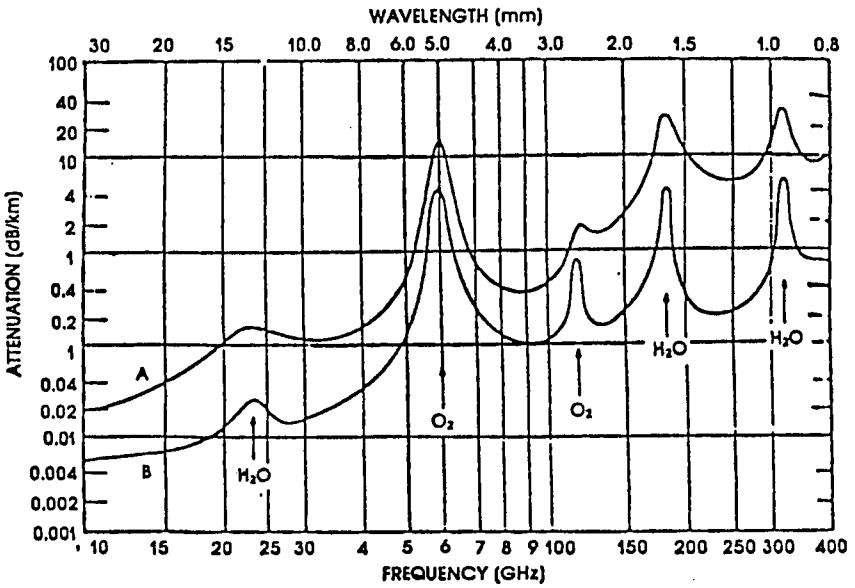

Fig. 1.2 Average atmospheric absorption of millimeter waves. A—Sea level: T = 20°C, P = 760 mm, P_{H_2O} = 7.5 g/m^3; B—4 km: T = 0°C: P_{H_2O} = 1 g/m^3 (from Wiltse [3], © 1981 Academic Press).

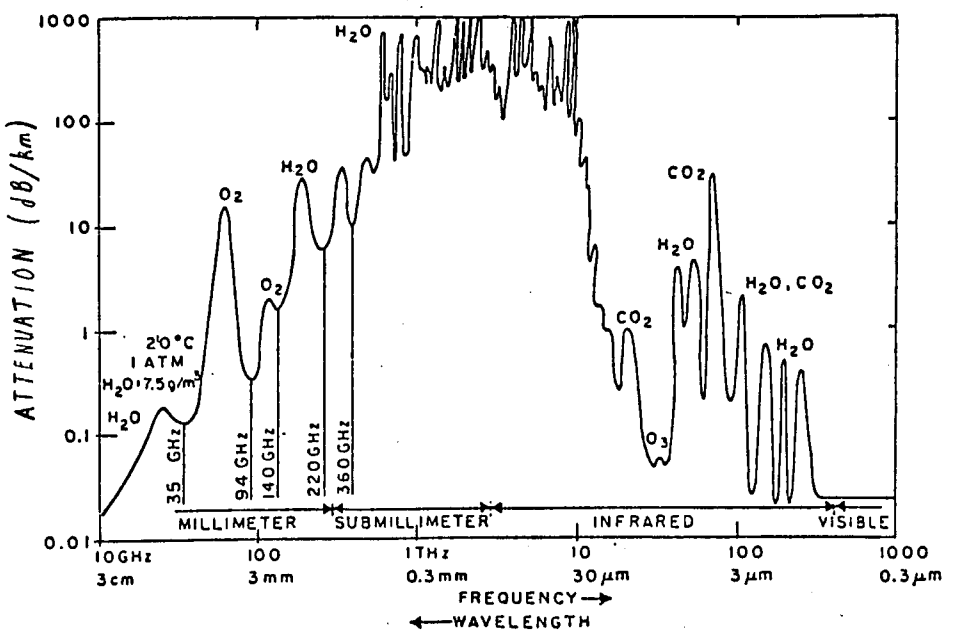

Fig. 1.3 Clear weather atmospheric attenuation (from Preissner, [4]).

The above are illustrative diagrams taken from Ref. [2]

There is also considerable interest in this region for diagnostics for fusion projects, where electron cyclotron resonances are in the 50-500 GHz region, and can give valuable information about the electron temperature.

Many molecules also have their natural resonances in the mm-wave part of the spectrum. The water molecule has resonances at 24 GHz and 180 GHz and the oxygen molecule at 60 GHz and 120 GHz. One very topical application is the monitoring of ozone and CO concentration in the atmosphere by exploiting molecular resonances near 180 GHz and 115 GHz respectively. MM-waves also finds uses in probing the structure of certain compounds via molecular spectroscopy as well as in in the growing field of molecular cloud astronomy, for the identification of molecules and free radicals. This has important applications in the study of star formation, and possibly gives clues to the very start of organic life in interstellar space.

1.2 MILLIMETRE WAVE SYSTEMS

Some of the main reasons why millimetre wave systems have taken so long to come to the fore, were the very high tolerances required, the lack of suitable sources, and the high losses associated with stripline and waveguide. The losses are inherent, due to the skin depth becoming smaller for waveguide systems, and the absorption loss becoming larger for every low loss dielectric, as the frequency is increased. These losses are important throughout the millimetre wave region, but if scaled down versions of microwave systems are applied, they start to become critical at frequencies not much greater than 100 GHz. However, atmospheric losses are still (relatively) negligible, and the smaller wavelength starts to allow traditional beam optics to become a viable proposition. Optical techniques have the advantages of allowing polarisation manipulation and optical filtering as well as having no dispersion and minimum losses. Waveguide systems have the advantage of size, single transverse mode behaviour, and compatibility with coherent solid state detectors and oscillators. Thus so called quasi-optical systems have evolved in the millimetre wave range that use a mixture of both optical techniques and waveguide techniques. In general, optics are used to transfer, filter and diplex signals, and waveguide systems are used with solid-state oscillators, multipliers and for coherent detection. The need for greater use of optical techniques becomes more and more apparent, as the frequency increases.

The lack of suitable sources is also a major problem, with both electron beam-devices and semiconductor devices starting to reach intrinsic transit time limitations for fundamental power generation. Because of the lack of high frequency low noise

amplification, millimetre waves do not lend themselves to direct electrical manipulation. Thus in almost every single application, whether it be remote sensing, communication, radar or spectroscopy, the need to analyse very small signals, almost invariably requires heterodyne techniques. Heterodyning is the process when a small signal is mixed with another known local oscillator signal in a non-linear device. The mixing products includes a difference frequency which can be detected, amplified and processed using conventional low noise low frequency electrical techniques. Using an ideal local oscillator, the difference frequency contains all the different spectral information of the original signal frequency. However this requires excellent F.M. and A.M. characteristics of the local oscillator if its noise sidebands are also not to be down converted and convolved with the original signal.

The F.M. noise can be substantially improved by phase locking which is normally achieved by locking to a temperature stabilised low frequency crystal oscillator (typically 100MHz), via a long frequency multiplication chain. This is not a trivial operation, and is certainly helped if the oscillator has low F.M. noise components, as it reduces the gain required in the feedback system and helps to prevent spurious oscillation. In many applications phase locking is not an option, and low F.M noise also becomes an important criterion. A.M. noise is usually significantly lower than the F.M. noise, and its effect can be further reduced by the use of a double balanced mixer which can effectively cancel the noise components on a double balanced mixer.

As the frequency increases it becomes more and more difficult to produce low noise local oscillators of suficient power to run mixer systems, and this has perhaps been the most important holdup in the advancement of millimetre and sub-millimetre wave technology.

1.3 OUTLINE OF THESIS

This thesis takes a look at transferred electron oscillators as a high frequency source, primarily as a local oscillator or test-bench source, and considers the way that they can be advantageously characterised and operated at high frequencies using quasi-optical techniques. The first three chapters consider the theory of Gunn oscillators from the viewpoint of a device engineer, solid-state engineer and circuit designer respectively. The next three chapters look at the theory, design and implementation of tunable high frequency oscillators. The last three chapters consider the design of quasi-optical systems that may be used to advantageously characterise millimetre wave oscillators, including the measurement of frequency, harmonic content, impedance, and FM and AM noise.

Chapter 2 looks at the theory of the transferred electron effect, and contains a general literature review of transferred electron sources. Chapter 3 looks at the solid-state characteristics that are required for a Gunn device and looks at the possibility of new materials emerging. Chapter 4 then looks at the general theory of solid-state oscillators from the point of view of the circuit designer and the theory of impedance matching. Chapter 5 is a general non-linear analysis of fundamental and harmonic oscillators, and predicts the theoretical behaviour of harmonic oscillators as well as outlining the impedance requirements . Chapter 6 looks at the actual design of the type of tunable high frequency source that was used in these studies and discusses the major design parameters. This particular type of oscillator has been sold to many leading laboratories in Britain. Chapter 7 gives many of the results that have been obtained with different types of Gunn diodes. It also discusses the results and looks at circuit optimistation as well as modelling of the circuit. Chapter 8 considers the theory of quasi-optics and Gaussian beams, and the design of various quasi-optical components including feedhorns, lenses, beamsplitters, polarisers and resonators. Chapters 9 and 10 then shows the design and operation of several quasi-optical systems used to characterise and operate the devices, including accurate frequency measurement and spectrum analysis, noise measurement and phase locking, impedance matching and impedance measurements. Chapter 10 looks specifically at the very important area of high frequency noise measurements where a state of the art high frequency noise bench has been constructed. This utilises a novel high Q open resonator as a carrier suppression filter and is a very good example of the advantages that quasi-optical techniques can bring to test-bench systems. Chapter 11 finishes off by taking an overview of present trends, looking at the state of progressing work, and suggesting work and ideas for the future.

There are then various Appendices which contain engineering drawings, computer code for filter and circuit analysis, and Fourier transforms. There is also a transmission-line analysis using ABCD matrices which was used extensively in modelling. In addition, there is a guide to electro-forming, as well as a few odds and ends that did not fit in anywhere else!

REFERENCES (CHAPTER 1)

1) D.M.Brookbanks, 'Millimetre wave solid state devices,' Allen Clark Research Centre Annual Review 1981, pp.35-42

2) 'Principles and Applications of Millimetre-Wave Radar,' 1987, Artech House

3) 'J.C.Wiltse, 'Introduction and Overview of Millimetre Waves,' Chapter 1, Infrared and Millimeter Waves, Volume 4, Academic Press, New York, 1981

4) J.Preissner, 'The Influence of the Atmosphere on Passive Radiometric Measurements,' AGARD Conference Reprint No.245. Millimeter and Submillimeter Wave Propagation and Circuits, 1978

2.0 TRANSFERRED ELECTRON OSCILLATORS

2.1 INTRODUCTION

One of the main requirements of almost any mm wave heterodyne system is for very low noise sources for use as local oscillators. Typically only a few mW are needed for room temperature mixers and less than 0.1 mW for cryogenic InSb mixers. High power is therefore not a prime consideration. However reliability, ruggedness wide tunability, efficiency and of course low noise are all important factors. A Gunn oscillator is a low power, low noise semiconductor device and in many respects is an ideal choice. It requires a low power constant bias voltage, and is typically a few percent efficient at around 100 GHz with better performance at lower frequencies. The circuits are reasonably simple, compact and sturdy, and often as much as an octave of circuit controlled tuning is possible. As a semiconductor device it also has the potential for reliable and economic bulk processing. In addition, with good circuit design, the Gunn oscillator is capable of giving a noise figure comparable with any other device.

Of its main rivals the IMPATT oscillator is also a semiconductor device, capable of producing higher frequencies and somewhat more power than a Gunn device. However, as its mechanism is based on the avalanche effect, it tends to be somewhat more noisy and considerably less reliable. The klystron is an electron beam device capable of very low noise. However, it requires large voltages, and is notoriously unreliable, with often only a few hundred hours of use. Carcinotrons too are electron beam devices, with wide tuning ranges and reasonable powers. They, however, are somewhat more noisy, and an order of magnitude more expensive, as well as requiring high voltage supplies.

Gunn oscillators therefore emerge as the cheapest, most reliable, low noise sources around at the present time.

2.2 THE GUNN EFFECT

The Gunn transferred electron effect is a bulk effect which leads to negative differential resistance (NDR) in certain materials, which possess a certain characteristic in their band structure. Many materials have been shown to have the requisite structure, however, only two have been studied in any detail. Namely the III-V compounds GaAs and InP. Their velocity/field characteristics and bandgap structures are shown in Figure 2.1 and Figure 2.2. The main feature to note is the fall in carrier velocity (current) with increasing field at a certain threshold field, leading to negative differential resistivity.

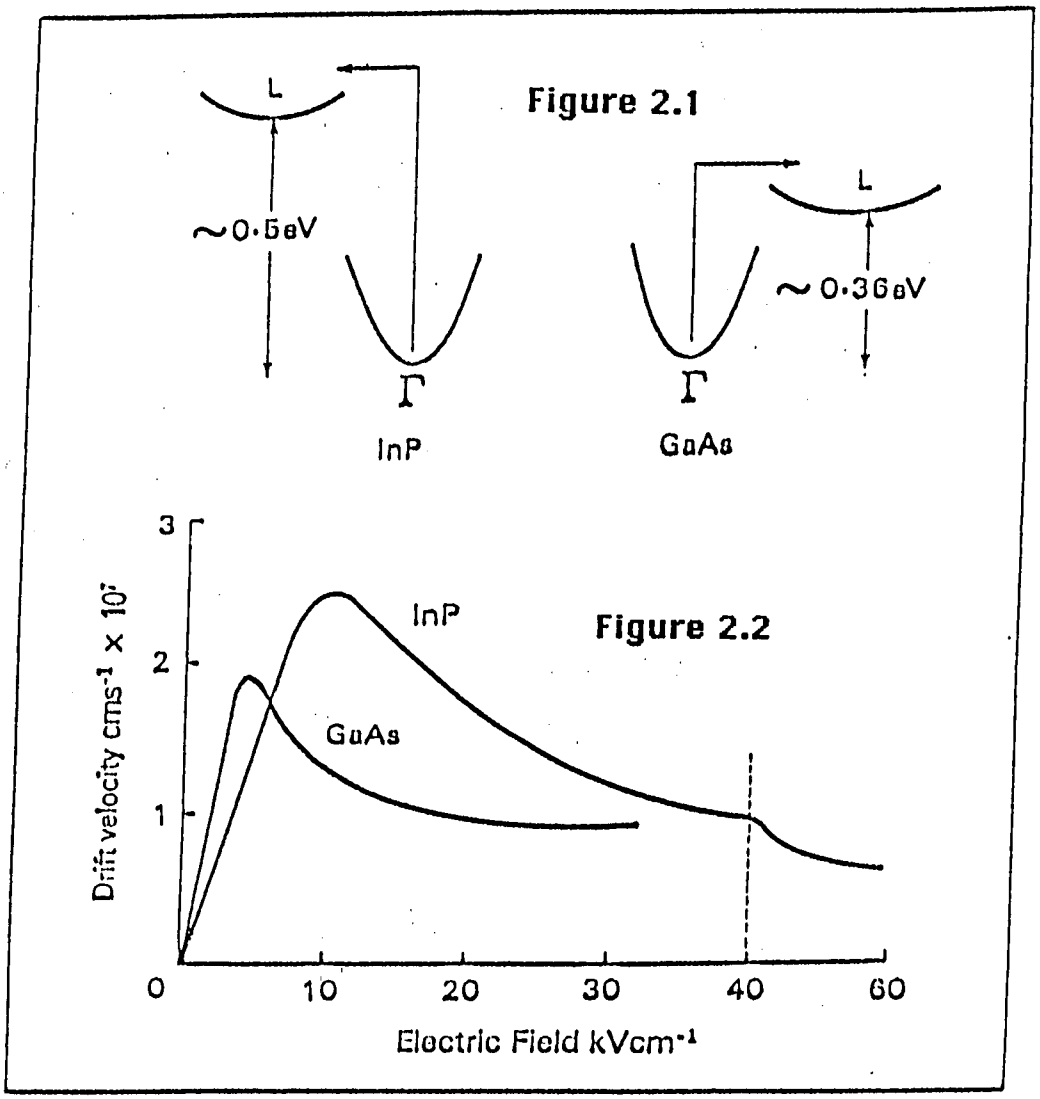

Fig. 2.1 and Fig. 2.2 showing respectively the comparative conduction band structure and velocity field curves of Indium phosphide and Gallium Arsenide taken from Ref.[27]

Essentially the mechanism is the transfer of high energy electrons from the high mobility central Γ valley to a low mobility (high density of states) satellite valley. Invariably this is the L (111) valley as opposed to the X (100) valley although some people have suggested that three valley dynamics could be a consideration in certain materials. It should be stressed though that the structure and dynamics of the valleys are not well parameterised, as is evidenced by the fact that it has only recently been accepted that the lowest valley in GaAs is indeed the L valley [48]. More recent evidence suggests that the electron dynamics at the top of the of the central Γ valley due to non-parabolicity may also play a part, particularly in materials with a large bandgap between the two conduction valleys.

At higher fields the velocity saturates in the upper valley due to increased phonon electron interaction. Finally at even higher fields, breakdown occurs.

The transferred electron effect, is a bulk effect, and therefore any oscillator essentially consists of a length of n-type material (GaAs or InP), between two electrodes. The length typically varying between 1 and 100 microns. At high frequencies (>20 GHz) the length of the active medium, normally determines the frequency range, while the active area is chosen to satisfy thermal and electrical impedance requirements [37]. The doping is another important parameter. Too low a doping and the negative resistance will always be stable (but can then be used to produce stable rf amplifiers), whereas too large a doping and breakdown, noise and reliability can become problems (as larger current flows for the same electric field). It is not the doping density that is important but the n.L product [49], where L is the active length. This imposes the following stability/breakdown criterion:

$$10^{13} > n.L > 5 \times 10^{11} \quad cm^{-2} \qquad (2.1)$$

although the usual recommended design values are normally in the range $1.2 - 2.0 \times 10^{12}$ cm^{-2}.

Along with the active layer doping, the electrode design is probably the most critical parameter at high frequencies and largely determines the electrical performance of the oscillator. In the usual 'low frequency' design the electrodes are usually chosen to be ohmic, and normally consist of very heavily doped n^{++} material which is lattice matched to the active layer. The anode is almost always ohmic, and normally forms the substrate, where further layers are subsequently grown epitaxially. This allows 'flip chip' mounting where the active layer of the device is positioned as close as possible to the heat-sink. Recently however, at the highest frequencies, interest has been shown in current limiting or current injecting cathodes. These either consist of direct metallic cathode contacts, which act as low height reverse biased schottky barriers, with current limiting properties, or the so called two zone cathode, or graded gap cathode which has similar current limiting properties. At high frequencies, this has been shown to lead to improvements in efficiency

as a more optimum current waveform is presented to the device. This is examined more closely later.

2.3 MODES OF OPERATION

In principle, any device which shows a net negative resistance at a given frequency can be made to oscillate at that frequency, if placed in an appropriate circuit. Any two terminal device which shows a negative differential resistance in its IV characteristic, is a candidate for for an oscillator or an amplifier, by biasing the device in its negative differential region.

However, as pointed out by Shockley [1], a bulk negative differential resistance does not necessarily imply a general negative resistance above d.c. Rather, there is a large negative resistance associated with the transfer of charge accumulations across the device, usually at frequencies roughly corresponding to the transit frequency. With appropriate feedback from the external circuit, the device can be made to tune around the transit frequency but at high frequencies the process becomes steadily more inefficient and therefore the frequency range (for fundamental power generation), for any device becomes banded.

Now whenever the gradient of the electron velocity electric field curve becomes negative ($dv/dE < 0$), accumulations of charge spontaneously grow within the active region. Associated with the formation of space charge within the device, are two distinct modes of operation. Namely:

1) The Classical Domain Mode
2) The Accumulation Mode

In addition the two modes can be further categorized into:

a) Transit Time Modes
b) Quenched and Delayed Modes
c) Harmonic and Sub-harmonic Modes
d) Harmonic and Sub-Harmonic Modes
d) Low Frequency Negative Conductance and Parametric Effects

As we shall see, it is the accumulation transit time mode that is thought to work at high frequencies, where harmonic extraction is often a useful means of reaching even higher frequencies.

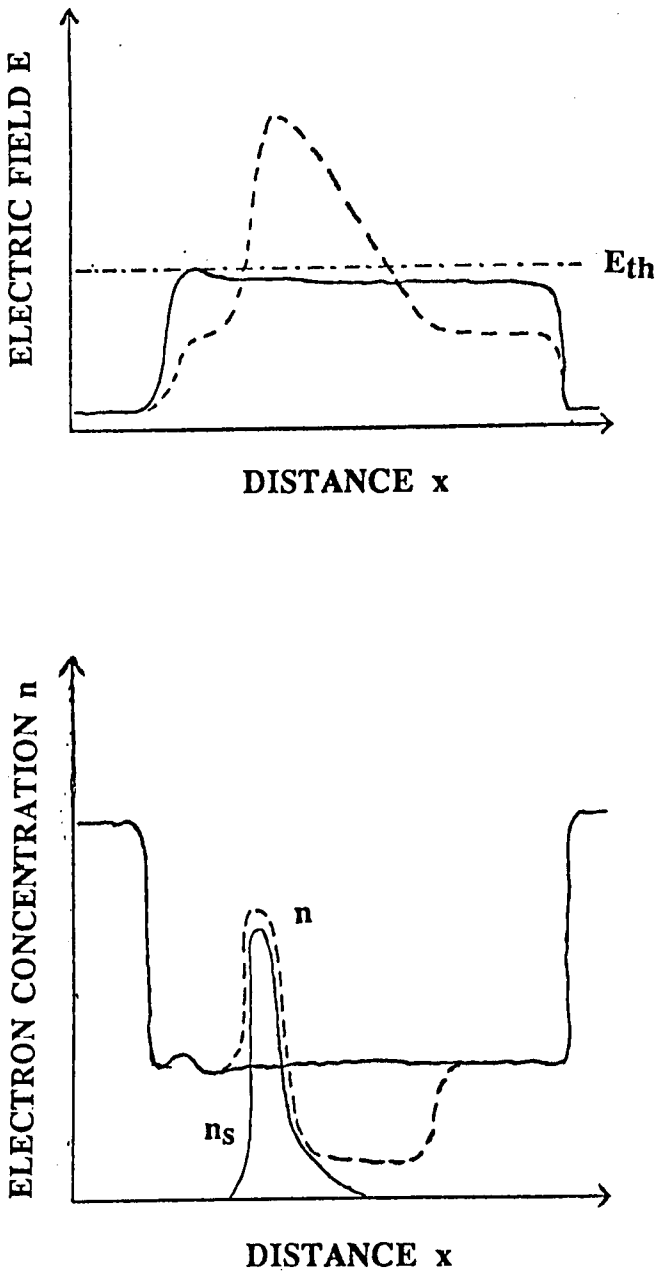

Fig. 2.3 Diagram showing the electric field (a) and electron concentration (b) for a Domain before formation and after formation. E_{th} is the threshold electric field, n is the total electron concentration, n_S is the concentration of satellite valley electrons.

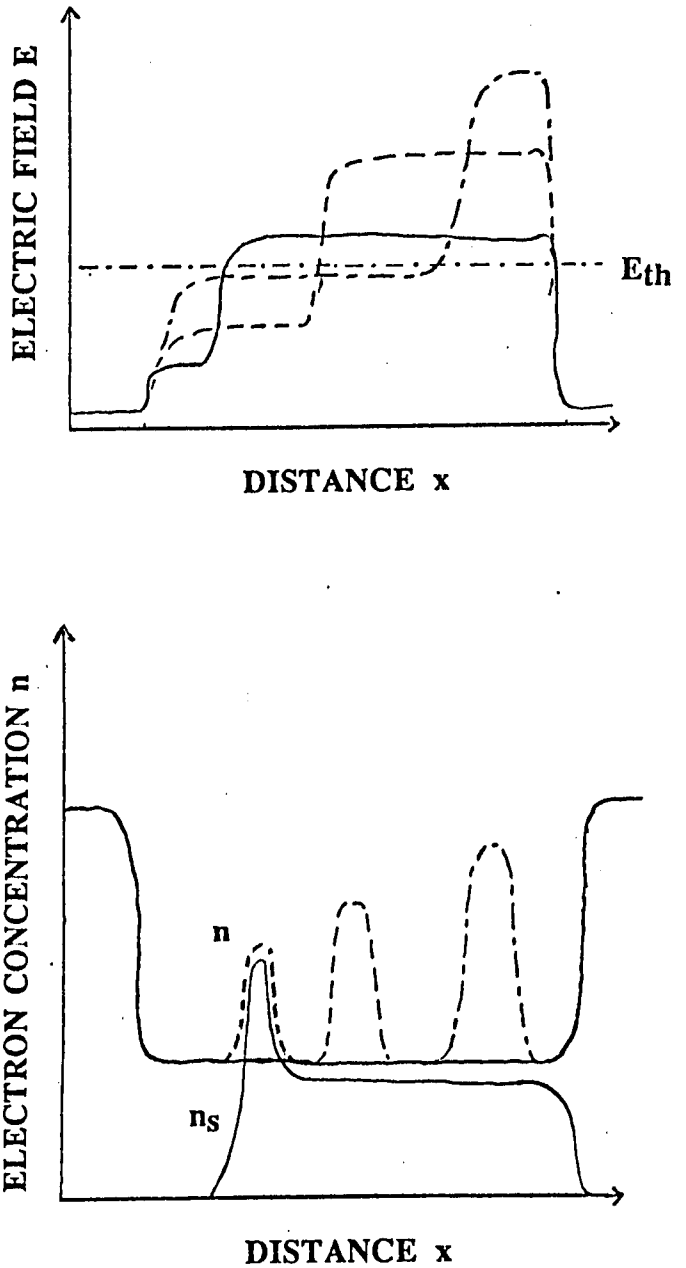

Fig. 2.4 Diagram showing the dynamic electric field (a) and electron concentration (b) for a propagating Accumulation layer. E_{th} is the threshold electric field, n is the total electron concentration, n_S is the concentration of satellite valley electrons.

that in the high field dipole domain). The rest of the sample acts as a positive resistance in series with the negative resistance, thus significantly reducing efficiency.

2.5 THE ACCUMULATION MODE

The accumulation mode in its simplest terms, is one where an accumulation layer develops in the normal way, but the depletion layer instead forms at the anode. This happens when the electric field rises so quickly, that the depletion region is unable to grow fast enough to absorb the voltage increase. The anode field therefore rises, lowering the negative differential resistance in the depletion region, which further inhibits its growth. Initially then, a high field NDR region will appear across the whole of the region between the accumulation layer and the anode, and will exist until either the high field region is quenched or runs into the anode. It is more efficient than the domain mode, because more of the material experiences the high field NDR, and there is less parasitic low field series resistance regions.

For this reason, the accumulation mode is to be preferred on the grounds of efficiency. In the early history of the development of TE oscillators though, it was felt that this mode would always be unstable, and that domains were the natural high field instability. As we shall see though, for high Q circuits there is experimental [8] and theoretical evidence [9] that the accumulation mode is nearly always present, and that many oscillations credited to the domain mode were in fact some form of accumulation mode.

2.6 TRANSIT, QUENCHED AND DELAYED MODES

When a TE device is placed in a high Q circuit, the voltage across the device will be a summation of the bias voltage, and the instantaneous value of the rf field.

$$V = V_b + V_{rf}\cos(wt) \qquad (2.2)$$

where w is the resonant frequency of the circuit.

If the rf voltage is comparable to the bias voltage, then at certain times the external voltage can be induced to fall below threshold. If the resonant frequency of the circuit is above that of the transit frequency, then the voltage will fall below the threshold voltage before the domain/accumulation has reached the anode. If it falls below the 'domain sustaining voltage' (which is about half the domain threshold voltage [7]), then the domain will collapse and a new domain will form at the cathode, as soon as the voltage again rises above threshold. This mode is known as the quenched mode. However, any form of

quenched mode, will never be as efficient as the equivalent transit device, as the region which is not traversed will always act as a series positive parasitic resistance.

If on the other hand, the resonant frequency of the circuit is above that of the transit frequency, then the domain will reach the anode. However, if the voltage of the rf signal is properly phased, then the voltage across the device can now fall below threshold, thus delaying the formation of a new domain. This is called the inhibited or delayed domain mode.

The importance of these modes is that the operating frequency is primarily controlled by the circuit, and it is these effects that can give TE oscillators more than an octave of tunability. However, it should be noted that at very high frequencies the situation becomes more complicated, as the extent of the charge accumulation becomes comparable to the transit length, and the time required for formation of the space charge becomes comparable to the frequency. Computer simulations have shown that these parameters are strongly influenced by the external frequency, and that the distinction between transit modes and delayed and quenched modes becomes more vague.

2.7 POWER / IMPEDANCE PRODUCT

Transit modes also become inherently more inefficient, as the frequency increases, as they are always subject to a power impedance product limit that scales as 1/f. In other words, there is usually a limit to the impedance level of a device that can be matched into a microwave circuit. Low impedance waveguides or transmission lines will have larger wall currents and larger rf losses, and any form of impedance matching will also incur rf losses. There is a limit therefore, to how much 'extra' power can be obtained by increasing the active area of a device, or by paralleling up devices. 'Extra' power is indeed obtained, as more current flows for the same voltage, however, the impedance level also drops, and eventually a point is reached where all the 'extra' power is just absorbed into the extra rf losses. To obtain more power, one therefore needs to increase the impedance level, which means increasing the voltage for the same current. This implies, using longer devices, or placing devices in series. It also gives a basis whereupon different devices can be compared; namely through their power impedance product.

It can now be understood why power for these oscillators can be expected to fall off as 1/f for any transit time device. As the frequency of operation increases, the active layer width (transit distance) decreases. Assuming a maximum permissible electric field across the device:

$$E_b = V_b/L = V_b \cdot (2f / v_s) \qquad (2.3)$$

it can be seen that the voltage must scale as the active width, which scales as 1/f. (The current must also scale with the voltage as it is limited by the minimum impedance requirement).

2.8 ACCUMULATION MODES

There now follows a brief historical survey, starting with the LSA mode, which was originally thought to be key to efficient operation at high frequencies. Subsequent research showed that at the highest frequencies Gunn diodes always operated in a type of accumulation transit mode, which was still largely tuneable.

2.8.1 THE LSA MODE

The LSA mode was originally proposed by J.Copeland in 1966 [10], as a way of producing very high power oscillators at high frequencies. The basic idea was to operate in accumulation mode so the whole sample 'experiences' the NDR, and to work with a quenched mode, so that the device is not limited by length. In theory, one could then have very long samples, with very large voltages across them. Carroll [5] suggested that difficulties in maintaining a uniform field across the sample may well limit the length, in conventional resonators, to no more than a quarter of a wavelength (electromagnetic wave). If one accepts this limitation, then one can still consider the device to have a power impedance product; which Carroll shows to be about five orders of magnitude greater than a conventional device working in the domain mode! One still has thermal limitations, but some very impressive results have been obtained in pulse mode at low frequencies. Over 6000W peak power [3] has been obtained at 1.75 GHz, and 2100W peak power at around 7 GHz. However, it has been shown that the time required for true quenching and rethermalization, limits the upper operating frequency to around 20 GHz, and higher frequencies always correspond to a type of transit or hybrid mode.

A critical factor in LSA operation is control of the build up of space charge to ensure that domains are not formed. A domain would attempt to 'absorb' all the voltage across the device, and in very long devices with large voltages, this can lead to high

localized electric fields, which in turn can lead to breakdown. One requirement is for very uniform material, both in donor density and cross-sectional area, as any non-uniformity will tend to produce local space charge accumulations.

Charge accumulation will also occur when the device is biased in the NDR region of the velocity/field curve. It is therefore usual to bias the device well above threshold, and into the saturated velocity region. Here, the voltage swing (as determined by the Q of the circuit) will ensure that the device spends a limited amount of time in the NDR region.

It is important that any voltage swing is sufficiently large, that it takes the field below threshold, so that a accumulation formed at the cathode is quenched completely, later in the device. If it is not, another accumulation will start to regrow at this point, which again can eventually lead to domain formation, or the production of sub-harmonic frequencies [11].

The point is that the load resistance determines the amplitude of the rf field. This must be large enough to permit quenching (otherwise breakdown can occur due to domain formation), however, too large a value and the diode may not be matched properly. As a general rule, the load resistance needs to be as small as possible while still permitting quenching.

In fact, it is the quenching condition, that imposes an upper frequency limit for LSA operation. As remarked before, it is important that the field remains below threshold for long enough to ensure that the space charge is completely quenched. However, not only must the space charge be quenched, but the electrons in the satellite valleys must 'cool' sufficiently, so that there is a significant transfer back to the central valley, otherwise the accumulation will again start at this point. This additional criterion was first identified by Jones and Rees [13] and imposes a limiting upper frequency for the operation of true LSA. Their Monte-Carlo simulations indicating a minimum time below threshold of about 20ps corresponding to an upper frequency limit of about 20 GHz for GaAs. Experimentally, true LSA operation has not been observed above 16 GHz (for GaAs), although claims for LSA operation at much higher frequencies are widespread throughout the literature. Due mainly to the work of Rees though, it now seems certain that most of these devices were working in some form of transit accumulation mode.

This frequency limit will be somewhat higher for InP [16], where theoretically high efficiencies (>15%) should be possible in an inductive circuit up to 50GHz. Mazzone and Rees [16], however point out that a small parasitic parallel capacitance can drastically cut the efficiency at high frequencies, making efficient operation difficult above 30 GHz. At 20 GHz though, efficiencies greater than 25% are predicted. At frequencies greater than 50GHz, maximum efficiency can only be expected to come from some form of transit mode.

2.8.2 ACCUMULATION TRANSIT MODE

LSA operation has been claimed for devices operating up to 90 GHz, but usually it was done on no more evidence than good circuit controlled tunability, and a frequency a few times larger than the expected transit time frequency, corresponding to a velocity of $1x10^7$ cm/s. However, as Jones and Rees [14], in their computer simulations, found, there are a number of effects that lead to good circuit tunability and operation at high frequencies.

a) First, unlike the domain mode which has a velocity of $1x10^7$ cm/s, small accumulation instabilities can have high velocities of around $3x10^7$ cm/s.

b) The accumulation velocity also tends to match its speed to the variation in device voltage. It will increase as the layer is quenched, (at the anode) and decrease as the layer is formed.

c) Also if the transient voltage conditions are correct, then, 1) the collapse of the layer at the anode can be delayed by maintaining a high enough device voltage and, 2) a new layer can grow (at the cathode) before the old one has collapsed at the anode. Both these effects extend the upper and lower operating frequencies.

2.9 TRANSIT ENHANCED COOLING EFFECT

As pointed out before, a critical frequency limitation on the LSA mode is that the electrons remain hot (i.e in the satellite valleys), for a considerable time, at the point where

the layer is quenched. However, this is not so for any transit effect, due to the so called transit-enhanced cooling or Jones-Rees effect. This effect can be understood by considering Figure 2.4 which shows the electron concentration and electric field in the vicinity of an accumulation. Most of the electrons in the accumulation will be in the satellite valleys, where they will be subject to large intervalley scattering rates. Any electron that is scattered into the central valley, will find itself moving with a large velocity v given roughly by:

$$v \sim (2 \mathcal{E}_s / m^*)^{1/2} \qquad (2.4)$$

where $\mathcal{E}_s$ is the potential energy of the electron in the satellite valley. Such an electron is essentially scattered in a random direction. If it is scattered in the direction of the field (towards the anode), it will rapidly overtake the accumulation layer, where it will find itself in a region of even higher electric field, where it will further accelerate. Such electrons are therefore rapidly scattered back into the satellite valley. An electron that is scattered in the opposite direction against the field, will also leave the accumulation layer quickly, being deaccelerated by the field. This electron will now find itself in a region where the field is below threshold, and unable to scatter the electron back into the satellite valley. The electron is therefore cooled all the way down to the satellite temperature in a time roughly equal to τ given by:

$$\tau = 1/_{qE} \cdot (2m^*\varepsilon_s)^{1/2} \qquad (2.5)$$

The time τ can be regarded as the characteristic time constant over which the electrons can redistribute themselves in response to a change in field [15]. Its value also defines the maximum frequency which can be obtained for any given material.

This process is highly advantageous as far as the TE effect is concerned as high energy electrons are placed where the accumulation layer needs them, whereas all the electrons behind the layer are left in a cooled state. After the accumulation has collapsed at the anode, the device will be free of any space-charge within its active region. A large improvement in frequency response can therefore be expected for any form of transit accumulation mode. Indeed, it is now generally accepted that all high frequency GaAs oscillators (>20 GHz) work in some sort of variant of this mode.

Jones and Rees have also done calculations on the optimum doping requirements for the transit accumulation mode [14]. They found that the n/f ratios still fall in the range normally associated with LSA operation, and the efficiency went up steadily with increase in the n.L product. For a reasonably efficient oscillation they suggest a lower limit of n.L $>= 5x10^{11}$ cm^{-2}, and an upper limit of n.L $<= 10^{13}$ cm^{-2} (otherwise excessive fields at the anode can develop). Short devices, not unsurprisingly were found to be less efficient than long devices, as is to be expected from consideration of the LSA mode. Jones and Rees showed that the preferred oscillation frequencies, corresponded to an effective transit velocity of $1.5x10^7$ cm/s (as opposed to a domain velocity of about $1.0x10^7$ cm/s). Taking this as the normal operating mode, Jones in a subsequent series of papers, showed that there was some advantage in efficiency to be gained by moving to overlength modes.

2.10 OVERLENGTH MODES

They discovered that there were three different types of overlength modes. The fully quenched or LSA mode, which has already been discussed; the so called incomplete quenched mode, and the accelerated transit mode.

As already mentioned, incomplete quenching can lead to transit effects, which manifest themselves as subharmonic components appearing in the waveform. However, if the quenching is nearly complete, then a field profile illustrated by curve d in Figure 2.5 can evolve [11]. Here, no subharmonic components exist, and the current can be higher at low voltages, leading to greater efficiency. However, there will be a limit on device length (for a particular frequency), if transit effects are not to dominate. Where they do, the field profile can ultimately evolve to a stable high field zone at the anode.

The third mode is the accelerated transit mode, and is probably the one most pertinent to efficient high (fundamental) frequency operation (>25 GHz for GaAs). It is a hybrid of the quenched and transit modes. As previously remarked, on quenching, large layer velocities of up to $4x10^7$ cm/s can occur. In this mode, therefore, the hot electrons (after quenching) reach the anode before they thermalise, leading to a better frequency response than the incomplete quenched mode, and a larger efficiency than the normal transit mode.

The existence or possibility of these modes, fully explains the high frequency operation of Gunn diodes in long samples, which were previously thought to be true LSA. The optimum circuit requirements are essentially the same for all three different modes, with bias voltages about three to four times the threshold voltage, and the operating currents, 0.6 to 0.7 of the threshold current [11]. Jones and Rees also give representative values of the parallel load resistance and reactance for each mode. For the accelerated transit mode, the load resistance is roughly the same as for the idealised LSA mode [10], at low frequencies (about $30R_0$ at 25 GHz where R_0 is the low field resistance), but increases at higher frequencies (e.g. $80R_0$ at 43 GHz) due to the effect of relaxation processes. Values of the reactance were given as $10R_0$ at 25 GHz, decreasing slowly to about $7.5R_0$ at 43 GHz. All these values were calculated for GaAs Gunn diodes.

2.11 TRANSIT DEVICES AT VERY HIGH FREQUENCIES

With the transit mode, it might be expected that to obtain higher and higher frequencies, all one needs to do is to shorten the device until the limit imposed by the response time of the bulk material is reached. In practice though, device and circuit requirements become much more stringent. Any reduction in the length of the sample, entails a reduction in resistance, if the n.L product and the cross-sectional area are to remain the same. At high frequencies (around 60 GHz for GaAs), this calls for critical device and circuit parameters, to ensure that any contact or spreading resistance does not swamp out the active layer resistance.

Acceleration times at the cathode also becomes an important factor [21]. Montecarlo simulations of devices [14,22] have shown that for n^+ ohmic cathodes (which in the past have almost invariably been used), that there is a 'dead space' region of at of at least 0.5 microns for GaAs. (This 'dead space' region will be somewhat larger for InP). This arises because a n^+ cathode imposes a low field boundary condition, and injects low energy, high mobility electrons, which need to gain energy before they can be scattered into the satellite valleys. This requires both space and time, and is relatively inefficient because of strong scattering from polar optic phonons ($h\upsilon_{pop} \approx 35$meV)[51] , and thus can effect the efficiency and the effective frequency cut-off. Having reached the requisite energy, the transfer to the satellite valley occurs fairly abruptly. The initial period of acceleration is

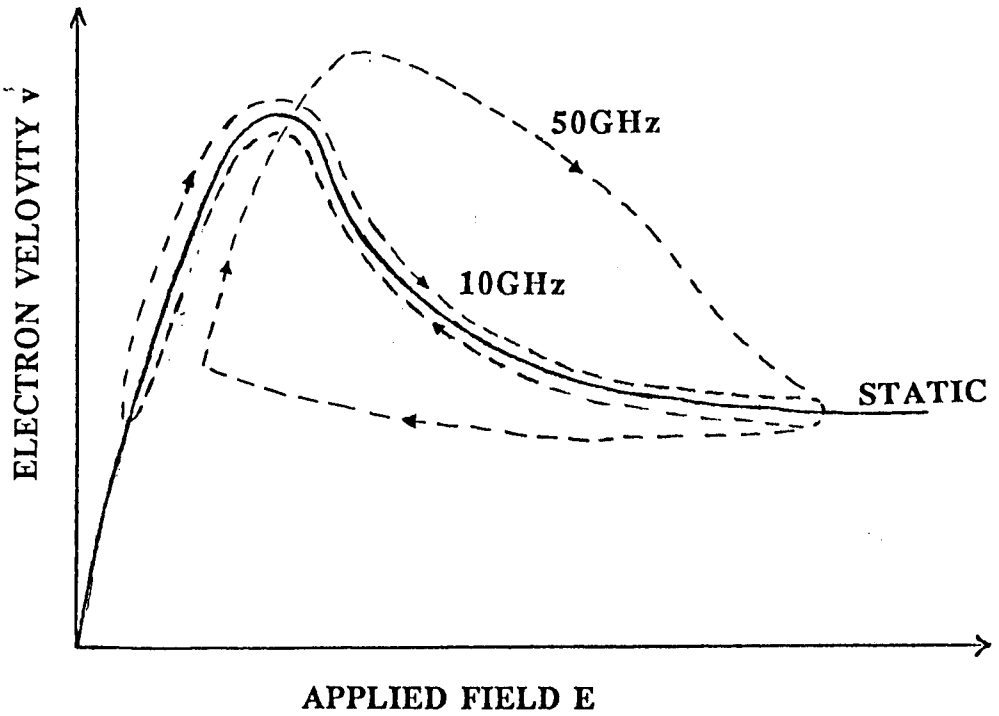

Fig. 2.5 Diagram showing the effects of high frequency hysteresis due to velocity overshoot. At high frequencies the current and voltage no longer follow the static IV curve which leads to a loss in r.f power.

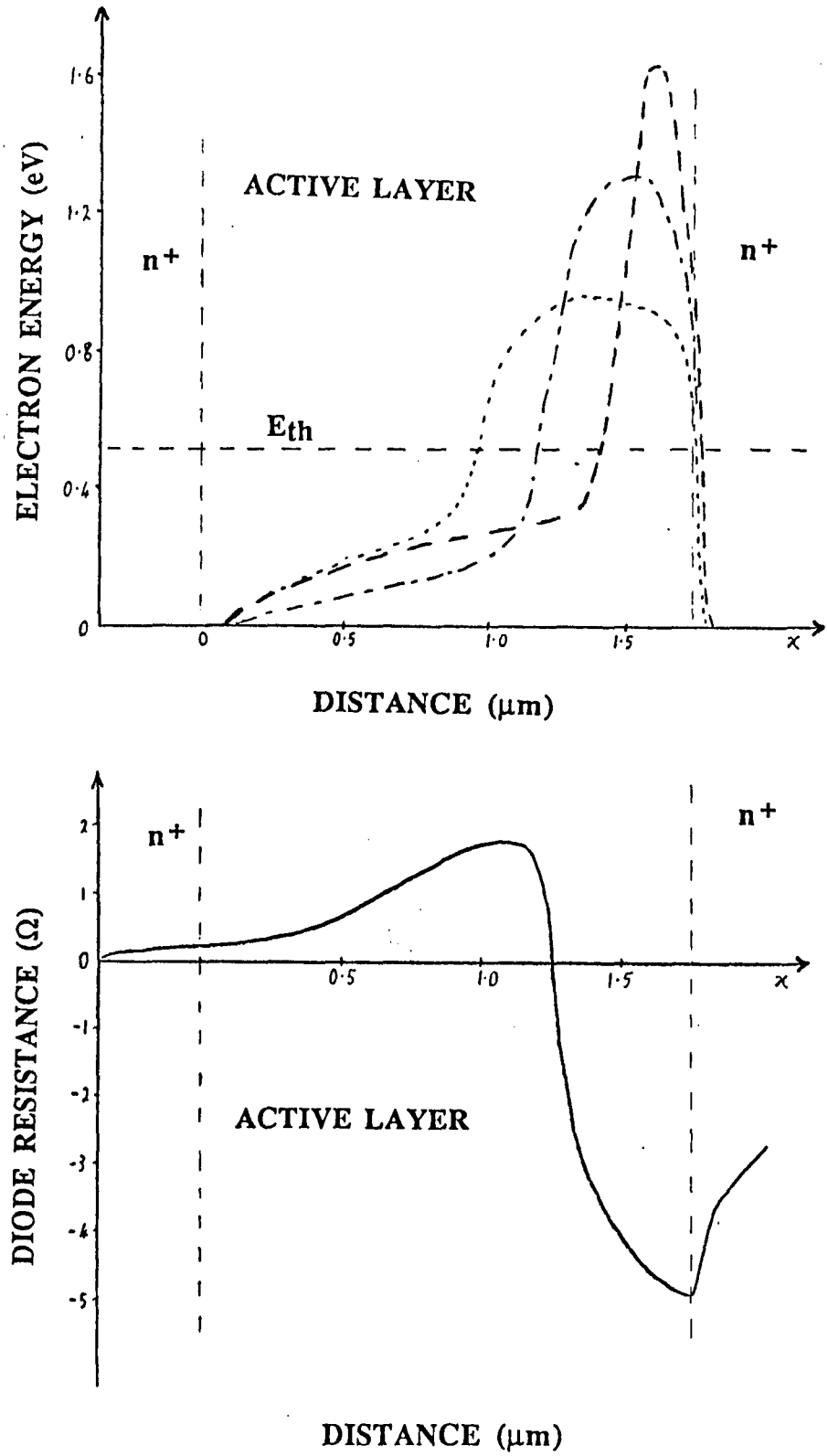

Fig. 2.6 Diagrams ilustrating (a) velocity overshoot in the dynamic propagation of an accumulation layer, and (b) the effective resistance across the layer due to the effects of velocity overshoot. Negative resistance is only achieved in the latter half of the active layer . The first half acts as a parasitic positive resistance lowering the total r.f. impedance and thus reducing total power output.

characterised by high velocities, of around twice the threshold velocity, which resembles ballistic motion of the electrons [23]. For a high frequency device of only a few microns, this effect can significantly increase the current relative to a longer lower frequency device. On transfer, the velocity decrease is greater, and this means that the electron accumulation becomes narrower and more intense. The rf current swing is therefore large. The voltage swing however is limited by the 'cathode dead space' which just acts as parasitic positive resistance region. The high field region, which generates the necessary negative resistance, is limited to a zone near the anode. It is thus clear that as the length of the device is made smaller for higher frequency operation a larger and larger percentage of the device acts as a positive resistance. This leads to a low net rf impedance, which makes matching difficult and contact and circuit losses more critical. The peak electric field can also be high, which can lead to breakdown problems. These effects are illustrated in Figs 2.5 and 2.6.

It is these limitations that have limited the frequency of operation to around 60 GHz (fundamental) for GaAs (n+ cathode) Gunn diodes [27], rather than any fundamental cut-off associated with the bulk properties of the material. GaAs Gunn diodes working to higher frequencies (>80 GHz) have invariably been found or assumed to be working in some form of harmonic mode. Friscourt et al.[37] however, has suggested that fundamental oscillation could be obtained in GaAs at 100 GHz, if 1 micron active lengths were used, although there are no reports of anyone getting any power out at this frequency using such diodes.

It also can be shown that the voltage/current waveforms produced by this structure are not conducive to high efficiency operation. Generally speaking, best efficiency is obtained when there is an abrupt change from a high voltage/low current state to a low voltage/high current state. (For fixed maximum and minimum values, a square wave, has the largest fundamental component of any waveform [24]). For the n^+ cathode, in addition to the rf voltage swing being limited, the voltage maximum occurs at a point where the accumulation layer is still growing, and thus, where the current is well above its minimum (valley velocity) value. This again acts to limit the efficiency [25,26].

For efficient operation it is thus highly desirable to be able to remove the dead space region, caused by the time required to accelerate the electrons to the requisite energy for efficient transferral to the satellite valley. To that end, various different cathode structures have been devised to try and inject hot electrons directly into the active region. These are considered below.

2.12 CATHODE STRUCTURES

Any improvement in these characteristics clearly requires a new cathode structure. In practice, two effects have been used to improve efficiency and extend the frequency range; namely hot electron injection and/or current limiting cathodes. Any form of hot electron injection, where the electrons are injected with an energy close to the satellite valley energy, will reduce the 'dead space' region. This in turn will increase the voltage swing, and lead to improved efficiency. There is still the problem that there is a low field condition imposed by an n^+ cathode. Nor is this helped by a large n^- doping notch or by a resistive layer close to the contact, which some workers have used, as this just imposes a high field boundary condition. This can be useful to stabilize amplifiers [28], but in oscillators it means that the device can not effectively go to a low voltage/high current state, due to formation of additional accumulation layers [26]. This leads to a very low efficiency.

2.12.1 CURRENT LIMITING CATHODES

These problems can be overcome with a current limiting cathode, where the electron current is made to saturate at a value corresponding roughly to the valley velocity, but the cathode field can vary between a value close to threshold and a very large value. This allows very efficient switching from a low voltage/high current state to a high voltage/low current state. Such a cathode also allows bias levels much greater than for n^+ cathodes and will have a higher power impedance product. Note, this cathode will have a more limited current swing, but this is more than made up for by the larger voltage swing and the improved voltage/current waveforms.

A current limiting cathode can be made by using a metal contact, which in effect creates a reverse-biassed Schottky barrier. This should have a potential drop just greater than E_S when the field goes above threshold, so that the cathode injects electrons with enough energy to immediately scatter into the satellite valleys [15]. This requires a very low barrier height which has been experimentally determined to be between 0.15 and 0.2

eV for optimum efficiency (in InP at around 12 GHz) [26]. Such low height barriers are difficult to achieve, and typically require a complex process of alloying metal films with the semiconductor surface. In addition, a contact will be optimum for only a small range of doping densities of the bulk material [28]. Also, as one of the primary processes of electron injection is through thermionic emission, the barrier height will have an exponential dependence on temperature. Optimum performance will therefore only be achieved over a limited temperature range. This technology is more suited to InP as the barrier height of a Schottky barrier contact on InP is low compared to GaAs [29]. For GaAs it would seem that metal contacts produce barrier heights which are too large, although it is believed that Varian may have found a way of producing a type of Schottky barrier on their GaAs diodes.

The area of InP diodes is usually limited by thermal requirements, to prevent device burnout, rather than impedance considerations (GaAs). However, this problem should be overcome with diamond heat sinking. Using current limiting contacts with diamond heat sinking, though, Varian [29] predict that 500 mW (10% efficiency) should be possible at 56 GHz, and 250mW (5% efficiency) at 94 GHz. The major limiting factor now being the matching capability of the circuit, for large area diodes.

A curious feature of these diodes is the current/voltage characteristic, where the bias current does not fall or stay steady above threshold, but increases with applied voltage until breakdown occurs. This is now believed to be due to the self heating of the diode, which lowers the effective barrier height at the cathode. It is also usually an indication of good device performance.

The temperature sensitivity can lead to a sharp peak in efficiency over a temperature range of just a few degrees ^{o}C as was shown for InP at 13 GHz in [26]. Varian have indicated though, that they now have the technology to specify the optimum efficiency at the desired temperature operating range. Alternatively, they state they have a cathode design that will give nearly flat efficiency and power over a large temperature range (-40C to 60C) [27], although this is achieved at the cost of some lowering of the output power. It has been reported that silver contacts have a weak temperature sensitivity, but do not give optimum efficiency [26], possibly because of a thin resistive layer being present, due to the diffusion of silver.

2.12.2 2-ZONE CATHODE

This structure was originally proposed to overcome the problems associated with the temperature sensitivity of the Schottky barrier, while still maintaining high efficiency. The structure of a 2-zone cathode is given in Figure 2.6. It comprises a very thin (< 0.3 microns) n^+ layer, next to the active layer, followed by an outer high field lightly doped semiconductor (few tenths of a micron), with a metal Schottky barrier contact. This device works on the principle of hot electron injection, although the thin n^+ layer also has current limiting properties. (The current being found to be well below that for an ohmic contact, thus giving a higher power impedance product). The principle of operation, is that the electrons are accelerated to high kinetic energies in the high field zone, and then retain a substantial amount of energy in crossing the thin n+ layer. Hot electrons are therefore injected at the cathode contact, which leads to an improvement in efficiency as discussed before. The metallisation process also becomes less critical, and sintered silver contacts have been shown to produce devices that have given 15-18% efficiency from -50 ^oC to 150 ^oC at 14.5GHz [30]. This is slightly less than that achieved by the best direct metal contact at this frequency (>20%), but the temperature stability is obviously an important consideration. It involves a more sophisticated materials technology though, which undoubtedly becomes more critical at higher frequencies. Varian report that they have made metal, ohmic and two zone cathodes for use at 90 GHz, where they found that metal current limiting contacts gave the highest powers and efficiencies [31]. They did not give details of results obtained for 2-zone or ohmic cathodes, although most of their efforts now seem concentrated on the technology of direct current limiting metal contacts for InP diodes.

2.12.3 GRADED GAP CATHODES

In 1975 Clark et al.[28] suggested an alternative approach to the Schottky barrier, with similarities to the two zone cathode. This involved the use of a semiconductor with a different bandgap to the bulk material, to provide a suitable current limiting contact. This scheme is more applicable to GaAs than Schottky barriers or two zone cathode schemes, which have just been used with InP diodes.

A refinement of this scheme has been studied recently with structures similar to that shown in Fig.2.7. The cathode consists of an undoped $Al_xGa_{1-x}As$ layer of graded Al/Ga

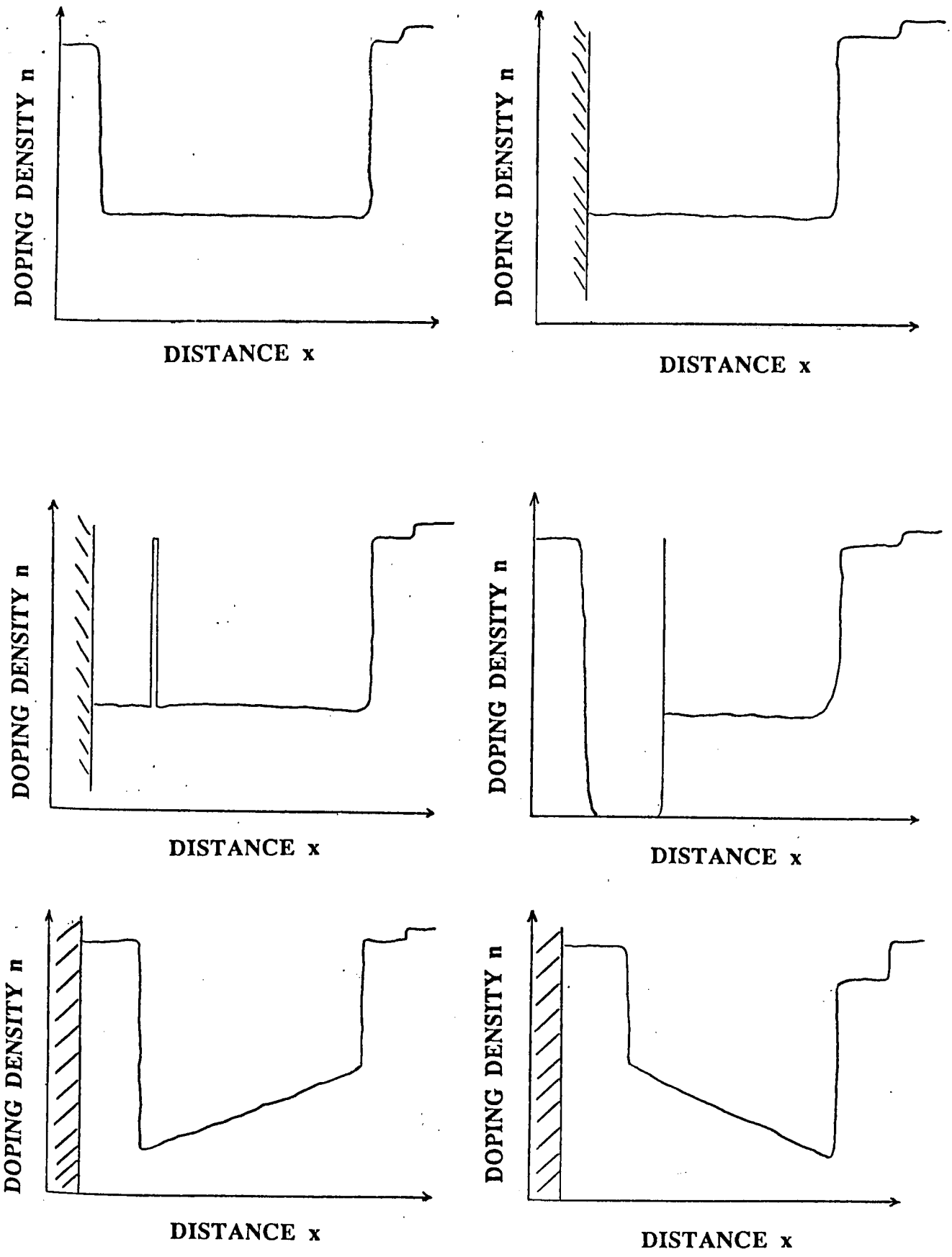

Fig.2.7 Diagams illustrating schematically some of the various different cathode structures used in the manufacture of Gunn diodes, including (a) the standard $n^{++}nn^{++}$ structure, (b) Metal Barrier, (c) Two Zone Cathode, (d) Graded Gap Cathode and (e) (f) structures with Graded Active Layers

ratio (from x=0 to x=0.3) which extends over a distance of 50nm. This forms a triangular barrier that acts as an injector of hot electrons of roughly 300meV, which is similar to the height to the satellite valley ($\Delta E_{\Gamma L} \approx$ 330meV)[51]. The barrier is triangular, to try and reduce the capacitance (relative to a square barrier) [52], and to try and make the barrier height independent of bias [50].

This is followed by a very thin (5nm) highly doped (10^{18} cm^{-3}) n^+ GaAs notch which effectively acts to control the electric field, by preventing the depletion region under forward bias, from extending into the active region of the device . However, it does not seriously affect the energy of the hot electrons, as the inelastic mean free path for hot electrons has been shown to be $\approx$ 45 nm at a doping density of 10^{18} cm^{-3} [51]. These two features in combination would appear to effect a very efficient hot electron injector, as devices have been made to oscillate very efficiently with active lengths too small (1μm), to allow operation with normal n+ ohmic contacts. Some very promising results have been obtained recently, and these are reported in greater depth later in this thesis. Most importantly, the length of the active region can now be chosen to accurately peak the power at any desired frequency in W band (second harmonic)[53], and power levels of up to 68mW have been achieved at 94 GHz.

2.13 GRADED DOPING ACTIVE LAYERS

Another very promising scheme which has been reported on recently is graded doping of the active layer [54]. This scheme has produced significant increases in power and efficiency for GaAs oscillators operating at 68 GHz and below (second harmonic), and has shown the potential for improved reliability. The idea is that in an ideal device we wish the resistivity or mobility of the active layer to be constant across its length. However, the mobility is a very strong function of temperature, and there is typically a large temperature gradient across the device (with the cooler end situated towards the heat-sink). According to the heat flow equation, this will have an exponential profile which means that the resistivity will vary exponentially across the active layer. It is possible to compensate for this by exponentially grading the doping layer to effectively keep the resistivity flat across the device. This is illustrated schematically in Figure 2.8.

This has given improved efficiencies and powers compared to flat profiled $n^+ n\ n^+$ devices, with maximum powers of 345mW (6.8% efficiency) at 31 GHz, and 90mW (1.8% efficiency) at 67.8 GHz (second harmonic). Accelerated life-time testing showed

little change in performance over 10,000 hours at 110^{0}C. Extrapolation of this result suggests continuous operation at room temperature of 19.4 yrs. Full results and details of profiles are given in ref.[54], where the importance of flip-chip mounting (to bring the active region as close as possible to the heat sink), and substrate thinning (to reduce skin depth losses) was also emphasised.

2.14 HARMONIC GENERATORS

The highest fundamental frequency that has been reported for GaAs is about 75 GHz, and for InP about 140 GHz. It is possible that these limits can be extended, but device and circuit parameters become critical, and efficiency starts to drop rapidly as one moves to higher frequencies. However, there is a growing need for oscillators at higher frequencies particularly at the atmospheric attenuation minima at 90, 140 and 220 GHz.

In practice there are two approaches to higher frequencies; both of which involve frequency multiplication. Usually this is achieved (using solid state devices) by using a frequency multiplier such as a varactor diode (non-linear capacitance/voltage), and pumping it with a fundamental oscillator. The very best frequency multipliers, however, are typically only a few percent efficient and add a new range of complexity to the circuit, as filters, idler circuits, and isolators are required.

Recently, interest has been shown in using the non-linearity of the bulk TED material itself to make multipliers. In addition to the non-linearity of the Gunn effect, two other mechanisms are found to cause non-linearity in GaAs [32]. These include the dynamic nonlinearity associated with a non parabolic central conduction band, and electron heating which alters the collision frequency. These last two effects can be expected to work at much higher frequencies than the Gunn effect, and have been used to generate third harmonics in n-type GaAs (without a static electric field) [32]. Efficiencies were very low however, and there are undoubtedly better materials than GaAs to exploit these effects.

A much more promising approach is to bias the GaAs with an electric field close to the Gunn value, and then pump it with a fundamental frequency wave. Here, the non-linear interaction can amplify simultaneously the fundamental frequency wave as well as the generated harmonics. The efficiency therefore can be very large, where in principle, the harmonic power may exceed the incident wave power [33,34]. This process has been analysed theoretically by several groups, however the only people to take relaxation effects

and the rf field components into account, have been Mazzone and Rees [34]. They showed that it is possible to have very efficient operation using a type of LSA multiplier mode, where strong second harmonic components allow operation to considerably higher frequencies than that allowed for the fundamental frequency mode. They suggest the frequency limit for second harmonic generation in GaAs should be between 120 GHz and 240 GHz, with efficiencies exceeding 100%. (The frequency limit, as usual, can be expected to be higher for InP). They also give values for the optimum impedances that should be presented to the diode at the fundamental and harmonic frequencies. As yet, no experimental results seem available.

It should be noted though, that it is the difficulties in designing a low loss circuit, where the harmonics are all properly terminated, that usually limits the efficiency at high frequencies, rather than the non-linear characteristic of the multiplier diode. However, the 8% efficient (250-280 GHz) frequency tripler (using a varactor diode), designed by J.Archer [12], which terminates the harmonics quasi-optically, shows that this problem can be overcome. The multiplier, however, uses state of the art circuit designs, which require high precision machining and electroforming techniques.

An alternative approach is to extract the appropriate harmonic from the fundamental oscillator itself, as the voltage and current waveforms will be non-sinusoidal. Fairly simple circuits can be built to achieve this and efficiencies can be surprisingly high. A 4.8% efficiency has been claimed for a 2nd-harmonic L.S.A. oscillator producing 170W peak power at 17.5GHz [47]. Also it has been, up to now, generally accepted, that all GaAs oscillators operating at 90 GHz, work in second or third harmonic mode, where an oscillator capable of giving 100mW at 45 GHz, can give more than 20mW at the second harmonic frequency. This is a sizeable improvement over what a commercially available multiplier might provide (from 100mW), and gives hope that such results might be extended to higher frequencies. (Although there is still some doubt about the mode of operation [37],[40]). In addition, because of the very high Q normally present at the fundamental frequency in these oscillators, they are found to possess very good noise and load pulling properties. Despite these advantages, very little theoretical work has been done on this mode, and most experimental results seem to have concentrated on the production of 60-120 GHz oscillations using GaAs diodes [35],[36],[38]. Impressive powers, and ultra wide-band oscillators have been made in this frequency range. It would seem likely

that it is possible to extend these results to higher frequencies using InP diodes, although it can be expected that the package parasitics will be a problem.

The published results for InP that have used n^+ cathodes, have shown the voltage/current waveforms are not optimum for fundamental operation, due to relaxation effects. However, such cathodes quite possibly have larger voltage/current components at second harmonic frequencies than current limiting cathodes, as well as offering greater temperature stability and longer lifetime . Ohmic cathodes, in fact, have been made to work successfully at 90 GHz with InP diodes, using active lengths of about 1 micron, at power levels of about 50 mW [39]. It remains to be seen whether they will be more efficient at producing harmonics than their current limiting counterparts. Another possibility might be to incorporate additional non-linear structures into InP diodes.

Friscourt et al. have written an excellent paper where they consider the fundamental and harmonic operation of GaAs devices at 100 GHz (using n^+ cathodes) [37]. Simulations indicated that the output power at the second harmonic increases almost linearly with the voltage swing at the fundamental (weak nonlinearity of the device). Therefore, one design criterion is that as large a Q as possible must be provided at the fundamental. Its efficiency is limited, by the negative resistance at the harmonic, which has a sharp maximum for a relatively low voltage swing at the second harmonic. This limits the maximum efficiency to around 1% (d.c to r.f.) at a second harmonic voltage swing of about 20% of that of the bias voltage. Allowing for circuit losses they suggest that at 100 GHz, for a well designed device, not much more than 35 mW should be possible. These results are in good agreement with experimental findings.

2.15 NEGATIVE RESISTANCE AND PARAMETRIC EFFECTS

It was stated previously that any low frequency oscillation would be unstable, and high frequency transit effects would dominate. This is true; however, low frequency negative conductivity can appear, when the device is oscillating at a higher frequency. It can then interact parametrically with the transit frequency to provide oscillations at several different frequencies at the output port [43]. Usually this is undesirable, and circuits should be designed so that they are lossy at low or sub-harmonic frequencies. However, the effect has been used to make u.h.f and v.h.f. oscillators, which have good frequency

stability, and wide-range mechanical or varactor tuning [44,45]. Reflection type amplifiers have also been made from Gunn diodes, that were simultaneously oscillating in a higher frequency domain mode [46].

The low frequency effect stems from the so called residual negative resistance, which exists when a domain or accumulation is traversing the sample. Any increase in voltage will push the domain/accumulation slightly lower down the velocity/field characteristic, leading to a slightly lower current, and similarly any decrease in voltage will lead to a higher current. Hence low frequencies can experience low gain amplification. An effect which can be quite marked in short samples, and which is most often seen through parametric amplification.

In LSA oscillators, Copeland has pointed out that this negative conductance can only exist up to frequencies of order f/Q, where f is the oscillation frequency and Q is the 'quality' factor of the cavity [10]. His arguments were based on the need to maintain space charge control, but they equally apply to transit modes. Essentially there is a limit to the frequency of modulation that has any effect on the device, because it takes the energy stored inside the cavity a finite time to change significantly. This is related to the Q of the device. Typically the low frequency negative conductance is also limited by thermal effects at very low frequencies (< 10 kHz), but parasitic oscillations between 10 MHz and 1 GHz are quite common. These have been found to limit the power output significantly in both Gunn and IMPATT oscillators. The traditional remedy is to surround the bias choke with a lossy ferrite as close to the cavity as possible.

It is also possible to have power output at higher frequencies which are not harmonically related to the fundamental, but which correspond to natural resonances of the circuit. This effect has been noted by several groups, notably by Taylor et al. [41] where their oscillation was undoubtedly an accelerated transit mode, rather than LSA as they claimed. H.Essen [40], recently, has also cast some doubt on the assumption that all GaAs oscillators above 80 GHz are working in second harmonic mode. He performed accurate measurements on the output power of a diode in a cross-guide circuit using heterodyne techniques. He discovered that the output frequency at W-band did not correspond exactly, to any harmonic of any oscillation at a lower frequency, (although there was one oscillation that was fairly close). He also found oscillations at lower frequencies, that were not harmonically related in any way. Indeed, his results would seem to indicate oscillation frequencies that are determined by the resonances of his somewhat complicated circuit,

although it seems likely that parametric effects were also responsible for at least some of the effects. Such evidence shows that oscillation is possible at many different frequencies, as long as there is an oscillation near the transit frequency. In fact, Kurokawa (see Chapter 4) has shown that it is possible to have several "sideband oscillations" about the fundamental frequency if there are loops in the impedance locus, which is entirely possible for the circuit in question.

Previous evidence of second or third harmonic operation was based on showing that a fundamental oscillation existed (through losses up the bias pin [36]), or through showing the existence of higher harmonics [42]. In both these cases, accurate measurements of the output frequencies were not performed, and it was merely assumed that it was harmonic operation. In fact, one would expect the negative resistance to be high near harmonic frequencies, and possibly for there to be a natural resonance, in a simple cavity, near to a harmonic frequency. Another possibility might be due to a parametric effect where the "sideband mode" is preferentially amplified due to greater gain (or less loss) appearing at that frequency. Indeed, Haaki (in an analysis for TE amplifiers), showed that the 'second harmonic' negative conductance maxima, exist at frequencies which are not quite harmonically related to the fundamental [39].

However, one would expect such oscillations not to exist much above the theoretical frequency cut-off for fundamental oscillation, which is currently believed to be about 100 GHz for GaAs [37]. (There should be no such cut-off for true second harmonic operation).

Such considerations go a long way to explain several anomalous effects noted in the literature, and it is clear that a full understanding of the modes of operation of these devices, is not yet complete.

2.16 NOISE IN TRANSFERRED ELECTRON OSCILLATORS

The effects of A.M. noise on a local oscillator in a heterodyne system can be reduced by the use of a double balanced mixer system and the F.M. noise can be substantially reduced by phase and/or frequency locking to a frequency standard. However, in many applications the free-running stability and noise is of primary concern.

In fact, the most important secondary characteristic of any local oscillator are probably its F.M. and A.M noise sidebands.

In this respect, the Gunn oscillator has excellent noise properties relative to other high frequency sources, and typical A.M. anfd F.M. noise plots are shown in Figs 2.8 and 2.9. As can be seen from these figures, the A.M noise characteristics of Gunn oscillators can be excellent, where noise levels are so low they can be difficult to detect with all but the most sensitive mixers. The free-running F.M. noise of a Gunn diode is somewhat larger, although it should be noted that it is dependent on the Q of the cavity. A more suitable indicator of the F.M. noise performance of a device being the noise measure M:

$$\text{Noise Measure } M = 10 \log_{10} [(P_o/kTB) (Q_e \Delta f / f_o)^2] \text{ dB}$$

As well as the Q of the cavity other various important contributions to the F.M. noise in Gunn diodes have also been identified, (although more work on this subject is required).

a) Bias Noise - There is usually a fairly strong correlation between bias noise and oscillator noise. Many oscillators have a typical voltage/frequency tuning of around 300 MHz/V and so a 1mV noise ripple on the bias supply will lead to noise components out to around 30 kHz.

b) Generation / Recombination Noise - Caused by impurities producing trapping centres. Measurements on Gunn diodes at 10GHz [56] have indicated this noise typically extends from 1 kHz out to around 1 MHz.

c) Excess or Flicker Noise - This is 1/f low frequency upconverted noise and is fairly temperature independent.

d) Thermal Noise - This is usually at a fairly low level with respect to the other forms of noise, although it usually becomes the dominant noise source at frequencies above 1MHz.

(If an oscillator becomes noisy during tuning it is normally attributable to an unusually low Q caused by a multiple resonance within the circuit).

Noise and noise measurement techniques are considered in much greater detail in Chapter 10

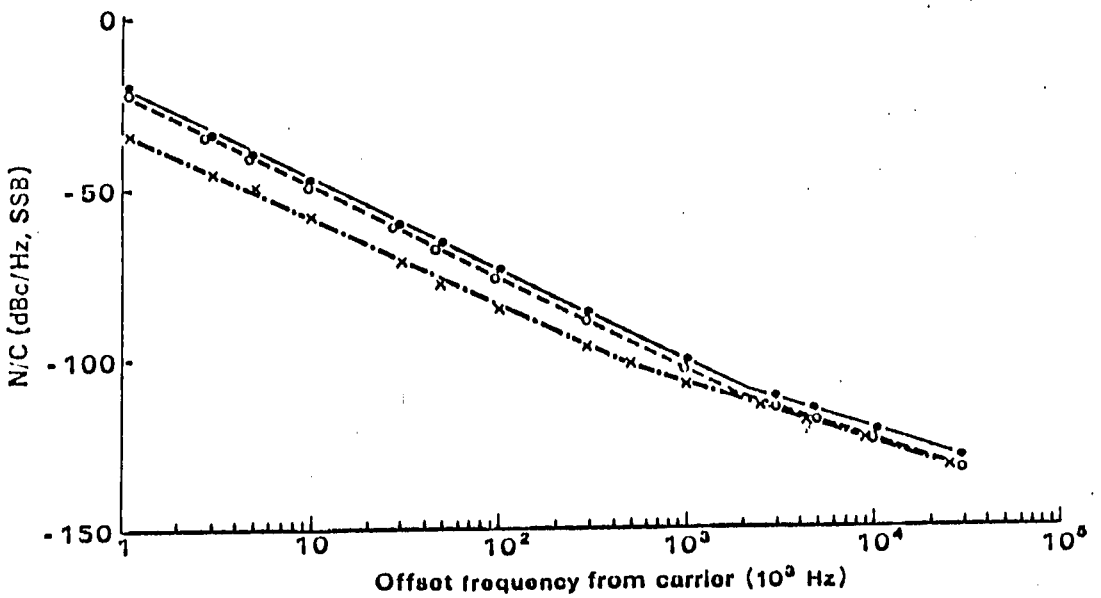

FM noise performance of InP and GaAs *M*-band TEOs (developed at Plessey Research, Ltd.): ●, InP, 60 mW, 2.5% Q_e = 125; O, GaAs, 29 mW, 1% Q_e = 690; ×, GaAs, 12 mW, 0.2% Q_e = 1390. (From Eddison and Davies, 1982a. © 1982 IERE.)

Figure 2.8

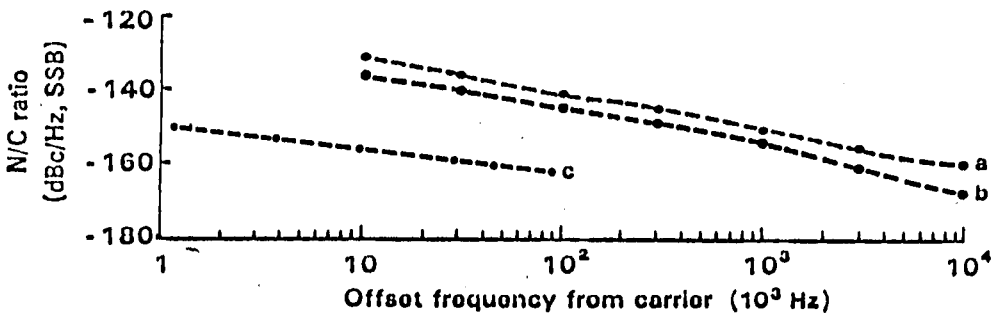

AM noise performance of InP and GaAs *X*- and *M*-band TEOs (developed at Plessey Research, Ltd.): curve a, 25-mW GaAs TED; curve b, 45-mW InP TED; curve c, 150-mW GaAs and InP TEDs, 40 GHz.

Figure 2.9

Figs. 2.8 and 2.9 showing typical F.M. and A.M. noise performance for different types of Gunn Oscillator operating at millimetre wave frequencies. Taken from Ref. [55]

REFERENCES (CHAPTER 2)

1) W.Shockley, 'Negative resistance arising from transit time in semiconductor diodes', Bell Syst. Tech. J., Vol.33, pp.799-826 1954

2) J.B.Gunn, 'Microwave oscillations of current in III-V semiconductors', Solid State Comm. Vol.1, pp.88-91 1963

3) L.F.Eastman, 'Transferred-Electron Devices', Microwave Devices, Edited by M.J.Howes,D.V.Morgan, John Wiley & Sons 1976

4) K.Mause et al., 'Monolithic integration of GaAs Gunn devices for digital circuits', Proc. Fourth Cornell Conference, Microwave Electron Devices, pp.211-23, 1973

5) J.E.Carroll, 'Hot electron microwave generators', Edward Arnold (publishers), 1970

6) H.W.Thim, 'Computer study of bulk GaAs with random one dimensional doping fluctuations', J.Appl.Phys., Vol.39, 3897-904, 1968

7) J.A.Copeland, 'Stable space charge layers in two valley semiconductors', J.Appl.Phys., Vol.37, pp.3602-9, 1966

8) W.O.Camp,Jr., 'Experimental observations of relaxation oscillator waveforms in GaAs from less than transit-time frequency to several times transit-time frequency', Proc. IEEE, pp.1248-50, Aug 1971

9) D.Jones,H.D.Rees, 'A reappraisal of instabilities due to the transferred electron effect', J.Phys C, Vol.6, pp.1781-93, 1973

10) J.A.Copeland, 'LSA oscillator-diode theory', J.Appl.Phys. Vol.38, No.8, pp.3096-101, 1967

11) D.Jones,H.D.Rees, 'Overlength modes of transferred electron oscillators', Electron.Lett., Vol.9, No.5, pp.105-6, 1973

12) J.W.Archer, 'A novel quasi-optical frequency multiplier design for millimetre and submillimetre wavelengths', IEEE Trans. MTT-32, No.4, 1984

13) D.Jones,H.D.Rees, 'Electron-relaxation effects in transferred-electron devices revealed by new simulation method', Electron.Lett., Vol.8, No.14, pp.363-4, 1972

14) D.Jones,H.D.Rees, 'Accumulation transit mode in transferred-electron oscillators', Electron.Lett., Vol.8, No.23, pp.566-7 1972

15) H.Kroemer, 'Hot-electron relaxation effects in devices', Solid State Electronics, Vol.21, pp.61-67, 1978

16) A.M.Mazzone,H.D.Rees, 'Overlength modes of InP transferred-electron devices', Electron. Letters, Vol.10, No.12, pp.234-5, 1974

17) J.A.Copeland, 'Theoretical study of a Gunn diode in a resonant cavity', IEEE Trans., Electron.Devices, ED-14, pp.55-8, 1967

18) S.Y.Narayan et al., 'Operation of transferred-electron oscillators in the ridge-waveguide circuit', Electron.Lett., Vol.7, No.2, pp.31-2, 1971

19) M.Wasse et al. 'Optimum loading for relaxation LSA mode', Electron.Lett., Vol.8, No.14, pp.364-6, 1972

20) B.C.Deloach,Jr., 'Coaxial versus rectangular waveguides for solid-state microwave circuits', Proc.IEEE, March 1978, pp.505-6

21) A.M.Mazzone,H.D.Rees, 'Transferred-electron oscillators at very high frequencies', Electron.Lett., Vol.17, No.15, pp.539-40, 1981

22) J.W.Tully, 'Montecarlo simulation of a millimetre-wave Gunn-effect relaxation oscillator', IEEE Trans.Electron Devices, Vol.ED-30, No.6, pp.566-71, 1983

23) L.F.Eastman et al., 'Ballistic electron motion in GaAs at room temperature', Electron.Lett., Vol.16, No.13, pp.524-5 1980

24) J.A.Copeland, 'LSA oscillator waveforms for high efficiency', Proc.IEEE, Sept. 1969, pp.1666-7

25) D.Jones,H.D.Rees, 'Transit modes of InP transferred-electron oscillators', Electron.Lett., Vol.11, No.1, pp.13-14, 1975

26) K.W.Gray et al., 'Current limiting contacts for InP transferred electron devices', Proc.Fifth Cornell Elec.Eng.Conf., 1975

27) D.M.Brookbanks, 'Millimetre wave solid state devices', Allen Clark Research Centre Annual Review, 1981

28) B.W.Clark et al., 'Cathode contact studies on transferred electron devices using transistor structures', Proc.Fifth Cornell Elec.Eng.Conf., 1975

29) B.Fank et al., 'Indium phosphide millimetre-wave devices and components', Int.J.of Infrared and Millimetre Waves, Vol.5, No.6 pp.859-67 1984

30) K.W.Gray et al., 'InP microwave oscillators with 2-zone cathodes', Electron.Lett., Vol.11, No.17, pp.402-403, 1975

31) J.D.Crowley et al., 'High efficiency 90 GHz InP Gunn oscillators', Electron. Lett., Vol.16, No.18, pp.705-6, 1980

32) V.N.Genkin et al., 'Nonlinear response of n-type GaAs in the millimetre wavelength range', Sov.Phys.Semicond., Vol.8, No.10, pp.1307-8, 1975

33) Z.F.Krasil'nik et al., 'Generation of the second harmonic of a millimetre electromagnetic wave in n-type GaAs', Sov.Phys.Semicond., Vol.9, No.6, pp.790-1, 1975

34) A.M.Mazzone,H.D.Rees, 'Transferred-electron harmonic generators for millimetre band sources', IEE Proc. Vol.127, Pt.I, No.3, pp.149-57 1980

35) J.E.Carlstrom et al. 'A Continuously tuneable 65-115 GHz Gunn oscillator', IEEE Trans., Vol.MTT-33, No.7, pp.610-19, 1985

36) W.H.Haydl, 'Fundamental and harmonic operation of millimetre-wave Gunn diodes', IEEE Trans., Vol.MTT-31, No.11, pp.879-89, 1983

37) M.Friscourt et al., 'Theoretical contribution to the design of millimetre-wave TEO's', IEEE Trans., Vol.ED-30, No.3, pp.223-29, 1983

38) G.Smith,J.Lesurf, 'Preliminary results for a tuneable W-band Gunn diode oscillator block', St.Andrews University, 1986

39) B.W.Hakki, 'Amplification in two-valley semiconductors', Jou. Appl. Phys., Vol.38, No.2, pp.808-18, 1967

40) H.Essen, 'Investigations of the operating modes of millimetre wave Gunn oscillators', Microwave Journal, Sept. 1982, pp.150-2

41) B.C.Taylor,S.E.Gibbs, 'Fundamental microwave oscillations in epitaxial GaAs by control of space-charge growth', Electron. Lett., Vol.4, No.22, pp.471-2

42) I.G.Eddison,D.M.Brookbanks, 'Operating modes of millimetre wave transferred oscillators', Electron.Lett., Vol.17, No.3, pp.112-113, 1981

43) C.S.Aitchson et al. 'Self-pumped Gunn-effect parametric amplifier', Electron.Lett., Vol.5, No.2, pp.36-37, 1969

44) G.A.Brunt, 'Low-frequency negative resistance of X-band Gunn diodes', Electron.Lett., Vol.5, No.7, pp.151-53, 1969

45) D.Cawsey, 'V.H.F and U.H.F Gunn-effect oscillators', Electron.Lett., Vol.3, No.12, pp.550-1, 1967

46) H.W.Thim, 'Linear microwave amplification with Gunn oscillators', IEEE Trans ., Electron Devices, Vol.ED-14, pp.517-22, 1967

47) J.Mun,G.M.Arbery, 'High-peak power 2nd-harmonic L.S.A sources', Electron. Lett., Vol.12, No.1, pp.10-11, 1976

48) D.E.Aspnes, 'GaAs lower conduction-band minima: Ordering and properties', Phys.Rev.B, Vol.14, No.12, pp.5331-5343, 1976

49) S.Y.Narayan,F.Sterzer, 'Transferred electron amplifiers and oscillators', IEEE Trans. Vol. MTT-18, No.11, pp.773-83 1970

50) N.R.Couch et al., 'High-Performance, Graded AlGaAs Injector, GaAs Gunn Diodes at 94 GHz', IEEE Electron Device Letters, Vol.10, No.7, July 1989, pp.288-30

51) P.H.Beton et al., 'Use of n+ spike doping regions as nonequilibrium Connectors', Electronics Letters, 31 March 1988, Vol.24, No.7, pp.434-5

52) A.P.Long et al., 'Hot-Electron Injection by Graded $Al_xGa_{1-x}As$', Electronics Letters, Jan.1986, Vol.22, No.3, pp.130-131

53) N.R.Couch, private communication

54) J.Ondria, R.L.Ross "Enhanced TED MMW Device Performance Using Graded Doping Profiles", Conf. Proceedings,. 17th European Microwave Conference, pp.673-680

55) I.G.Eddison, "Indium Phosphide and Gallium Arsenide Transferred-Electron Devices", Chapter 1, Infrared and Millimeter Waves , Vol.11

56) H.R. Gnerlich, J.Ondria, "A New Look at Noise in Transferred Electron Oscillators", Vol. MTT-25, No.12, December 1977, pp.977-81

3.0 TRANSFERRED ELECTRON MATERIALS

3.1 MATERIAL PARAMETERS

Essentially the key properties of a potential transferred electron material are determined by its velocity/field characteristics which come from knowledge of its band structure and phonon interaction. A full list of those properties for GaAs and InP are given in Table 1. The values given should be treated qualitatively as many parameters are not known accurately, and others are functions of temperature and donor density. In addition, one must be aware of relaxation effects associated with the finite time required for an electron to respond to a given applied field: the more so at high frequencies. In particular, there can be velocity overshoot effects at n^+ cathodes and limiting relaxation times for any form of quenched mode, which can seriously affect the efficiency at high frequencies. These will be discussed at greater length later.

The most salient features of any transferred electron device are:

1) The Peak Velocity
2) The Valley Velocity
3) The Threshold Field
4) The Breakdown Field
5) Frequency Cut-Off (Intrinsic and for Quenched Mode)
6) Noise figure

Ridley [1] in an excellent paper has considered the above quantities in terms of the band structure and dynamics of the central and satellite valleys, and his main conclusions are given qualitatively below.

The dynamics of the central valley are thought to be dominated by polar optical phonon scattering, and can be characterised by two parameters: the phonon energy at zone centre, and the polar coupling strength or ionicity, as measured by effective charge. The latter quantity being a measure of the interaction between the phonons and the electrons. A large phonon energy and ionicity, implies a large momentum and energy relaxation time, implying low mobility and more energy absorbed by the lattice from the electrons.

The dynamics of the upper valley and intervalley are thought to be governed by low wavelength, easily excited, transverse and longitudinal acoustic (TA and LA) phonons. The scattering is also believed to be much faster than that of the central valley, and normally dominated by the LA phonon. The amount of scattering can also be expected to

be a sensitive function of temperature, as the phonon density is subject to Bose-Einstein statistics.

3.1.1 THE PEAK VELOCITY

The peak to valley velocity ratio is the key factor in determining the efficiency of any oscillation, and most of the attempts at band-gap engineering have been directed to increase this ratio, mainly through increasing the peak velocity. This is mainly determined by low field mobility, and the energy separation between the Γ and the L valleys. Low field mobility in turn, is associated with a low energy gap between the valence and conduction bands, and low values for ionicity, and the energy of the optical polar phonon. Most of the interest in new materials has been directed to finding high mobility high Γ-L bandgap materials, although as we shall see, this can lead to low breakdown fields, and frequency limiting effects. InP has a lower mobility than GaAs but because of its larger bandgap, it has a higher peak velocity, although at a much higher threshold field. Overshoot effects at the cathode can increase the actual peak velocity, especially in GaAs due to its high mobility, however they do not increase the efficiency of operation.

3.1.2 THE VALLEY VELOCITY

Monte Carlo simulations [2] in GaAs and InP, show that by the time an appreciable fraction of electrons have been transferred, electrons in the upper valley are hot enough to have reached saturation drift velocity. The velocity therefore does not increase after transfer at higher fields but saturates to a steady value.

At high fields the velocity of the electrons in most semiconductors eventually saturate to a steady value before breakdown. This saturation process occurs because at high fields the characteristic energy relaxation time and momentum relaxation time of the electron become the same. This occurs when the amount of energy lost per collision approximates to the most energetic phonon.Using the two simple definitions:

$$e\,v\,E = (\mathcal{E}_{phonon} / \tau_e) \qquad (3.1)$$

$$e\,E = m^* v / \tau_m \qquad (3.2)$$

we have the relation:

$$v = v_s = (\mathcal{E}_{phonon} / m^*) \qquad (3.3)$$

The valley or saturation velocity is thus mainly determined by the size of the dominat acoustic phonon. The smaller the phonon the smaller the saturation velocity. Ideally for a Gunn effect device it should be as small as possible to increase the peak/valley ratio.

InP has a lower saturation velocity than GaAs, primarily because it has the lowest average phonon energy, mainly due to the small value of the zone edge LA phonon. This in turn largely stems from the large mass of the Indium atom. (Simple theory indicating that the maximum energy of an acoustic phonon is inversely related to the mass of the atoms).

3.1.3 THE THRESHOLD FIELD

The threshold field is an important quantity in transferred electron oscillators. Too high a field can cause problems due to overheating. In the early history of Gunn Oscillator design this was a significant problem, and it was felt it was a telling factor against InP. Indeed, InP oscillators normally have to be run in pulse mode at low frequencies (10-30 GHz) for high power operation. However, with modern integrated heat-sinking techniques, and the drive to higher frequencies, (smaller active widths) this has not proved to be such a limiting problem. In addition, as is shown in the next section, the intrinsic frequency cut-off is directly proportional to the threshold field, due to inertial effects. Thus much higher frequency operation should be able to be attained for InP compared to GaAs. Indeed a rough 2:1 ratio has been shown in both theory and practice.

The threshold field, not unsurprisingly, increases with the Γ-L energy gap and decreases as the mobility increases, due to greater scattering, and more energy absorbed by the lattice. Therefore, the threshold field increases with ionicity and zone centre phonon energy.

3.1.4 THE BREAKDOWN FIELD

The breakdown field is difficult to predict analytically, however, certain trends can be noted. It occurs when electron/hole pairs are created faster than they can recombine. To produce an electron hole pair an electron must acquire a threshold energy which is directly related to the energy gap. For a spherical parabolic conduction and valence band this is given by:

$$\varepsilon_{TH} = \varepsilon_g \left(\frac{1+2\mu}{1+\mu}\right) \qquad (3.4)$$

where $\mu = m_e^*/m_h^*$.

Suitable corrections can be made for non-parabolicity [1], however it is clear that the larger E_g the larger the threshold energy and the breakdown field. The question now, is where electrons of sufficient energy can be found. The answer is in the high energy tail of the electron distribution in the satellite valley. The breakdown field can also be seen to increase with Γ-L bandgap, as the larger the gap the more potential energy and the nearer the electrons will be to the threshold energy. The breakdown field will also increase with decreasing acoustic phonon energy due to the lower saturation velocity. (Less chance of an electron obtaining sufficient kinetic energy to create an electron-hole pair). This is an important effect, as is shown by the fact, that, despite InP having a smaller energy gap E_g and larger Γ-L separation, it still has a higher breakdown field (due to the low value of the zone edge LA phonon energy).

3.1.5 THE CUT-OFF FREQUENCY

There are different fundamental frequency cut-offs for different modes of operation. Here we will consider two of them, although it should be noted that they are in no sense sharp cut-offs but a gradual fall off in efficiency can be expected at their values.

As pointed out by Jones and Rees [3] and Kroemer [4] the fundamental frequency limits are governed by the rate which electrons can gain or lose energy in the central Γ valley, as opposed to the intervalley scattering rate which is much faster. The central valley dynamics in turn are governed by two time constants. The characteristic inertial time constant, caused by the finite acceleration-deceleration time of the electrons, and the energy relaxation time τ due to phonon/electron collisions. Considering first the inertial relaxation time required for an electron to gain or lose an energy ε_s:

$$\tau = (1/qE)\,(2\,m^*\,\varepsilon_s)^{1/2} = \tau_0 \,.\, E_{th}/E \qquad (3.5)$$

where τ_0 is the characteristic inertial time constant given by:

$$\tau_0 = (1/qE_{th}) \,.\, (2\,m^*\,\varepsilon_s)^{1/2} \qquad (3.6)$$

For InP this works out to be 0.75 ps and for GaAs 1.5 ps. The smaller time constant for InP being almost entirely due to the larger threshold field. τ_0 should be viewed as the time constant with which the electron distribution adjusts itself to any change in electric field and as such represents the ultimate frequency limit for any mode.

For any form of quenched mode, one not only requires the space charge to disperse (governed by the inertial time τ), but for the electron temperature, at the point of quenching, to go down, otherwise the space-charge would merely regrow at this point. This requires the lattice to absorb the energy from the electrons through electron/phonon interaction. We can therefore expect that the frequency response will increase with zone centre phonon energy and ionicity. This implies that certain low mobility materials may have a very good frequency response.

Ridley [1] has carried out an analytical calculation which shows that the energy relaxation time can be given by an expression of the form:

$$f_c \sim 9x10^{14} \ (e^*/e)^2 \, . \, (h \, w_0)^2 \, . \, F \qquad (3.7)$$

where F is approximately constant at 0.8 for a wide range of III-V materials. This again predicts a 2:1 frequency advantage for InP over GaAs. Rolland et al. [5] have also considered this frequency cut-off, and have noted that during the central intravalley transfer the energy-relaxation time remains close to its maximum value, and can be averaged by the following relation:

$$\tau_\varepsilon = A \, (\mathcal{E}_s - \mathcal{E}_0) \, / \, (q \, E_{th} \, v_{th}) \qquad (3.8)$$

where $\mathcal{E}_s$ is the transfer energy (Γ-L bandgap), $\mathcal{E}_0$ is the thermal energy, v_{th} and E_{th} are the threshold values of the static drift/velocity field characteristic, and A is a constant of proportionality.

They therefore suggest a simple comparative criterion could be given by a factor of merit F*:

$$F^* = q \, E_{th} \, v_{th} \, / \, (\mathcal{E}_s - \mathcal{E}_0) \qquad (3.9)$$

InP again showing a better frequency response by almost a factor of 2:1 from this figure.

The actual frequency cut-off predicted by $1/\tau_e$ in these simple models tend to give ultimate frequency limits where the negative differential resistance disappears entirely. Efficiency however can be expected to degrade long before these limits are reached. In

practice many authors then incorporate fairly arbitrary factors of 2 and pi in there calculations, to bring the frequency limit roughly to where they feel it ought to be! It is this factor more than anything else that accounts for the wide range of different frequency cut-offs found quoted in the literature. A more accurate approach is through Montecarlo simulation, which has been shown to give many valuable results, both qualitatively and quantitatively, despite many of the scattering parameters not being known to any great degree of accuracy.

Montecarlo simulations by Jones and Rees [3,6,7] have shown that this imposes a 20 GHz frequency limit for true L.S.A. operation in GaAs, although this may be relaxed for active lengths a few times the 'transit-time length'. Experimentally, true L.S.A. operation has not been observed above 16 GHz.

3.1.6 THE NOISE FIGURE

As stated by Ridley the basic noise in TE devices is thermal, with a useful measure of the noise being given by:

$$M = T_e'/T \qquad (3.10)$$

where T is the lattice temperature and T_e is the electron temperature. The highest noise power per unit frequency being equal to kT_e, where the effective temperature of the electrons is essentially a measure of the energy of the electrons averaged over a cycle.

We can therefore expect the noise figure to increase with band gap E_g, and decrease with increasing Γ-L energy gap. Calculations and experiment [1,8] again showing almost a 2:1 advantage of InP over GaAs.

3.1.7 SUMMARY

In conclusion then we can note the following points:

a) It is desirable to have as small a zone-edge phonon energy as possible to reduce the saturation velocity and increase the breakdown field. The reason the InP value is so small, is largely due to the large mass of the Indium atom.

b) The ionicity and zone centre phonon energy are also important quantities, and are a measure of the scattering and energy relaxation rate in the central valley. Low values imply

high mobility, which implies a large peak velocity and good efficiency. Large values, however, imply a large threshold field and much better frequency response, leading to greater efficiency at high frequencies. Low mobility materials, therefore, tend to have a higher frequency cut-off. InP has larger values than GaAs by around 20%.

c) Generally the transfer energy (Γ-L separation) needs to be as large as possible to reduce noise, and temperature sensitivity, and to increase the peak velocity and the threshold field. On the other hand, the breakdown field decreases with increasing transfer energy. Also, above a certain threshold energy (>0.5eV for III-V materials), the NDR can become dominated by the central valley due to its non-parabolicity. This is discussed more fully in the next section. In addition, too high a threshold field can cause heating problems with long active lengths.

d) Lastly, it is usually useful to have as large a bandgap as possible, to have as large a breakdown field as possible. A large band-gap, however, will also increase the noise, and is also associated with low mobility materials.

InP therefore emerges superior to GaAs in every respect, except possibly at low frequencies (<20GHz), where the heating effect, due to its high threshold field, is a possible limitation. (Although it should be noted that it has twice the thermal conductivity of GaAs). This superiority principally derives from its large zone-centre phonon energy and ionicity, giving it a higher frequency cut-off, and small zone edge phonon energy (LA), giving it a low saturation velocity and large breakdown field.

On this basis Ridley has suggested a figure of merit W for high frequency transferred electron oscillators given by:

$$W = (e^*/e) \cdot (hw_0 / hw_{LA}) \qquad (3.11)$$

This gives a criterion for which to compare new materials and to choose possible alloys. This is discussed more fully in the next section.

3.2 NEW MATERIALS

So far only InP and GaAs have been seriously developed as Gunn oscillators, and so the question is whether any other material could have improved characteristics. In particular, various III-V alloys have been suggested, as well as some II-VI materials. A list of materials which have been found to possess the Gunn effect is given in Table II with some of their relevant parameters. Most of the recent efforts seem to have concentrated in

producing materials with high peak velocities via bandgap engineering, with a view to improve the efficiency. This can be achieved in materials with:

a) a large low field mobility and
b) a large Γ-L energy separation.

The large low field mobility needed, requires low bandgap materials with low effective masses. Too low a bandgap, though, can lead to low breakdown fields. For example the only III-V material with a larger Γ-L separation than InP, is InAs, with a value of 1.11eV. However, with a bandgap of only 0.36eV, it has a very low breakdown field, and the Gunn effect has only been observed under high pressure (14 kbar).

InP therefore clearly emerges as the best binary III-V material available for transferred electron effects. The ternary and quaternary III-V materials though, have a wider range of bandgaps and valley separations, of which the most promising are:

a) $Ga_{1-x}In_x As$ - where x can vary from 0.4 to 0.6. At x = 0.4 the bandgap is 0.86eV and the valley separation is 0.72 eV. The large valley separation and the large mobility [9] lead to a larger peak velocity, and greater negative differential mobility, than GaAs. This, together with its fairly low threshold field of 3 kV/cm [10], and established technology, suggest that it will rival GaAs at low frequencies. Indeed GaInAs oscillators have been made at X band [11] where without optimisation they produced 40mW of power (9GHz) at 3% efficiency. However, it was reported that the limit on the output power was caused by the onset of current runaway, indicating that low breakdown field is a problem.

b) $Ga_{1-x}In_xP_{1-y}As_y$ alloys, when they are matched to an InP substrate have also been of interest, as they possess the largest theoretical peak velocity (of any suitable material for TE effects) with a value exceeding $3x10^7$ cm/sec even with significant alloy scattering [12]. Their higher saturation velocity, however does not give as good a peak to valley ratio as GaInAs. It, however, is obviously a valuable material for other microwave applications, such as field effect transistors.

c) $Ga_{1-x}In_xSb$ is another interesting material. It has a good peak velocity, but of most interest is its very low threshold field of 0.6 kV/cm. This may give it an advantage in certain low power applications, although its small energy gap of 0.36 kV/cm indicates a low breakdown field.

d) $Al_{1-x}In_xAs$ - where if x is 0.75, the energy gap is 0.91eV and the G-L separation is 1.12eV. Of all the III-V ternary and quaternary materials (that have a reasonably large energy bandgap i.e around 1eV) this one has the largest Γ-L valley separation. Monte

Carlo calculations [9] also indicate a very large mobility of around 11700 cm/Vsec, and thus this material can be expected to have have a very large peak velocity. This turns out to be about 2.7×10^7cm/s which although high, (about the same as InP) is perhaps not as high as expected.

The reason for this, is that the negative differential resistance becomes dominated by the dynamics of the central Γ valley [9]. The mobility by definition is given by:

$$\mu = \tau_m e / m^* \qquad (3.12)$$

where m*, the effective mass is given by:

$$m^* = h^2 / (d^2E / dk^2) \qquad (3.13)$$

Now in most alloys based on GaAs the E/k slope starts to change sign at around 0.5eV, which means that d^2E/dk^2 will be very small at this point, implying a large effective mass and low mobility. For most GaAs type materials with bandgaps greater than 0.5 eV, the high field dynamics becomes dominated by the central valley and polar optical scattering. Hauser et al. [9] have calculated an expression for the maximum peak velocity which can be achieved in a semiconductor because of this effect. It is given by:

$$v_{max} = [(hw_0 / m^*) . \tanh(hw_0 / 2kT)]^{1/2} \qquad (3.14)$$

where hw_0 is the optical phonon energy and m* is the effective mass at low fields (constant).

In practice, because there are other scattering effects in the central valley, the peak velocity is usually found to be 80-90% of the value predicted above. For increasing non-parabolicity, the threshold field will increase, but the peak velocity will go down, due to lower mobility.

Because of the above effect, it would appear that such materials cannot hope to compete with InP. However, a point that is not stressed in the literature, is that these materials also have potentially very low saturation velocities. Also, because of the high negative differential mobility, they occur at fields which are not significantly greater than the threshold field. One of the problems with InP, is that to take full advantage of its good peak to valley ratio, it requires biasing well above threshold, and a large rf voltage swing must develop. This can produce circuit and thermal limitations. A feature of central valley dominated materials, would appear to be a low saturation velocity and a large NDR. Indeed it is the scattering into the satellite valleys that limits the size of the NDR. For Ga In As the saturation velocity would appear to be close to 0.6×10^7 cm/sec, whereas that for Ga Al As

. is close to 0.5×10^7 cm/sec [9]. The main reason for these low velocities is the presence of the high mass Indium atom making the zone-edge acoustic phonon energy small.

Ridley [1] has suggested possible potential alloys based on his suggested figure of merit:

$$W = (e^*/e) \cdot (hw_0/hw_{LA}) \qquad (3.15)$$

On this basis, he suggested alloying GaAs with In or InP, but remarked that there seemed little advantage in alloying InP with any of the common III-V materials. However he suggested that alloying with InN (to increase e* and hw_0), or TIP (to increase e* and decrease hw_{LA}) might be possibilities. But, as he also points out, alloying introduces an additional scattering mechanism, and it is unclear how well conclusions derived from consideration of binary materials, can be applied to ternary or quaternary materials.

As yet no experimental or theoretical evidence seems to have appeared in the literature on these materials, in conjunction with TE oscillators.

As remarked before, most of the research into new transferred electron materials has centred on materials with high mobility, in an effort to improve peak velocity. Such considerations though, are almost diametrically opposed to operation at very high frequencies where low mobility, high threshold field materials are a requisite. The highest fundamental frequency so far attained in a TE oscillator, is about 140GHz by an InP diode. It is clearly of interest to move to higher frequencies, particularly where high power is not of prime consideration.

The only known TE materials that possess a higher threshold field than InP, are the II-VI materials CdTe and ZnSe. Of these, the threshold field of CdTe is only marginally larger, and this coupled with its low peak to valley ratio of about 1.5 does not make it a serious competitor of InP.

ZnSe, however, with a threshold field of 38 kV/cm [13], is a promising material for very high frequencies, as it has an inertial time constant two thirds that of InP, although, because of its low peak to valley ratio of 1.5, its efficiency would be limited. The figure of merit associated with quenched operation cut-off indicates that ZnSe would be slightly worse than InP. It should be stressed here though, that this figure assumes electron dynamics associated with the III-V materials. To find a material with an even higher threshold field, one presumably needs even lower mobilities. Here ZnS suggests itself as a very strong candidate, as it has a low field mobility of about 1/4 that of ZnSe, and a marginally larger valley separation. It, however, has an almost identical band structure [14] suggesting that the Gunn effect should be possible in this material too.

As yet though, no experimental or theoretical evidence exists for the Gunn effect in ZnS, and the only reference to the Gunn effect in ZnSe is from a paper published in the mid 1960s, by Ludwig and Aven [13]. In that paper, they concluded that it could not compete with GaAs because the input power per unit volume was 100 times greater (10 times the threshold field), while the thermal conductivity was less than half that of GaAs. They also experienced difficulty in making good contacts, and noticed a tendency towards current runaway at voltages only moderately above threshold. They however were working with long samples (50-200 um), and in a low Q circuit where the domain mode was clearly evident.

A characteristic of the domain mode is that the domain attempts to 'absorb' all the voltage across the material, which can lead to very high localized fields within the sample, which in turn can lead to breakdown. All commercial GaAs and InP devices that work to high frequencies, are transit time devices, that work in the accumulation mode. Here domains cannot develop because the sample is so small (1-2μm), and because they normally operate in high Q circuits.

Current runaway and thermal limitations can therefore hope to be avoided, or reduced, for smaller samples operating in the accumulation mode. Contact problems to a large extent have also been solved [14], with current limiting cathodes having been made on long samples. It has also been shown, that the breakdown field is of the order of 1000 kV/cm [15], so breakdown should not really be a problem.

It is thus clearly evident that further work deserves to be done on these and other similar materials.

TABLE I

SEMICONDUCTOR CHARACTERISTICS OF GaAs AND InP

	GaAs	InP
ENERGY GAP E_g (eV)	1.43	1.34
Γ-L ENERGY SEPARATION E_s (eV)	0.36	0.52
Γ-X ENERGY SEPARATION (eV)	0.48	0.76
m* Γ MINIMUM	0.067m	0.078m
m* L MINIMUM	0.4m	0.4m
LOW FIELD MOBILITY (cm V s) 300K	8000	4750
LOW FIELD MOBILITY (cm V s) 500K	5000	3000
PEAK VELOCITY V_p ($*10^7$ cm/s)	2.0 (2.1)	2.5
SATURATION VELOCITY (cm/s)	0.95 (0.8)	0.5
PEAK TO VALLEY RATIO (300K)	2.2	3.5
INERTIAL ENERGY TIME CONSTANT (ps)	1.5	0.75
ENERGY RELAXATION TIME	0.4	0.2
THRESHOLD FIELD (kV/cm)	3.2 (3.5)	10.0
ELECTRON VELOCITY TEMP. DEPENDENCE	-0.5%/K	-0.1%/K
THERMAL CONDUCTIVITY (W/cmK at 300K)	0.54	0.68
BREAKDOWN FIELD (kV/cm at N = 10)	400	500
COLLISIONAL ENERGY RELAXATION TIME (ps)	6	3
POLAR OPTICAL PHONON ENERGY (eV)	0.037	0.043
NON-POLAR ACOUSTIC PHONON ENERGY (eV)	0.028	0.011

TABLE II

TRANSFERRED ELECTRON CHARACTERISTICS OF KNOWN GUNN MATERIALS

SEMICONDUCTOR	E_g(eV)	E_s(eV)	E_{th}(kV/cm)	V_p(*10^7cm/s)
GaAs	1.42	0.31	3.2	2.1
InP	1.35	0.53	10.5	2.5
Ge (a)	0.74	0.18	2.3	1.4
InAs (b)	0.36	1.11	1.6	3.6
InSb (c)	0.28	0.41	0.6	5.0
CdTe	1.5	0.51	11.0	1.5
ZnSe	2.6	1.3	38.0	1.5
Ga In Sb	0.36	0.36	0.6	2.5
Ga In Sb	0.24		0.6	2.9
In As P	1.1	0.95	5.7	2.7
Ga In As P	1.05		5.5-8.6	3.1-3.6*
In Ga As	0.75	0.55	3	2.2-2.8
Al In As	0.91	1.12	4	2.7

a) At 77K

b) Under 14kBar pressure

c) At 77K under 8 kBar pressure

* Obtained from Monte-Carlo Simulations

REFERENCES (CHAPTER 3)

1) B.K.Ridley,'Anatomy of the transferred electron effect in III-V semiconductors', J. Appl. Phys. Vol.48, p754-764, Feb. 1977

2) W.Fawcett,D.C.Herbert, 'High field transport in GaAs and InP', J.Phys.C, Vol.7, pp.1641-54

3) D.Jones,H.D.Rees, 'Electron relaxation effects in transferred electron devices revealed by new simulation method', Electron. Lett. Vol.8, pp.363-4, 1972

4) H.Kroemer, 'Hot electron relaxation effects in devices', Solid St. Electronics, Vol.21, pp.61-67 1978

5) P.A.Rolland et al., 'Comparative frequency behaviour of GaAs, InP, and InGaAs transferred electron devices - derivation of a simple comparative criterion', IEEE Trans. Electron Devices, Vol.ED-28, No.3, pp.341-3, 1981

6) D.Jones,H.D.Rees, 'Accumulation transit mode in transferred electron oscillators', Electron.Lett., Vol.8, pp.566-7 1972

7) D.Jones,H.D.Rees, 'A reappraisal of instabilities due to the transferred electron effect', J.Phys.C, Vol.6, pp.1781-93 1973

8) B.Fank et al., 'Indium Phosphide millimetre wave devices and components', Int.J. of infrared and millimetre waves, Vol.5, No.6 pp.859-67 1984

9) J.R.Hauser et al., 'Negative resistance and Peak Velocity in the central (000) valley of III-V semiconductors', Solid State Electronics, Vol.22, pp.487-93 1979

10) W.Kowalsky et al., 'Transferred-electron domains in InGaAs in dependence on the nl product', Solid St. Electronics, Vol.27 No.2, pp.187-9 1984

11) W.Kowalsky et al., 'InGaAs Gunn oscillators', Electron.Lett. Vol.20, No.12, pp.502-3 1984

12) M.A.Littlejohn et al., 'Velocity-field characteristics of GaInPAs quaternary alloys', Applied Phys. Letts., Vol.30, No.5, pp.242-4, 1977

13) G.Ludwig,M.Aven, 'Gunn Effect in ZnSe', J.Applied Phys., Vol.38, No.13, pp.5326-31, 1967

14) J.W.Allen, Private communication

15) A,W.Livingstone,J.W.Allen, 'Electron-hole pair production by impact ionization in ZnSe', J.Phys.C, Vol.3, pp.2468-73 1970

4.0 HIGH FREQUENCY OSCILLATOR CIRCUIT THEORY AND IMPEDANCE MATCHING

4.1 INTRODUCTION

Gunn and Impatt diodes, when appropriately biased can be made to have an effective negative differential resistance in the millimeter wave frequency range, and will convert dc power into rf power at millimeter wave frequencies, if a suitable circuit impedance is presented to the device. It is the purpose of this section to discuss the interaction of such diodes, which are inherently non-linear, with millimeter wave circuits, which can usually be represented as linear passive networks.

An oscillation is the continuous cyclic transfer of stored energy from one state to another. In a pendulum it is the transfer of kinetic energy to potential energy and potential energy to kinetic energy. In the electrical case, it is the continuous interchange of electric and magnetic energy within the circuit. If we have a generator feeding power into a circuit, resonance will occur in that circuit if the total energy stored in the electric field is equal to the total energy stored in the magnetic field over one cycle. If it is not, then power will be reflected back towards the generator.

For an oscillation to start there must be a mechanism to put energy into the system. The amount of energy added per cycle is known as the gain of the system, and in the context of millimeter semiconductor oscillators, it can be represented by an effective negative resistance, at a given frequency. Usually, there will be losses in the system; either to useful rf power, or to other forms of energy such as thermal energy. In the electrical context, these are represented by positive resistances. The loss must be smaller than the gain of the system if oscillation is to start, or existing oscillations are not to be exponentially damped. If the gain is greater than the losses, then the oscillations should exponentially increase continuously. However, in any real system the amplitude is eventually limited by higher order effects. Nonlinearities usually mean losses increase, and gain decreases with oscillation amplitude, so a steady-state value will normally eventually be attained at a point where the loss in the system is equal to the gain. Most semiconductor oscillators are highly non-linear, and it is found typically that the negative resistance decreases with oscillation amplitude. In terms of Gunn oscillations, we can imagine that as the rf voltage amplitude increases, then the diode will spend less and less time biased in the negative differential resistance region, and so the effective negative resistance will decrease.

There are therefore two main conditions for a resonant steady-state electrical oscillation.

1) At resonance the time averaged energy stored in the magnetic field equals the time averaged energy stored in the electric field of the system. This is normally only true for a set of discrete frequencies, and therefore this condition determines the resonances of the system.

2) For steady-state the gain of the system must equal the losses in the system. Both gain and losses are normally functions of the oscillation amplitude, and therefore will only be equal for certain discrete amplitudes. This condition will determine the amount of energy lost from the system either through resistive losses or useful power output. It is difficult to calculate though, as knowledge of the diodes nonlinearity is required.

At low electrical frequencies, an oscillator circuit will typically consist of lumped discrete elements such as capacitors for storing the electric field, inductors for storing the magnetic field and resistors representing losses and useful power delivered to a load. As one moves to higher frequencies, adjacent wires through their mutual capacitance and inductance, will have larger associated electric and magnetic fields associated. Also, as the wavelength of the radiation starts to approach the length of the wires or elements in the circuit, the electric and magnetic fields will interact to produce electromagnetic radiation, and the elements will radiate power away from the circuit. Except for antennae applications, this is usually undesirable, and mediums such as waveguide and coaxial cable, have to be used to transfer power at such frequencies (microwave/millimeter wave). At even higher frequencies resistive losses associated with decreasing skin depth in waveguide, and smaller wavelength make optical techniques more suitable (millimeter wave and above). Although there is obviously a transition period where many techniques are viable and application dependent.

At millimeter wave frequencies, for highest power and lowest noise, solid-state oscillators will usually use some form of short-circuited transmission line, to form a resonant cavity. This is because they have low losses, which permits a large Q, and provide a well defined mode pattern which is easy to couple into.

The theoretical study of non-linear active devices tends to be quite complicated and often not that fruitful, in the sense of being able to predict useful experimental values. More often it is experiments that are required to prove the theory. However, the study of millimeter wave oscillators in high Q circuits, has brought some useful results, and explained, at least qualitatively, many experimental observations. That progress can be made is mainly due to the fact we are usually working at one frequency as defined by the

high Q cavity. It was Kurokawa [1,2,3,4] who provided most of the initial work, and understanding in this field. Most of his main predictions and criteria are outlined below.

4.2 FREE-RUNNING OSCILLATORS

We can consider the interaction between an active negative resistance device, and any resonant circuit (including the load), by considering the equivalent circuit shown in Figure 4.1. It is convenient to consider the impedance of the circuit and the device separately and choose the reference plane to be at the device terminals.

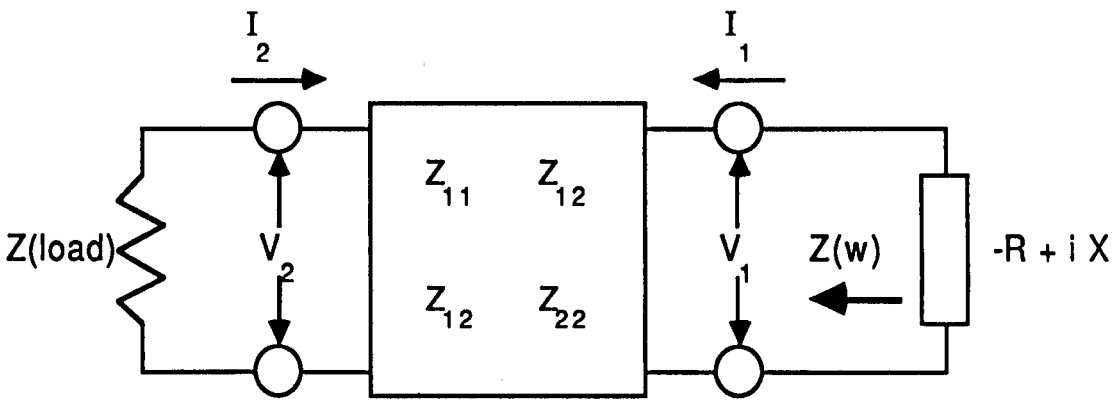

FIGURE 4.1
Two-terminal network representing the oscillator circuit

4.2.1 CIRCUIT IMPEDANCE

The cavity can be taken to be a linear passive network and will have an impedance Z (at the device terminals), that will be a strong function of frequency. It may also be a slight function of temperature due to expansion of the cavity, however, generally such effects will be small.

Looking out from the device, the circuit impedance will be a strong function of frequency w and is represented as:

$$Z_c(w) = R_c(w) + iX_c(w) \qquad (4.1)$$

where R_c represents both the load resistance and resistive loss in the circuit. It is related to the energy lost from the circuit and will always be positive. X_c is the reactance of the circuit, and is related to the ratio of the electric field and the magnetic field of the standing wave at the device. It will be negative if there is more energy stored in the magnetic field,

and positive if more energy is stored in the electric field in the circuit over one cycle. It is also the ratio of the voltage max. to the current max. of the standing wave in the cavity.

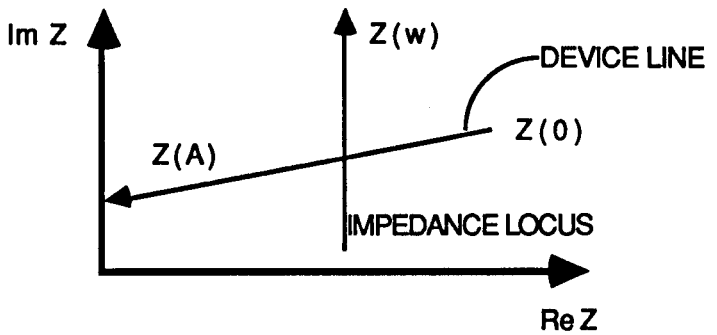

(a) Impedance locus and device line

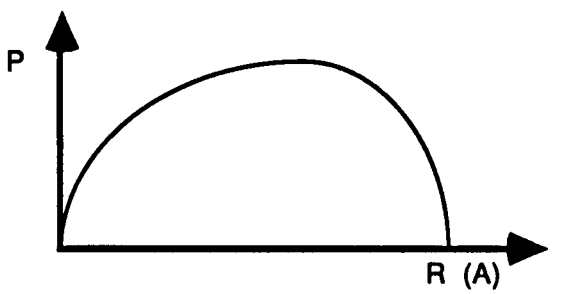

(b) Generated Power as a function of device resistance

FIGURE 4.2

In simple ideal circuits we can expect the reactance to be a very strong function of frequency and the resistance to be a very slow function, as shown in Figure 4.2a.

As a general rule this will be true for simple high Q circuits with very little power reflected from the load. (For a single tuned resonant circuit the impedance locus will be a vertical straight line). The impedance seen at any frequency will be mainly determined by the cavity around the device, and will be a relatively slow function of frequency. However, for tuning elements or reactive loads located a number of wavelengths from the active device, we can expect the impedance to change very rapidly with frequency. This can lead to bends and loops forming in the impedance locus as shown in Figure 4.3 which can lead to hysteresis and frequency jumps during tuning. This is discussed more fully later.

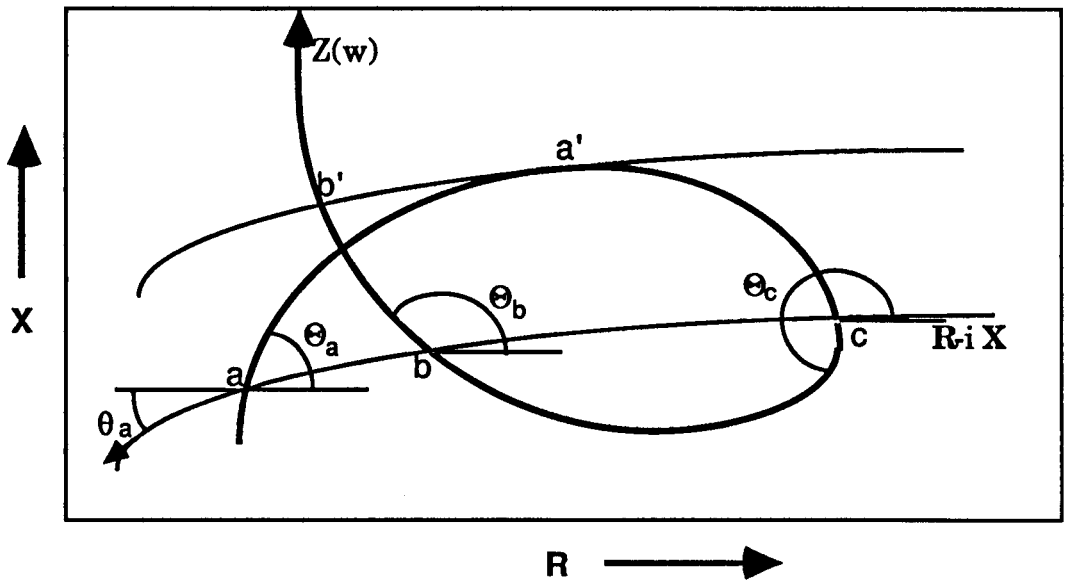

FIGURE 4.3

Z(w) and -Z(A) on the complex plane where Z(w) has a loop in its locus

The stability condition is that $\sin(\Theta-\theta) > 0$

4.2.2 ACTIVE DEVICE IMPEDANCE

The active device is essentially non-linear and its impedance will depend on many parameters although it is mainly a function of current amplitude A. The device impedance is represented as:

$$Z_d(A) = -R_d(A) + iX_d(A) \qquad (4.2)$$

In general it will have an impedance that is a very strong function of current or voltage amplitude, but which will also be a function of bias, temperature, frequency and the current and voltage waveform. The shape of the waveform being a function of how the harmonics are terminated. The bias and the temperature are very important operating parameters, however, under normal optimum operating conditions they are usually sufficiently constant not to change the impedance significantly for most applications, and their variation will be neglected for the moment. The variation of device impedance with frequency is also slow, (at least compared to the variation of circuit impedance with frequency) and it can normally be considered constant for single frequency operation. Therefore, for the purposes of analysis the impedance will just be taken as a function of current amplitude, as shown in Figures 4.2a and 4.3. A typical characteristic is that the negative resistance of the device will decrease with current amplitude and the reactance

will not change much. It should be noted, however, that the impedance will change over the full frequency range of the device and a typical example (for a 6GHz Impatt diode) is shown in Figure 4.4. It should also be realised that this is the impedance for a fundamental resonance, and that once the device is oscillating the impedance will change at other frequencies. In particular, regions of negative resistance can appear at low frequencies, harmonics and sub-harmonics of the fundamental. This is discussed more fully later.

The condition for fundamental oscillation can be found by considering Figure 4.1 . The entire circuit can be imagined as a simple series connection between the device and resonant circuit. Now because there is no applied voltage at the resonant frequency the total impedance times the current must be equal to zero, and the equation for free-running oscillation is given by:

$$[Z_c(w) - Z_d(A)]\, I = 0 \qquad (4.3)$$

which leads to the two oscillation conditions:

$$R_c(w) - R_d(A) = 0 \qquad (4.3a)$$

$$X_c(w) + X_d(A) = 0 \qquad (4.3b)$$

Thus an operating point is given by the intersection of the device and circuit impedance locus as shown in Figure 4.2a.

4.2.3 POWER

The generated power produced by the negative resistance device is given by:

$$P = R_d(A) \times (A^2 / 2) \qquad (4.4)$$

where A is the current amplitude and R_d is the negative resistance of the device. If the operating point along the device line is changed by altering the circuit impedance then we can expect the power generated to vary in a way shown schematically in Figure 4.2b. If we consider the device line, then, at one extreme we have a large negative resistance for zero current amplitude, and at the other, a small negative resistance for large current amplitude. Therefore, we expect there to be some point in the middle where the device will generate the most power, for some critical current amplitude. In fact, a simple model [9] indicates that the maximum generated power will be produced at a point where the negative resistance is half that of its maximum value. It is also quite easy to show [2] that the

maximum power corresponds to the condition when the value of s (often referred to as the saturation parameter) is equal to 2, where s is given by:

$$s = -\frac{A}{R_L}\frac{\delta R_d(A)}{\delta A} \tag{4.4b}$$

4.2.4 CIRCUIT EFFICIENCY

Due to circuit losses, the power output will not be the same as the generated power but be given by the circuit efficiency multiplied by the generated power. If we consider the equivalent circuit in Figure 4.1 the circuit efficiency [3] can be shown to be given by:

$$\eta = \frac{R_L}{R_d(A_0)}\left|\frac{Z_d'(w_0)}{Z_{out}'(w_0)}\right| \tag{4.5}$$

where Z_d is the impedance looking into the device and Z_{out} is the impedance seen looking into the circuit from the load resistance and $Z_c'(w_O)$ and $Z_{out}'(w_O)$ are their rate of change with frequency at w_O.

The circuit efficiency can be expected to decrease with increasing current amplitude due to greater resistive losses within the circuit. The maximum output power point, can therefore be expected to be slightly on the low current side of the maximum generated power point [4]. A device which can be shown to be at this point is said to be critically coupled to the circuit.

To increase the circuit efficiency η but keep the optimum current amplitude across the device it is often found useful to have some form of impedance transformer near the active device. A "low" impedance section at the device, so that the device sees the optimum current at the desired frequency, and a higher impedance cavity and output waveguide to reduce resistive losses.

It is also not too difficult to construct a single frequency tuned circuit which has variable coupling. A typical example is a circuit consisting of a waveguide cavity which is then coupled to a separate output waveguide. The variable coupling is achieved by having a rotary joint at the junction between the two waveguides [6], enabling almost any amount of coupling to be achieved. This is a little inconvenient to use, as either the output

waveguide, or the whole circuit has to be rotated. However, if the amount of coupling required is known then it is possible to replace the rotary joint with some form of iris, whose effects and parameters have been well characterised in the literature [7]. Such techniques though, are inherently single frequency and unsuitable for broadband applications as well as leading to difficult fabrication problems at the highest frequencies. The amount of coupling required may also be diode and frequency dependent.

4.2.5 STABILITY

If we now consider whether an oscillation will be stable with respect to small signal fluctuations it is shown in [1] that the point must satisfy the following equation:

$$A_0\left(\frac{-\delta R_d(A_0)}{\delta A}\right)\left(\frac{\delta X_c(w_0)}{\delta w}\right) - A_0\left(\frac{\delta X_d(A_0)}{\delta A}\right)\left(\frac{\delta R(w_0)}{\delta w}\right) > 0 \qquad (4.6a)$$

where A_0 and w_0 are the amplitude and frequency of the oscillation. This condition has a direct graphical interpretation as it can be shown that (4.6a) is equivalent to:

$$|Z_d'(A)|\,|Z_c'(w)|\sin(\phi-\theta) > 0 \qquad (4.6b)$$

Thus $\sin(\phi-\theta) > 0$ for stability. If we consider Figure 4.3 then, points (a) and (b) will be stable but point (c) will be unstable. As Kurokawa points out [1], which of the two stable points the oscillator selects depends on the oscillators history, and a jump from one to the other can be effected, by changing the impedance of the circuit or the device. (The device reactance is normally sensitive to bias variations). The jump will occur either because of transient voltage and current variations during tuning, or because one point will cease to exist, if one tunes far enough. This is illustrated in Figure 4.3 where an oscillation at (a') will jump to (b') with any increase in device reactance. If the device reactance is then decreased, the oscillation will occur on the "b loci" until the device and circuit locus cease to exist at the bottom of the loop. A hysteresis effect is therefore seen, as the device reactance is changed, with both the power and frequency varying and jumping discontinuously. A more detailed description is given in Refs.[1,2,3]. This has frequently been observed experimentally, and is usually due to loops in the impedance locus rather than a device effect. Loops in the impedance locus are usually indicative of a low effective Q, multi-resonant circuit, often associated with reflections from the load.

Another effect, which is also seen experimentally is the appearance of sidebands at displacements of order 0.1 to 1 percent away from the oscillation frequency, just before a

jump in frequency[3]. This is due to a very subtle device circuit interaction which was first explained by Kurokawa[1].

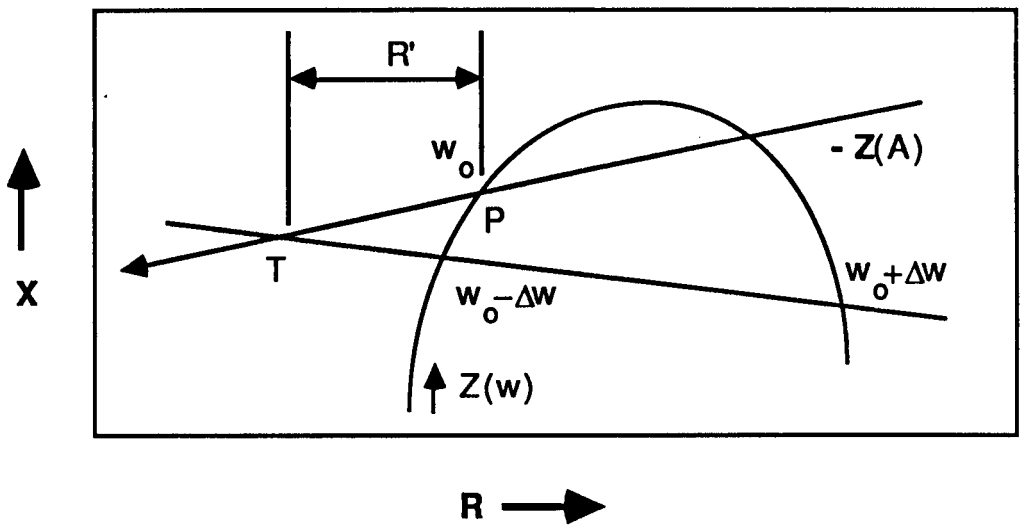

Diagram illustrating condition for spurious sidebands
FIGURE 4.5

In Figure 4.5, we define the intersection between the tangent of the device line at the oscillation point P and the line through the frequency points $w_0 \pm \Delta w$ on the circuit line to be at the point T.

Now if the resistive component R satisfies

$$R' = -1/2\, A_0(\delta R_d(A_0) / \delta A) \qquad (4.7)$$

then spurious oscillations can grow at $w_0 \pm \Delta w$. This condition is never satisfied for a single resonant circuit (vertical circuit line) but is often satisfied when there are loops present in the circuit locus. Indeed several spurious oscillations can appear on either side of the oscillation. This is another indication that loops in the circuit loci are to be avoided.

Another hysteresis effect that is seen experimentally is due to a loop in the device locus, as shown in Figure 4.6.

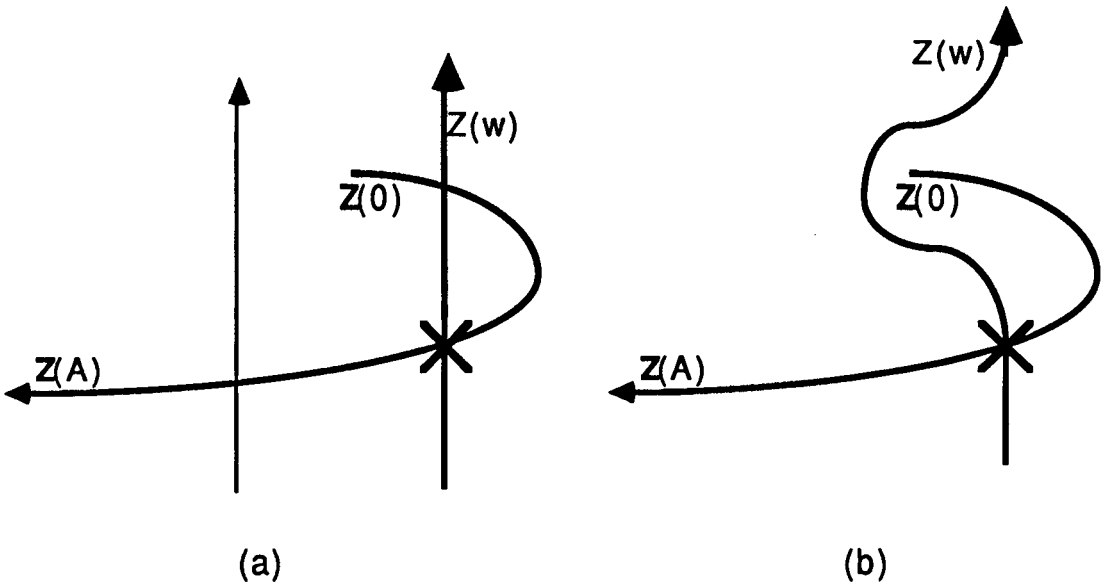

a) Diagram illustrating typical switch-on hysteresis effect

(Device will not start to oscillate even though previosly it was operating at the maximum power point denoted by X)

b) A possible solution - where the coupling to the load is reduced initially.

FIGURE 4.6

This type of loop is not uncommon for frequencies above the transit time frequency [3] and can lead to a switch-on hysteresis if the circuit locus is like that illustrated. The impedance of the circuit is chosen so that the device can operate at the maximum power point. However, if the device is switched off there will be no oscillation because the small-signal device impedance Z(0) is not on the right-hand side of the impedance locus [3]. Thus initially the load resistance is greater than the devices initial negative resistance. This means that small oscillations will experience a positive resistance and be exponentially damped. Therefore to start oscillation the circuit impedance locus Z(w) in Fig.4.6a must be brought to the left (less coupling to the load) and then retuned to achieve maximum power. An alternative is to try and design a circuit like that shown in Figure 4.6b, however, this would be very difficult for all but single frequency applications.

4.2.6 NOISE

The active device will always produce noise which can be modelled as a noise voltage source in series with the active device. The oscillation condition therefore becomes:

$$[Z_c(w) - Z_d(A)]\, I = e \qquad (4.8)$$

which can be rewritten as:

$$Z_c(w) = Z_d(A) + (e / I) = Z_d(A) + |el|/A_O \exp(-i\Theta) \qquad (4.9)$$

where |el| and Θ will change randomly with time, producing FM and AM noise components. Note that the larger the current amplitude, and the smaller the noise voltage, the smaller the FM and AM deviations. Thus for lowest noise, one generally wants to work at a point on the device locus that is undercoupled to the load, although the noise voltage can also be expected to be a function of position.

Noise can also be considered in terms of the impedance loci of the circuit and the device, and Kurokawa has indicated [2] that it can be thought of as a vibration of the device line. longitudinal vibrations producing AM noise and transverse vibrations producing FM noise. This can predict several useful results (assuming the device and circuit loci intersect roughly at right angles). Firstly, a higher circuit Q can be expected to reduce FM noise, as the same change in impedance, corresponds to a smaller change in frequency,but not change the AM noise much. (The same is true of injection locking [2]).

Also, both FM and AM noise components can be expected to grow very large if the angle of intersection between the device and circuit locus becomes very small, as the same amount of vibration of the device line will correspond to larger amplitude and frequency variations. It is shown in Ref.1 that for small fluctuations that the FM and AM noise can be approximated as:

$$|dA(f)|^2 = \frac{2\,|el|^2}{w^2\,|Z_c'(w_0)|^4 + A_0^2\,|Z_d'(A_0)|^2 \sin^2(\phi - \theta)} \qquad (4.10)$$

$$|\Phi(f)|^2 = \frac{2\,|e|^2}{w^2 A_0^2\,|Z_c'(w_0)|^2} \cdot \frac{w^2\,|Z_c'(w_0)|^4 + A_0^2 |Z_c'(w_0)|^2\,|Z_d'(A_0)|^2}{w^2\,|Z_c'(w_0)|^4 + A_0^2\,|Z_c'(w_0)|^2\,|Z_d'(A_0)|^2 \sin^2(\phi - \theta)} \qquad (4.11)$$

where |e(f)| represents the magnitude of the noise voltage at a given frequency. We can see as the intersecting angle becomes sharp (0^0 or 180^0) then one of the terms in the denominator becomes zero and the oscillation becomes much more noisy.

Now, putting,

$$|e(f)|^2 = 4\,K\,T\,R_L/\eta \qquad (4.12)$$

where η is the circuit efficiency and T is the effective noise temperature (at frequency f). And making the approximation,

$$Q_{ext} = w_0\,Z_c'(w_0)/2R_L \qquad (4.13)$$

and assuming $(\phi-\theta) \approx 90^o$. Then we can make the following approximations:

$$|\phi|^2 = \frac{\frac{k\,T}{\eta\,P_0}}{\left(Q_{ext}\frac{w}{w_0}\right)^2} \qquad (4.14)$$

$$|\delta A(f)|^2 = \frac{\frac{2\,k\,T}{\eta\,R_L}}{\left(Q_{ext}\frac{w}{w_0}\right)^2 + \left(\frac{A_0\,|\,Z'(A_0)\,|}{2\,R_L}\right)^2} \qquad (4.15)$$

(where it should be noted that the second term in the denominator in Eq.4.15 is equal to 1 at the maximum power point, from Eq. 4.4b)

Typically the AM noise in Gunn oscillators is very low [7], although it has been reported that oscillator combining can reduce the AM noise.

There will of course be some dependence on Q on the high frequency AM (and FM) components. A vibration of the device line will cause a shift in the position of stable oscillation, indicating a new frequency and oscillation amplitude. However, the RF voltage and frequency cannot change instantaneously, because of the large amount of energy stored in the microwave circuit. Essentially, the requirement is for that energy to "decay away" and be "replaced" by the energy generated under the new oscillation condition. The "decay" will be exponential and the time constant will be inversely proportional to the Q of the circuit. This is hardly surprising as the Q of an oscillator is proportional to the amount of energy stored in the circuit divided by the amount of energy lost per cycle.

It is therefore clear that if the device line "vibrates" at too high a frequency, then the circuit will not be able to respond quickly enough, and some average value will be maintained. AM noise will therefore, drop away at the half power point of the oscillator. FM noise will also be affected, although as already observed the Q of the oscillator will also effect the low frequency FM components.

With Impatts and Gunn devices a low frequency negative resistance can appear when the device is oscillating. This can amplify noise from the bias circuit or cause low frequency oscillations, which can then appear as sidebands about the carrier due to parametric upconversion. With cw Gunn devices, this can normally be solved by placing a large capacitor on the bias lead [7]. However, for Impatts which require a constant current supply, and pulse applications of Gunn diodes, this is not feasible and some sort of resistive termination of the bias circuit must be used [7,8].

4.2.7 THE Q OF THE OSCILLATOR

The Q of an oscillation is defined as:

$$Q = \frac{\text{ENERGY STORED AT RESONANT FREQUENCY}}{\text{ENERGY LOST PER UNIT CYCLE}} \qquad (4.16)$$

where these quantities are all measured at resonance. This quantity is also the loaded Q_L. Now the energy loss will be made up of, useful power (delivered to a load), and non-useful losses, (such as joulean heating or diffraction out of the system). We therefore also define:

$$Q_{ext} = \frac{\text{ENERGY STORED AT RESONANT FREQUENCY}}{\text{ENERGY LOST AT OUTPUT PORT PER CYCLE}} \qquad (4.17)$$

$$Q_U = \frac{\text{ENERGY STORED AT RESONANT FREQUENCY}}{\text{ENERGY LOST RESISTIVELY PER CYCLE}} \qquad (4.18)$$

where the loaded Q, unloaded Q and external Q will all be related by:

$$1/Q_L = 1/Q_{ext} + 1/Q_u \qquad (4.19)$$

An alternative and perhaps more useful definition of Q is:

$$Q = \frac{w_0 \left|\frac{dZ}{dw}\right|_{w_0}}{2R} \qquad (4.20)$$

where R represents the appropriate resistive loss.

We can also define the Q of the active device as:

$$Q = \frac{w_0 \left|\frac{dZ}{dw}\right|_{w_0}}{2\,|R_d|} \tag{4.21}$$

where **Z** is the impedance of the diode and $\mathbf{R_d}$ is the negative resistance.

Ideally the Q of the active device wants to be as small as possible so that it has as large a bandwidth as possible, over which it will oscillate. The more energy that is stored within the device the more tuned it will be, and the more difficult it is to use and characterise. The Q of the circuit must be higher than the Q of the oscillator, and is usually so by an order of magnitude. The higher the frequency, the smaller the package to reduce parasitic capacitances and inductances.

Generally speaking, it is useful to have as large a loaded Q as possible to reduce the FM noise and improve the stability of the oscillator. However, increasing the energy stored, normally entails a consequent increase in the resistive losses in the circuit, which will reduce the circuit efficiency, and the output power. (Although the generated power will be the same).

There are also occasions where it is useful to make the oscillator electronically tunable, which can be achieved either by changing the reactance of the active device through bias tuning, or changing the reactance of the circuit through varactor tuning. Usually one wants as large a frequency change as possible for a given change in reactance, and this will be determined by the device circuit loci. For a single tuned series resonant circuit the circuit impedance locus is a vertical straight line, like that shown in Figure 4.2, and the rate of frequency change with reactance will be related to the external Q. The relative frequency change for a change in reactance ΔX [1], is given by:

$$\frac{\Delta w}{w} = \frac{-1}{2\,Q_{ext}} \cdot \frac{\Delta X}{R} \tag{4.22}$$

However, this is only for the simple case of the single tuned circuit. With high frequency oscillators, it is almost impossible to make such simple equivalent circuits and the impedance locus is often distorted. In these cases, the actual Q of the circuit is no longer such a useful parameter, and we define an effective Q [3] given by:

$$Q_{eff} = \frac{w_0 \left|\frac{dZ}{dw}\right|_{w_0} \sin(\phi - \theta)}{2 R_L} \qquad (4.23)$$

This is the Q that is usually measured in any injection locking experiment.

Kurokawa [1] has shown that it is possible to get a very low effective Q if one uses multi-resonant circuits. For example, if one has a double resonant circuit where both series and resonant parts are tuned to the same frequency the n we can expect the loading of the circuit to change away from resonance, so the circuit impedance locus will no longer be a straight line. If we consider the individual Q's of the series and parallel elements as shown in Figure 4.7, then Kurokawa showed that near resonance the effective Q can be approximated by:

$$Q_{eff} = (Q_1 - Q_2) \qquad (4.24)$$

and that the impedance of the circuit line will look roughly like the set shown in Figure 4.8 depending on the relative magnitudes of Q_1 and Q_2.

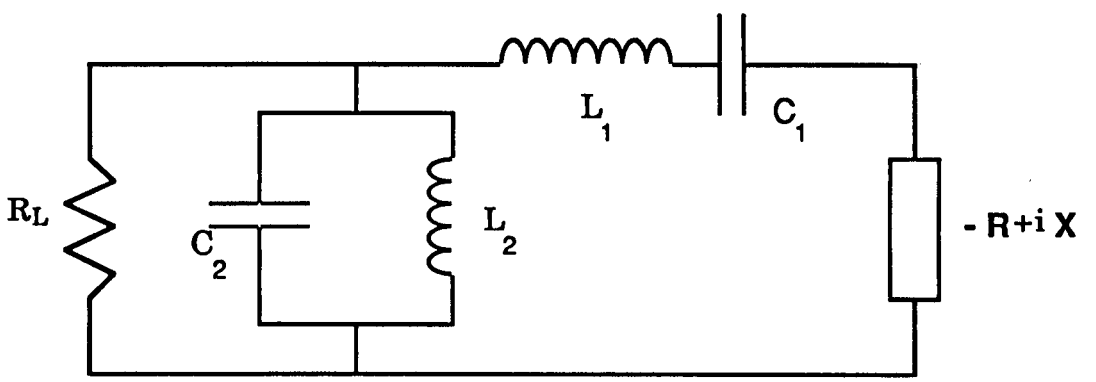

FIGURE 4.7

Diagram illustrating a double resonant circuit where both circuits are resonant at the same frequency

This can lead to a broadbanding effect near resonance as the frequency markers become closer together. Note that a loop appears in the impedance locus for $Q_1<Q_2$, and for $Q_1=Q_2$ there is a cusp. The former can lead to tuning hysteresis as discussed before, and both can suffer from noisy output if the angle of intersection between the device and

circuit locus becomes very acute. Therefore, for any double resonant circuit it is important to have $Q_1 > Q_2$, to have a smooth variation in Z(w) as shown in Figure 4.8b.

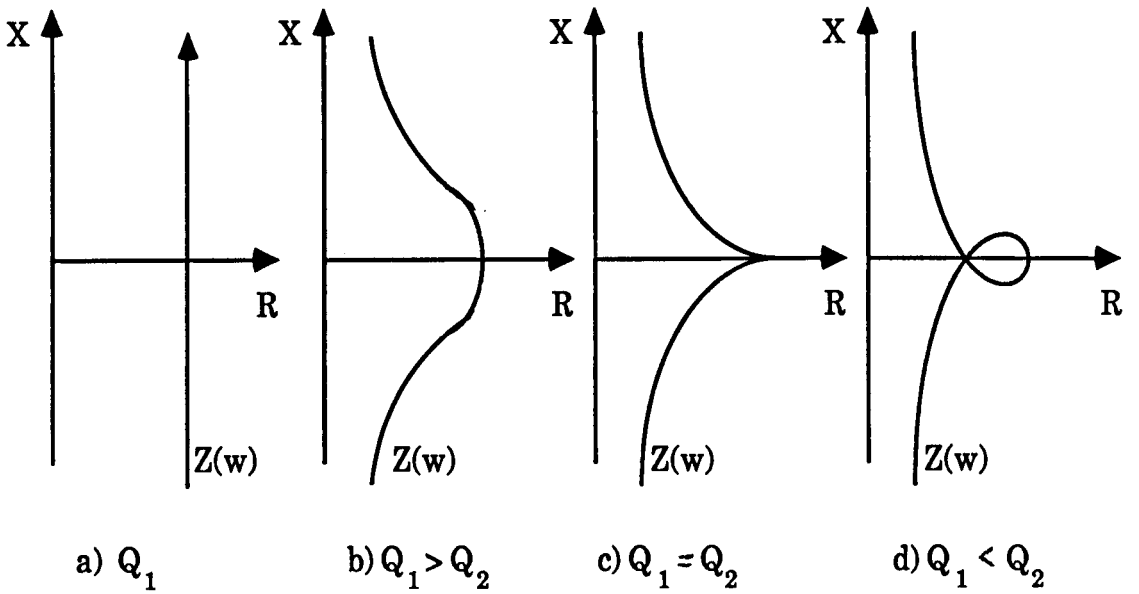

FIGURE 4.8

Diagrams showing the impedance for the circuit shown in Fig. 4.7

Such circuits can increase the locking range for injection locking, and help to explain the very low Q's sometimes measured for certain oscillators. They can suffer from several problems though, if the effective Q becomes too low. Firstly, the output will become noisy as the angle of intersection becomes acute; and the power can vary substantially away from resonance, as the device becomes less heavily loaded. Lastly the frequency deviation can be very non-linear with change in impedance, which can be a problem with some applications. Kurokawa has suggested that the situation might be improved with higher order resonant circuits, although as he states, the rate of return rapidly diminishes as we increase the complexity of the circuit.

In conclusion, due to the complexity of microwave oscillators we must reconsider what is meant by the Q of the oscillation and we define two Q's. The first is defined in terms of the energy stored and the energy lost per cycle and is given by Eq. 4.16 (or Eq. 4.20). It can be applied to any oscillating system and will essentially just be a function of the circuit. It will define the value of dZ/dw near resonance, for the circuit. The second is the effective Q and depends on the circuit and device loci, and is given by Eq.4.23. It will always be smaller than the "real Q". It is more "complex", in that it depends on the orientation of the device and circuit lines, but it is more appropriate to the circuits

considered here, in terms of what is actually measured. It is perfectly possible to have a high Q, but a low effective Q, if the angle of intersection between the device and circuit loci is small.

4.3 INJECTION LOCKING

Injection locking is a very important topic. Kurokawa has written an excellent paper on the subject [2], and was the first to clarify the theory for microwave oscillators [1]. Injection locking can stabilise and generate a fixed frequency signal as well as amplify, amplitude limit and detect FM signals. It is also a very useful experimental tool for the characterisation of microwave and millimeter wave oscillators. However, just the basic theory of small signal injection with a circulator will be outlined here.

The injection signal seen by the device can be represented as a voltage source E in series with the load impedance, as shown in Figure 4.9.

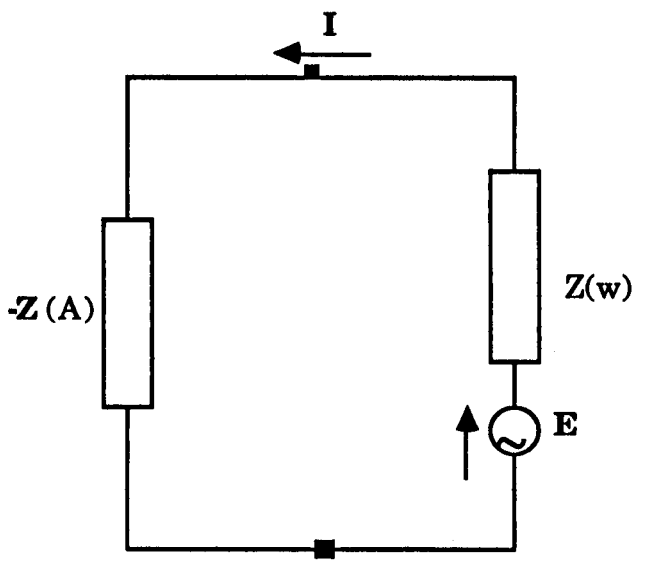

FIGURE 4.9

Diagram illustrating equivalent circuit of an injection locked oscillator

Because a circulator is used, the circuit impedance remains the same as before. If the injection frequency is close enough to the free running oscillation frequency then frequency locking will occur, and the locked oscillator equation becomes:

$$[Z_c(w_i) - Z_d(A)]\ I = E \qquad (4.24)$$

where for small signal injection the RF current amplitude remains roughly the same as the free running amplitude A_0. Rearranging:

$$Z_c(w_i) = Z_d(A) + (|E|/A_0)\exp(-i\Phi)$$

$$= Z_d(A) + 2R_0(P_i/P_0)^{1/2}\exp(-i\Phi) \qquad (4.25)$$

where Φ is the phase difference between **E** and **I**, and $|E|/A_0$ is the distance from $Z_d(A)$ to $Z_c(w_0)$, under locked conditions. It can also be shown that that this equals $2R_0(P_i/P_0)^{1/2}$ where P_i is the injected power and P_0 is the output power. This can be seen graphically in Figure 4.10 which also indicates the limit for locking i.e. the point where the perpendicular from $Z_c(w_0)$ to the device line equals $|E|/A_0$. The effect of the injection signal is therefore to add to $Z_c(w_0)$ an impedance corresponding to $(|E|/A_0)\exp(-i\Phi)$.

Now for constant injection power, the voltage |E| can be expected to be roughly constant, (although it must be transformed through the circuit impedance, so it will depend on how the circuit efficiency varies with frequency). Stability considerations [1] also indicate that locking will only occur if the angle β in Figure 4.10 is less than $\pi/2$, so in general there will only be one stable locking point.

Other stability conditions also apply [1], but these will almost always be valid for reasonably behaved circuit and device loci e.g. no loops present within the locking range.

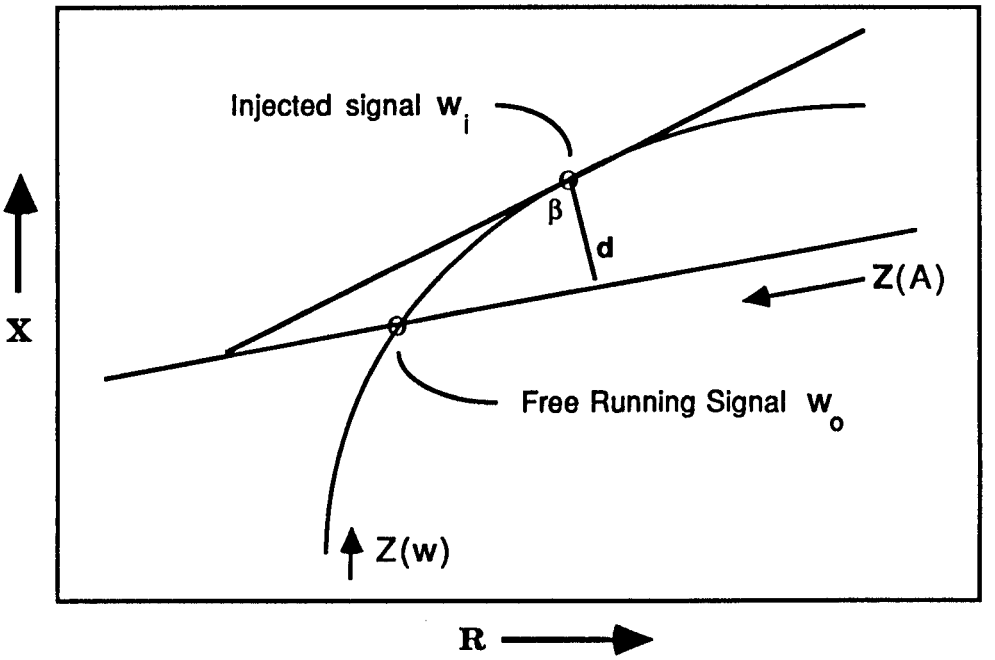

FIGURE 4.10

Diagram illustrating the injection locking limit
d is the injection locking vector = $2 R_L (P_i/P_0)^{1/2}$
β must be less than $\pi/2$ for stability

The device will operate at the point on the device line, under the condition that the distance from $Z_c(w_0)$ to the device line must equal $|E|/A_0$. By varying the injection frequency w_i the operating point will move along the device line as shown in Figure 4.11a, and the power will vary accordingly depending on the value of A and the negative resistance.

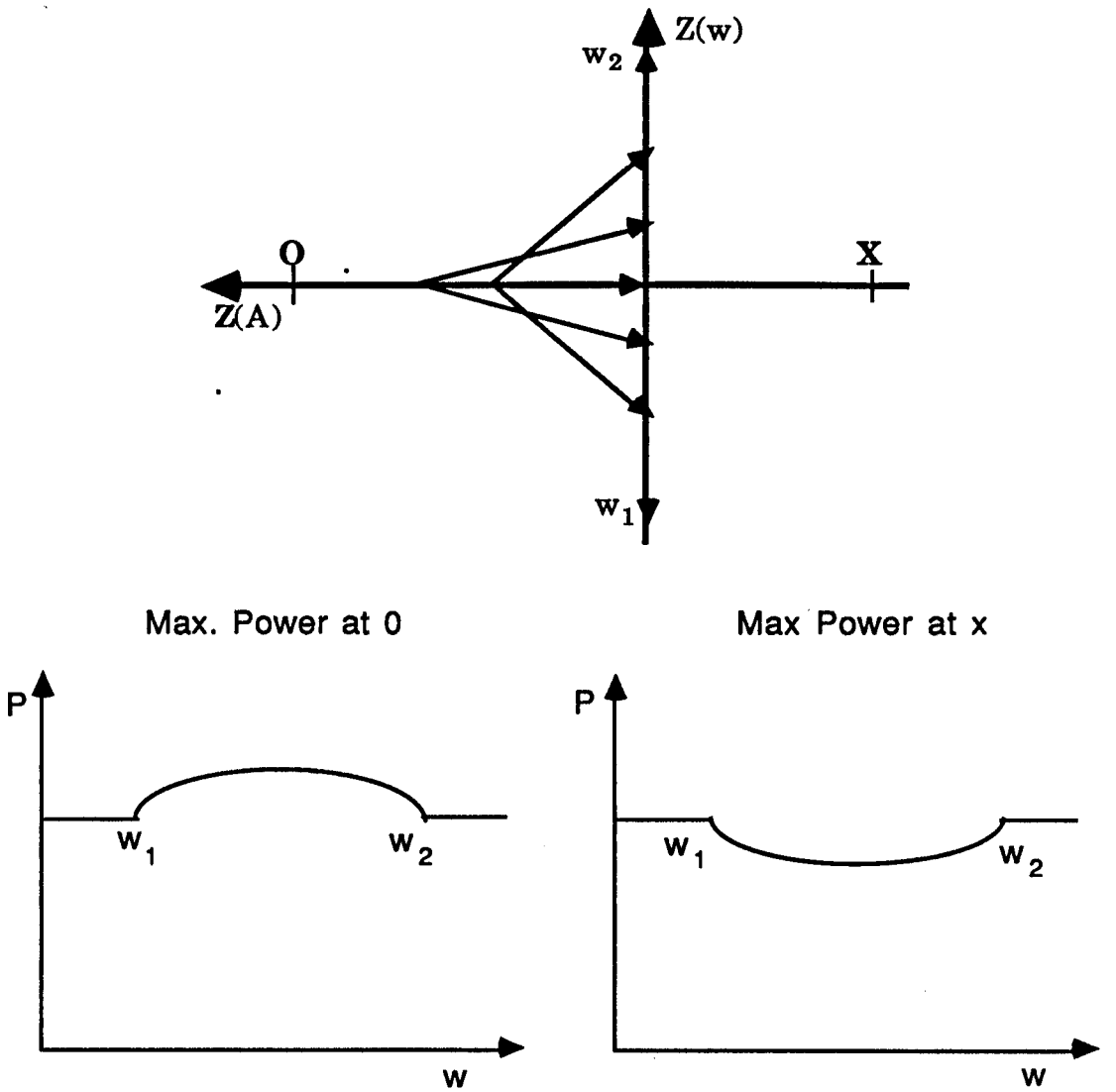

FIGURE 11a

Graphs showing schematically the power variation as the injection frequency is varied from w_1 to w_2

It is therefore possible to find the maximum power point, for that particular frequency, and characterise the device and circuit loci using injection locking experiments [3].

It is also possible to characterise the device or circuit line by injection locking experiments. A typical result for a slanting device line is shown in Fig.11b.

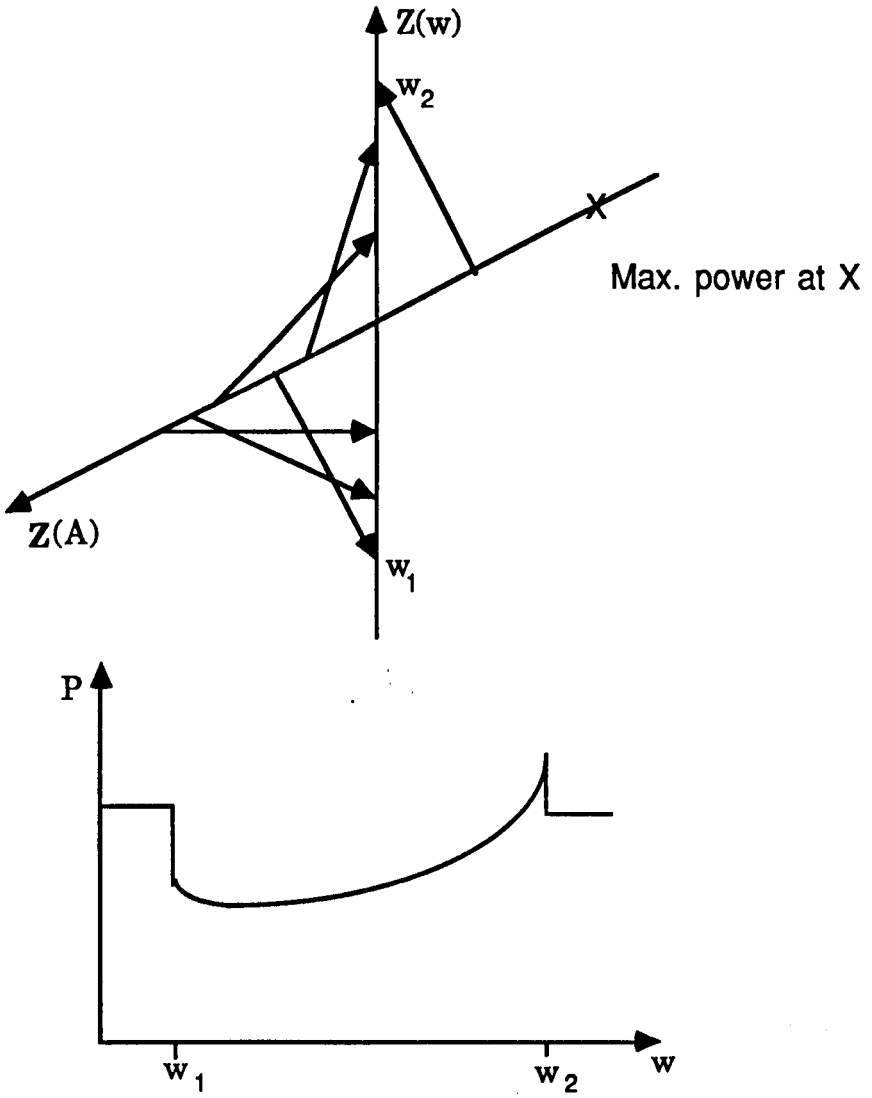

FIGURE 11b

Typical power variation when the device line is slanted

4.3.1 NOISE WITH INJECTION LOCKING

Noise in locked oscillators can still be thought of in terms of the device line vibrating, except we now have two operating points. The point on the circuit line determining the frequency, and the point on the device line determining the current. Now, the FM noise is essentially dependent on movement of the operating point along the circuit locus. However, because the injection frequency is usually fixed, (which fixes the operating point on the circuit loci), we can expect a dramatic decrease in FM noise for a locked oscillator. It will not disappear entirely though, because vibrations of the device line will cause the direction of the injection vector to change. Thus the phase of the current will change randomly, which is just the same as FM noise. The change in phase will increase

away from the centre of the locking range (see Figure 4.12), and be inversely proportional to the size of the injection vector.

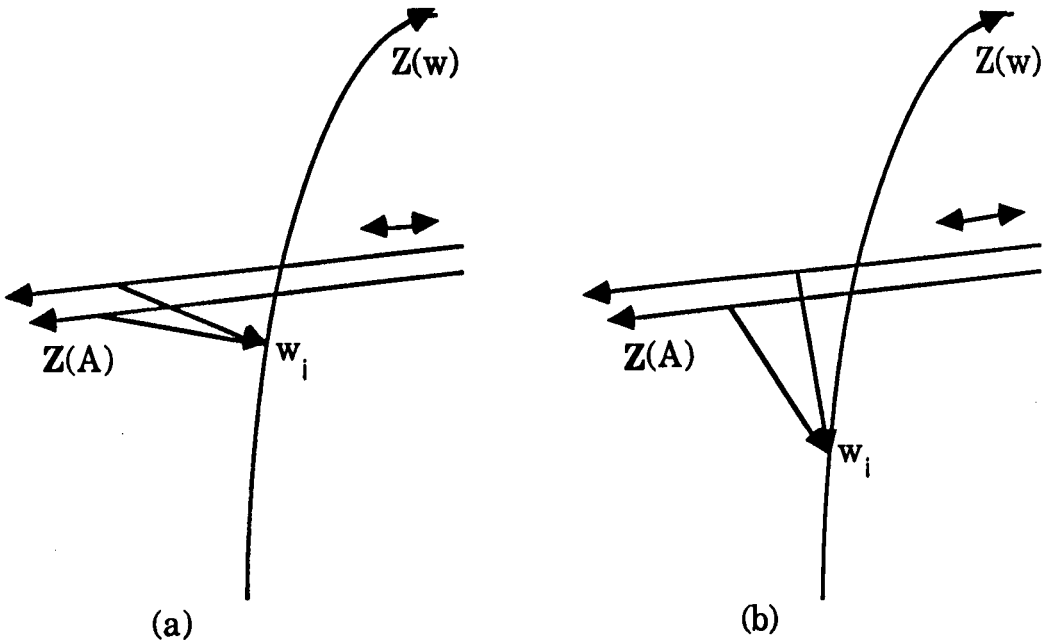

FIGURE 12

Graphical explanation of the FM and AM noise behaviour of a locked oscillator as one changes the injection frequency

Thus the FM noise can be expected to improve with increasing injection power. The AM noise on the other hand will be approximately the same, as it is just dependent on the operating position on the device line. In fact, it can increase as, in addition to any longitudinal vibration, the transverse vibration will cause the operating point to move along the device line giving AM noise. This is a result of having to keep the length of the injection vector constant and is illustrated in Figure 4.12b. This effect can be expected to increase near the locking boundary.

It is shown in [2] that for $\sin(\phi-\theta) = 0$, that the FM and AM noise is given by:

$$|\phi|^2 = \frac{\frac{kT}{\eta P_0}}{\left(Q_{ext}\frac{w}{w_0}\right)^2 + \frac{P_i}{P_0}\cos^2(\Phi)} \qquad (4.26)$$

$$|\delta A|_i^2 = |\delta A|_f^2 \cdot \frac{\left(Q_{ext}\frac{w}{w_0}\right)^2 + \frac{P_i}{P_0}}{\left(Q_{ext}\frac{w}{w_0}\right)^2 + \frac{P_i}{P_0}\cos^2(\Phi)} \qquad (4.27)$$

where $|\delta A|_f^2$ is the free running AM noise given by Eqn. 4.15. It can be seen that the FM noise will improve but that the AM noise actually gets worse under injection locking! Although in practice it is not a significant effect with Gunn oscillators.

4.4 SUMMARY OF THEORY

In conclusion, the microwave oscillator circuit can be very much more complex than its low frequency counterpart, and is capable of producing a whole range of spurious effects. This is essentially due to the difficulty in preventing unwanted reflections, and stray circuit reactances, at these high frequencies. However all the above theory equally applies to low frequency devices as Kenyon has illustrated by, making equivalent lumped circuits [4].

With broadband negative resistance devices care must be taken to:

a) Provide the right reactance to give the desired frequency.

b) Optimise the coupling to give the maximum power output

c) Avoid loops and acute angle crossings in the device circuit loci, as they can lead to noise and tuning problems. Usually it is preferable to have the circuit and device line, crossing at right angles.

d) Optimise the effective Q for the desired application. A high Q for stable, low noise applications, and a low Q for electronic tuning or injection locking.

e) Reduce the circuit losses as much as possible to improve the circuit efficiency.

f) Provide a suitable low frequency impedance to the device to stop bias oscillations and upconversion of noise, due to low frequency negative resistance appearing when the

device is oscillating. i.e. large resistive impedance or short circuit to ground (over the desired frequency range).

g) Correct termination of harmonic frequencies to optimise the power output at the fundamental (or harmonics).

4.5 IMPEDANCE MATCHING

In this section, we shall look at the problem of matching devices to transmission lines whose characteristic impedances considerably differ from the device impedance. This normally requires some sort of resonant circuit to resonate up (or down) to the desired impedance level. All the techniques are applicable to both generators or detectors, although it should be noted that the situation is considerably more complicated for oscillators as, altering the load may also significantly alter the resonant frequency of the oscillator, which in turn alters many of the reactances.

4.5.1 MATCHING WITH A RESONANT CIRCUIT

If we first consider the simplest case of resonant matching - using a simple resonant circuit as shown in the diagram below.

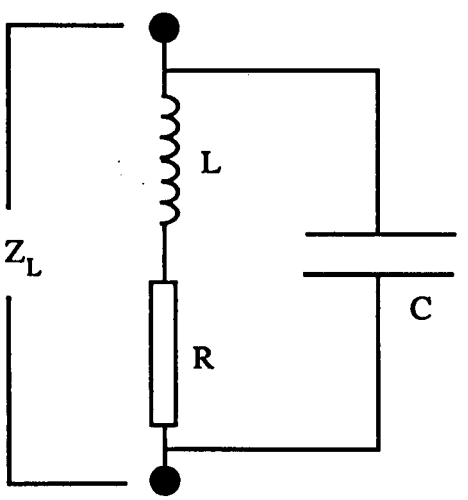

SIMPLE RESONANT TRANSFORMER

The impedance Z_L presented to the terminals is given by:

$$Z_L = \frac{1}{\frac{1}{R + iwL} + iwC} \qquad 4.28$$

After some manipulation the resonant frequency (when $X_L = 0$) is found to be given by:

$$w_0^2 = \frac{L - CR^2}{L^2 C} \qquad 4.29$$

where an expression for the Q of the circuit can be found by substituting for w_0:

$$Q^2 = \frac{w_0^2 L^2}{R^2} = \frac{L}{C R^2} - 1 \qquad 4.30$$

At this resonant frequency the real part of the load can now be calculated as:

$$R_L = \frac{L}{C} \cdot \frac{1}{R} = (Q^2 + 1) R \qquad 4.31$$

Most lumped circuit transformers rely on a parallel resonance of this type and Eq. 4.31 is a general equation that indicates the order of the Q that is required to effect the necessary impedance transformation. For example, to match a negative resistance of 5 ohms to a waveguide of characteristic impedance 500 ohms requires a Q of about 10.

In fact it is comparatively simple to extend this treatment using lumped constants to a general transmission line.

Consider a load which has impedance $Z_T = R_T + iX_T$ at a frequency f, which is placed across (in parallel) a transmission line of characteristic impedance Z_0.

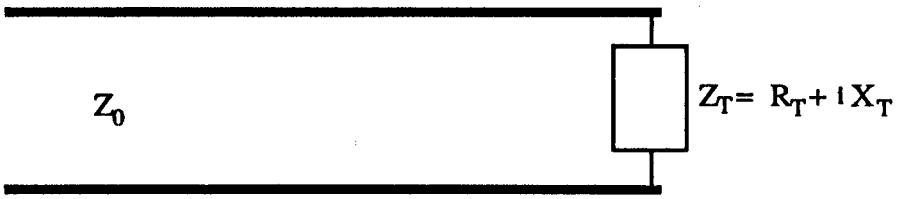

A LOAD Z_T TERMINATING A TRANSMISSION LINE OF IMPEDANCE Z_0

Therefore, for perfect matching to the transmission line we require:

$$R_T = Z_0$$

$$X_T = 0 \qquad (4.32)$$

This means that power at frequency f will be completely absorbed by the load and there will be no reflected wave from the load back down the transmission line.

If however, R_T or X_T differ from the above there will be a reflected wave back down the line, and not all the power is absorbed by the load. This clearly is undesirable for applications involving mixers, power detectors, or indeed oscillators. Most loads will differ considerably from the above, so additional matching structures must be incorporated to match a given load to a transmission line.

4.5.2 MATCHING WITH A BACKSHORT

The simplest means of matching a load to a transmission line is to have an adjustable backshort behind the load. This is a short circuited line placed an arbitrary distance L beyond the load. By an appropriate adjustment of X_T and the length L, a series resonant circuit can be formed of the necessary Q, to effect the appropriate impedance transformation. Thus the impedance Z_T 'sees' an impedance Z_L which is just Z_0 and $i Z_0 \tan(\beta L)$ in parallel.

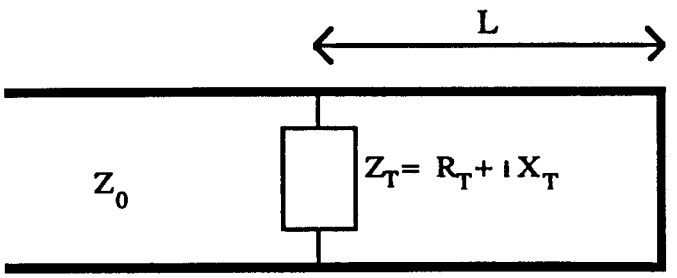

MATCHING A LOAD Z_T TO A TRANSMISSION LINE OF IMPEDANCE Z_0 USING A BACKSHORT

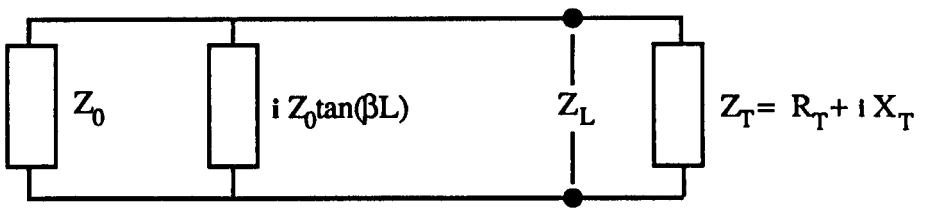

EQUIVALENT CIRCUIT FOR BACKSHORT MATCHING

The impedance which must be matched is now:

$$1/Z_L = 1/Z_0 + 1/(i Z_0 .\tan(\beta L)) \qquad (4.33)$$

Thus the new matching condition is given by $Z_L = Z_T$ which after some manipulation gives:

$$Z_L = Z_0 .\sin^2(\beta L) + i (Z_0/2) .\sin(2\beta L) \qquad (4.34)$$

i.e. for perfect matching

$$R_T = Z_0 .\sin^2(\beta L) \qquad (4.35a)$$

$$X_T = (Z_0/2) .\sin(2\beta L) \qquad (4.35b)$$

This expression bears closer examination and indicates some interesting results.

Given that it is normally possible to manipulate the reactive part of the impedance across the guide with a suitable mount, it is the resistive part that is normally the problem.

The equation indicates that using only a backshort, it is impossible to exactly match a resistive impedance greater than Z_0 placed across a transmission line of characteristic

impedance Z_0. However, for $R_T < Z_0$ we can always get critical coupling if we can arrange for X_T to be some appropriate critical reactance X_C. This value after some manipulation of Eq. (4.34) is given by:

$$|X_T| = (Z_0 R_T)^{1/2} (1 - (R_T / Z_0))^{1/2} = X_C \qquad (4.36)$$

If $X_T < X_C$ then $R_T > Z_0$ and the load is overcoupled to the waveguide. If $X_T > X_c$ then $R_T < Z_0$ and the load is undercoupled to the waveguide. For $X_T = X_C$ we have critical coupling where all the power is absorbed (or maximum power generated, for an oscillator). For swept frequency impedance measurements, we would expect to see less and less reflection and a 180 degree phase change as we pass through this point.

If we now consider two special cases:

1) For $R_T = Z_0$ the line will be matched resistively when $\beta L = (n+1).\pi/2$. i.e. when the backshort is one quarter of a wavelength away. However, for there to be no reflection, this also leads to the requirement that X_T must also equal 0. This condition can approximately be met for a resistive film evaporated onto a thin dielectric sheet such as mylar. The resistance per square is made equal to Z_0 and as long as the dielectric is very thin, $X_T \sim 0$. This technique has been used to design bolometric detectors. Four detectors in fact were designed and manufactured where the thin film coating was a layer of bismuth whose resistance per square was chosen to be approximately the same as the characteristic impedance of a waveguide. With a backshort almost ideal matching was obtained with most of the power being absorbed in the bismuth film. By recording the resistivity of the bismuth film (which is a strong function of temperature), with reference to another bismuth film in a reference waveguide, an accurate power meter can be made. This technique has given promising results, but problems with the bismuth's resistance changing with time has for the moment delayed their use as laboratory instruments.

Another interesting application is the use of thermoplastics. These are regularly used to determine the position of infrared laser beams, where the heat generated by absorption causes a change in colour of the plastic. Initial experiments showed they were not very absorbing at millimetre wave frequencies, where the power per unit area is also often significantly less than infrared beams. This gave a very poor contrast even at moderate power levels (35mW). However, a significant improvement in contrast was achieved by coating bismuth on the back of the plastic, of resistance per square roughly that of free space, and positioning a backshort a quarter of a wavelength away. This

allowed the visual imaging of focussed millimeter beams after they had traversed an optical system. This is an area that deserves further research. At the moment the technique can accurately indicate the position of a focussed beam of around 10mW but further improvements in sensitivity are possible, and there is the potential to observe real time antennae patterns. Further discussion is outside the scope of this thesis.

2) For $R_T << Z_0$ the line is resistively matched for βL tending towards $n\pi$. i.e. when the backshort is roughly one half of one wavelength away. Again Eq.4.35 implies that X_T must also be very small (compared to Z_0). In fact for $R_T << Z_0$, it can be seen from the Eq.4.35 that we have the condition:

$$X_T \sim (Z_0 R_T)^{1/2} \qquad (4.37)$$

To illustrate this, we can consider a low resistance diode (detector or oscillator) that is connected by an inductive post across a waveguide. Equation 4.35 says that the post across the transmission line, which contacts the device, must have a very low impedance over the desired operating frequency range. For high frequency and very low resistance devices, it is difficult to arrange for the inductance to be low enough to satisfy the matching condition. Note, lowering the height of the waveguide to reduce the inductance, also reduces the required reactance (given by Eq.4.35), as Z_0 is also reduced. One solution, is to try and make the mount series resonant at the desired frequency. This has the effect that X_T can be small and the resistive part can be matched to the waveguide. However, it can also significantly reduces the bandwidth over which adequate matching can be achieved. Note that the Q wants to be as small as possible for maximum bandwidth. i.e. small inductance and large capacitance.

This series resonant condition can be achieved by introducing discontinuities in the post or post/diode transition, to create extra capacitance between the post and the waveguide walls. The post can now be viewed as a length of transmission line with capacitances in parallel along its length. These capacitances have the effect of making the line resonant, at a considerably shorter distance than half a wavelength.

The situation is not quite as simple as this, however, as if the post is thick (in terms of wavelength), it will also have some sort of impedance transforming effect down the waveguide. It can also create capacitance between the discontinuity and the floor of the waveguide which may shunt the diode.

Capacitances shunting the diode should be avoided as it makes the matching more critical. If the resistance of the diode R_D is comparable to 1/wC then the effective resistance R_T across the waveguide is reduced considerably and the required impedance transformation is that much greater.

4.5.3 ADDITIONAL MATCHING

It may not always be possible to change X_T to the desired value and critical coupling will probably only be available at one or two spot frequencies with backshort tuning. If we consider, the Smith chart in terms of admittance then it is clear that, for backshort tuning to give critical coupling, the admittance Y_T must initially lie somewhere on the unit circle. The backshort can then provide the necessary susceptance to bring the impedance to the 1,0 point for critical coupling. Note, that if Y_T does not lie on the unit circle then the best backshort match is to bring the admittance on to the zero susceptance line (minimum VSWR).

Perfect coupling can always be arranged for any lossless transmission line if we can produce a reflection of the appropriate phase and amplitude further down the line. This in effect cancels the VSWR set up by the initial mismatch of the line, beyond the reflection. There are a number of ways that this can be achieved.

4.5.3.1 SINGLE STUB TUNING

A stub in parallel with the line (or in series) can provide any magnitude of reflection, and if its distance L from the load is adjustable then any arbitrary phase can be achieved.

On the Smith chart, from any arbitrary load Y_L the length of line L (or phase) is chosen to bring the load onto the unit circle (via a constant S circle). The susceptance of the stub is then chosen to move along the unit circle to the 1,0 point and match the line.

In practice, providing an adjustable length L is difficult unless a phase changer can be placed between the stub and the load, so a single stub will always have a limited

bandwidth. For matching to a very low impedance we have the condition that the distance from the load to the stub tends towards half a wavelength, and the tuning becomes critical.

4.5.3.2 DOUBLE STUB TUNING

Double stub tuners are capable of matching a larger variety of impedances, however for matching to very low resistances (high conductances), there is a requirement that the distance between the stubs be close to a multiple of a half wavelength. Not only does this again limit the bandwidth, but it also has the effect of making the tuning exceptionally critical.

4.5.3.3 THE MAGIC TEE

A better way of producing an arbitrary phase and reflection is to use a magic tee as shown in Fig.4.13 By symmetry, a wave entering the E arm is split equally between arms 1 and 2, and none is transmitted to the H arm of the tee. If backshorts are placed symmetrically in arms 1 and 2, then there is a total reflection back down the E arm. If however, one of the backshorts is one quarter of a wavelength from the symmetry position, then all the power is transmitted to the H arm and there is a perfect match. Thus any arbitrary reflection can be generated by changing the symmetry of the backshorts, and any arbitrary phase can be produced by moving both backshorts in or out together by equal amounts. In practice, this requires the tee to be manufactured to high tolerances often with additional matching structures, to ensure equal splitting and good isolation between the ports, which becomes more and more difficult at the higher frequencies. Adjusting the phase by moving both backshorts accurately together, can also be quite tricky.

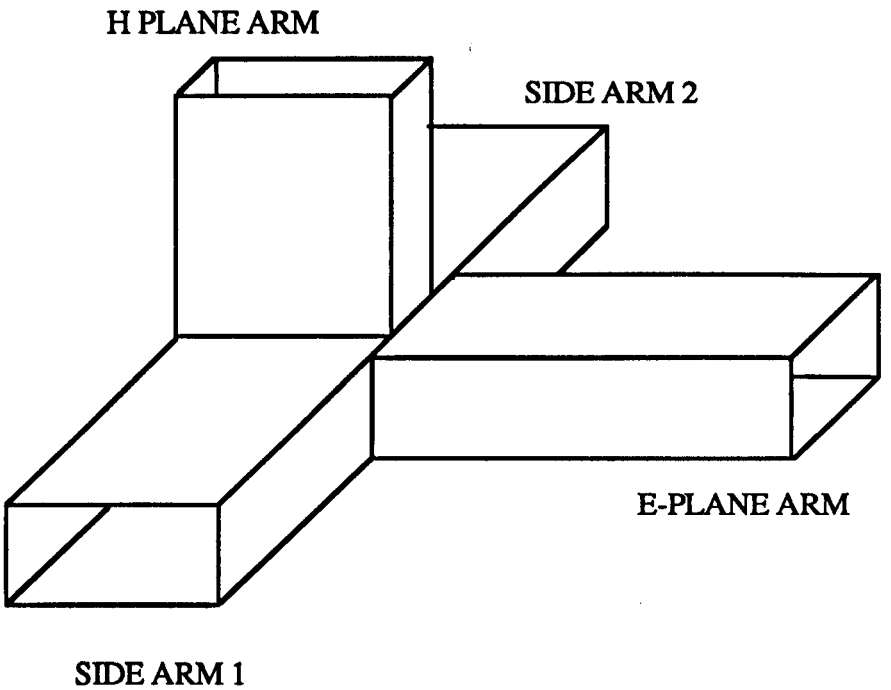

FIG. 4.13

MAGIC TEE STRUCTURE USED FOR IMPEDANCE MATCHING

4.5.3.4 FREE SPACE MATCHING

At higher and higher frequencies it becomes more and more difficult to produce the tolerances required by waveguide, and matching using free space techniques can become more appropriate. In this technique, the transmission line is coupled out into free space using a feedhorn and lens to produce a Gaussian linearly polarized beam. It passes completely through an angled polariser, onto a rotatable movable roof mirror. If the roof line is parallel or perpendicular to the polariser the beam will be completely reflected back into the system, whereas if the roof line is 45 degrees to the polariser, all the beam will now be reflected by the polariser into the load. Thus by rotating the roof mirror, any arbitrary reflection back into the feedhorn and waveguide can be created, and by moving the roof mirror linearly, this reflection can have any appropriate phase. This has the advantage that the phase and amplitude is controlled by independent easily adjusted

movements. In addition, the phase should vary linearly with mirror position, and the accuracy of the reflection coefficient is now independent of frequency, but just depends on rotation. This is a very convenient way of impedance matching at the highest frequencies, although careful design of feedhorn and lens must be used to ensure maximum coupling and low transmission losses through the horn and lens. The scheme is shown in Fig.4.14 , to try and provide optimal matching for an oscillator.

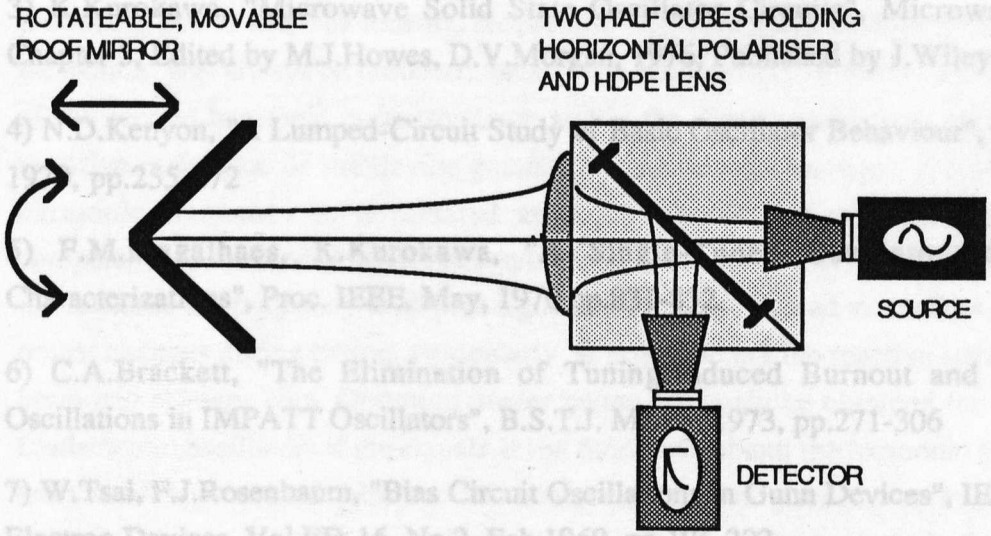

OPTICAL IMPEDANCE MATCHING CIRCUIT

FIG 4.14

REFERENCES (CHAPTER 4)

1) K.Kurokawa, "Some Basic Characteristics of Broadband Negative Resistance Oscillator Circuits", B.S.T.J. July-Aug, 1969, pp.1937-1955

2) K.Kurokawa, "Injection Locking of Microwave Solid-State Oscillators", Proc. IEEE, Vol.61, No.9, Oct.1973, pp.1386-1410

3) K.Kurokawa, "Microwave Solid State Oscillator Circuits", Microwave Devices, Chapter 5, Edited by M.J.Howes, D.V.Morgan, 1976, Published by J.Wiley & Sons

4) N.D.Kenyon, "A Lumped-Circuit Study of Basic Oscillator Behaviour", B.S.T.J. Feb, 1970, pp.255-272

5) F.M.Magalhaes, K.Kurokawa, "A Single-Tuned Oscillator for IMPATT Characterizations", Proc. IEEE, May, 1970 pp.831-832

6) C.A.Brackett, "The Elimination of Tuning-Induced Burnout and Bias-Circuit Oscillations in IMPATT Oscillators", B.S.T.J. March, 1973, pp.271-306

7) W.Tsai, F.J.Rosenbaum, "Bias Circuit Oscillations in Gunn Devices", IEEE Trans. on Electron Devices, Vol.ED-16, No.2, Feb.1969, pp.196-202

8) L.Wandinger, V.Nalbandian "Millimeter-Wave Power Combiner Using Quasi-Optical Techniques", Vol. MTT-31, No.2, Feb.1983, pp.189-191

9) K.Solbach, "Simulation Study of Harmonic Oscillators", Vol. MTT-30, No.8, Aug.1982, pp. 1233-1236

5.0 FUNDAMENTAL AND SECOND HARMONIC EFFECTS IN NON-LINEAR DIODES

5.1 INTRODUCTION

Many high frequency oscillators, including IMPATT, Gunn, quantum-well and tunnel devices have been shown to produce significant amounts of second harmonic power. Essentially any device which has a negative differential resistance is capable of producing power at a fundamental frequency, when placed in an appropriate circuit, and harmonics will always be produced through the non-linearity of the diode. The magnitude of the second harmonic current/voltage across the diode can be very significant if the negative resistance of the device persists to the second harmonic frequency, and the harmonic frequency is terminated appropriately. If this voltage/current becomes comparable to the fundamental voltage/current, it can cause the admittance of the diode at the fundamental frequency to change significantly. This can lead to marked frequency and power changes during tuning, particularly at points where the reactive termination of the harmonic changes sign. Optimum power output will only be obtained for harmonic and fundamental oscillators if the signals at the fundamental and the harmonic frequencies are terminated appropriately. In practice, however, for Gunn oscillators, the third harmonic voltage/current is so low its effect on the output can be neglected, for most circuit conditions. (Experimentally, and from varactor theory [3], to produce any third harmonic power, large currents at the second harmonic frequency are needed. i.e. the second harmonic needs to be reactively terminated).

This chapter examines a relatively simple non-linear analysis of a second-harmonic diode to look at how the fundamental and second harmonic impedance terminations can affect the frequency and power output of the diode at the fundamental and second harmonic frequrencies.

5.2 DIODE MODEL

To look at the type of effect harmonics can have on the admittance of a diode we will follow the analysis performed by Solbach [1], where he models the diode as a real non-linear resistance, which has an I/V curve which can be represented as,

$$I = C_1 V + C_2 V^2 + C_3 V^3 \qquad (5.1)$$

at the frequencies of interest, where C_1 is a negative conductance, C_3 is the term which limits the voltage across the diode and C_2 is the term which largely controls the symmetry

of the I/V characteristic. The larger C_2, the more unsymmetrical the I/V curve. The type of I/V curve which it represents is shown in Fig.1. (This is a simplified model and in the more general case C_1, C_2 and C_3 would be complex).

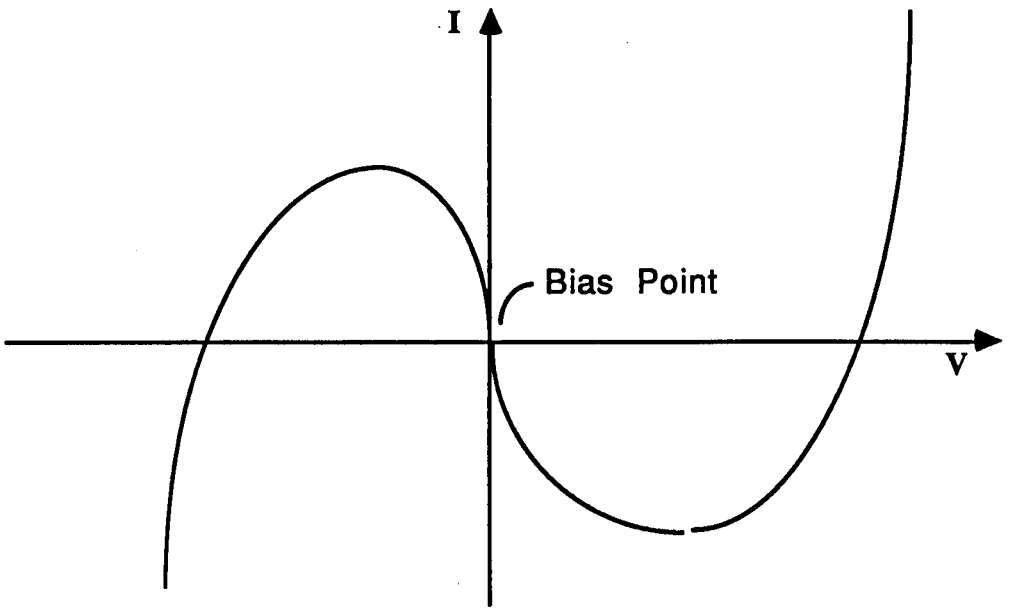

FIGURE 5.1

Figure showing schematically the type of I/V curve modelled

In the steady-state we assume the actual terminal voltage across the active device is,

$$V = V_1 \cos(wt) + V_2 \cos(2wt + \phi) \qquad 5.2$$

where all higher harmonics are set to zero.

If this is then substituted in (1) and expanded then we get a d.c term and components up to the sixth harmonic for the current. (Terms containing cos(wt) and cos(2wt+ϕ) are real and those containing -sin(wt) and -sin(2wt+ϕ) are imaginary). Ignoring the higher harmonics where no significant voltage is allowed to develop, this leads to the evaluation of the rf currents as,

$$I_1 = C_1V_1 + C_3\left(\frac{3V_1^3}{4} + \frac{3V_1V_2^2}{2}\right) + C_2V_1V_2\cos(\phi) + i\,C_2V_1V_2\sin(\phi)$$

$$I_2 = C_1V_2 + C_3\left(\frac{3V_2^3}{4} + \frac{3V_2V_1^2}{2}\right) + C_2\frac{V_1^2}{2}\cos(\phi) + i\,C_2\frac{V_1^2}{2}\sin(\phi) \quad 5.$$

Now because there are no voltage sources the circuit must obey the equations,

$$I_1 + V_1.Y_c(w) = 0 \qquad 5.5$$
$$I_2 + V_2.Y_c(2w) = 0 \qquad 5.6$$

where $Y_c(w) = G_c(w) + iB_c(w)$ and $Y_c(2w) = G_c(2w) + iB_c(2w)$ are the admittances presented to the diode by the circuit at the fundamental and second harmonic frequencies. They are essentially just functions of frequency. Note that I_1/V_1 and I_2/V_2 are the admittances of the diode at the fundamental and harmonic frequencies. These give:

$$G_d(w) = C_1 + C_2V_2\cos(\phi) + C_3\left(\frac{3V_1^2}{4} + \frac{3V_2^2}{4}\right) \qquad 5.7$$

$$B_d(w) = C_2V_2\sin\phi \qquad 5.8$$

where $Y_d(w) = G_d(w) + i\,B_d(w)$

$$G_d(2w) = C_1 + C_2\frac{V_1^2}{2V_2}\cos(\phi) + C_3\left(\frac{3V_2^2}{4} + \frac{3V_1^2}{4}\right) \qquad 5.9$$

$$B_d(2w) = -C_2\frac{V_1^2}{2V_2}\sin(\phi) \qquad 5.10$$

where $Y_d(2w) = G_d(2w) + i\,B_d(2w)$

Thus the diode admittance is a function of V_1, V_2, and ϕ as well as w, and can be subdivided into three distinct parts. This simple treatment allows analytical expressions to be derived, however the basic Physics will be the same for all diode characteristics. We can note that the diode admittance expression contains three distinct terms.

Note that C_1 is negative and represents the negative conductance or gain of the device.

The C_3 term is positive, and is the term which limits the voltage amplitude of the device i.e. it represents the resistive loss in the diode as the the voltage and current swing into positive regions of the diode characteristic. The C_3 term wants to be as small as

possible for maximum power output at the fundamental or the second harmonic. It is represented as A(w) or A(2w) later.

The C_2 terms are the ones which represent the interaction and conversion between the fundamental and second harmonic voltages. Depending on the phase ϕ, power will be converted from the fundamental to the second harmonic or vice-versa. It is interesting to note that this term is complex and is a circle in admittance space. Qualitatively, this is very similar to the treatment given by Brackett [4] although he uses a slightly simpler representation of his diode admittance. It is the reactive part that can lead to the phenomenon of frequency jumping, as one tunes through a second harmonic resonance. This is discussed in more detail later. The value of C_2 wants to be as large as possible for the maximum possible conversion to second harmonic. An analogy with laser second harmonic generation is that the frequency doubling crystal must have a quadratic polarisation term. This implies that the crystal must not have a centre of symmetry or inversion centre, otherwise no second harmonic is generated (although it is still possible to generate third harmonic).

From (7) and (8) the respective circuit and diode admittances must be equal and opposite for steady-state oscillations.

$$G_c(w) = -G_d(w) \qquad 5.11a$$

$$B_c(w) = -B_d(w) \qquad 5.11b$$

$$G_c(2w) = -G_d(2w) \qquad 5.12a$$

$$B_c(2w) = -B_d(2w) \qquad 5.12b$$

These yield four basic equations from which we can evaluate w, ϕ, V_1 and V_2 given the diode characteristic and the circuit admittances. The question that must now be answered, is what are the optimum admittances at the fundamental and second harmonic, for maximum power output at the desired resonant frequency. To understand this, it is perhaps easiest to look at a graphical representation of the admittances where we show $-Y_d$ and Y_c in the admittance plane. Where the two curves intersect, represent the operating point of the diode.

5.3 THE RESONANT FREQUENCY

If we now look at the fundamental resonant frequency of the diode and circuit, and see how it is affected by the presence of second harmonic voltages.

Figure 1 shows the intersection of $Y_c(w)$ and $-Y_d(w)$ in the admittance plane, where Y_c is represented, as usual, by a vertical line (constant conductance) but whose susceptance varies with frequency. The diode is represented as the sum of the three terms given in Equations 9 and 10, and this is shown graphically. The A(w) term representing the third amplitude limiting expression involving C_3.

The first item of interest is that there will now normally be two intersection points, P_1 and P_2, and two resonant frequencies possible at w_1 and w_2. However, usually only one point is stable and this depends on the susceptance of the circuit at the second harmonic frequency. If the susceptance at 2w is negative, then w_1 is stable, and if the susceptance at 2w is positive then w_2 is stable.

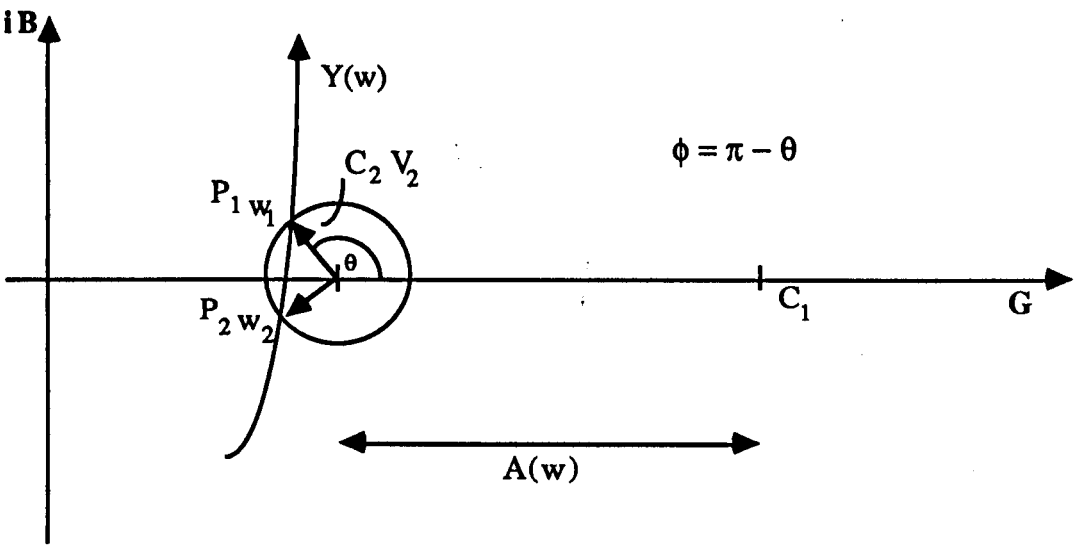

FIGURE 5.2

DIAGRAM ILLUSTRATING THE IMPEDANCE OF THE DIODE AT ITS FUNDAMENTAL FREQUENCY WHERE THERE IS A LARGE SECOND HARMONIC FREQUENCY COMPONENT

This follows from combining (10),(12),(13b) and (14b) to give,

$$\left(\frac{V_2}{V_1}\right)^2 = -\frac{B_c(w)}{2\,B_c(2w)} \qquad 5.13$$

As the right hand term must be positive it follows that the sign of the susceptances at the fundamental and second harmonic frequencies must always be opposite. This selects the

point on the diode admittance curve where the circuit will operate. Equation (15) can be rearranged to give the resonant condition,

$$B_T = |B_c(w)| - 2\left(\frac{V_2}{V_1}\right)^2 |B_c(2w)| = 0 \qquad 5.14$$

where B_T is the total reactance of circuit and diode at the resonant frequency w.

When V_2 or $B_c(2w)$ is zero the resonant condition is the same as the single frequency case (note that any other associated susceptance of the diode is lumped in with the circuit susceptance in this model. In fact, the second term will normally be small, and the resonant condition will approximate that of the fundamental frequency. However, the second term can become large when the second harmonic is resonant in the circuit (large V_2), or at anti-resonance when $B_c(2w)$ tends to infinity or negative infinity. Both these points, are at positions where the sign of the second harmonic susceptance is about to change sign and it is therefore possible for frequency jumps to occur, as one tunes in frequency. We can further distinguish between the two cases of resonance and anti-resonance because of the different tuning characteristics that are predicted.

5.4 SECOND HARMONIC RESONANCE

Here we look at the case where the second harmonic susceptance passes through zero. In a simple circuit this condition corresponds to a minimum positive conductance, and V_2 will build up in the cavity/circuit. If $(V_2/V_1)^2$ increases faster than $B_c(2w)$ decreases as we tune in frequency, then we can get the situation illustrated in Figure 2, where frequency jumps can occur. The critical parameter determining whether a frequency jump occurs is given by,

$$\mu = \frac{1}{2}\left(\frac{V_1}{V_2}\right)^2 \frac{d\,B_d(w)/dw}{d\,B_d(2w)/dw} \qquad 5.15$$

Normally this parameter is very large, however whenever the value of μ passes through unity, a frequency and power jump can be expected.

A very similar expression was obtained by Brackett [4] using a slightly different treatment. In fact, if we allow the C coefficients to be a function of frequency, then we obtain,

$$\mu = \frac{1}{2}\left(\frac{V_1}{V_2}\right)^2 \frac{d\,B_d(w)/dw}{d\,B_d(2w)/dw} \frac{C_2(w)}{C_2(2w)} \qquad 5.16$$

which has exactly the same form as the expression obtained by Brackett.

Clearly, μ will not always pass through unity for all circuits and diode combinations, however, one would nearly always expect a slight distortion of the frequency tuning curve as μ approaches unity, as well as a change in power at the fundamental, or second harmonic. The frequency jumps can be more clearly understood by examination of Figures 3 and 4. which show graphically how frequency jumps can occur and the associated hysteresis, depending on the direction of tuning. Points b,c,f and g all correspond to points where μ is equal to unity.

5.5 SECOND-HARMONIC ANTI RESONANCE

In this case $B_d(2w)$ tends to infinity or negative infinity and so the second term in Eq.16 can become large, and frequency jumps and hysteresis of the type shown in Figs 5 and 6 can occur if μ reaches unity. Note that μ can approach unity as although $dB_d(2w)/dw$ becomes very large at an anti-resonance, the second harmonic voltage tends towards zero. However this also means that the C_2V_2 term is very small, and so any frequency jumps will also necessarily be extremely small.

It is interesting to note that similar type of frequency jumps can also occur when a fundamental oscillator is attached to a tank circuit or cavity which is situated an odd number of quarter wavelengths away, when one tunes through the resonance of the cavity. This was noted by Pound [5] back in 1946 in his excellent paper on microwave stabilisation.

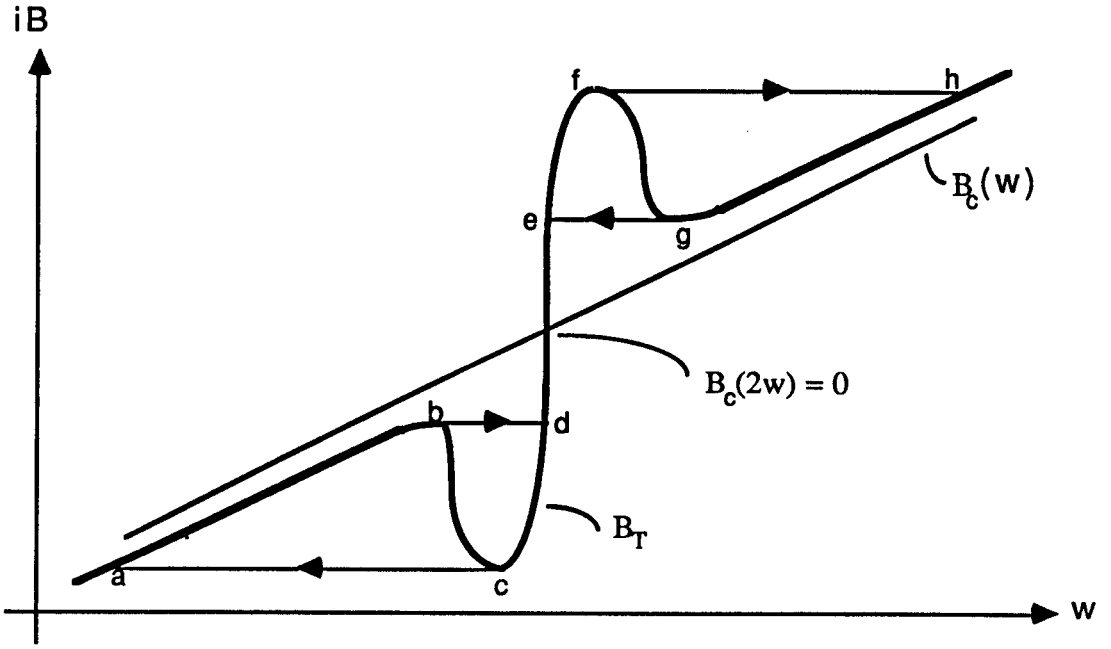

FIGURE 5.3

Diagram illustrating schematically the type of tuning and frequency jumps possible when tuning through a second harmonic resonance

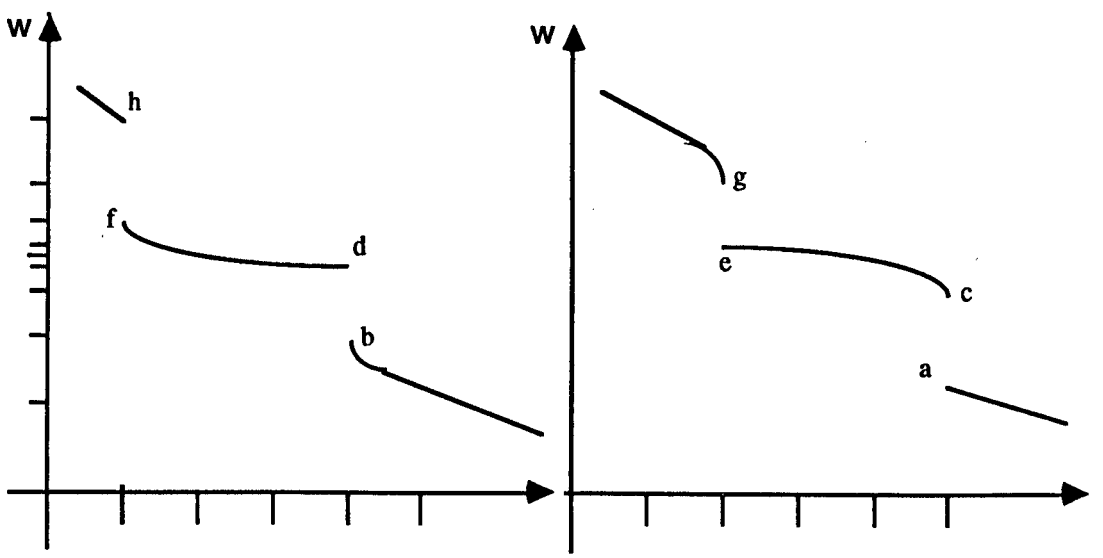

Cavity Length L

a) Tuning up in frequency
Down in Cavity Length

Cavity Length L

b) Tuning down in frequency
Up in Cavity Length

FIGURE 5.4

Graphs showing expected tuning characteristics as one passes through a second harmonic resonance during tuning

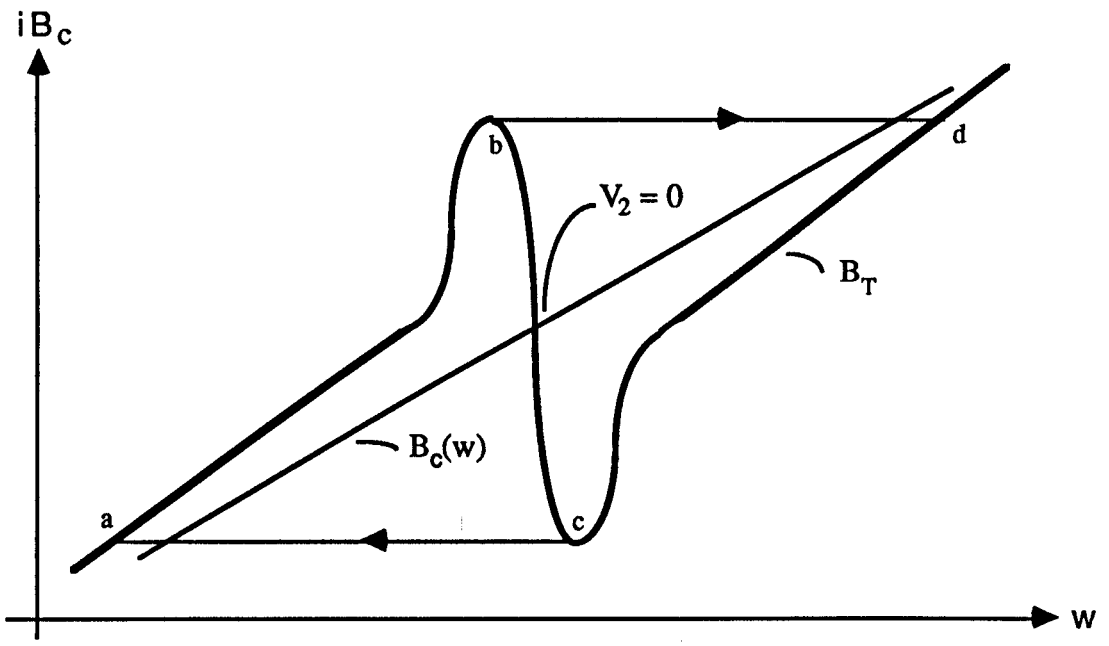

FIGURE 5

Graph showing tuning characteristics as one approaches an anti-resonance of the second harmonic

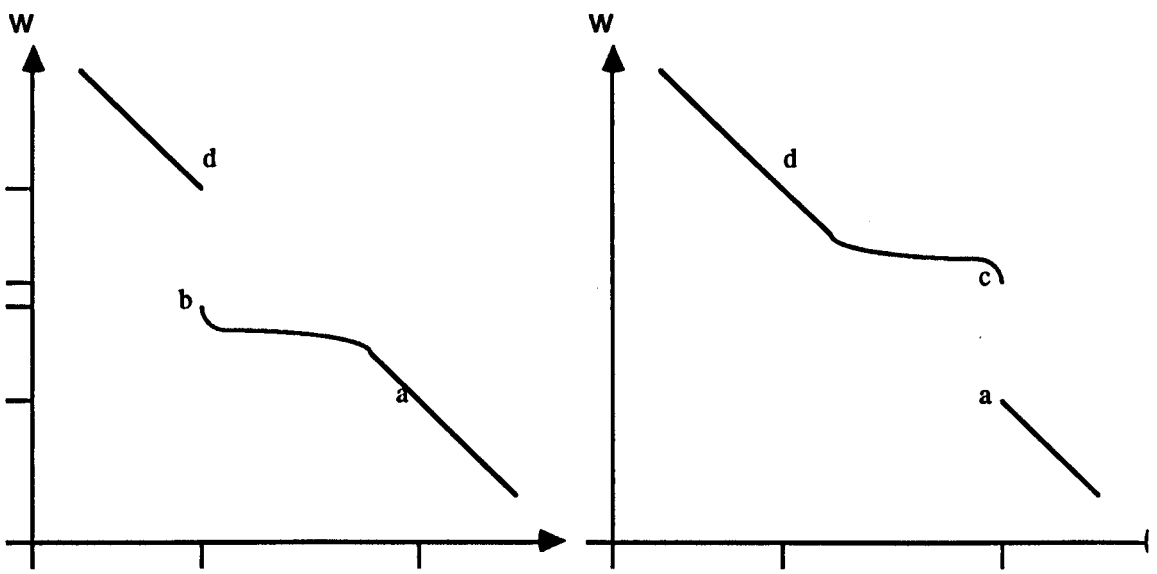

a) Tuning up in frequency
Down in cavity length

b) Tuning down in frequency
Up in cavity length

FIGURE 6

Graph showing schematically the possible tuning characteristics as one passes through a second harmonic anti-resonance

5.6 POWER OPTIMISATION IN A FUNDAMENTAL OSCILLATOR

If we first consider the simple case where the second harmonic voltage V_2 is zero then from Eq.9 we can calculate the value of the power produced as,

$$P(w) = \frac{G_c(w)\ V_1^2}{2} = \frac{2G_c(w)}{3C_3}\ (-C_1 - G_c(w)) \qquad 5.17$$

where C_1 is of course negative. If $G_c(w)$ is greater than C_1 then the device will of course not oscillate. The power output will have a maximum when $G_c(w)$ is one half the value of C_1 (obtained by differentiating with respect to $G_c(w)$).

If we allow a second harmonic component to exist then we have the situation shown in Fig.1. Clearly, depending on the phase of ϕ the C_2V_2 term can have a resistive component that is either positive or negative, and for maximum power output ϕ wants to equal π, so the resistive component is maximally negative i.e. power is converted from the second harmonic to the fundamental. Indeed, in many oscillators it has been found to be advantageous to provide a second harmonic resonance, where both $G_c(2w)$ and $B_c(2w)$ will tend towards zero. As will be shown later, having $B_c(2w)$ approximate zero, forces the phase ϕ to approximate π, and having $G_c(2w)$ approximate zero allows the second harmonic voltage to build up. This allows the C_2V_2 term to add a large effective negative resistance to the diode characteristic. In many low frequency oscillators, this can have the effect of dramatically increasing the fundamental output power. However, it should also be noted that as V_2 increases, the resistive term ($3/2\ C_3\ V_2^2$) in Eq. 9 also increases and so the effect is always limited, and will depend on the ratio of C_2 to C_3. If C_3 is large there may be little value in using this effect. As one is operating near a second harmonic resonance there is also the possibility of frequency jumps during tuning.

5.7 POWER OPTIMISATION IN A SECOND HARMONIC OSCILLATOR

The second harmonic is produced through the diodes non-linearity, and as such can be expected to be roughly proportional to the fundamental voltage across the diode. This means that to achieve maximum second harmonic power, the fundamental should not be loaded, but be trapped inside the oscillator cavity. There is thus a large amount of fundamental energy stored inside the cavity, for very little energy dissipated (resistive losses in the cavity walls). The fundamental voltage being eventually limited by the non-linearity of the diode.

Thus a good approximation is to put $G_c(w) = 0$, which is true apart from small resistive losses. The fact that the fundamental is not loaded means that the fundamental circuit can be very well defined. In fact, one can try and build a true single frequency parallel (or series) resonant circuit, which is untroubled by reflections from a distance. This means effectively that the circuit loci will nearly always be perpendicular to the device loci, meaning that the effective Q will be as large as possible, and that good stability and low noise can be expected during tuning.

Thus for our simple parallel resonance, the circuit line for the fundamental frequency $Y_c(w)$ is a vertical line along the imaginary axis in Fig.7. The line for $Y_c(2w)$ is a little more arbitrary and just depends on the circuit. If we make the reasonable assumption that V_2 is fairly small compared to V_1 for most circuit conditions, then the amplitude limiting terms in Eqs. 9 and 11 will be dominated by V_1, and we can make the approximation that $A(2w) = 2A(w)$.

This leads to the type of admittance characteristic shown in Fig. 7. Note that the angle ϕ for both the fundamental and second harmonic admittances must be equal and opposite, and is largely determined by the admittance at the second harmonic.

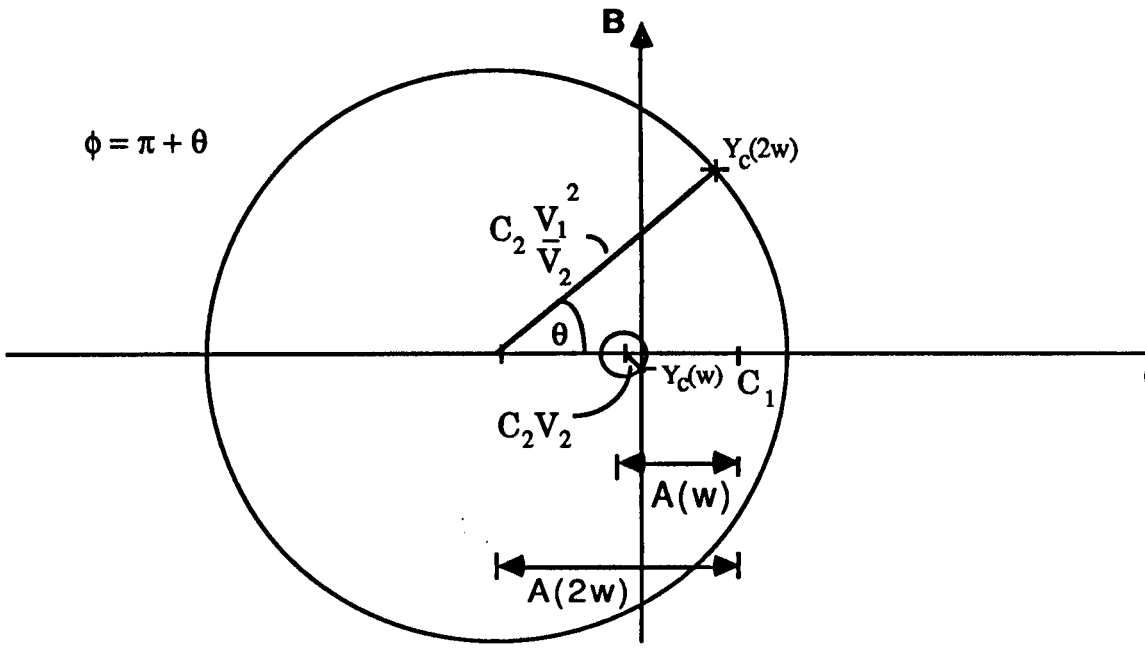

FIGURE 5.7

Diagram illustrating the impedance conditions for a stable oscillation when the second harmonic voltage is fairly small

The second harmonic power output is given by,

$$P(2w) = \frac{G_c(2w) \cdot V_2^2}{2} \qquad 5.18$$

where we are trying to pick circuit conditions which will maximise this value. Again it is clear from Figure 7 that the value will be maximised for ϕ approaching π, which will be found as $B_c(2w)$ approaches zero. (Note that any reactance associated with the diode has been lumped with the circuit in this simplified model). For the condition that $B_c(2w)$ equals zero, Solbach [1] has calculated the optimum conductance $G_c(2w)$ to be exactly equal to the value of C_1, with the 3dB fall off points at 5 C_1 and $C_1/5$.

Thus the source impedance of a second harmonic oscillator should be around half that of the equivalent fundamental oscillator. This may make it more difficult to match, for optimum coupling at the second harmonic, however, the coupling is less critical than in the case for a fundamental oscillator. In particular, a fundamental oscillator will not oscillate if the load resistance is greater than the maximum negative resistance. This is not the case for

second harmonic oscillator where power output can be expected over a wide range of load conductances.

It should be noted that in most simple single cavity circuits as $B_c(2w)$ approaches zero, then $G_c(2w)$ approaches zero (resonance condition) and thus the circuit may become undercoupled to the load. The details will of course depend on the admittance of the diode in question, but maximum power output can be expected when $B_c(2w)$ is fairly small. It should also be noted that one is operating near the point where frequency jumps may occur during tuning.

As a result of these factors, it is possible to build a fairly simple second harmonic oscillator that is tunable over almost the entire frequency range where a Gunn diode exhibits negative resistance. This can be as high as an octave. Moreover, the output can be expected to be stable, have low noise, and exhibit no hysteresis during tuning, as well as providing almost constant power output over bandwidths as large as 20 GHz (at 90 GHz). The full tuning range being over 50 GHz, around 90 GHz.

5.8 THE Q OF A SECOND HARMONIC OSCILLATOR

As shown by Solbach the external Q of a second harmonic oscillator is approximated by,

$$Q_{e2} = \frac{w \left| \frac{d B_c(w)}{dw} \right|}{2G_c(2w)} \cdot \frac{1}{2} \cdot \left(\frac{V_1}{V_2}\right)^2 \qquad 5.19$$

where Eq.20 is derived from Eq.16. This compares to a fundamental oscillator whose external Q is approximated by,

$$Q_{e1} = \frac{w \left| \frac{d B_c(w)}{dw} \right|}{2G_c(w)} \qquad 5.20$$

where all values in Eqs. 20 and 21 are calculated at the resonant frequency w_0.

Now for maximum power output at the fundamental $G_c(w) = C_1/2$, and at the second harmonic $G_c(2w) = C_1$. Substituting for these values in Eqs. 20 and 21, we have the ratio of the Q-factors as,

$$\frac{Q_{e2}}{Q_{e1}} = \frac{1}{4}.\left(\frac{V_1}{V_2}\right)^2 \qquad 5.21$$

Thus if V_2 is very small, which will be the case for large $B_c(2w)$ and $G_c(2w)$, the external Q will be extremely large (although the power output will be low). In fact, Solbach reports that the ratio of the Q's approximates the ratio of the output power of the harmonic to the power of the matched fundamental for a wide variety of load conditions. For fundamental GaAs/InP Gunn oscillators, the external Q is typically between 50 and 100, whereas for second harmonic oscillators it is typically found to lie between 500 and 1500.

(For an InP oscillator operating in fundamental mode at 90GHz in a resonant cap oscillator, the frequency pulling by the backshort is usually over 1GHz, whereas for an InP oscillator operating in the second harmonic mode at the same frequency, the frequency pulling is less than 100MHz).

As the power output of a second harmonic oscillator is typically 10% of its fundamental equivalent, the model would thus appear to give very acceptable answers. In any case it is clear that measurement of the second harmonic Q can give information about the relative magnitudes of V_1 and V_2.

5.9 MODEL LIMITATIONS

In many respects it is not an ideal model, however it lends itself to analytical solutions and illustrates and explains some of the characteristics of harmonic oscillators. In particular, it describes a huge range of solid-state diode oscillators which have a negative resistance at a particular frequency and thus can build up oscillations which are eventually limited by the diodes non-linearity.

The main limitations of the model are:

1) The I/V curve shown in Fig.1 is probably quite a good representation of the characteristic of tunnel diodes and quantum well oscillators. However it is not strictly applicable to Gunn diodes which have a N-shaped characteristic as shown in Fig.2. A better approximation to this kind of characteristic is [2],

$$I = \frac{V/R + I_S\,(V/V_0)^k}{1 + (V/V_0)^k} \qquad 5.22$$

where R is the low field resistance, I_S is the saturation current and V_0 is the threshold voltage. k is an excitation coefficient and approximates 4 for GaAs. However, this type of characteristic does not lend itself to the simple analytical solutions of (1). In addition, it is is a d.c representation of the I/V curve, which is not necessarily valid at high frequencies.

2) The circuit is modelled as a parallel resonance, and therefore the voltage across the diode and circuit elements will be the same and taken as having components at the fundamental and second harmonic voltages. The non-linearity then produces higher current harmonics. However in coaxial or resonant cap type circuits, the circuit is essentially in series resonance, where the current is forced to be sinusoidal, and it is the voltage that is allowed to contain higher harmonics. Essentially, one should substitute current for voltage and resistances for conductances etc. However, the V/I curve cannot be represented quite as simply as the corresponding I/V curve, which makes analytical solutions more difficult with this approach. The final results though, should be qualitatively similar.

3) The validity of any I/V curve has to be questioned at very high frequencies where collisional, space charge and hot-electron ballistic effects may become dominant. At 100GHz the model may still be valid for quantum well oscillators, however for Gunn oscillators which are essentially transit time devices, computer models have shown that not only does the diode not follow the d.c. I/V curve, but there is significant hysteresis over the current and voltage swing. Thus at the very least, the values of C_1, C_2 and C_3 will be a function of frequency, with C_1 decreasing at higher harmonics.

The assumption, inherent in Eq.3, that the voltage has a second harmonic term, implies that there is a net negative resistance at the second harmonic frequency, but not at higher frequencies. This is probably quite a good approximation for the Gunn diode which is essentially a transit-time device.

4) The diode is modelled as a pure resistance, however, as nearly all diodes contain a thin "resistive" active region in between two highly conducting planes they usually have significant capacitance. This is generally modelled as a capacitance in parallel with the net negative resistance.This modifies the real and imaginary parts of the diodes impedance to give,

$$Z_d(w) = \frac{-R - i\,wCR^2}{1 + w^2 (RC)^2} \qquad 5.23$$

which for $w << 1/RC$ reduces to $Z_d(w) \cong -R - i\,wCR^2$.

However, as w approaches 1/RC the effective negative resistance of the diode is significantly reduced, from its low frequency value. At 100GHz in Gunn diodes this effect is starting to become significant with C≈0.5pF and R≈10Ω. It is likely to be far more significant for quantum-well oscillators which have very large negative resistances and capacitances per unit area (at the moment).

Gunn diodes are now, just about limited by the intrinsic speed of the electron transfer process (the rate at which electrons can gain or lose energy in the central G valley and overshoot effects at the cathode). The intrinsic process in quantum well oscillators is certainly much faster, and it is to be expected that they will be limited by high capacitance and parasitic resistances in the diode.

Note that in a typical circuit (vertical circuit impedance line) no stable oscillation is possible for $w>1/RC$ as $dZ_d(w)/dw$ becomes negative at this frequency. The circuit is therefore unstable from the stability criteria given in Chapter 4. Additionally as one approaches this critical value, the output will become much more noisy as the slope of the circuit line approaches the device line.

REFERENCES (CHAPTER 5)

1) K.Solbach, "Simulation Study of Harmonic Oscillators", IEEE. Trans. Microwave Theory and Techniques, Vol. MTT-30, No.8, August 1982, pp.1233-1237

2) H.Yamamoto, H.Iwasawa, A.Sasaki, "Optimum Conditions for Second Harmonic Generation by Hot-Electron and Electron-Transfer Effects in Semiconductors", Solid-State Electronics, Vol.22, 1979, pp.271-275

3) P.Penfield and R.P Rafuse, Varactor Applications, Cambridge, MA: MIT Press, 1962

4) C.A.Brackett, "Characterisation of Second-Harmonic Effects in IMPATT Diodes", Bell System Tech. Journal, October 1970, pp.1777-1810

5) R.V.Pound, "Microwave Stabilisation Techniques", Rev. Sci. Instrum. Vol.17, pp. 490-505, 1946

6.0 OSCILLATOR DESIGN

6.1 INTRODUCTION

As outlined in Chapter 5 the main design criteria of any tuneable oscillator or multiplier is the control and manipulation of the impedances at the fundamental frequency and its harmonics. This becomes more and more difficult as the frequency of the device increases, as the circuit resistive losses increase and the package parasitics start to have a larger and larger effect.

The type of oscillator used for most of the characterisation is based on the design given by Carlstrom et al. [1] and also by Haydl [2] and is shown schematically in Figure 6.1. It consists of a standard resonant post circuit but with a variable post length. This takes the form of a coaxial cavity which intersects with a reduced or full-height waveguide. The diode package is screwed into the waveguide floor and also acts as the bottom of the coaxial cavity. A choke structure forms the top of the coaxial resonator and ensures high reflectivity at both the fundamental and the second harmonic.The design of the choke structure is outlined at the end of this chapter. For second harmonic operation, the waveguide is chosen to be below cut-off at the fundamental and single mode at the second harmonic. The fundamental is therefore confined to the quasi-coaxial cavity and defines the operating frequency. The radial cap acts as a very efficient wideband impedance transformer at the second harmonic frequency and helps to match the diode to the waveguide. The backshort tunes out the reactance at the second harmonic and provides a resonant load at this frequency. There is no absolute control of the resistive load at the second harmonic, but in practice this can be altered by changing the dimensions of the cap/post structure. The optimum dimension varying from diode to diode. Varying the length of the cavity can thus tune the frequency, and a waveguide backshort can almost independently tune out the power without significantly altering the frequency.

A scale drawing of the assembled oscillator is shown in Fig. 6.2. It is essentially a standard split block design which is made in four parts. The Gunn diode is screwed into the centre of the bottom section, so its flange is either flush or just above the waveguide floor. The second or choke bloke contains the cavity, waveguide structrue and the choke itself which forms the top of the coaxial cavity. Into the choke is inserted a small pin (<= 1mm diameter) with a thin disc at the end. This forms the resonant cap structure and provides the cavity's central conductor as well as providing a means of biasing the Gunn diode. The cavity length can be adjusted by moving the choke structure over the central

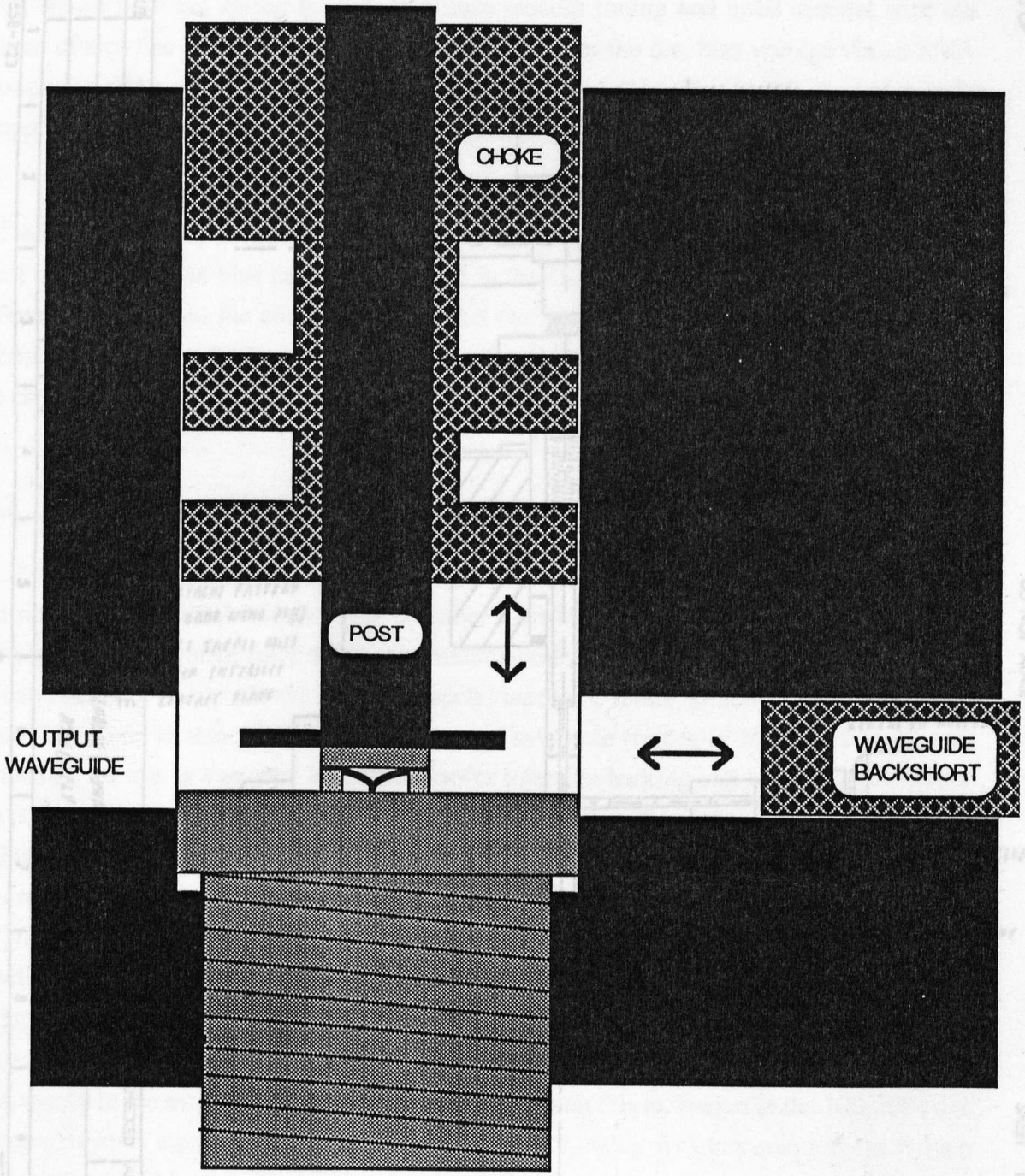

FIGURE 6.1

SCHEMATIC OF RESONANT CAP CAVITY

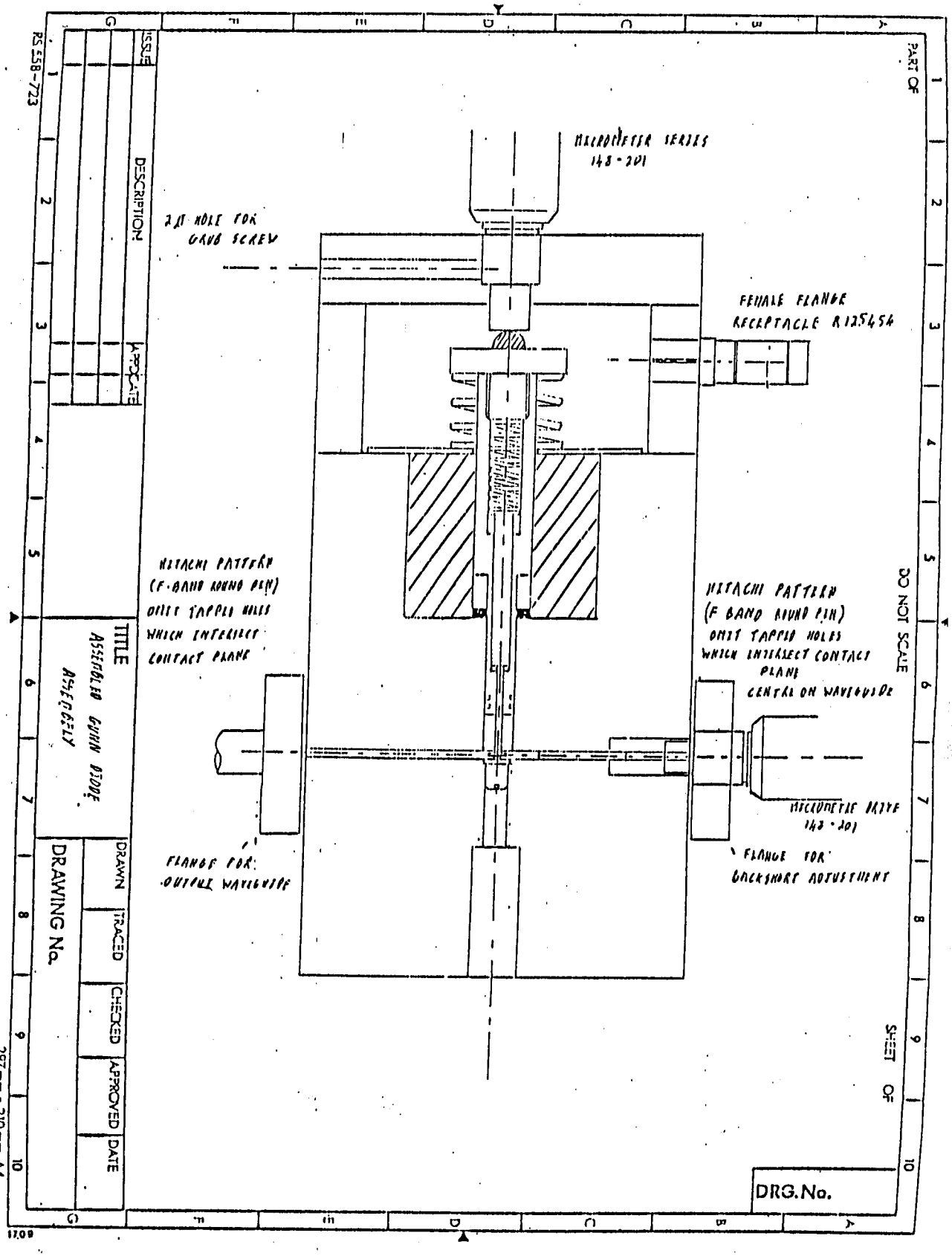

FIGURE 6.2 SCALE DRAWING OF ASSEMBLED OSCILLATOR

pin, where both are spring loaded, to ensure smooth tuning and good contact with the Gunn diode. The third section or bias section brings in the d.c. bias voltage via an SMA connector and a small safety circuit, to the choke assembly. The fourth section merely supplies the support for the tuning micrometre.

All the blocks, choke structure and pin are made from aluminium, mainly for ease of manufacture. The central choke structure is annodised to electrically insulate it from the rest of the block, so bias can be brought in to the Gunn diode via the cap and post. The connection between the choke assembly and the tuning micrometre is via a small glass hemisphere to provide electrical insulation and a one point contact. The rest of the block is at earth potential.

6.2 SECOND HARMONIC MATCHING

Over the last ten years or so it has been realised that the GaAs Gunn oscillator has an upper fundamental frequency of no more than 80 GHz [1], with higher frequencies being achieved through some form of harmonic mode. The commonly used 95 GHz GaAs Gunn oscillator nearly always works in second harmonic mode, although extraction of the third harmonic is also possible [2]. The power available (typically 20mW) is more than adequate for use as a general lab source, or for injection locking and mixing applications. In addition, the second harmonic circuit possesses many advantages over its fundamental counterpart including wide mechanical tunability, and a high effective Q, leading to low noise and good stability over a very wide frequency range (that can be as large as an octave [3]). In many ways, it is also easier to optimise and more reliable than a fundamental oscillator, and this has led people to use the second harmonic at low fequencies, even where fundamental power is available [4,8]. Its major use though, at the moment, is extending the available frequency range upwards, although it can be expected that parasitic reactances in the available packages will eventually limit this technique in the 100-200 GHz range. Beyond that, frequency doublers and triplers, using whisker contacts (to reduce capacitance) will have to be used to provide solid state sources.

A detailed discussion of the impedance requirements for a second harmonic diode is given in the previous chapter. In practice it is difficult to make high frequency circuits to exactly match at two different frequencies over any sort of frequency range, however the resonant cap oscillator has shown that it is capable of giving excellent matching over large frequency ranges. It is this type of impedance matching that is concentrated on in the following sections.

6.3 RESONANT CAP OSCILLATORS

The most successful second harmonic oscillators at frequencies around 90 GHz have been the resonant cap and post circuits first suggested by Bell Labs [6]. Ruttan [7] was the first to report a 95 GHz oscillator using a radial cap circuit, although he thought that the device was working in fundamental mode. Since then it has been realised that GaAs oscillators were working in harmonic mode [10],[13], although fundamental InP oscillators have been shown to work well in this type of resonator too.

Many resonant cap type circuits have been described in the literature, of which the key papers are given below. Haydl [2] gave detailed measurements, describing the effect on the frequency, of changing many dimensional parameters. Ondria [11] described an oscillator that was tunable from 75-110 GHz, by changing the height of the diode and cap assembly within the cavity. Arora and Sarma [12] also described the successful operation of cap structures in circular waveguide and gave details of many frequency and power measurements. All the circuits described in the above operated in the 75-110 GHz range where 5-20mW output power at 95 GHz is a typical requirement, although Ondria has claimed 65mW at 94GHz and recently 80mW was obtained at 94GHz [24]. It has also been shown that the standard circuit can be successfully scaled to work at other frequencies. Solbach et al.[8] describe a 60GHz second harmonic oscillator delivering 30mW of power, and recently Essen and Wennerscheid [14] described a 140GHz second harmonic InP oscillator that delivered 5mW of power.

At first it was not clear how the cap type circuit was working, but it now seems clear that the capacitance associated with the cap allows a quasi-coaxial resonance to exist at the fundamental frequency (in the below cut-off guide). In addition, the cap helps to form an efficient impedance transformer at the second harmonic which allows good coupling to the high impedance waveguide. Realisation of this, enabled Carlstom et al.[3] to design a very wideband and efficient oscillator by using a variable height coaxial resonator at the fundamental frequency, and coupling out the second harmonic using a reduced height below cut-off waveguide. It is oscillators of this type that have been designed and tested.

6.4 THE RESONANT FREQUENCY

In early oscillators, the disc and post was incorporated into a full height waveguide, and the desired resonant frequency was achieved by changing the diameter of the disc, on which there was a large frequency dependence. The actual resonance depends

on several parameters, including the diode and package used, and therefore this approach relied heavily on previous measurements, and trial and error to achieve the desired frequency. Most commercial single frequency GaAs oscillators, around 95 GHz, will be of this type. They are fairly easy to build but it is difficult to predict accurately the resonant frequency (+-500MHz).

Haydl [2] has made extensive measurements of the effect on the resonant frequency, of varying various dimensional parameters of disc post resonators in waveguide and coaxial circuits. In analysing the results he used the standard model for the disc post resonator, where he considers the disc to act as a capacitance and the post to act as an inductance. Such a model based on lumped circuit parameters is not strictly valid, but it provides a good qualitative "feel" for what can be expected by changing various dimensions. His results can be summarised as follows:

1) A large frequency dependence on the diameter of the disc. The larger the diameter of the disc, the lower the frequency.

2) A decrease in frequency with the thickness of the disc.

3) A decrease in frequency as the height of the disc is raised from the waveguide walls up to the point where it reaches half way up the waveguide. (All of these results can be explained in terms of an increase in the fringing capacitance between the disc and the waveguide walls).

4) A decrease in frequency with decreasing post diameter but remaining fairly constant for thin posts.

5) A decrease in frequency with an increase in post length.

These results were attributed to an increase in the inductance of the post. But with hindsight it is possible to say that most oscillators of this type are operating in a quasi-coaxial mode. Increasing the length of the post, serves to increase the effective length of the cavity. Decreasing the diameter of the post, rather than increasing any inductance (associated with magnetic fields around the post), serves to increase the fringing capacitance (associated with the electric fields around the disc). This is explained more clearly later on.

As mentioned in the previous chapter a resonant condition is given when the sum of all the reactances within the circuit total zero. With this condition, it is normal to consider the two terminals of the diode as the reference plane. The requirement then is that the reactance of the diode and package must be equal and opposite to the reactance

presented by the circuit. This condition determining the resonant frequency as discussed in Chapter 4.

If we consider the reactances associated with the diode and package first. These will include the capacitance associated with the diode, the parasitic capacitance associated with the package, and the inductance associated with the bonding wires inside the package. Care must be taken to ensure that these reactances are small enough to ensure that there are no resonances possible within the package and that the oscillation frequency is defined by the circuit.

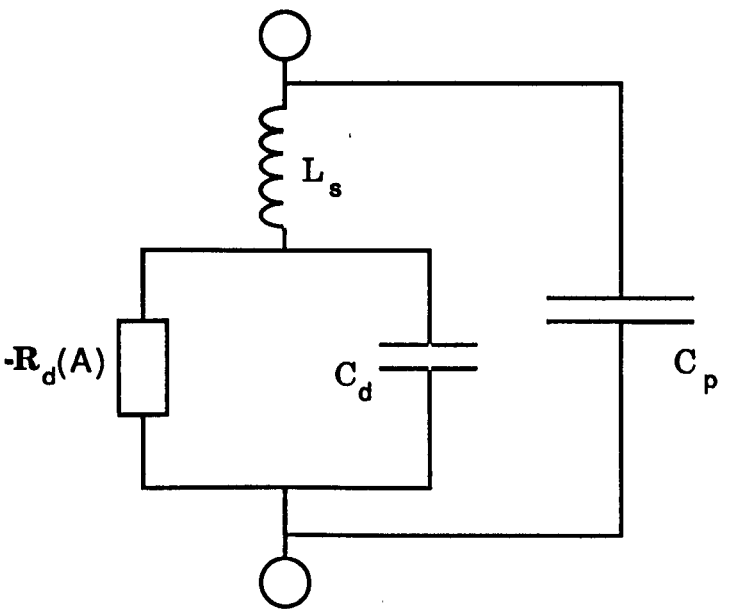

FIGURE 6.3 EQUIVALENT CIRCUIT OF A GUNN DIODE AND PACKAGE

6.5 DIODE AND PACKAGE REACTANCE

The usual model for the package and diode is illustrated in Fig.6.3. It shows the diodes negative resistance R_d in parallel with the diodes capacitance C_d. This is in series with an inductance L_S due to the bonding wires that connect with the top of the package. The whole lot is then shunted by the package capacitance C_P which exists between the top and the bottom of the pack.

6.5.1 DIODE IMPEDANCE

A rough estimate of the capacitance of the diode can be calculated from the following expression, [3] which shows that the capacitance C_d ought to be linearly related to the threshold current I_{th}:

$$I_{th} = D_d^2 (\frac{\pi}{4}) E_{th} n q u = C_d . \frac{L_d E_{th} n q u}{\varepsilon_0 \varepsilon_r} \qquad (6.1)$$

where E_{th} is the threshold field, n the carrier density, u the electron mobility, L_d the diode active length and D_d the diameter of the diode. Note this formula assumes that the n.L product will be the same for most diodes. (However, one can also expect the capacitance to vary slightly with the dc current and voltage).

Calculations show that for typical GaAs Gunn devices operating at 95GHz, the capacitance will be of the order 150-550 fF. In very high frequency circuits one way of increasing the resonant frequency is to reduce the device area to reduce the device capacitance, although this does limit the power handling capability of the device [15]. It also must be remembered that the device capacitance is essentially in parallel with the device negative resistance.

The device impedance is therefore given by:

$$Z_d = \frac{-R - i\,wCR^2}{1 + w^2(RC)^2} \qquad (6.2)$$

Because the capacitance and the resistance are in a sense inseperable, it is this impedance that should be considered as the device line. This is shown graphically in Fig.6.4 for C_d = 0.2pF and w = 2π. 50GHz, where the negative impedance Z_d is shown as a function of the negative resistance R_d of the diode. R_d varying from 0 to -100Ω in steps of 1Ω. (Note the negative resistance of the diode will be a function of the current amplitude which in the steady state is determined by the value of the load resistance).

Fig. 6.4 Graph showing negative impedance of Zd as R is varied from 0 to -100 ohms Frequency = 50GHz, Capacitance = 0.2pF

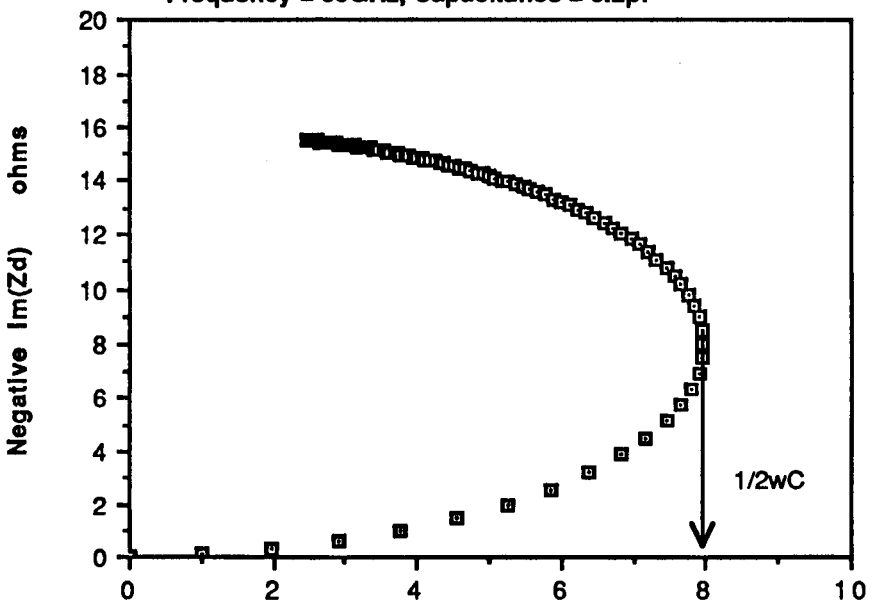

It should be noted that the the upper part of the curve will normally be unstable for most circuits, from the stability criteria described in Chapter 4. Thus this diagram indicates, for these fairly typical parameters, that no oscillation is possible if the load resistance is greater than $1/2wC_d$. For a frequency of 50GHz this turns out to be just under 8Ω, and reducing with increasing frequency. It is therefore important to choose the device capacitance such that the resonant frequency w_o is always less than the RC time constant for the device negative resistance and capacitance. For most circuits, no oscillation can exist if this condition is violated, and the oscillation can be expected to become more noisy as this point is approached.

6.5.2 RESISTIVE LOSSES

As the operating negative resistance of the diode depends on the load resistance it is clearly of value to discuss the magnitude of the load resistance at the fundamental frequency, where it will just be made up of the circuit losses. Many people have pointed out the need to reduce circuit losses to a minimum [19] especially in cases where the load resistance is very low. Clearly if the load resistance appears as only a few ohms to the diode, then a resistance of 1Ω in the substrate or due to a bad contact is going to significantly reduce the output power, not to mention the introduction of thermal effects. The d.c resistance of a typical 95GHz GaAs Gunn diode is of the order of 4Ω (which

hopefully is mostly due to the active layer). It should be noted though, that the series resistance can be expected to rise at higher frequencies due to the skin effect.

In particular we can identify several specific areas where series resistance will exist.

a) Significant positive resistance exists within the active layer because of the "low doping". One of the device physicists main aims is to ensure that the whole length of the diode is biased into the negative resistance regime and that as little as possible is biased in the positive resistance regime. This is possibly more of a problem at low frequencies and with long diodes, where any sort of domain mode will encounter a large series resistance. It may however also be a factor in 2-zone cathode type oscillators which although capable of increasing the potential efficiency of oscillation, may fall foul of increased series resistance due to the thin undoped layer (where the electrons are initially accelerated). This might explain why InP diodes utilising Schottky barrier cathode contacts tend to work better than 2-zone cathode structures.

b) It has also been pointed out that the substrate can introduce losses and that these can become more apparent at millimeter wave frequencies as the skin depth decreases. Where the skin depth δ is given by:

$$\delta = \sqrt{\frac{2}{w \mu_0 \sigma}} \qquad (6.3)$$

In particular, in [19] dimensioning rules were suggested to keep the losses to a minimum of which the most important was that the length of the substrate should not be much more than two or three times the skin depth. They suggested that for an InP substrate with a doping level of 3.10^{18} cm^{-3}, that the maximum thickness should be 12μm for CW operation in W-band.

c) The resistance of the millimeter wave resonator must also play an important part in the total circuit losses. These can be estimated from the predicted loss of a length of waveguide. The attenuation constant for a copper guide is given by [20] to be:

$$\alpha_{coax} = \frac{5.17 \times 10^{-4}}{(\lambda_0)^{1/2}} \left(\frac{1}{b} + \frac{1}{a}\right) \frac{1}{\ln (b/a)} \quad dB\ cm^{-1} \qquad (6.4)$$

where [20] also points out that this is less than rectangular guide for impedance levels of less than 135Ω. Putting in suitable values (l_0=3mm, b=3mm, a=1mm) this gives a value of 0.014 dB cm-1. However this is for a "perfect" copper coaxial circuit, and because of bad

surface finishes this can always be expected to be an absolute minimum. It is to be hoped that this is the major source of load resistance at the fundamental, and thus gold or silver plating of waveguide cavities can ultimately be hoped to increase the amplitude of the fundamental within the cavity, thus leading to more power at the harmonic.

6.5.3 PACKAGE CAPACITANCE

The normal argument is that the parasitic capacitance associated with the package needs to be as small as possible to avoid shunting the diode, and allowing circulating rf currents that are then dissipated in the resistive parasitics. In typical modern hermetic packages for GaAs diodes the capacitance is of the order of 100fF. (Varian quote 120fF for their standard package). Again, though, this capacitance is usually measured at low frequencies, across the diode terminals, and it should only be used as a guide at very high frequencies, when the wavelength becomes comparable with the dimensions of the diode. It should also be noted, that with radial line circuits, one can hope to "resonate out" this capacitance with the backshort (at the output frequency).

6.5.4 PACKAGE INDUCTANCE

The inductance of the connecting lead often has a nonminimum optimum value [16], in that it can act as an impedance transformer in the range of interest. With IMPATT diodes it has been found that sometimes a larger inductance can provide a better performance than that obtainable by tuning adjustments, although the required inductance becomes very small at high frequencies [15]. One suggestion has been that the bonding leads can also act as effective antennae at high frequencies, and this view is supported by the experimental fact that rotation of the diode in the block can lead to higher power output.

Haydl [2] has also indicated that the inductance of the bias lead is a much more important parameter in optimising the power output of Gunn diodes than the package capacitance.

Varian quote 0.2nH for the inductance of their leads for their standard packages (for the "95 GHz" GaAs diodes), although it should be noted that this inductance is measured at low frequencies and should be treated wiuth some caution when the wavelength becomes commensurate with the actual dimensions of the lead.

There is also some confusion over the equivalent circuit of the device. For both Gunn and IMPATT devices the theoretical derived circuit is that shown in Figure 6.3,

where the device capacitance shunts the negative resistance. Kramer [16] however reports that swept frequency impedance measurements made on millimeter Gunn diodes usually correspond to a series RLC circuit. Unfortunately, he does not quote the frequency of operation or give experimental details.

6.6 THE CIRCUIT IMPEDANCE

In most useful oscillators the diode couples into a transmission line mode which is then short circuited to give the desired resonance. Normally one ensures that only one travelling mode is possible. One now has a case of distributed capacitance and inductance along the transmission line, for the travelling wave. This gives an impedance which can be calculated in the normal way. However, in any real oscillator, in order to couple into the resonator, or couple power out of the resonator there must be some form of discontinuity in the form of coupling loops or posts across the waveguide. These will set up other modes (in fact an infinute number) that need to exist to ensure that Maxwells conditions still hold at any discontinuity. These modes are usually below cut-off and die away exponentially very quickly, however they are capable of storing energy close to the regions where they exist. Specifically, E or TM waves represent electric fields and H or TE waves represent magnetic fields. Thus electric and magnetic energy can be stored within the cavity and, as was shown originally by Hahn [17], be represented by lumped capacitances and inductances. In fairly simple cases these can be calculated by the approach of matching electromagnetic wave solutions across the discontinuity although the solution is usually not trivial.

In order to find the reactance of the circuit it is necessary to calculate the capacitances and inductances of the local waves as well the impedance of the travelling wave. This is not so easy for a cap and post in a waveguide. However, for the case of the variable coaxial type circuit it is possible to make significant progress.

6.7 MODEL FOR RADIAL LINE IN COAXIAL CAVITY

Any attempt to exactly model a high frequency oscillator is doomed to failure as there are too many factors that influence the frequency, of which too many are unknown. For example, the package parameters are all measured at low frequencies, and it is not clear at all, that they can be treated as lumped capacitances and inductances at high frequencies, particularly when the package dimensions become commensurate with the wavelength. The device capacitance may be a function of bias voltage and temperature as well as active

length and doping. These will vary from diode to diode in a fairly unpredictable way. Haydl has also indicated that the capacitance associated with the first section of the bias choke can also change the frequency.

Moreover, these effects are not altogether negligible. Haydl [2] showed frequency shifts (in the second harmonic frequency for radial cap resonators) of:

a) 91 GHz to 99GHz by roughly quartering the diode capacitance by changing the active area.

b) 95 GHz to 103 GHz by reducing the package capacitance from 160fF to 50fF by removing part of the ceramic ring of the package.

c) 93GHz to 96GHz by reducing the inductance of the package by changing from a single ribbon to a cross ribbon.

However, Lazarus et al. [17] found in experiments where a diode was placed in a simple coaxial cavity that the resonance (monitored by measuring the weakly coupled second harmonic) corresponded very closely to that predicted by the half wave TEM resonance of the coaxial cavity. They took that to be an indication of the very low encapsulation parasitics and the low capacitive susceptance associated with their diode, (which was supplied by Plessey). It is clear that any model of the diode must attempt to explain all of these effects.

Previous attempts to model the circuit have relied on lumped reactance circuits [2]. These give a reasonable qualitative view, but in no way provide quantitative results. It is clear that more quantitative results can only come via a distributed reactance model, where full account is taken of the different modes that can be set up.

On that basis, it was decided as an initial step to the modelling of the oscillator, to examine the modes that could be supported by the cavity (i.e. initially assuming the diode to be a short piece of post). This led to the evaluation of the equivalent circuit shown in Fig. 6.5.

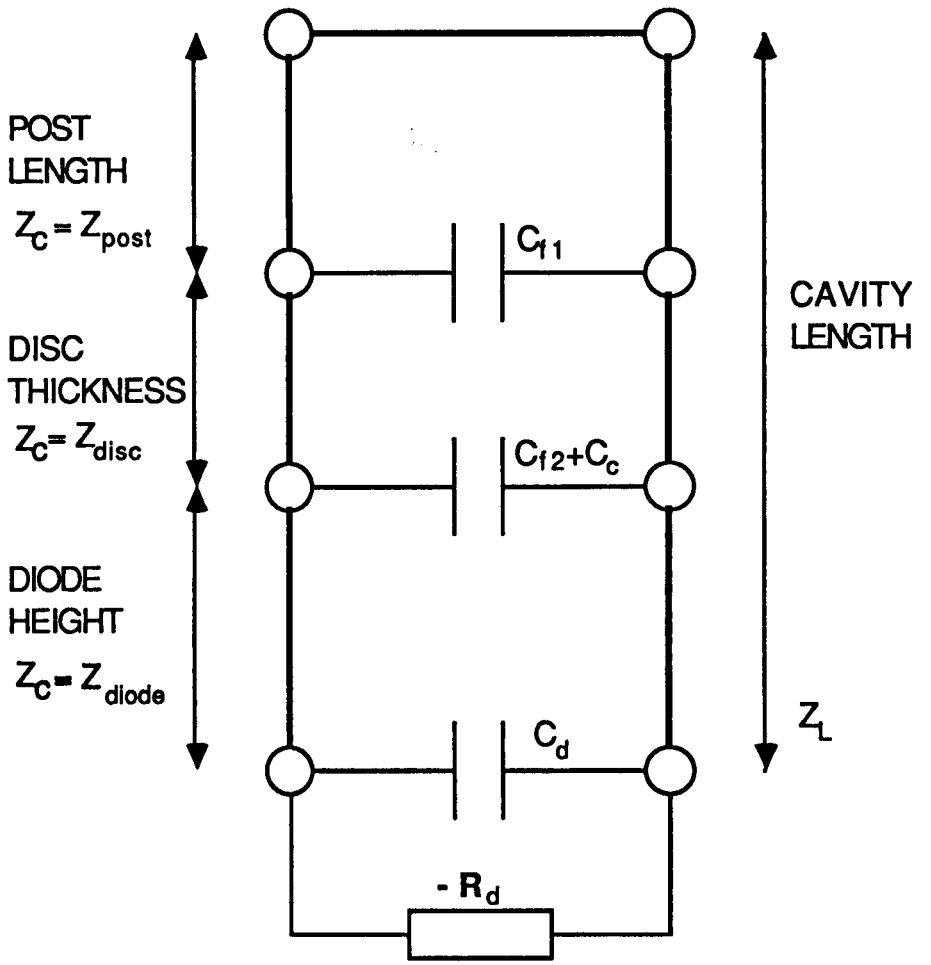

FIGURE 6.5 DIAGRAM SHOWING THE EQUIVALENT CIRCUIT OF A RESONANT CAP OSCILLATOR AT THE FUNDAMENTAL FREQUENCY

This consists of representing the circuit as three coaxial transmission lines in series, where the presence of other modes are represented as discontinuity or fringing capacitances. The diode itself is represented as a transmission line (representing the height of the package) in series with the device, which is given by the device capacitance in parallel with the device negative resistance. It should be noted that lumped parameters are acceptable here as the dimensions of the active layer of the device are small compared to the wavelength.

If there was no cap in the cavity it would be a simple coaxial resonator and resonances would be predicted whenever the length of the resonator was a multiple of a half wavelength. Any discontinuity, however, will modify the field and lead to electric or magnetic energy being stored at that point which will alter the resonance condition.

We know from the work of Whinnery et al. [18] that radial coaxial discontinuities will mainly produce TM modes above cutoff, and that it can be modelled exactly by an effective capacitance at the discontinuity. This capacitance is mainly a function of the dimensions of the inner and outer conductors across the discontinuity, although it will also be frequency dependent to a certain extent, especially when the distance between the two conductors r_o-r_i approaches a half-wavelength. It will also be influenced by other discontinuities a short distance away, (although the effect only becomes significant at distances less than r_o-r_i). The capacitance can be worked out by matching the electromagnetic fields at the discontinuities, which will be Hankel functions, and then summing them to find the energy stored and hence the effective capacitance. This is not exactly trivial, but fortunately Whinnery et al. have provided curves for typical cases, including frequency and proximity corrections. These are shown in Figure 6.6. The values of the capacitance C_{f1} and C_{f2} are then plugged into the model of the circuit shown in Fig.6.5. It is asumed that they will be independent of each other, which is a reasonable assumption as the cap will effectively screen the TM modes associated with the post and those associated with the diode.

The model must then be modified to take into account the fact that there is a diode underneath the cap rather than a cylinder of metal. The diode may be approximated to a thin coaxial section (bias leads) surrounded by a cylindrical piece of dielectric (hermetic seal). To first order, the resonance predicted by the coaxial TEM mode will be unchanged, and to that extent the representation of the diode as a short piece of post is a reasonable one, however we can expect a much larger discontinuity or fringing capacitance to exist. In addition, one can expect the TM modes to be significantly modified by the presence of the dielectric. i.e. more electric field to be stored in the dielectic.

(With regard to this, it might also be noted that the package capacitance is usually measured for an electric field across the diode (as for TM modes), and not perpendicular (as for the coaxial TEM mode)).

To incorporate these two effects, a (constant) correction capacitance C_c is also included in the model. This was initially chosen so that there was a good fit for one particular resonator at one particular frequency. Because the impedance of the diode was unknown, (and assumed to be fairly small and capacitive because of the small loading at the fundamental), it was initially ignored as it was felt that its effect could be allowed for within the value for the correction capacitance C_c. The chosen value was 0.04pF.

As an initial test of the validity of the equivalent circuit the experimental results of Carlstrom et al. shown in Fig.6.7 were modelled. The procedure was to input initial

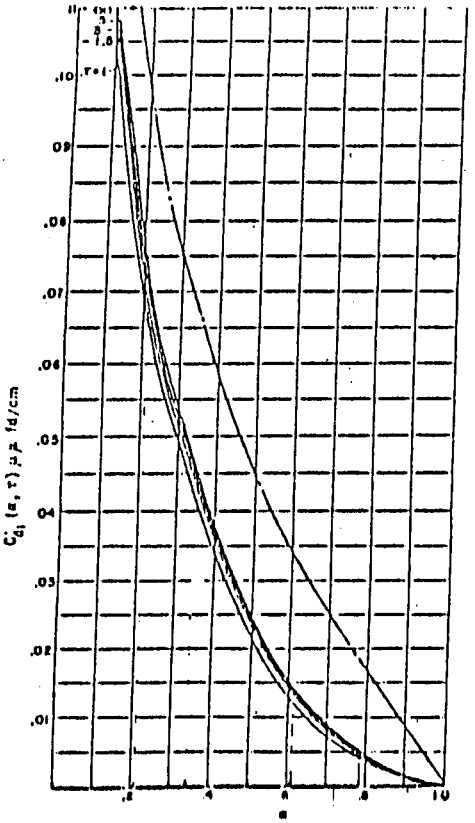

—Curve of $C_{d_1}'(\alpha, \tau)$. When multiplied by outer circumference, gives directly the discontinuity capacitance for Fig. A with $\alpha = a/b$, $\tau = r_1/r_1$.

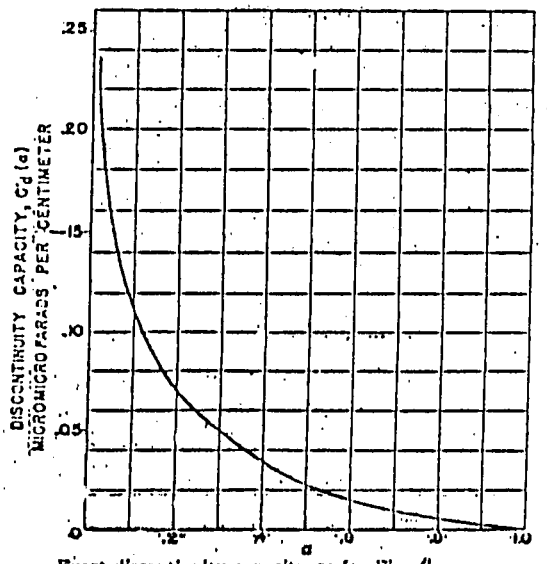

—Exact discontinuity capacitance for Fig. A. Results given for air dielectric; for other dielectrics multiply by dielectric constant.

FIG. A

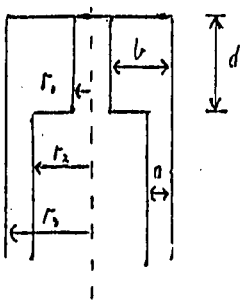

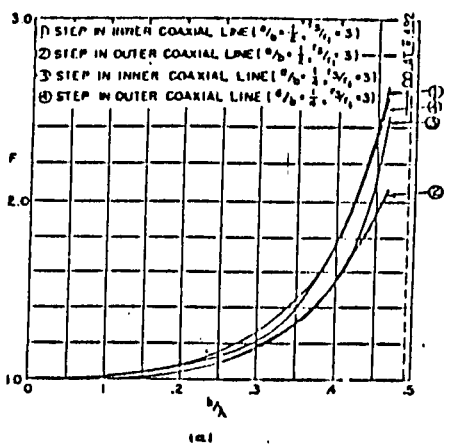

—Frequency factor F,

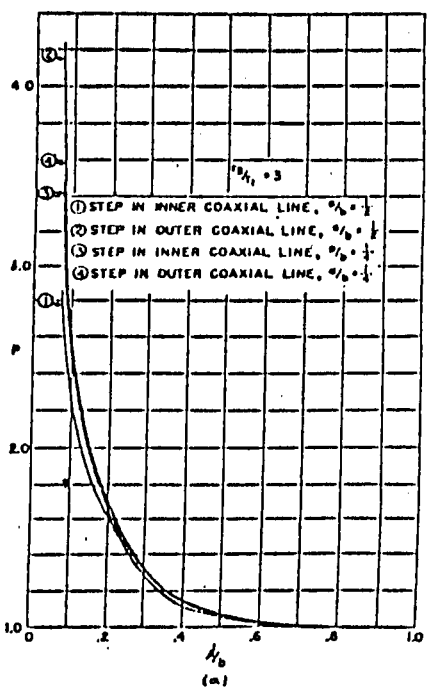

—Proximity factor P,

FIGURE 6.6 GRAPHS SHOWING THE CALCULATED VALUES FOR THE DISCONTINUITY CAPACITANCE FOR THE CASE SHOWN IN FIG. (A)
THE CAPACITANCE IS GIVEN BY C' x P x F
TAKEN FROM WHINNERY et al. [18]

parameters such as the diameter, thickness and height of the disc and a particular frequency. The reactance of the circuit was then calculated for different post heights. The post heights being incremented at each iteration. The point where the total reactance of the circuit passes through zero is the resonant condition, and the resonant cavity length was found by a linear fit between the two closest calculated values. The procedure was then repeated for different frequencies and different cap configurations. The results are shown in Fig 6.8.

Comparison of Fig 6.7 and Fig. 6.8 immediately show both an excellent qualitative and quantitative fit. There is possibly a slight discrepancy for the graph where the cap height is altered (Figs. 6.7b,6.8b), by adding another post section below the cap. However, this is to be expected as there will now be a small discontinuity, between the new section of post and the diode which is not taken into account ; and more importantly, the value for the correction capacitance is no longer valid as the diode is further from the cap. Despite this there is still excellent qualitative agreement and initial computer experiments have shown that an even better fit can be accomplished if one also allows for the capacitance of the diode. We can also point out various other successful features of the model.

a) Viewing the diode package in a cavity, as a length of coax where the reactive part of the active layer is small under light loading, obviously fits in well with the experimental result of Lazarus [17]. Under these assumptions it is to be expected that the resonances will approximate those predicted by the coaxial cavity as the discontinuity capacitance will be very low.

b) We can also explain the fact that the resonant frequency does not change very much (3GHz), when the inductance is halved, by changing from a single ribbon to a cross ribbon [2]. A lumped parameter model predicts a large change in resonant frequency, however when viewed from a transmission line point of view, the coaxial TEM mode will not be affected much, and the discontinuity capacitance cannot be expected to change hugely, as the total effective diameter of the bias leads will not have changed that much.

c) On the other hand, because the discontinuity mainly sets up TM modes which store electric energy around the diode, any change in the amount of dielectric (by removing part of the ceramic ring that surrounds the diode) can be expected to change the energy stored and hence the resonant frequency. In terms of the model this will manifest itself in a modification of the correction capacitance C_C. Computer experiments indicate that reduction of C_C to roughly 0.03pF can accomodate the change in frequency found by Haydl [2] (95-103GHz) for such an experiment.

d) Haydl also found, by quartering his device capacitance by reducing the are of the diode, that the resonant frequency changed from 91 to 99 GHz. This indicates the device capacitance cannot be completely ignored, but is comparable to the correction capacitance. As already mentioned, initial computer experiments (putting in suitable values for the device reactance based on this result) seem to indicate an even better fit to the experimental results.

e) The model also predicts the next coaxial resonances, as the cavity is lengthened even further. These have been found to correspond almost exactly to those found in our own oscillators, thus providing further evidence of the validity of the model.

f) Because of the discontinuity capacitance, the second harmonic resonance, will usually not coincide with the fundamental resonance, although the model does predict that there will be a cavity length where the two resonances will be the same. This point can be expected to manifest itself as a dip in the power output at the second harmonic frequency, as is clearly seen from the results of Carlstrom et al. in Fig.6.7.

The resonances predicted by the model and from the experiment do not quite coincide (few GHz different) although again there is excellent qualitative agreement. It is believed the slight difference can be accounted for, by the fact that the reactive component of the device at the second harmonic will be larger, because it is more heavily loaded, and that the correction capacitance C_C must have a frequency dependence not dissimilar to the discontinuity capacitance.

g) In chapter 7 it is shown that it is possible to get a small but definite frequency jump during tuning in some oscillators. Haydl [2] also reported a similar phenomenon, although it was not seen in the results given by Carlstrom et al. The effect seems to be related to the height of the waveguide, in that it often occurs in oscillators with full height waveguide to coax transitions but not with half height waveguide transitions. It is also not seen for small caps. It is suggested that the jump may be due to a transition to some sort of radial mode, or possibly even a type of TE waveguide mode that can exist across the width of the guide. Note that, although the cavity may appear too small to sustain such a resonance, because of the energy stored in other modes (such as a below cut-off coaxial type mode) it is still possible to have a resonant condition, in the same way that the coaxial mode has a resonance at suprisingly small cavity lengths.

This possibility is under further investigation.

In fact, it has been suggested [11] that the resonance of the cap post circuit is entirely due to coupling to the radial TEM mode that can exist under the cap, although it is

FIGURE 6.7 TYPICAL TUNING CURVES FOR DIFFERENT CIRCUIT PARAMETERS, TAKEN FROM CARLSTROM et al. [3]

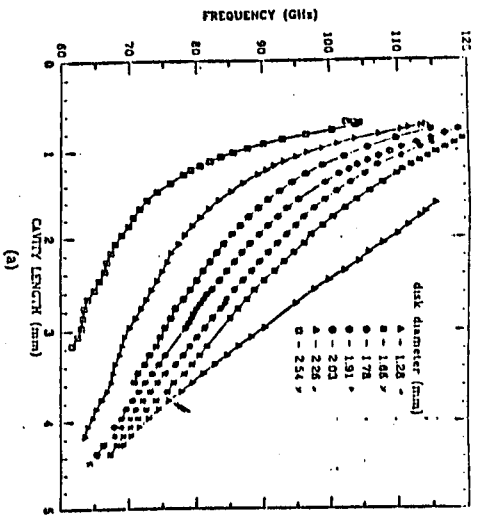

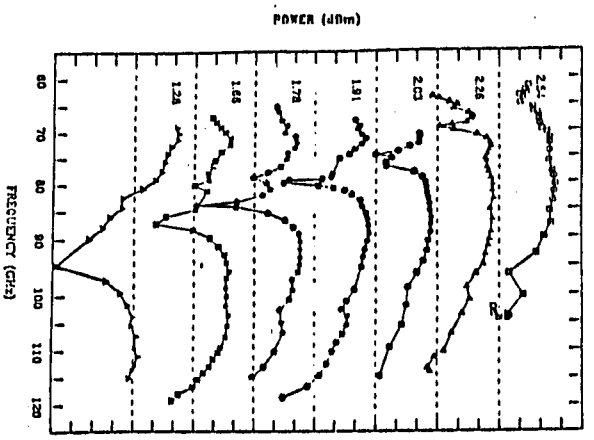

Fig. A (a) Tuning curves for one oscillator and diode, and seven disks of different diameter, $t = 0.10$ mm, and $h = 0$ for all disks. The turnover in the curve for the 2.54-mm-diam disk presumably is due to a slow transition in the electric-field configuration from a TEM mode to a radial line mode as the post length is made small. (b) The corresponding output power curves. The dashed line for each curve is at 0 dBm. The tick marks on the vertical axis are at 5-dB increments.

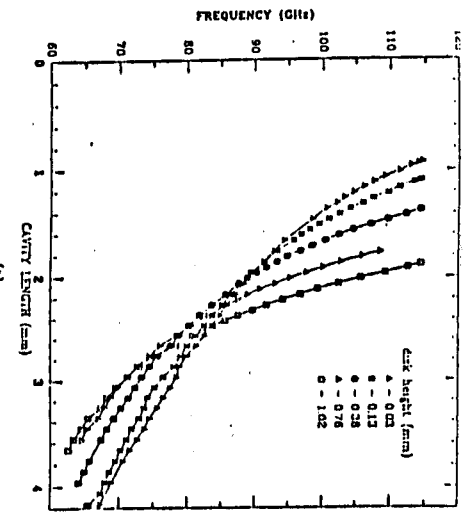

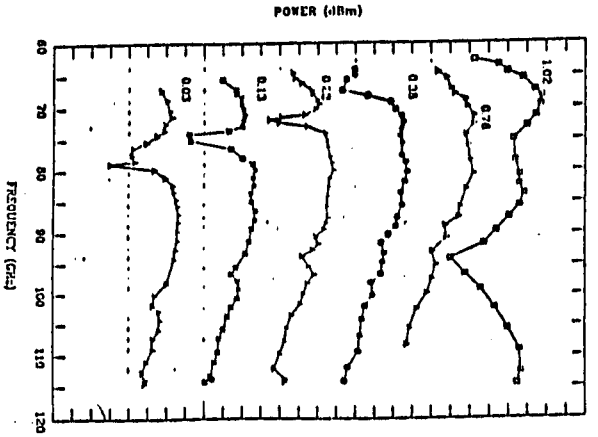

Fig. B (a) Tuning curves for five values of the disk height h above the diode package. The data were obtained from the same oscillator and diode. The disk diameter was 1.9 mm; $t = 0.13$ mm. The same coaxial pin was successively shortened between measurements. (b) The corresponding output power curves. The power output curve obtained for a disk height of 0.25 mm is also shown. The dashed line for each curve is at 0 dBm. The tick marks on the power scale are at 5-dB increments.

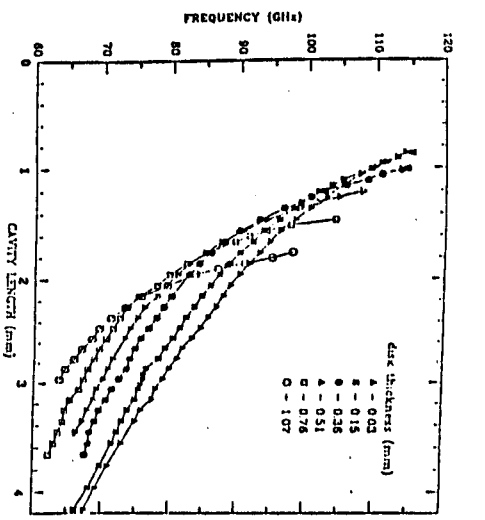

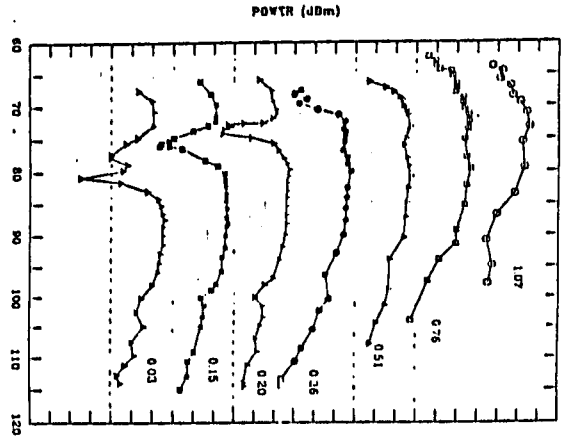

Fig. C (a) Tuning curves for six values of the disk thickness t. The data were obtained from the same oscillator and diode. The disk diameter was 1.9 mm; $h = 0$. The same disk was successively machined thinner between measurements. (b) The corresponding output power curve. The power output curve obtained for a disk thickness of 0.20 mm also shown. The dashed line for each curve is at 0 dBm. The tick marks on the power scale are at 5-dB increments.

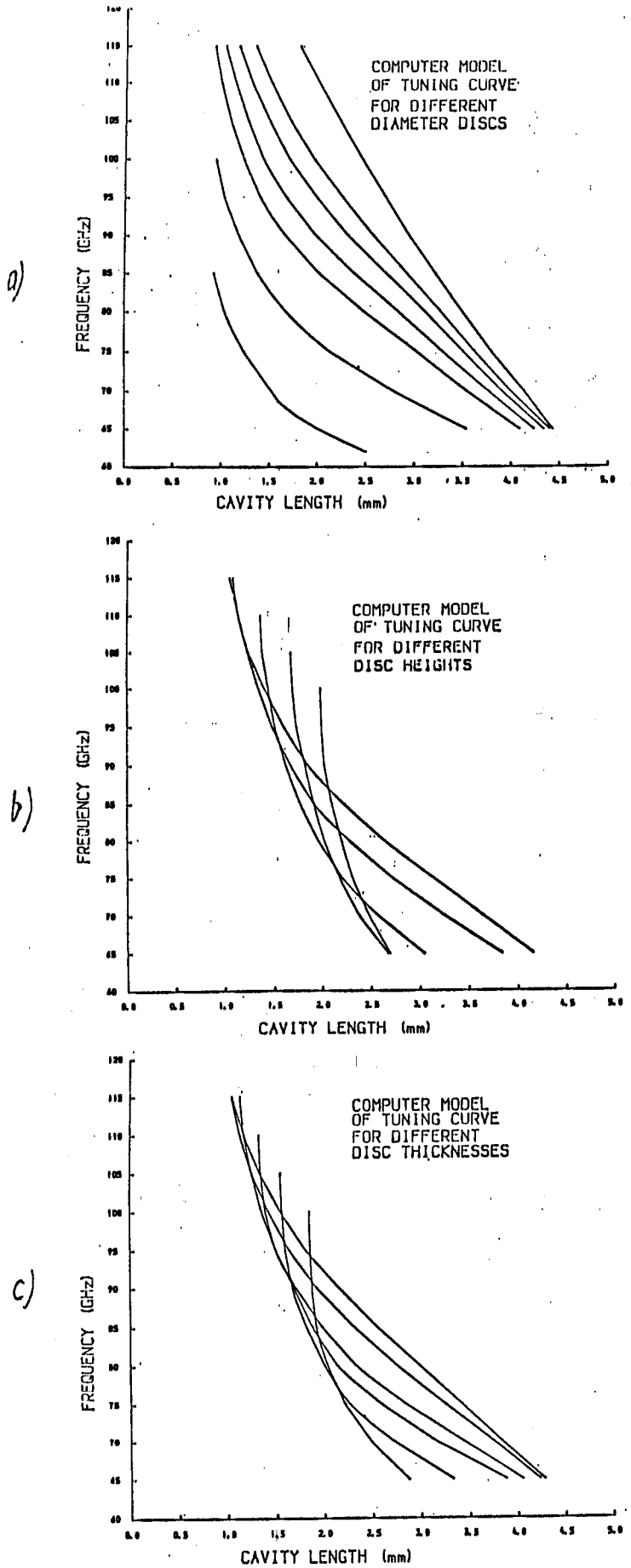

FIGURE 6.8 COMPUTER MODEL OF TUNING CURVES OF CARLSTROM et al. (SHOWN IN FIGURE 6.7)

unclear how this works, as there must be energy stored above the cap as well! . On this point though, it should be noted that the radial TEM mode can be regarded as as superposition of radial TE and TM modes. The effects of these modes are allowed for in the calculation of the discontinuity capacitance, so the two theories are not totally mutually exclusive as long as you allow the existence of other modes. Note that the results of Whinnery et al. actually imply that the coupling to the TEM mode is low for the dimensions of the package (i.e 0.46mm high).

6.8 THE POWER OUTPUT

As already mentioned the power output primarily depends on the loading at the fundamental and the harmonic. The fundamental must be loaded as little as possible to develop the maximum voltage swing across the diode. In terms of the external circuit this can only be improved by reducing the resistance of the cavity which might be achieved by gold or silver flashing, or in the limit by placing the diode in a superconducting cavity.

Note that for a high power diode we are always operating at a point where the resistive losses are (or should be) significant, and so we can expect a distinct increase in power output if these losses are decreased. Alternatively, one can argue that it should be possible to produce larger area, and hence higher power diodes if the losses are decreased significantly. (Although it is unclear whether the resistive loss associated with the diode and the package, or the loss associated with the circuit predominates).

Now the harmonic, will have an optimum loading that is determined by the non-linearity of the diode, as discussed in Chapter 4. A theoretical calculation showing how the power varies for fundamental and harmonic operation is shown in Fig. 6.9. The power output at the second harmonic is limited by the rapidly falling negative resistance with harmonic voltage swing leading to an optimum load condition which is calculated to be just a few ohms for a typical diode.

In fact, the area of a high power diode is chosen so that there is generally an optimum load of only a few ohms. The argument is that by increasing the area of a diode, to first order one will decrease the negative resistance R_d (at which the maximum power point exists) but increase the amount of current I by the same amount. As the power is given by:

$$P_{out} = 1/2.R_L.I^2 = 1/2.(R_d - R_c).I^2 \qquad (6.5)$$

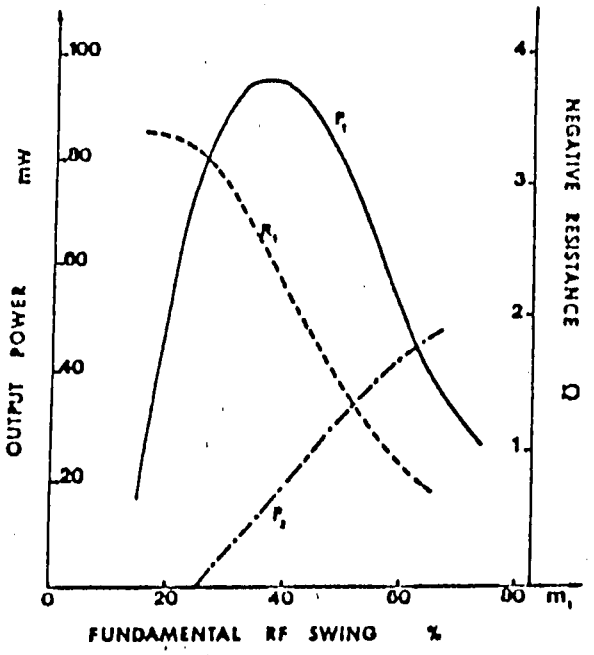

a) Harmonic operation: Evolution of the output power and negative resistance at the fundamental frequency, and of the output power at the second-harmonic frequency versus the fundamental RF voltage swing. $V(t) = V_0[1 + m_1 \sin 2\Pi f_0 t + m_2 \sin (4\Pi f_0 t + \varphi)]$ where $f_0 = 50$ GHz, $\varphi = 0$, $m_2 = 20$ percent, $L = 2.0$ μm, $N \# 10^{16}$ cm^{-3}, $T = 430$ K, $\phi = 75$ μm.

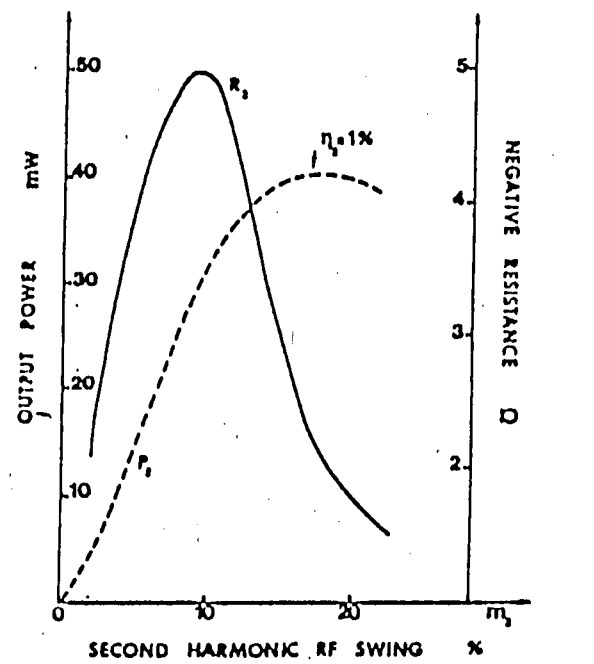

b) Harmonic operation: Evolution of the output power and negative resistance at the second-harmonic frequency versus the RF voltage component at this frequency. $V(t) = V_0[1 + m_1 \sin 2\Pi f_0 t + m_2 \sin (4\Pi f_0 t + \varphi)]$ where $f_0 = 50$ GHz, $\varphi = 0$, $m_1 = 60$ percent, $L = 2.0$ μm, $N \# 10^{16}$ cm^{-3}, $T = 430$ K, $\phi = 75$ μm.

FIGURE 6.9 DIAGRAMS SHOWING THE CALCULATED VARIATION OF OUTPUT POWER AND NEGATIVE RESISTANCE AS A FUNCTION OF VOLTAGE SWING FOR a) FUNDAMENTAL and b) HARMONIC OPERATION FOR TYPICAL OPERATING PARAMETERS
TAKEN FROM FRISCOURT et al. [25]

this will lead to a greater power output until R_L starts to become comparable to the circuit series resistance R_c. In fact a simple analysis suggests that the maximum power will be obtained when the optimum negative resistance $\mathbf{R_d}$ is equal to twice the circuit resistance R_c. This assumes that the optimum negative resistance is going to scale with the inverse of the device area, which for a non-linear device is possibly not strictly true. However, it is a fairly safe assumption that the maximum power delivered from an optimum diode will be at a point where the negative resistance is of the order of a few times the series resistance, which should be a few ohms. Although for reliability it is possible that it is chosen to be considerably higher.

This of course though, can vary from diode to diode depending on the active area and any excess series resistance that might be present, due to, say, a bad contact. For example , the active area of a diode is often limited by thermal considerations, rather than any impedance matching criteria. The optimum loading can therefore be expected to be quite different for different types of diodes. This explains why different circuits can give more power for one particular type of diode but not for another.

6.9 IMPEDANCE TRANSFORMATION AT THE SECOND HARMONIC

As the effective resistance of the output waveguide is several hundred ohms it is clear that there is the problem of effecting the necessary large impedance transformation between the diode and tbe waveguide. i.e so the waveguide impedance appears as only a few ohms to the diode. This is achieved in two ways.

Firstly there is the normal argument that the cap acts as an effective radial line transformer. Doring and Seebald [20] published impressive experimental results for a 3.5-6.5GHz test circuit that showed that large impedance transformations could be obtained over large bandwidths by a radial line transformer. Their results were later confirmed theoretically in [21] and they are shown in Fig.6.10. The main features are:

1) the impedance transformation mainly depends on the height of the radial line above the waveguide floor as shown in Fig.6.10a. For cap heights less than 1mm in WG/11 (29x59mm) it is possible to achieve low loss impedance transformation ratios of up to 300:1. We can think of this as a simple parallel resonance between the inductance of the package and the capacitance associated with the disc. The impedance transformation will be greater as we lower the inductance associated with the packaged device or increase the capacitance associated with the cap. That is why at low frequencies more power can

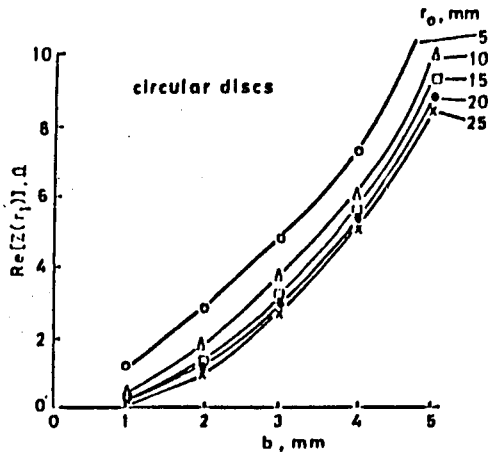

a) *Measured real part of the input impedance of the radial line against its height. Parameter is the radius*

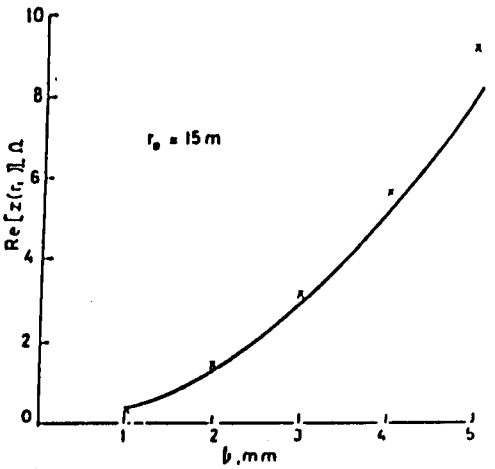

b) *Our calculation and measured values for F = 3·5 GHz*
× data from Reference 1
— this method

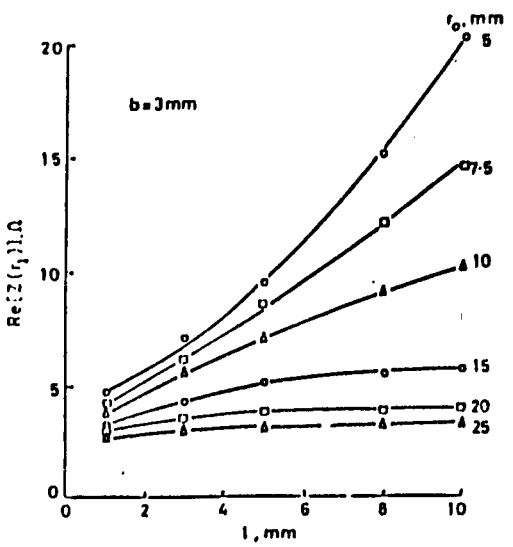

c) *Measured real part of the input impedance of the radial line against thickness of the discs. Parameter is the radius*

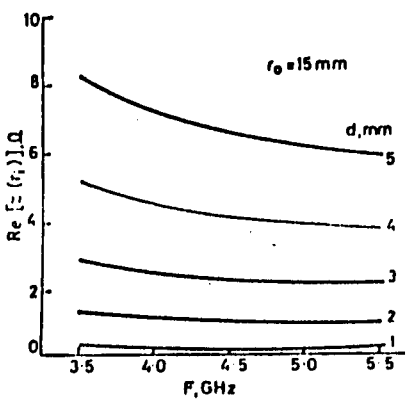

d) *Variation of Re [z(r_1)] with frequency*

FIGURE 6.10 THEORETICAL AND EXPERIMENTAL IMPEDANCE TRANSFORMATION WITH RESONANT CAP OSCILLATORS AS A FUNCTION OF a)b) CAP SIZE, c) CAP THICKNESS and d) FREQUENCY AT 3.5-6GHz. TAKEN FROM DORING AND SEEBALD [20]

sometimes be obtained by raising the height of the package to increase the inductance, and there are significant problems with matching devices at very high frequencies.

2) it works over a fairly large bandwidth for an appropriate disc. i.e. 3.5 - 5.5GHz in the experiment. In other words, there is a fairly small dependence on the radius of the disc for the impedance transformation. This can be seen in Fig 6.10a and Fig.6.10d. This is because of the low effective Q of the resonance as the inductance below the cap is very small. The larger the value of the inductance, the more the impedance transformation will become tuned.

It has been suggested that these results can be extended to higher frequencies and that the post cap circuit works as a radial line transformer at 95GHz [2],[3]. This assumes that the second harmonic couples into the TEM radial mode which can then couple efficiently into a waveguide mode. However, it is also true that the cap can also couple into the quasi-coaxial mode, and the impedance seen by this mode can significantly effect the impedance transformation. The following considerations should be noted:

a) Firstly, the results of Doring and Seebald [20] were taken at low frequencies where large impedance transformations were found for cap heights that were very small compared to the dimensions of the waveguide and the frequency. This is clearly not so at 95 GHz where the height of the package means that the cap height is almost half the height of the waveguide. Also, in their experimental setup they did not have a post extending from the cap to the top of the waveguide floor, as in the normal oscillator configuration. Addition of this post would set up further currents which would create fields above the cap that almost certainly change the results.

b) If the cap acted as a perfect impedance transformer to the waveguide, one would expect the frequency of oscillation to just be controlled by the backshort for a fundamental 80GHz oscillation. Results shown later for fundamental 80GHz InP diodes, indicate that the quasi-coaxial mode also plays a strong role in the tuning of the oscillator. One of the original papers on resonant caps [6] also showed that it is possible to have effective tuning with the backsort, although it should be noted that in this case, the cap made contact to the diode directly and was thus only 0.056mm from the waveguide floor. The results of Lazarus et al.[17] can thus be expected to be valid. It should also be noted that backshort tuning was also seen with fundamental InP diodes when absorbing material was placed above the cap structure, to make the quasi-coaxial mode very resistive.

c) Reflection experiments on second harmonic oscillators indicate that maximum power is obtained when the diode is well matched at the second harmonic. i.e. There is a position of the backshort when no or very little power is reflected.

Power dips in the second harmonic, correspond to points where the cavity is very badly matched to the waveguide and most of the second harmonic power is reflected, no matter what the position of the backshort.

As pointed out earlier, the existence of the cap normally means that the fundamental and the harmonic quasi-coaxial resonances will not coincide. When they do coincide, we can expect a substantial change in loading at the second harmonic as there will be two 'competing resonances' - one effectively in parallel and one in series with the diode. It is believed that this effect can be explain the results of Carlstrom et al. in Figure 6.7, where a fairly sharp power dip is seen at a particular frequency for a given cavity configuration. They also noted that the backshort had very little effect on the second harmonic in the region of the power dip, but that the third harmonic power appeared unaffected. This again would appear to be clear evidence of some type of resonance at the second harmonic within the cavity.

Thus the impedance transformation, at any one frequency can be expected to be a function of the impedance seen by the quasi-coaxial mode at the second harmonic, as well as a function the impedance transforming effects of the radial disc. Changing the size of the disc changes both parameters in a non trivial way, but this can be used to optimise the power output at any one frequency.

One can now consider ways of optimising the load coupling for a particular diode. Clearly the impedance the second harmonic sees will be a function of the cap height, thickness, diameter and the cavity length and varying these parameters can be expected to change the load resistance for a given resonant frequency. This explains why in [8] an increase in cap height was found to increase the power output (for a second harmonic output frequency of 60GHz). However, it is difficult to alter just one parameter, without significantly changing the resonant frequency.

One way of achieving this, with minimal change to the tuning characteristics of the oscillator, is to vary the position of the coaxial cavity relative to the output waveguide. Initial experiments, raising the diode by about 0.2mm with respect to a full height waveguide have been shown to more than double the output power over a very large frequency range. More experiments are planned to quantify this result.

Clearly, it is of great value to find the optimum or critical coupling point of a given diode. This could be achieved by injection locking experiments for different cavity configurations as outlined in Chapter 4. Furthermore, it is hoped to quantify the coupling provided by resonant cavities, by performing accurate phase and amplitude reflection

measurements at millimetre wave frequencies using optical techniques. This is discussed further in Chapter 10. Such data could then be used to design effective stripline oscillator circuits at millimetre wave frequencies, for which there is potentially a very large market.

6.10 THE BLOCK DIMENSIONS

The width of the block was determined by the criteria that it was necessary to have a backshort assembly that could tune through at least 5mm of travel (approximately one wavelength at 95 GHz in WG-28). The height of the diode block, was chosen to allow any suitable feedhorn to be attached (and still be above the bottom of the oscillator). The choke block and the choke were designed with the criteria that the cavity height should be tunable through at least 5mm so as to be able to cover the full frequency range of interest [1]. This meant the compression springs used to load the choke assembly and the pin structure had to be about 10mm long. In addition 5mm was allowed for the choke structure, all of which determine a minimum length for the choke assembly. A suitable margin of error was allowed for, which led to the choke assembly being designed 40mm in length. This in turn determines the length of the choke block and the bias block so the micrometre can tune over the appropriate range. The PTFE insert in the second block is merely for electrical insulation and to allow the choke assembly to run smoothly up and down.

In addition, sufficient room must be allowed inside the third block to allow a small safety circuit to be incorporated into the d.c bias for the diode. This consists of a simple RC filter to remove voltage spikes and stop any possible low frequency oscillations of the diode with the power supply, and a zener diode to stop reverse biasing or application of too many volts. The circuit is shown in Figure 6.11.

6.10.1 THE CAVITY DIMENSIONS

It is found that the power output and operating frequency depend critically on small changes in the cavity dimensions. The design criteria and implications behind each of the cavity dimensions is now discussed.

6.10.1.1 THE OUTER DIAMETER

Altering the outer dimension of the cavity, will effect the magnitude of the inductance normally associated with the bonding wire, and the fringing capacitance associated with the cap. The bonding wire inductance in particular, would appear to be a

very critical parameter affecting the impedance transformation, and altering the outer diameter of the coaxial circuit is the only obvious way of altering its magnitude. The inductance of the bonding wire controls the energy stored by the magnetic fields around the wire(s), and will increase as the cavity size increases. For operation at the highest frequencies, it would seem that very low values of inductance are necessary, which would indicate the necessity of much smaller cavities. Other considerations include the size of the packaged device and the size of the output waveguide.

The outer diameter of most of the cavities was chosen to be 3mm as this was successfully used by Carlstrom et al., and also coincides with the diameter of the screw head of Varians Gunn diode package, allowing the diode to be raised slightly above the waveguide floor. In some cases, this has been found to increase the output power by over 200%. Raising the diode changes the resistive coupling to the cavity at the second harmonic, as experimentally it is found there is little effect on the frequency tuning of the device. It has also been suggested that this effect may also be associated with the orientation of the bonding wires relative to the waveguide [12].

Carlstrom also mentions that he tried using a 3.94mm cavity but that it "exhibited several power dips across the frequency band possibly due to the cavity supporting additional waveguide modes at the fundamental frequency"[3]. It is unclear from this whether the output waveguide was below cut-off at the fundamental. The cavity itself, cannot support additional coaxial TEM modes and should not be able to couple into any TE modes (circumferential variations of the electric field). It is also well above cutoff for TM modes in coax (radial variations in the electric field), however, as noted in Chapter 5, it is still possible to have a resonance if enough energy is stored in other modes. It is also possible then the second harmonic may now have been able to couple into a radial mode, in addition to the coaxial resonance that has been observed (see last chapter and [1]). In addition, because of the physical disparity between the cavity and the width of the waveguide it may have been more difficult to couple power into the waveguide effectively and provide an optimum match.

Carlstrom also reported that he tested smaller cavities of diameters 2.06mm and 2.39mm but that it was now necessary to have much smaller caps to be able to tune up to the highest frequencies (115GHz). This is because the discontinuity capacitance will be very much larger for discs approaching the size of the cavity, making it more difficult to tune to high frequencies. However, small discs will start not to offer the necessary impedance transformation at low frequencies thus cutting the output there, as Carlstrom reported. As mentioned above however, that they may offer a better impedance transformation at high frequencies where the power output may increase. Arora and

Sarma[3] reported powers of 1-2 mW at 120GHz where they used discs of 1.4mm diameter in circular waveguide of diameter 2.4mm, as opposed to discs of approx. 1.8mm diameter in 3mm circular waveguide for optimum output in the 75-85 GHz range.

Thus the major effect of altering the size of the outer diameter will be to affect the coupling to the output waveguide and as a general rule, the size of the cavity wants to be roughly the same as the output waveguide. Obviously other considerations are machining difficulties and the size of the Gunn diode package.

6.10.1.2 THE INNER DIAMETER (POST DIAMETER)

There are a number of considerations here. Firstly, purely from a resistive point of view the attenuation constant for coaxial guide [5] is given by:

$$\alpha = \left(\frac{R_a}{a} + \frac{R_b}{b}\right) \frac{1}{2\zeta \ln (a/b)} \qquad (6.6)$$

where R_a and R_b are the characteristic resistances of the metals that make up the outer radius (a) and inner radius (b), and ζ is the impedance of free space (377Ω). When R_a and R_b are the same, it can be shown (by differentiating w.r.t. a/b) that the attenuation constant is a minimum when a/b = 3.6. For an outer diameter of 3mm this criteria predicts an optimum inner diameter of 0.83mm, which is roughly the dimension used by Carlstrom et al. This is probably the best value just from the point of view of achieving the highest Q at the fundamental. It corresponds to a characteristic impedance of nearly 77 ohms.

Other published results are for a coaxial line [4] weakly coupled to a WG-27 waveguide (5mm diameter cavity and no disc). This showed that for maximum power produced at the second harmonic the impedance level needed to be around 77ohms, although it was found that as a general trend the post needed to be slightly thinner at the higher frequencies. However, because the cavity was so weakly coupled and the impedance change small the results are not really conclusive. Arora and Sarma [3] also gave values for their power output as they altered the post diameter but their results are complicated by the fact they were working in circular waveguide with different caps, and no obvious trend can be seen.

From a tuning point of view, the larger the post diameter the less capacitance associated with the discontinuity between the post and the cap. This means that the resonant frequency will be higher for a thicker post, everything else being equal, as is shown by some of the results given by Haydl [2]. Most of the energy change due to a

change in the post diameter will be due to evanescent radial waves above the cap (associated with the discontinuity capcitance). There may also be losses associated with a large capacitance, due to more energy being stored in the local waves, and being dissipated in the cavity walls.

It is not clear which of the above is the most important, but a good starting point is clearly an impedance level of around 77ohms (or a 0.83mm post in a 3mm diameter cavity). This also coincides with the diameter of the Gunn diode package cap.

Other considerations include the more mundane difficulty of machining. It is not too difficult to make a fixed frequency oscillator, where the bias plug, cap and post are all made from the same block, however to make a scaled down version of a variable height coaxial cavity is more difficult. In particular, it is difficult to machine much smaller posts than 1cm long 0.8mm diameter posts and drill 1cm long 0.8mm holes. To ensure a large element of repeatability a post diameter of 1.0mm was initially chosen for the design which corresponds to an impedance of 66ohms. This has been found to give good power outputs in practice. Later oscillators incorporated a post of diameter 0.8mm whivch also gave good results.

6.10.1.3 THE CAP DIAMETER

Ideally the cap is meant to act as a quarter wavelength radial line transformer, although the transformation is undoubtedly affected also by the quasi-coaxial resonance at the second harmonic. It is certainly found that the radial cap can work well over a very large frequency range around the quarter wavelength value, although small caps can limit the power in the lower frequency range. On the other hand very large caps can limit tuning in the upper frequency range because of the larger discontinuity capacitance(see [4]).

In a fixed height cavity the discontinuity capacitance associated with the disc will be a major factor in determining the resonant frequency and its size will normally be chosen to give the required frequency. For a variable height cavity the major factor will be to keep the second harmonic resonance away from the desired tuning range. The smaller the disc the higher the frequency and the wider the frequency band where the resonance occurs. From Carlstrom's results [4] this is clearly a very important factor, and so the size of the disc should be chosen depending on the frequency range that is required. Note that the primary requirement of the disc is to provide the right amount of coupling at the second harmonic which may vary from diode to diode. High power diodes may therefore require

different circuits compared to lower power diodes at the same frequency, in order to optimise the power output, because of the different resistive loading required.

This impedance transformation is mainly achieved by the disc acting as a radial line transformer, but it will also clearly be affected by the impedance of the quasi-coaxial circuit at the second harmonic, as well as any package resonances.

From Carlstrom's data, a disc size of 2mm was chosen for most of the experiments as it seemed to offer a large tuning range and put the second harmonic resonance below 80 GHz for the particular diode that he used.

6.10.1.4 THE DISC HEIGHT

The disc height will affect both the resonant frequency and the second harmonic resonance, by changing the value of the total inductance below the cap as well as altering the discontinuity capacitance slightly. It also introduces another discontinuity between the package and the first post section which brings further complexity. For diodes with a large optimum negative resistance it is possible that a better match can be achieved by increasing the height of the cap [6], but at high frequencies where a smaller inductance is required to effect the necessary impedance transformation, there is nothing to be gained as reported by Haydl [2]. Indeed, it maybe that a lower height package might be useful to try and match very low negative resistances. In the limit this can provide a direct impedance transformation to the waveguide [10] and give output frequencies that are controlled by the waveguide backshort. In conclusion, there seemed little to be gained, except extra complexity by increasing the height of the cap, so it was allowed to sit directly on top of the package.

6.10.1.5 THE DISC THICKNESS

The disc thickness too changes the tuning characteristics of the oscillator by acting as a short piece of low impedance coax separating the discontinuity capacitances. The thicker the disc, the lower the resonance at the second harmonic, which can lead to improved tuning ranges. On the other hand, the the disc thickness will eventually limit the tuning range, and as a piece of very low impedance guide, will contribute to the losses. From Carlstroms results, the optimum thickness appears to lie between 0.15mm and

0.36mm. Results obtained, seem to show best performance for the thinnest discs, of thickness between 0.15mm and 0.2mm.

6.10.2 THE OUTPUT WAVEGUIDE

Haydl [2] showed that a fundamental waveguide can lead to frequency pulling of several GHz by the backshort and lead to frequency discontinuities whilst tuning. Therefore the output waveguide must be below cut-off at the fundamental and preferably single mode at the harmonics. For operation at 95GHz, (and to have the ability to couple to standard test gear) this means the choice is WG-27 (75-110 GHz) or WG-28 (90-140) GHz. In terms of the frequency coverage of the diodes available (60-120 GHz) [4], for lower losses, ease of machining, and perhaps more optimum coupling to the cavity, WG-27 would appear to be the ideal choice, although good results have been obtained with both WG-27 and WG-28.

The local height of the waveguide at the cavity is also a consideration, as it will affect the coupling from the cavity to the waveguide. Carlstom et al. used half height WG-27 waveguide successfully. Experiments with WG-28 waveguide have shown that quarter height guide is clearly worse. Results with full height waveguide, are just as good if not better than those with half-height waveguide. There seems little reason therefore, not to prefer full-height waveguide.

6.10.3 THE BIAS CHOKE

The bias choke ideally must have a stopband at both the fundamental and second harmonic frequencies (30-120GHz), as well as being able to supress low frequency oscillations in the range 10-100MHz, caused by the diodes low frequency negative resistance resonating against some part of the bias supply.

For the stopband filter, the usual choice is to make a non-contacting design based on having several high and low impedance coaxial sections, each a fraction of a wavelength long as shown in Fig.6.12. A travelling wave will then suffer a reflection at each interface. With an appropriate design these reflections can be made to add up in phase giving a total reflection much greater than if no filter had been present. Such a design is based on quarter wavelength sections at a particular frequency. Of course, it is also possible to design a system where the reflections are out of phase and in effect increase the transmissivity of the system at a particular frequency. Such a design would involve half wavelength sections and in effect be a type of Fabry-Perot.

The design procedure followed the approach used by Brewer and Raisanen [23] and is outlined in the following section.

6.10.4 COAXIAL CHOKE FILTER DESIGN

We now consider the design and modelling of the filter structure which forms a short circuit at one end of a coaxial circuit. This is done by modelling, each element of the filter as a length of transmission line, which in turn is modelled as a lumped reactance. Standard filter theory is then used to derive the necessary lengths, to produce a wideband short circuit. It is interesting to note that impedance matching and filter theory are essentially the same problem.

6.10.5 LUMPED CIRCUIT REPRESENTATION

It is useful to note that a length l of transmission line can be represented as a series of lumped components in series and in parallel. Either, as two capacitances in parallel connected by a series inductance, or two inductances in series separated by a capacitance in parallel as illustrated below

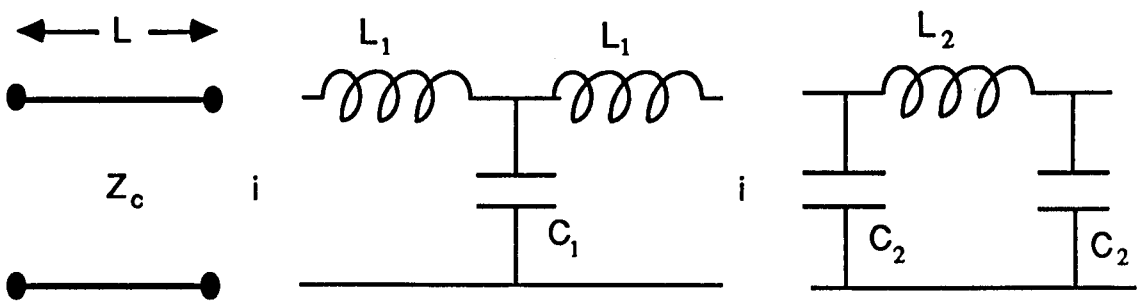

EQUIVALENT CIRCUITS FOR A TRANSMISSION LINE

where $wL_1 = Z_C \tan(\beta l/2)$ and $wC_1 = Y_C \sin(\beta l)$

and $wL_2 = Z_C \sin(\beta l)$ and $wC_2 = Y_C \tan(\beta l/2)$

This is easily proved by multiplying out the respective individual capacitance and inductance matrices.

This representation is very useful when trying to design waveguide or coaxial-circuit filters as standard lumped circuit filter theory can be used.

If we take the standard model of the coaxial filter choke, shown in Fig.6.12a, then, we can represent the transmission line model by the quasi-lumped circuit shown in Fig.6.12b. This can be further lumped with little approximation to the lumped structure shown in Fig.6.12c. At each discontinuity there is a capacitance associated with evanescent modes (which is not entirely negligible), but these values are easily found by the graphs given by Whinnery et al.[3] and are included in the model.

With this reduced lumped circuit, standard lumped circuit filter theory can be used. The values of the L's and C's are determined by the desired filter response.

These give a system of equations which can be solved to find the optimum values of the lengths of the individual sections of the choke. For example, we can assign the elements g values:

$$g_0 = R_0 = Z_{C0}$$
$$g_1, g_3 = w_1 L_A, w_1 L_C$$
$$g_2, g_4 = w_1 C_B, w_1 C_D$$

Therefore, we obtain 4 equations for the four lengths of the individual sections.

$$g_1 x\, g_0 = Z_{C1} \sin(\beta_1 z_1) + Z_{C2} \tan(\beta_2 z_2 / 2) \qquad (6.7a)$$

$$g_3 x\, g_0 = Z_{C2} \tan(\beta_2 z_2 / 2) + Z_{C3} \sin(\beta_3 z_3) + Z_{C4} \tan(\beta_4 z_4 / 2) \qquad (6.7b)$$

$$g_2/g_0 = Y_{C1} \tan(\beta_1 z_1 / 2) + Y_{C2} \sin(\beta_2 z_2) + Y_{C3} \tan(\beta_3 z_3 / 2) + w_1(C_{F1} + C_{F2}) \qquad (6.7c)$$

$$g_4/g_0 = Y_{C3} \tan(\beta_3 z_3 / 2) + Y_{C4} \sin(\beta_4 z_4) + w_1(C_{F3} + C_{F4}) \qquad (6.7d)$$

Note that C_{F0} and L_4 are fairly small and they can be neglected without affecting the result significantly.

All the values apart from the values of the sections can be calculated a priori:

Because coax is a TEM transmission line, the value for all β is of course, $\beta = 2\pi/\lambda$ where λ is the free space wavelength. In this model it also represents the wavelength at the passband edge of the filter.

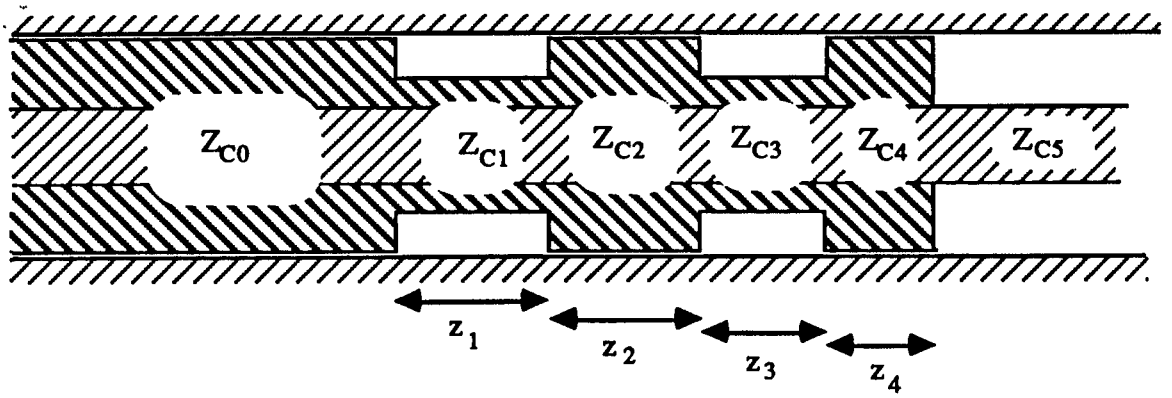

FIGURE 6.12a SCHEMATIC OF CHOKE STRUCTURE IN GUNN OSCILLATOR

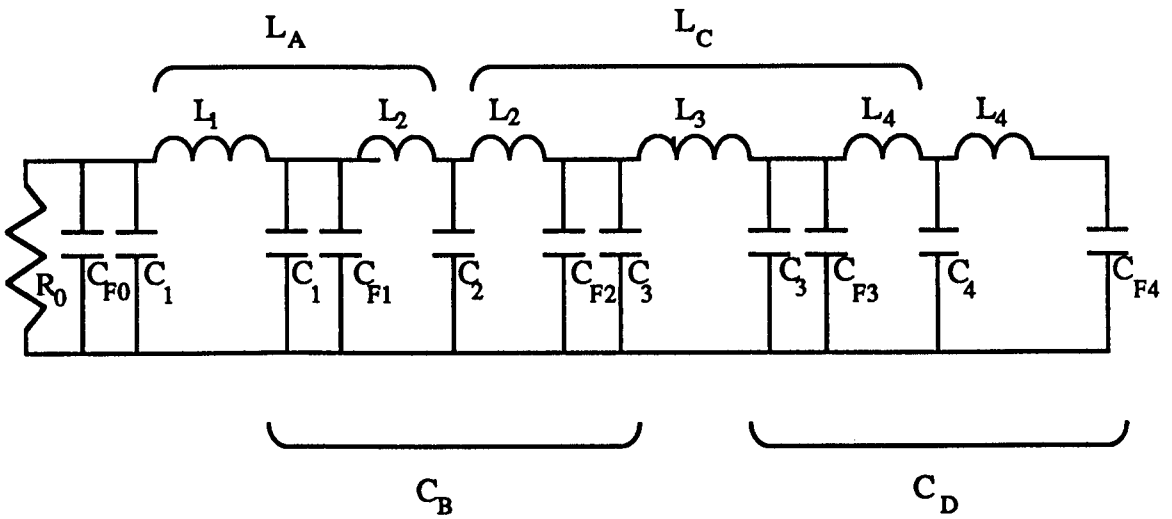

FIGURE 6.12b EQUIVALENT LUMPED CIRCUIT FOR CHOKE STRUCTURE

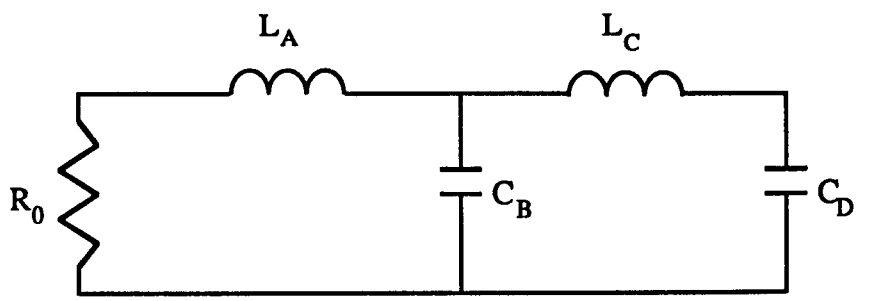

FIGURE 6.12c REDUCED LUMPED CIRCUIT USED TO CALCULATE FILTER CHARACTERISTICS

The values of the discontinuity capacitances can be found from the graphs of Whinnery et al. [4] and are typically of the order of 0.15pF. The values for Z_c for a coaxial line, are found from the formula,

$$Z_c = \frac{1}{2\pi}\left(\frac{\mu}{\varepsilon}\right)^{1/2} \ln (b/a) \qquad (6.8)$$

where b is the outer radius and a is the inner radius.

Therefore we just have to solve for z_1, z_2, z_3 and z_4. At first this appears a tricky problem, but it can be easily solved using an iterative process [23]. The values of the tan functions are comparatively small, and are ignored in the first iteration. Approximations to the values of z_1, z_2, z_3 and z_4 can be found directly from the sin functions. These values are then substituted into the tan functions and new values of z_1, z_2, z_3 and z_4 are calculated from the sin functions again. This process is repeated until convergence is reached, which is normally after only a few iterations. A program was written to perform this iteration and for a five section structure produced the results that are quoted in 6.10.5.3.

6.10.5.2 DESIGN CONSIDERATIONS

To design a choke filter, it is usual to specify a low pass filter where the passband edge is above the lowest frequency to be used. Note however, that although the design is a low pass filter configuration, because we are not dealing with true lumped components, there will eventually be 'holes' in the stopband where the length of each section approaches half a wavelength. However the section lengths cannot be too small, otherewise they beome ineffective at the larger wavelengths. The bandwidth is always limited and section lengths should therefore end up roughly between $\lambda/8$ and $3\lambda/8$. This should always be borne in mind when designing a choke which is required to work over a very large frequency range and in some cases it is necessary to empirically adjust a given design. In general there is a payoff between the steepness of the cut-off and the bandwidth obtainable. When using lumped circuit theory, the following design considerations should be noted.

a) The more sections that are included the higher order the filter, and the more steep the cut-off slope and reflection coefficient. However resistive losses also go up and the stopband is reduced. In general, five sections is normally considered optimum [23].

b) In general, the ratio of the heights of the low and high impedance sections wants to be as large as possible to maximise the reflection coefficient. The only limitation is that the height of the low impedance sections must again not approach half wave resonance,

although in practice it is normally considerations of mechanical rigidity that will limit the ratio.

c) When specifying a Chebyshev filter the passband ripple is an important parameter. The larger the ripple the steeper the cut-off at the band edge. However, it is also found that the stoband is also reduced. For this application, where the operating frequencies are well above the band edge, the bandwidth is the most important parameter. It is therefore useful to specify, a very small ripple, or to use a maximally flat Butterworth filter.

6.10.5.3 DESIGN OF COAXIAL CHOKE

The dimensions of each of the sections of the coaxial choke are constrained by the size of the diode and/or by mechanical considerations and are given as,

Outer Diameter = 3mm

Inner Diameter (Sections 0,2,4) = 2.95mm

Inner Diameter (Sections 1,3) = 2.2mm

Inner Diameter (Section 5) = 0.8mm

Referring to Eq. 6.8 and the graphs of Whinnery et al. (Fig.6.6) this gives values of

$$Z_{C0} = Z_{C2} = Z_{C4} = 1\Omega$$
$$Z_{C1} = Z_{C3} = 30\Omega$$
$$Z_{C5} = 80\Omega$$
$$C_{F0} = C_{F1} = C_{F2} = C_{F3} = 150fF$$
$$C_{F4} = 170fF$$

Using a maximally flat Butterworth filter we have,

$$g_0 = R_0 = Z_{C0} = 4$$
$$g_1 = w_1 L_A = 0.383$$
$$g_2 = w_1 C_B = 1.082$$
$$g_3 = w_1 L_C = 1.577$$
$$g_4 = w_1 C_D = 1.531$$

When these parameters, along with a nominal terminating impedance of $Z_{C0} = 4\Omega$ and a cut-off frequency of 15GHz are substituted into the program we have the following calculated structure:

$z_1 = 0.15mm$

$z_2 = 0.8mm$

$z_3 = 0.8mm$

$z_4 = 0.7mm$

Using similar parameters but for a Chebyshev filter with a 1dB ripple, with cut-off at 15GHz, gave the following structure.

$z_1 = 0.45mm$

$z_2 = 0.8mm$

$z_3 = 0.8mm$

$z_4 = 0.7mm$

All the lengths scale approximately with cut-off frequency.

A program was also written to calculate the reflectance of any coaxial filter over the desired frequency range. This was used to plot out the theoretical reflectance and phase angle of the calculated design. This plot is shown in Fig. 6.13 for the Chebyshev filter structure. The reflectance of the choke without a filter section, is also given for comparison. Both give excellent theoretical VSWR over the range from 30-120 GHz and this and similar designs have been employed in the choke structures for the oscillators. In fact, machining tolerances are not stringent, as it was found that the exact dimensions did not matter in detail, as long as the sections do not approach half wave resonance.

(The capacitor/resistor combination in the bias block is usually sufficient to inhibit any low frequency oscillations. If not, the addition of a lossy microwave ferrite situated closely around the choke structure has been shown to work well [9].)

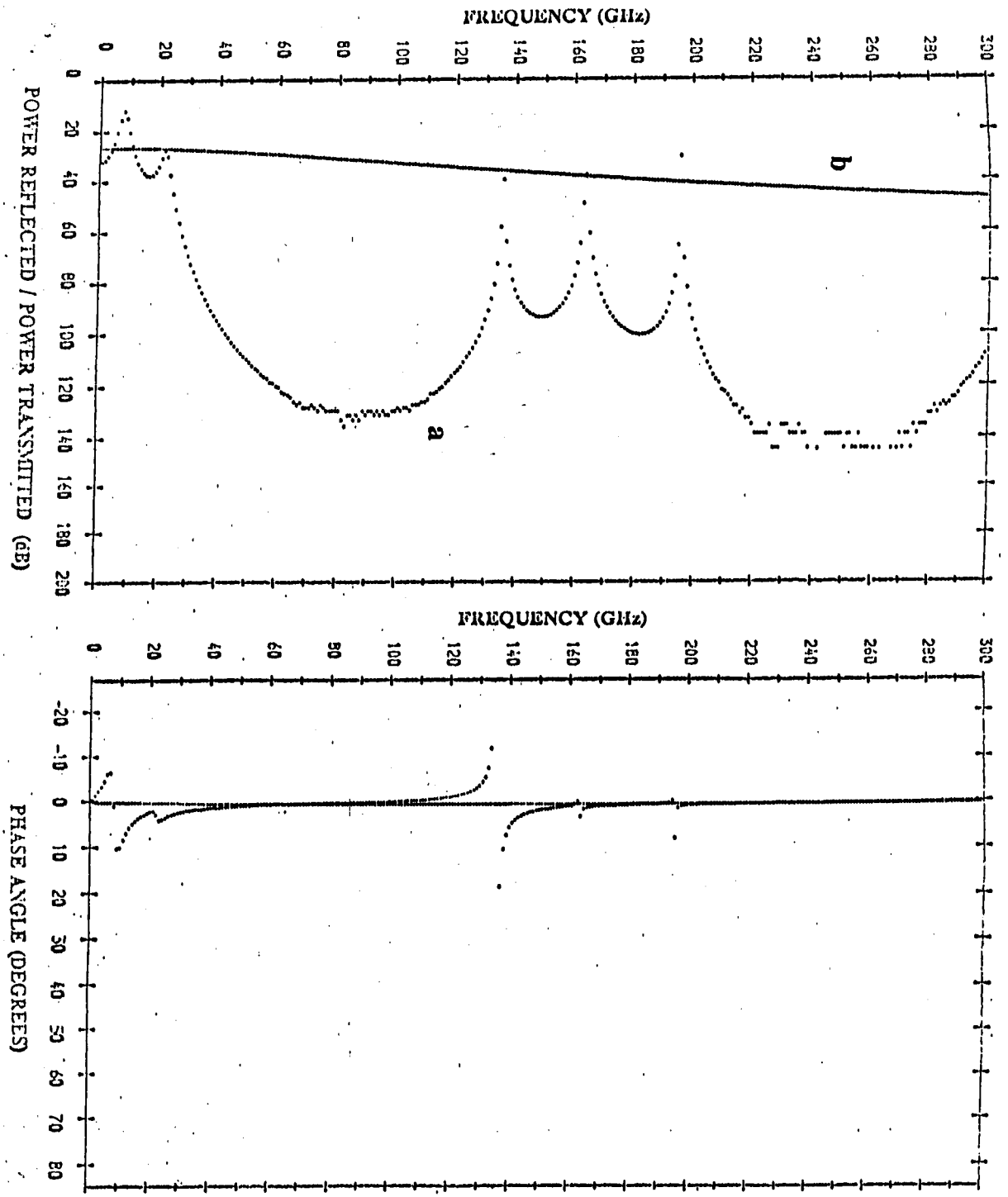

FIGURE 6.13 DIAGRAM SHOWING THEORETICAL REFLECTANCE AND PHASE ANGLE FOR THE CHOKE STRUCTURE DESIGNED FROM THE CHEBYSHEV FILTER a) WITH CHOKE b) WITHOUT CHOKE
(z_1=0.45mm, z_2=0.8mm, z_3=0.8mm, z_4=0.7mm)

REFERENCES (CHAPTER 6)

1) L.F.Eastman, "Transferred-Electron Devices", Microwave Devices, Chapter 2, J.Wiley & Sons, 1976

2) W.H.Haydl, "Fundamental and Harmonic Operation of Millimeter-Wave Gunn Devices", Vol. MTT-31, No.11, Nov.1983, pp.879-889

3) J.E.Carlstrom, R.L.Plambeck, D.D.Thornton, "A Continuously Tunable 65-115 GHz Gunn Oscillator", Vol.MTT-33, No.7, July 1985, pp.610-619

4) J.W.Archer, "Millimeter Wavelength Frequency Multipliers", Vol. MTT-29 No.6, June, 1981 pp.552-557

5) K.Solbach, "Simulation Study of Harmonic Oscillators", Vol.MTT-30, No.8, Aug.1982, pp.1233-1237

6) T.Misawa, N.D.Kenyon, "An Oscillator Circuit with Cap Structure for Millimeter Wave IMPATT diodes", IEEE Trans. MTT-18, 969, 1970

7) T.G.Ruttan, "Gunn-Diode Oscillator at 95 GHz", Electron. Lett., Vol.11, July 1975, pp.293-294

8) K.Solbach, F,Sickling, H.Barth, "Harmonic Gunn Oscillators Allow Frequency Growth", Microwaves & RF, April 1983, pp.75 onwards

9) I.G.Eddison, "Indium Phosphide and Gallium Arsenide Transferred-Electron Devices", Infrared and Millimeter Waves, Volume 11, Millimeter Components and Techniques, Part III, Chapter 1, Academic Press, 1984

10) W.H.Haydl, "Harmonic Operation of GaAs millimeter wave transferred electron oscillators", Electron Lett. Vol.17, pp.825-826, Oct.1981

11) J.Ondria, "Wide-band mechanically tunable and dual in-line radial mode W-band (75-110 GHz) cw Gunn diode oscillators", in Proc. 7th Biennial Conf. Active Microwave Semiconductor Devices and Circuits (Cornell Univ. Ithica N.Y), Aug. 1979

12) R.S.Arora, N.V.G.Sarma, "Experimental Investigation Of Millimeter Wave Gunn Oscillator Circuits in Circular Waveguides", International Journal of Infrared and Millimeter Waves, Vol.6, No.10, 1985

13) I.G.Eddison, D.M.Brookbanks, "Operating Modes of Millimeter Wave Transferred Electron Oscillators", Electron Lett., Vol.17, pp.112-113, Feb.1981

14) H.Essen and E.Wennerscheid, "Low Noise Oscillator Approaches at 140GHz", International Journal of Infrared and Millimeter Waves, Vol.8, No.2, 1987

15) K.P.Weller, R.S.Ying, D.H.Lee, "Millimeter IMPATT Sources for the 130-170 GHz Range", IEEE MTT, Vol. MTT-24, No.11, Nov.1976, pp.738-43

16) N.B.Kramer, "Millimeter-Wave Semiconductor Devices" IEEE MTT, Vol. MTT-24, No.11, Nov. 1976, pp.685-693

17) M.J.Lazarus, F.R.Pantoja, S.Novak, M.G.Somekh, "Wideband Tunable MM-Wave Gunn Oscillator Design", Electronics Letters, Vol.17, No.20, October 1981

18) J.R.Whinnery, H.W.Jamieson, T.E.Robbins, "Coaxial-line Discontinuities", PROC IRE, Vol.32, Nov. 1944, pp.695-709

19) J.F.Luy, R.Kuehne, "Current Distribution in Oscillating mm-Wave Diodes", Solid State Electronics, Vol.29, No.4, 1986 pp.471-476

20) K.H.Doring, E.Seebald, "High Transformation Ratio for Impedance Matching with a Radial Line", Electronics Letters, Jan.1980 Vol.16, No.2, pp.50-51

21) Wu Zheng-de, "Theoretical Study on the Radial Line Transformer in a Rectangular Waveguide", Electronics Letters, March 1984, Vol. 20, No.6, pp.256-258

22) N. Marcuvitz, Ed., "Waveguide Handbook", New York: McGraw-Hill, 1951, pp.307-310

23) M.K.Brewer, A.V.Raisanen, "Dual-Harmonic Noncontacting Millimeter Waveguide Backshorts: Theory, Design, and Test", IEEE Trans. Microwave Theory Tech., Vol. MTT-30, pp.708-14, May. 1982

24) S.Neylon, M.E.D.L. Personal Communication

7.0 OSCILLATOR RESULTS

7.1 INTRODUCTION

This section traces the development of a set of different Gunn Diode oscillators and describes the power output and frequency tuning range that has been obtained with these type of oscillators with various different types of diodes. Initial experiments used low power (5mW) Varian GaAs Gunn diodes which are all believed to have a Schottky barrier current limiting type contact. These provided some useful initial results to determine the important features of the oscillator design. Later, more powerful GaAs Gunn diodes became available and typical results are given. Results obtained with second harmonic operation show that continuous tuning ranges of over 40GHz are possible with good power output over 20GHz tuning ranges. Under some circuit conditions they also illustrated features such as power dips and frequency jumps in the tuning range of the oscillator.

An ohmic contact n+ n n+ diode manufactured by M.E.D.L. is also examined in some detail, to illustrate the optimisation of a diode to a circuit. This diode gave a large power output and some interesting results.

Various experimental GaAs Gunn diodes with graded gap cathode structures were also characterised in a number of different circuits. The data was used to determine the optimum operating frequency of the diode versus active length, with good agreement with theoretical results[13].

Lastly, both second-harmonic 94GHz InP diodes and fundamental 80GHz InP diodes have been tried in various circuits, and results on 140GHz second-harmonic InP oscillators are also reported.

7.2 POWER AND FREQUENCY MEASUREMENTS

A number of different set-ups were employed in the measurement of frequency and power. They are considered in greater detail in Chapter 9 and are outlined below.

1) For absolute power measurements, the power was measured using a WG/27 ANRITSU power meter which is calibrated only for the 75-110 GHz region.

2) For the main frequency/power measurements the block was attached via a 10dB coupler to a corrugated feedhorn, which fed into a quasi-optical Martin Puplett Interferometer system that used a Golay as the detector. This measured the second harmonic frequency to an accuracy of about 10MHz using a fringe counting technique. In addition, via a Fast Fourier Transform, it allowed the examination of any 3rd harmonic frequencies, and the magnitude and frequency of any large frequency sidebands. The other arm of the 10dB coupler was connected to a crystal detector, which gave a simultaneous indication of the power output. The voltage and backshort position were adjusted for maximum power output. This is illustrated in Figure 7.1.

7.3 FREQUENCY PULLING MEASUREMENTS

In the second set-up, an additional 10dB coupler was used to couple in power from a low noise high power InP oscillator also operating in second harmonic mode. The couplers were arranged so the oscillators effectively did not 'see' each other, and a crystal was used to detect any mixing or upconversion of bias oscillations. The mixed signal, typically of a few hundred MHz, was amplified and viewed on a spectrum analyser. The r.f frequency was monitored simultaneously by coupling to the interferometer system. This experimental set-up is illustrated in Figure 7.2. This approach worked well with Varian diodes, however there were certain problems with other diodes as it was discovered that spurious bias oscillations could be induced by reflection from the crystal detectors.

In both set-ups an oscilloscope and spectrum analyser was used to monitor any oscillations on the bias supply.

7.4 INITIAL RESULTS AND BLOCK DESIGN

Initially, a large variety of different blocks were built, all with slightly different dimensions. These are described briefly below. Unless otherwise stated, the blocks had 3mm diameter cavities with 1mm diameter posts and used a 2mm diameter cap. Tuning characteristics and power output are also given, although it should be noted that these will also be very dependent on the particular diode used.

BLOCK 1 - The Prototype Block was a first attempt to produce a widely tuneable Gunn Oscillator. As such it had a number of design and machining faults, but it worked well enough to give confidence in the design. Its main features were:

GUNN DIODE MEASUREMENT SYSTEM

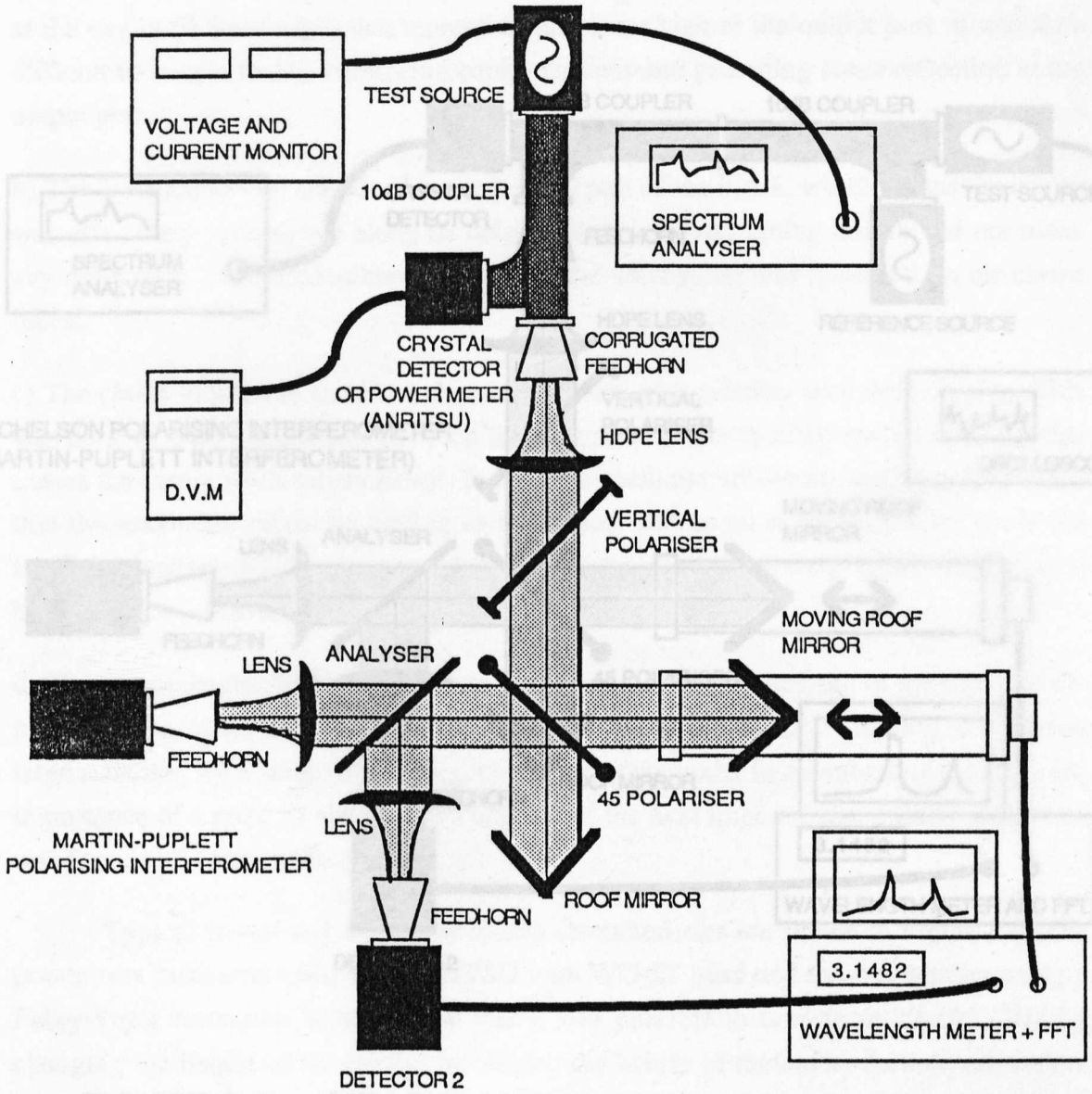

FIGURE 7.1 SCHEMATIC OF SYSTEM USED TO MAKE POWER / FREQUENCY MEASUREMENTS ON GUNN OSCILLATORS

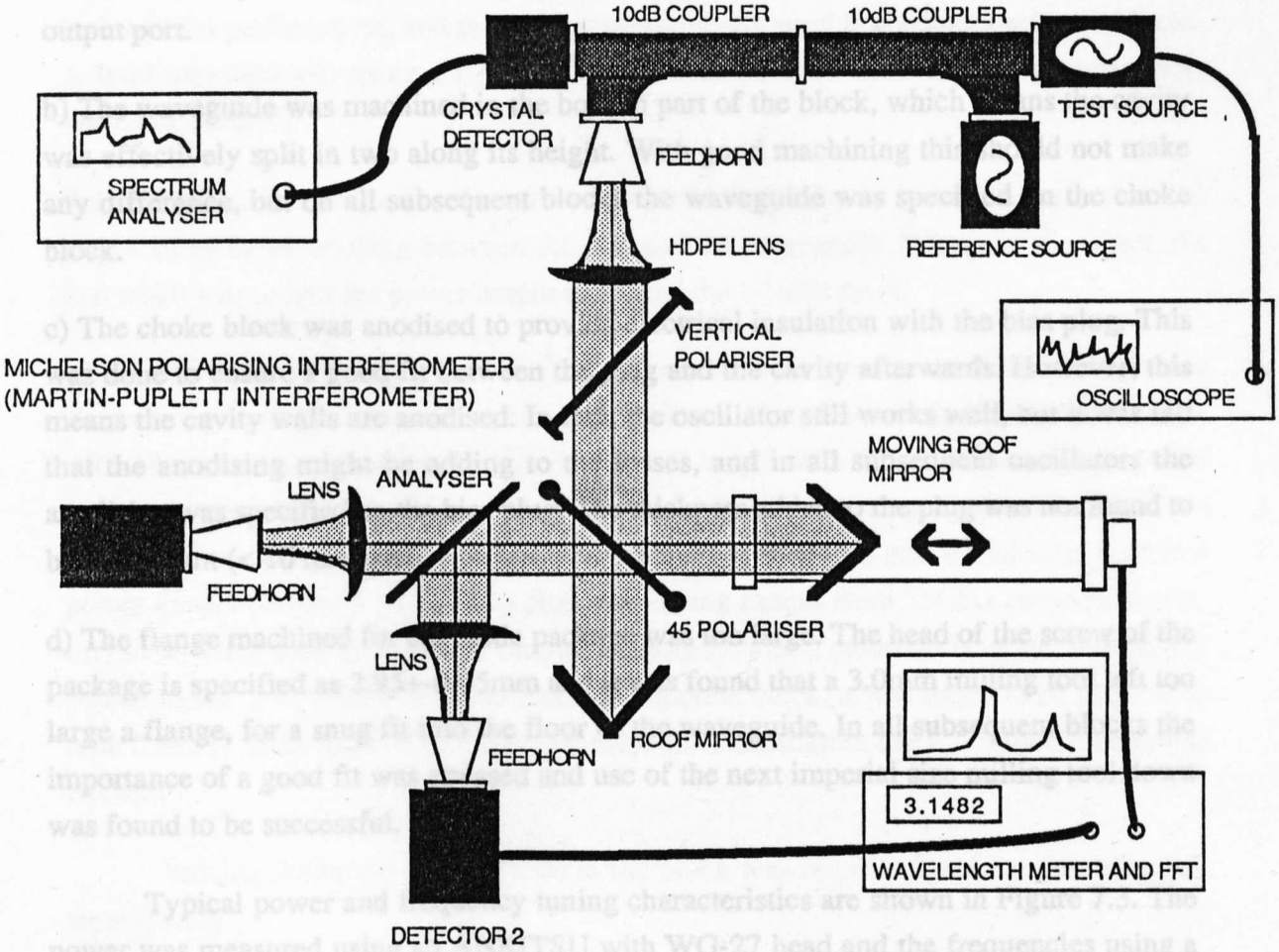

FIGURE 7.2 MEASUREMENT SETUP FOR INVESTIGATION OF FREQUENCY PULLING AND BIAS OSCILLATIONS

a) Due to a machining error it had a waveguide that essentially was reduced height WG-27 at the cavity (0.5mm high) that tapered to just 1mm high at the output port. It was thus difficult to couple to any measuring equipment without providing some reflection at the output port.

b) The waveguide was machined in the bottom part of the block, which means the cavity was effectively split in two along its height. With good machining this should not make any difference, but on all subsequent blocks the waveguide was specified on the choke block.

c) The choke block was anodised to provide electrical insulation with the bias plug. This was done to ensure a good fit between the plug and the cavity afterwards. However, this means the cavity walls are anodised. In fact, the oscillator still works well, but it was felt that the anodising might be adding to the losses, and in all subsequent oscillators the anodising was specified on the bias plug. The thickness added to the plug was not found to be significant (< 10 microns).

d) The flange machined for the diode package was too large. The head of the screw of the package is specified as 2.95+-0.05mm and it was found that a 3.0mm milling tool left too large a flange, for a snug fit into the floor of the waveguide. In all subsequent blocks the importance of a good fit was stressed and use of the next imperial size milling tool down was found to be successful.

Typical power and frequency tuning characteristics are shown in Figure 7.3. The power was measured using an ANRITSU with WG-27 head and the frequencies using a Fabry-Perot resonator. It was found that it was possible to tune from 77-105 GHz by changing the height of the cavity. Increasing the height of the cavity further, allows the next coaxial mode to appear as is indicated in Figure 7.3. Typically though the power output is down by a factor of about 3 on the "fundamental cavity mode". On some measurements there was evidence of power being produced around 60GHz before the diode jumped to the next mode at 103 GHz. This would indicate a power dip, possibly analogous to that found by Carlstrom rather than any frequency cut-off at 76 GHz due to the diode. The frequency jump from 81 GHz to 76GHz is a common feature in many tuning curves, and bears a close resemblance to a result obtained by Haydl [2] for a similar oscillator. This feature is discussed in greater detail later.

Generally, over a number of measurements, the power output was found to vary very quickly with frequency, which was taken to be an indication of a strong reflection at the output port due to the mismatch.

It was later found that by raising the diode slightly above the waveguide floor (by a few tenths of a millimeter) that a power increase of almost 50% could be achieved over a large frequency range. It was also quickly established that the thinnest discs (< 0.2mm) had the best performance, and these were subsequently used in the later oscillator blocks. A later measurement using a ANRITSU with WG-28 head showed a maximum power output of 2.8mW.

Subsequently, the flange for the screw head was deepened as it was thought that this might allow better coupling between the disc and the waveguide. Whatever the effect, the end result was to half the power output to around the 1.5mW level.

BLOCKS 2 AND 3 - Blocks 2 and 3 were made commercially at "Browns Precision Engineering" using numerically controlled machines. They were designed with half height WG-28 waveguide at the cavity tapering to full height WG-28 at the output port. After some initial machining problems, the only final minor fault was a slight widening of the cavity at the waveguide. They were found to work very well and initial tests with low power diodes (5-10mW at 94GHz) produced tuning ranges from 75GHz (waveguide cut-off) to 98 GHz with good power output, (measured with a calibrated crystal detector) as shown in Fig. 7.4. With a different diode in the same block, it was found to be possible to tune from 77 GHz to 123 GHz continuously. Both oscillators used 2.0mm diameter cap circuits.

Raising the height of the diode in the block was not found to increase the power significantly.

BLOCKS 4 AND 5 - Blocks 4 and 5 were well made and were identical to Blocks 2 and 3 except one had a quarter height WG-28 waveguide at the cavity, whereas the other had a full height WG-28 waveguide. It was quickly established that the full height waveguide worked well (>5mW power) whereas the power output of the quarter-height waveguide was low (< 1mW) for the same diode. This clearly suggests that the quarter-height waveguide is badly coupled to the radial cap cavity.

The full-height waveguide oscillator was subsequently loaned to QMC before further measurements could be made. Measurements made there, suggested powers around 8mW at 95GHz and 5mW at 100GHz with tuning limited by the mechanics of the springs inside the oscillator. However it was also reported that the power tended to go down slightly and the frequency could jump by 100MHz while the oscillator was running. This was presumably due to thermal problems. It was subsequently found that the diode used (rated at 13mW at 95GHz) was capable of much higher powers at lower frequencies.

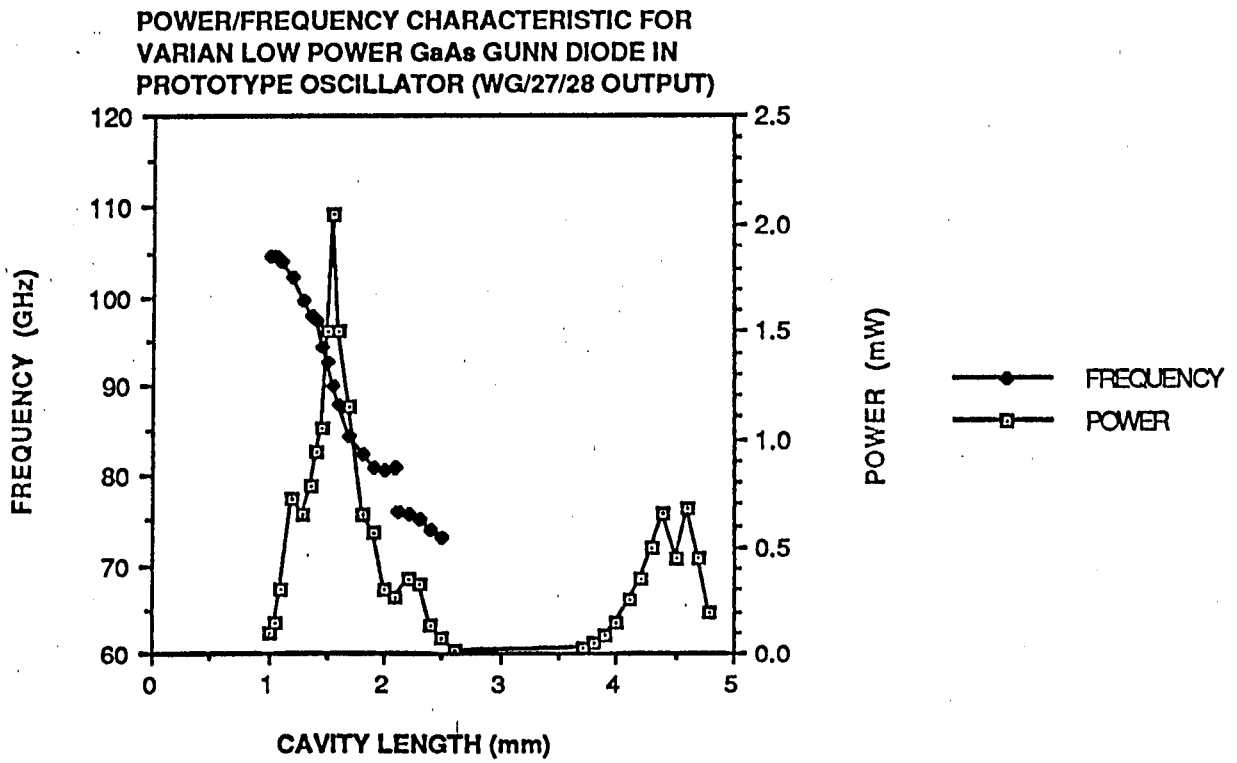

FIGURE 7.3

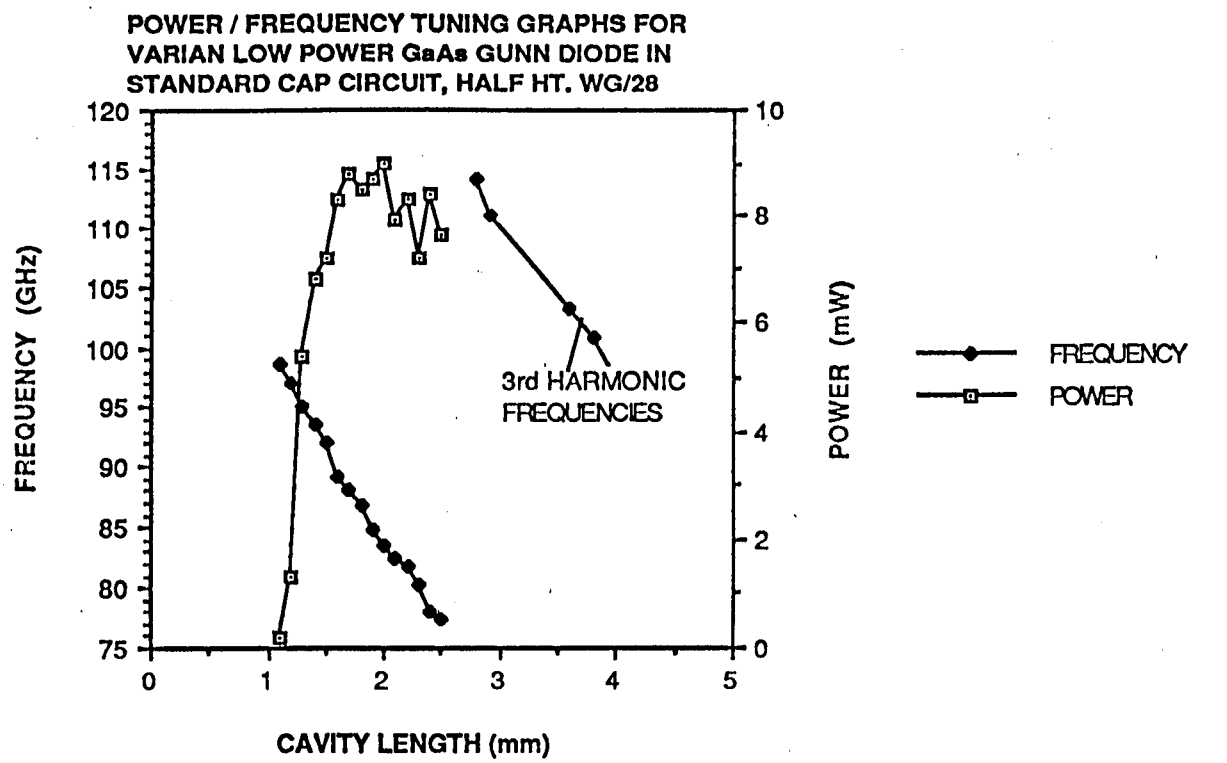

FIGURE 7.4

On return of the block, it was found that raising the diode by a few tenths of a millimetre within the block, significantly increased the power output, and addition of heatsink compound around the screwthread of the diode package, substantially improved the long term stability of the diode. The best power output obtained was 25mW at 90GHz, and typical results are shown in Fig.7.5. Power output greater than 10mW was obtained from 85GHz to 99GHz. Note that the power output at 95 GHz was over 16mW, compared to Varians quoted value of 13mW. The fact that their measurement was taken at 5.0V bias while ours was at 6.0V probably explains this anomaly. However, the choke assembly which the bias is brought through, typically has a resistance of about 1Ω, and so the results are comparable. In addition, the highest powers were all measured at the maximum allowed bias of 6V, and so it is possible that more power could have been obtained by further increasing the bias voltage. Of course, this may also pay a price in increased thermal dissipation and reduced lifetime.

This particular diode was then transferred to Blocks 13 and 14 where even larger power output was obtained.

BLOCKS 6 AND 7 - Blocks 6 and 7 were characterised by use of circular output waveguides and the absence of split blocks. They were based on the designs given by Arora and Sarma [3], where they showed that high power output was available in blocks that were essentially easy to manufacture. For example, circular waveguide allows easy manufacture of backshorts with high reflectance choke structures. In both, a special assembly was made to hold the diode, to allow it to be brought up through the waveguide floor. Its position within the cavity is therefore variable.

Block 6 had three output ports of circular waveguide of 3.0mm diameter corresponding to a frequency cut-off of 78 GHz. Two ports were used to tune the power out of the third port. Arora and Sarma reported an increase in output power of around 50% for such a scheme at a fundamental frequency of around 50 GHz, although it is not clear how advantageous the use of a second backshort is, to the coupling out of the harmonic power.

Unfortunately, the problem of coupling to any measuring equipment prevented any accurate power measurements being made, although when coupled to a calibrated crystal detector through a short piece of WG-28 waveguide, power levels comparable to those obtained in waveguide were indicated. In addition, measurements using polarisers showed that the output was essentially vertically polarised. Tuning ranges seemed very similar to those achieved with rectangular waveguide (80-105 GHz), although several adjustments

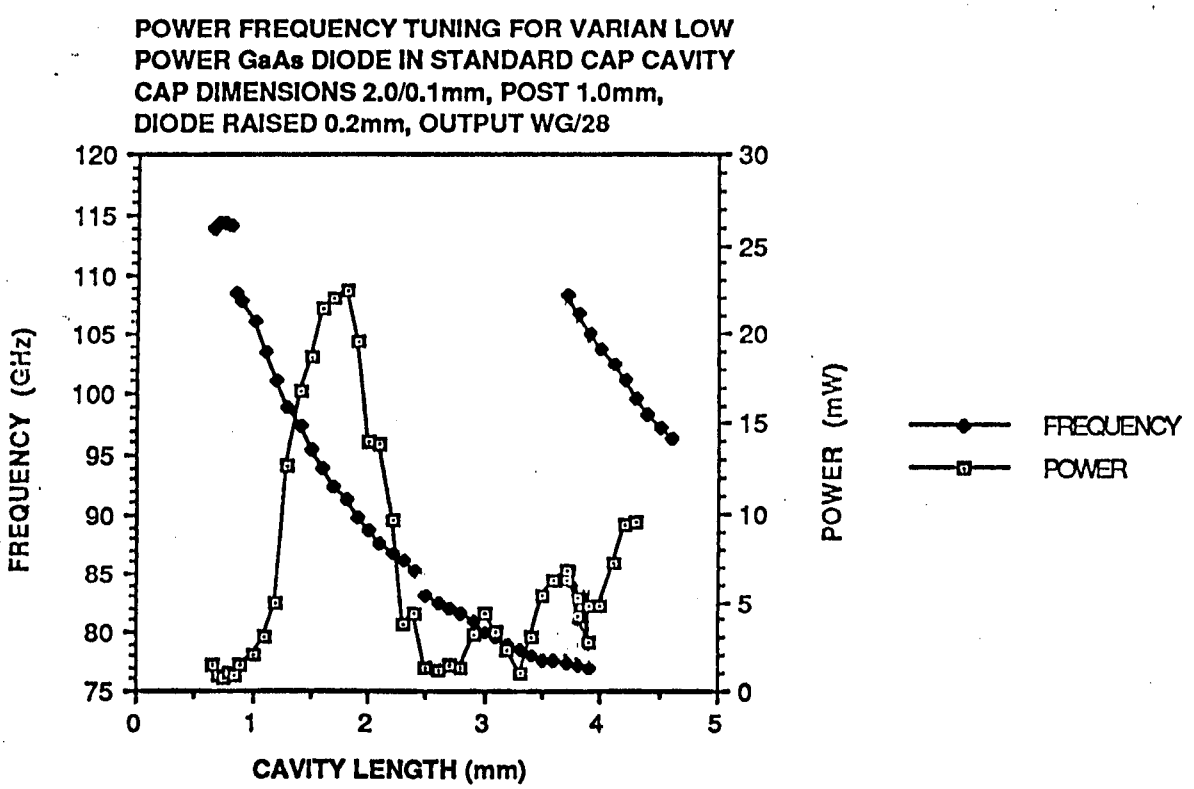

FIGURE 7.5

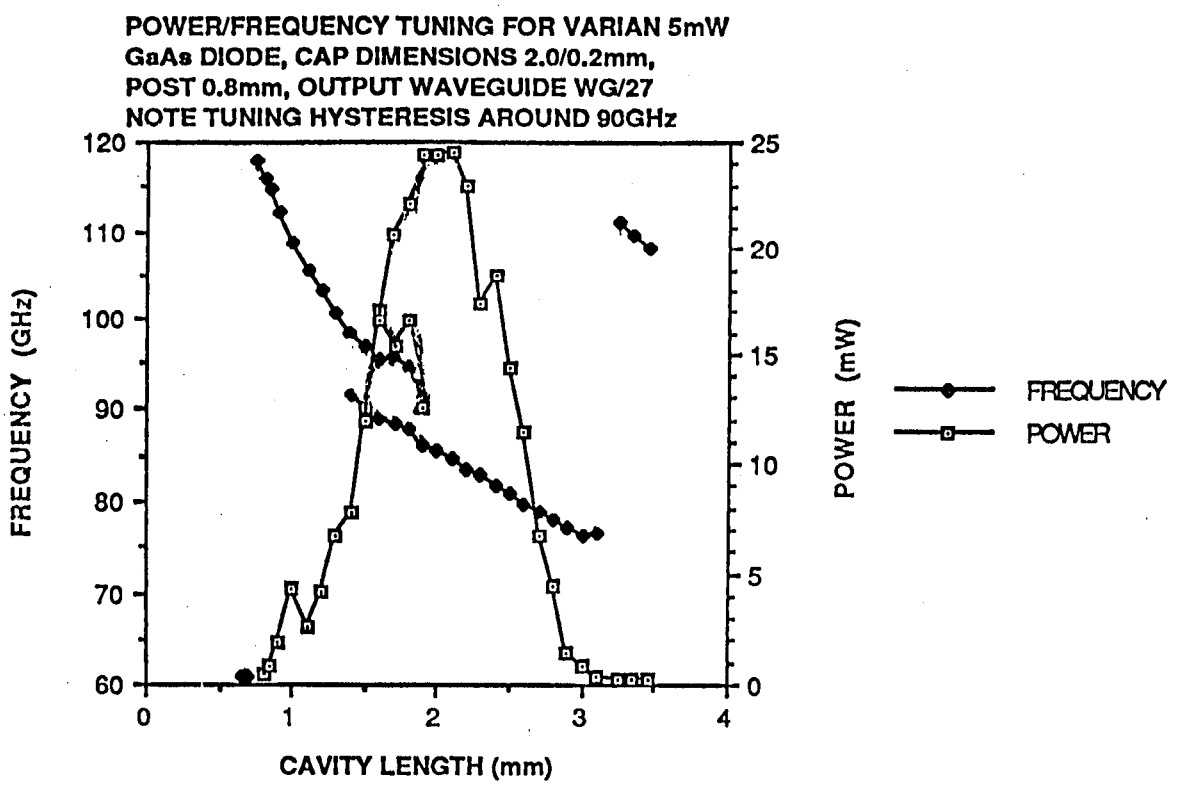

FIGURE 7.6

were needed to obtain optimum power over the full frequency range. It should also be noted that, because of the effective height of the guide, a large portion of the bias choke structure was within the guide, although this did not seem to have an appreciable effect. Largest powers were obtained when the cavity was positioned centrally with respect to the waveguide.

Block 7 was originally a reject because of a tool breaking in the circular waveguide. The waveguide was then enlarged to a diameter of 6mm approximately, to allow a test of whether the "95 GHz" Gunn diodes were fundamental or were working at a lower frequency. Tuning appeared limited, but it was apparent that the diode was capable of producing a large amount of power at frequencies around 45 GHz. This was taken as strong evidence that the diodes were producing power in second harmonic mode at 90GHz.

BLOCK 8 - Block 8 was made with a quarter height WG-28 waveguide with a 2.5mm diameter cavity. This was designed to accommodate a whole range of fixed height post/cap structures that had been made earlier for a different block design. It was hoped to be able to tune to the higher frequencies available using these structures, because of the smaller cavity and the smaller caps used. However, very low powers were always obtained and so not much further work was done, although frequencies of 110, 115 and 117 GHz were measured, which at the time, were the highest frequencies achieved. With hindsight, the quarter height waveguide was too small to allow good coupling to the radial mode set up below the cap. There was thus no effective impedance transformation at the second harmonic. Very low powers were also obtained whenever a coaxial circuit was used in any block for any harmonic oscillator.

BLOCKS 9 and **10** were full height WG-27 waveguide and **BLOCKS 11** and **12** were full height WG-28 waveguide. Initial results indicated very successful operation, although the importance of positioning the diode centrally beneath the cap also became apparent. Very low power outputs were achieved with one block, that was nominally identical to another. The problem was eventually traced to the fact that the diode was not centrally positioned in one block, but was out by about 0.1mm. Removal of the steel pins and positioning of the split block by hand, before screwing the blocks back together, considerably improved the output power.

BLOCKS 13 and **14** were made by EEV. Block 13 consisted of the normal cavity intersecting with a full height WG/27 waveguide and Block 14 had a full height WG/28 waveguide. Both were very accurately machined and had an improved spring loaded backshort drive. In addition, choke structures and caps were manufactured so that post

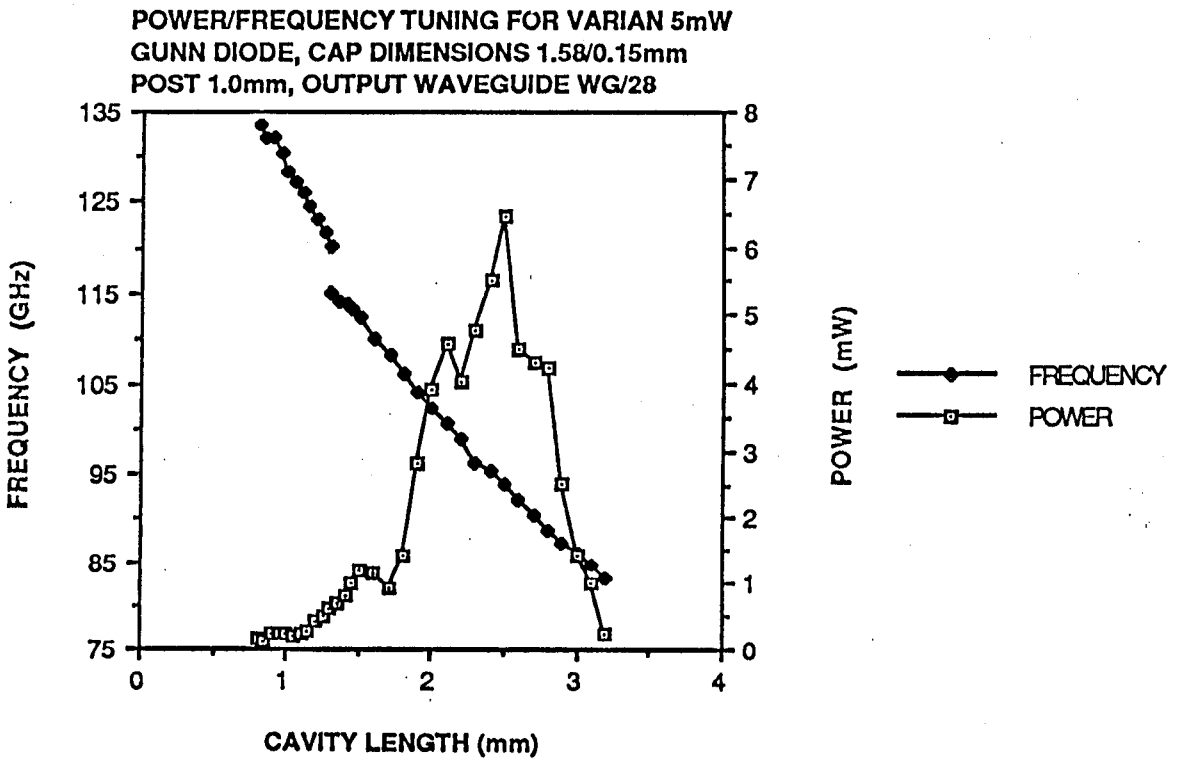

FIGURE 7.7

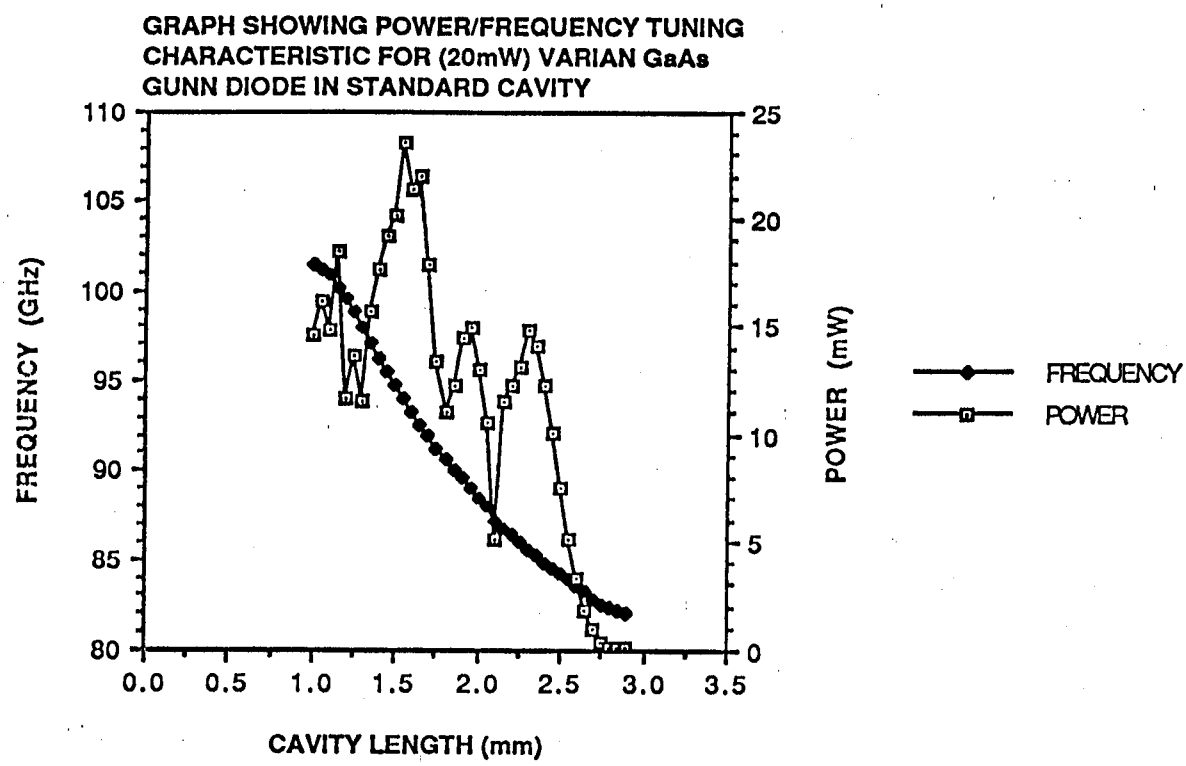

FIGURE 7.8

diameters of 0.8mm could be accommodated. The only initial difficulty was that the third section of the block had been shortened significantly, which made it difficult to fit in the safety circuit, and limited the tuning range. In addition, the spring that loaded the choke structure had to be very small and comparatively weak, which gave some initial problems involving backlash. Nevertheless, these blocks have given output powers in excess of 29 mW at 90 GHz (for a diode rated at 13mW at 95GHz), which shows that these oscillators are inherently capable of producing high power outputs given an appropriate diode. The achievement of 29mW required very critical adjustment of the diode though, and more repeatable results are shown in Fig 7.6 for the WG/27 waveguide.

To see how far the diode could tune, the same diode was then placed in the WG/28 waveguide (cutoff 75GHz) with a 1.58mm diameter cap, which should lower the coupling as well as allowing tuning to higher frequencies. The results are shown in Fig. 7.7, and show that power can be obtained up to a frequency of at least 133GHz.

All the results quoted above were from Varian diodes which were bought nominally at a power rating of 5mW at 94GHz, (although the power quoted at 94GHz was typically in the range 5-14mW). Since then higher power 20mW Varian diodes have been used, which have shown similar tuning characteristics but at higher power levels. A typical result is illustrated in Figure 7.8.

7.5 INITIAL OBSERVATIONS

From the above results the following general conclusions and observations were drawn.

a) It is possible to obtain power outputs at the manufacturers specification with over large tuning ranges using this type of tuneable cavity.

b) The importance of accurate machining of the waveguide and cavity, and the central and accurate location of the diode with respect to the cavity.

c) There appeared to be no advantage of having half-height waveguide (to reduce the impedance transformation) rather than full height waveguide at the cavity, and quarter height waveguide was clearly worse. Full height waveguide was therefore specified in the design of all future blocks.

d) Frequency jumps of a few GHz were noted in many of the tuning curves. At the time this was an unexpected and unwelcome feature, as it had not been seen in the results

reported on by Carlstrom. The position of the frequency jump was influenced by the size of cap.

e) As previously noted power output and tuning characteristic are a strong function of cap size. Very little power is produced for a coaxial type cavity when the diode is operating in harmonic mode.

f) For a particular cap power output could be maximised by changing the position of the diode with respect to the cavity. This has also been reported by others who have indicated significant power increases by rotating the diode within the block. Presumably this changes the effective inductance of the bonding leads, depending on their proximity to the waveguide walls.

g) Power output and frequency tuning characteristics can vary from diode to diode in nominally identical circuits. It would appear in most cases each Gunn diode needs individual matching to the circuit for optimum performance.

7.6 M.E.D.L. n+ n n+ 94GHz GaAs GUNN DIODE

A more detailed study of the effect of certain circuit parameters was made on a n+ n n+ second harmonic GaAs diode supplied by MEDL. It was tested in a number of different cavity configurations and found to exhibit a number of interesting properties. The diode had a large d.c negative differential conductance, and and operated at significantly higher current levels than the Varian diodes. It was capable of producing large amounts of power (50mW+) when optimally matched into a resonant cap circuit. The power maximum seemed to be situated around 87-88GHz, falling off below 80GHz and above 110GHz. Power output was obtained at second harmonic frequencies as high as 124GHz and as low as 70GHz.

7.6.1 THE TEST DIODE

The diode was specified as:

$V_{th} = 1.2V$
$I_{th} = 920mA$
$I_{op} = 550mA$

V_{op} = 5.76V
F_{op} = 95.0GHz
P_{op} = 41mW

7.6.2 THE I/V CURVE

I/V curves measured at d.c have to be used with some care when applied at rf frequencies, as heating effects, electron scattering, velocity overshoot and current limiting cathode structures may all contribute, to significantly change the rf characteristic. However, some general comments can be made on the I/V curves obtained. The IV characteristic was a function of frequency and typical results are shown in Figs. 7.9a, b and c. There is a large current drop above threshold, and this begins to flatten out about 2.5V above threshold. Jumps in the voltage occur at the steepest part of the negative region and frequency jumps between 1 and 2GHz occur between these voltage jumps. Bias oscillations tended to disappear, when the flat part of the characteristic was reached. This was often at fairly high voltages around 5V. This tended to occur at higher voltages, at the lower frequencies.

Our circuits have a series resistance of between 1-2Ω and so threshold and optimum power output occurred at slightly higher voltages than the diode specification, although the threshold and optimum current values were the same (as one might expect).

Figure 7.19b has a lower threshold voltage than is indicated in Figs. 7.9a and 7.9c, because a parallel inductor/resistor arrangement was removed from the block which was adding to the series d.c resistance (and having little effect on the bias oscillations).

The jumps in the I/V curve are primarily an effect caused by the the large negative conductance. The power supplies that were used did not have sufficiently low d.c. output impedance to match the diode at the point of maximum negative conductance. The comparatively large frequency jumps on either side of the voltage jump, are either signs that the device capacitance varies greatly with voltage or that the bias oscillations are having a significant effect on the rf impedance. As is shown later there can be a large change in frequency (≈1GHz) just above threshold in many diodes.

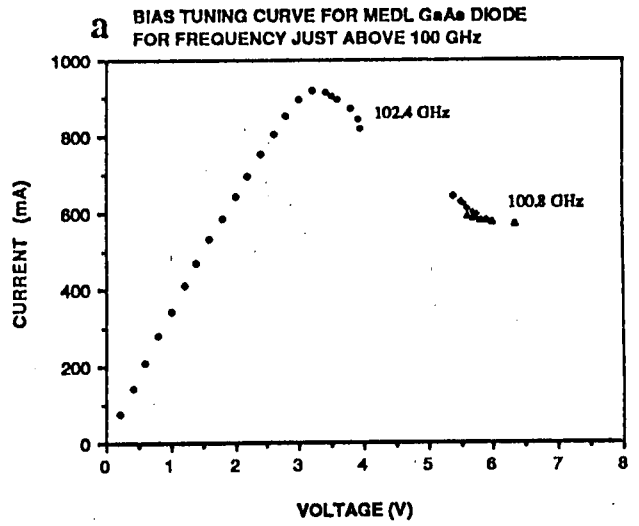
a
BIAS TUNING CURVE FOR MEDL GaAs DIODE
FOR FREQUENCY JUST ABOVE 100 GHz
102.4 GHz
100.8 GHz
CURRENT (mA)
VOLTAGE (V)

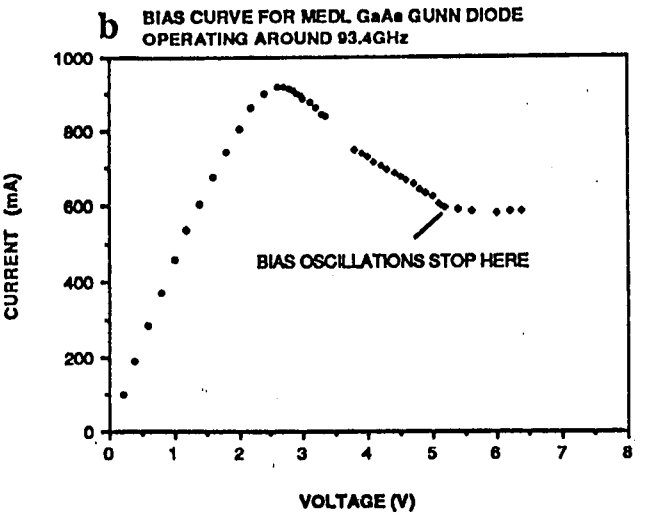
b
BIAS CURVE FOR MEDL GaAs GUNN DIODE
OPERATING AROUND 93.4GHz
BIAS OSCILLATIONS STOP HERE
CURRENT (mA)
VOLTAGE (V)

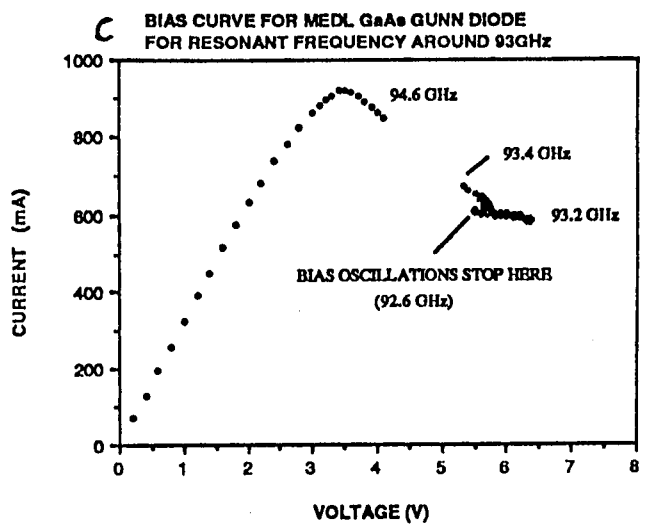
C
BIAS CURVE FOR MEDL GaAs GUNN DIODE
FOR RESONANT FREQUENCY AROUND 93GHz
94.6 GHz
93.4 GHz
93.2 GHz
BIAS OSCILLATIONS STOP HERE
(92.6 GHz)
CURRENT (mA)
VOLTAGE (V)

FIGURE 7.9

7.6.3 BIAS OSCILLATIONS

Bias oscillations invariably occurred just above threshold and only disappeared after the voltage jump to the flat part of the IV characteristic. However, in addition some difficulty was experienced in mixing experiments as it was found that it was also possible to induce bias oscillations, and chaotic type noise at low frequencies (<1GHz) if rf power at a slightly different frequency was shone at the diode.

Typically, these ranged from large 3-10 MHz oscillations at amplitudes of about 50-200mV which typically occurred just above the voltage jump, to smaller oscillations around 80MHz just above threshold. Spurious noise and oscillations at various frequencies up to 700MHz, were also observed.

The detailed behaviour of the bias oscillations, depended on the frequency of oscillation, bias voltage but also seemed to be induced by rf shone back at the diode. In one particular measurement, power from two oscillators were sent into a fast crystal detector via two 10dB couplers (without a circulator) in order to make appropriate heterodyne measurements. Subsequent measurement showed that the type of crystal used was very badly matched to the waveguide, and it is likely that a substantial VSWR was set up between the detector/backshort combination and the oscillators. The oscillations were sometimes seen to disappear with adjustment of the backshort on the detector and on the test oscillator, and with adjustments to the bias. They were less common at high bias voltages. They also disappeared when the second oscillator was switched off. This would seem to imply that the oscillations observed were induced by the coupling of rf power at a slightly different frequency into the diode/circuit. This may have practical implications in certain system applications.

It should be noted that no such oscillations had been seen with Varian diodes in exactly the same experimental set-up.

7.6.4 FREQUENCY AND POWER CHARACTERISTICS

The frequency and power tuning characteristics of the diode are illustrated in Figs. 7.10 to 7.17. At the time of testing the ANRITSU power meter was not available and a crystal detector was used to measure relative power output. These power readings were subsequently calibrated by an ANRITSU power meter and which showed a calibration of 6.3mW per unit with good accuracy across the band.

It soon became apparent that careful matching was needed to obtain optimum power outputs at any desired frequency. Most power was obtained when the diode was raised very significantly compared with the waveguide (0.6mm). It may well be that optimum matching may be most easily achieved with an oscillator with a reduced height waveguide input to the cavity.

As with the Varian diodes it was also noted that the bias level for maximum power output went down with increasing frequency.

The impedance transformation at the second harmonic and the tuning characteristic at the fundamental frequency, can be altered as outlined in Chapter 6 by changing the capacitance associated with the cap. Increasing the capacitance can be achieved by increasing the size of the cap or reducing the diameter of the post. In addition, any change which puts a discontinuity further into the region of high electric field can be expected to have a similar effect.

The first experiment used a cap of diameter 2.0mm, thickness 0.1mm, and post diameter 0.8mm at three different positions of the diode. The results are shown in Figs 7.10 - 7.12. There was an unwanted frequency jump roughly between 94 and 102GHz, and between 78 and 73GHz. The power maximum occurred roughly between 83 and 88Ghz and was most apparent when the diode was raised 0.6mm in cavity height. At a cavity length of 3.85mm simultaneous oscillation at 70 and 91GHz were obtained in this configuration, just before the oscillation jumped to the next cavity mode. Multiple oscillations were a feature of the behaviour of the diode, and they typically occurred just before or after a frequency jump at fairly low voltage levels.

Changing the thickness of the cap to 0.2mm introduces slightly more capacitance as one of the discontinuities is placed in a region of higher electric field. (Although this will not necessarily be true as the disc thickness is further increased). The jump now occurs between the frequencies of 80 and 92GHz and also exhibits a "flat frequency region" at around 83GHz. The multiple frequencies obtained at very short cavity heights are not really understood, but are probably related to the effect of a multiple resonant circuit as outlined in Chapter 4.

The diode can now oscillate at 94-95GHz, although the frequency jump, now clearly occurs in the region of maximum power output (Fig 7.13), which is not very satisfactory. Ideally, the jump should be at a lower frequency, which would probably be best achieved by slightly increasing the diameter of the cap, or reducing the diameter of the

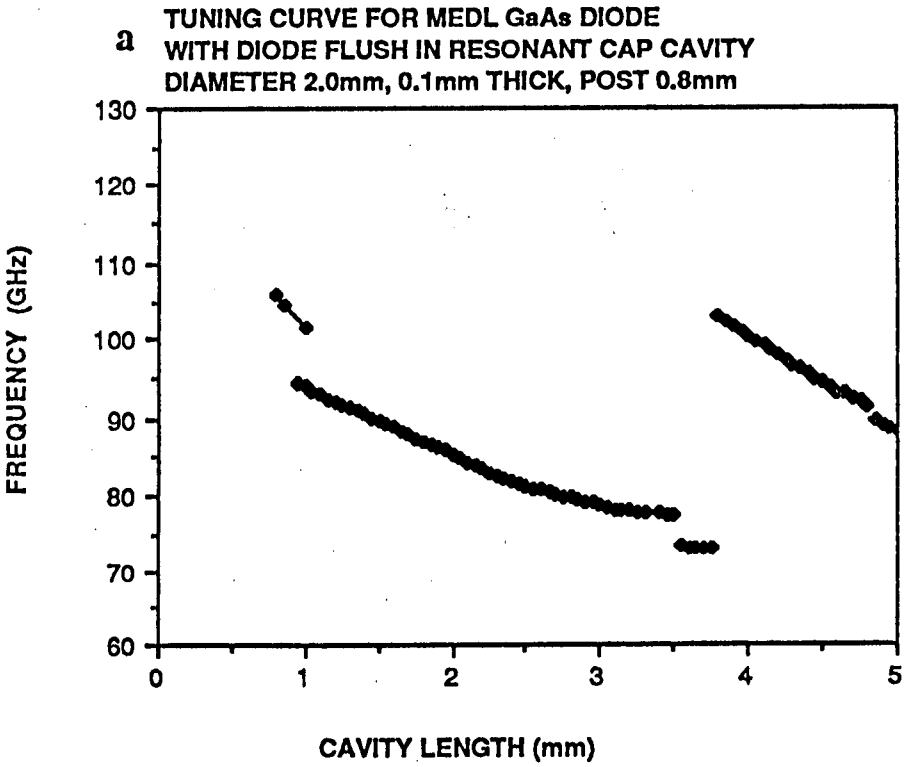
a
TUNING CURVE FOR MEDL GaAs DIODE
WITH DIODE FLUSH IN RESONANT CAP CAVITY
DIAMETER 2.0mm, 0.1mm THICK, POST 0.8mm
FREQUENCY (GHz)
130
120
110
100
90
80
70
60
0
1
2
3
4
5
CAVITY LENGTH (mm)

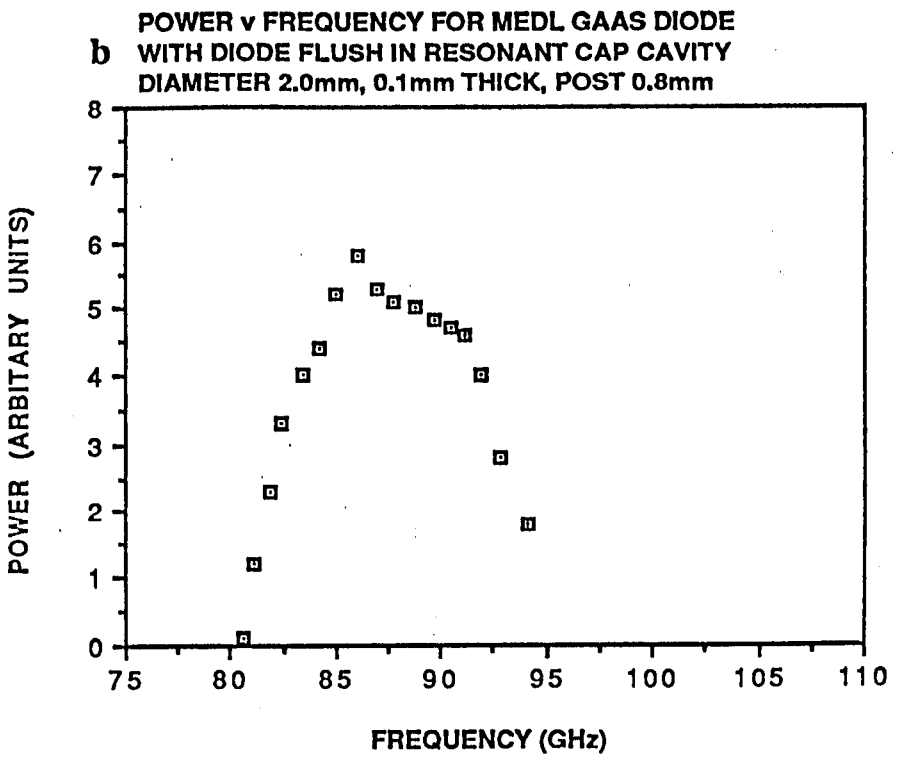
b
POWER v FREQUENCY FOR MEDL GAAS DIODE
WITH DIODE FLUSH IN RESONANT CAP CAVITY
DIAMETER 2.0mm, 0.1mm THICK, POST 0.8mm
POWER (ARBITARY UNITS)
8
7
6
5
4
3
2
1
0
75
80
85
90
95
100
105
110
FREQUENCY (GHz)

FIGURE 7.10

a

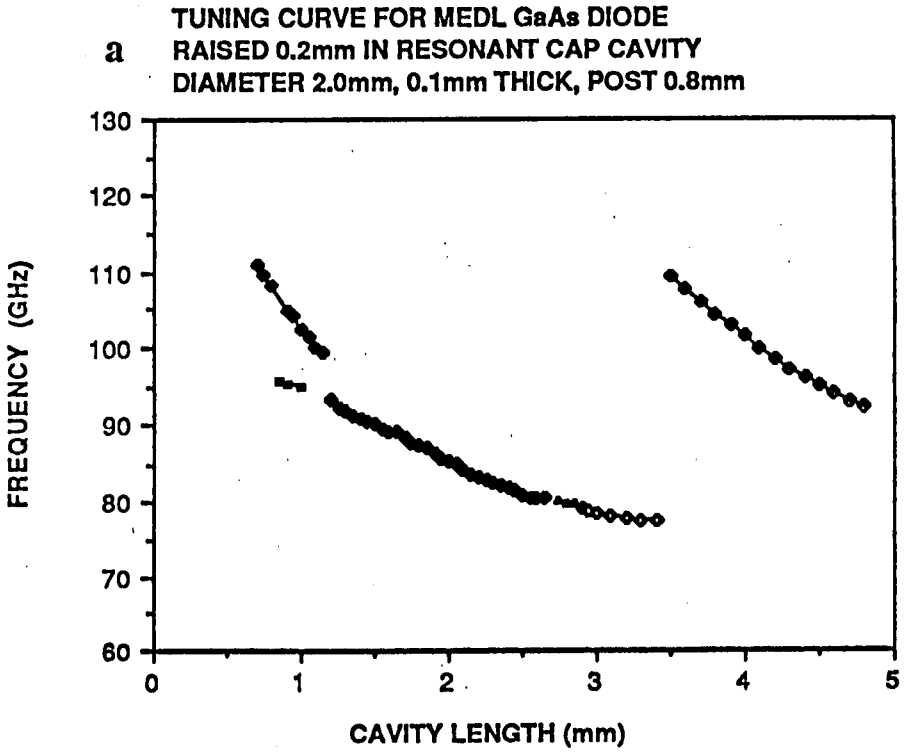

b

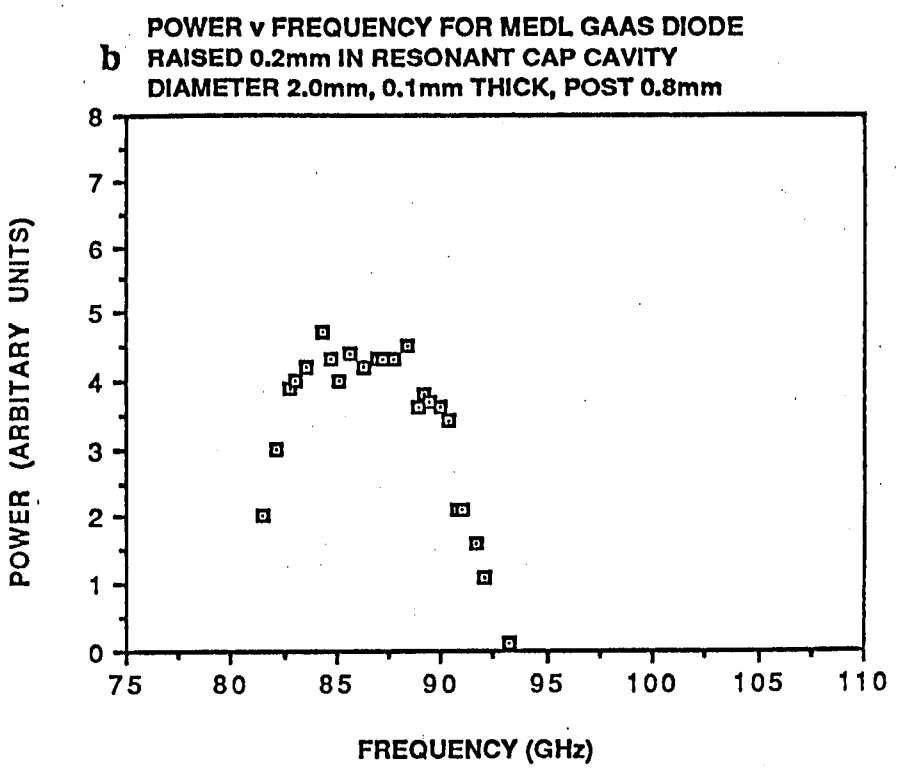

FIGURE 7.11

a TUNING CURVE FOR MEDL GaAs GUNN DIODE
RAISED 0.6mm IN RESONANT CAP CAVITY
DIAMETER 2.0mm, 0.1mm THICK, POST 0.8mm

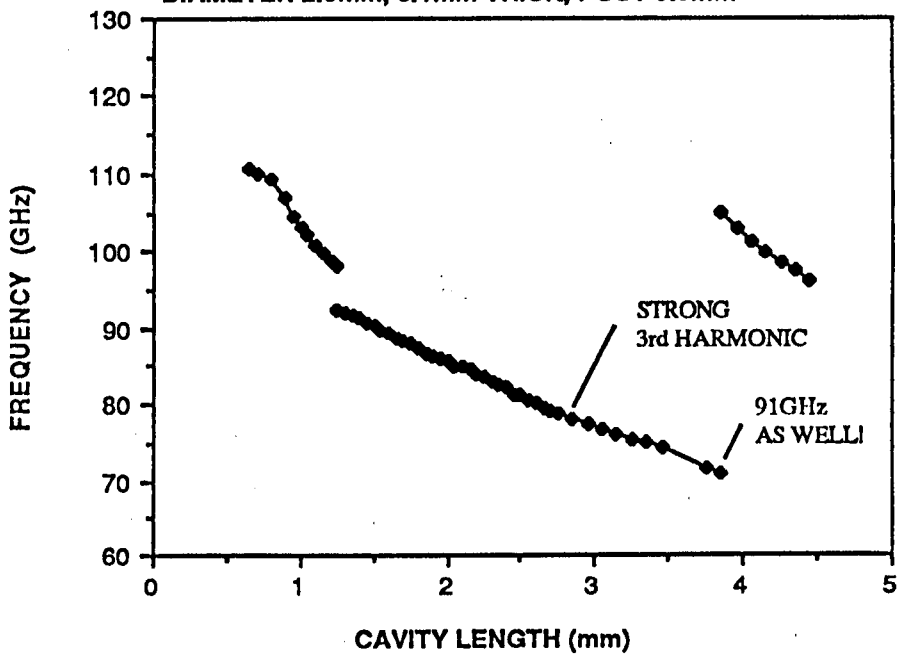

b POWER v FREQUENCY FOR MEDL GaAs DIODE
RAISED 0.6mm IN RESONANT CAP CAVITY
2.0mm DIAMETER, 0.1mm THICK, 0.8mm POST

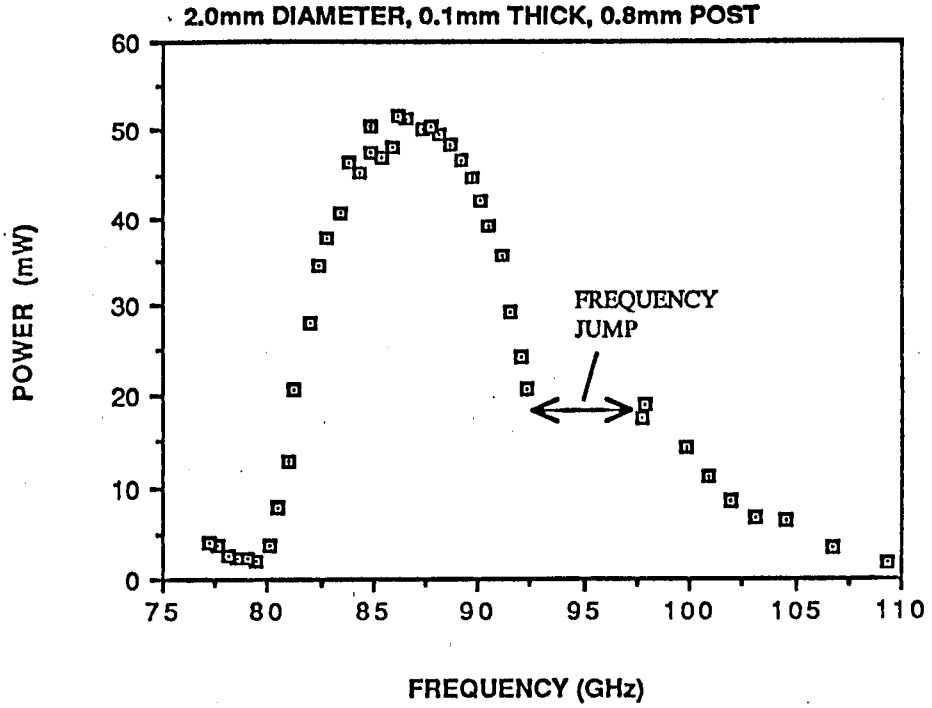

FIGURE 7.12

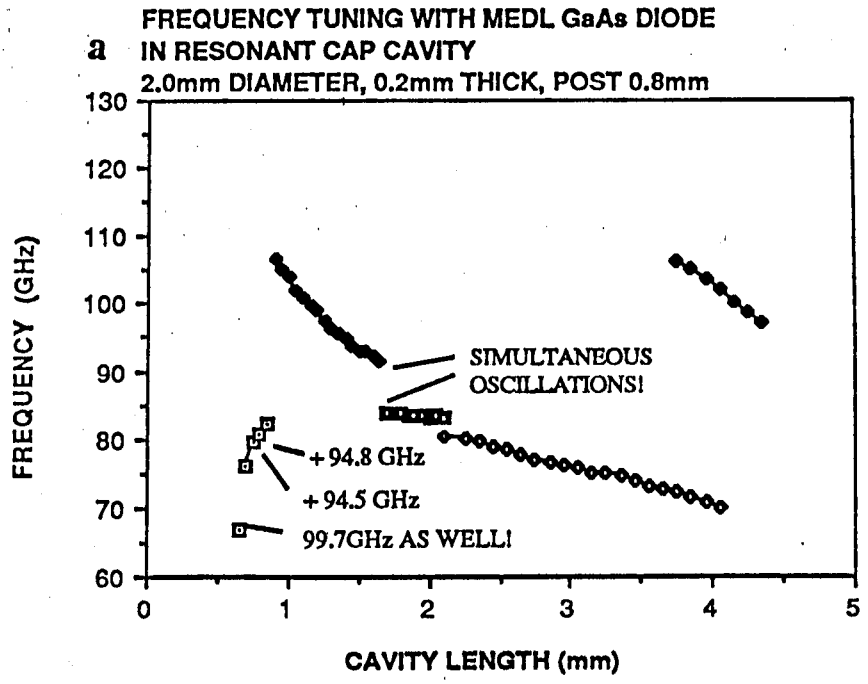
a
FREQUENCY TUNING WITH MEDL GaAs DIODE
IN RESONANT CAP CAVITY
2.0mm DIAMETER, 0.2mm THICK, POST 0.8mm
FREQUENCY (GHz)
130
120
110
100
90
80
70
60
0
1
2
3
4
5
CAVITY LENGTH (mm)
SIMULTANEOUS
OSCILLATIONS!
+94.8 GHz
+94.5 GHz
99.7GHz AS WELL!

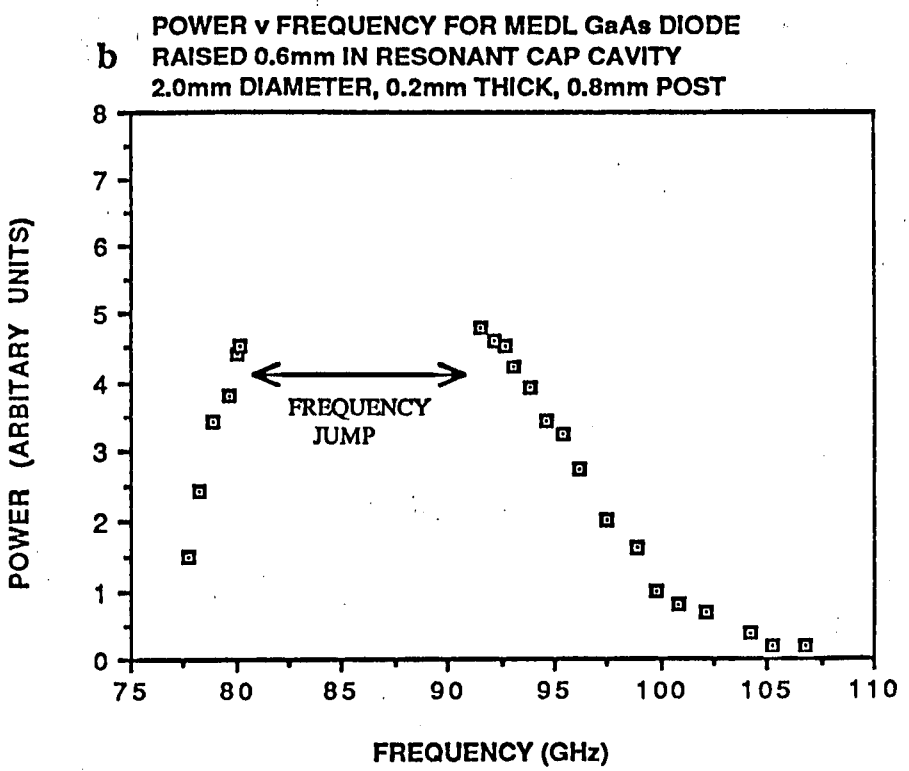
b
POWER v FREQUENCY FOR MEDL GaAs DIODE
RAISED 0.6mm IN RESONANT CAP CAVITY
2.0mm DIAMETER, 0.2mm THICK, 0.8mm POST
POWER (ARBITARY UNITS)
8
7
6
5
4
3
2
1
0
75
80
85
90
95
100
105
110
FREQUENCY (GHz)
FREQUENCY
JUMP

FIGURE 7.13

post. However, moving the resonance well away from the desired frequency, does not necessarily allow optimum coupling at 94-95 GHz.

The alternative is to move the resonance above 95 GHz which can be achieved by reducing the capacitance. This was achieved by using a larger diameter post, although a similar affect could almost certainly be achieved by using a slightly smaller diameter cap. Using a 2.0mm diameter cap, 0.2 mm thick, but a post 1.0mm in diameter, the results shown in Figs 7.14-7.16 were obtained. Here the frequency jumps occur between 107 and 116GHz, and 78-81GHz which allows a much more satisfactory tuning range. There is also a small jump around the 87-88GHz frequency. In one oscillator at low voltages, six simultaneous oscillation frequencies were obtained all separated by about 5GHz, just after a frequency jump.(Fig.7.15)

Lastly, to try and look how far the oscillator would tune, the diode was placed in a coaxial cavity of inner diameter 0.8mm, and Fig. 7.17 shows the tuning characteristic. Power was obtained at frequencies as high as 124GHz, where the fundamental frequency was above cut-off and also present in the output. The power output was low throughout the whole tuning range due to the bad coupling between the coaxial cavity and the full-height waveguide.

Figure 7.18 shows the variation of power with backshort position. As expected, the output is a strong function of backshort position and the characteristic is repeated every half guide wavelength. This type of characteristic was very typical of all diodes tested.

7.6.5 CONCLUSIONS

The MEDL diode is a low impedance device capable of high output power for a GaAs Gunn diode with a tuning range very similar to that found with Varian/GEC diodes. The largest power output was obtained at 88GHz and usable power output was obtained in the 78-105 GHz range. However, the diode/circuit did seem susceptible to bias and multiple oscillations, under certain circuit conditions. These problems arose whenever the diode was biased in the region of high negative differential resistance which typically existed beyond 5V. (Fig.7.9)

It can be seen that raising the diode relative to the waveguide floor did not significantly affect the tuning characteristic of the diode, but strongly affected the second harmonic power output. This would indicate that it does not affect the impedance seen at the fundamental frequency but strongly affects the impedance transformation at the second

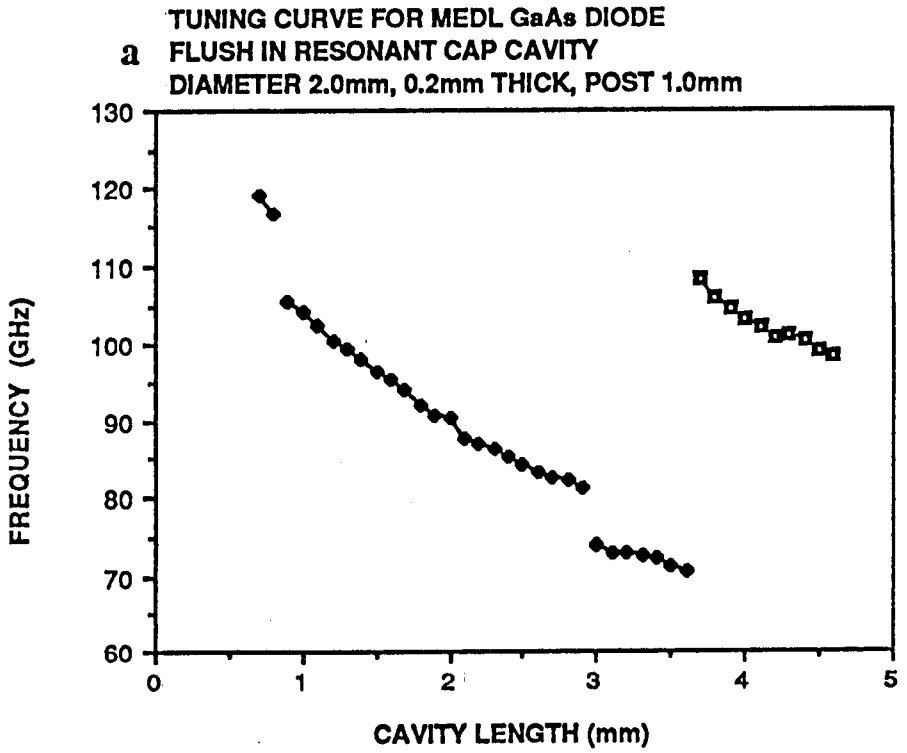
a
TUNING CURVE FOR MEDL GaAs DIODE
FLUSH IN RESONANT CAP CAVITY
DIAMETER 2.0mm, 0.2mm THICK, POST 1.0mm
FREQUENCY (GHz)
130
120
110
100
90
80
70
60
0
1
2
3
4
5
CAVITY LENGTH (mm)

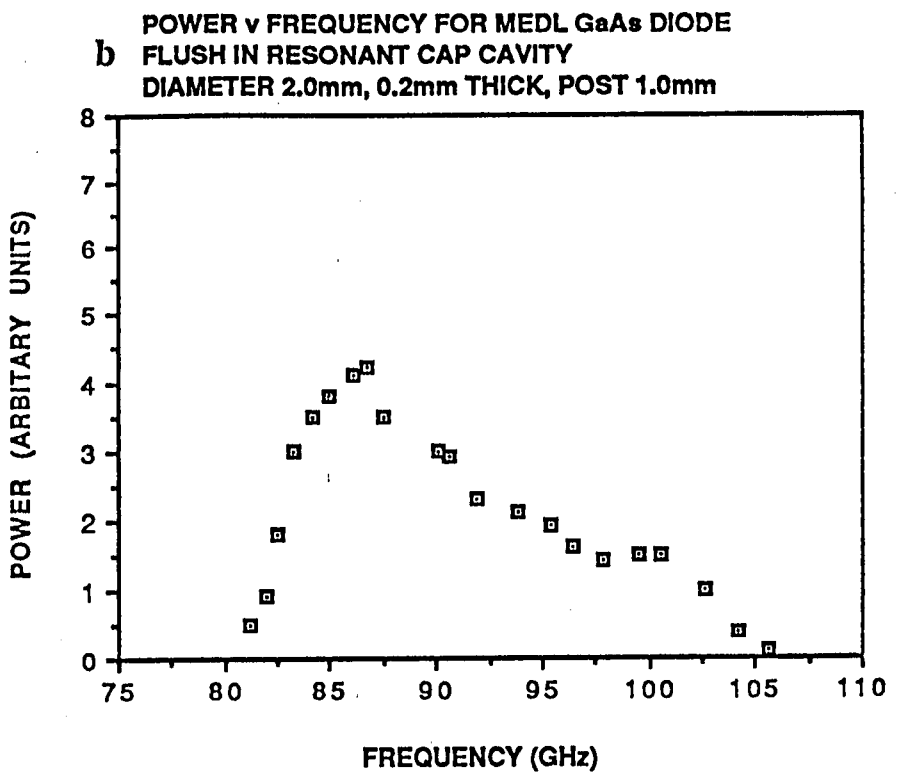
b
POWER v FREQUENCY FOR MEDL GaAs DIODE
FLUSH IN RESONANT CAP CAVITY
DIAMETER 2.0mm, 0.2mm THICK, POST 1.0mm
POWER (ARBITARY UNITS)
8
7
6
5
4
3
2
1
0
75
80
85
90
95
100
105
110
FREQUENCY (GHz)

FIGURE 7.14

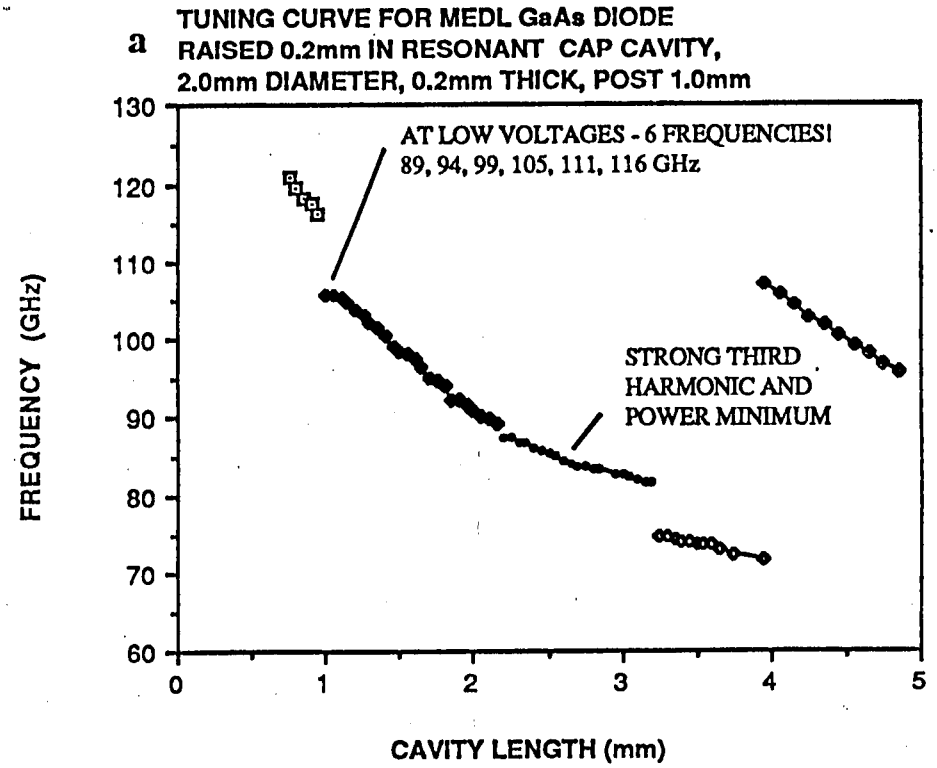
a
TUNING CURVE FOR MEDL GaAs DIODE
RAISED 0.2mm IN RESONANT CAP CAVITY,
2.0mm DIAMETER, 0.2mm THICK, POST 1.0mm
AT LOW VOLTAGES - 6 FREQUENCIES!
89, 94, 99, 105, 111, 116 GHz
STRONG THIRD
HARMONIC AND
POWER MINIMUM
FREQUENCY (GHz)
130
120
110
100
90
80
70
60
0
1
2
3
4
5
CAVITY LENGTH (mm)

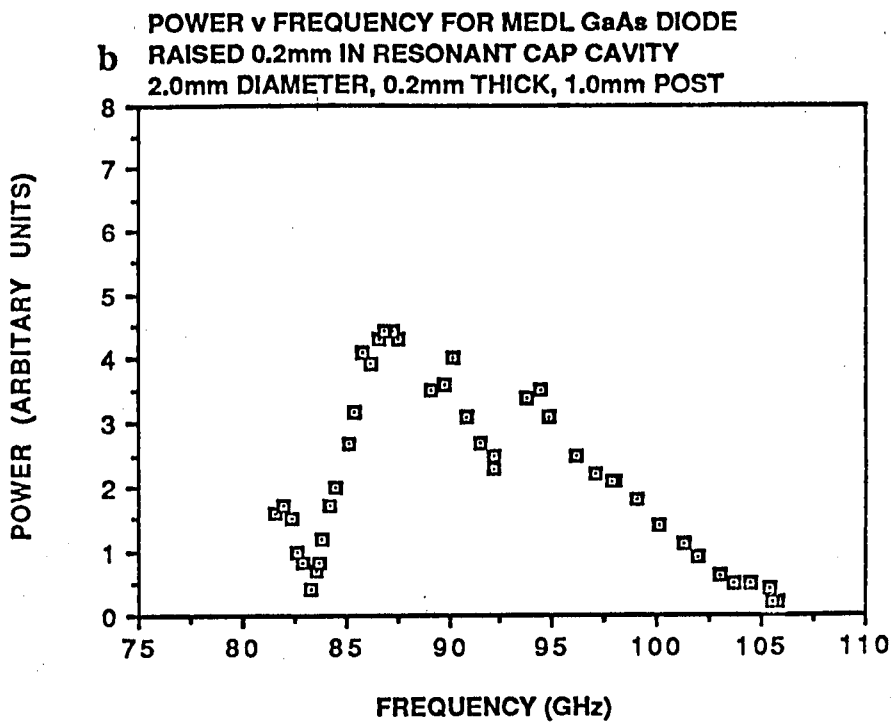
b
POWER v FREQUENCY FOR MEDL GaAs DIODE
RAISED 0.2mm IN RESONANT CAP CAVITY
2.0mm DIAMETER, 0.2mm THICK, 1.0mm POST
POWER (ARBITARY UNITS)
8
7
6
5
4
3
2
1
0
75
80
85
90
95
100
105
110
FREQUENCY (GHz)

FIGURE 7.15

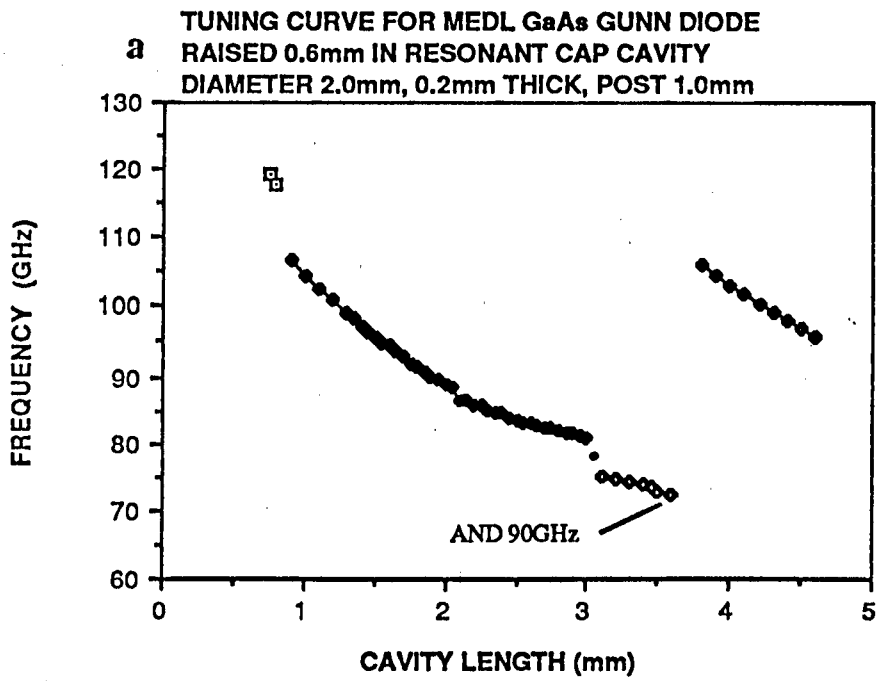
a
TUNING CURVE FOR MEDL GaAs GUNN DIODE
RAISED 0.6mm IN RESONANT CAP CAVITY
DIAMETER 2.0mm, 0.2mm THICK, POST 1.0mm
FREQUENCY (GHz)
130
120
110
100
90
80
70
60
AND 90GHz
0
1
2
3
4
5
CAVITY LENGTH (mm)

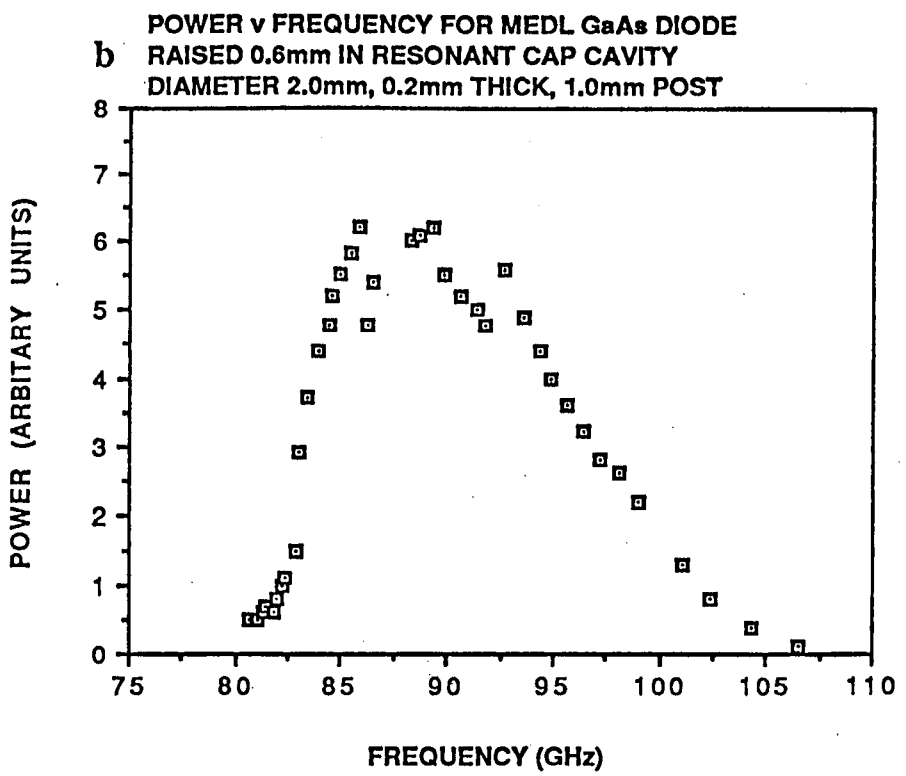
b
POWER v FREQUENCY FOR MEDL GaAs DIODE
RAISED 0.6mm IN RESONANT CAP CAVITY
DIAMETER 2.0mm, 0.2mm THICK, 1.0mm POST
POWER (ARBITARY UNITS)
8
7
6
5
4
3
2
1
0
75
80
85
90
95
100
105
110
FREQUENCY (GHz)

FIGURE 7.16

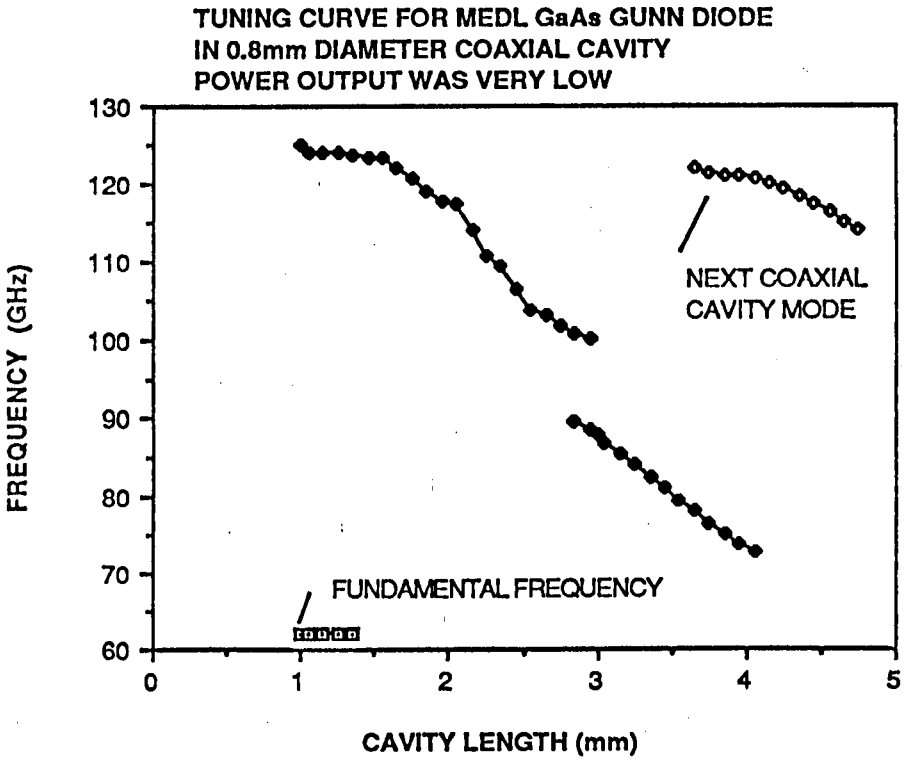

FIGURE 7.17

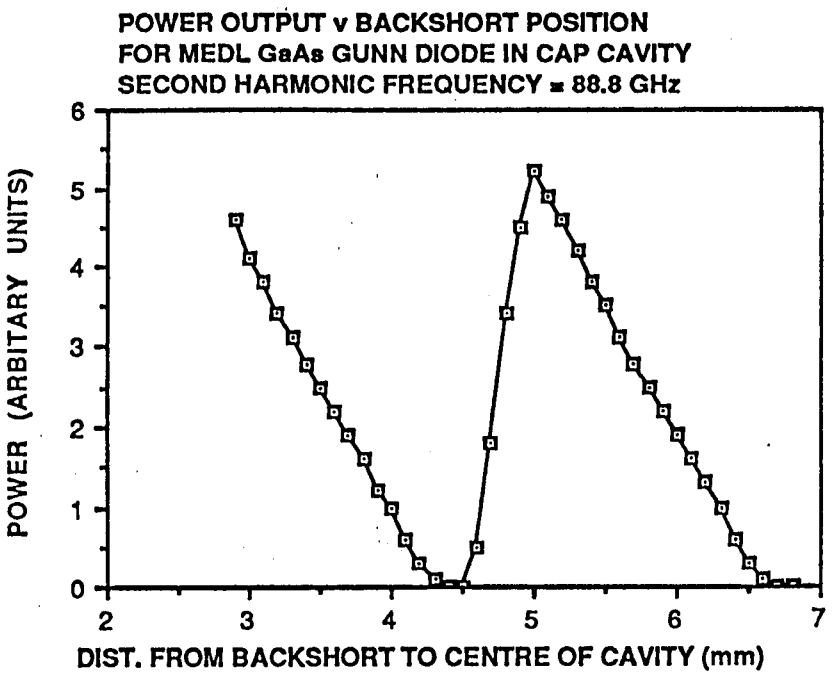

FIGURE 7.18

harmonic. A change of cap size changes the impedance seen at both the fundamental and second harmonic, which makes its effect difficult to determine beforehand. However, this parameter can be used to change the position of frequency jumps and power dips effectively which are assumed to be effects at the fundamental and harmonic frequencies respectively.

Great care was observed in handling and tuning, and no attempt was made to take the voltage over 6.3V, which was below the optimum voltage at many of the lower frequencies. It is still not clear how close the diode was to critical matching, although the maximum power output obtained at 94 GHz was slightly greater than the specification given at MEDL.

7.7 G.E.C./M.E.D.L. GaAs GRADED GAP GUNN DIODES

Another set of diodes that were tested were various second harmonic GaAs diodes with graded gap cathode structures (see Chapter 2) manufactured by MEDL and GEC. Five different batches of diodes were received and tested in various tuneable cavities. They differed in the respect of having different active carrier lengths and doping parameters, and it was hoped to use the tuneable cavities to find the optimum operating frequency for each batch. One of the advantages of looking at the second harmonic frequency when characterising a diode is that some power is always produced (Chapter 5), almost no matter how bad the coupling (at the 2nd harmonic). This compares with the fundamental frequency where oscillation can not be attained if the loading is too great. Thus the full tuning range of the diode can be examined by looking at the second harmonic output.

The diodes were designated as:

GEC DB742/1 (DIODE NUMBERS 3,4,5,6,7)
GEC DB736/1 (DIODE NUMBERS 3,4,5,6(1),6(2)) Two 6's!
GEC CAV 223 (2 DIODES)
GEC CAV 224 (3 DIODES)
GEC CAV 225 (4 DIODES)

Both DB742 and DB736 were similar structures and gave good power around 80GHz, when placed in resonant cap circuits. The maximum power achieved was greater than 62 mW from DB742/1/6 at 80GHz. The other diodes had shorter active lengths with CAV 223 giving good fundamental power around 60GHz and second harmonic power

between 90 and 140 GHz. CAV 224 gave second harmonic power between 110 and 150 GHz. CAV 225 which was the shortest device could not be made to oscillate at all and did not appear to have a IV characteristic typical of a Gunn diode.

7.7.1 DB742 and DB736

DB742 and DB736 had the same active carrier length but different doping characteristics. In terms of the power maximum frequency, it was found that DB742 and DB736 were quite similar, and capable of giving over 50 mW around 82 GHz, when placed in the appropriate resonant cap cavity. Power was achieved over the 65 GHz -120 GHz range and all the diodes gave broadly similar results. DB742 giving marginally more power, at slightly higher frequencies.

All the diodes were tested in a large variety of different circuits and gave results consistent with maximum power being around 82 GHz (for matching with resonant cap circuits). Highest powers were obtained for relatively large diameter caps. Best power was achieved for a resonant cap diameter of 2.35 mm, thickness 0.15 mm, where diode 6 from DB742/1 gave over 62mW at 80GHz and 52mW at 74GHz. (Diode 3 from DB736 gave over 45mW near 70GHz in this circuit). Nearly all the diodes gave good power over the 78-90 GHz range (20 mW).

7.7.1.1 IV CURVES

IV curves were measured for each diode and at a number of different frequencies. All the diodes from each batch behaved qualitatively the same, although the characteristic of the IV curve was also a function of frequency. This can be clearly seen in Fig 7.19 which shows Diode 4 (DB742/1) operating at two different frequencies (80GHz and 115GHz). This shows that the d.c current can be quite a strong function of the r.f across the diode, (which of course is a function of frequency and the circuit).

Threshold occurred around 1450 mA for DB736 and 1200 mA for DB742. Typical IV curves for DB736/1 are shown in Fig. 7.20.

Apparent jumps in some of the IV curves are again caused by the fact that the power supplies used did not have sufficiently low d.c. output impedance to match the large negative conductance of the diode at this point. (Again it should be noted that the bias circuits typically have a d.c. series resistance of between 1Ω to 2Ω, and so threshold and

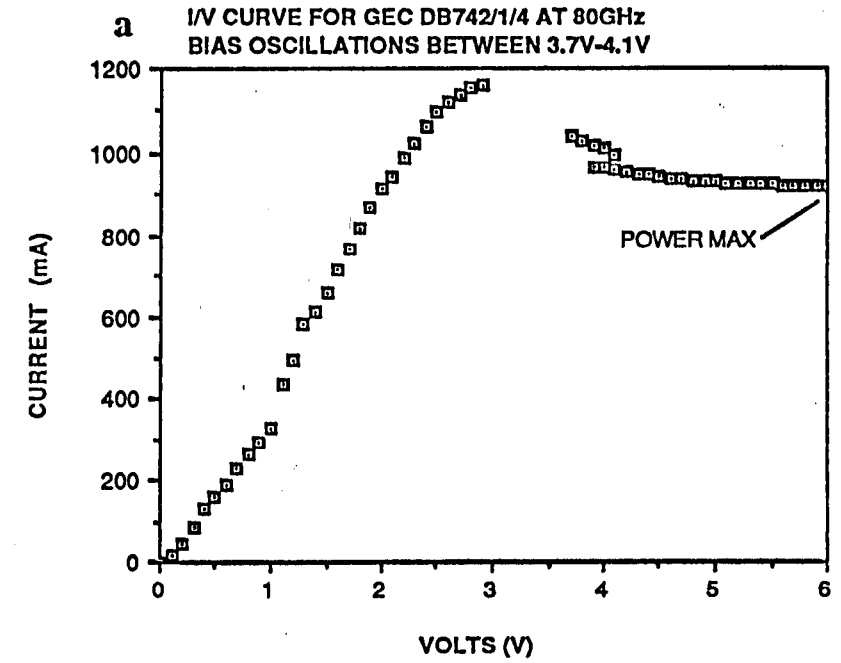
a
I/V CURVE FOR GEC DB742/1/4 AT 80GHz
BIAS OSCILLATIONS BETWEEN 3.7V-4.1V
CURRENT (mA)
VOLTS (V)
POWER MAX
0
200
400
600
800
1000
1200
0
1
2
3
4
5
6

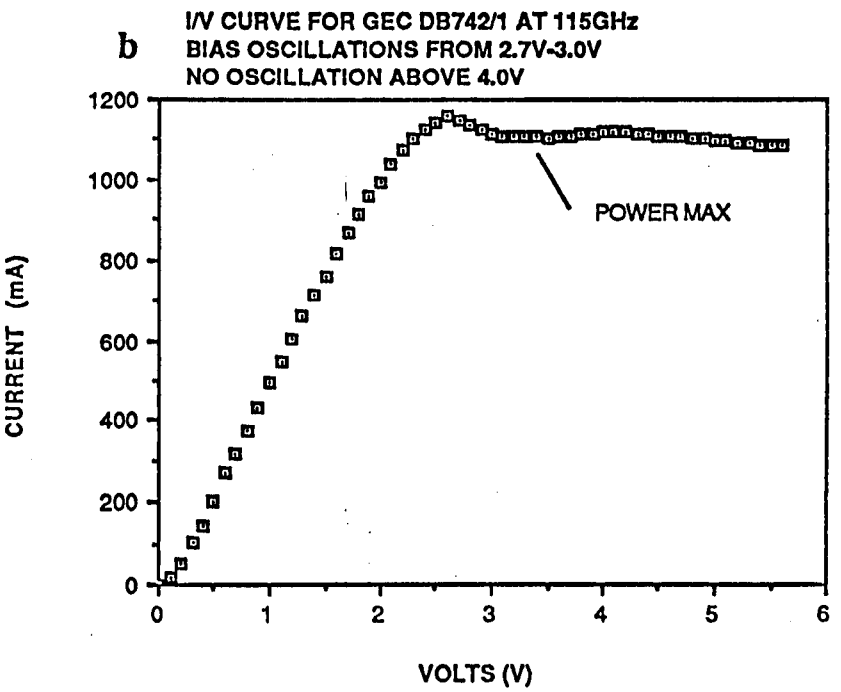
b
I/V CURVE FOR GEC DB742/1 AT 115GHz
BIAS OSCILLATIONS FROM 2.7V-3.0V
NO OSCILLATION ABOVE 4.0V
CURRENT (mA)
VOLTS (V)
POWER MAX
0
200
400
600
800
1000
1200
0
1
2
3
4
5
6

FIGURE 7.19

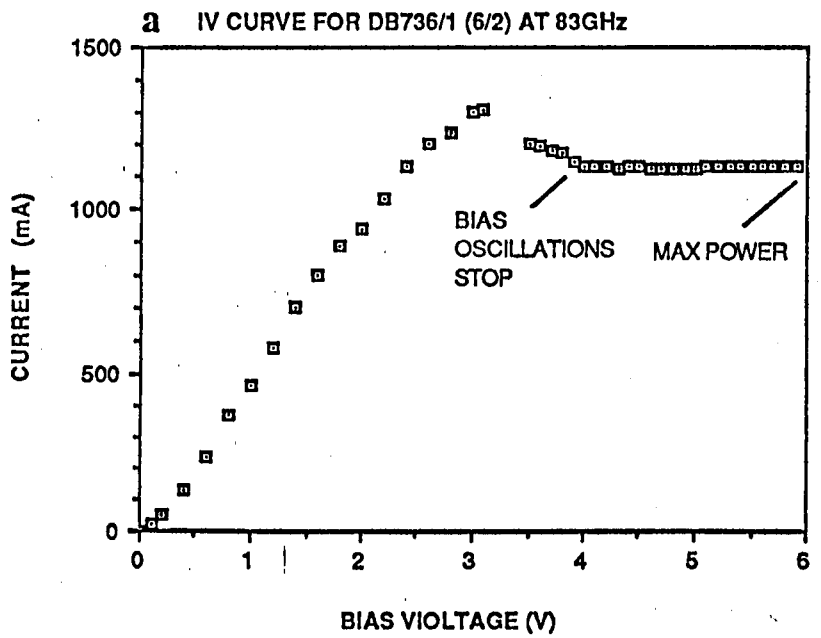
a
IV CURVE FOR DB736/1 (6/2) AT 83GHz
1500
1000
500
0
CURRENT (mA)
BIAS
OSCILLATIONS
STOP
MAX POWER
0
1
2
3
4
5
6
BIAS VIOLTAGE (V)

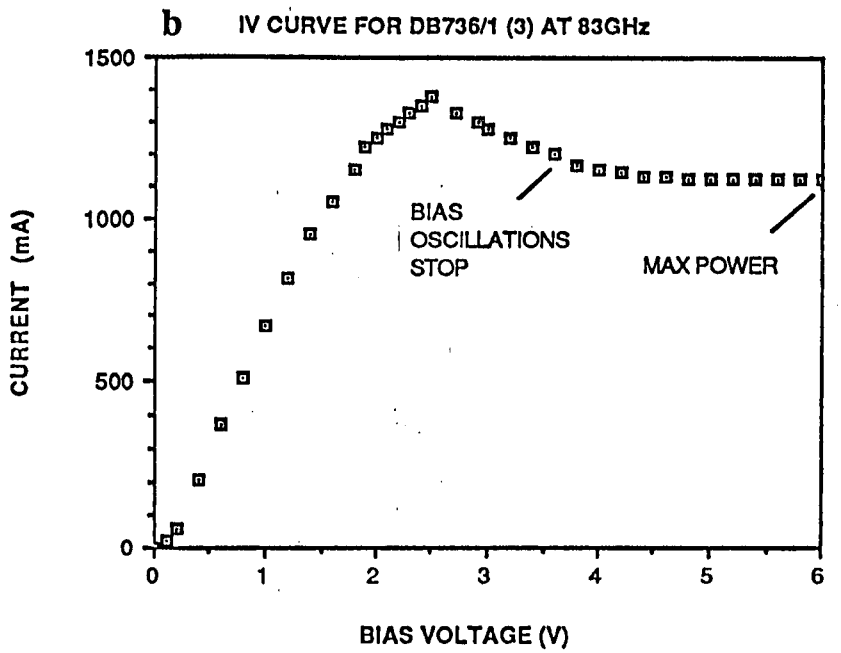
b
IV CURVE FOR DB736/1 (3) AT 83GHz
1500
1000
500
0
CURRENT (mA)
BIAS
OSCILLATIONS
STOP
MAX POWER
0
1
2
3
4
5
6
BIAS VOLTAGE (V)

FIGURE 7.20

optimum power output occur at slightly higher power supply voltages than might be expected).

The current generally reached a minimum value between 3V and 6V (depending on the frequency) and then started to increase slightly. Maximum power nearly always occurred at this current minimum. This was also a function of frequency. As the frequency was increased, the optimum power point occurred at lower and lower voltages. Indeed, as shown in Fig. 7.26b, no oscillation occurred above a bias voltage of 4V at 115GHz. There was also a definite correlation between power output and optimum current. The optimum current tended to be lowest at the frequency where the power output was greatest (i.e. around 80 GHz). This suggests that the amplitude of the fundamental field across the diode is at its greatest at 80 GHz (as one might expect). At 80 GHz the optimum current was around 1100-1200 mA for DB736 and 950-1100 mA for DB742.

These IV curves should be compared to the MEDL diode where the flat stable part of the IV curve occurred at much higher voltages, resulting in a much narrower voltage tuning range.

7.7.1.2 BIAS OSCILLATIONS

Threshold occurred around 1450 mA for DB736 and 1200 mA for DB742. Above threshold there was a large negative differential conductance accompanied with bias oscillations. The oscillations were essentially broadband/multi-frequency - typically a comb of frequencies at 1.5 MHz, with larger components at 80 MHz and multiples of 100 MHz, which could extend as far out as 1.5 GHz from the carrier, but were fairly low above 500 MHz. (The exact spectrum will of course vary with the oscillator and power supply as it depends on the impedance that the diode sees at these 'low' frequencies). These measurements were made by looking at the frequency of a fast detector and monitoring the bias voltage simultaneously. Oscillations appeared on the bias line just above threshold (turn on), and simultaneously appeared as upconverted noise/oscillations on the output of the oscillator. About a volt above threshold the oscillations on the power supply line suddenly disappear, as the IV curve flattens out. The noise on the rf output power also completely disappears at this point.

Up to about 1V above this point, very occasionally sidebands on the oscillators output were observed without accompanying bias oscillations. There was evidence to suggest that this was again due to rf power from another reference oscillator reaching the

test oscillator. (Oscillations of this nature were not seen near the 'optimum voltage' and were only noted for DB736 diodes).

7.7.1.3 POWER AND FREQUENCY CHARACTERISTICS

Initially Diode 4 from the **DB742** batch was selected and tested in a variety of different circuits of varying cap/post diameters and raised to different levels to find the optimum circuit. (Typically a 94GHz Varian diode requires a cap of around 2.0mm diameter). A selection of the different frequency/power curves for are given in Figs 7.21 to 7.24, (although many other variations were tried!). Most power was obtained with a large diameter cap of 2.2mm with the diode raised significantly (Fig.7.24), with small diameter caps giving clearly worse results (Fig.7.23). The other diodes from DB742 were tested with this circuit and some typical results are shown in Figs. 7.25-Fig7.29. Figure 7.27 shows the typical effect on the power of raising the diode relative to the waveguide floor, with results not dissimilar to those found with the MEDL diode. Figure 7.28 shows the tuning characteristic of this set-up with very similar results obtained for all cavity heights.

Figure 7.30 shows the optimum bias and current as a function of frequency. The optimum voltage decreased steadily with increasing frequency and the bias current increased dramatically. This was a feature of all the diodes tested.

Subsequent testing of the critical coupling condition (see Chapter 10) indicated that the diodes were probably still not fully matched. More recently, placing diode 6 in a cavity with a cap of 2.35mm gave a power output of over 62mW at 80GHz and 52mW at 74GHz (see Fig. 7.37).

The **DB736** batch were all initially tried with caps of diameter 2.0mm (the largest available at the time). Various circuit configurations were tried with the optimum power appearing around 82 GHz. Typical results are shown in Figs. 7.31-7.34. Only one diode was found to have a significantly different characteristic to the batch, and that was DB736/1/6(1) which had a low threshold current (1140 mA) compared to the other diodes, which typically had threshold currents around 1440 mA. This diode had a power maximum at 85 GHz and a slightly different tuning characteristic (Figs. 7.35-7.36).

More recently diode 3 was placed in a cavity where the cap diameter was 2.35mm and a maximum power of 45mW was obtained at 70GHz (Fig. 7.38).

In addition to the graphs given, all the available diodes (at the time) were tested in a circuit with a cap diameter of 2.2mm (4 from DB742, 3 from DB736) They all had maximum power greater than than 45 mW, and the maximum power obtained is shown below.

DB742

Diode 3 - 49 mW at 82GHz
Diode 4 - 52 mW at 82GHz
Diode 5 - 47 mW at 81 GHz
Diode 6 - 46 mW at 82 GHz

DB736

Diode 3 - 45 mW at 80 GHz
Diode 5 - 49 mW at 82GHz
Diode 6/2 - 49 mW at 82GHz

All the diodes showed frequency jumps in their tuning characteristics not dissimilar to those seen previously with other diodes. The d.c current was observed to increase noticeably in the vicinity of a frequency jump indicating that the jumps are due to an impedance loop at the fundamental. Measurements were made of the optimum current and voltage for every diode tested in every circuit, and all were found to have the same general characteristics. The effects are illustrated in Figs 7.39 and 7.40 which show the optimum current and voltage as a function of frequency. It is interesting to note that the bias current increases close to a frequency jump. Note these correspond to the tuning curves illustrated in Figs 7.37 and 7.38.

7.7.1.4 DIODE FAILURES

There were two diode failures, from each batch. In DB742, diode 4 went short circuit after being taken to a bias voltage of 7.0V. This diode had operated successfully for approximately 100 hours, with no sign of degradation, at bias voltages of no greater than 6.2V. Probably over-voltaged!

Diode 7 (DB742) also failed after what was probably a momentary loss of contact with the bias supply. This was due to a compression spring suddenly seizing up within the block. We have had other diodes fail because of this problem, and it is not considered to be due to any failing of the diode. (All suspect springs have now been replaced!).

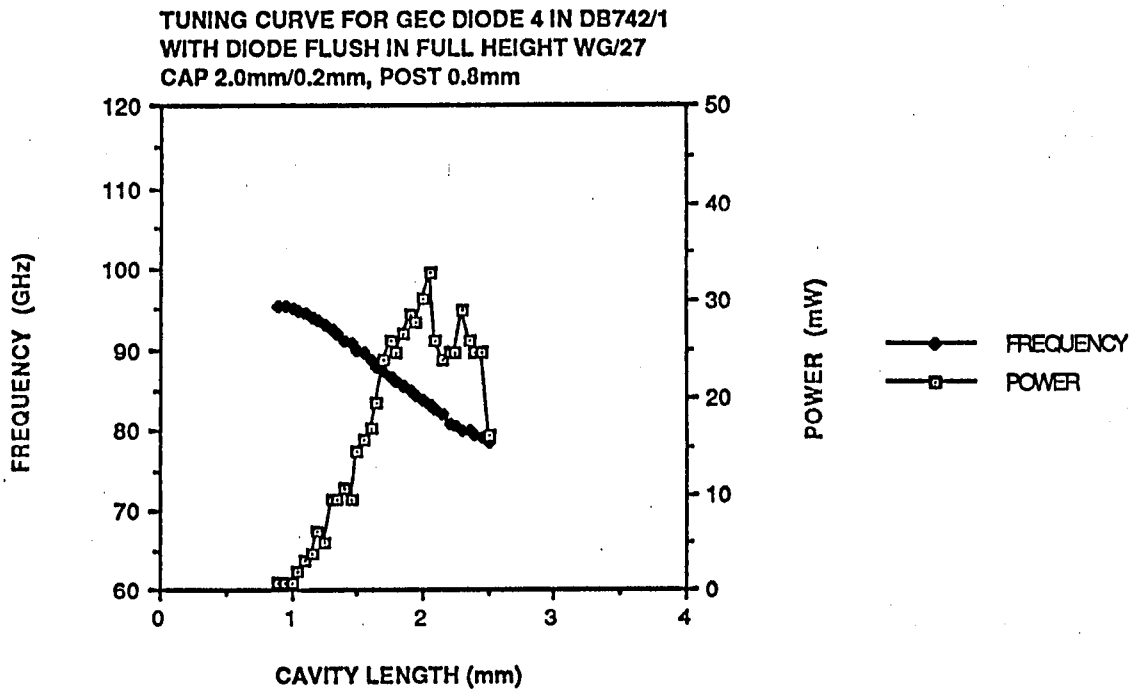

FIGURE 7.21

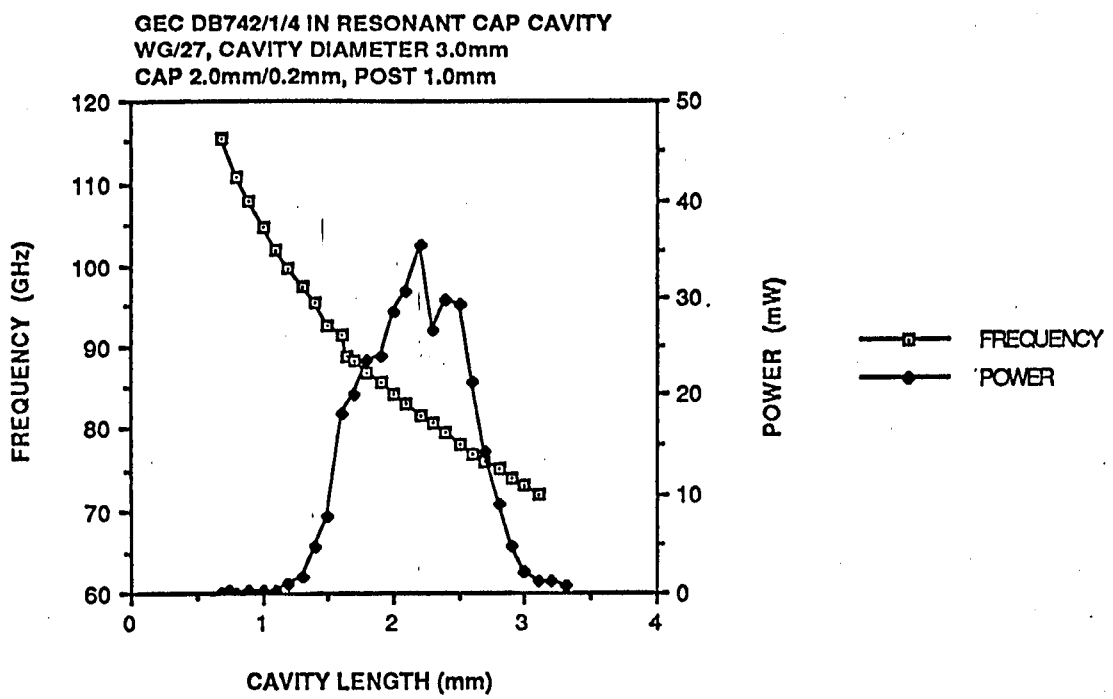

FIGURE 7.22

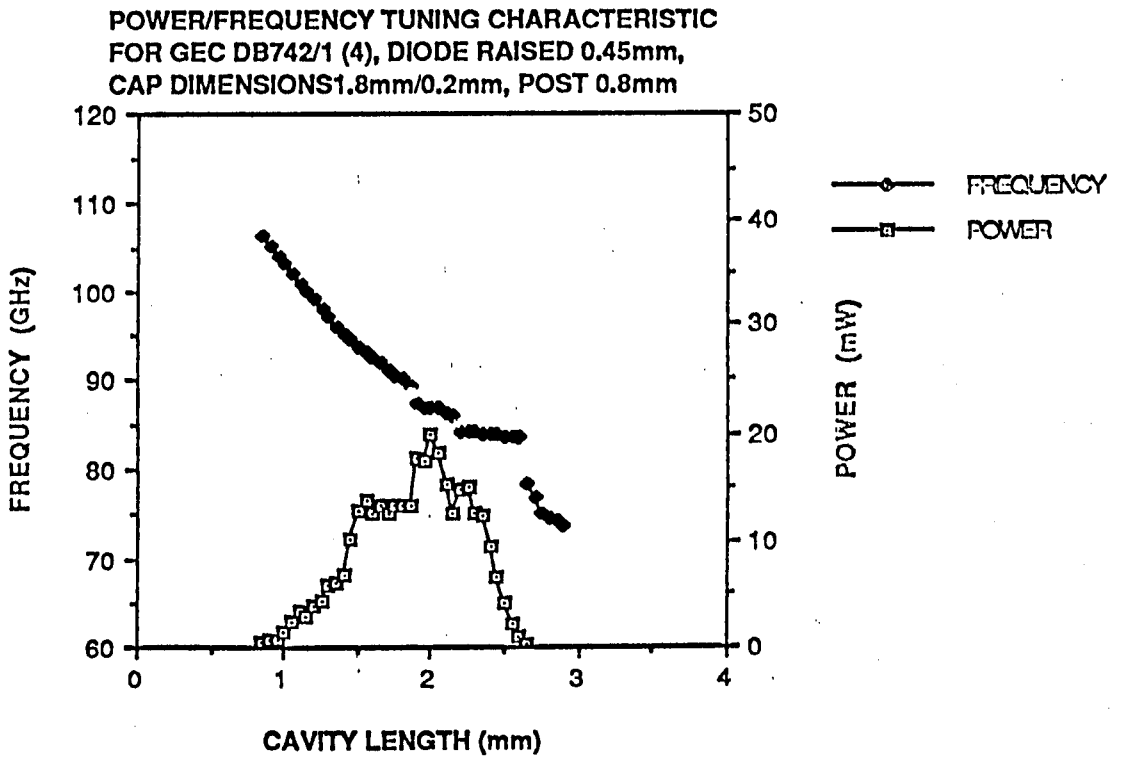

FIGURE 7.23

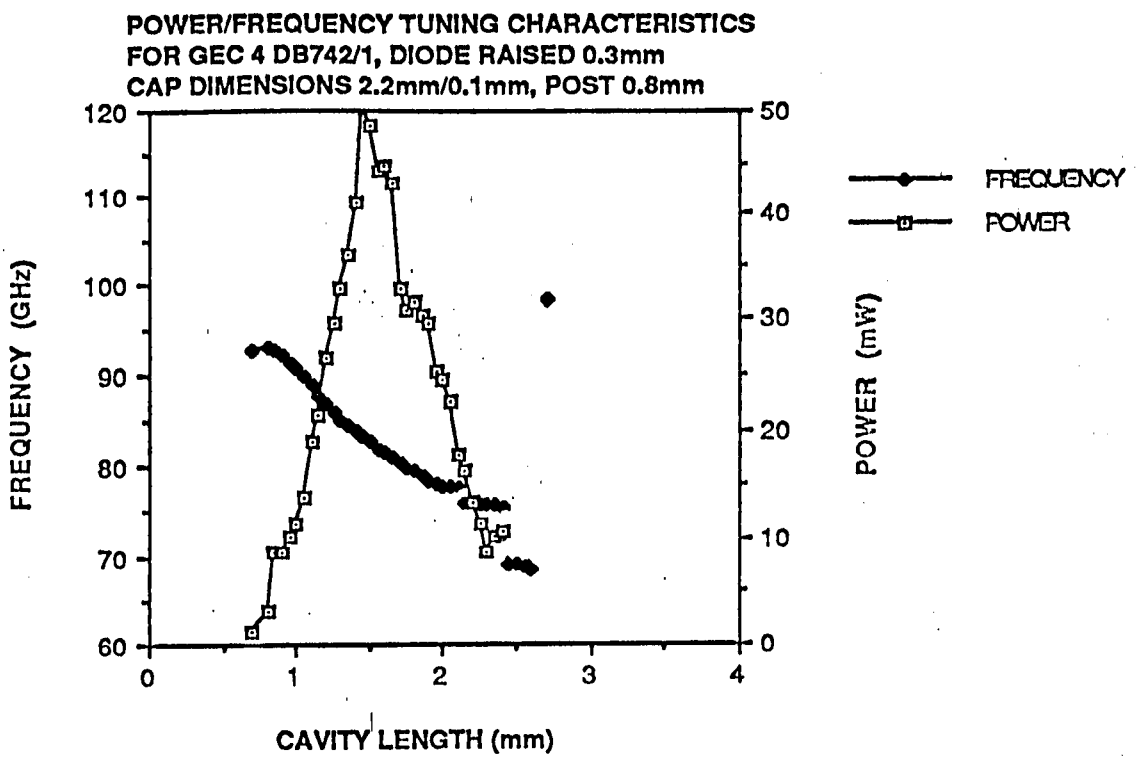

FIGURE 7.24

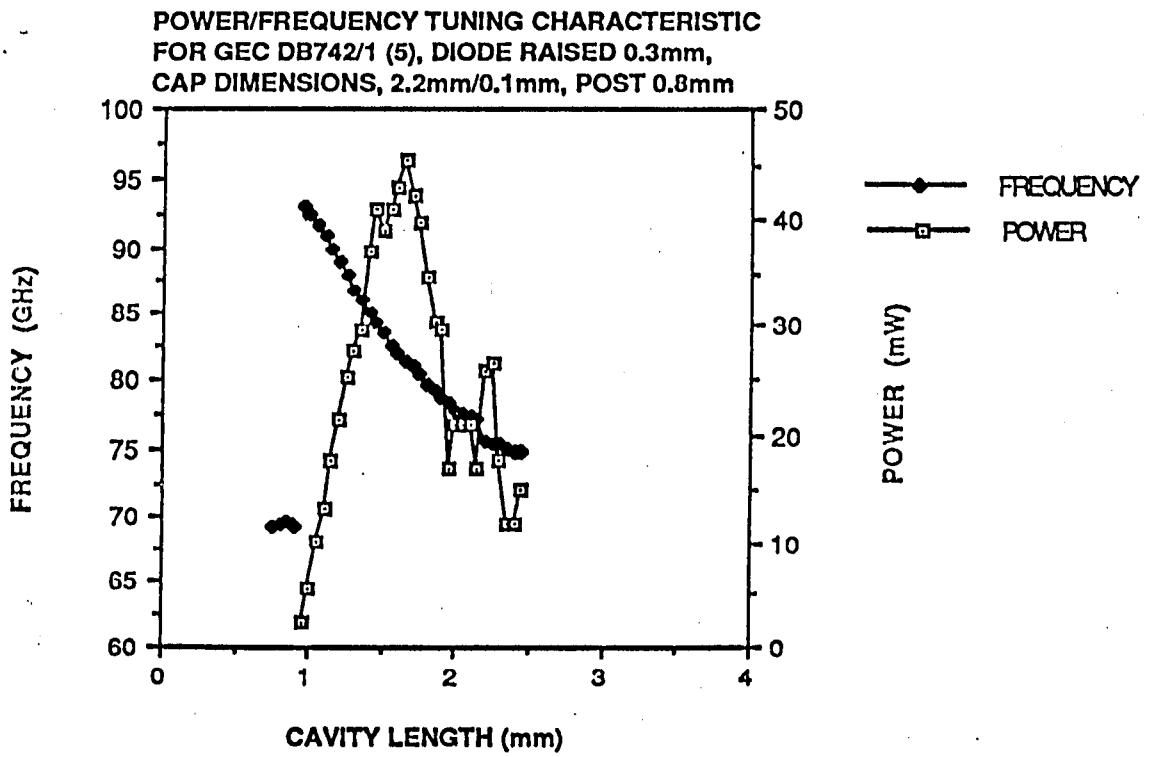

FIGURE 7.25

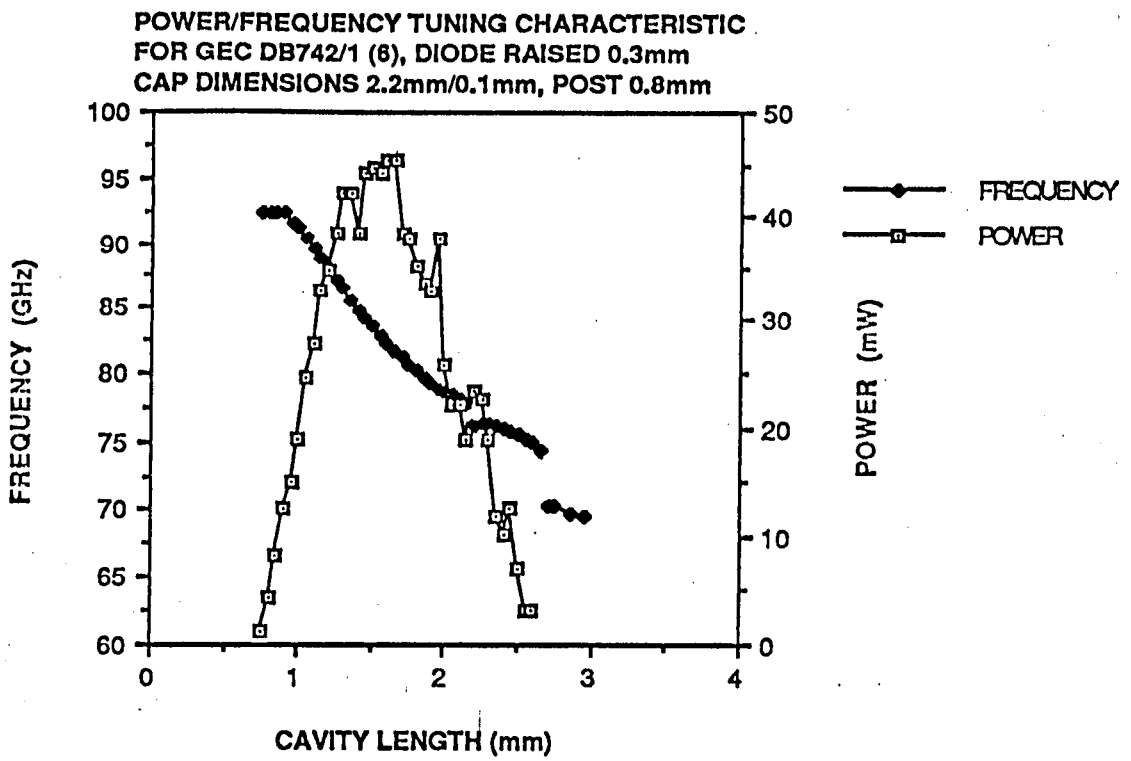

FIGURE 7.26

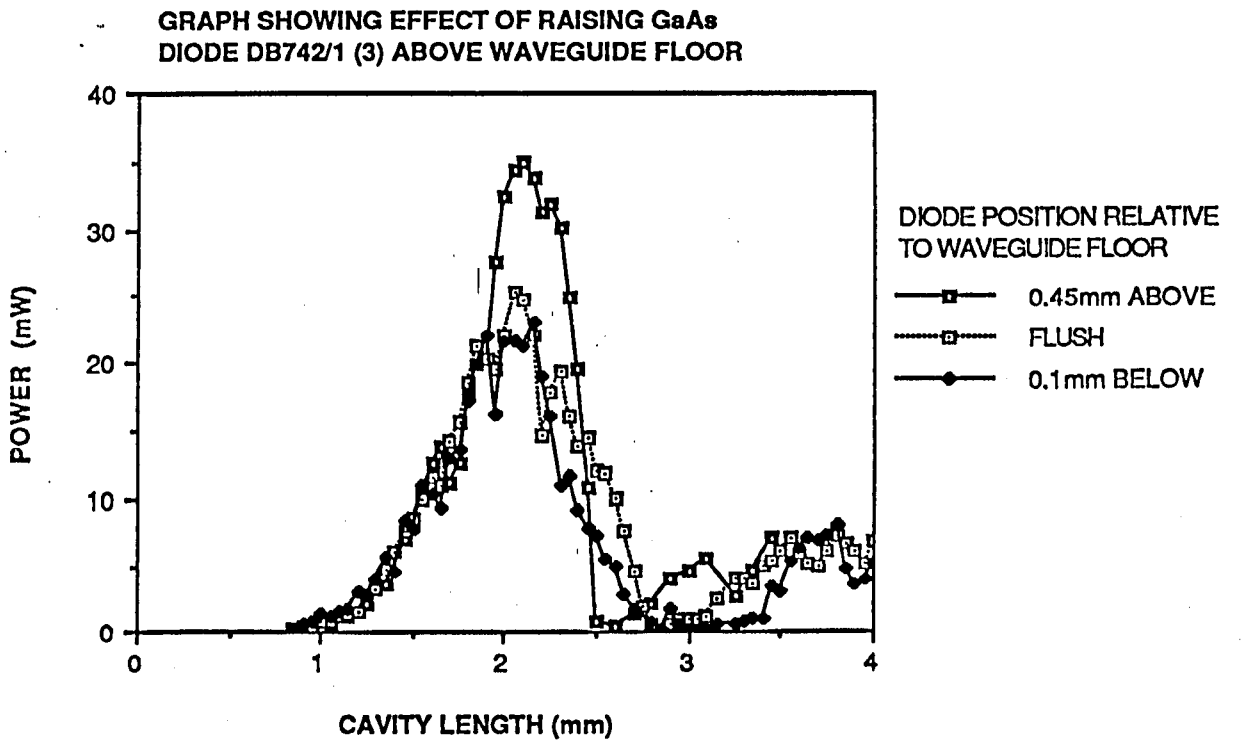

FIGURE 7.27

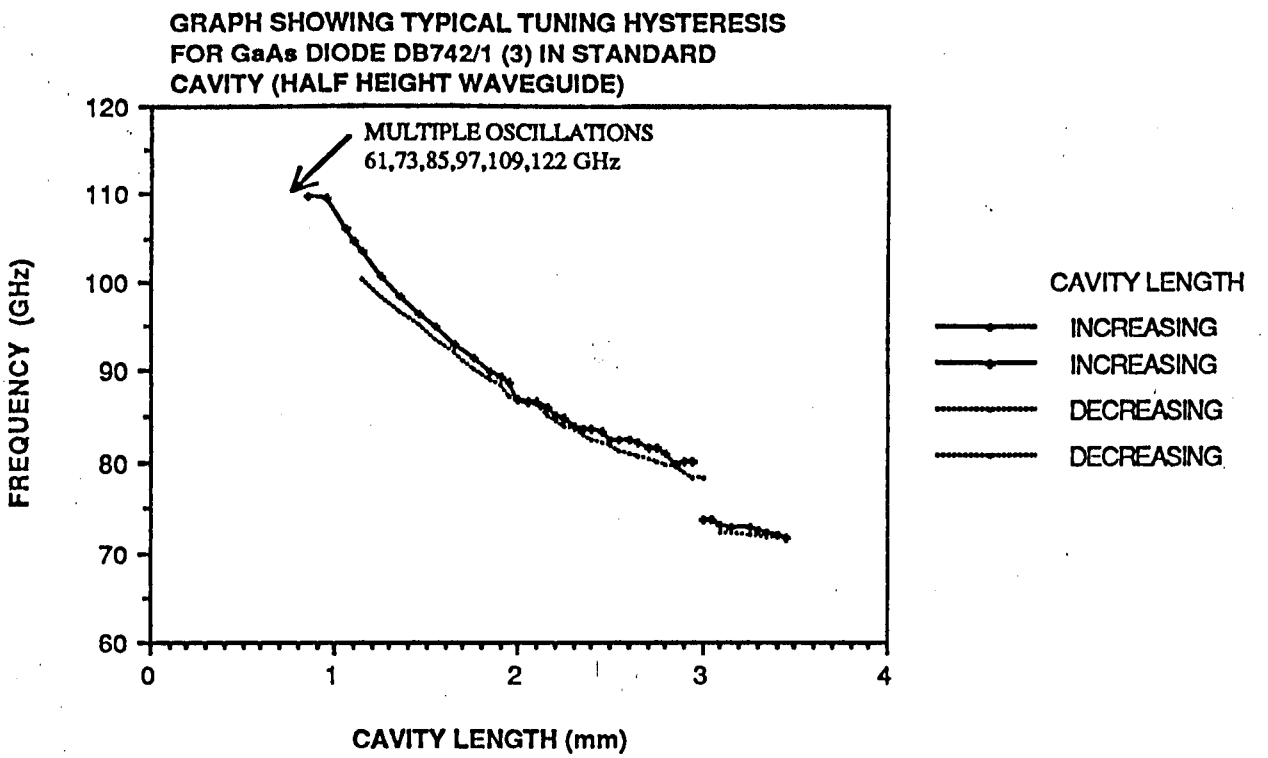

FIGURE 7.28

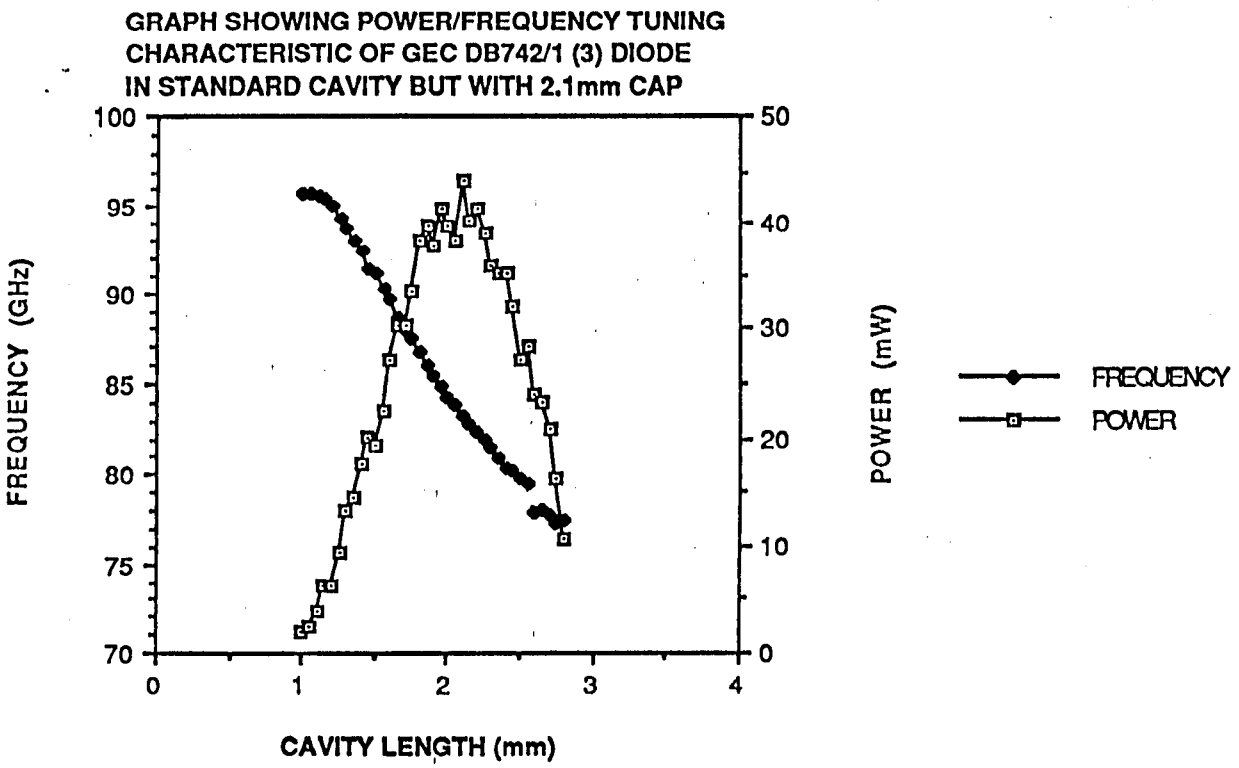

FIGURE 7.29

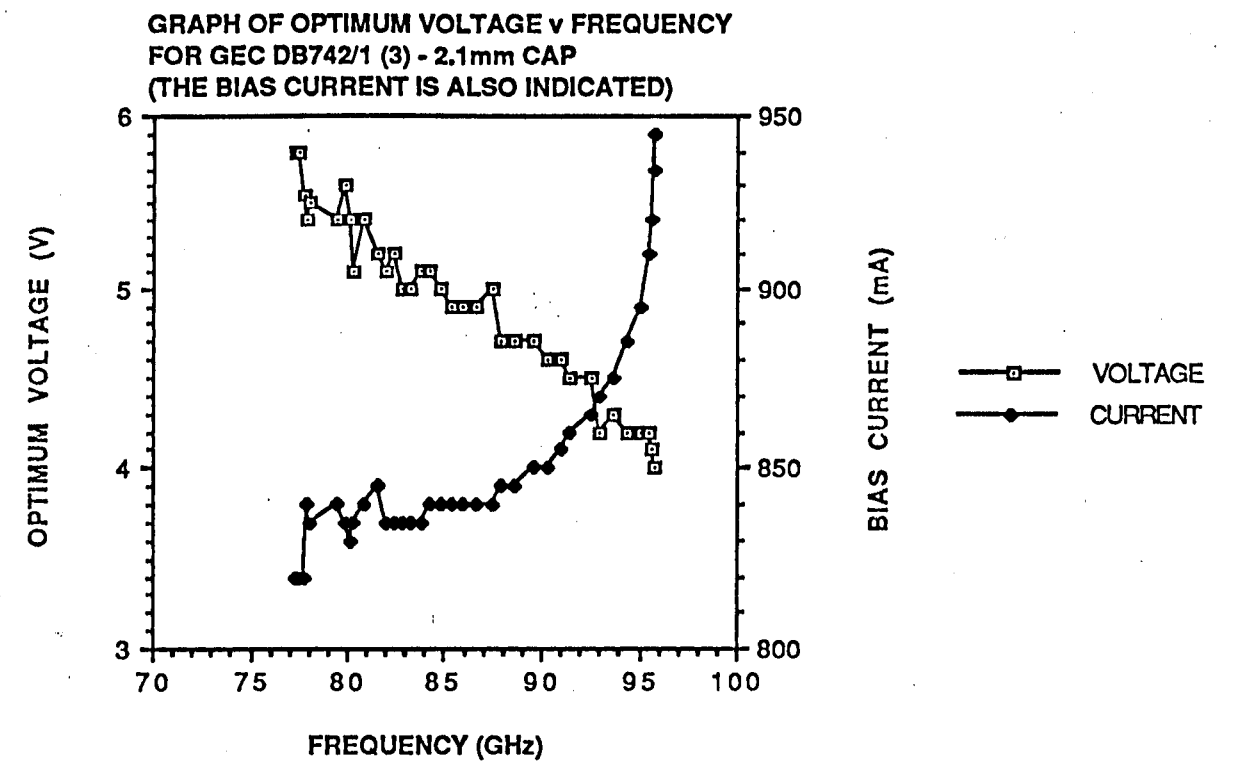

FIGURE 7.30

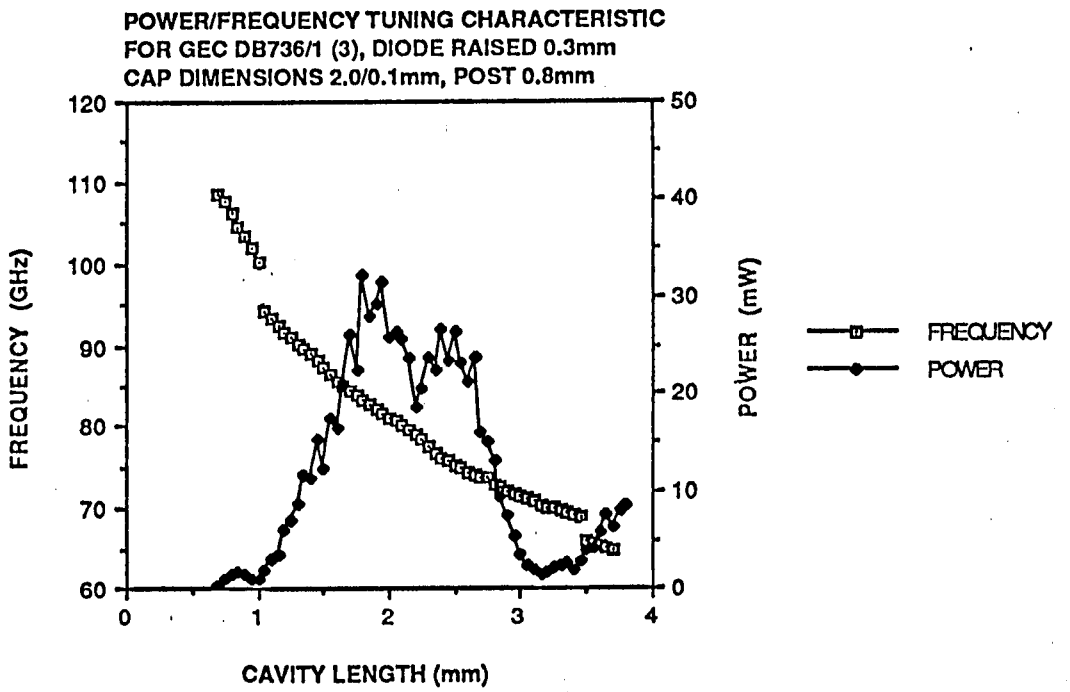

FIGURE 7.31

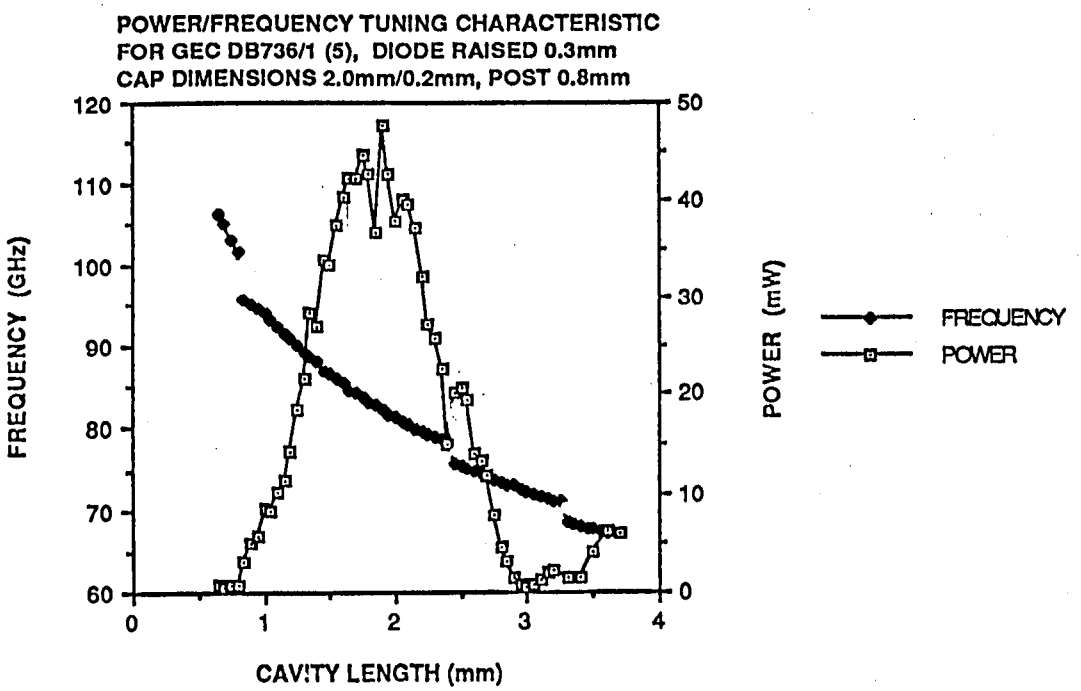

FIGURE 7.32

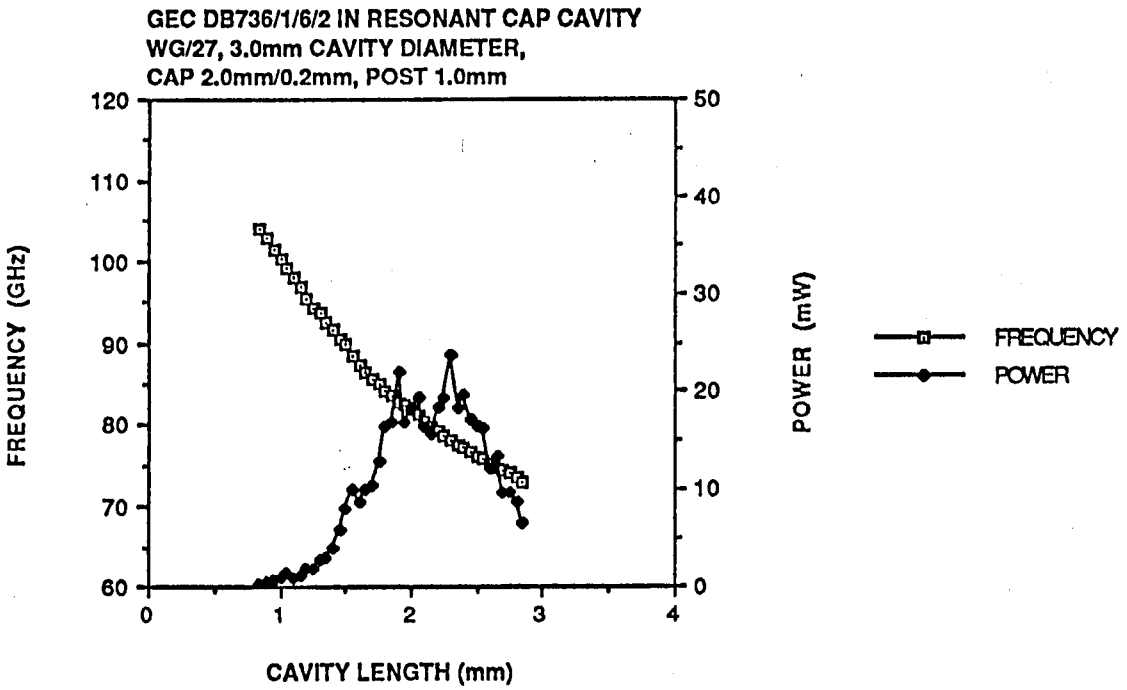

FIGURE 7.33

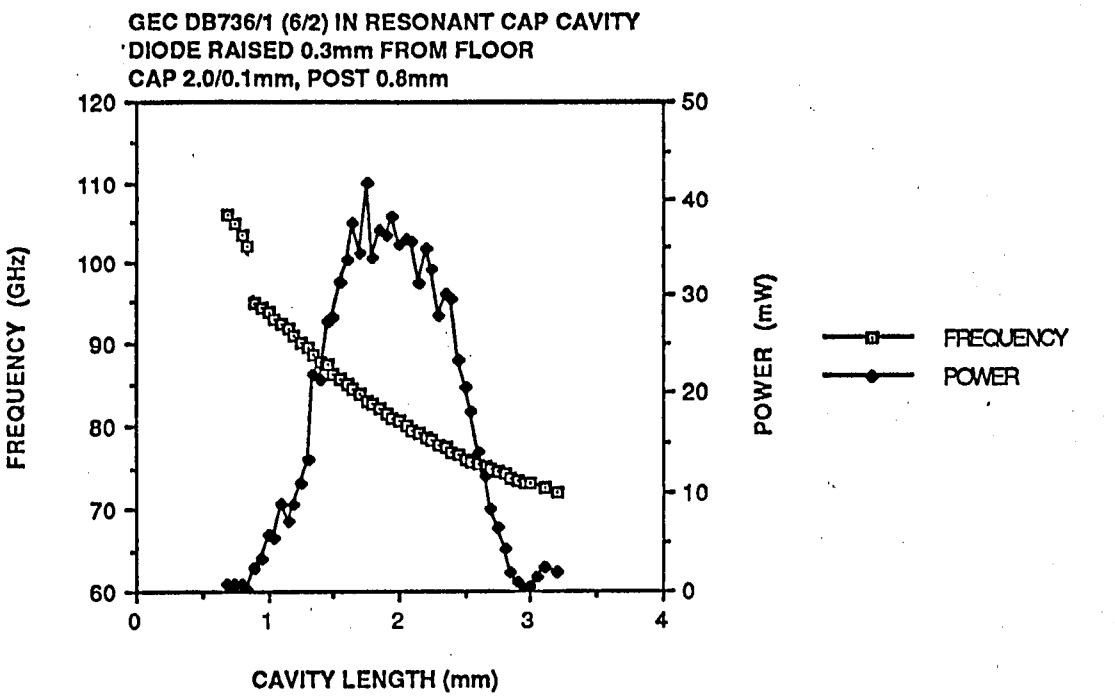

FIGURE 7.34

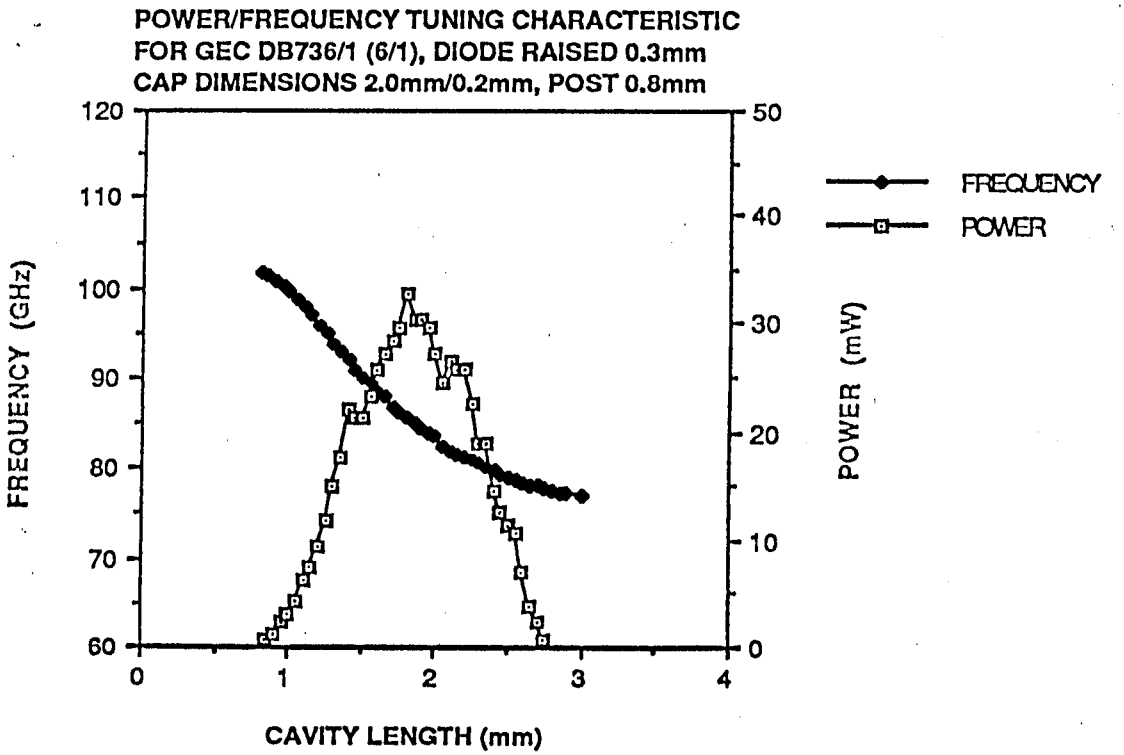

FIGURE 7.35

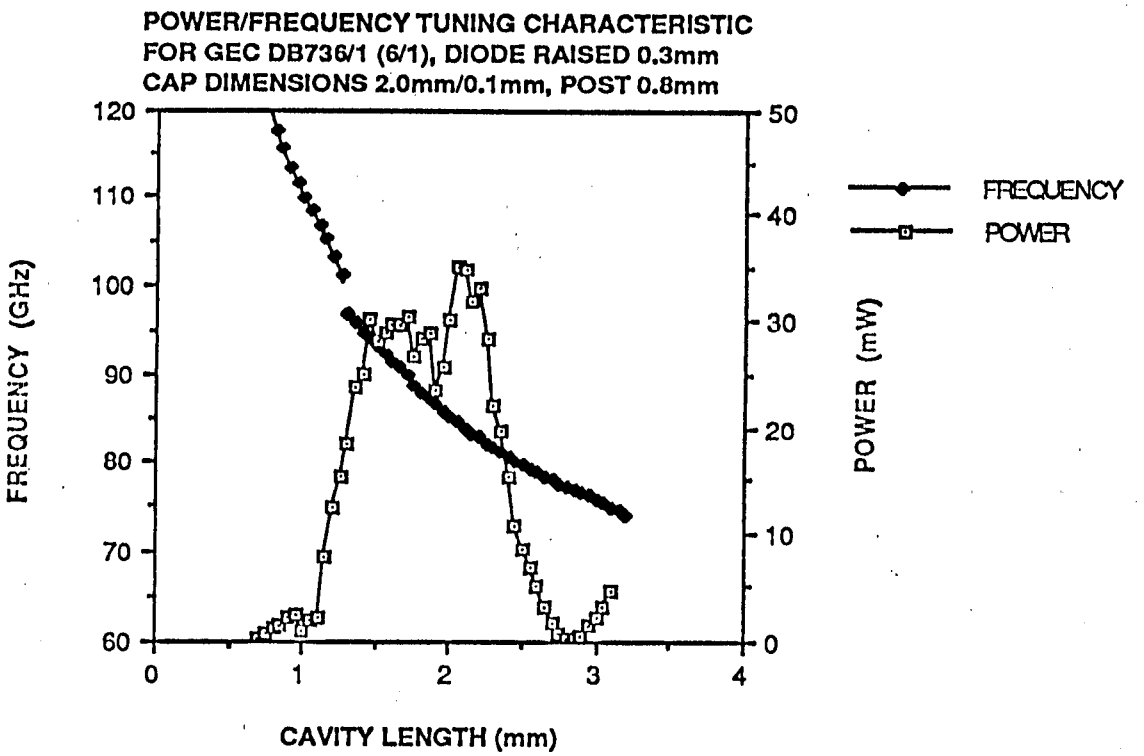

FIGURE 7.36

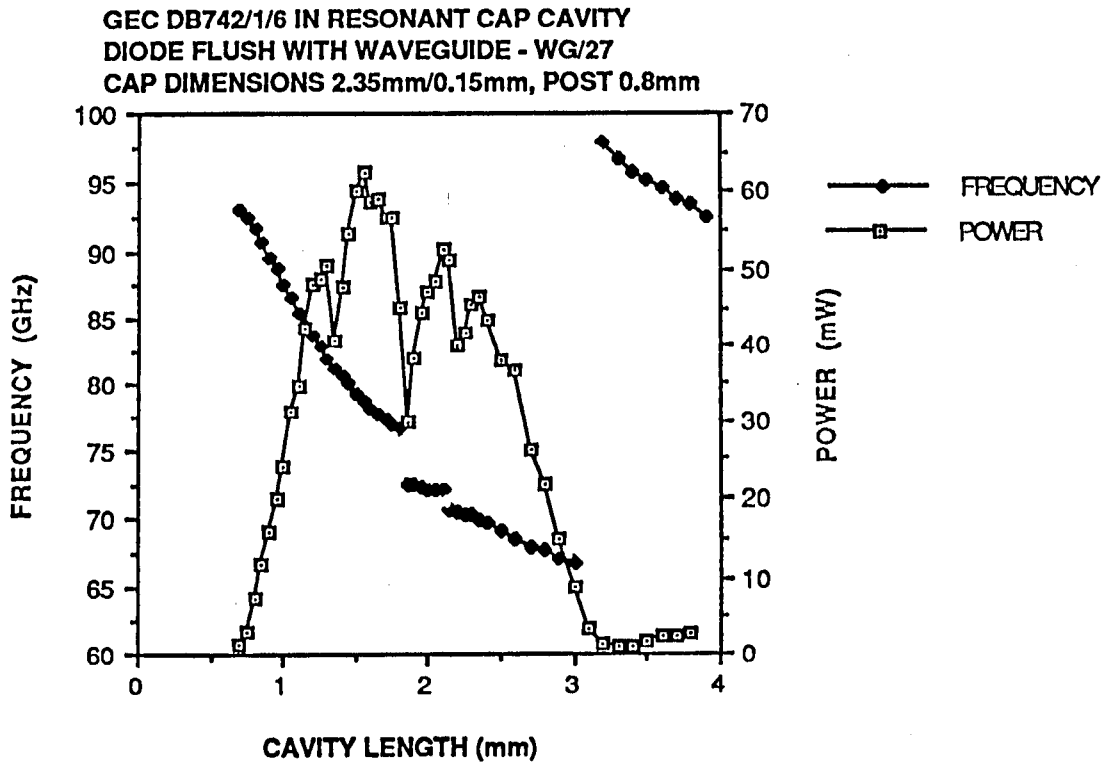

FIGURE 7.37

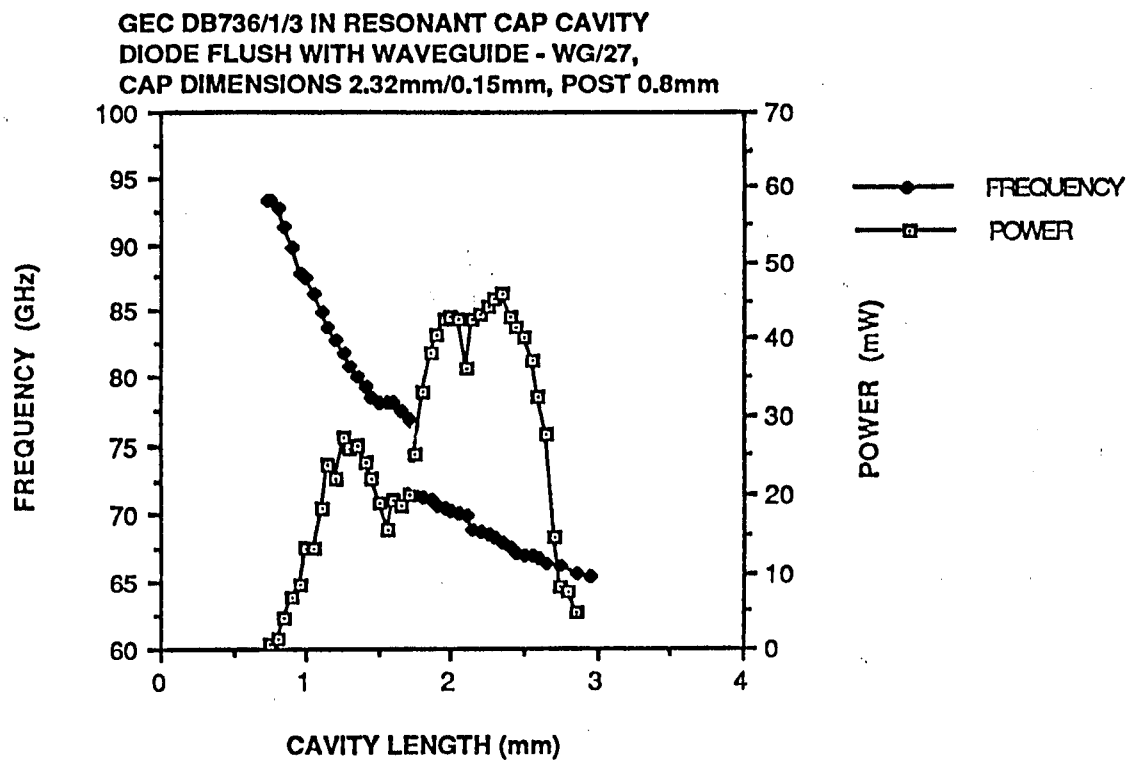

FIGURE 7.38

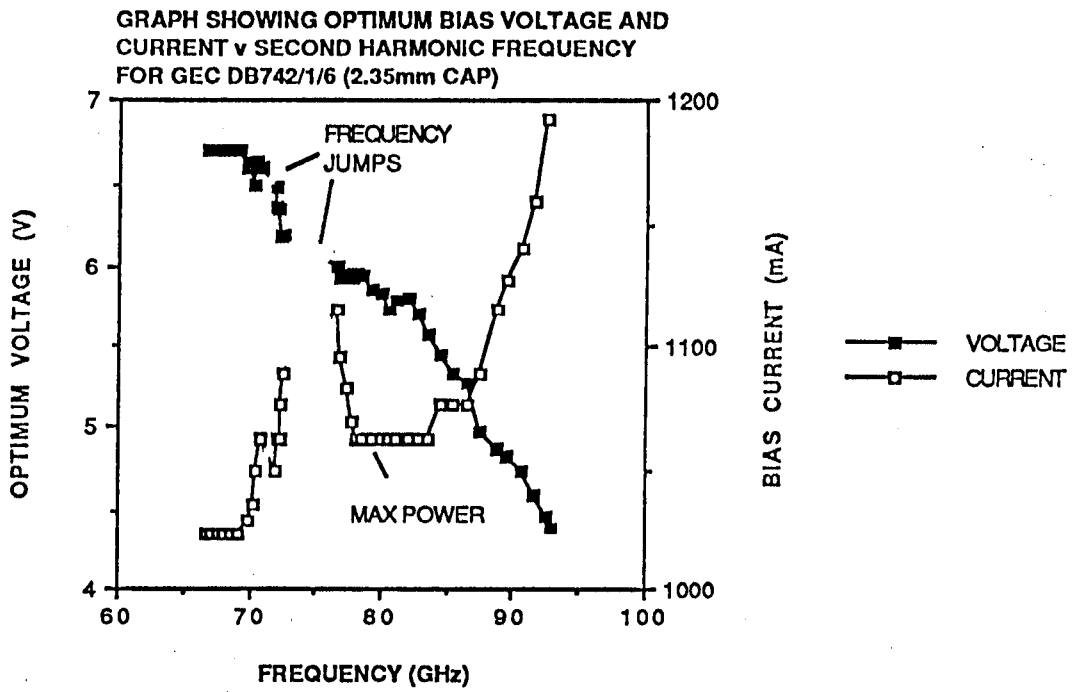

FIGURE 7.39

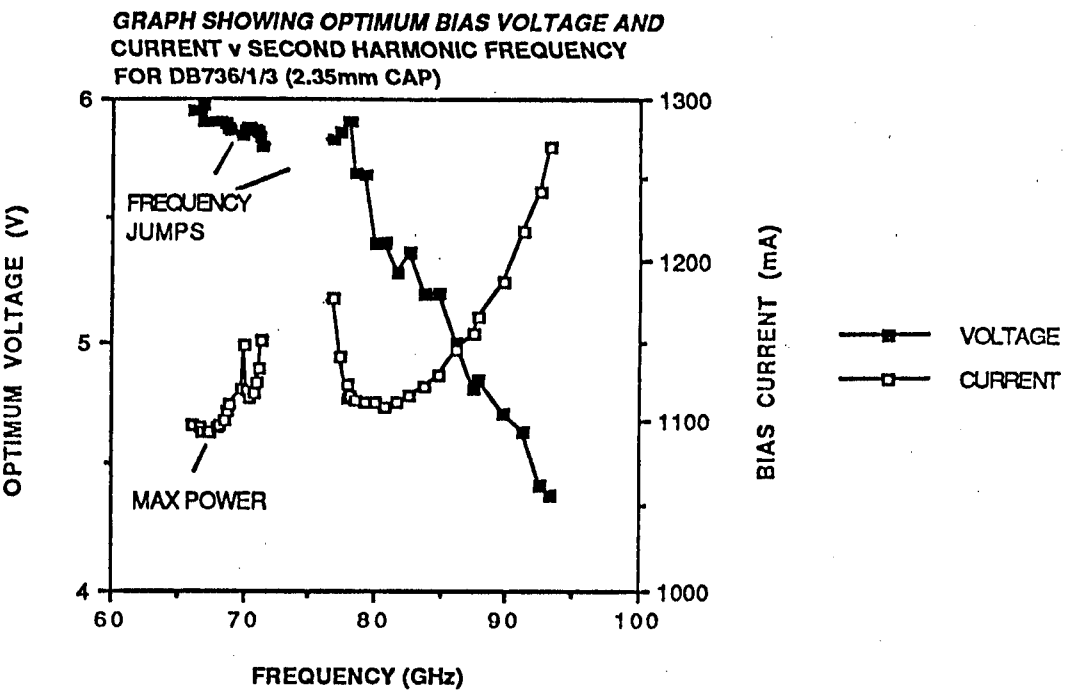

FIGURE 7.40

There were also two diode failures from DB736. Diode 6/1 suddenly went short circuit for no apparent reason, although the block was not particularly well heat sunk at the time. Diode 5 also went short circuit after possibly being overbiased (>6.5V).

7.7.2 CAV 223,224

These diodes had much shorter active lengths than 94GHz diodes, and were expected to operate at a much higher frequency. Attempts to use them in resonant cap circuits were generally unsuccessful as the devices either did not oscillate at all, or had limited power and frequency tuning. Instead they were operated in various coaxial type cavities which were available with different output waveguides (WG/27,WG/28,WG/29). Power output was still low but the circuit has the advantage that at second harmonic, they are usefully used to see the full frequency range of the diode.

Note that cap type circuits don't seem to match much better above about 110 GHz (for this type of package). The power output should therefore be treated as a very rough indication as to the optimum frequency. The cavities used for the second harmonic measurements were much smaller than those used before, in an effort to prevent spurious resonances at the second harmonic (and allow greater tuning of the fundamental). Power output was also greater for the small cavity.

Both CAV 223 and CAV 224 had smooth (current-limiting type) IV curves with no sign of any bias oscillations. The IV curves were much flatter than those from the DB742 or DB736 batch and typical results are illustrated in Figures 7.41 and 7.42. There was no sign of any bias oscillations.

7.7.2.1 CAV 223

From the CAV 223 batch one diode (Diode 3) gave power from 91-138 GHz (second harmonic) - Fig 7.43. In a cavity with WG/27 output , this diode also gave out over 60 mW of power at 65 GHz (4.5V, 1090 mA). However, it seemed to be dominated by a package resonance at 65 GHz, and coaxial tuning had little effect on the fundamental frequency. The optimum current and voltage ranged from 4.0V, 1100 mA at 138 GHz to 5.5V, 1010 mA at 100 GHz. Threshold voltage was 1.8V.

The other diode (Diode 4) gave power between 90 and 130 GHz (Fig.7.44). It subsequently failed during measurement of the frequency spectrum at a bias voltage of

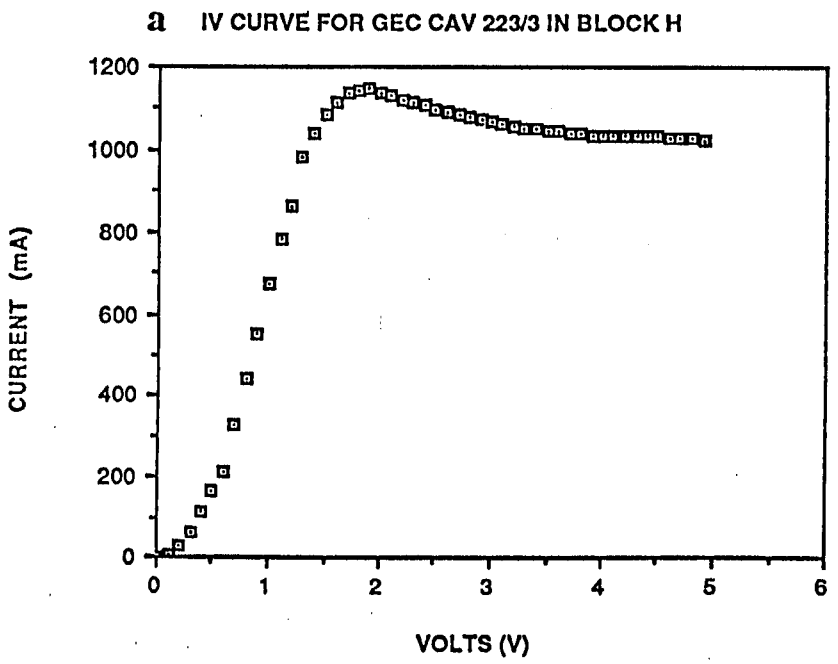

FIGURE 7.41

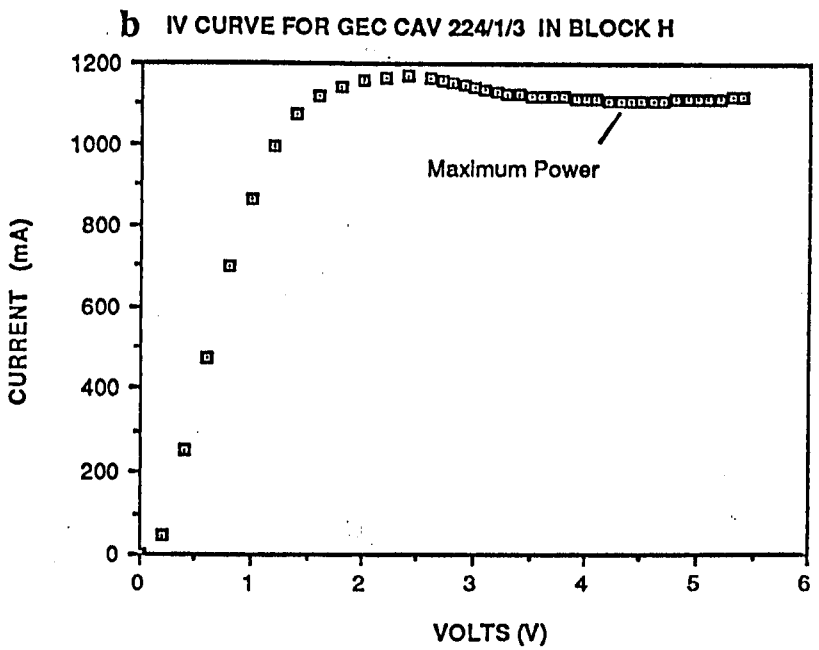

FIGURE 7.42

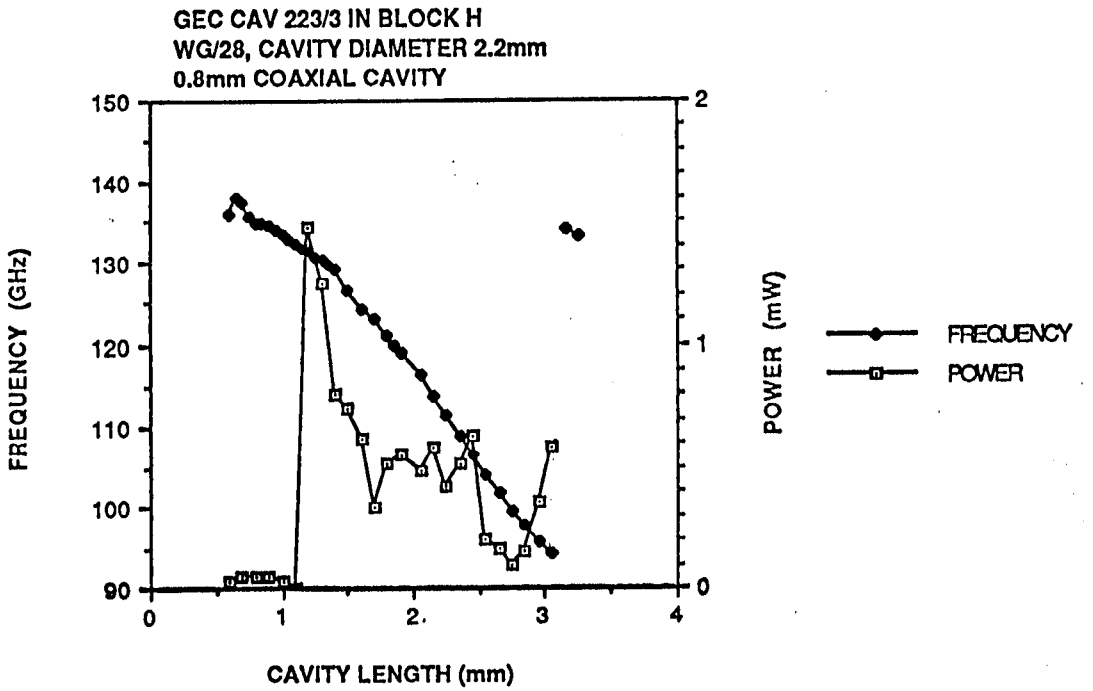

FIGURE 7.43

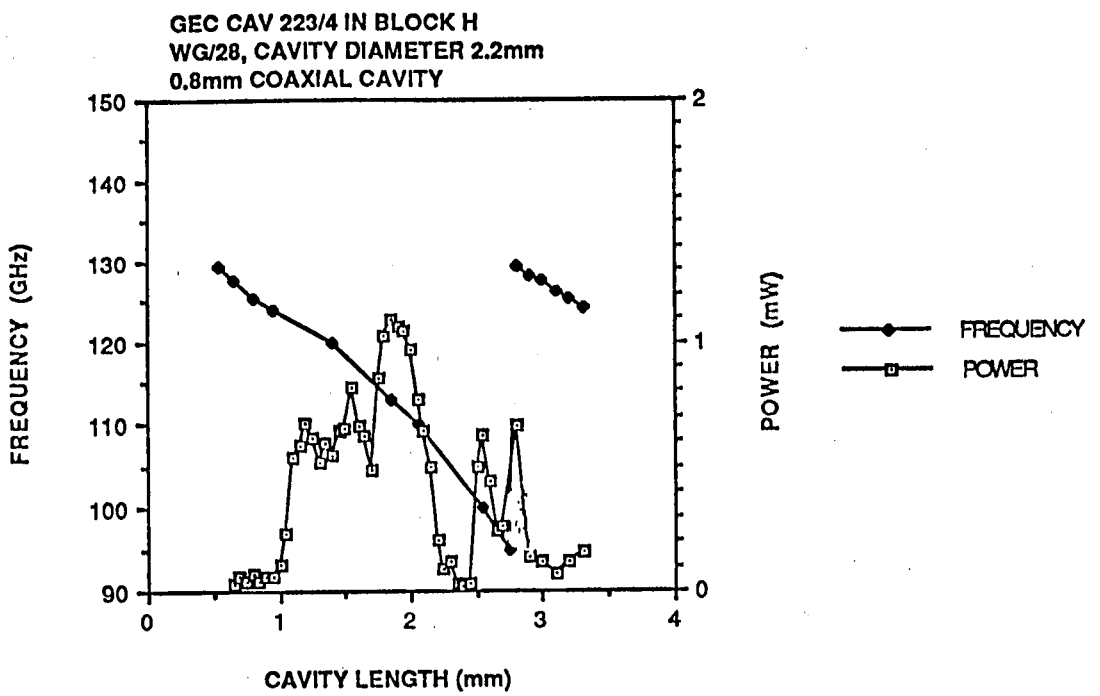

FIGURE 7.44

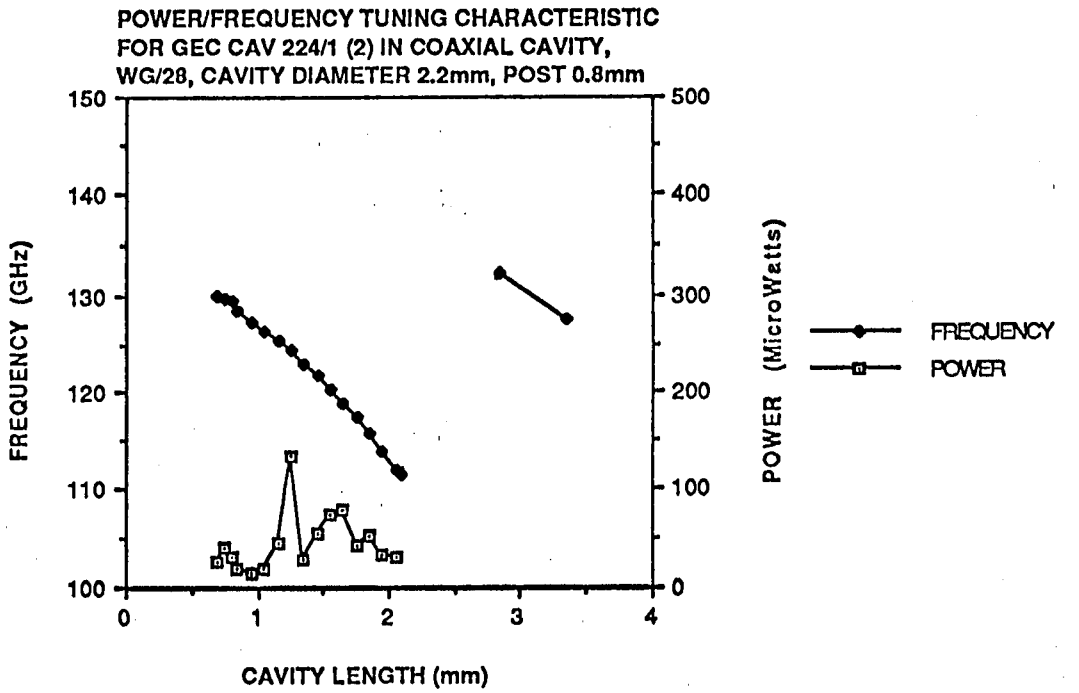

FIGURE 7.45

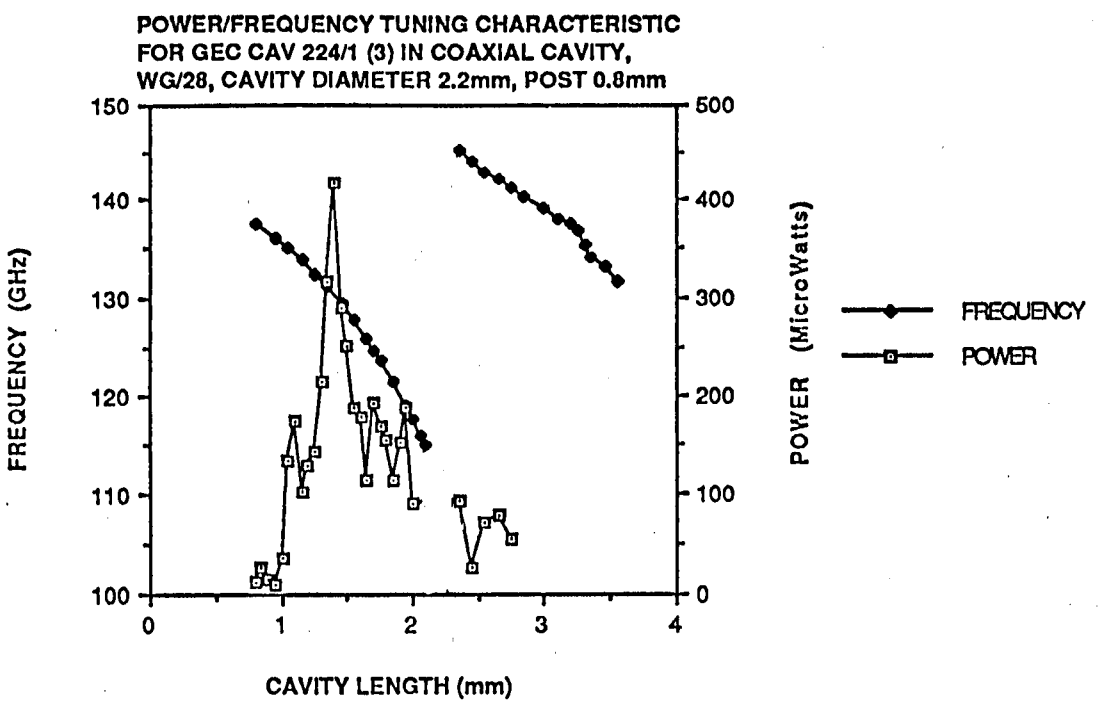

FIGURE 7.46

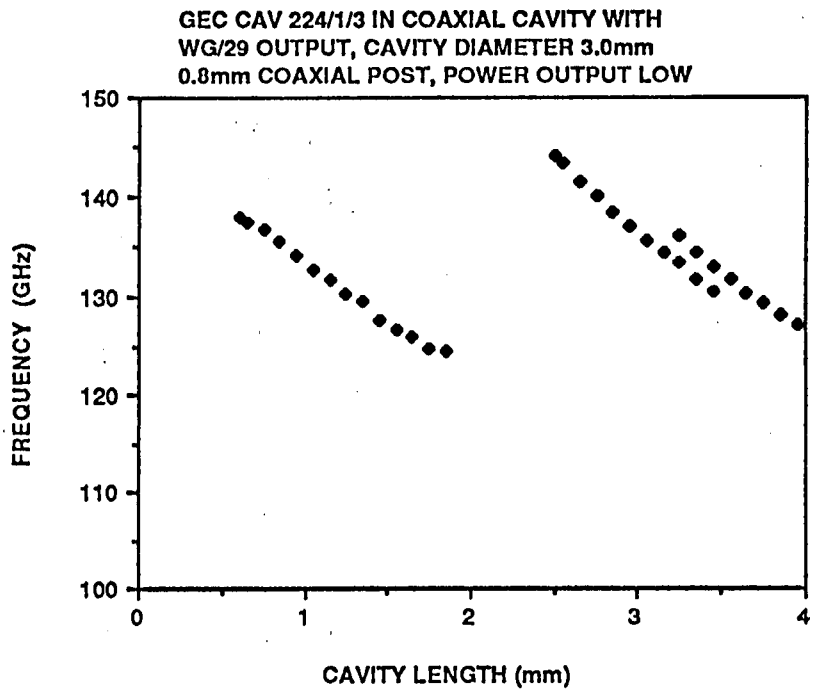

FIGURE 7.47

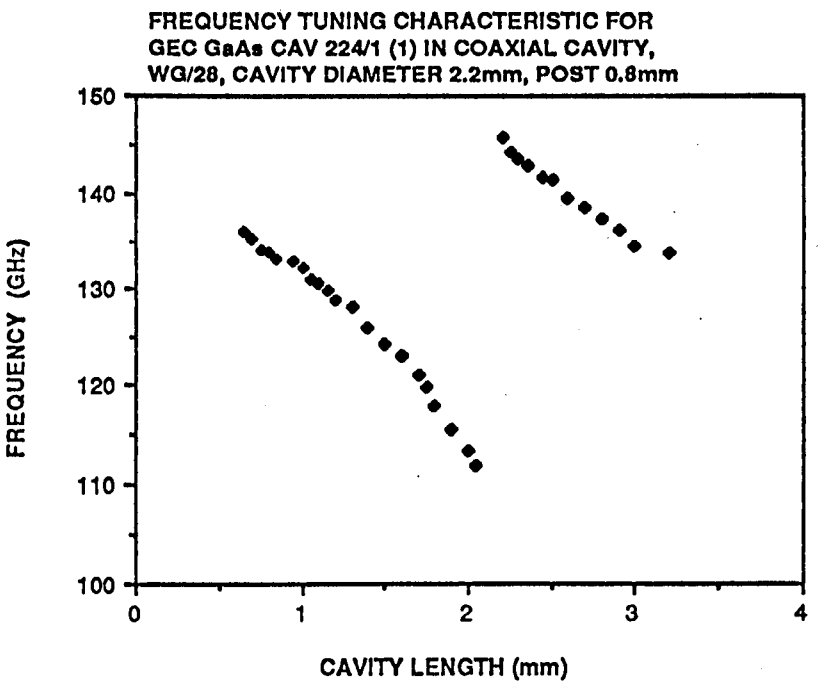

FIGURE 7.48

5.8V. The optimum current and voltage ranged from 3.8V, 895 mA at 130 GHz to 5V, 890mA at 100 GHz.

7.7.2.2 CAV 224

The CAV 224 batch gave out power in the 110-150 GHz range, and one diode gave 50 mW at 66 GHz. (It was difficult to persuade them to oscillate at all in resonant cap type circuits, and all the results were achieved with coaxial circuits.) In a coaxial circuit with a WG/27 output Diode 2 could not be made to oscillate at all , although Diode 3 gave 50 mW at 66 GHz, and Diode 1 gave 17 mW at 62 GHz, although the tuning appeared fairly critical. Diode 2 also gave significantly less second harmonic power than the other diodes in the same circuit.

To look at their tuning ranges the diodes were transferred to a coaxial cavity with a small outer diameter (2.2mm) and coupling to WG/28.

It was found that there was some variety between the three diodes in their tuning ranges, but in general they operated at higher frequencies than CAV 224.

CAV 224/1 - 114-146 GHz (17 mW at 62 GHz) (Fig.7.47)
CAV 224/2 - 112 -130 GHz (Fig.7.45)
CAV 224/3 - 115 -150 GHz (50 mW at 66 GHz) (Fig.7.46)

The diodes were also tested in cavities with WG/29 outputs where the frequency cut-off is at 88GHz. These indicated similar results for the second harmonic frequency tuning range and the tuning curve for 224/3 is given in Fig.7.48.

It should be noted that the package and diode are resonant at around frequencies of 60-75 GHz (for coaxial operation). This resonant frequency can be increased by reducing the cavity diameter/WG output, but in some cases this may have influenced the maximum frequency that was obtainable.

7.7.2.3 CAV 225

Cav 225 had the shortest active length and most of the IV curves indicated short circuit behaviour on testing. It is unclear whether there was a problem in manufacturing or whether the device length was too small for operation as a Gunn device. Other

experimental results have indicated that there is a minimum length of active region where oscillation is not seen.

7.8 InP GUNN OSCILLATORS

InP Gunn diodes are superior to GaAs diodes in almost every respect. They have a larger peak to valley velocity ratio leading to higher efficiency, and smaller relaxation times leading to higher frequency operation. This is essentially due to the higher threshold field, which is attributable to the large energy separation between the central and satellite valleys. This also leads to a less temperature dependent power frequency characteristic.

The highest fundamental frequency reported for GaAs is around 80GHz, whereas Varian have reported fundamental frequency operation in InP at 140GHz.

At the important 95GHz frequency GaAs oscillators work in a second harmonic mode, and are capable of delivering powers of up to 50mW. Second harmonic InP oscillators operating at the same frequency are typically quoted at 60mW power output , but in fundamental mode power outputs in excess of 100mW have been obtained. Varian have suggested that powers around 0.25W may be possible with diamond heat sinking. In addition, they should be capable of higher output powers when operating in harmonic mode at 95GHz.

The material however, is much harder to work with than GaAs and manufacturing and processing problems are known still to exist.

7.8.1 94GHz SECOND HARMONIC InP DEVICES

Although InP devices are capable of good fundamental operation at 94GHz, it is also possible to operate them at 94GHz in second harmonic mode, in the same way as has been described with GaAs devices. Because of the larger peak to valley ratio, the typical operation of these devices is at a bias voltage of 10V, but with operating currents of only 200-300mA. This means that there is less power dissipation within the block than with equivalent GaAs devices.

Several InP devices working in second harmonic mode have been tested in resonant cap type cavities, and found to have similar tuning characteristics to second harmonic GaAs diodes, usually at very good power levels. Some typical results are illustrated in Figures.7.49 to 7.52. It can be seen that many of the same problems of GaAs

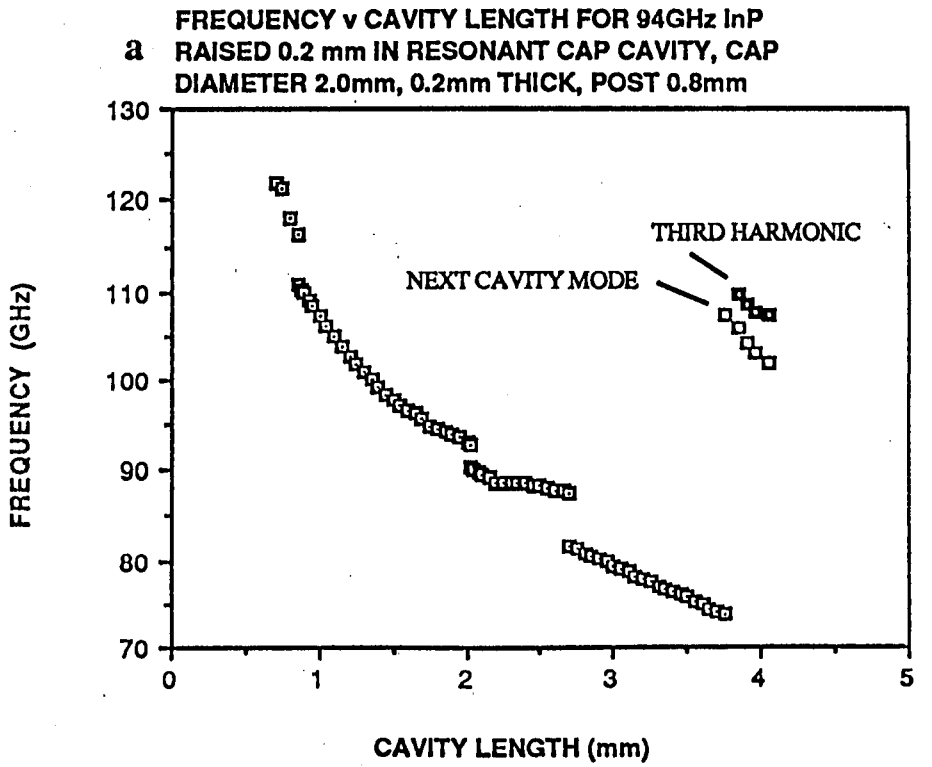
a
FREQUENCY v CAVITY LENGTH FOR 94GHz InP
RAISED 0.2 mm IN RESONANT CAP CAVITY, CAP
DIAMETER 2.0mm, 0.2mm THICK, POST 0.8mm
THIRD HARMONIC
NEXT CAVITY MODE
FREQUENCY (GHz)
CAVITY LENGTH (mm)
130
120
110
100
90
80
70
0
1
2
3
4
5

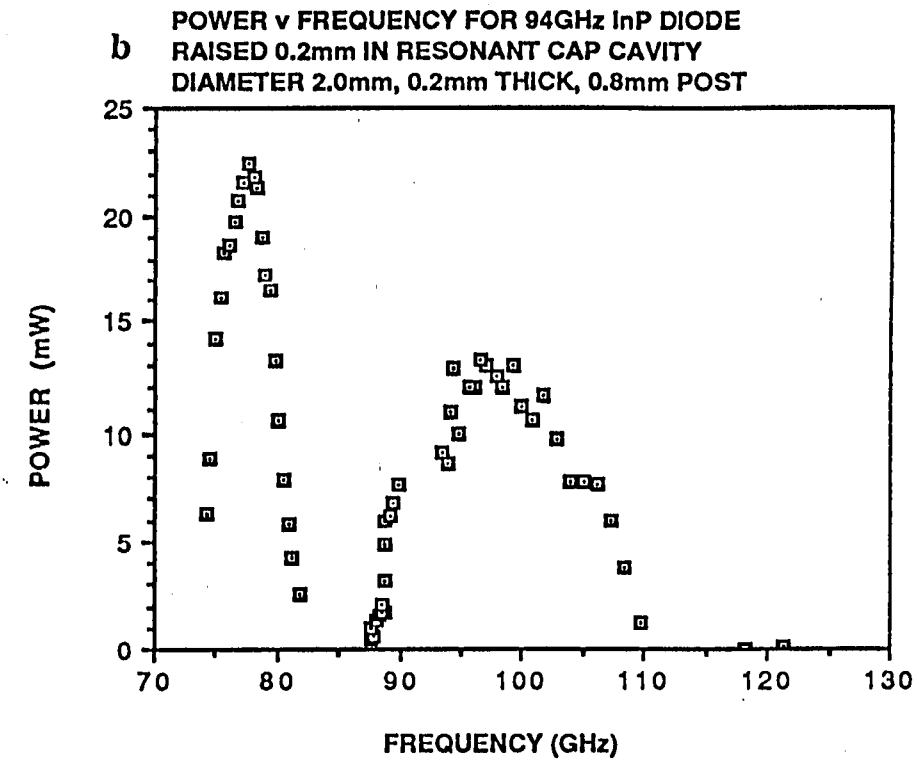
b
POWER v FREQUENCY FOR 94GHz InP DIODE
RAISED 0.2mm IN RESONANT CAP CAVITY
DIAMETER 2.0mm, 0.2mm THICK, 0.8mm POST
POWER (mW)
FREQUENCY (GHz)
25
20
15
10
5
0
70
80
90
100
110
120
130

FIGURE 7.49

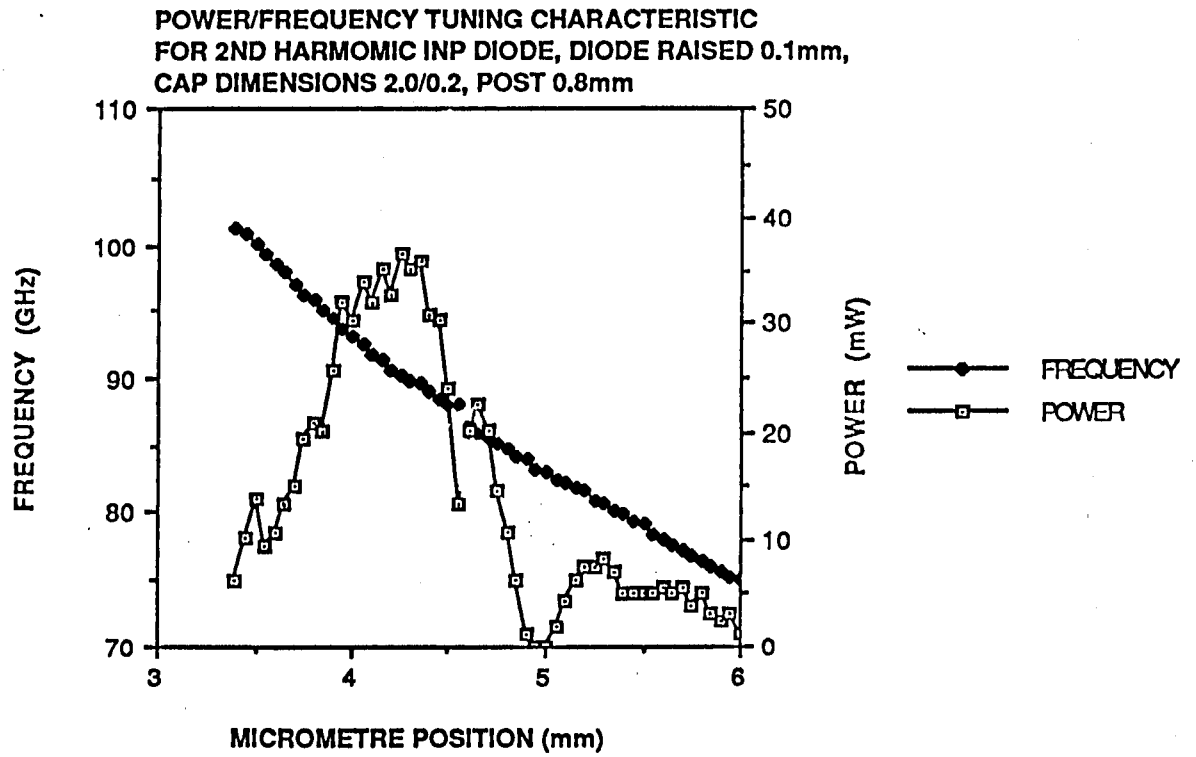

FIGURE 7.50

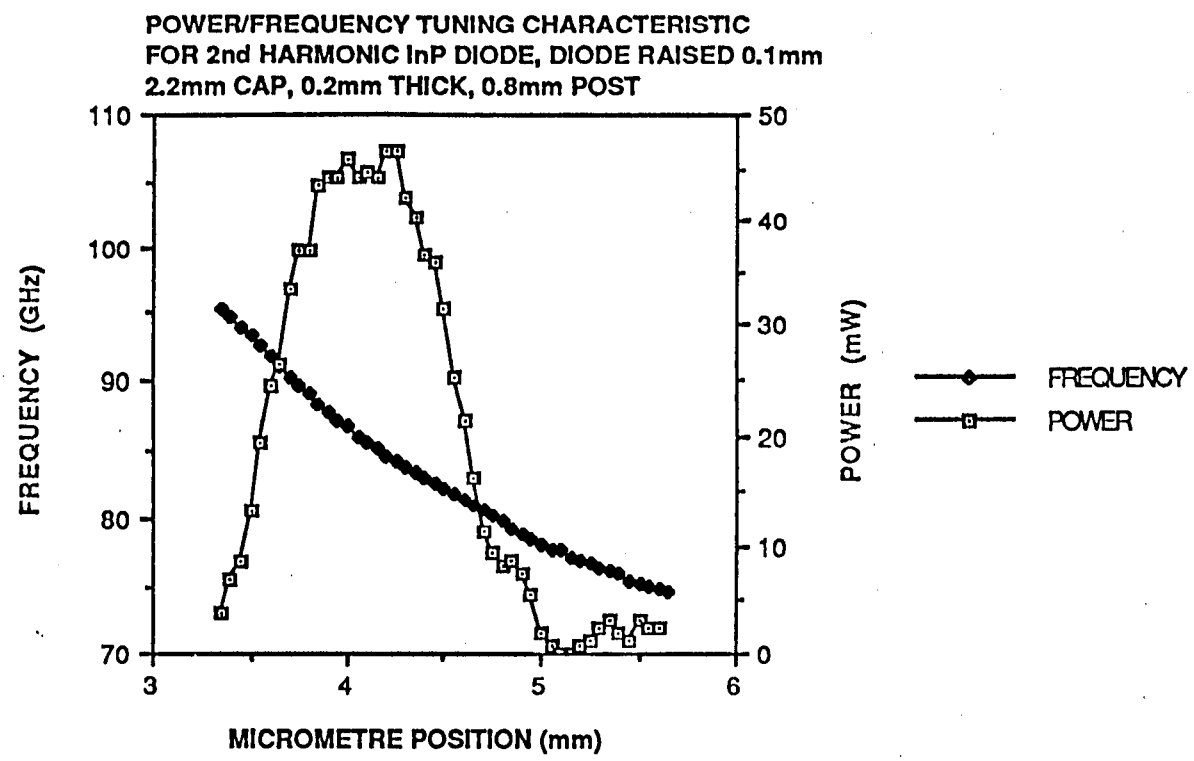

FIGURE 7.51

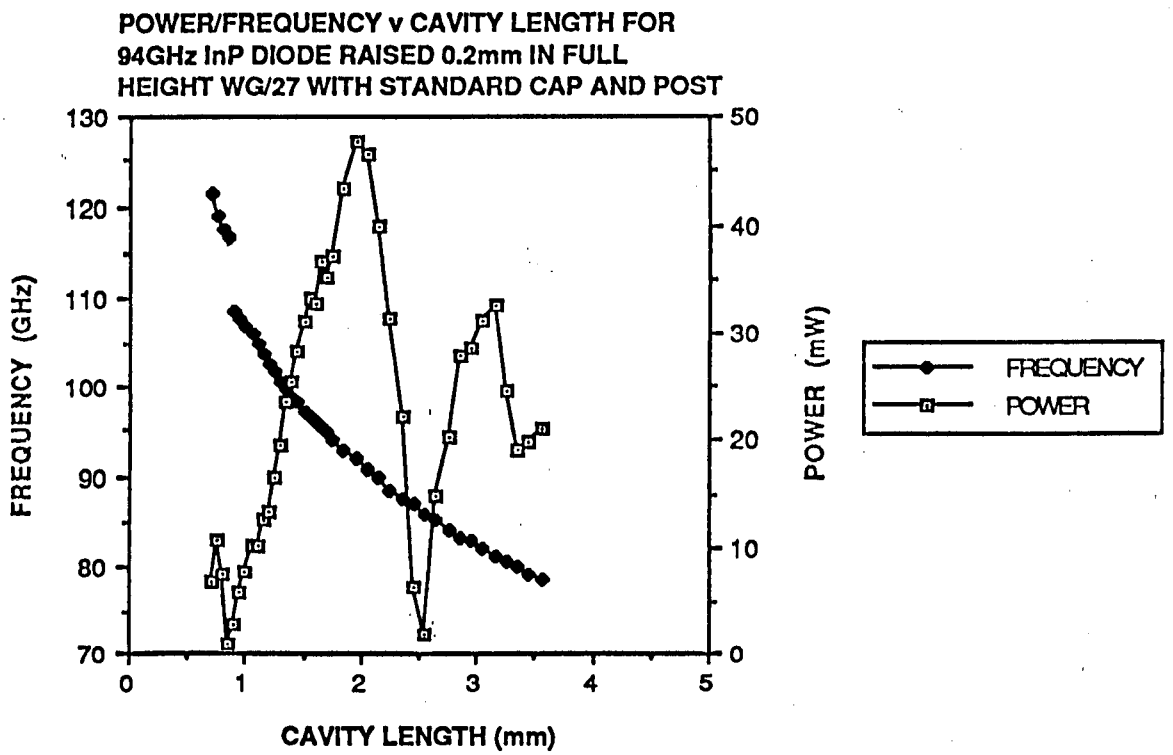
POWER/FREQUENCY v CAVITY LENGTH FOR
94GHz InP DIODE RAISED 0.2mm IN FULL
HEIGHT WG/27 WITH STANDARD CAP AND POST
FREQUENCY (GHz)
130
120
110
100
90
80
70
0
1
2
3
4
5
CAVITY LENGTH (mm)
50
40
30
20
10
0
POWER (mW)
FREQUENCY
POWER

FIGURE 7.52

devices, such as frequency jumps can still exist (Fig.7.49). It can also be seen that power and frequency characteristics can vary considerably from diode to diode in nominally identical circuits (7.49 and 7.52). This again illustrates the need for individual tuning of each diode circuit combination (Fig 7.50 and 7.51). One feature that is clearly present in Fig 7.52 is a power dip at the second harmonic that is similar to the effect seen by Carlstrom et al.

7.8.2 80GHz FUNDAMENTAL InP GUNN DEVICES

This section gives initial results of the use of InP diodes, which nominally provide fundamental output at 80 GHz in the type of oscillator blocks that have been successfully used to provide second harmonic power over wide tuning ranges using GaAs diodes. High power was achieved at frequencies ranging from 60GHz to 95GHz, and useful power was achieved at harmonic frequencies up to 150GHz. Small but clearly detectable third harmonic power was obtained at 180GHz and 226GHz. 140GHz harmonic oscillators are discussed in greater detail in the next section.

In some ways fundamental operation is just as difficult to optimise as harmonic operation at at very high frequencies. Because the fundamental frequency is now coupled to the load, the effective Q of the oscillation is generally lower for the same sort of circuit, which can lead to increased problems due to load pulling and greater noise. At 95GHz it also becomes very much more difficult to ensure that there is only one possible mode of oscillation within the cavity, as package parasitics can effect tuning and coupling. In addition, because the negative resistance of the diode can cover a very large bandwidth it may be easy for the diode to jump to a harmonic mode where the fundamental frequency is below the cut-off of the output waveguide.

No detailed circuits for use with InP diodes seem to have been published within the literature, although Varian have reported that best results at 60GHz have been obtained with a coaxial cavity coupled to a waveguide, and that best results at 95GHz have "used a 2mm cap", presumably in full height WG/27 waveguide. Circuits using IMPATT diodes at 95GHz (fundamental) have also successfully used caps.

7.9.1 RESULTS

A Varian InP diode rated at 80mW at a frequency of 80GHz was used in the initial tests. It was placed in a block that had provided good results with GaAs diodes operating

in second harmonic mode between 75-110 GHz . It consisted of a WG/28 waveguide tapering to half height, intersecting with a variable height coaxial cavity. The inner conductor of the coax consisting of the standard post circuit with the diode package screwed into the waveguide floor acting as the bottom of the cavity.

In the initial experiment the cap diameter was 2mm, the cap thickness 0.2mm, the post diameter 1mm and the coaxial cavity diameter 3mm. The results are shown in Fig 7.53 and are typical of the type of tuning that is obtained with InP diodes in this type of circuit. No calibrated power meter was available when the results were taken , but the power obtained around 95GHz was estimated to be between 20 and 50mW. The power obtained at all other frequencies was thought to be less than 1mW.

Although no "third harmonic" could be detected in the output, the frequencies above 115 GHz were identified as second harmonic for the following reasons:

1) They were very stable, low power oscillations, where the frequency did not change with backshort position within the accuracy of the measurement (about +- 100MHz). This indicates a very high Q resonance (>1000) which is typical of harmonic oscillators.

2) The spacing of the modes indicate a fundamental frequency one half of the output frequency, as the modes should repeat themselves at spatial intervals corresponding to $\lambda/2$ in the coaxial line. For example, at 120GHz the modes are separated by ~2.5mm which indicates a fundamental wavelength of 5mm (60GHz).

However, the frequencies centred on 95GHz were identified as fundamental because:

1) The power output was very high, and the backshort could pull the frequency by as much as 1GHz possibly indicating a Q of around 100, which is typical of resonant cap oscillators operating at this fundamental frequency.

2) The spacing of the modes ($\lambda/2 \sim 1.6$mm) indicates that the fundamental frequency is at 95GHz.

No "backshort pulling" measurements were made on the mode that exists between 100 and 108GHz (low power output), although it would appear likely that the output was also a harmonic frequency, with a frequency jump occurring between 115 and 108GHz. Evidence for this assumption is a frequency of 90.5GHz which was identified at a cavity length of 1.8mm at a low bias voltage which fits in well with the other fundamental resonances.

Other observations included:

a) With a 2mm cap, the smallest permissible cavity height of 0.8mm gives the lowest order resonance at 67GHz. This frequency is somewhat higher than that achieved with typical Varian "95GHz" GaAs diodes in the same package and circuit, indicating that the effective diode/package parasitics of the InP diodes is somewhat smaller.

b) A corollary of the above, is that these types of resonant cap circuit do not operate in the lowest order mode in the cavity, at fundamental frequencies greater than 70GHz. Operating with high order cavity modes has several inherent problems. Although the Q of the cavity may increase, (more energy stored) this is offset by an increase in losses within the cavity which must help to decrease the power output. More importantly, the spacing between resonant frequencies becomes closer and this can lead to mode jumping problems and unwanted frequency jumps during tuning. This is particularly problematic for these type of InP diodes, as they can exhibit negative resistance over octave bandwidths. Thus even operating with second order cavity modes, can lead to problems tuning to the desired frequency. In particular, switching to a mode below cut-off can be a problem.

c) The results shown in Fig 7.53 were obtained with a WG/28 waveguide which has a cut-off frequency at 75GHz. Operation below 75GHz is obviously possible as the harmonic frequencies are clearly evident, and appear to be favoured over above cut-off modes. This is not unnatural as they clearly have the lowest losses, (as the fundamental frequency is not loaded). They can thus appear to have the highest effective gain when the oscillation initially builds up from noise, even though the negative resistance of the diode may be larger at frequencies above cut-off.

Therefore if fundamental operation is to be achieved, a requisite is an output waveguide with a low frequency cut-off, to ensure there is no switch to harmonic operation. Optimum operation of 80GHz fundamental InP diodes has been obtained with a coaxial cavity and a WG/27 output waveguide where the cut-off is at 60GHz. Typical tuning is illustrated in Fig.7.54 where power levels exceeded 75mW between 70 and 75 GHz at a bias of 5.5V. At a bias of 6.2V power outputs in excess of 100mW were obtained in this frequency range. In this circuit it was difficult to obtain a frequency at 80GHz, and it was only obtained for the smallest possible cavity length. This would indicate that the diode/package is resonant around 80GHz in this cavity.

Attempts to produce tuneable fundamental oscillators with a resonant cap structure have not proved so successful. A typical result is shown in Fig. 7.55 where the tuning by the cap cavity is limited, and where small frequency jumps are prevalent for the high

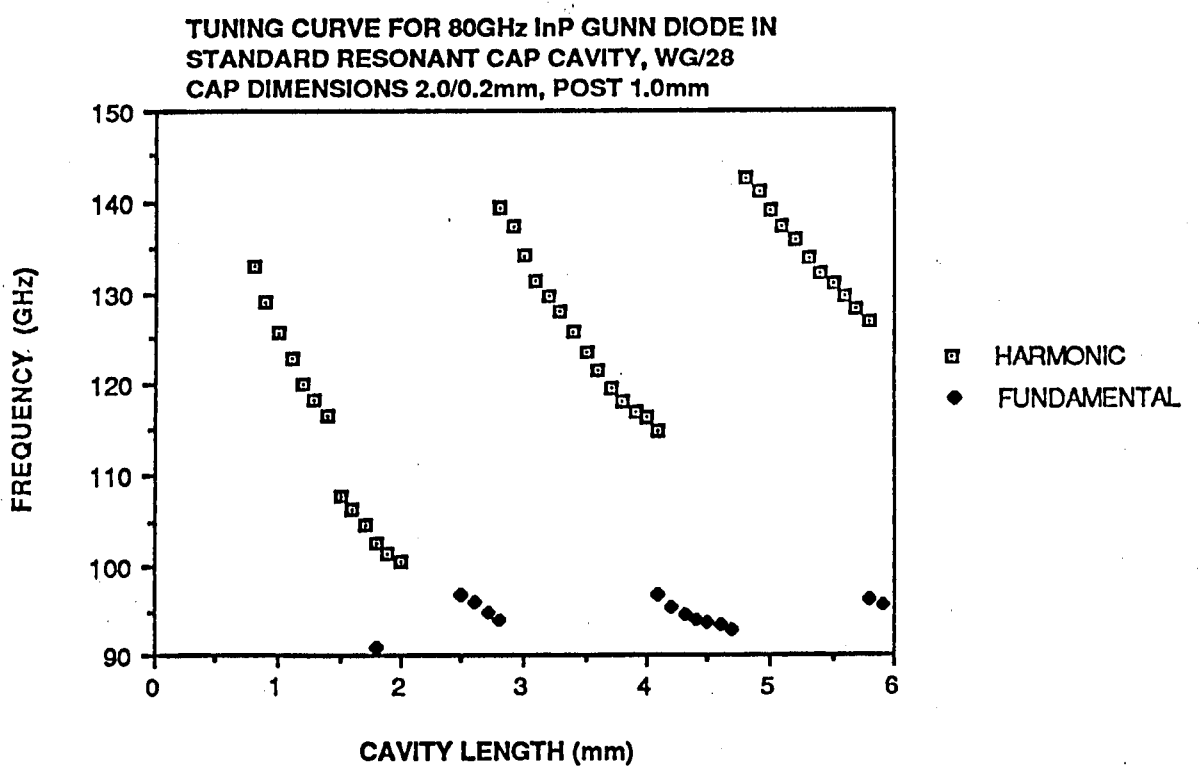

FIGURE 7.53

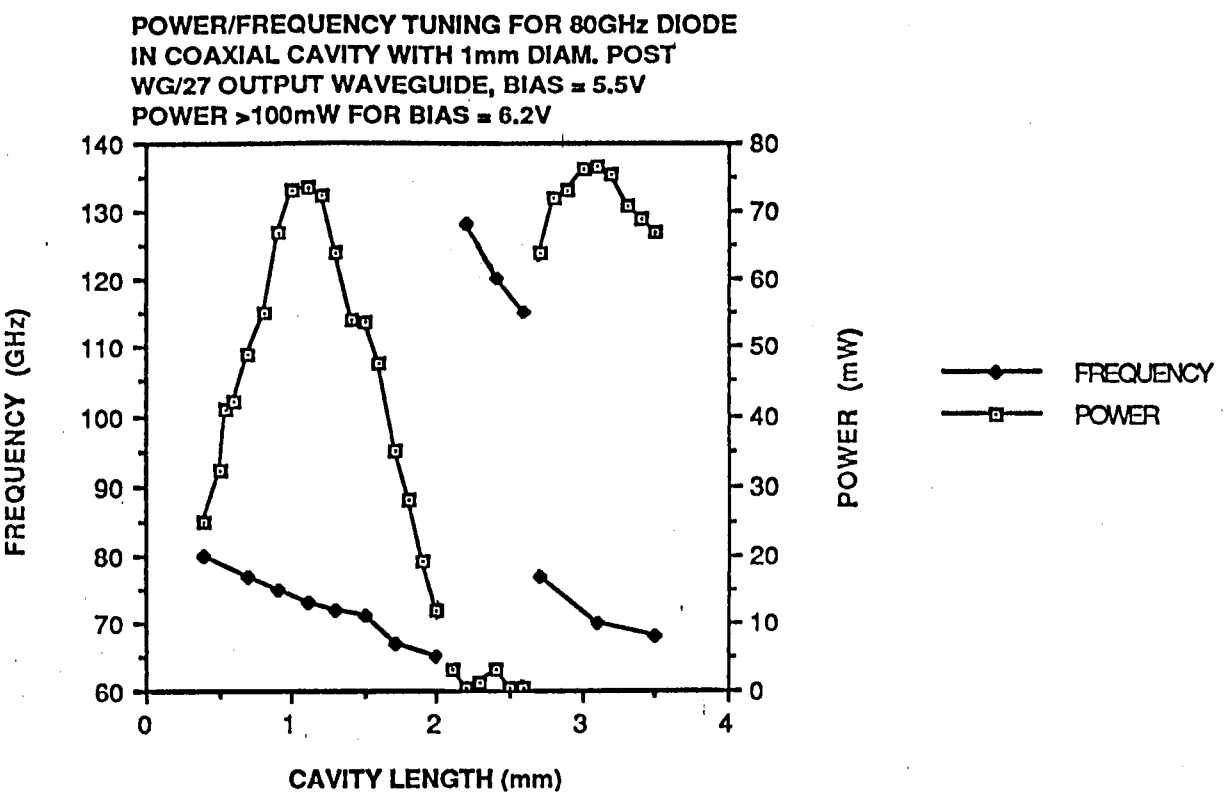

FIGURE 7.54

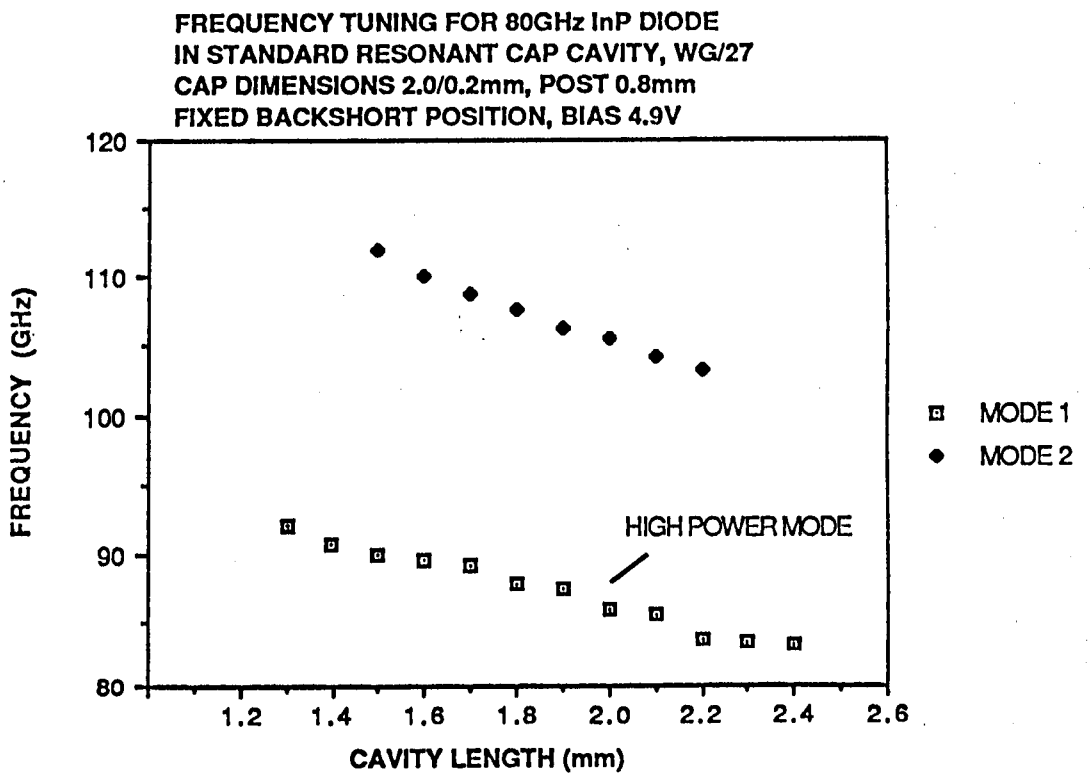

FIGURE 7.55

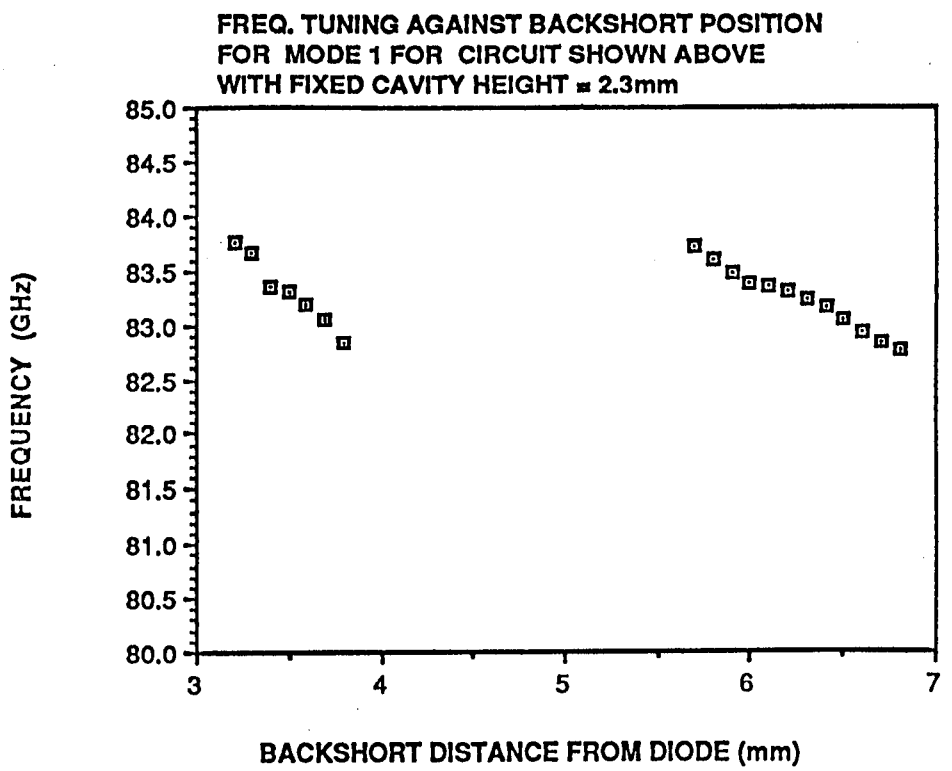

FIGURE 7.56

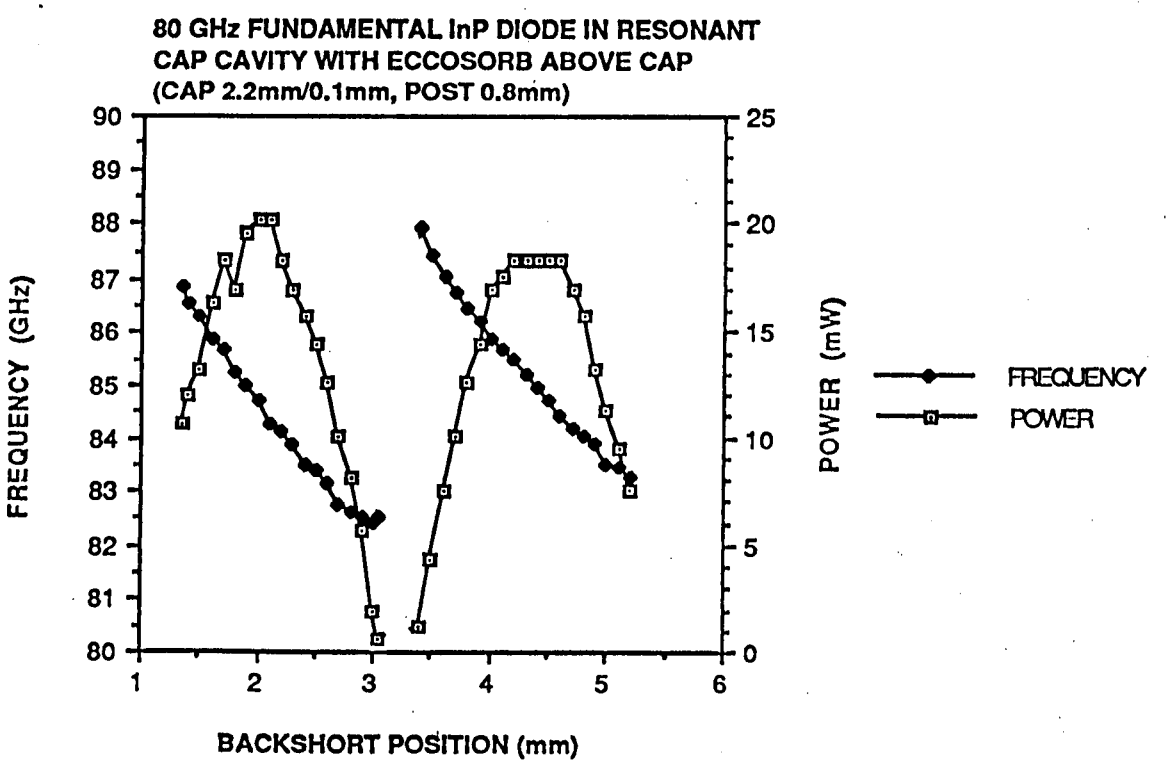
80 GHz FUNDAMENTAL InP DIODE IN RESONANT CAP CAVITY WITH ECCOSORB ABOVE CAP (CAP 2.2mm/0.1mm, POST 0.8mm)
FREQUENCY (GHz)
POWER (mW)
BACKSHORT POSITION (mm)
FREQUENCY
POWER
90
89
88
87
86
85
84
83
82
81
80
25
20
15
10
5
0
1
2
3
4
5
6

FIGURE 7.57

power mode below 92GHz. In addition, oscillation was only possible for certain backshort positions, and the backshort could pull the frequency by more than 1 GHz (Fig.7.56). Also, a jump to a second harmonic mode (mode 2) was still found to be possible. Power levels for the 'high power mode' were thought to be of the order of 30mW, although no power meter was available at the time.

The jumps in the frequency are taken to be caused by the effect of two modes 'competing' against one another. The quasi-coaxial mode, and the backshort mode. The resonant cap allows good coupling to the waveguide and strong resonant reflection from the backshort. We therefore have in effect a series and parallel circuit which may be resonant at the same time, and thus produce frequency jumps as is explained in Chapter 4. To confirm that resonant reflection against the backshort was possible, a piece of ECCOSORB was placed above the cap circuit, to make the coaxial mode look like a 80Ω resistive termination. The rather impressive result is shown in Fig.7.57 and to first order was independent of small changes in cap diameter, and changes in the height of the coaxial cavity. The backshort could pull the frequency around by over 5GHz and most power was produced at a centre frequency of roughly 84.5GHz. This power/frequency tuning characteristic strongly suggests that, for this diode, there is a package resonance at 84.5 GHz which is then heavily loaded by the backshort.

7.10 140GHz SECOND-HARMONIC InP GUNN DEVICES

The original approach here, was to use an InP (or even a GaAs device) again in 2nd harmonic mode, in the same type of circuit that had been successfully used to provide powers from 65-110 GHz with GaAs devices. It was clear from Fig. 7.53 that with a WG/28 output waveguide that 80GHz InP diodes could be made to oscillate in second harmonic mode, and Fig. 7.54 indicates that it is certainly possible to produce a large fundamental oscillation at 70GHz. There seemed to be good prospects of producing power at 140GHz. This was confirmed in the results shown in Figs.7.58 to 7.61, which shows typical results obtained for two coaxial cavities (0.8mm and 1mm diameter posts) and a resonant cap circuits of cap diameter 2.0mm and 1.55mm. Fig.7.59 shows for a resonant cap type oscillator there is a problem associated with reaching 140GHz in the lowest order mode, because of the capacitance of the cap. Reduction of the size of the cap can reduce this effect (Fig.7.61) but even with a coaxial type cavity, it appears that the tuning is eventually limited by the resonance of the package which in the case of the diode shown in Fig.7.58 and Fig.7.60 is just over 70GHz.

No power meter was available for these results, but it was conservatively estimated that below 130 GHz the power level was of the order of 0.5-1.0mW, between 130GHz-140GHz it was 0.1-0.5mW, and above 140GHz it was less than 0.1mW.

It is also clear that it was possible to obtain harmonic output up to 150GHz with this diode (at higher order coaxial modes). This is the point where the frequency cut-off of the waveguide at the fundamental is approached (75GHz). In one oscillator at particular tuning points it was possible to produce clear third harmonic output at frequencies of 163GHz and 226GHz accompanied by a reduction of power output at the second harmonic. Presumably at these frequencies the second harmonic is also resonant in the coaxial cavity and acts as an idler frequency, thus dramatically increasing the power output at the third harmonic, (which was nevertheless estimated to be only of the order 10μW).

The power output was generally low for these type of circuits, and typical measured results are shown in Figs 7.62 and 7.63. Power output was always very low in any cap circuit at 140GHz, rarely exceeding 100μW. The power maximum always occurring at a much lower frequency (110GHz in Fig.7.62). The power output at 140GHz was usually greater in a coaxial type circuit but again rarely exceeded 400μW (Fig.7.63).

It was felt that this was due to two reasons. Firstly the impedance transformation at 140GHz is probably now dominated by the parasitics of the package which would appear to be resonant at 70GHz. It may be that this fundamentally limits the impedance transformation that is possible.

Secondly, the distance between the post and the cavity wall is 1mm which is a half wavelength at 150GHz. There can be a transverse resonance at this point, and harmonic energy may be stored in the cavity, rather than transmitted to the load. Moreover, as this frequency is approached one can expect more energy to be stored in the below cut-off radial modes, and for this also to limit the potential tuning range.

The only plausible way of increasing the resonant frequency of an existing package is by reducing the size of the cavity to reduce the inductance associated with the bonding leads in the package. The reduction in the size of the cavity, also has the useful feature of removing any unwanted transverse resonances that might exist at the second harmonic frequency.

It was therefore decided that to try and improve the power output that a scaling of the whole cavity would be necessary. This has the rather unfortunate effect of meaning

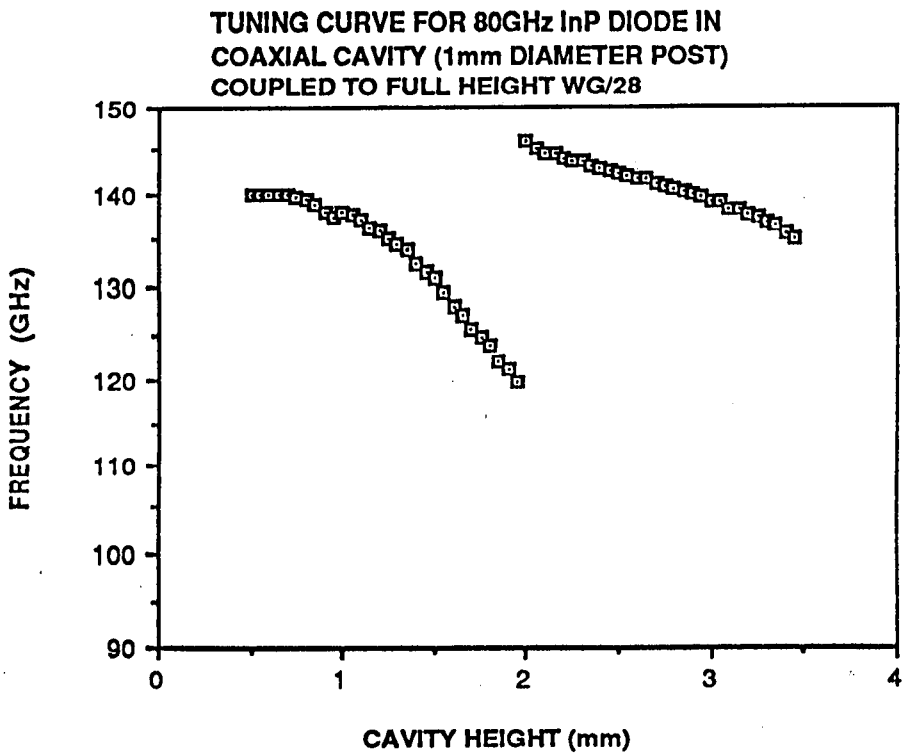

FIGURE 7.58

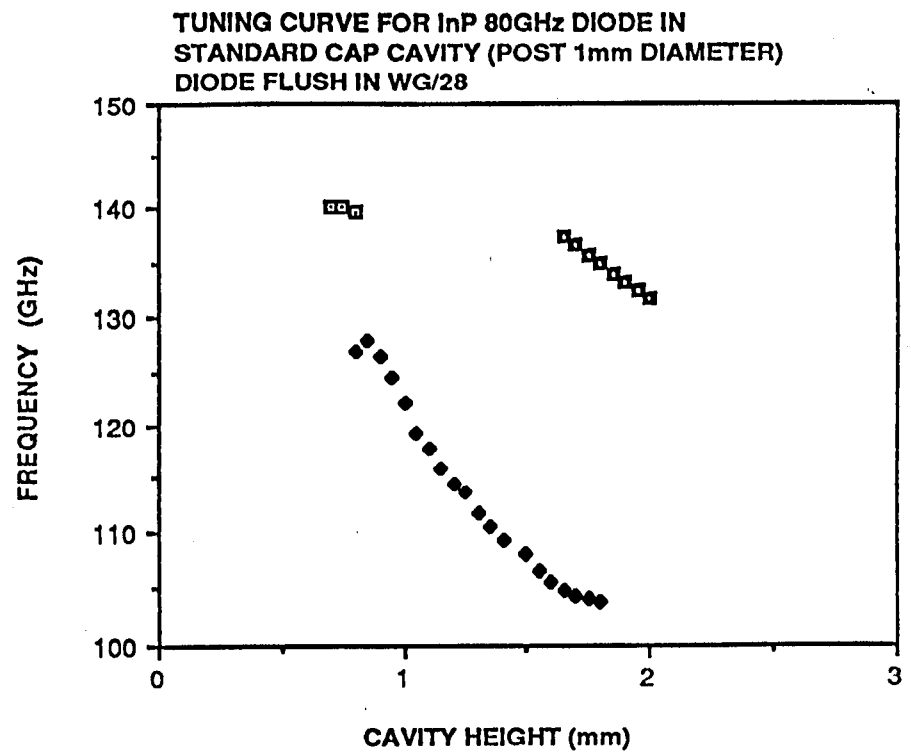

FIGURE 7.59

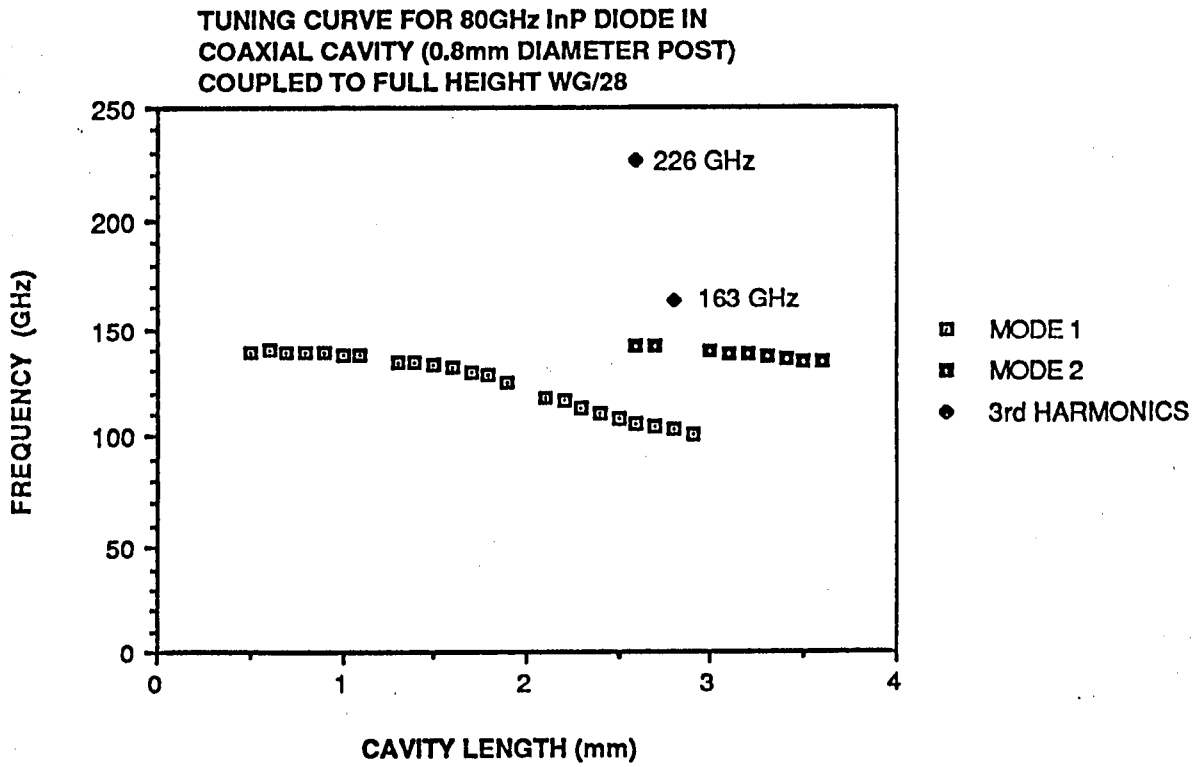

FIGURE 7.60

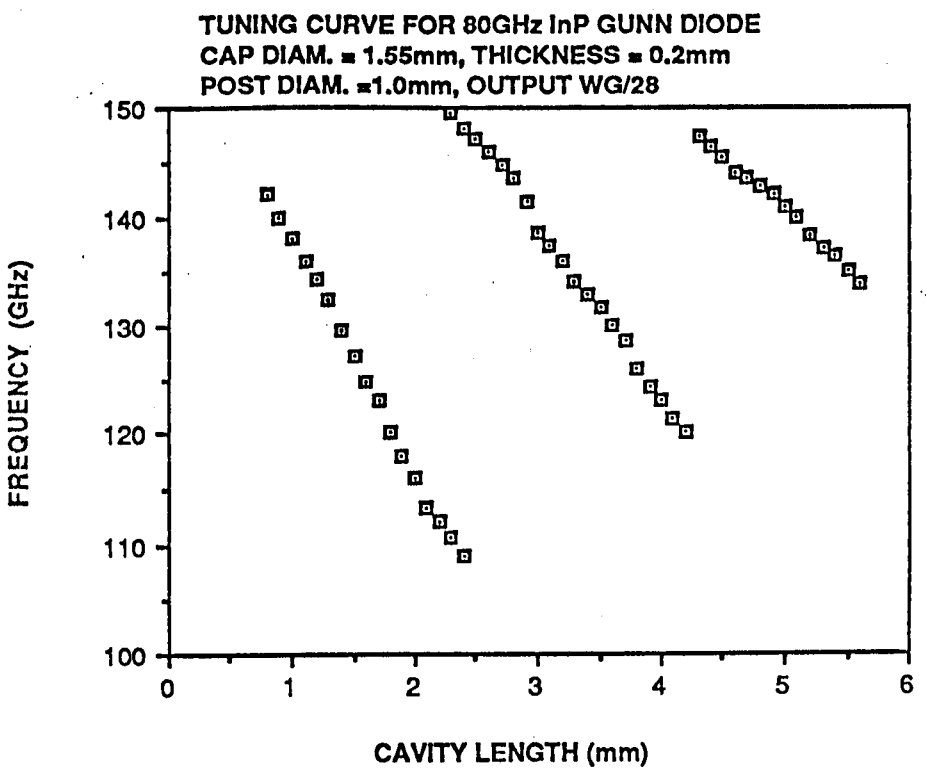

FIGURE 7.61

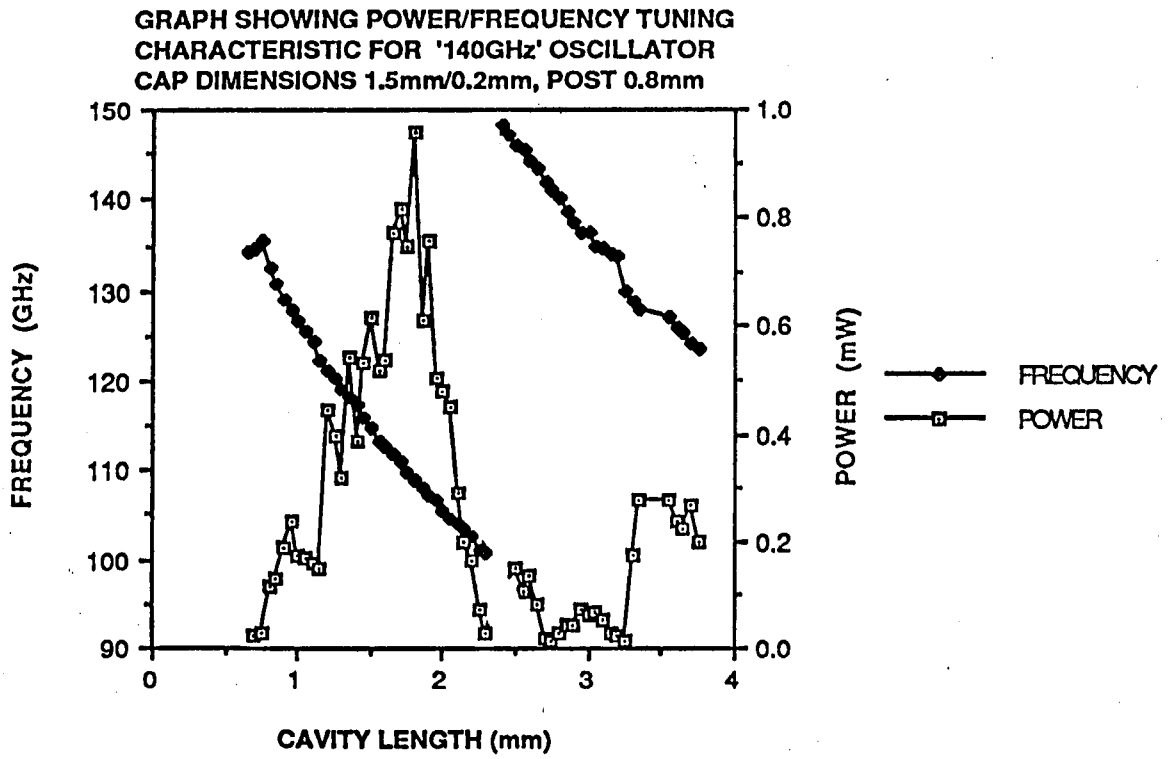

FIGURE 7.62

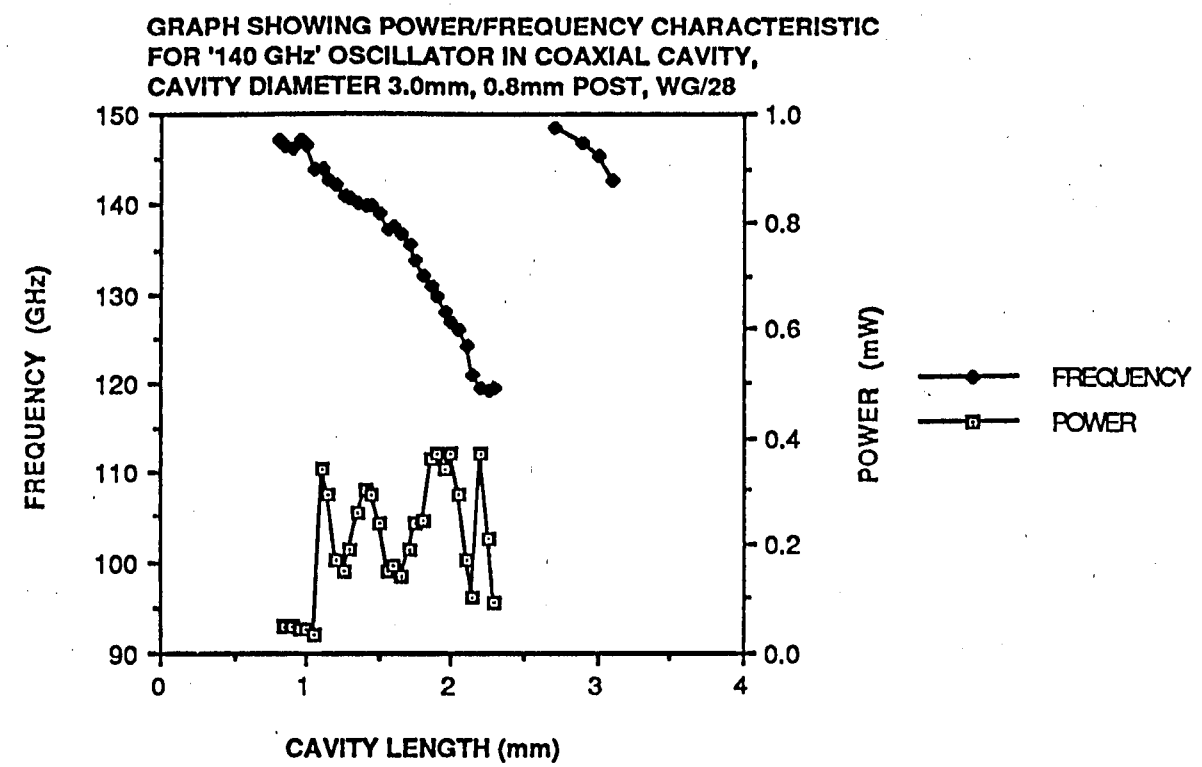

FIGURE 7.63

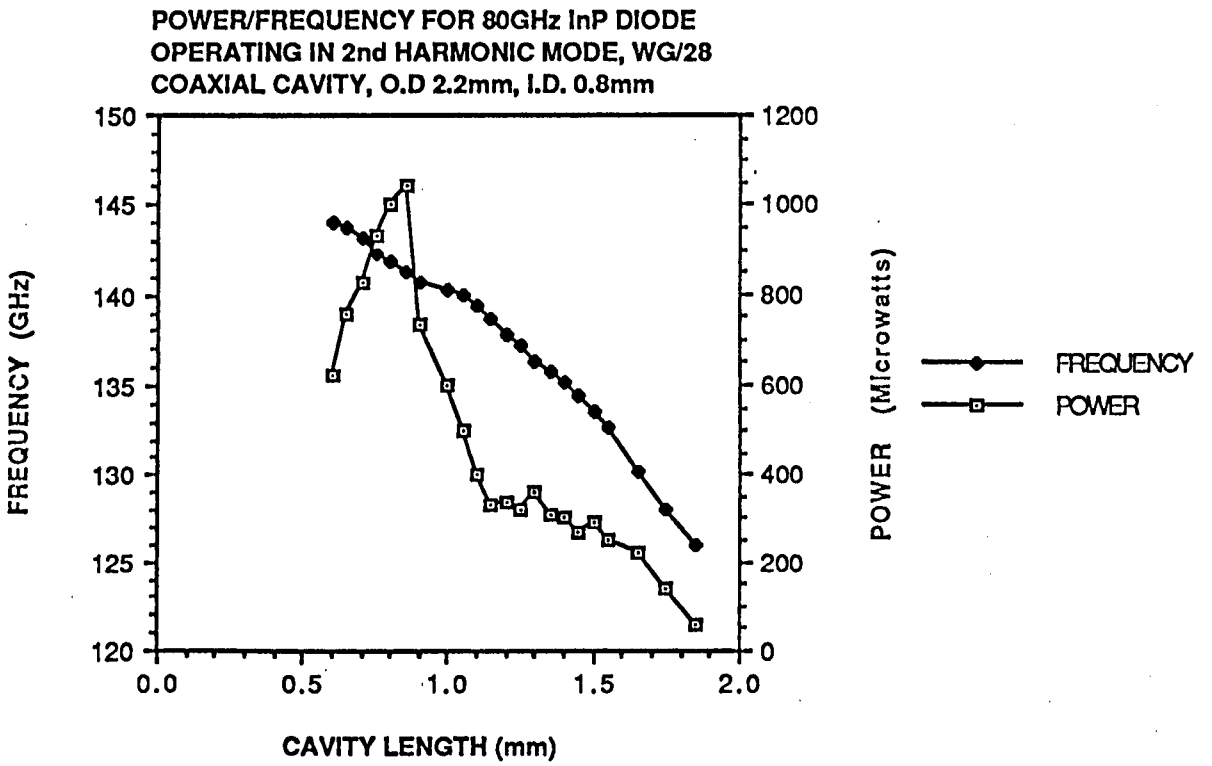
POWER/FREQUENCY FOR 80GHz InP DIODE
OPERATING IN 2nd HARMONIC MODE, WG/28
COAXIAL CAVITY, O.D 2.2mm, I.D. 0.8mm
FREQUENCY (GHz)
150
145
140
135
130
125
120
1200
1000
800
600
400
200
0
POWER (Microwatts)
0.0
0.5
1.0
1.5
2.0
CAVITY LENGTH (mm)
FREQUENCY
POWER

FIGURE 7.64

that the top of the "diode screw" must now be completely flush with the bottom of the waveguide. However, the only result I have found in the literature quoted a best power of 5mW at 140 GHz with a Varian diode (and 2mW for other diodes), for a circuit "scaled directly from a 95GHz oscillator". This gave some confidence that this approach may be successful.

A cavity of diameter 2.2mm was therefore manufactured with a 0.8mm diameter post, with output waveguide WG/28. This gave consistently higher powers than the old circuits with a 3mm diameter cavity, with the best result shown in Fig. 7.64, where a power output greater than 1mW was achieved at 140GHz in a coaxial cavity. Other 80GHz InP diodes typically gave between 400 and 500μW at 140GHz in this circuit.

This was still disappointing in terms of power output, however it was noticed that a slight mismatch at the output port of the oscillator could increase the power to as much as 1.4mW. A magic T structure was therefore designed and manufactured in WG/28 to try and optimise the output coupling. However, no increase in power was ever obtained using the Magic T, over that shown in Fig.7.64, with waveguide losses in the Magic T presumably negating any marginal improvement in output coupling.

At present, it is felt that the parasitics of the package is probably the major problem in effecting a large impedance transformation at the second harmonic. The next logical step would therefore be, either, to obtain diodes with reduced parasitics, or to design cavities with even smaller outer diameters, although the manufacturing difficulties are not to be underestimated.

7.11 GENERAL DISCUSSION OF RESULTS

It is clear that high power outputs have been obtained over large frequency ranges, and that this type of circuit is capable of providing near critical coupling for second-harmonic GaAs and InP diodes operating around 80-95GHz. The critical parameter in optimising these devices is the impedance seen at the second harmonic. This would appear to be a complicated function of circuit and diode parameters. From the results obtained from fundamental InP diodes operating in resonant cap and coaxial cavities it would appear that there are at least three resonances possible at the second harmonic frequency, all of which can load each other.

Firstly there would appear to be a resonance associated with the diode and package itself. Measurements made in resonant cap circuits where ECCOSORB was placed in the

space above the cap, showed that the power and frequency of fundamental InP diodes could be pulled, by the backshort, around a strong oscillation frequency centred at 84GHz (Fig.7.57). This effect was independent of small changes in size of the cap, and the position of the ECCOSORB relative to the cap. This resonance is presumably associated with the inductance of the bonding leads and capacitance of the package or diode, and must be a very important parameter in determining the impedance transformation at the second harmonic. In fact, it has been found experimentally [12] that the inductance of the bonding leads is a very important parameter in maximising the power output of a diode, independent of external tuning. Clearly the impedance of the diode and package is important here, although it should be noted that the inductance associated with the wires should be a function of the diameter of the cavity/waveguide in which the diode is placed. The effective inductance is reduced for small diameter cavities and it is likely that very small cavities may be required for very high frequency operation. It has also been noted that rotation of the diode within the cavity can dramatically increase the power output [12]. I would suggest that this has the effect of changing the inductance associated with the leads by bringing the leads closer or further from the waveguide wall. This may well be the critical resonance in determining optimum performance of second harmonic Gunn oscillators operating at 94GHz and may well limit performance at higher frequencies.

The second important resonance is clearly that associated with reflection from the backshort. This would appear critical to successful coupling to the waveguide. It is certainly clear that the backshort can be positioned to couple out virtually no power or a maximal amount of power. Coupling to the waveguide and backshort is via a radial mode set-up beneath the cap which then acts as a quarter wave impedance transformer to the waveguide. This quarter wave transformation is expected to be wide-band, but clearly it can be expected that lower frequencies may require larger caps.

Another important resonance that will effect the impedance seen at the second harmonic is that of the quasi-coaxial mode at the second harmonic frequency. This is the mode that (usually) determines the oscillation frequency at the fundamental. Reflection experiments indicate that the harmonic impedance of the circuit is a fairly strong function of the cavity size. The relation between the impedance seen at the harmonic and fundamental of this mode can also be expected to be a strong function of the capacitance associated with the cap. Results from fundamental InP diodes illustrated that the resonant cap is not an ideal choice for a tuneable oscillator as the waveguide mode and coaxial mode strongly load each other resulting in frequency jumps and erratic power output.

A very great deal of time has been spent attempting to model the impedance at the second harmonic but only with limited success. It is difficult to model a multi-resonant

circuit, where different modes and coupling parameters are involved, using lumped circuit theory where so many of the circuit and diode parameters are unknown. It is now my personal view that the easiest option in characterising circuits is to have a detailed experimental program to measure the change in impedance of the diode circuit combination. This would examine the impedance as a function of diode, diode package, cap and cavity size as well as backshort position. It is hoped that these measurements will be possible in 1990 when the quasi-optical impedance bridge being built at St Andrews will be completed. The impedance bridge is discussed in Chapter 10.

Some initial reflection experiments have been done which have given some interesting results, and are discussed in section 7.11.5.

7.11.1 THE BIAS VOLTAGE

The optimum bias voltage was found to change with frequency for all the diodes and a typical variation is shown in Fig.7.30, 7.39 and 7.40, which were measured for GEC diodes although the general trend was observed in all types of diode. The main feature, which was seen in all the results was that the optimum bias got lower as the frequency became higher. (In some experiments it was also noted that that the optimum bias became lower at very low frequencies, although often it was not possible to see any variation as the best power output over large frequency ranges was obtained at the maximum allowed safe bias voltage). This is to be expected as the diode is essentially a transit time device, and so requires 'faster' electrons at the higher frequencies, which calls for less scattering into the upper valley, and operation nearer threshold.

In diodes with a large negative conductance the IV characteristic is seen to be a function of frequency. Another common feature is that the maximum power is usually obtained at a d.c current minimum. This is in keeping with the idea that there is a maximal fundamental voltage and current swing.

7.11.2 VOLTAGE PULLING

Heterodyne measurements have showed that these diodes had very large frequency pulling with bias voltage. At typical operating voltages the voltage pulling was of the order 400-500 MHz/V at 85 GHz (Fig 7.67). This is possibly useful in certain applications but it may also contribute significantly to the flicker noise in the diode. (Previous experiments on low frequency Gunn diodes showed that voltage pulling was roughly proportional to

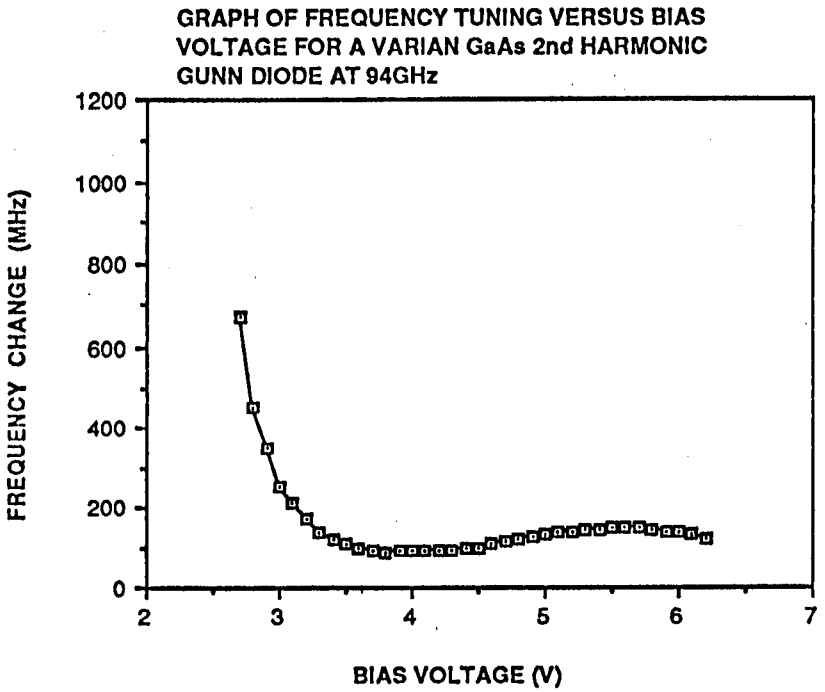

FIGURE 7.65

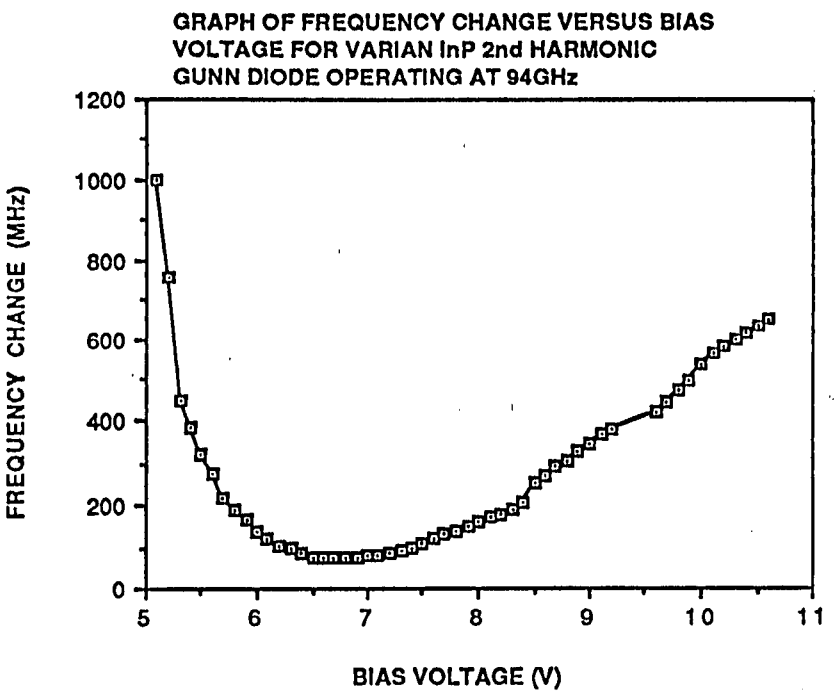

FIGURE 7.66

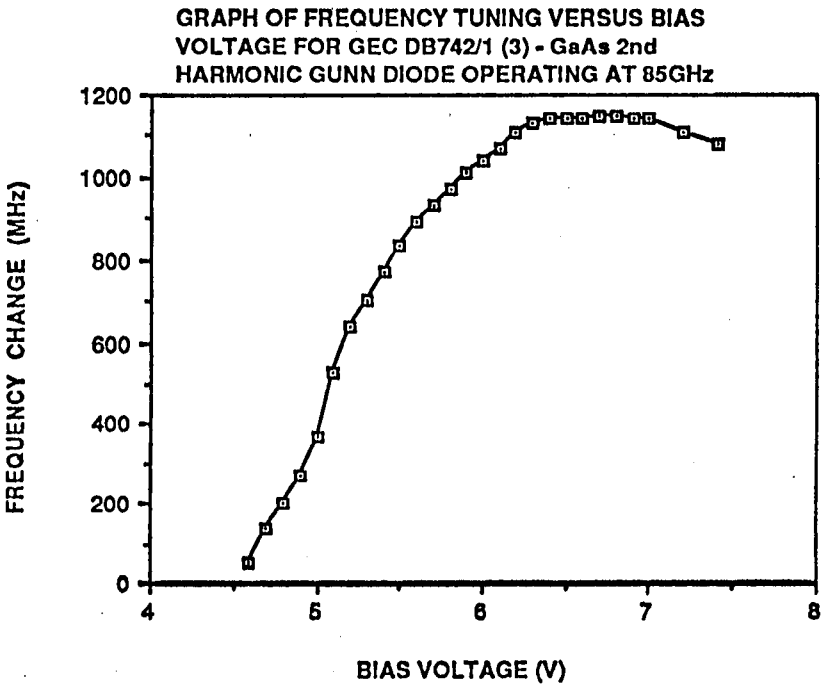
GRAPH OF FREQUENCY TUNING VERSUS BIAS VOLTAGE FOR GEC DB742/1 (3) - GaAs 2nd HARMONIC GUNN DIODE OPERATING AT 85GHz
FREQUENCY CHANGE (MHz)
1200
1000
800
600
400
200
0
4
5
6
7
8
BIAS VOLTAGE (V)

FIGURE 7.67

flicker noise [16]). Certainly care would need to be taken to reduce any noise on the bias line being upconverted.

This value is to be compared with a Varian InP diode operating at second harmonic at 85 GHz which has voltage pulling of about 100 MHz/V (Fig 7.66), and a Varian GaAs diode operating at the same frequency which had an optimum power point where the voltage pulling was very small (Fig. 7.65). For DB742/1/3 a zero slope for the voltage pulling was seen at 7V - well above the desired operating point.

There is evidence to suggest that the frequency variation with voltage is dominated by thermal rather than electrical effects within the diode. The capacitance of the diode being a strong function of diode temperature, and the diode temperature being raised by an increase in voltage. (The direct change of capacitance with voltage being very much smaller). The change in frequency with voltage is therefore a comparatively "slow" effect, with hysteresis in the tuning and a limited modulation bandwidth. Both effects having been observed experimentally.

7.11.3 HEAT SINKING AND TEMPERATURE EFFECTS

Temperature effects are definitely significant with these type of diodes. In one experiment the power output of a diode in a standard resonant cap circuit with full height WG/28 output was monitored continuously with an ANRITSU power meter. 6mW was initially obtained when the device was switched on. The block was placed on a piece of ECCOSORB and the power slowly dropped to 2mW after about one hour. The block was then cooled (until condensation started to appear) by placing it on a sheet of metal which had a metal finger that extended into a dewar of liquid nitrogen. The power output then rose steadily to saturate at a value of 9mW! In addition, small frequency jumps (~100MHz) have been seen, when the device is left running, which presumably are related to an expansion of the cavity or a variation in the device impedance.

Subsequently it was found that this problem could effectively be solved by placing heatsink compound around the screwthread of the diode package, although the power output has still been seen to drop (by up to 25%) if the block is not in good thermal contact with a large heatsink. Many of the powers reported in the initial experiments may have suffered from this problem. It also indicates that raising the diode in the cavity by unscrewing it, may well incur a thermal penalty and that a well designed movable holder might be a better design.

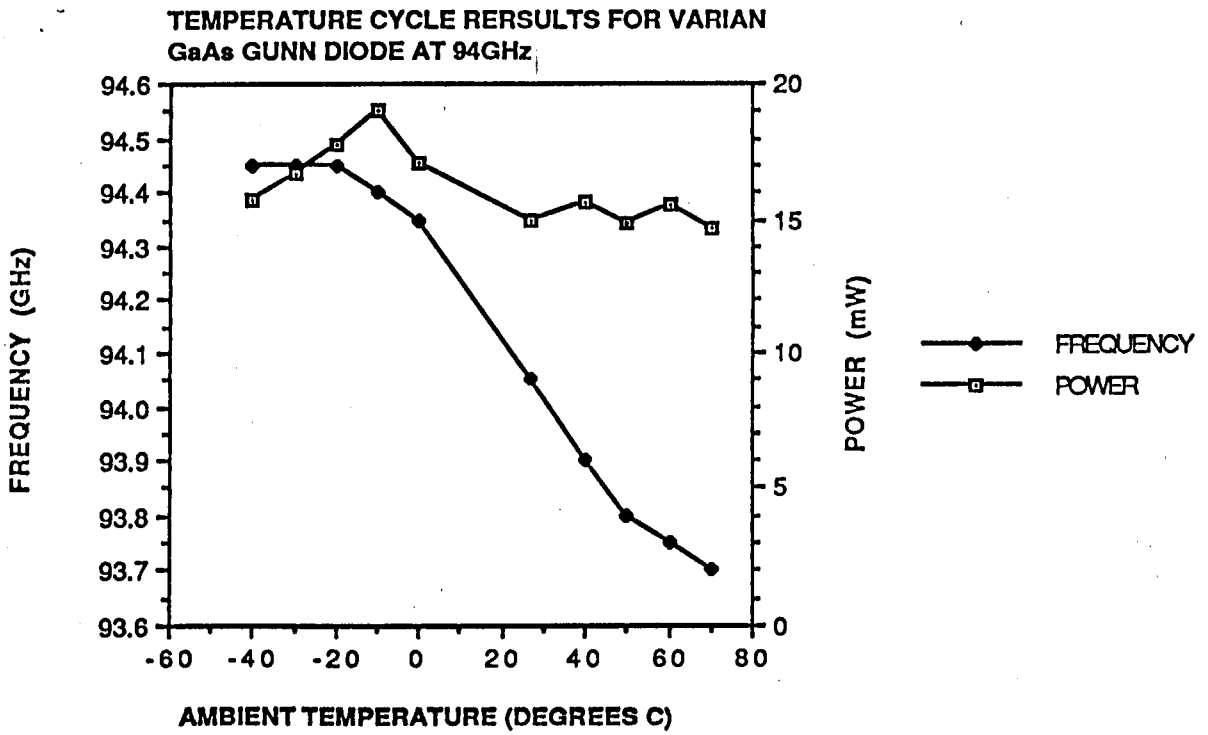

FIGURE 7.68

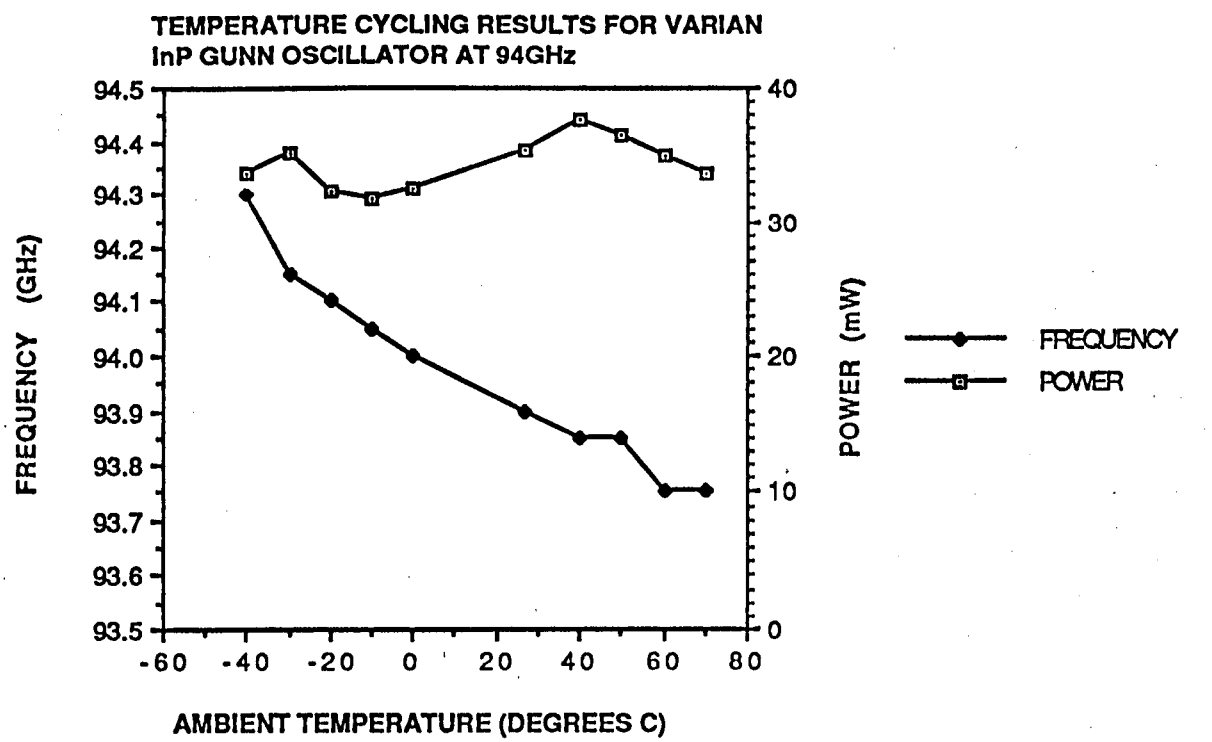

FIGURE 7.69

To look further at the effect of temperature two oscillators operating at 94GHz were tested in a temperature controlled oven at EEV. The oscillators used Varian second harmonic InP and GaAs diodes and the results are shown in Figs 7.68 and 7.69. Experiments at MEDL on devices with graded gap cathode structures have shown considerably less frequency sensitivity. Both Varian devices are expected to have metal Schottky barrier type cathodes which are expected to have a strong temperature dependence. One of the potential advantages of the graded gap cathode structure is considerably less temperature dependence.

7.11.4 CRITICAL COUPLING OF HARMONIC OSCILLATORS

As previously stated, for maximum power output, the most important criteria is to optimise the coupling at the second harmonic. For the standard cavity and waveguide it appears that it is possible to match diodes using both full and half height waveguide. A full height waveguide appears to offer more hope for critical adjustment by varying the height of the cavity in relation to the output cavity, although it should be noted that the adjustment is often fairly critical. The optimum coupling condition can be expected to change with frequency, and there is probably no static value that is completely optimum.

Ideally, in the operating mode specified above, this type of circuit potentially offers very wideband impedance transformations at the second harmonic and good power output over a very large frequency range. In practice, several unwanted circuit related effects tend to distort this performance, and appear as spurious dips or jumps in the power frequency characteristics of the diode.

1) Unwanted narrow band (3-4 GHz) power dips are sometimes seen in the output spectrum, with high power output often seen at frequencies slightly higher than the dip. The effect is also sometimes seen to be accompanied by a small distortion in the frequency tuning curve.

2) Smaller power dips are also seen near unwanted frequency jumps, during the tuning of the oscillator. Near these power dips the output can become relatively noisy and there is often a noticeable change in the IV characteristic with the d.c current increasing slightly.

3) At very high frequencies there is a limit to how far the oscillator will tune, mainly due to the capacitance associated with the cap, and ultimately by the parasitics associated with the package. For large caps, as the height of the circuit is reduced, the effective capacitance

associated with the cap increases. This can be comparable with the reduction in inductance associated with the post, and the frequency can in fact decrease. At the low frequency end, the tuning can be limited, because of a mode jump to the next highest coaxial mode as the cavity height is increased.

Higher frequencies can be reached by reducing the size of the cap, but this is normally at the cost of somewhat reducing the impedance transformation. Lower frequencies can sometimes be reached by increasing the size of the cap, or reducing the diameter of the post.

In the limit, one reaches a coaxial line type circuit, which offers the maximum range of tuning, but typically provides very low power outputs, as the second harmonic is very badly matched to the output waveguide, and sees a reactive impedance for the coaxial mode, to which it is strongly coupled.

7.11.5 THE FREQUENCY JUMPS

In several of the tuning curves for the different oscillators, frequency jumps have been observed. These fall into two categories. Firstly, there are some strange effects seen when the post height becomes very small. The resonant frequency can start to decrease with the cavity height, as is shown in Fig.7.5. This is presumably due to the increase in capacitance between the cap and the cavity roof, outweighing the decrease in cavity length. Another effect, is a jump to a constant high frequency, also shown in Fig. 7.5, when the post length becomes almost negligible. It is likely that there is a switch to some sort of radial mode or package resonance, as we reach the point where no modes are set up above the cap.

Lastly and more significantly, frequency jumps of several GHz can occur in certain oscillators. These can occur at more than one frequency in the tuning range, and are often characterised by a loss of second harmonic power, an increase in bias current and a noisy output near the jump. In addition, from the results, it would appear that it is possible to change the frequency at which the jump occurs by changing the dimensions of the cap. The greater the capacitance associated with the cap the lower the frequency at which the jump occurs. It would thus appear to be a circuit related effect rather than a device-orientated effect. The jump would also appear to be distinct from a simple jump to the next higher order mode. The results would appear to be more consistent with a loop appearing in the impedance locus of the circuit at the fundamental frequency. These type of jumps were also reported by Haydl [2].

At first it was thought that the jump could be related to resonance effects at the second harmonic, for reasons that are outlined in Chapter 5. However, with some oscillators the frequency jumps could be very large, and there was a substantial increase in bias current near the frequency jumps. The size of the current change with backshort position (which would destroy any second harmonic resonance across the diode), was always at least an order of magnitude smaller than that seen near the jumps. It was felt therefore that the jumps must be due to a loop in the impedance locus at the fundamental frequency.

As outlined in Chapter 4, loops in the impedance locus can occur across the device terminals, when a parallel and series circuit become resonant at the same frequency if the Q of the 'external' circuit is larger than that of the resonant circuit 'closest' to the device. It would appear that a resonance can occur beneath the cap, associated with the inductance of the bonding lead, and the capacitance due to radial modes beneath the cap, and the package. This is supported by several experiments where the space above the cap has been filled with the absorbing material ECCOSORB.

In one case this experiment was done for the 2nd harmonic GaAs oscillator illustrated in Figure 7.37 which showed frequency jumps centred on 75 and 72GHz. Initially it was expected that no oscillation would be possible when the ECCOSORB was inserted, but low power output was obtained either at frequencies of 75GHz and 72GHz! (the mode depending on bias and backshort position). Thus power output was obtained at frequencies where there was normally a frequency jump seen in the 'normal' tuning curve. These frequencies changed with the dimensions of the cap, but to first order were independent of the height of the coaxial cavity loaded with ECCOSORB. The conclusion is that there exists a fundamental resonance associated with the cap and the package. At certain cavity heights this resonant frequency is the same as that associated with the quasi-coaxial resonance, and a double resonant condition can exist, which can lead to loops in the circuit impedance locus and frequency jumps during tuning.

A double resonance of this type has the effect of resonantly increasing any losses in the cavity which can reduce the fundamental voltage and hence the second harmonic output. This reduction in r.f across the diode can also be expected to produce a small increase in the d.c current. Near frequency jumps, the effective Q of the cavity is expected to be reduced which can lead to more noisy output [1]. The frequency at which this occurs will be related to the parasitics of the package and the surrounding cap structure. The position where the jumps occurred would be expected to be altered by changing the dimensions of the cap. These effects are all observed experimentally.

When this experiment was repeated with an InP diode operating in fundamental mode near 80GHz the tuning curve shown in Fig.7.57 was obtained, which to first order was independent of small changes in cap diameter (2.2mm to 2.0mm) and the height of the coaxial cavity loaded with ECCOSORB. This would indicate that at higher frequencies there is a strong resonance associated with the diode package assembly.

This resonance can lead to frequency jumps in fundamental InP oscillators operating near this frequency. Fig.7.55 showed the danger of having two strong resonant competing modes in parallel and in series with one another, when operating fundamental frequency oscillators in resonant cap circuits. Many small frequency jumps were observed when tuning with both the backshort and the height of the coaxial cavity. Better tuning was obtained in coaxial circuits, when the coaxial mode is dominant, although the backshort was observed to have a less important effect in 'tuning out' the power.

No evidence of frequency jumps was reported in Carlstrom's results (half height WG/27), although he did mention that frequency jumps and anomalous tuning behaviour was obtained in a large diameter cavity (4mm). It would thus appear that any parasitic resonances with his oscillators occur at much higher frequencies than the fundamental frequency, and reduction in the size of the cavity may reduce the problem.

7.11.6 POWER DIPS

Although Carlstrom did not see any frequency jumps in his cavity he reported large drops in second harmonic power output at certain frequencies, which had a strong correlation with the dimensions of the cap. These were also observed in some of the results obtained with the diodes tested in our circuits, although it should be noted that these power dips are distinct from those associated with frequency jumps. A clear example is illustrated in Fig. 7.52 where a strong power dip exists at 85GHz. Little or no change in the IV characteristic is observed during these power dips, and often third harmonic power output becomes apparent, which strongly suggests that these power dips are associated with a resonance or impedance matching problem at the second harmonic frequency.

To test this hypothesis some simple reflection experiments were performed on a test oscillator with a GEC DB742 diode in a resonant cap cavity. Firstly the power output of the test oscillator was ascertained at three frequencies as a function of backshort position. The test oscillator was then turned off and the reflection coefficient of the oscillator was examined at these three frequencies as a function of backshort position,

using a reference oscillator and a 10dB coupler. The results are shown in Figs 7.70 to 7.72 where normalised power output and reflected power output are shown as a function of backshort position. Figs 7.70 and 7.71 show frequencies where the power output was high and Fig 7.72 indicates a frequency which had an anomalous power dip.

It is immediately clear from the results that best power output is obtained when the reflection coefficient is at a minimum and lowest power output is obtained when the reflection coefficient is very low. This suggests that the diodes may be consistently undercoupled to the load. The result also indicate that the diode is sensitive to the phase of the reflection from the backshort, as would be expected from the considerations outlined in Chapter 5.

In the case of the power dip (Fig.7.72), it was found that the reflection coefficient was always very low and almost independent of the backshort position. This suggests that the power dip is caused by a narrow-band poor impedance transformation at the second harmonic. It has not yet been definitively established what causes this effect, but one plausible theory is that it is caused by the second harmonic becoming resonant in the quasi-coaxial mode, with less power being coupled into the radial mode. The waveguide looks like a large impedance for the quasi-coaxial mode and so the coupling is dramatically reduced. One criticism that has been levelled at this theory is that the resonance is too narrow band to be associated with a coaxial resonance. However, there is also energy stored associated with the the cap structure which must increase the Q of the quasi-coaxial resonance compared to a simple coaxial resonance. Simple modelling of the second harmonic impedance (for the quasi-coaxial mode) has given rough qualitative agreement with the change in frequency of the power dip with cap dimensions.

Another plausible alternative is that there may be a resonance associated directly with the diode parasitics and the radial cap modes, similar to the resonance associated with frequency jumps at the fundamental frequency.

7.11.7 HIGHER HARMONICS

The harmonic spectrum of the diodes were investigated by coupling power into a Martin Puplett Interferometer as is discussed in greater detail in Chapter 10. A typical transform is shown in Figs. 7.73

There was clear evidence of third harmonic power output from several low power Varian diode (see Fig. 7.4), because it was easily detected below 111GHz when the second harmonic went below cut-off at 75GHz. (The power level at this frequency though,

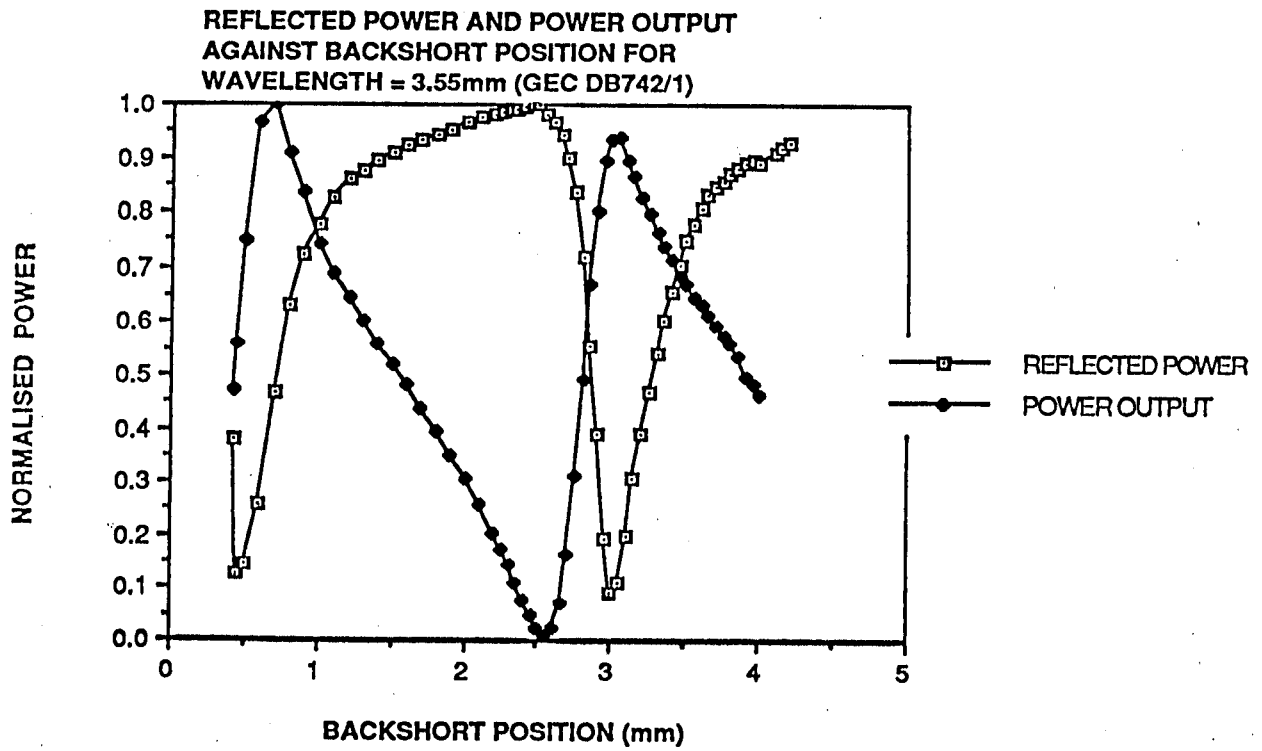

FIGURE 7.70

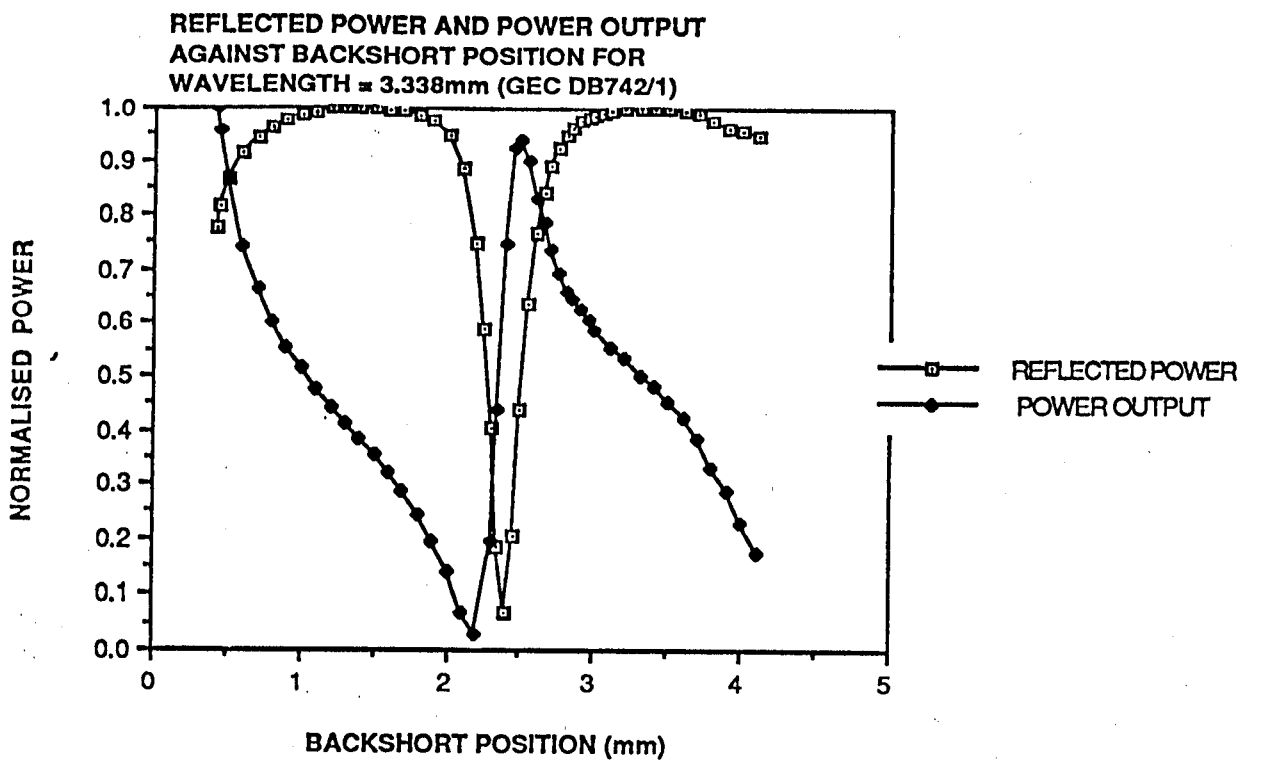

FIGURE 7.71

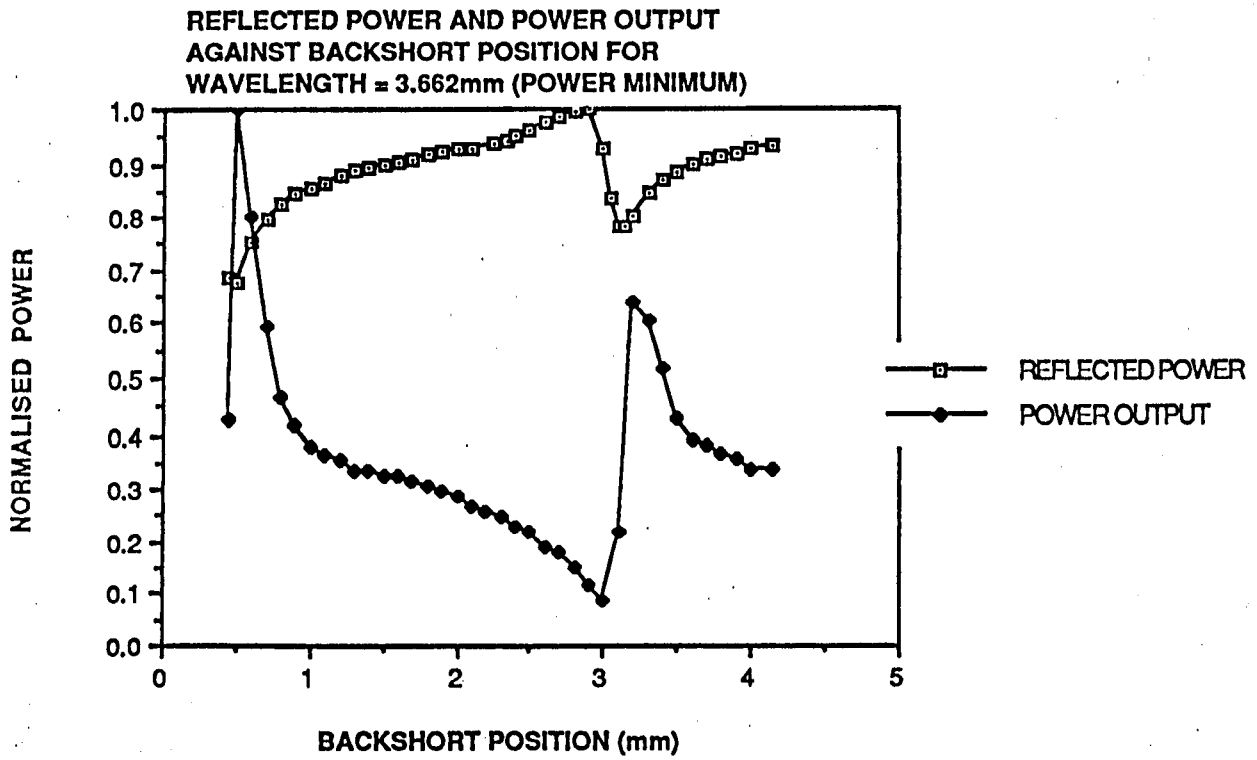
REFLECTED POWER AND POWER OUTPUT
AGAINST BACKSHORT POSITION FOR
WAVELENGTH = 3.662mm (POWER MINIMUM)
NORMALISED POWER
1.0
0.9
0.8
0.7
0.6
0.5
0.4
0.3
0.2
0.1
0.0
0
1
2
3
4
5
BACKSHORT POSITION (mm)
REFLECTED POWER
POWER OUTPUT

FIGURE 7.72

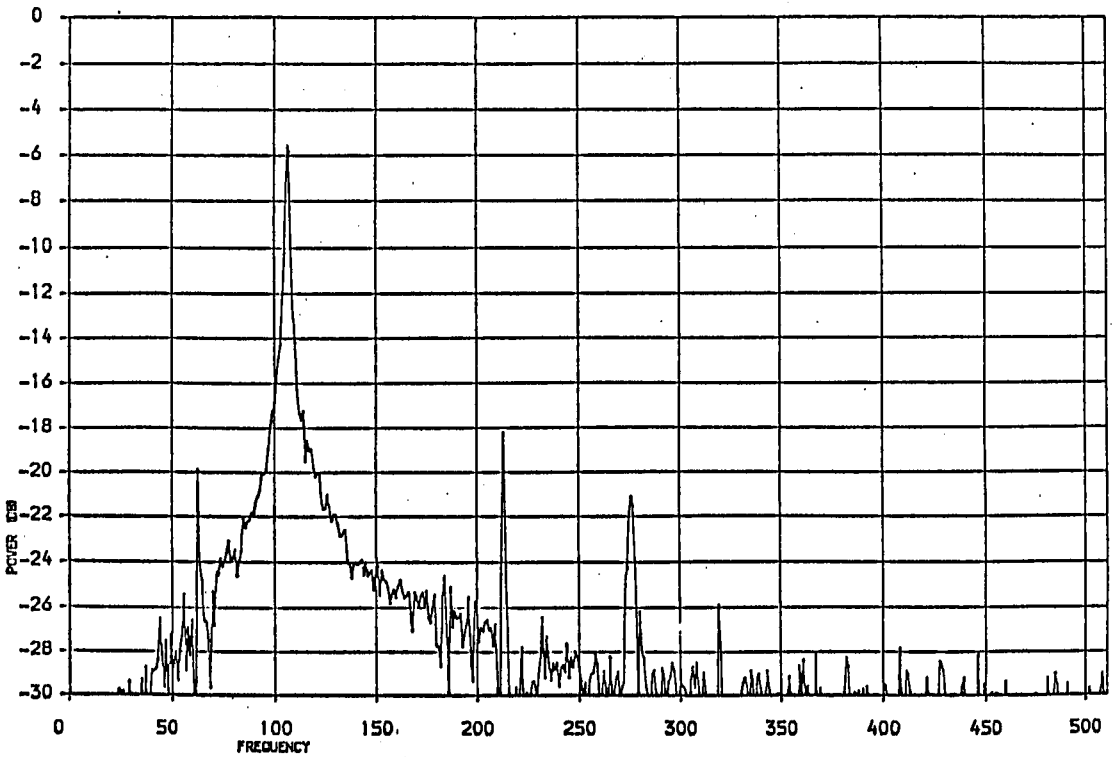

FIGURE 7.73

PLOT SHOWING THE TYPICAL FOURIER TRANSFORM OBTAINED FROM A 1024 PT SCAN ON A MARTIN-PUPLETT INTERFEROMETER. THE MAIN FREQUENCY COMPONENT IS AT ≈ 107GHz.

IT HAS BEEN SHOWN (SEE CHAPTER 9) THAT THE APPARENT SECOND HARMONIC COMPONENT CAN BE CAUSED BY STANDING WAVES IN THE SYSTEM, AND THE FREQUENCY COMPONENTS AT 65GHz AND 280GHz ARE CAUSED BY PERIODIC FLUCTUATIONS IN THE MIRROR MOVEMENT ASSOCIATED WITH THE ROTATION OF THE LEAD SCREW DRIVING THE MIRROR.

HOWEVER ANY COMPONENT AT ONE AND A HALF TIMES THE MAIN FREQUENCY (3rd HARMONIC OF SECOND HARMONIC OSCILLATOR) IS LIKELY TO BE GENUINE.

was considerably less than 0.1 mW). Moreover, there was interferometric evidence of a third harmonic frequency up to about 120GHz. The highest second harmonic frequency obtained with this diode was 99 GHz.

Third harmonic output was occasionally seen with high power 80GHz InP diodes, with clear power output obtained at 163 and 226GHz, under certain tuning conditions (Fig. 7.60).

In general, however, it was very rare to observe third harmonic with the GEC and MEDL devices and indeed for many of the Varian diodes. The measurement of the third harmonic was normally observed interferometrically by Fourier Transforming the output from a Martin-Puplett Interferometer. This is discussed further in Chapter 9. This measurement implies that the third harmonic must usually be at least 25-30dB down on the second harmonic output.

This is perhaps not surprising as a large third harmonic output would require appropriate terminations of the fundamental and second harmonic frequencies, as well as a large impedance transformation at the third harmonic. This impedance transformation is likely to be severely limited by the parasitics associated with the diode and package.

7.12 CONCLUSIONS

Basically the above can be summarised as saying that most of the structure in the power and frequency tuning characteristics in the results presented are due to circuit related effects, and that the powers obtained should always be taken as an underestimate. At the moment, the usual way to optimise the power output is to test each diode in a number of different circuits, although it has to be said that it is an extremely time-consuming process. In practice, this is achieved by adjusting the cap/post parameters and the position of the diode/cavity relative to the output waveguide. As can be seen from many of the results, the operation of the oscillator can be sensitive to very small dimensional changes in any of these parameters. For a resonant cap oscillator operating at 94GHz, the critical parameters are probably the resonant transformation effect of the diode/package, and the impedance of the quasi-coaxial mode at the second harmonic. Frequency jumps would appear to be due to an unwanted resonance at the fundamental associated with the cap and package. Power dips of the type seen by Carlstrom are clearly associated with a resonance at the second harmonic. It is strongly suspected that this is due to the "quasi-coaxial resonance" existing at the harmonic, although this needs full experimental confirmation.

It is likely that the increasing value of the inductance associated with the bonding leads at high frequencies starts to seriously limit the impedance transformation at high frequencies (>100GHz). The only effective solution being different packages and/or smaller cavities.

There is an obvious need to characterise cavities by the coupling they give at different frequencies. In addition, there is a requirement to characterise and specify what coupling a diode requires for optimum power output. It is hoped to do this in subsequent experiments, by making accurate phase and amplitude reflection measurements on cavities at 95GHz using optical techniques.

REFERENCES (CHAPTER 7)

1) J.E.Carlstrom, R.L.Plambeck, D.D.Thornton "A Continuously Tuneable 65-115 GHz Gunn Oscillator", Vol. MTT-33, No.7, July 1983 pp.610-619

2) W.H.Haydl, "Fundamental and Harmonic Operation of Millimeter-Wave Gunn Diodes", Vol. MTT-31, No.11, Nov. 1983, pp.879-889

3) R.S.Arora, N.V.G.Sarma, "Experimental Investigations of Millimeter Wave Gunn Oscillator Circuits in Circular Waveguides", International Journal of Infrared and Millimeter Waves, Vol.6, No.10, 1985 pp.951-971

4) M.J.Lazarus, F.R.Pantoja, S.Novak, M.G.Somekh "Wideband Tuneable MM-Wave Gunn Oscillator Design", Electronics Letters, Vol.17, No.20, Oct.1981, pp.739-741

5) N.Marcuvitz "Waveguide Handbook", McGraw-Hill 1951

6) M.K.Brewer, A.V.Raisenen "Dual-Harmonic Noncontacting Millimeter Waveguide Backshorts: Theory, Design and Test", Vol. MTT-30, No.5, May 1982 pp.708-714

7) J.R.Whinnery, H.W.Jamieson, "Equivalent Circuits for Discontinuities in Transmission Lines", Proc. IRE, Feb. 1944, pp.98-114

8) J.R.Whinnery, H.W.Jamieson, T.E.Robbins, "Coaxial-line Discontinuities", Proc. IRE, Vol.18, Nov. 1944, pp.695-709

9) J.Ondria, "Wide-Band Mechanically Tuneable and Dual In-Line Radial Mode W-Band (75-110 GHz) CW GaAs Gunn Diode Oscillators", in Proc. 7th Biennial Conf. Active Microwave Semiconductor Devices and Circuits (Cornell Univ. Ithica N.Y.), Aug. 1979

10) T.Misawa, N.D.Kenyon, "An Oscillator Circuit with Cap Structure for Millimeter Wave IMPATT diodes", IEEE Trans. MTT-18, pp.969, 1970

11) H. Kroemer, "Hot-Electron relaxation effects in devices", Solid State Electronics, Vol.21, pp.61-67, 1978

12) M.E.D.L., Private Communication.

13) Nigel Couch, Private Communication.

14) K.Kurokawa, "Some Basic Characteristics of Broadband Negative Resistance Oscillators", B.S.T.J.,July-Aug,1969, pp.1937-1955

15) I.G.Eddison, "Indium Phosphide and Gallium Arsenide Transferred Electron Devices at Millimeter Wavelengths", Infrared and Millimeter Waves, Volume 11, Chapter 1, 1984 (Edited by K.J.Button)

16) A.A.Sweet, L.A. Mackenzie, "The FM noise of a CW Gunn Oscillator", Proceedings of the IEEE, May, 1970, pp.822-823

17) MEDL, Private Communication

8.0 QUASI-OPTICAL DESIGN

8.1 INTRODUCTION

This section discusses the design of most of the key components that make up the quasi-optical systems that are discussed in the next chapter. It is not meant to be a complete review of quasi-optics or indeed of the components used, but it indicates the main design and manufacturing ideas that were used in the systems described in the next chapters. Most millimetre wave optics are based on the propagation of Gaussian beams and the section starts by looking at their basic properties. It then looks at the production of a highly pure Gaussian beam from a waveguide mode using corrugated horns, and their manufacture using electroforming techniques. To propagate the highly divergent Gaussian beam through a system, the design of millimetre wave lenses are briefly considered. These are used to form the so called 'beam waveguide' through a system , as well as to to efficiently match into receiving antennae or into resonators.

The design of quasi-optical resonators including coupling mechanisms and matching techniques are then examined, followed by the design and performance of optical beamsplitters, both of the dielectric sheet type, and the wire grid polariser. Lastly the use of roof mirrors are considered as a means of rotating the plane of polarisation of a beam.

8.2 GAUSSIAN BEAMS

A TEM_{00} Gaussian beam is completely defined by the size w_0 and position of its beam waist (for a given frequency). The beam radius a distance z from the beam waist is given by:

$$w(z) = w_0 \sqrt{1 + \left(\frac{\lambda z}{\pi w_0^2}\right)^2} = w_0 \sqrt{1 + \left(\frac{z}{z_R}\right)^2} \qquad 8.1$$

and the radius of curvature of the wavefront a distance z from the beam waist is given by:

$$R(z) = z\left[1 + \left(\frac{\pi w_0^2}{\lambda z}\right)^2\right] = z\left[1 + \left(\frac{z_R}{z}\right)^2\right] \qquad 8.2$$

where z_R is the so called Rayleigh Range and given by $z_R = \pi w_0^2 / \lambda$.

8.3 THE DESIGN OF CORRUGATED FEEDHORNS

Millimetre waves represent a transition region between optics and waveguide systems, where both sets of techniques are applicable and useful. To make best use of both techniques it is obviously desirable to be able to transform effectively from the TE_{10} mode in waveguide, to a symmetrical beam in free space suitable for lens optics, or illumination of paraboloidal reflectors. Such a beam can be suitably represented as a summation of cylindrical or spherical hybrid modes (or indeed any infinite set of modes!), however in many circumstances it is easier to represent a symmetrical beam by a summation of Gaussian modes. This is essentially because most beams can be adequately represented by just the lowest order Gaussian mode, and so it becomes easy to trace the path of a beam through a system without recourse to large computation.

The basic problem therefore, is to create a symmetrical beam from the TE_{10} waveguide mode. Pyramidal horns tend to have significant side lobe levels, and better radiation patterns are obtained with simple conical horns, where the TE_{11} mode is dominant. However, although the H-plane pattern is very good the electric field tapers slowly in the E-plane. This field can cause excitation at the rim of the horn, which then appears as spurious sources at the edge of the aperture, which can then distort the main beam and create sidelobes in the E-plane. One solution to this problem is to set up the higher order TM_{11} mode, and then combine it in phase with the TE_{11} mode. The fields can then cancel at the edge in the E-plane to provide a highly symmetric beam. Diagrams of the field patterns of the two modes are shown in Fig.8.1, which indicates the first 30 modes for circular waveguide. (The TM_{11} mode is normally set up by having a circular step discontinuity at the throat of the horn as in the dual mode Potter horn). However, in a normal smooth horn the TE_{11} and TM_{11} modes see different boundary conditions, and have different cutoffs, and therefore have different propagation velocities. It is difficult to combine them in phase at the aperture and the dual-mode Potter horn therefore usually has a very limited bandwidth.

The best solution to this problem is the corrugated horn. Under certain conditions, a corrugated surface presents a reactive boundary which approaches the same condition for TM and TE waves at grazing incidence. The propagation velocity for the TE_{11} and TM_{11} modes is therefore the approximately the same and they can combine to form the so called HE_{11} mode, which produces a highly symmetric beam over a reasonably large bandwidth.

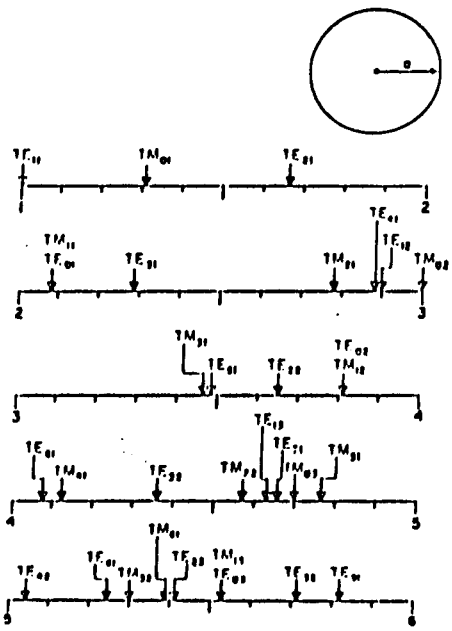

Normalized modal cutoff frequencies for a circular waveguide.

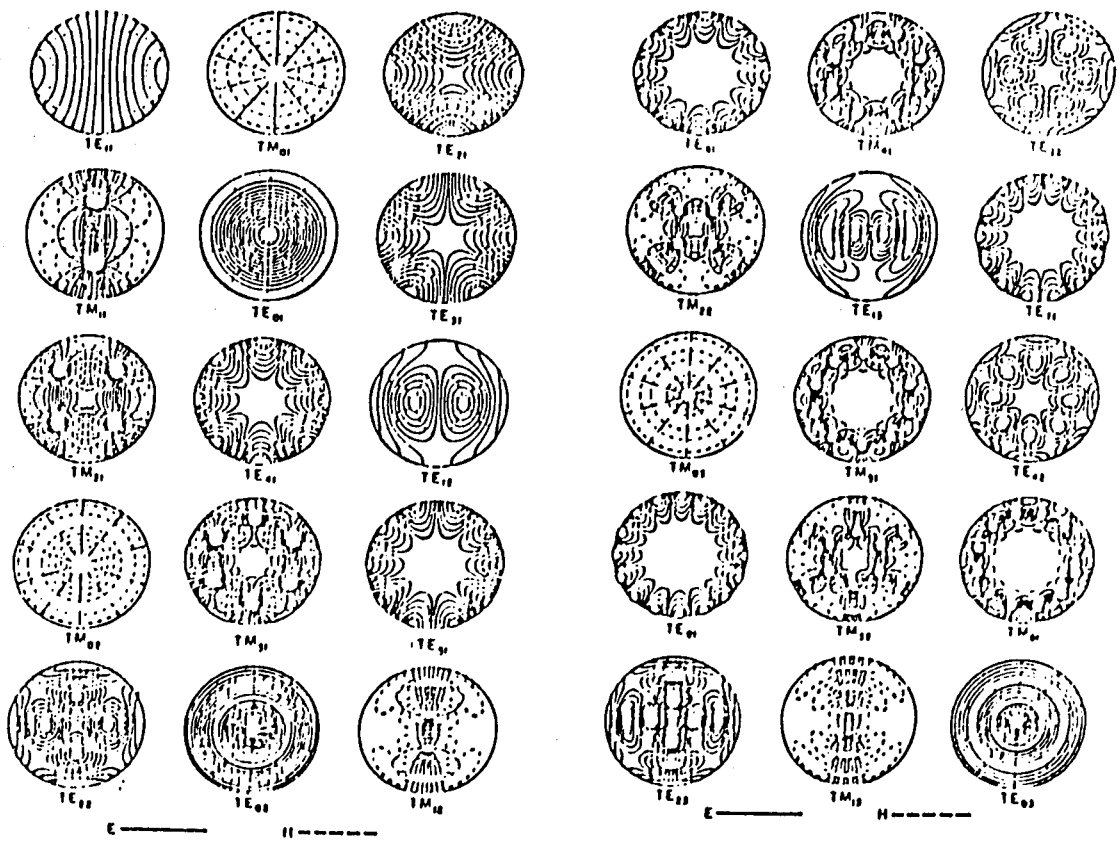

Transverse modal field distribution for a circular waveguide (fl modes).

FIGURE 8.1 DIAGRAM ILLUSTRATING THE FIRST 30 CIRCULAR MODES AND THEIR CUT-OFF FREQUENCIES. IN A CORRUGATED FEEDHORN THE TE_{11} and TM_{11} MODES ARE COMBINED IN PHASE TO PRODUCE THE HIGHLY SYMMETRICAL HE_{11} MODE. TAKEN FROM [26]

As R.Wylde [2] has pointed out, this type of beam can then be very accurately represented by just the lowest order fundamental Gaussian beam (contains 98% of the power). Relatively straightforward Gaussian beam optics can then be used to design the appropriate optical system.

8.3.1 THE HORN MODES

As previously mentioned, the corrugated horn is meant to work by setting up the TE_{11} and TM_{11} modes which combine in phase to produce the highly symmetric HE_{11} mode. This is a naturally propagating mode for a long corrugated feedhorn, however the feed is capable of supporting other less desirable modes. If the corrugations do not provide a capacitative surface ($\lambda/4 < d < \lambda/2$) then a surface mode becomes possible which can illuminate the rim of the horn causing sidelobes. In addition, another naturally propagating mode is the HE'_{11} (note the dash!) where the TE_{11} and TM_{11} modes are out of phase. This can cause cross-polarization components to appear in the radiation pattern. This effect can be reduced by having as large an aperture as possible (relative to wavelength), tapering the horn very slowly (small θ_o), and keeping the thickness of the teeth as small as possible. Another key factor is the input of the horn. It is important that the corrugated feed only supports one mode at the input if only the HE_{11} mode is to be set up. This limits the bandwidth of a horn to about 1:1.68, where this value is obtained for b/a = 1.8309, where b and a are the inner and outer radii of the corrugations. It is also possible to set up higher order HE and HE' modes which can distort the beam pattern if one does not maintain good circular symmetry within the horn.

Thus long, narrow angle flared horns with thin teeth are likely to have the best symmetrical gaussian-type radiation patterns.

8.3.2 THE RADIATION PATTERN

The critical parameter which determines the radiation pattern is the aperture phase error, which is the difference in distance between the slant length R (apex to edge of aperture) and the horizontal distance Z (apex to centre of aperture) in wavelengths. It is given by (in terms of the slant angle θ_o),

$$\text{Aperture Phase Error} = \Delta = M/2\pi = R/\lambda \sin(\theta_o) \tan(\theta_o/2) \qquad 8.3$$

where for small θ_o the approximation $\Delta = a^2 / 2\lambda R$ can be used (where a is the aperture radius). It can also be shown that the aperture phase error is also the ratio of the horn

opening angle θ_0 to the characteristic beam diffraction angle for the aperture. At large Δ (>0.7) the open angle exceeds the diffraction angle and we have the so called frequency independent limit. Here the radiated energy is confined to the angular sector determined by θ_0. The normalised characteristic radiation patterns are shown in Fig.8.3a.

For small Δ the beam waist radius becomes independent of frequency, but the radiation pattern becomes frequency dependent as is shown in Fig.8.3b.

(Note Figs.8.2 and 8.3 are produced by calculating the propagation of each Gaussian mode from the aperture and summing them in the far field. The analysis is therefore only strictly valid for narrow flare angle horns where the paraxial approximation is valid $|E| = E_y$).

Essentially, one uses Fig.8.2. and Fig.8.3 to choose the horn angle θ_0 and the slant length R to provide the desired radiation pattern. Note that Figs. 8.2 and 8.3 are applicable for any horn where just the HE_{11} mode is excited under balanced conditions, within the horn, (which is essentially true for narrow angle flared horns). One proviso, is that, it can be unwise to chose a slant angle between 12^o and 45^o. This can be seen by examination of Fig.8.4 which shows the direction of the scattered radiation when it first encounters the grooves. For certain slant angles (from a geometric optics point of view) the scattered ray can directly illuminate the horn rim as shown in Fig.8.5, which then sets up spurious current elements at the aperture which can add to the sidelobe level. This has been observed experimentally.

8.3.3 GAUSSIAN BEAM TRANSFORMATION

As stated earlier R.Wylde showed that the radiation pattern produced by the HE_{11} mode in a conical horn could be very accurately represented by a single fundamental Gaussian beam, if the appropriate beam parameters were chosen. In particular 98% of the power in the beam would be in the fundamental mode if, at the aperture, the following beam parameters were assigned:

$\mathbf{w}_{aperture} = 0.6435\ a$ where a is the radius of the aperture

$\mathbf{R}_{aperture} = R$ where R is the slant length

and $\mathbf{R}_{aperture}$ is the radius of curvature of the beam and $\mathbf{w}_{aperture}$ is the beam waist at the aperture.

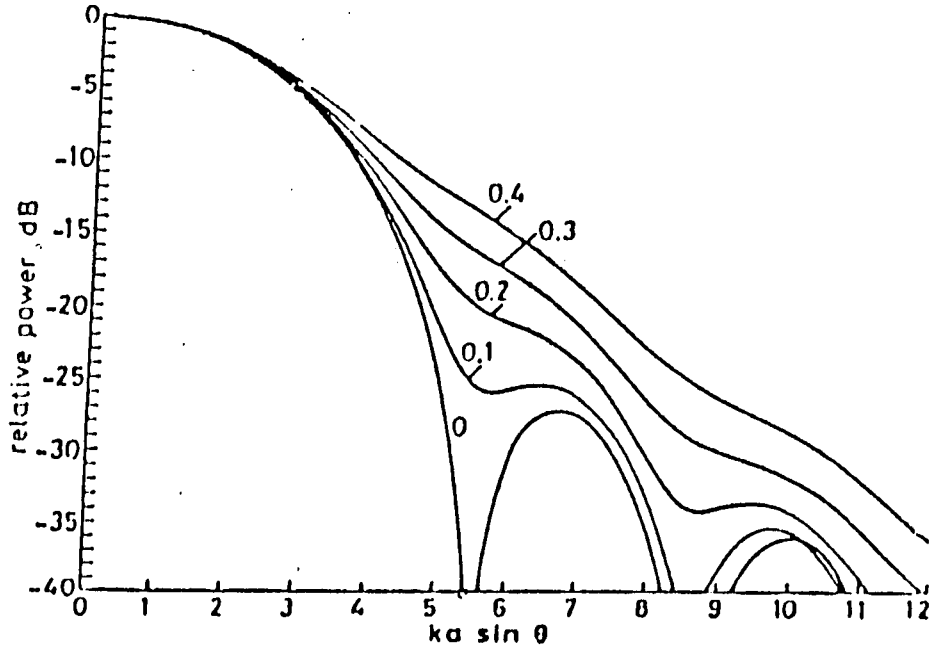

FIGURE 8.2 SHOWS THE NORMALISED FAR-FIELD ANTENNA PATTERN OF A NARROWBAND CORRUGATED HORN [2] PARAMETER IS APERTURE PHASE ERROR = $\Delta = M/2\pi$

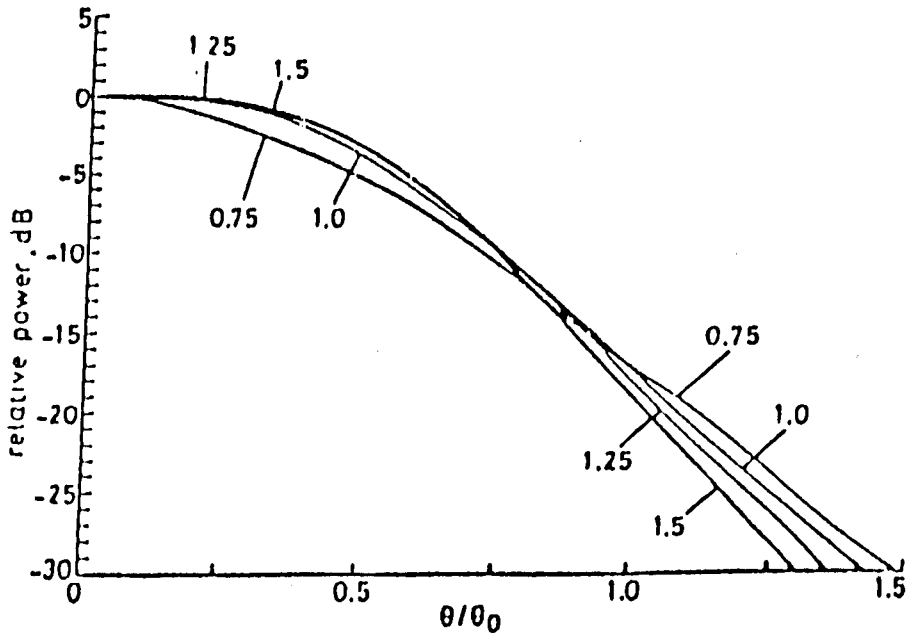

FIGURE 8.3 SHOWS THE NORMALISED FAR-FIELD ANTENNA PATTERN OF A WIDEBAND CORRUGATED HORN [2] PARAMETER IS APERTURE PHASE ERROR = $\Delta = M/2\pi$

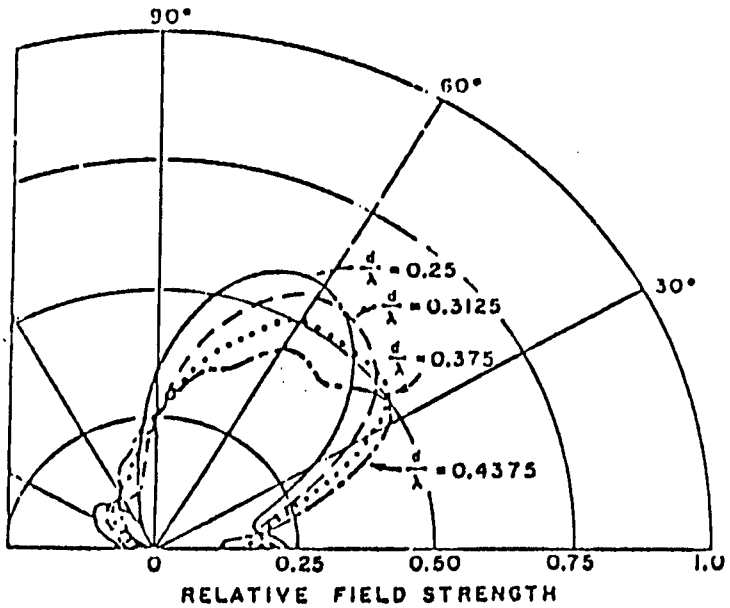

FIGURE 8.4 DIAGRAM ILLUSTRATING THE DIRECTION OF THE SCATTERED FIELD WHEN A CYLINDRICAL WAVE FIRST ENCOUNTERS A CORRUGATED SURFACE

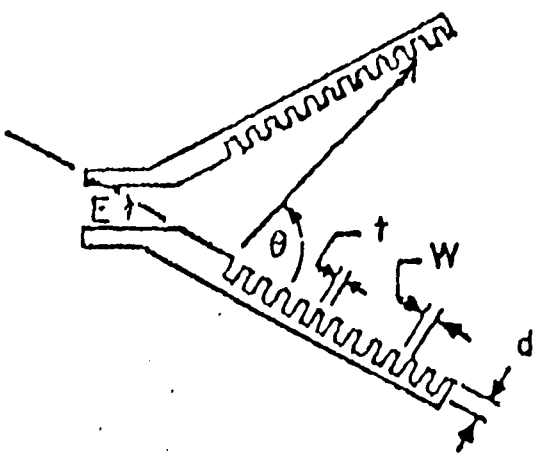

FIGURE 8.5 DIAGRAM ILLUSTRATING ILLUMINATION OF THE RIM OF THE HORN FOR A HORN WITH A WIDE SLANT ANGLE

These values can then be used to calculate the size and the position of the imaginary beam waist radius within the horn.

$$w_0^2 = \frac{(0.6435)^2 a^2}{(1 + (0.6435)^4 (2\pi\Delta)^2)} = \frac{0.4141\, a^2}{(1 + 6.77\,\Delta^2)}$$

$$R_0 = \infty \quad \text{(by definition of the beam waist)}$$

and the distance z_0 from the apex of the horn to the beam waist as a fraction of the total horn length Z is given by,

$$T = \frac{z_0}{Z} = \frac{1}{1 + 6.77\,\Delta^2}$$

Thus for small Δ the beam waist is located just inside the aperture of the horn. These values can then be used to calculate the size and radius of curvature of the beam at any point further on in the system. Note that because of the paraxial approximation, the above expressions are probably only valid for $\Delta < 0.5$.

For a typical commercial corrugated feedhorn for W-band, we have 2a = 14mm and a slant angle of 4.7^0. If we define z as the distance from the horn aperture to the beam-waist (within the horn). This gives for example:

$$\Delta = 0.287/\lambda$$

$$w_0^2 = 20.3/(1 + 0.55/\lambda^2)$$

$$z = 46.9/(0.55 + \lambda^2)$$

where in each case λ is measured in mm.

For λ = 3mm this gives w_0 = 4.37mm and z = 5.0mm, and for λ = 4mm this gives w_0 = 4.43mm and z = 2.83mm. This is illustrated in Fig.8.6 which shows the theoreticaal beam waist size and position or such a horn, as a function of frequency. Thus the size and position of the beam-waist within the horn does not change very much with frequency at least compared to the size of a typical optical system. However, because the beam waist size is essentially frequency independent, the Rayleigh range is now a function of frequency (Fig.8.7). By substituting in Eq.8.1 and Eq.8.2 we can calculate the Gaussian

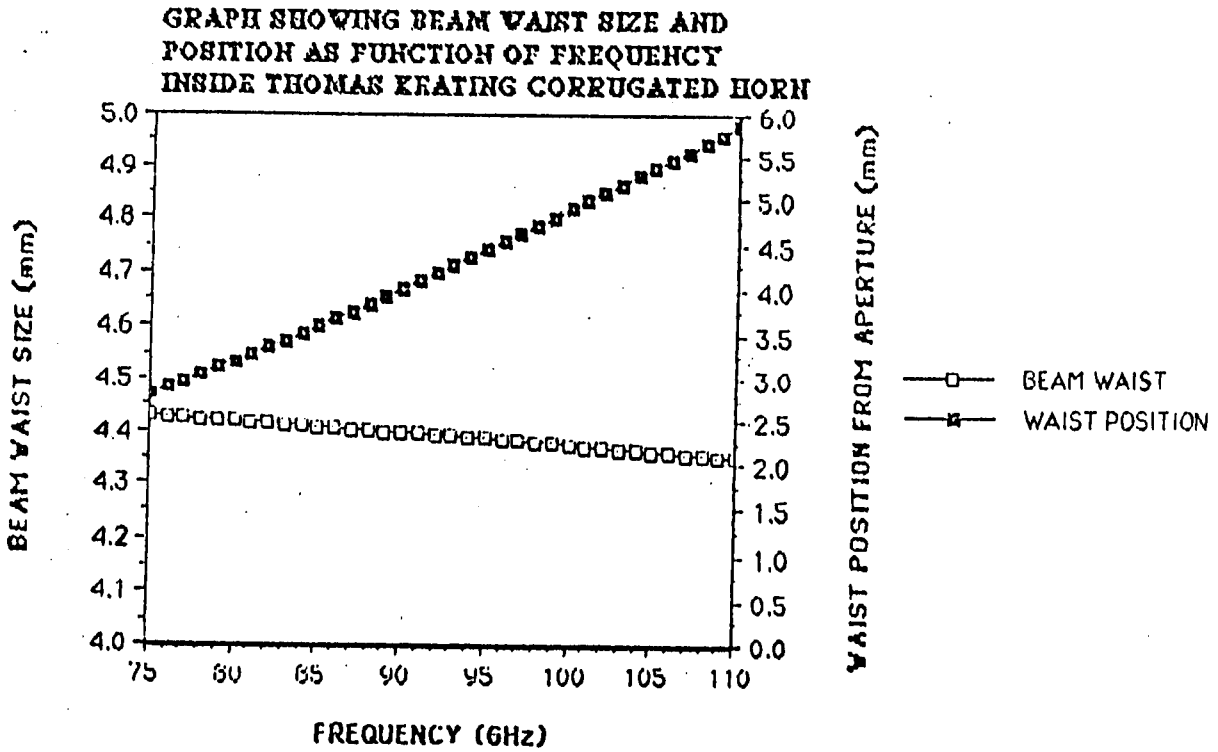

FIGURE 8.6

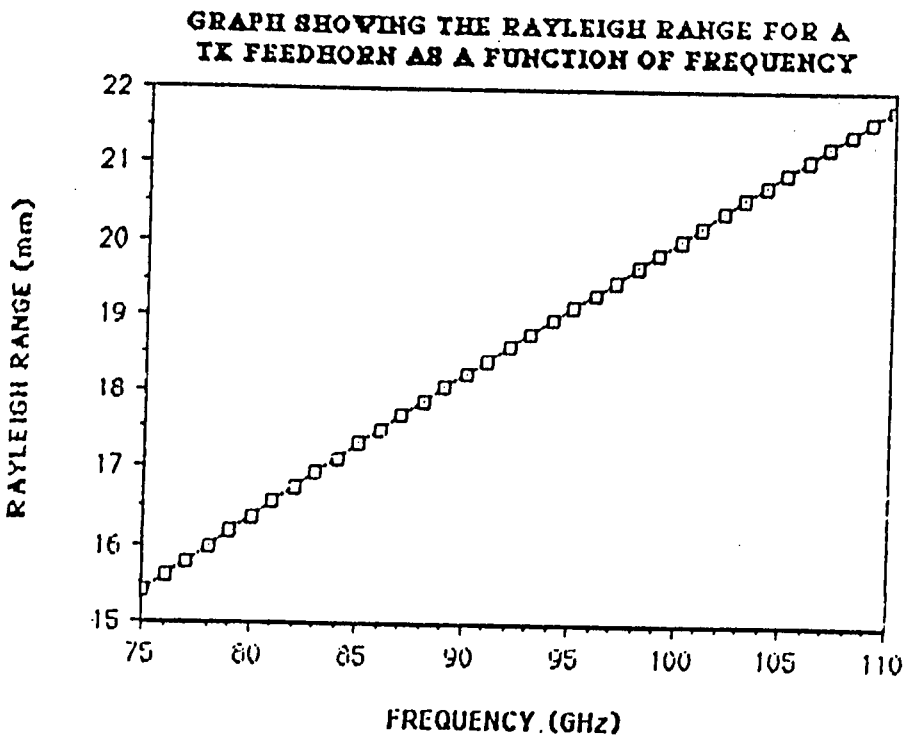

FIGURE 8.7

GRAPH SHOWING GAUSSIAN BEAM SIZE FROM A TK FIEDHORN AT FREQUENCIES OF 75GHz, 85GHz, 95GHz AND 110GHZ

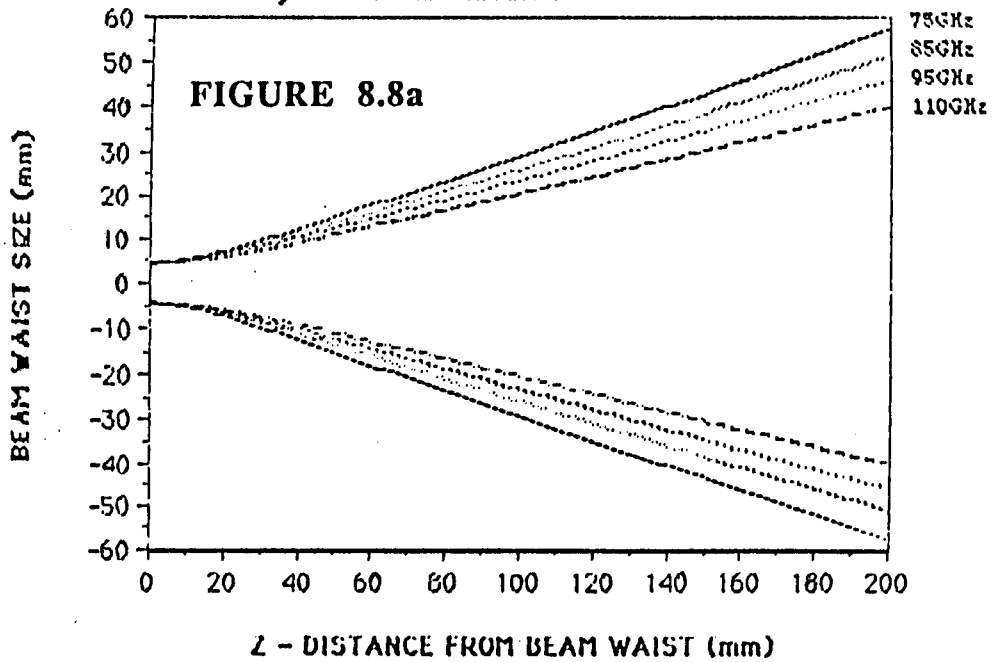

GRAPH SHOWING RADIUS OF CURVATURE OF BEAM FROM A TK FEEDHORN AT FREQUENCIES OF 75GHz, 85GHz, 95GHz AND 110GHz

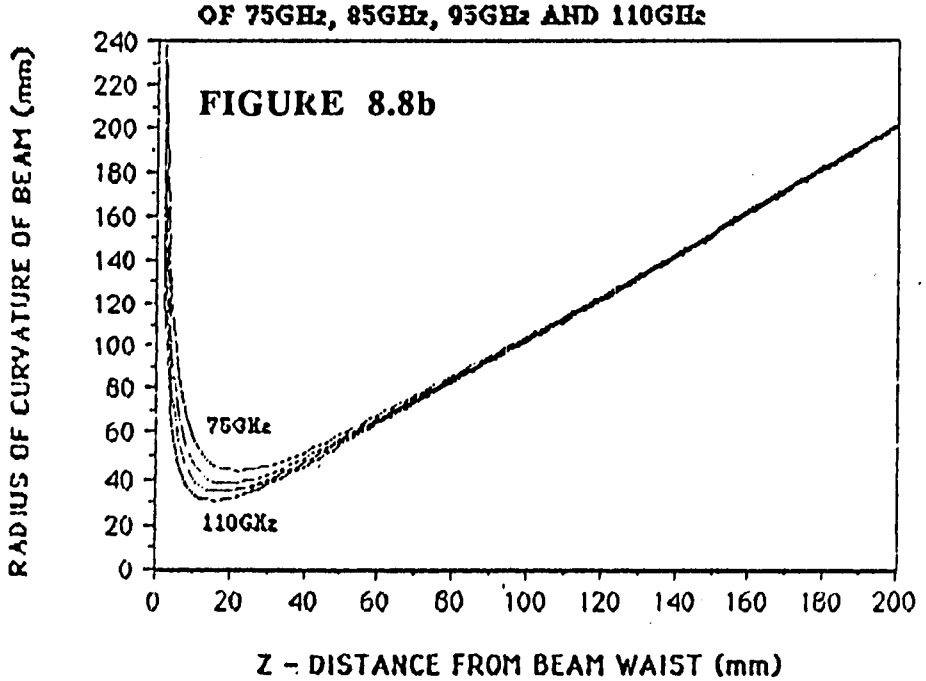

beam size and the radius of curvature of the beam, as a function of distance from the beam waist. This is illustrated in Fig.8.8a and 8.8b respectively. Such diagrams have been found to be very useful in the design of coupling optics to quasi-optical systems.

8.3.4 CORRUGATION DESIGN

This section examines the diferent design considerations in specifying the size and shape of the corrugations in a feedhorn.

8.3.4.1 CORRUGATION DEPTH

To prevent illumination of the edges of the edges of the horn it is very important that the surface reactance is capacitative, so the walls cannot support a surface wave. The corrugation depth d should therefore lie between $\lambda/4 < d < \lambda/2$. Under these conditions the grooves will scatter radiation away from the walls, which will result in a decay of surface current. This is obviously desirable as one would like as little current as possible to be flowing at the rim of the horn to reduce sidelobes. Now it is shown in Fig.8.9a that the most rapid decay of current is for $d=\lambda/4$ and there is no decay of current for $d=\lambda/2$. However $\lambda/4$ grooves near the throat of the horn can give a large VSWR, and they are also not the optimum choice for resistive loss, as is shown in Fig.8.10a. As one also does not wish to allow surface modes, this means that the corrugation depth is usually chosen to be a little larger than a quarter wavelength at the lowest frequency. This depth is often tapered towards a half wavelength near the throat of the horn to reduce the VSWR. (Note that in the grooves it is the radial TEM mode that propagates, so all wavelengths are free space wavelengths).

8.3.4.2 CORRUGATION DENSITY

Now the phase of the signal scattered by one slot compared to the next is going to dependent on the distance between slots (in wavelengths). Thus to reduce frequency sensitivity, it is desirable to have as many slots per wavelength as possible. It is also found that this reduces the VSWR, however the decay of current is found to be almost independent of corrugation density (Fig.8.9b) and the resistive losses increase significantly, as is shown in Fig.8.10b. In addition it becomes very difficult to manufacture large corrugation densities (>10 per wavelength) at millimetre wavelengths. Therefore around 95GHz corrugation densities of between 2-4 per wavelength are found to

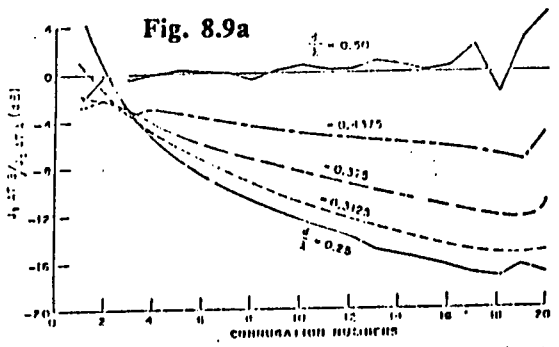

Decay of surface current on corrugated surface due to energy being lossed away from corrugation.

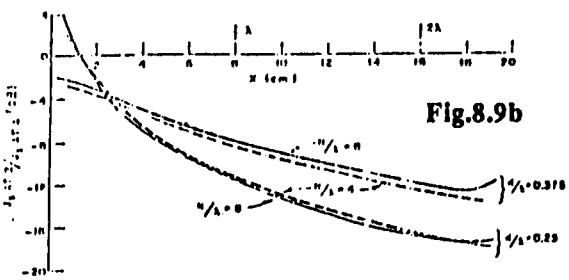

Decay of surface currents on corrugations as function of corrugation density.

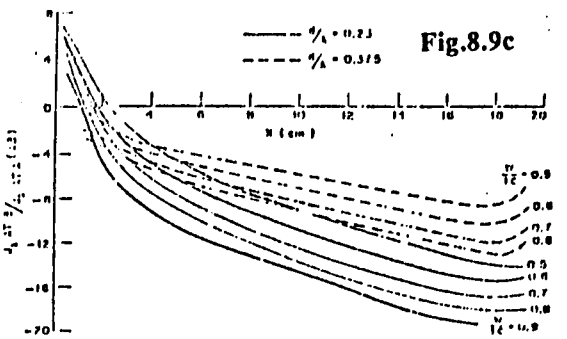

Decay of surface currents on corrugations as function of corrugation shape.

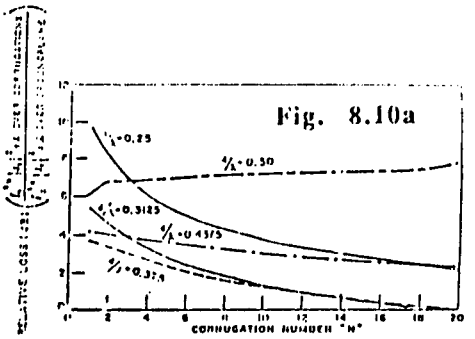

Power loss in corrugated surface for various corrugation depths.

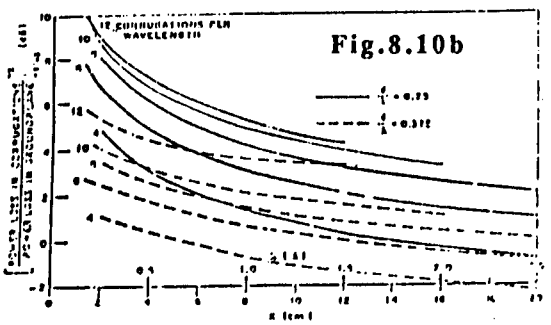

Power loss in corrugations as function of corrugation density

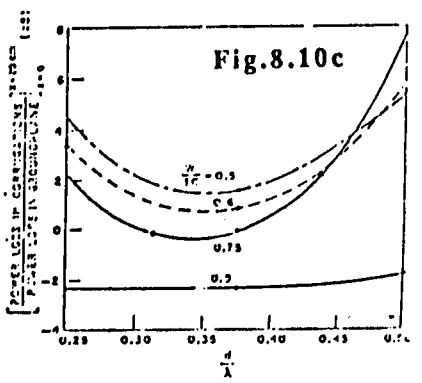

Power loss in corrugated surface with 8 corrugations per wavelength for various corrugation shapes versus corrugation depth.

LEFT - FIGURE 8.9 ILLUSTRATING THE DECAY OF SURFACE CURRENT [4] AS A FUNCTION OF a) CORRUGATION DEPTH b) CORRUGATION DENSITY c) CORRUGATION SHAPE

RIGHT - FIGURE 8.10 ILLUSTRATING THE POWER LOSS [4] AS A FUNCTION OF a) CORRUGATION DEPTH b) CORRUGATION DENSITY c) CORRUGATION SHAPE

be acceptable. One might also consider increasing the density near the throat of the horn to reduce the VSWR, although one should be aware that a significant part of the loss is in the first few corrugations.

8.3.4.3 SLOT TO TOOTH WIDTH RATIO

The parameter here, is the slot (W) to tooth (t) width ratio with the corrugation density already specified. One consideration is that the slot should only allow the TEM mode to be reflected from the slot and that the higher modes should be attenuated. This is equivalent to saying that the slot width W should be small compared to the wavelength λ and the depth d. Although in practice serious effects will only be seen when the width starts to approach $\lambda/2$ or the depth d itself. In fact, the decay of current along the wall can be shown to be faster for large slot widths (Fig.8.9c), and small teeth imply low conversion to the HE'_{11} mode. In terms of VSWR and loss, a large slot width tends to increase the VSWR but decrease the loss (Fig.8.10c). Therefore in some designs the slot width is narrowed towards the throat of the horn to try and reduce reflections, as is shown in Horn 1 which is taken from a design by Dragone.

8.3.5 MANUFACTURE

The only practical way of manufacturing corrugated horns at millimetre wavelengths is by the process of electroforming using disposable mandrils. Usually a former made of aluminium is made and then copper is electroformed on top until a sufficient thickness is achieved. The aluminium is then etched away using concentrated hydrochloric acid to leave the copper horn. The horn then can be nickel and gold plated to give a durable low loss finish to the horn. Best results are achieved when the aluminium has a high purity. An alternative is to use a wax or plastic former, when a conducting metal is either evaporated or sprayed on the surface prior to electroplating. The wax or plastic is then melted or dissolved out.

8.3.5.1 THE ELECTROFORMING

Some care must be taken with the electroforming process for copper corrugated horns, to ensure that the copper is plated all the way into the corrugations. In particular, it must be free from nodules, cracks and inclusions that can exist when trying to electroform down small holes or sharp bends. The normal technique of using copper sulphate (or

some other electrolyte using an inorganic salt) with a direct current has in general not proved satisfactory in terms of quality and speed of growth.

There has been notes in the literature that an improvement can be effected by the process of periodic-reverse-current-plating [7] where the mandrill is made alternately cathodic and anodic. The principle is that, in the anodic cycle, unsound metal or copper nodules will be preferentially deplated leaving a smooth finish to the plating and even growth. Harvey [7] stated that best results are found when the anodic and cathodic currents are nearly the same, although obviously the time spent in the cathodic cycle must be greater. He stated the optimum periods depend on the shape and size of the former but are typically of the order 20-100 and 10-40 secs for each cycle. A high power amplifier was designed that could give up to 3A with these type of switching speeds, and with any desired mark space ratio, using simple digital electronic techniques. Initial attempts to electroform waveguide transitions, using this technique, however proved unsuccessful and more recent literature has indicated that little improvement is to be gained over a simple constant voltage source.

More important criteria, would seem to be the purity of the aluminium, copper and copper solution as well as the cleanliness and finish of the aluminium mandril.

There are several "recipes" for copper electroplating. These are given in more detail in the APPENDIX (also see [8]).

8.3.6 W-BAND HORN DESIGN

Both corrugated and smooth horns have been designed and manufactured to operate in W-Band, and a smooth horn has also been made for 140GHz. Smooth horns are comparatively simple to design and manufacture and have given quite good beam patterns. Their design will not be considered any further here, although an excellent critique can be found in Ref. However, it should be noted that smooth horns become very competitive with corrugated feeds as the frequency increases towards 200GHz, as not only is the manufacture considerably easier, but the resistive losses in the corrugations starts to become prohibitive. The first corrugated horns manufactured gave good beam profiles but were lossy and had significantly worse VSWR's than commercial horns. This was attributed to the fact that the corrugated mandrils were manufactured by hand and had a number of imperfections, especially at the throat of the horn. The electroplating and etching process appeared to have been successful.

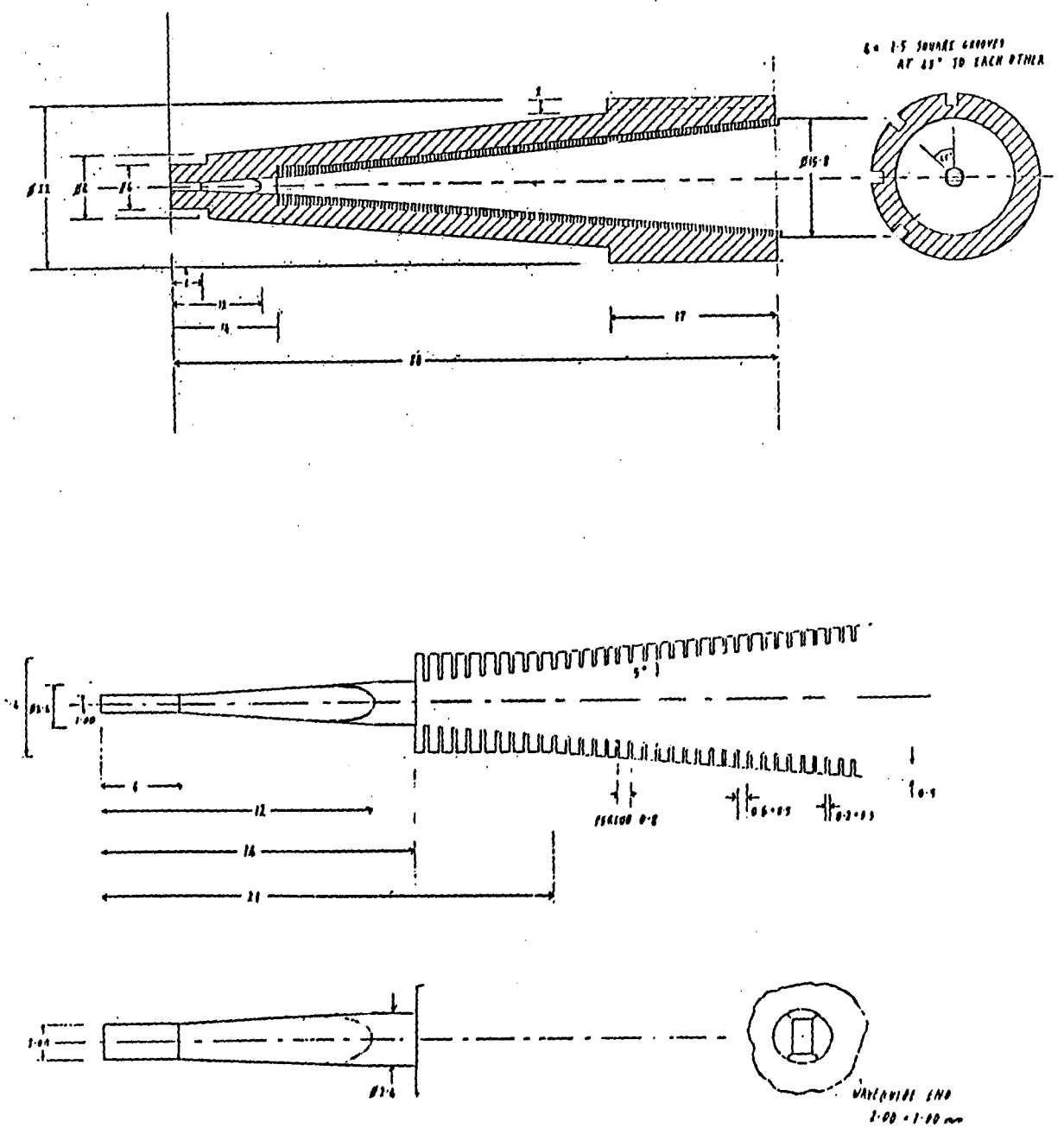

FIGURE 8.11 SCHEMATIC DIAGRAM ILLUSTRATING THE DESIGN OF THE MANDRIL FOR A CORRUGATED HORN

More recently a NC machine has become available and the difficulty and time of machining has been reduced dramatically. A large program of horn manufacture has been instigated and a number of different types of mandril with different corrugations have been made, which are at present being grown and due to be tested in early 1990. A schematic diagram illustrating the general design of a manril for a corrugated horn is illustrated in Fig.8.11

8.4 LENS DESIGN

This section will consider the very important area of design of a quasi-optic lens for the focussing of Gaussian beams in the millimetre wave range. Much of the original design work was done by A.Harvey [9] who derived Eq. 8.13 and the iterative process to calculate the lens profile. Firstly, the Gaussian beam theory of lenses is coinsidered, and then the design and manufacture of lenses.

8.4.1 GAUSSIAN BEAM TRANSFORMATION WITH LENSES

It is possible to transform the position and size of any Gaussian beam using mirrors or lenses as spatial phase transformers. Both have advantages and disadvantages. Off-axis mirrors are difficult to machine, and tend to have problems involving cross-polarisation. Lenses introduce some absorption loss and reflection. However, in general, the easiest and most adjustable option is matching using lenses, and th ey were used in most of the work described. The focal length of a lens is defned by the relationship:

$$\frac{1}{f} = \frac{1}{R} - \frac{1}{R'} \qquad 8.4$$

where R is the radius of curvature of the Gaussian beam on one side of the lens, and R' is the radius of curvature on the other side of the lens. Note, that although several sign conventions exist in the literature, f is usually regarded as positive for a converging lens.

Having obtained a lens of focal length f, (the design of which is considered in the next section), the following Gaussian beam lens formulae can be calculated by substituting from Eqs. 8.1 and 8.2 into Eq.8.4. If a beam waist w_{01} is situated a distance z_1 from an

ideal lens of focal length f then the location of the new beam waist w_{02} is a distance z_2 from the lens where:

$$z_2 = f + \frac{(z_1 - f)\, f^2}{(z_1 - f)^2 + (\frac{\pi w_{01}}{\lambda})^2} \qquad 8.5$$

and the size of the beam waist w_{02} is given by:

$$w_{02}^2 = \frac{1}{\frac{1}{w_{01}^2}(1 - \frac{z_1}{f})^2 + \frac{1}{f^2}(\frac{\pi w_{01}}{\lambda})^2} \qquad 8.6$$

In the absence of absorption in the lens (thin lens) which would affect the spatial distribution of power in the beam, both these equations are exact. It should be noted that if one beam waist is placed at the focal length of the lens, then the transformed beam waist is also situated at the focal length of the lens (independent of frequency), and will be of size:

$$w_{02} = (\frac{f\lambda}{\pi w_{01}}) \qquad 8.7$$

Thus, two lenses separated by the sum of their respective focal lengths make very efficient beam expanders, as using the above equation, a beam waist w_{01} located at the focal length of the first lens will be transformed to a beam waist situated at the focal length of the second lens but of size:

$$w_{02} = \frac{|f_2|}{|f_1|} w_{01} \qquad 8.8$$

where the expansion factor is independent of frequency.

8.4.1.1 THE BEAM WAVEGUIDE

Unfortunately the deleterious effects of standing waves between lenses can limit the use of this effect in optical design. In many cases it is suitable to use just one lens to do the focussing. Here one usually wants to focus a rapidly expanding Gaussian beam (as from a

feed-horn) and 'throw' the beam for as large a distance as possible, i.e. before the beam becomes too large for the optics. If we have the largest possible beam w_L at one lens, then by analogy with a resonator analysis, the confocal arrangement gives the furthest distance we can throw the beam, before the beam size increases to w_L again. Here, the beam-waist of this quasi-parallel beam is given by $w_L/\sqrt{2}$, and rearanging 8.5 the maximum throw distance is given by:

$$\text{Maximum throw between lenses} = d_{max} = \pi.w_L^2/\lambda \qquad 8.9$$

A series of confocal lenses propagating a beam through a system is known as a beam waveguide. The exact analysis of how to design a lens to couple from one beam waist to another at a set frequency is given in the next section.

8.4.2 LENS PROFILE DESIGN

The design of a lens profile to produce a lens of focal length f to couple from one known beam waist size to another beam waist size is now considered. For perfect coupling these profiles are not spherical as is usually assumed in geometrical optics, but a Gaussian beam analysis shows that the ideal profile is slightly more complex. For most applications considered later, two lenses are sufficient to couple from one output feedhorn through a system and into an input feedhorn for detection. Typically we wish to couple from a rapidly diverging beam (as from a feedhorn), into a quasi-parallel beam (to send through an optical system). Here a planar convex lens is suitable, where the planar side should face the rapidly diverging beam, and the convex side should face the quasi-parallel beam. Any reflection will couple into a very different Gaussian beam, which will tend to diffract out of the system, thus significantly reducing any VSWR problems. It was these type of lenses that were used in all the optical systems that are to be described. To consider the design it is best to consider the two interfaces seperately. [9]

8.4.2.1 PLANAR AIR/DIELECTRIC INTERFACE

As in geometric optics it can be shown for a beam of radius of curvature R incident normally on a planar dielectric interface, the radius of curvature inside the dielectric is

increased by a factor n. By substituting this into Eq.8.2 and using Eq.8.1 it can be shown [10] that the Gaussian beam propagates inside the dielectric as if:

a) The beam has the same size beam waist as in air

b) The beam-waist is now a distance n times further away than in air

c) The wavelength in the dielectric is reduced by a factor n (of course).

It is therefore relatively easy to plot the path of a Gaussian beam at a planar dielectric interface.

8.4.2.2 GENERAL AIR/DIELECTRIC INTERFACE

First if we consider the general form of a Gaussian beam we have an amplitude term multiplied by a phase term:

$$\Psi_{mn} = A_{mn}(x,y,z).\exp\left(-i\left[kz + \frac{k r^2}{2R(z)} - (m+n+1)\tan^{-1}\left(\frac{\lambda z}{\pi w_0^2}\right)\right]\right) \qquad 8.10$$

If we consider the coupling between two Gaussian beams at a general air/dielectric interface as shown in Fig 8.12. To be able to couple perfectly from one beam waist to another we must insure that there is an equal phase change for all paths between the two beam waists. If we consider the phase change over path a and the general path b we have, with reference to Eq 8.10:

$$\phi_a = nkz - \tan^{-1}\left(\frac{2z}{nkw_0^2}\right) + kz' - \tan^{-1}\left(\frac{2z}{kw'^2_0}\right) \qquad 8.11$$

$$\phi_b = nk(z - z_L) + \frac{nkr^2}{2R[z - z_L]} - \tan^{-1}\left(\frac{2(z - z_L)}{nkw_0^2}\right)$$

$$+ k(z' + z_L) - \frac{kr^2}{2R'[z' + z_L]} - \tan^{-1}\left(\frac{2(z' + z_L)}{kw'^2_0}\right) \qquad 8.12$$

where k has been replaced by nk in the dielectric and $R[z - z_L]$ is the radius of curvature of the beam in the dielectric at the position $z - z_L$, and $R'[z' + z_L]$ is the radius of curvature of the beam outside the dielectric at position $z' + z_L$. These phase differences must be the same, which means that an expression relating r and z_L can be found. This is given by:

$$r^2 = \frac{1}{\left(\frac{nk}{2R[z - z_L]} - \frac{k}{2R'[z' + z_L]}\right)} \cdot \left((n - 1)k z_L - \tan^{-1}\left(\frac{2z}{nkw_0^2}\right) - \tan^{-1}\left(\frac{2z}{kw_0'^2}\right) + \tan^{-1}\left(\frac{2(z - z_L)}{nkw_0^2}\right) + \tan^{-1}\left(\frac{2(z' + z_L)}{kw_0'^2}\right) \right) \qquad 8.13$$

Using the above formula a lens profile can be calculated using an iterative process given the two beam waists and the size of the waist at the lens (which is equivalent to specifying z and z')[11]. A program was written to calculate the lens profile in a form which allowed easy manufacture on a N.C. lathe. This was done in the manufacture of all the lens used in the experiments. Many of the above terms can be very small however, and in some cases suitable simplifications can be made.

8.4.3 SPHERICAL LENS COMPARISON

In the following analysis the approximations required to produce the lens makers and Gauss formulae are examined (spherical lenses).

Now to first order,

$$R[z-z_L] = R[z] - z_L(1 - (z_R/z)^2)$$

$$R'[z'+z_L] = R[z'] + z_L(1 - (z_R'/z')^2)$$

If z_L is small enough compared to the radius of curvature R we can apply the thin lens approximation $R'[z' + z_L] \approx R'[z']$ and $R[z - z_L] \approx R[z]$. The thin lens approximation basically assumes that the radius of curvature of the beam on each side of the profile does not change much over the thickness of the lens profile.

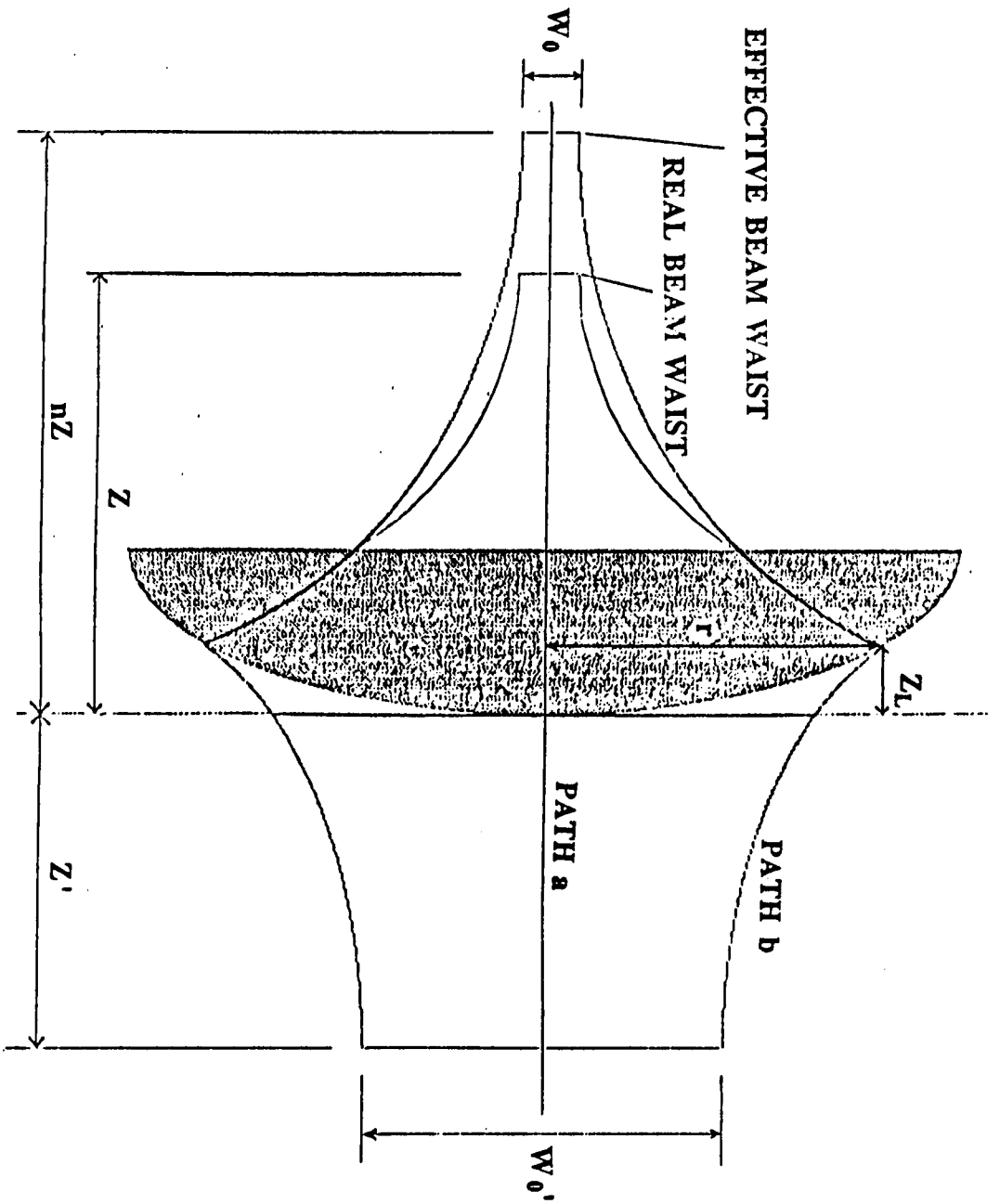

FIGURE 8.12 DIAGRAM ILLUSTRATING THE COUPLING FROM ONE BEAM WAIST TO ANOTHER BEAM WAIST THROUGH A PLANAR CONVEX LENS

Another suitable approximation for the curvatures required of the lens can be found by neglecting the tan terms which tend to cancel one another for small z_L. For small z_L and $z > z_R$, by using Taylor expansions, good first order approximations for the tan terms are:

$$\tan^{-1}((z - z_L)/z_R) - \tan^{-1}(z/z_R) = - z_L z_R / z^2$$

$$\tan^{-1}((z' + z_L)/z_R') - \tan^{-1}(z'/z_R') = z_L z_R' / z'^2$$

For z several times greater than z_R the tan terms will be small compared to the $(n-1)kz_L$ term, although it should be noted that this is not necessarily always the case.

However, making the above two approximations we can thus put:

$$r^2 = \frac{(n - 1) . z_L}{\frac{n}{2R} - \frac{1}{2R'}} \qquad 8.14$$

Now if the term multiplying z_L is large compared to z_L, then we can then make the spherical lens approximation: $r^2 \approx 2R_L z_L$, where R_L is the radius of curvature of the lens. R_L is therefore given by:

$$R_L \approx \frac{(n - 1)}{(\frac{n}{R} - \frac{1}{R'})} \qquad 8.15$$

For a planar convex lens the denominator of the above expression is just equal to the inverse of the focal length from Eq.8.4.We thus have:

$$R_L = (n - 1)f \qquad 8.16$$

If we compare this with the normal geometrical lens fomula (using spherical optics):

$$\frac{1}{f} = (n - 1)(\frac{1}{R_{L1}} - \frac{1}{R_{L2}}) \qquad 8.17$$

(where R_{L1} and R_{L2} are the radii of curvatures of the two sides of the lens) we can see that it is essentially the same formula with $R_{L2} = \infty$ for a planar surface.

8.4.4 ANTI-REFLECTION TECHNIQUES

One of the major problems with lenses, are reflections from the surface, which can set up standing waves within the optical system. To reduce this problem, a number of different precautions can be taken. Firstly, the system should be designed to have the minimum number of lenses possible. Secondly, the lens profiles should be chosen to couple very little reflected power back into the incident Gaussian beam by making the planar side face the rapidly diverging beam and the convex side face the quasi-parallel beam as discussed before. It is also useful to choose a material which has a low refractive index to reduce the size of the reflection. Typical low loss materials used are PTFE (Teflon) and HDPE (High density Polyethylene).

Lastly, the equivalent of quarter wavelength anti-reflection coatings can be placed on the lenses. These normally take the form of thin concentric grooves which are approximately quarter of a wavelength deep. As long as the grooves are small compared to the wavlength (i.e at least 6 per wavelength), then the beam sees a layer which has an effective refractive index which is some average of the air and the lens material. The mark space ratio of the grooves is chosen to provide the ideal match match between the lens and the air. If the air has a free space impedance of Z_0 (= $(\mu_0/\varepsilon_0)^{1/2}$) and the lens has an impedance Z_L (= $(\mu/\varepsilon)^{1/2}$), then from standard transmission line theory, the matching impedance of the quarter wave layer should be $(Z_0Z_L)^{1/2}$. If we take the refractive index of the air to be n_A ($\approx$ 1) and the lens as n_L it follows that that the average refractive index of the layer should be $(n_An_L)^{1/2} \approx n_L^{1/2}$. The grooves are normally machined using a NC machine. (Note, in principle, although it is possible to use a single outward spiral groove, in practice, the quality of the groove is such that it is preferable to have concentric radial grooves).

8.5 RESONATOR DESIGN

This section will look at the design of very high Q open resonators and the associated optics. This is definitely an area where quasi-optics offers potentially a very much greater performance over traditional closed waveguide-type cavities. Up to now their main use at millimeter wave frequencies has been the very accurate measurements of the real and imaginary parts of the dielectric constant of low loss materials [20], but they can

also find uses in the measurement and reduction of phase noise in oscillators, and as narrow bandwidth frequency filters.

Resistive losses in any waveguide cavity normally limits the Q to something of the order of 10,000 at 95 GHz, for a well designed non-tuneable system. Using curved open resonators, Q's of the order of 1,000,000 can be attained which allow tuning without loss of performance, and in some cases easy adjustment of the coupling factor.

Any high Q open resonator can be thought of as an analogue of a Fabry-Perot etalon system, and finds uses where frequency discrimination or noise reduction is necessary. It is also an analogue of any waveguide cavity system, although the propagating wave is now usually a Gaussian beam rather than a waveguide mode.

8.5.1 THE FABRY-PEROT

A Fabry-Perot traditionally consists of two highly reflecting mirrors facing one another to form a resonator. Its special properties derive from the fact that when power is incident at one of the mirrors, very large fields can build up within the resonator at appropriate resonant frequencies. At these resonant frequencies the power inside the cavity can become large enough, such that the transmission through the mirrors of the resonant field becomes comparable to the amplitude of the incident and reflected field. The leakage field from the resonator however is 180 degrees out of phase with the reflected field. In the lossless case this results in resonant transmission of all the incident power through the Fabry-Perot (for identical mirrors). In the microwave case, however, losses are usually not negligible, and limit the Q that is obtainable.

There are many expressions quoted in the literature for the performance of a Fabry-Perot of which many are only approximations. For an exact treatment one must take into account separately, the absorption and scattering at the mirrors as well as the loss within the resonator medium.

8.5.2.1 ANALYSIS OF LOSSY FABRY-PEROTS

A very clear account of the theory of lossy Fabry-Perots is given by Siegman [10]. This is expanded upon in the following treatment to obtain the expressions given in Eqs.8.25 and 8.26.

If we have two mirrors of amplitude reflectivity r_1,r_2, and amplitude transmission t_1, t_2 (where due to absorption, $r_1^2 + t_1^2$ and $r_2^2 + t_2^2$ do not necessarily equal 1). We can also define a round trip gain within the cavity $G_{rt}(w)$ which is given for a passive resonator by,

$$G_{rt}(w) = r_1 . r_2 . \beta . \exp(i2\delta) \qquad 8.18$$

where β is the round trip amplitude transmission coefficient (or the one way power transmission coefficient) and 2δ is the round trip phase change through the cavity. We ignore any phase change at the mirrors (other than π).

It can then be shown [10] that in the steady state the circulating field just inside mirror 1 within the cavity, must be equal to the incident field multiplied by transmission of the first mirror + the circulating field which has undergone one full round trip around the cavity.

$$E_{circ} = it_1 E_{inc} + G_{rt} E_{circ} \qquad 8.19$$

or rearranging,

$$\frac{E_{circ}}{E_{inc}} = \frac{i t_1}{1 - G_{rt}(w)} \qquad 8.20$$

Note for large reflectivities and low losses G_{rt} approaches 1 at resonance ($\exp(i2\delta)=1$) and the circulating field becomes very large compared to the incident field.

The transmitted field is given by the circulating field at mirror 2 multiplied by the transmission coefficient of mirror 2. (Where the circulating field at mirror 2 is equal to the circulating field at mirror 1, multiplied by the one way amplitude transmission coefficient ($\beta^{1/2} \exp(i\delta)$). This gives:

$$E_{trans} = it_2 \beta^{1/2} \exp(i\delta) E_{circ} \qquad 8.21$$

or rearranging using 8.4.2

$$\frac{E_{trans}}{E_{inc}} = \frac{-t_1 t_2 \beta^{1/2} \exp(i\delta)}{1 - G_{rt}(w)} \qquad 8.22$$

Now the reflected field will be made up of that portion of the incident field that is reflected + a contribution that is transmitted through the input mirror from the circulating field within the cavity. This contribution is given by the circulating field that left mirror 1 (E_{circ}) after it has traveled one round trip (except for the reflection off mirror 1).

It is therefore given by:

$$E_{refl} = r_1 E_{inc} + (i\, t_1/r_1)\, G_{rt}(w)\, E_{circ} \qquad 8.23$$

Again rearranging using 8.4.2

$$\frac{E_{refl}}{E_{inc}} = r_1 - \frac{t_1^2}{r_1} \frac{G_{rt}(w)}{1 - G_{rt}(w)} \qquad 8.24$$

Both 8.23 and 8.24 can be brought into more familiar form by substituting for $G_{rt}(w)$ and multiplying by the complex conjugate of the fields to give the transmitted intensity and reflected intensity coefficients. After suitable mathematical manipulation and putting $R_1 = r_1^2$ and $T_1 = t_1^2$ where $R_1 + T_1 + A_1 = 1$, the transmission coefficient for a lossy Fabry-Perot was calculated to be:

$$T = \frac{\dfrac{\beta T_1 T_2}{(1 - \beta\sqrt{R_1 R_2})^2}}{1 + \dfrac{4\beta\sqrt{R_1 R_2}}{(1 - \beta\sqrt{R_1 R_2})^2} \sin^2(\delta)} \qquad 8.25$$

and the reflection coefficient whichisobtained by similar means is given by:

$$R = \frac{\dfrac{(1 - A_1)}{R_1} \dfrac{4\beta\sqrt{R_1 R_2}}{(1 - \beta\sqrt{R_1 R_2})^2} \sin^2(\delta) + \dfrac{(R_1 - (1 - A_1)\beta\sqrt{R_1 R_2})^2}{R_1 (1 - \beta\sqrt{R_1 R_2})^2}}{1 + \dfrac{4\beta\sqrt{R_1 R_2}}{(1 - \beta\sqrt{R_1 R_2})^2} \sin^2(\delta)} \qquad 8.26$$

Both these expressions simplify to the expressions normally found in the literature when various simplifying assumptions are made i.e $R_1 = R_2$, $\beta = 1$ and $A = 0$ etc. The equations are of the form:

$$T = \frac{T_{max}}{1 + (2F/\pi)^2 \sin^2(\delta)} \qquad 8.27$$

$$R = \frac{\frac{(1 - A_1)}{R_1} (2F/\pi)^2 \sin^2(\delta) + R_{min}}{1 + (2F/\pi)^2 \sin^2(\delta)} \qquad 8.28$$

where F is the Finesse of the cavity (ratio of free spectral range to the cavity bandwidth) and is given by:

$$F = \frac{\pi \sqrt{G_{rt}}}{1 - G_{rt}} = \frac{\pi (\beta \sqrt{R_1 R_2})^{1/2}}{(1 - \beta \sqrt{R_1 R_2})} = \frac{\Delta\omega_{ax}}{\Delta\omega_{cav}} \qquad 8.29$$

The last two terms apply at resonance when $\sin^2(\delta) = 0$.

Sometimes, 8.27 and 8.28 are put in terms of the Airy Function $A(\delta) = (1 + (2F/\pi)^2 \sin^2(\delta))^{-1}$

$$T = T_{max} \cdot A(\delta) \qquad 8.30$$

$$R = ((1-A_1)/R_1).(1 - A(\delta)) + R_{min} A(\delta) \qquad 8.31$$

On resonance $A(\delta) = 1$ and the transmission is given by:

$$T = T_{max} = \frac{\beta T_1 T_2}{(1 - \beta \sqrt{R_1 R_2})^2} \qquad 8.32$$

and the reflection on resonance is given by:

$$R = R_{min} = \frac{(R_1 - (1 - A_1) \beta \sqrt{R_1 R_2})^2}{R_1 (1 - \beta \sqrt{R_1 R_2})^2} \qquad 8.33$$

From Eq.8.33 it is easy to see that the critical coupled condition when $R_{min} = 0$ is given when

$$R_1 = (1 - A_1)^2 \beta^2 . R_2 \qquad 8.34$$

Thus in the presence of finite losses critical coupling will never be achieved when $R_1 = R_2$, but can only occur if $R_2 > R_1$. It is also worth noting that if the second term in 8.4.12 becomes very small compared to R_1 (large losses or low R_2) then the reflectivity just tends to R_1 as one might expect. The other interesting case is when the second term is larger than R_1 (low losses and high R_2). In this case the cavity field becomes very large on resonance and there is a relatively large transmission back out through mirror 1. The reflectivity from the cavity will therefore always be large although there will now be a sharp phase change on resonance. For the Gires-Turnois Interferometer (losses = 0, $R_2 = \infty$) ,the cavity field becomes four times larger than for the case of identical mirrors. The reflectivity is unity for all frequencies but there is a 180^0 phase change on resonance.

8.5.2 STABILITY CONSIDERATIONS

For completeness, the stability and nature of resonator modes are now briefly considered. The analyses can be found in almost any good laser text of which [15] provides a useful summary. In the case of a millimetre wave resonator it is important to know the spot size at the mirrors and at the beam waist to provide low loss and efficient coupling to any external system, such as the one considered in Chapter 10.

If we consider two mirrors facing one another of radius R_1 and radius R_2 separated by a distance L, then the resonator modes are best analysed by considering the resonator g parameters, where:

$$g_1 = 1 - L/R_1 \qquad 8.35a$$

$$g_2 = 1 - L/R_2 \qquad 8.35b$$

It can be shown that the resonator supports stable modes if the stability condition

$$0 < g_1 g_2 < 1 \qquad 8.35c$$

is satisfied. The most stable configuration is a confocal resonator where $g_1 = g_2 = 0$. The plane parallel resonator ($g_1 = g_2 = 1$) and the concentric resonator ($g_1 = g_2 = -1$) operate at points where alignment is most critical.

The different resonant frequencies of the resonator for the different transverse modes (designated by **m** and **n**) are given by the expression:

$$f_{mnq} = [\, q + (m + n + 1)\frac{\cos^{-1}\sqrt{g_1 g_2}}{\pi}\,]\,\frac{c}{2nL} \qquad 8.36a$$

where **q** represents the qth axial mode or the number of half waves in the cavity. (Note **n** is a mode number and n is the refractive index of the medium).

The axial mode spacing is given by:

$$f_{\Delta q} = f_{mn(q+1)} - f_{mnq} = \frac{c}{2nL} \qquad 8.36b$$

and the spacing between adjacent tranverse modes is given by:

$$f_{\Delta mnq} = (\cos^{-1}\sqrt{g_1 g_2})\frac{c}{2nL} \qquad 8.36c$$

Note that for the confocal configuration $g_1 = g_2 = 0$, and all the TEM_{mn} modes are degenerate and have exactly the same frequency (for the same axial mode). If we move slightly off the confocal configuration then the TEM_{00} mode becomes non-degenerate. It is normally distinguishable from the other modes as it has the lowest diffraction loss, and hence the highest Q.

For the TEM_{00} mode the spot size at the beam waist in the resonator is given by [15]:

$$w_0 = (\frac{\lambda L}{\pi})^{1/2}\,\frac{[g_1 g_2(1 - g_1 g_2)]^{1/4}}{(g_1 + g_2 - 2\,g_1 g_2)^{1/2}} \qquad 8.37$$

This means that for a resonator the Rayleigh range is independent of frequency and given by:

$$z_R = \frac{\pi w_0^2}{\lambda} = L.\frac{[g_1 g_2 (1 - g_1 g_2)]^{1/2}}{(g_1 + g_2 - 2g_1 g_2)} \qquad 8.38$$

and for a confocal resonator this simplifies to $z_R = L/2$ and $w_0 = (\lambda L/2\pi)^{1/2}$. The theoretical beam sizes and radius of curvatures for a Gaussian beam propagating from two confocal resonators of radii of curvature 360mm and 520mm is shown in Figs.8.13 and 8.14 respectively. Note that the radii of curvature of the beam is independent of frequency as the Rayleigh range is also independent of frequency. These diagrams were useful in designing the coupling optics to and from the resonator in the F.M. noise measurement system discussed in Chapter 10.

The beam waist is positioned a distance z_1 away from mirror 1 where z_1 is given by:

$$z_1 = \frac{g_2(1 - g_1)L}{g_1 + g_2 - g_1 g_2} \qquad 8.39$$

The spot size at mirror 1 is given by:

$$w_1 = \left(\frac{\lambda L}{\pi}\right)^{1/2} \left(\frac{g_2}{g_1(1 - g_1 g_2)}\right)^{1/4} \qquad 8.40$$

and the spot size at mirror 2 is given by:

$$w_2 = \left(\frac{\lambda L}{\pi}\right)^{1/2} \left(\frac{g_1}{g_2(1 - g_1 g_2)}\right)^{1/4} \qquad 8.41$$

It is these spot sizes (relative to the size of the mirrors) that determine the diffraction losses. This is discussed in more detail in the next section.

8.5.3 CAVITY LOSSES

Cavity/mirror losses are very important in microwave resonators as it is these that eventually limit the size of the Q that can be obtained.

GRAPH SHOWING BEAM WAIST SIZE FOR TWO CONFOCAL CAVITIES OF TOTAL LENGTH 360mm AND 520mm (RAYLEIGH RANGE = L/2)

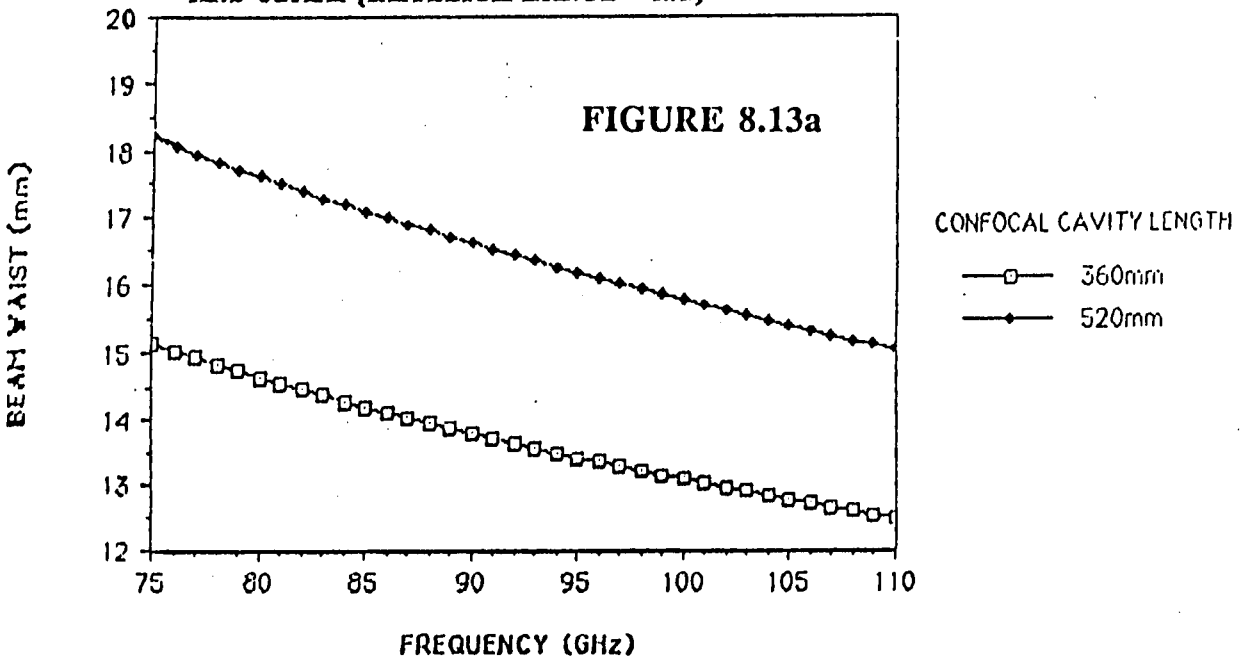

FIGURE 8.13a

GRAPH SHOWING RADIUS OF CURVATURE OF BEAM FROM CONFOCAL CAVITIES OF LENGTH 360mm AND 520mm

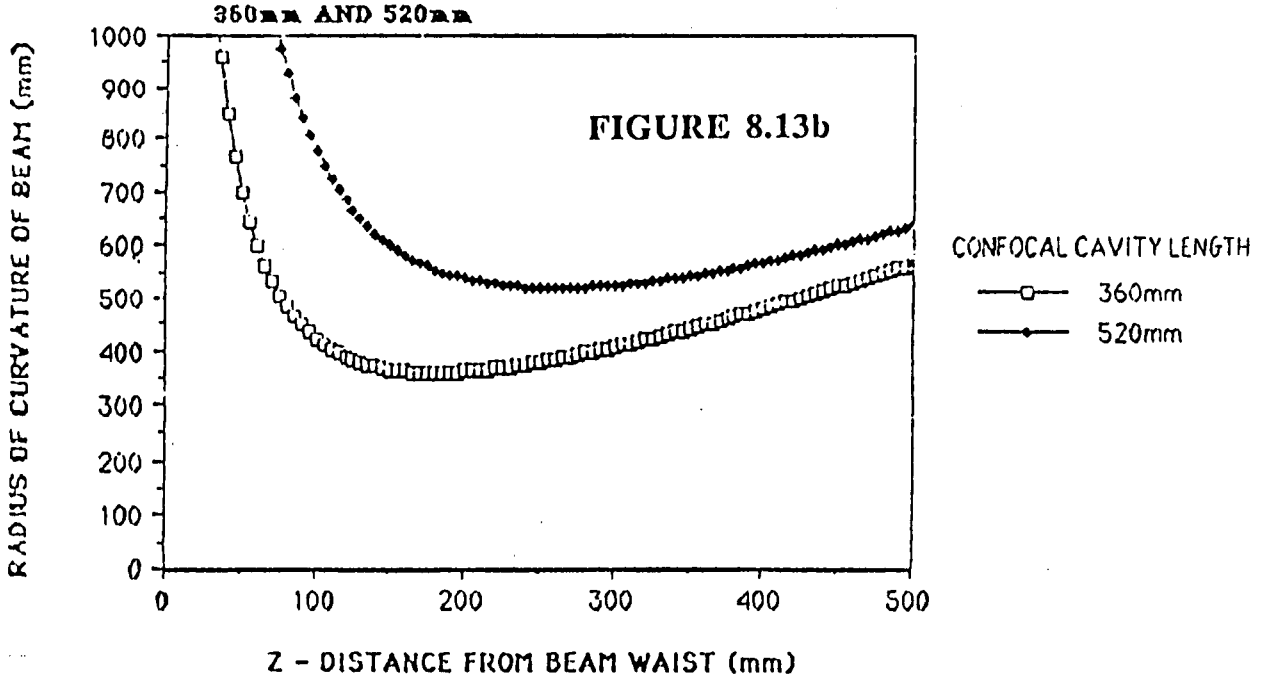

FIGURE 8.13b

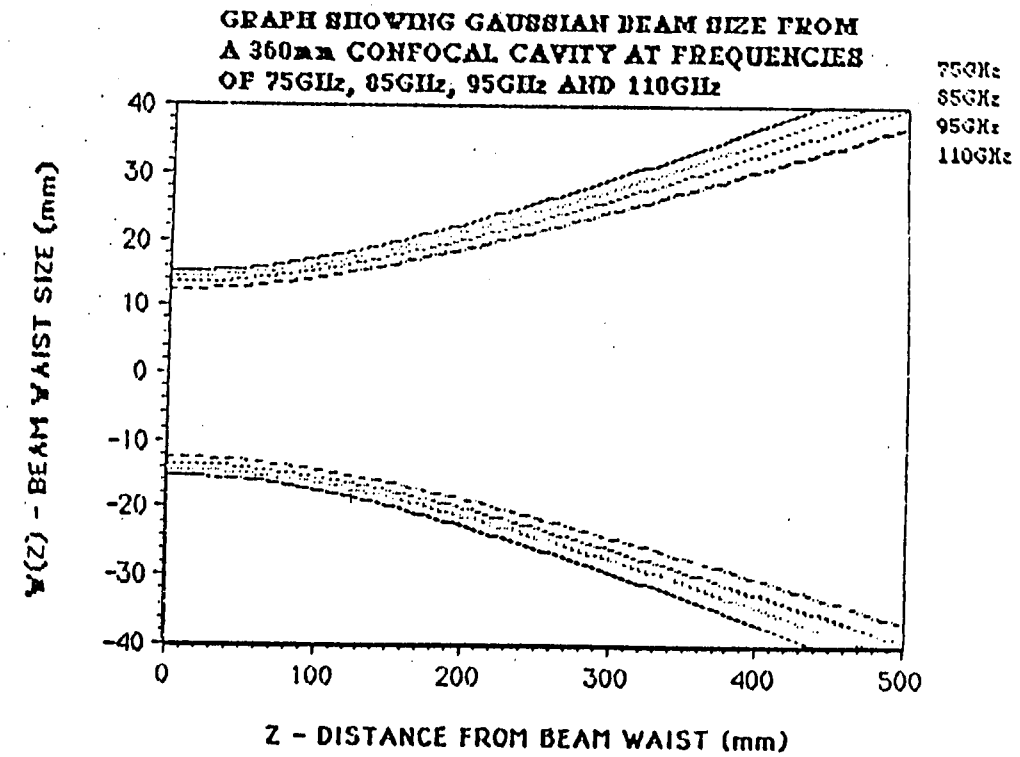
GRAPH SHOWING GAUSSIAN BEAM SIZE FROM
A 360mm CONFOCAL CAVITY AT FREQUENCIES
OF 75GHz, 85GHz, 95GHz AND 110GHz
75GHz
85GHz
95GHz
110GHz
W(Z) - BEAM WAIST SIZE (mm)
40
30
20
10
0
-10
-20
-30
-40
0
100
200
300
400
500
Z - DISTANCE FROM BEAM WAIST (mm)

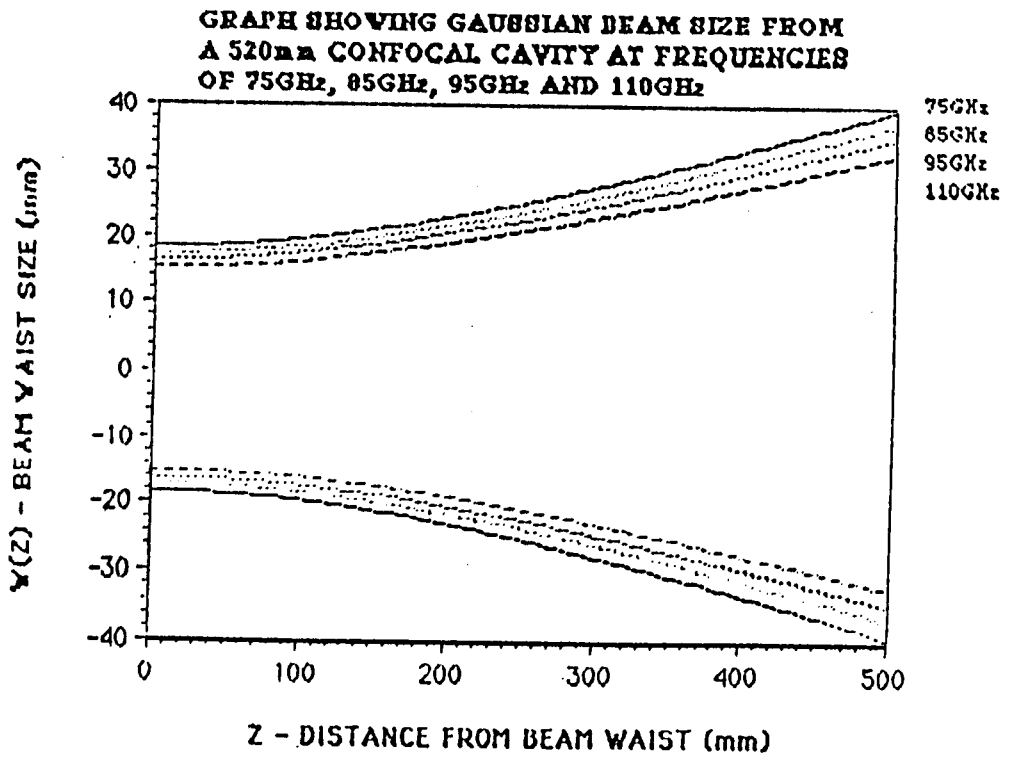
GRAPH SHOWING GAUSSIAN BEAM SIZE FROM
A 520mm CONFOCAL CAVITY AT FREQUENCIES
OF 75GHz, 85GHz, 95GHz AND 110GHz
75GHz
85GHz
95GHz
110GHz
W(Z) - BEAM WAIST SIZE (mm)
40
30
20
10
0
-10
-20
-30
-40
0
100
200
300
400
500
Z - DISTANCE FROM BEAM WAIST (mm)

FIGURE 8.14

The Q of the cavity is given by the number of half wavelengths in the cavity multiplied by the Finesse:

$$Q = F.q = \omega/\Delta\omega_{cav} \qquad 8.42$$

where $q = 2L/\lambda$ and F is given by Eq 8.4.9 and is a function of β, R_1 and R_2. Clearly the longer the cavity the larger the Q, although for any given mirror size the Q will eventually be limited by diffraction losses as the mirrors are moved apart.

We can consider five general types of losses within the cavity.

1) Diffraction Losses
2) Absorption Losses at the Mirror
3) Absorption Losses within the cavity medium
4) Scattering Losses
5) Coupling Losses

8.5.3.1 DIFFRACTION LOSSES

The diffraction losses associated with Gaussian beams are well understood, mainly thanks to the early work of Li [13] and the early research that was prompted by the advent of the laser in the early 1960's. The most useful parameter in discussing diffraction losses is the Fresnel number N which is given by:

$$N = a^2 / L\lambda \qquad 8.43$$

The diffraction losses are determined from the size of the spot size at each mirror and the radius of the mirror. The diffraction loss of a TEM_{00} Gaussian beam which is of spot size w(z) when reflected off a mirror of radius a (or transmitted through a circular aperture of radius a) is given by:

$$P_{diff}(a)/P_T \sim \exp(-2a^2/w^2(z)) \qquad 8.44$$

Therefore the cavity which has the least loss due to diffraction is the one which has the smallest spot size, for a given cavity length. This is the confocal cavity, where the spot size is given by:

$$w_m = (L\lambda / \pi)^{1/2} \qquad 8.45$$

and the beam waist is symmetrical with regard to the mirrors and is given by:

$$w_0 = (L\lambda / 2\pi)^{1/2} \qquad 8.46$$

Substituting 8.45 into 8.44 we have the diffraction loss for a single mirror (confocal cavity) as:

$$P_{diff}(a)/P_T \sim \exp(-2\pi N) \qquad 8.47$$

The above expression gives the total power lost by 'missing' the mirror. But because the reflected TEM_{00} mode is now effectively truncated, power is also lost from the TEM_{00} mode to higher order modes which are also reflected back down the cavity. A more exact analysis gives the round-trip loss (two mirrors) for the TEM_{00} mode in a confocal cavity system as:

$$\alpha_{diff} = P_{diff}(a)/P_T \simeq 16\pi^2 N \exp(-4\pi N) \qquad 8.48$$

The diffraction loss for N=1 in this system is of the order 0.055% and rapidly decreases for N>1.

For the general TEM_{mn} mode the losses are approximately given by [13]:

$$\text{Diffraction Loss } \alpha_{mn} \approx \frac{2\pi (8\pi N)^{2m+n+1} \exp(-4\pi N)}{\Gamma(m+1)\,\Gamma(m+n+1)} \qquad 8.49$$

It should be noted that it is not necessarily good to have N much greater than 1, as it is often desirable to have significant cavity loss for the higher order modes. A more detailed discussion of this can be found in [13] from which Fig.8.15 is taken illustrating the loss for a symmetric confocal cavity as a function of N.

8.5.3.2 MIRROR LOSSES

For a well designed system the largest loss will be the resistive loss associated with the reflecting metallic mirrors. For mirrors of conductivity σ the loss is given by [12]:

$$\alpha_{refl} = 4R_S / Z_0 = 4 / (Z_0 \sigma \delta_S) = 2 (4\pi\varepsilon_0 f / \sigma)^{1/2} \qquad 8.50$$

where σ is in SI units. This theoretical loss is shown as a function of frequency for various different types of metals in Fig.8.16. This means that for all the highly conductive mirrors such as copper, the losses will always be of the order of 0.1%. This will normally be the limiting loss for any high Q millimetre wave system.

8.4.3.3 ABSORPTION LOSSES

Losses due to the atmosphere are of the order of between 0.1dB/km and 1dB/km over the mm wave range and are in most instances negligible. At 94 GHz a 1m cavity would have a round trip loss of around 0.002% in laboratory conditions. Absorption losses will only start to become noticeable near molecular resonances (e.g. At 60 GHz and 120 GHz). Losses are usually defined in terms of the power attenuation coefficient α where:

$$P(z) = P_0 \exp(-\alpha z) \qquad 8.51$$

or in terms of the loss tangent $\tan\delta$ where:

$$\tan(\delta) = (\varepsilon''/\varepsilon') \qquad 8.52$$

The power attenuation coefficient α and $\tan(\delta)$ are related by:

$$\alpha = \left(\frac{2\pi\sqrt{\varepsilon'}}{\lambda}\right)\tan(\delta) \qquad 8.53$$

For most low loss dielectrics, $\tan(\delta)$ can vary from 50-1000 μradians. It should be noted however, that the loss can vary considerably from sample to sample, depending on the manufacturing process.

For a 100 μm thick dielectric film , the loss should still be negligible compared to the resistive loss in the mirrors.

8.4.3.4 SCATTERING LOSSES

Scattering losses can be caused by non-perfect mirror surfaces which may cause excitation of higher order modes which are subsequently lost by diffraction. It is difficult

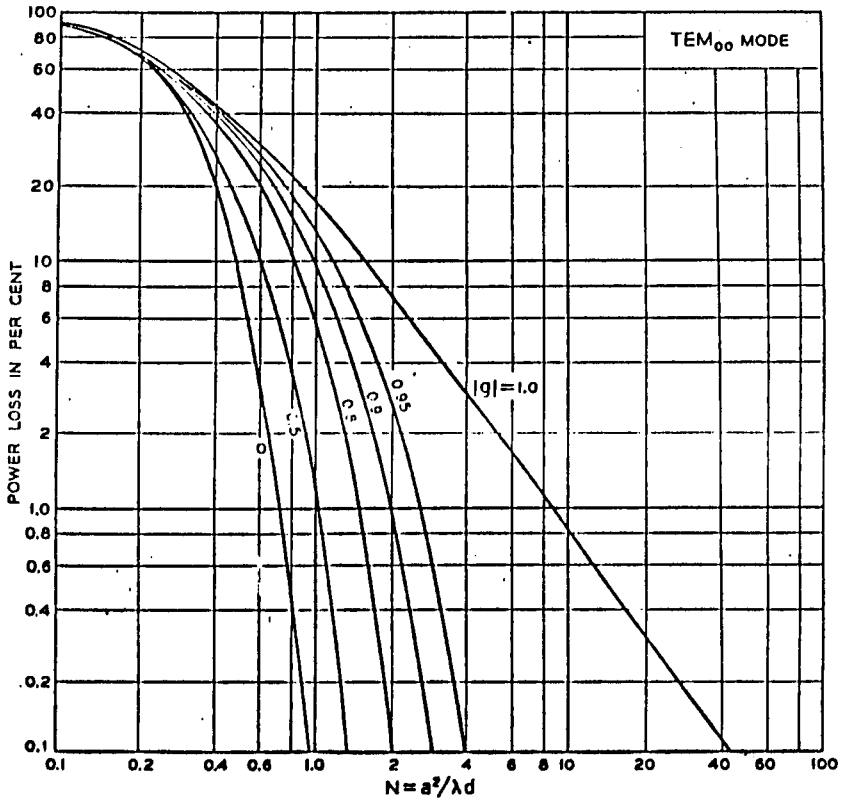

FIGURE 8.15 DIAGRAM ILLUSTRATING THE PERCENTAGE POWER LOSS PER PASS DUE TO DIFFRACTION, OF A SYMMETRIC RESONATOR CAVITY, AS A FUNCTION OF FRESNEL NUMBER N, FOR DIFFERENT VALUES OF THE STABILITY PARAMETER G. TAKEN FROM [13]

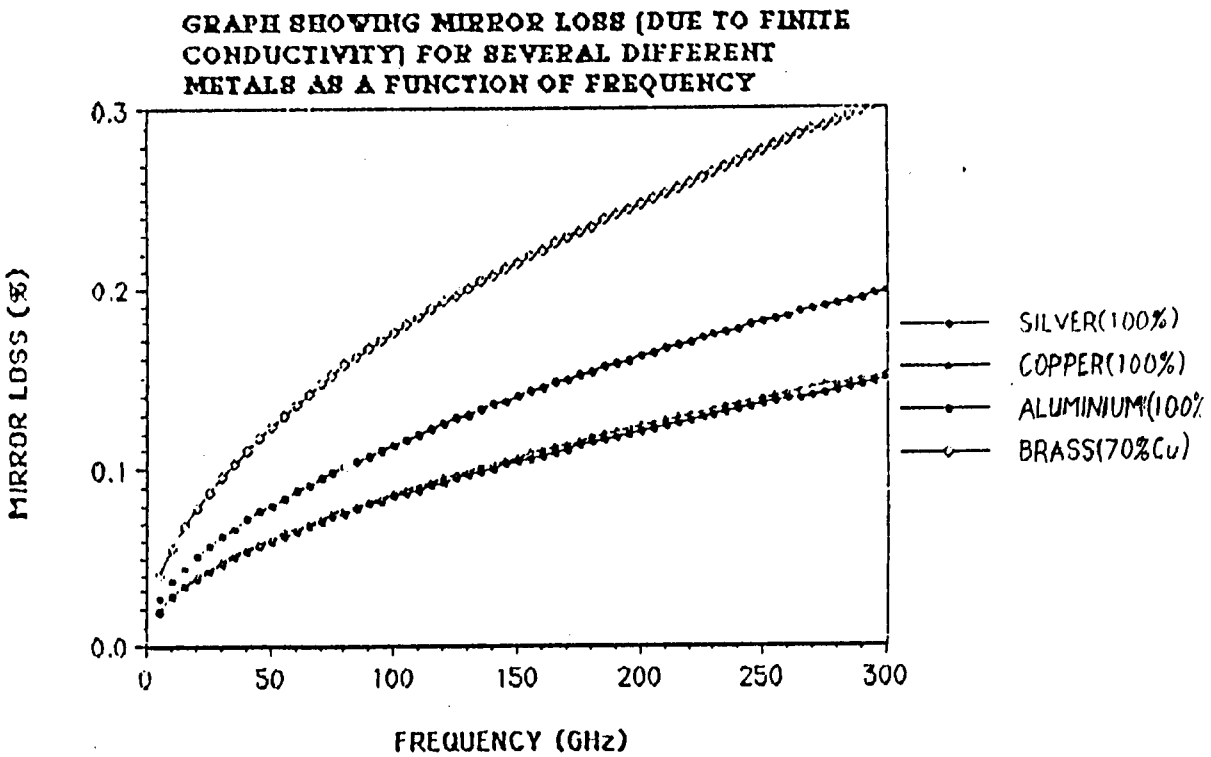

FIGURE 8.16

to be quantitative about this, but sufficient to say that the mirrors should be as accurate as possible to reduce this effect.

8.4.3.5 COUPLING LOSSES

Coupling losses refer to the absorption or scattering loss that is present when power is transmitted in or out of the resonator, and obviously has to be very small for a high Q system. These losses are distinct from the cavity losses which are represented by the loss parameter β. In Eqs. 8.4.5 and 8.4.6 the coupling losses refer to the absorption A, which obviously is also related to the reflectivity R through the relation $R+T+A = 1$. Losses can be both due to absorption and scattering. Semi-reflecting metallic films have significant resistive losses and small coupling holes in the mirrors have significant scattering losses.

8.4.4 COUPLING

Coupling is extremely important and largely determines the whole 'efficiency' of the system. The eventual use of the resonator determines the type of coupling that is required and each type of coupling has both advantages and disadvantages. Coupling wants to be low for the highest possible Q, but, the ratio of the coupling to the loss in the cavity is also an important factor, which determines the overall values of the transmission, reflection and loss of the system on resonance.

8.4.4.1 SMALL HOLE COUPLING

The traditional way of coupling to a microwave resonator is to use direct coupling from a waveguide through a small hole or iris situated centrally in one of the mirrors. Output is through another iris situated next to the first iris or in the other mirror. This has the advantage of direct compatibility with waveguide systems, and the resonator is largely free from the vibrational problems associated with free standing grids or metallic films on dielectric sheets or the losses associated with multi-layer dielectric films. It has the disadvantage that the coupling is a very sensitive function of the diameter of the iris, which also means the Q of the cavity will be frequency sensitive. It is also difficult to

change the coupling without replacing the whole mirror. There are also increased scattering losses associated with the excitation of higher order modes by the coupling hole.

When coupling to the resonator is achieved by small holes in one or both of the mirrors, initially a dipole field is set up which radiates in all directions. Some of this power can couple into a resonator mode, and a large resonator field can build up on resonance. However, there will always be the scattering losses from the initial dipole field, and thus large mirrors may be required to 'capture' most of the power. For matching to the cavity (critical coupling), it may be possible to use a small screw situated at the entrance of the iris to alter the coupling. However this may be frequency sensitive, and care must be taken to ensure that it does not distort the sidebands.

In most systems to achieve the highest Q, the coupling (transmission) is usually chosen to be very small so that the scattering losses are small compared to the losses in the cavity. This means from Eq. 8.4.10 that the net transmission on resonance is very low and these systems are often chosen to be operated with insertion losses of around 40 -50 dB [15].

8.4.4.2 OPTICAL COUPLING THROUGH THE MIRRORS

The traditional 'optical' way of coupling to resonators is through a partially transparent mirror, which is usually a multi-layer (quarter wavelength) dielectric stack. Unfortunately at millimetre wave frequencies, the absorption losses make such a system less than ideal. Another way of obtaining a highly reflective surface is to have a semi-silvered metallic surface on a thin dielectric sheet. This can work well, but the resistive losses in the metal start to become important when the metal becomes semi-transparent.

A better method is to use free standing metallic wires or grids. These can offer very high reflectivities coupled with much lower losses than the equivalent continuous metallic surface. They have much lower loss because, to use a transmission line analogue, the "reflecting discontinuity" is now largely inductive rather than resistive in nature (when the condition $a \ll g \ll \lambda$ holds where a is the size of the wire or grid, and g is the grid spacing). A more detailed survey can be found in references [14,18,21,22].

They offer the potential of having a critically coupled reflection cavity on resonance by having a "100%" curved reflector, and a grid in a near semi-confocal configuration.

(The losses in the cavity are chosen to match the reflection of the grid to satisfy Eq.8.34) The disadvantages of such a system is that there will be a certain degree of frequency sensitivity in the reflection coefficient, and that any grid or 'thin' structure will be more susceptible to acoustic or vibrational noise. It is also difficult to change the coupling of the structure.

8.5.4.3 BEAMSPLITTER COUPLING

Another interesting way of coupling to a high Q resonator is through a highly transmitting beamsplitter [19,23], which is placed at 45^0 to the axis of the resonator and the incident beam. On resonance (for a lossless system), the beam is completely reflected, and none is transmitted. In fact, Eqs.8.4.5 and 8.4.6 still apply in form, but the reflectivity R is replaced by the transmission T and vice-versa. In this system of coupling, the use of mode-matching optics also allows the possibility of exciting only the main TEM_{00} mode within the resonator, and preventing the excitation of higher order lossy modes, which may lead to ambiguous low Q resonances.

The non-normal incidence reflection off the beam-splitter means that the system is polarisation sensitive. This has the potential advantage that the coupling and the Q of the system can be continuously varied by altering the incident polarisation. The stability of the resonator (to vibration) will be good as it is governed mainly by the 'external' mirrors, although the alignment of the beam-splitter with the resonator is fairly critical. One potential disadvantage is that power is reflected on resonance, rather than transmitted which may require isolation of the transmitting source (although it may also provide a means for self injection locking). Also, in this system because the input and output coupling to the resonator (via the beam-splitter) are exactly the same, this means from Eq.8.4.12 that critical coupling can never be obtained in the presence of finite losses, (with two mirrors). However, the addition of a third mirror on the output port can provide an ideal means of completely matching the cavity, where all the power is now absorbed in the cavity near resonance. This was the method used to provide a high Q resonator for a F.M. noise measurement system. It is discussed at greater length in the next chapter.

8.6. DIELECTRIC BEAMSPLITTER DESIGN

In many ways it is easier to make a highly transmitting low loss beam splitter, than it is to make a highly reflective low loss mirror, at microwave and millimetre wave frequencies. This is mainly due to the fact that the wavelength is large compared to a thin dielectric sheet. To analyse a dielectric beamsplitter we must take into account the multiple reflections from each of the two interfaces. Thus for net reflection and transmission we must use the Fabry-Perot equations given by 8.4.5. and 8.4.6.

For a thin dielectric A=0 and β can be calculated using Eqs 8.4.28 - 8.4.30. At λ=4mm for a 100μm thick sheet of MELINEX where $n = \sqrt{\varepsilon} = 1.72$, $\tan(\delta) \approx 10^{-4}$ we have $\beta = 0.99996$, which implies the absorption loss is usually negligible. The reflection R off one interface at non-normal incidence can be calculated from the Fresnel Equations [17] and depends on the polarisation. For polarisation parallel to the beamsplitter we have:

$$R_{parallel} = \left(\frac{n_t \cos(\theta_i) - n_i \cos(\theta_t)}{n_i \cos(\theta_t) + n_t \cos(\theta_i)}\right)^2 \qquad 8.54$$

and for the polarisation perpendicular to the beamsplitter we have:

$$R_{perp} = \left(\frac{n_i \cos(\theta_i) - n_t \cos(\theta_t)}{n_i \cos(\theta_i) + n_t \cos(\theta_t)}\right)^2 \qquad 8.55$$

where θ_i is the angle of incidence and θ_t is the angle transmitted through the dielectric which can be found from Snells law: $n_i \sin(\theta_i) = n_t \sin(\theta_t)$. For $\theta_i = 45^0$ and $n_i = 1$ and $n_t = 1.72$ we have $R_{parallel} \approx 2\%$ and $R_{perp} \approx 14\%$. A graph illustrating the reflectivity off a single air/dielectric interface as a function of refractive index is shown in Fig.8.17

The phase change 2δ between adjacent beams on transmission or reflection is given by:

$$2\delta = k_0 \Lambda = (2\pi/\lambda).2d \cos(\theta_t) = (2\pi/\lambda).2d.(n_t^2 - n_i^2 \sin^2(\theta_i))^{1/2} \qquad 8.56$$

where d is the thickness of the sheet (and we ignore any additional 2π phase changes due to reflection at the interfaces). Because d is very small compared to the wavelength λ, the phase change δ will be small, which means that the net transmission through the dielectric

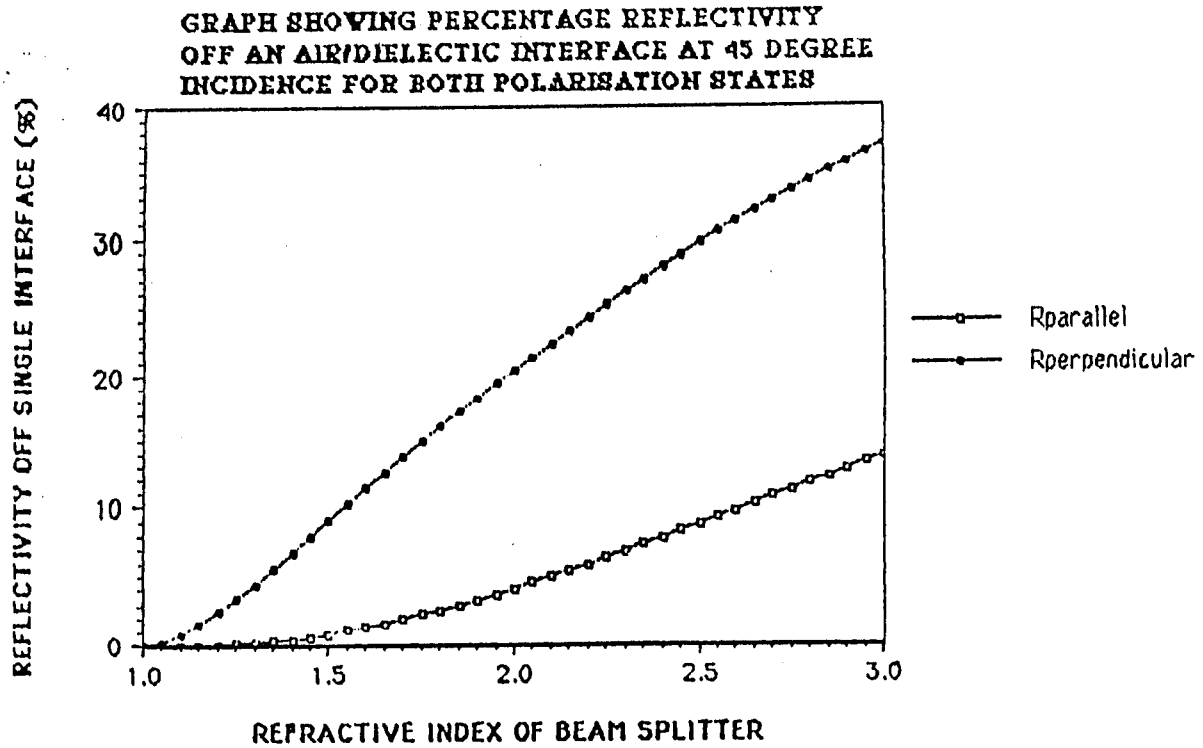

FIGURE 8.17

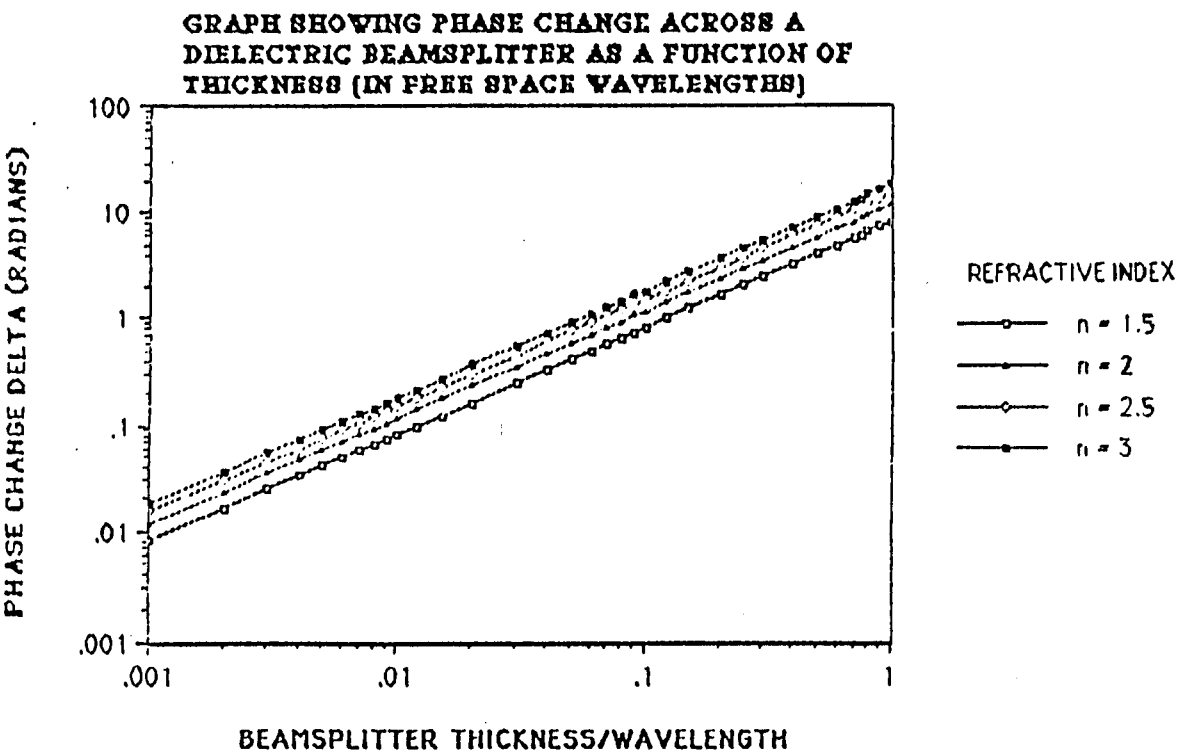

FIGURE 8.18

will be very high. A graph illustrating the phase change as a funtion of beam-splitter thickness is shown in Fig.8.18.

For a 100μm thick sheet of MELINEX (n=1.72), λ = 3mm, $\theta_i=45^0$ and $n_i=1$, we calculate the phase change δ = 0.33 radians. Substituting this value into Eq.8.25 we have for the net transmission $T_{parallel}$ = 0.991 and T_{perp} = 0.927. For the same values but a 10μm sheet these transmissivities are increased to $T_{parallel}$ = 0.99991 and T_{perp} = 0.9992, all with negligible loss (compared to the loss in the mirrors). The operation of dielectric beam-splitters is considered in further detail in Chapter 10.

8.7 WIRE GRID POLARISERS

A wire grid polariser is a set of parallel conducting wires usually suspended in free space or on a thin substrate. Any electric field component parallel to the wires sets up currents in the wires, which then reradiate and effectively reflect the radiation (as they would in a thin metal sheet). However, if the wires are thin compared to the wavelength of the radiation, then currents cannot be set up in the wires for electric field components perpendicular to the wires and the beam passes completely through the polariser. Interestingly, the wires must not be too small however, as they still need to be significantly greater than the skin depth (associated with the conductivity of the wires and frequency of radiation), otherwise currents will be set up on the other side of the wire and the parallel component will start to be transmitted.

At millimeter and submillimeter frequencies it is possible to make wire grid polarisers that act as almost perfect elements. The wire grid polarisers used in the systems described here were wound on to rectangular frames using 10μm tungsten wire on an adapted coil-winder, at a spacing of 25μm. The wires were then glued to the frame, and a second frame is bolted to the first to sandwich the wires and the glue together. The wires are then cut away around the outer rim to produce the polariser. The method of manufacture is more fully described in [9,24,25].

Using grids of this type the measured cross polarisation is usually substantially better than 30dB and the loss less than 0.01dB throughout the millimeter wave range.

8.8 ROOF MIRRORS

Roof mirrors form an integral part of many optical systems and can be used to rotate the polarisation of the beam or change the phase of a signal. They consist of two conducting plane reflecting mirrors set at right angles to one another. If the plane of polarisation is at an angle of α to the roof line then it can be shown that the incident radiation on reflection is rotated through an angle of 2α [9]. (The analysis is not difficult and depends on the condition that the electric vector must be perpendicular to the surface of the mirror).

If the incident radiation is is at 45 degrees to the roof line, the returning beam will be orthogonally polarised to the incident beam. Thus any beam that was reflected off a polariser towards a roof mirror will now be transmitted through that polariser and vice-versa.

The loss in the roof mirror should be determined by the resistive loss in the mirrors and any specular reflection. In a system built at 230GHz the loss was measured to be less than 0.02 dB for a polished and gold flashed roof mirror [25]. The importance of having the two faces of the roof mirror at 90 degrees, and having the roof mirror aligned relative to the phase front of the beam is discussed in [24].

The roof mirror is another almost perfect optical element, and in conjunction with polarisers they are used extensively in many types of quasi-optical instrumentation. They can be used to accurately change the phase and amplitude of an optical signal [9], and their use forms the basis of the Martin-Puplett Interferometer.

REFERENCES (CHAPTER 8)

1) C.Dragone, "Reflection, Transmission, and Mode Conversion in a Corrugated Feed", Bell System Technical Journal, Vol.56, July-August 1977, pp. 835-867

2) R.J.Wylde, "Millimetre-wave Gaussian beam-mode optics and corrugated feed horns", IEE Proceedings, Vol.131, Pt.H, No.4, Aug. 1984

3) A.J.Simmons, A.F.Kay, "The Scaler Feed - A High Performance Feed For Large Paraboloid Reflectors", Design and Construction of Large Steerable Aerials, IEE Conf. Publ. 21, 1966, pp.2213-217

4) C.A.Mentzer, L.Peters Jr., "Properties of Cutoff Corrugated Surfaces for Corrugated Horn Design", IEEE Trans. Antennas Propagat. Vol. AP-22, pp.191-196, March 1974

5) R.E.Lawrie, L.Peters Jr., "Modifications of Horn Antennas for Low Sidelobe Levels", IEEE Trans. Antennas Propagat., Vol. AP-14, pp. 605-610, Sept. 1966

6) P.F.Goldsmith, "Quasi-Optical Techniques at Millimetre and Submillimetre Wavelengths", Chapter 5, Infrared and Millimetre Waves, Vol.6

7) A.F.Harvey, "The Electroforming Of Components And Instruments For Millimetre Wavelengths", Proc.IEE., March 1955, pp. 223-230

8) C.W.Ammen, "The Electroplaters Handbook", Tab Books Inc., 1986

9) Andrew Harvey "PhD Thesis" St. Andrews University, to be submitted 1990

10) Andrew Harvey, Private Co mmunication

11) Siegman,"LASERS", Chapter 11

12) A.Battaglia, A.Gozzini,G.Boudouris, "Experimental Study of Confocal Fabry-Perot Microwave Resonators", Il Nuovo Cimento, Oct 1970, pp.121-151

13) Li, Bell System Technical Journal, May 1965, pp.917-932

14) J.P Casey, Jr., E.A.Lewis, "Interferometer Action of a Parallel Pair of Wire Gratings", Journal of the Optical Society of America, Vol.42, No.12, pp.971-977

15) H.Weichel, L.S.Pedrotti, "A Summary of Useful Laser Equations - An LIA Report", Dept. of Physics, Air Force Institute of Technology, Wright-Patterson AFB OH

16) R.N.Clarke, Private Communication.

17) Hecht, Zajak, "Optics"

18) B.Walker, E.A.M.Baker, A.E.Costley, "A Fabry-Perot Interferometer for plasma diagnostics", J.Phys.E:Sci.Instrum., Vol.14, 1981, pp.832-837

19) P.F.Goldsmith, "Quasi-Optical Techniques at Millimeter and Submillimeter Wavelengths", Infrared and Millimeter Waves, Vol.6, Chapter 5

20) R.N.Clarke, C.B.Rosenberg, "Fabry-Perot and Open Resonators at Microwave and Millimetre Wave Frequencies, 2-300 GHz", J.Phys. E: Sci.Instrum., Vol.15, 1982, pp.9-24

21) E.A.M.Baker, B.Walker, "Fabry-Perot Interferometers for use at Sub-millimetre Wavelengths", J.Phys. E: Sci.Instrum., Vol.15, 1982, pp.25-32

22) R.Ulrich, K.F.Renk, L.Genzel, "Tunable Submillimeter Interferometers of the Fabry-Perot Type", IEEE MTT, Vol.11, 1963, pp.363-371

23) I.P. French, T.E. Arnold, "High Q Fabry-Perot Resonator for Nitric Oxide Absorption Measurements at 150 GHz", Rev. Sci. Instrum., Vol.38, pp.1604-1607

24) D.H.Martin, "Polarizing (Martin-Puplett) Interferometric Spectrometers for the Near- and Submillimeter Spectra", Infrared and Millimeter Waves, Vol. 6, Chapter 2, Academic Press, 1982

25) J.C.G.Lesurf, "A Quasi-Optical Astonomical Receiver", PhD Thesis, University of London, 1981

26) A.F.Harvey, "Microwave Engineering", Acadmic Press, London 1963

9.0 FREQUENCY AND IMPEDANCE MEASUREMENTS

9.1 INTRODUCTION

In this chapter and the next, the use of quasi-optical systems to characterise oscillators is considered. A Martin-Puplett Interferometer system is used to give accurate measurements of frequency and give indications of the harmonic content of oscillators. The ability of a rotatable, moveable roof mirror with a polariser to obtain almost any desirable impedance, can be used to give external impedance matching to oscillators, as well as to make passive impedance measurements on oscillators.

9.2 FREQUENCY MEASUREMENT

Accurate knowledge of the resonant frequency or frequencies is important to determine the behaviour of the oscillators, as frequency jumps, higher order harmonics, and sideband oscillations can be present during tuning and can give important clues to the interaction of the diode and the circuit. This section outlines the use of a Martin-Puplett Interferometer as a means of analysing this type of behaviour

The traditional microwave frequency measurement technique is to use an adjustable resonant cavity which is weakly coupled to a waveguide via a small coupling hole. This can be adjusted to give either absorption or transmission on resonance. The most common kind, is the cylindrical cavity coupled to the broad wall of the waveguide which operates in the low order TE_{111} mode, to avoid ambiguity in the resonance across a waveguide band. The cavity is adjusted using a very fine precision differential screw thread, and there is a small absorption of power on resonance. The use of a low order mode and high resistive losses at millimeter wave frequencies means the cavity Q is limited. Typically at 100 GHz an adjustable electroformed cavity, operating in this mode, has a Q of around 1600, and is typically only adjustable to 50MHz, and absolutely accurate to 250MHz.[1,2] In addition, the weak coupling, (necessary to ensure that the resonant frequency is not coupling dependent), means that with some wavemeters, the absorption can be very small, and can be seriously affected by standing wave effects along the waveguide. The system must be calibrated, and is limited to a single waveguide band. The losses increase and the relative accuracy decreases rapidly as one moves to higher frequencies.

9.2.1 THE MARTIN PUPLETT INTERFEROMETER

A more accurate and versatile system and the one which was used extensively in the measurement of the oscillator sources, is the Martin-Puplett interferometer employed as a frequency counter. A diagram of a Martin-Puplett Interferometer (M.P.I.) is shown in Fig 9.1. It is a four port device and relies on polarisation to perform the interferometry. An extensive study of the performance and uses of the M.P.I. can be found in [3,4,5]

It was used in two distinct modes: firstly as a fringe counter, and secondly as a Fourier Transform Instrument. Its principle advantages over a wavemeter are its wide bandwidth and very low loss. It has the advantage over the Michelson interferometer, that all the power is delivered to the output ports, and none is reflected back at the source.

The major problem which affects the performance of the instrument, is signal reflection from the detector which can then re-enter the interferometer and be returned towards the source. This can then manifest itself as a spurious harmonic frequency by A.M modulating the source, or by simply reflecting from the source and back through the system to the detector. If the reflection is strong enough, then pulsing of the source can occur. This then appears in the transform as multiple harmonics of the fundamental all of similar magnitude. These problems all stem from the fact that it is very difficult to make a detector that is wide-band matched.

Despite careful matching it was difficult to reduce the spurious second harmonic component to below 15dB down on the main frequency. Many many hours of experimentation were required to show that this was almost entirely due to standing wave effects. The evidence that the frequency component is usually spurious includes,

a) For an oscillator operating in second harmonic mode the next frequency component would need in effect to be the 'fourth harmonic'. A third harmonic component was very rarely seen and its amplitude varied with backshort position. The 'fourth harmonic' relative amplitude did not vary substantially with backshort position. It should be noted that standing waves cannot produce a spurious frequency component at one and a half times the main frequency and so any frequency component observed here is almost certainly real.

b) A substantial reduction in the relative amplitude of the harmonics were observed when the VSWR was reduced by placing appropriate attenuation before the Golay detector, although it was very difficult to remove completely.

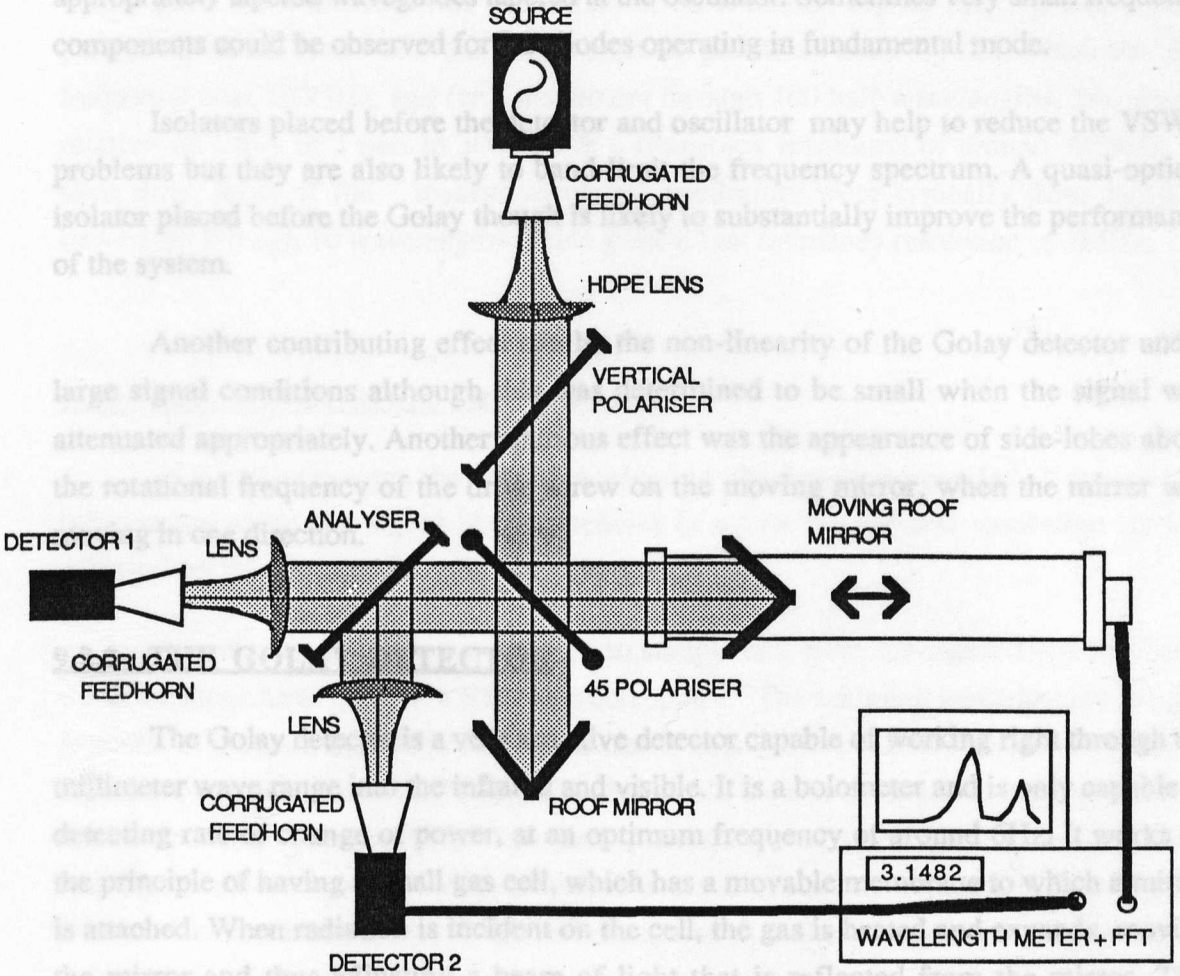

FIG. 9.1 MICHELSON POLARISING INTERFEROMETER (MARTIN-PUPLETT INTERFEROMETER)

c) No higher frequency components could be observed for oscillators operating in second harmonic mode when filters to remove the main frequency were used. The filtering was done both interferometrically using another Martin-Puplett Interferometer and by using appropriately tapered waveguides tapered at the oscillator. Sometimes very small frequency components could be observed for InP diodes operating in fundamental mode.

Isolators placed before the detector and oscillator may help to reduce the VSWR problems but they are also likely to band-limit the frequency spectrum. A quasi-optical isolator placed before the Golay though is likely to substantially improve the performance of the system.

Another contributing effect can be the non-linearity of the Golay detector under large signal conditions although this was determined to be small when the signal was attenuated appropriately. Another spurious effect was the appearance of side-lobes about the rotational frequency of the drive screw on the moving mirror, when the mirror was moving in one direction.

9.2.2 THE GOLAY DETECTOR

The Golay detector is a very sensitive detector capable of working right through the millimeter wave range into the infrared and visible. It is a bolometer and is only capable of detecting rate of change of power, at an optimum frequency of around 6Hz. It works on the principle of having a small gas cell, which has a movable membrane to which a mirror is attached. When radiation is incident on the cell, the gas is heated and expands, moving the mirror and thus adjusting a beam of light that is reflected from the mirror. This movement of light is then detected and an output voltage is produced which is proportional to the movement of the light. To prevent damage and improve the signal to noise ratio, the infrared is effectively filtered out of the response by placing a piece of black bin liner over the detector. This is still relatively transparent to millimetre waves, whilst protecting the detector from stray or spurious thermal sources, such as draughts, sun-light, lamps or soldering irons.

9.2.3 FREQUENCY MEASUREMENT USING FRINGE COUNTING

For a single frequency component (with small harmonics) entering the system, the output of the Golay should be a periodic waveform, where the waveform repeats itself everytime the moving roof mirror travels through half a wavelength. A system was built to count the number of zero crossings as the roof mirror moved through a large number of

wavelengths. The distance the roof mirror moved was determined by the rotation of a lead screw which was monitored by a counter which gave out 2000 digital pulses every revolution to the system. The movement of the mirror was also controlled by the system which gave the wavelength of the radiation on a L.E.D. digital display. For a 1mm periodicity on the lead screw this gave a nominal positional accuracy of 0.5 microns. At a frequency near 100GHz, and for a movement through 100 half-wavelengths, this gives a relative accuracy of 1 part in 300,000 or a frequency resolution of around 300kHz. To save time, most of the measurements on oscillators were typically done using a movement through 10 wavelengths which gives a best frequency resolution of 3MHz.

9.2.4 FAST FOURIER TRANSFORMS

In a perfect system, the signal received by the detectors contains all the spectral information about the signal. At frequencies of a few Hz spectral resolution is best achieved by Fast Fourier Transforming the output.

A computer program was written to sample and store the signal from the Golay using the input AtoD ports of a BBC microcomputer. The sampling was triggered at equal intervals of distance as determined by the rate of rotation of the lead screw on the moving mirror (or at equal intervals of time). The data could then be averaged to remove the large d.c. component. It could also be apodised if necessary, to change the response due to the rectangular measurement window (which has the effect of convolving a sinx/x response with the true spectrum). Data storage and manipulation limited the number of measurement points to 512 in the original system which limits the frequency resolution to 1 part in 256 of the Nyquist frequency.

9.2.5 OTHER FREQUENCY MEASUREMENT TECHNIQUES

The fringe counting technique provides a quick and convenient measure of the frequency, for calibration of the oscillators, however it only uses the the number of zero crossings and the distance between them to calculate the frequency. Although the accuracy is improved in direct relation to the number of zero crossings, the accuracy is still dependent on the accurate measurement of the start and final crossing points. Measurement of these points may still be affected by spurious noise or signal components at higher frequencies and thus limit the potential accuracy of the system.

One method to improve the accuracy, is to try and use all the information contained in the signal again by Fourier Transforming. As we have already seen, the resolution accuracy of the Fast Fourier Transform is limited by the number of points taken. However, in general we are only concerned with one large signal component and this can be found approximately from the Fast Fourier Transform. It is then possible to take 'Slow' Fourier Transforms near this frequency and iterate towards the exact frequency which has the largest amplitude. (Alternatively, it may be possible to find a solution by curve fitting around the largest component in the Fast Fourier Transform).

9.3 EXTERNAL IMPEDANCE MATCHING

As has already been outlined in chapter 4, external impedance matching can be achieved by the use of a polariser, and a rotateable, moveable roof mirror in the configuration shown below in Fig. 9.2.

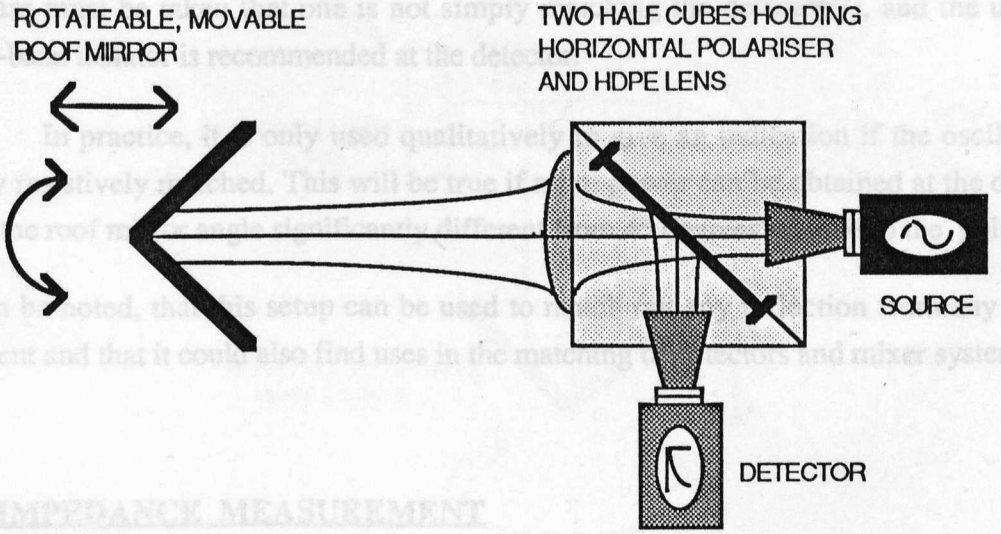

OPTICAL IMPEDANCE MATCHING CIRCUIT

FIG 9.2

By changing the position of the roof mirror the phase of the signal returned to the oscillator can be altered, and by changing the angle of the roof mirror relative to the polariser, the amplitude of the return signal can be adjusted. Thus the load impedance of

the oscillator can be changed over a fairly large range. Some care must be taken in interpretation of the results as there are a number of spurious effects that must be taken into account:

a) There will always be a constant resistive loading due to the losses in the feedhorn and the coupling loss. This resistive loss is always likely to be of the order of 1.5dB.

b) There may also be significant standing waves between the two feedhorns, which will affect the results.

c) In addition, a change in resistive or reactive loading can affect the resonant frequency of the oscillation. Although this is likely to be no more than a few tens of MHz, because of the large distance (in terms of wavelengths) between the roof mirror and the oscillator, a significant phase change can occur at the roof mirror. Thus, for every different resistive loading, the phase of the return signal should also be swept to look for maximum power output.

d) Care must be taken that one is not simply matching the detector(!), and the use of a wide-band isolator is recommended at the detector.

In practice, it is only used qualitatively to give an indication if the oscillator is badly resistively matched. This will be true if more power can be obtained at the detector with the roof mirror angle significantly different from 45 degrees relative to the polariser.

It can be noted, that this setup can be used to match out any reflection from any optical element and that it could also find uses in the matching of detectors and mixer systems.

9.4 IMPEDANCE MEASUREMENT

It is also possible to use quasi-optical techniques to make passive impedance measurements, and it is eventually hoped to be able to use these to accurately characterise oscillator packages and to successfully de-embed devices at W-band and higher. At the moment an impedance measurement system is being constructed at St Andrews to be used as a national standard at the National Physics Laboratory. The design of the impedance measurement system is discused in detail in [3, 4] and so the system will only be outlined here. A schematic of the system design is shown on the next page in Fig 9.3.

The system is essentially a quasi-optical impedance bridge that uses a null measurement technique to achieve accurate impedance measurements, that can be made over a very wide range of frequencies. Power from the oscillator passes completely

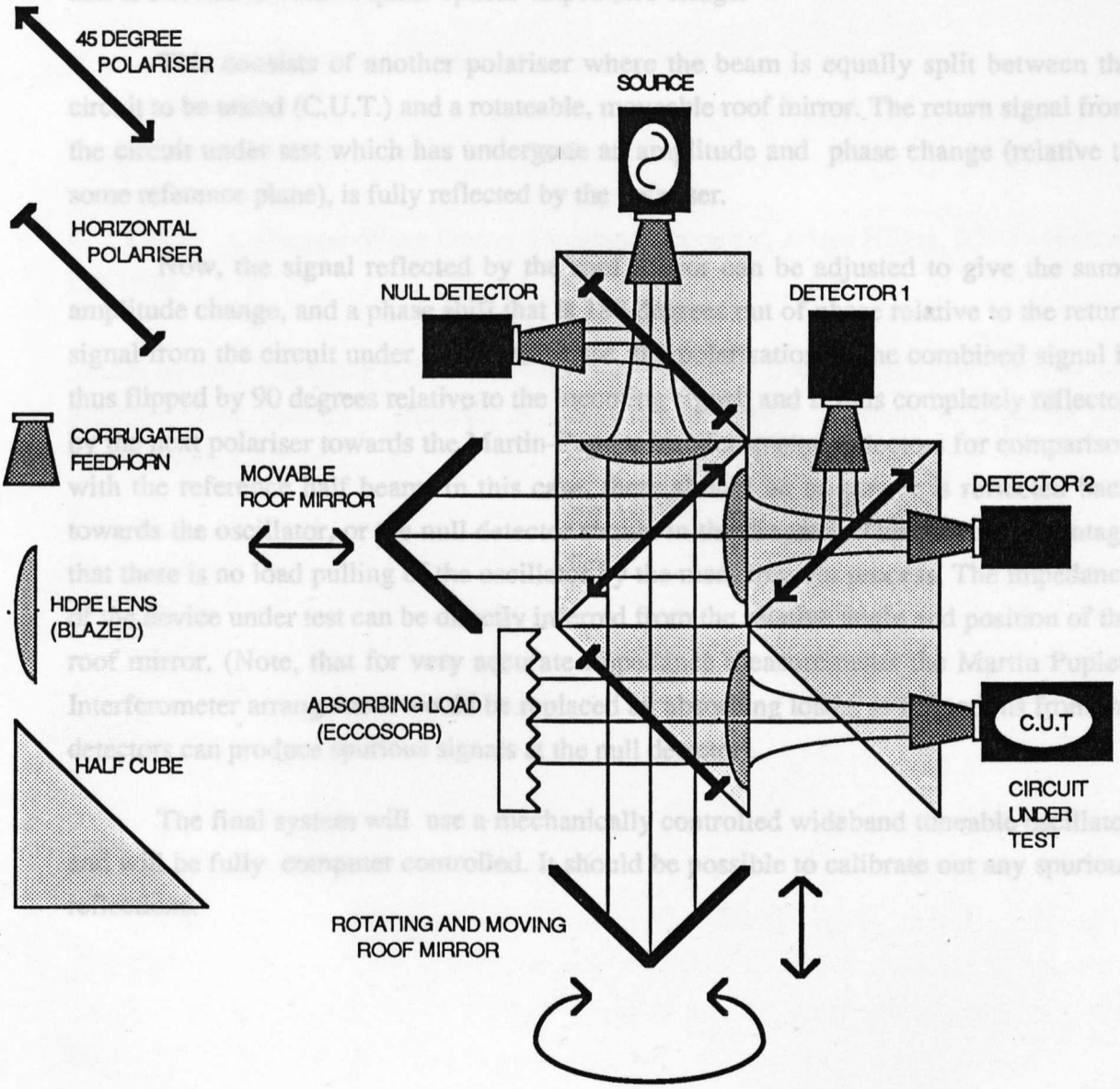

FIG. 9.3 IMPEDANCE MEASURING SYSTEM

through the first polariser and is split into two at the second polariser. One part is directed towards a Martin-Puplett interferometer for accurate frequency measurement. The other half is directed towards a quasi-optical impedance bridge.

This consists of another polariser where the beam is equally split between the circuit to be tested (C.U.T.) and a rotateable, moveable roof mirror. The return signal from the circuit under test which has undergone an amplitude and phase change (relative to some reference plane), is fully reflected by the polariser.

Now, the signal reflected by the roof mirror can be adjusted to give the same amplitude change, and a phase shift that is 180 degrees out of phase relative to the return signal from the circuit under test. In this case, the polarisation of the combined signal is thus flipped by 90 degrees relative to the incoming signal, and is thus completely reflected by the next polariser towards the Martin-Puplett Interferometer detectors for comparison with the reference half beam. In this case, there should be no power is reflected back towards the oscillator, or the null detector shown in the diagram. This has the advantage that there is no load pulling of the oscillator by the measurement process. The impedance of the device under test can be directly inferred from the relative angle and position of the roof mirror. (Note, that for very accurate impedance measurements the Martin Puplett Interferometer arrangement would be replaced by absorbing loads, as reflections from the detectors can produce spurious signals at the null detector).

The final system will use a mechanically controlled wideband tuneable oscillator and will be fully computer controlled. It should be possible to calibrate out any spurious reflections.

REFERENCES (CHAPTER 2)

1) Flann Microwave Instruments Catalogue, 1987

2) Hughes Millimeter-Wave Products Catalogue, 1985

3) A. Harvey, PhD Thesis, to be submitted, 1990

4) J. Lesurf, 'Millimeter-Wave Optics, Devices & Systems', Adam Hilger, IOP Publishing Ltd 1990

5) D.H Martin, 'Polarizing (Martin-Puplett) Interferometric Spectrometers for the Near and Submillimeter Spectra', Infrared and Millimeter Waves, Volume 6, Systems and Components, Chapter 2

10.0 NOISE MEASUREMENTS

10.1 SIGNIFICANCE OF NOISE IN MM-WAVE DEVICES

There has been an increasing interest in the use of MMW frequency bands for communication, radar and measurement systems because of the higher bandwidth, directivity, and precision offered at these higher frequencies. If however, full advantage of the bandwidth offered by MMW frequencies is to be achieved, precise frequency and phase control is essential. Doppler radar especially requires a large degree of frequency control for the determination of target velocities. However, it is the growing trend of more and more sophisticated signal processing techniques for the detection and identification of targets that has provided much of the impetus to significantly reduce total system noise. With continuing improvements in receiver/detector sensitivity, and increasing use of solid-state transmitters, noise associated with the injection locked/phase locked sources and local oscillators can become an important concern to the system engineer. In addition, in many cases (such as 'smart' missiles) it is not economically or sometimes mechanically viable to have phase locked sources in many systems and so noise and frequency drift, have to be carefully evaluated.

In MM-wave astronomy where detectors are reaching the highest sensitivity, the noise associated with a phase locked local oscillator can often be the dominant source of noise.

With the development of new devices and processing technologies, the noise characteristic of a device (i.e white noise, 1/f, $1/f^2$) and its variance with operating parameters (i.e temperature, bias voltage) can often give important clues as to problems in the device technology.

Along with the frequency and power, the noise is by far and away the most critical parameter to the system engineer. EEV have stated that this is the specification which is requested most, when inquiries are made about oscillators, and the ability to give a specification is likely to have a direct impact on sales.

10.2 AM AND FM NOISE

AM Noise is amplitude modulation noise and FM noise is frequency modulation noise. They can both be considered as small signal sidebands on either side of an

oscillator. AM noise manifests itself as symmetrical sidebands which are in phase with one another. The FM noise sidebands are 180 degrees out of phase. A.M. noise measurements are relatively straight forward and can use a direct detection system, followed by low noise amplifiers and filters, and a R.M.S. voltage detector.

F.M. measurements are slightly more involved because the sidebands cancel in any direct measurement as they are 180 degrees out of phase with one another. It is thus necessary to introduce some type of F.M. to A.M. conversion, and then to measure the noise contribution. This usually requires careful calibration. In addition, the measured F.M. noise of a diode is dependent on the Q of the cavity in which it operates. This also needs to be measured to calculate the noise measure M for a particular device, and to enable comparisons with previous measurements. This can be achieved using injection locking experiments [6].

10.3 NOISE MEASUREMENT TECHNIQUES

Essentially, every waveguide system has an optical analogue that offers potential advantages at W-band frequencies and above. Those systems utilising closed high Q cavities may benefit by using open resonator techniques where higher Q and ease of tuning are clear advantages [3], [9]. The systems that use reflection cavities however, require the use of circulators which limit the bandwidth and are not generally available above W-band. It is possible to make optical circulators that will work at much higher frequencies, (not dissimilar to those used in laser applications) but they are fairly lossy and require matching to free space (using quarter-wave anti-reflection coatings) which will limit the bandwidth anyway.

There are essentially two approaches to noise measurement at high frequencies. The first technique is to phase lock another low noise source in quadrature to the source to be tested. This introduces full A.M. to F.M. and A.M. to F.M. conversion, but adds the noise of the original source, although this can be found if three sources are available. The other methods are single oscillator techniques, where the carrier is used as the 'local oscillator' and is phase shifted relative to the noise sidebands. If the carrier is shifted by 90 degrees we have full AM to FM and FM to AM conversion.

For the FM to AM conversion, a number of system configurations may be utilised. These either involve using a discriminator directly such as a high Q cavity either in reflection [7] or transmission [3], or delay line (interferometer) [1],[4], or using the Ondria phase bridge method [2],[6].

In the Ondria phase bridge method, the carrier is suppressed using a high Q reaction cavity in one arm, and reintroduced into the system shifted by 90 degrees. The high Q cavity itself introduces a frequency dependent phase shift and attenuation across the width of the cavity which also needs to be taken into account.The total effect is partial FM to AM conversion and AM to FM conversion, within the half-width of the cavity and full FM to AM conversion outside this half width. Balanced mixers are used to distinguish the contributions from AM and FM noise, and to measure the mixer noise under operating conditions. Because the carrier is suppressed the sensitivity of the mixer system may also be improved, as there is less danger of saturating the mixer. An absolute calibration for FM can be performed by introducing a known amount of frequency modulation on to the source and measuring the corresponding output voltage. (i.e. The Crosby zero crossing method). If the mixer is sensitive enough, absolute calibration can also be made by comparison with a black body source such as an absorber in liquid nitrogen.

To achieve the highest sensitivity with F.M noise measurements, a key requirement is to have a frequency discriminator, with as high a discriminator slope as possible. It is generally regarded that using single oscillator techniques this is best achieved with an Ondria Bridge type arrangement. This utilises a carrier supression filter of the highest possible Q, and the highest possible supression. Waveguide cavities have Q's which are severely limited by resistive losses, and often are untuneable. In the system devised an open resonator is used to achieve Q,s in excess of 100,000 and optical techniques are utilised to obtain almost perfect matching to the cavity. (An increase in Q by a factor of 10 can be expected to decrease the noise floor by a factor of 20dB).

10.4 WORLD AND U.K. STATE OF THE ART

Until recently, the only dedicated noise bench at W-band in the U.K. was made by Plessey in 1982. It utilises the delay line technique in waveguide which was initially outlined by Peebles [8]. As described in 1982, it required 10mW of oscillator power to provide adequate sensitivity. This was mainly determined by the detector diodes used, and waveguide/component losses. (The 30cm of WG/27 delay line alone had an insertion loss of 4dB). This technique also requires a high quality circulator which significantly reduces the bandwidth. (About 2GHz per circulator).

Another approach which has been utilised in France and the U.S. is to use a very low noise phase locked source and downconvert the oscillator signal, and then use a conventional low frequency noise test bench. This has given good results, but is expensive

and adds the unknown noise of the phase locked source. Phase locked sources are expensive and inherently single frequency.

Yet another approach used by Hewlett-Packard at the moment is to phase lock a low noise multiplied source in quadrature with the oscillator. This also can give good results, but it is difficult to make wideband tuneable and adds the noise of the phase locked source. Power output required from the oscillator for a good measurement is typically 10mW.

John Ondria reported in 1980 that he had extended his microwave noise measurement system to W-band. This utilises the phase bridge technique with the possibility of carrier suppression in one arm by use of a high Q reaction cavity ($Q \approx 6500$) and a circulator. No noise figures or sensitivities were given in this paper, but the system was capable of measuring -160dBc/Hz at 100kHz from the carrier for an input power of 12mW.

It is difficult to compare systems, but in the end the system sensitivity is determined mainly by the quality of the detector, and then secondly by the system configuration. An InSb detector will be more sensitive than any of those used previously and an optical system will be less lossy than any equivalent waveguide system. This should enable us to perform state of the art measurements at W-band and above.

10.5 DETECTORS

The detectors and low noise if amplifiers are critical in determining the overall sensitivity of the system. The critical parameters are noise temperature, voltage sensitivity, if bandwidth, rf bandwidth and ease of use. In this system two different types of detectors are intended to be used. For the lowest noise and local oscillator requirements it is proposed to use a set of matched cooled InSb detectors, which will probably be primarily used for A.M. measurements. For F.M. measurements where i.f bandwidth is a consideration, and the noise levels to be measured are much higher it is proposed to use a pair of Schottky diode mixers to be used in a tuneable mount.

10.5.1 InSb DETECTORS

InSb detectors have produced system noise temperatures of 200-300 degrees over the range 100-400GHz. This compares with the very best Schottky barrier detectors which have noise temperatures of nearer 1000 degrees (500 degrees when cooled). Moreover the noise temperatures for InSb mixers are typically specified 100kHz away from the carrier, compared to Schottky barriers where they are specified 1GHz away from the carrier. The noise temperature may be considerably worse close in to the carrier where the 1/f noise of the mixer may start to dominate. Only SIS mixers have had lower noise temperatures, but the ruggedness, and ease of matching of InSb are clear advantages over both SIS and Schottky mixers. InSb detectors may only require 1μW of local oscillator power for efficient operation, compared to 500μW for the very best Schottky devices. This is an important consideration for the potential characterisation of high frequency low noise quantum-well devices, which certainly in the initial stages of development will only be capable of producing a few tens of μW.

InSb is also capable of very broadband performance as it remains absorbing up to 0.3mm (1000GHz), and being a bulk mixer it has the advantage that it often becomes easier to match power into the mixer at the higher frequencies and over a broader bandwidth than point contact diodes.

10.5.2 SCHOTTKY BARRIER MIXERS

Schottky barrier mixers are not nearly as sensitive as InSb detectors but they have the advantage of room temperature operation, a considerably larger if bandwidth, as well as low noise operation. This makes them ideal candidates for the F.M. noise measurements.

Several mixers mounted in low parasitic pill packs were bought from FARRAN technology, and mounted in blocks similar to the type used for the GUNN oscillators in the work described before. The principle was that by altering the height of the cavity and the position of the backshort it should be possible to match most of the power into the diode, and thus make the detector wide-band tuneable. Using a 2mm cap structure it quickly became apparent that it was possible to obtain excellent sensitivity throughout W-band by this method. However, it was also apparent that matching power into the cavity was not the same thing as matching power into the diode, and highest sensitivity could occur when significant amounts of power were still being reflected from the cavity. Further

experimentation indicated that a small cap of diameter 1.4mm offered a reasonable combination of good matching and sensitivity, although more detailed experiments are indicated.

10.6 DELAY LINE SYSTEM

The delay line system utilised by Plessey is essentially just simple interferometry but performed in waveguide. The signal is split into two and made to travel two different path lengths. The paths are chosen so that the signals cancel at the carrier frequency, but at frequencies slightly offset from this frequency they will begin to interfere. For offset frequencies of only 1MHz it is clear that for maximum sensitivity, the difference in path lengths essentially just wants to be as large as possible. In practice, the losses associated with the longer line (and limited oscillator power) determine an optimum path difference. In WG/27, as a rule of thumb, the losses are taken as 0.1dB per cm, which means that the optimum path difference may be relatively small. In comparison, the atmospheric attenuation at 94GHz in laboratory conditions is negligible (0.3dB km^{-1}).

A low loss optical analogue is a Martin-Puplett polarising interferometer system. Feedhorns are used to couple power into the system from waveguide, and can provide up to 98% coupling to a fundamental Gaussian beam. HDPE lenses couple the beam through the system with losses of only 0.1-0.2dB, and wire-grid polarisers are used as beam-splitters with losses of only 0.01dB. With a well designed system based on Gaussian Beam optics it is possible to get coupling from the oscillator, through the system and into the detector with a loss of only 1dB, although 1.5-2dB might be more typical over a large frequency range (20GHz). The maximum path difference that could be allowed depends on the coupling between the recombined Gaussian beams, and diffraction losses, but a path difference of 1m can be managed without problem. This should give an effective Q of around 2500.

10.7 CARRIER SUPRESSION SYSTEM

A more sensitive configuration is the carrier supression system which utilises a high Q cavity. Again quasi-optics offers a great improvement in performance, and a novel optical resonator has been devised which not only allows simple frequency tuning, but almost perfect suppression of the carrier over an ultra-wideband frequency range. It is

expected this will allow high sensitivity F.M. measurements to be made from W-band to at least 300GHz in the present system. With larger optics, the frequency range could be extended to lower frequencies to give improved performance over waveguide noise benches at millimetre wave frequencies. With adjustments to the polarisers and beam-splitter it is considered that sensitive measurements up to 1000 GHz should be possible.

A high Q near confocal open resonator, with dielectric sheet beam-splitter coupling, has been built and tested using a variety of different mirrors and beam-splitters. Best results so far have given an unloaded Q of at least 200,000, and a loaded Q (fully matched cavity) of at least 100,000 at 83GHz. This is starting to approach the maximum Q that can be achieved, for the size of cavity (36cm length), and compares well with previous published results. It is anticipated that at 94GHz, the final system will have a larger cavity (52cm) , and that unloaded Q's of 500,000, and loaded Q's of 250,000 will be readily achieved.

The system is also completely tuneable, with simple adjustment of one of the end mirrors allowing performance that is essentially only band-limited by the feedhorn/lens combination. In addition, a novel and very effective matching configuration has been designed, that should be capable of giving complete carrier suppression at any frequency (diffraction losses allowing).

The necessary frequency discriminant has also been demonstrated, and frequency (phase) locking of a Gunn oscillator to the passive cavity was achieved without difficulty. Because of the very narrow-linewidth associated with the cavity (<600 kHz), frequency (phase) locking will be necessary over a narrow band, to stop the oscillator frequency drifting with respect to the cavity during a measurement.

This must be compared with the best W band waveguide noise measurement system which used a closed cavity. Here resistive losses limited the loaded Q to 7000 at 94GHz, where matching was achieved using a screw at the entrance to the cavity. The system gave accurate results, but to achieve the high Q, the cavity was also untuneable. We can also compare the waveguide delay line system designed by Plessey which had an equivalent Q of around 1,200.

10.8 F.M NOISE CARRIER SUPRESSION SYSTEM DESIGN

A schematic of the initial system that has been used to test the resonator and noise set-up is shown in Figure 10.1. The beam from the test source has its polarisation defined

FIG. 10.1 F.M. NOISE MEASUREMENT SYSTEM

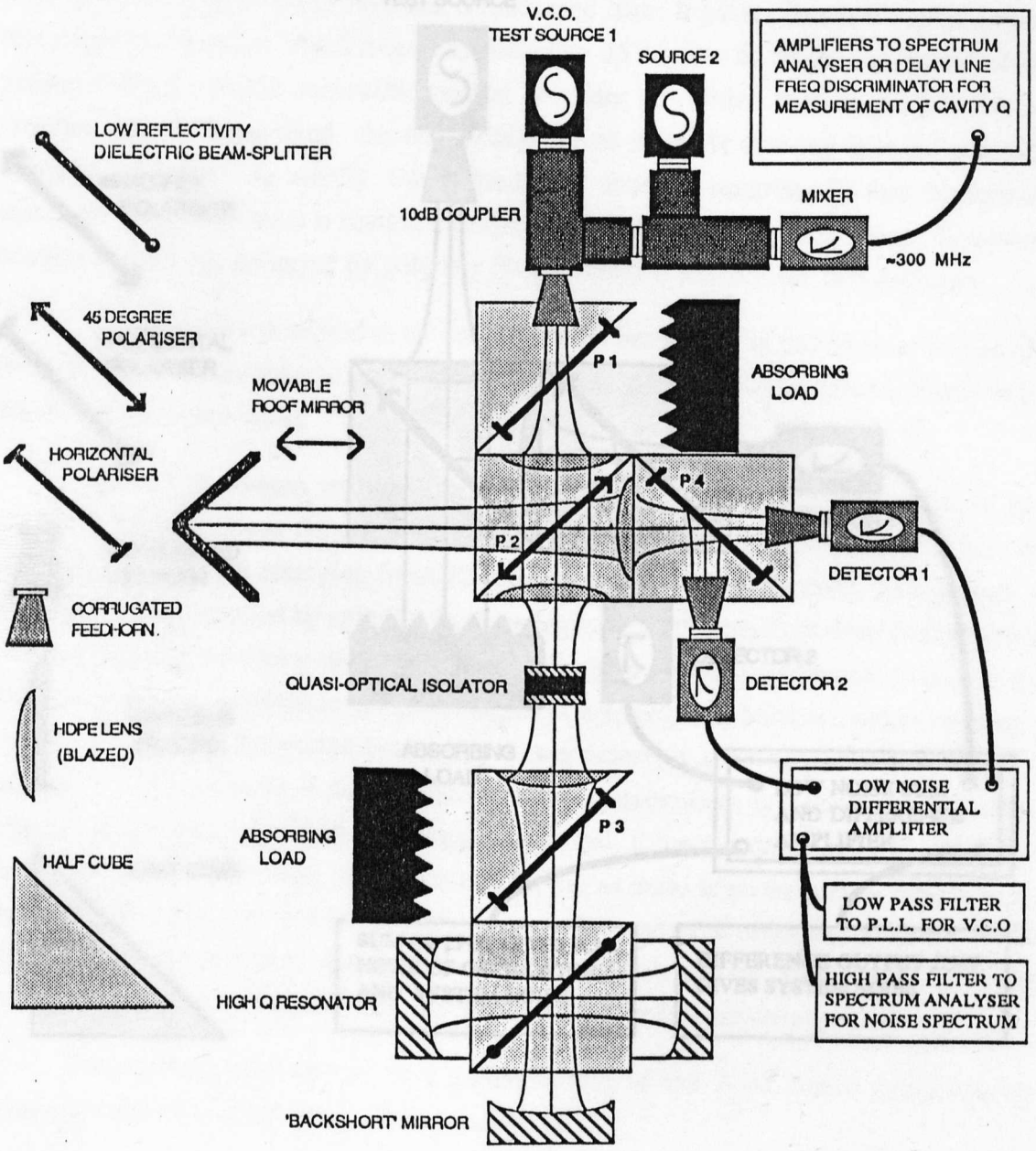

FIG. 10.2 A.M. NOISE MEASUREMENT SYSTEM

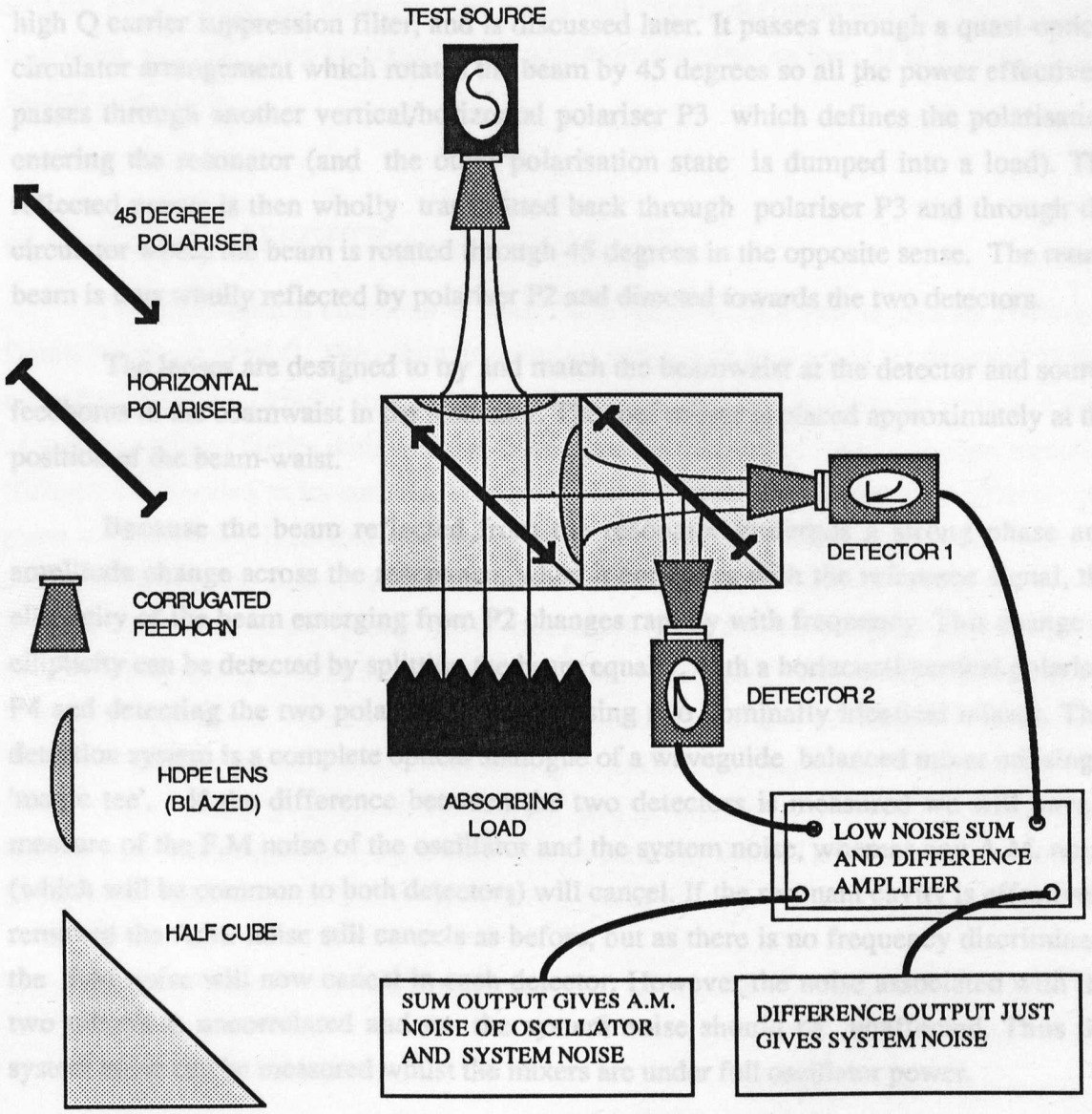

by polariser P1 and it is then split into two using a 45 degree polariser P2. One arm acts as the reference arm. In this arm, the beam reflects off a roof mirror and is transmitted to the detector system. The phase of this beam can be adjusted by changing the position of the roof mirror. The other beam is sent towards the 'three mirror system' which acts as a very high Q carrier suppression filter, and is discussed later. It passes through a quasi-optical circulator arrangement which rotates the beam by 45 degrees so all the power effectively passes through another vertical/horizontal polariser P3 which defines the polarisation entering the resonator (and the other polarisation state is dumped into a load). The reflected power is then wholly transmitted back through polariser P3 and through the circulator where the beam is rotated through 45 degrees in the opposite sense. The return beam is thus wholly reflected by polariser P2 and directed towards the two detectors.

The lenses are designed to try and match the beamwaist at the detector and source feedhorns to the beamwaist in the resonator. The roof mirror is placed approximately at the position of the beam-waist.

Because the beam reflected from the resonator undergos a strong phase and amplitude change across the resonance, when it combines with the reference signal, the ellipticity of the beam emerging from P2 changes rapidly with frequency. This change in ellipticity can be detected by splitting the beam equally, with a horizontal/vertical polariser P4 and detecting the two polarisation states using two nominally identical mixers. This detection system is a complete optical analogue of a waveguide balanced mixer utilising a 'magic tee'. If the difference between the two detectors is measured we will have a measure of the F.M noise of the oscillator and the system noise, whereas any A.M. noise (which will be common to both detectors) will cancel. If the resonant cavity is effectively removed the A.M. noise still cancels as before, but as there is no frequency discriminant the F.M noise will now cancel in each detector. However the noise associated with the two mixers is uncorrelated and so the system noise should be unaffected. Thus the system noise can be measured whilst the mixers are under full oscillator power.

This system also allows easy measurement of the A.M. noise using similar techniques and the simple set-up shown in Fig. 10.2.

10.9 A.M. NOISE MEASUREMENT

In the A.M. noise measurement system of Fig. 10.2 the beam is split equally between the two detectors where the A.M. noise will be common to both. Thus if we take the sum of the two detectors we will measure both the A.M.noise of the local oscillator

and the noise of the mixers and amplifiers. (The anti-symmetrical F.M. noise sidebands cancel in each detector). However, if we take the difference between the two detectors, the A.M.noise which is correlated will now cancel, but the system noise from the two mixers and amplifiers (which is uncorrelated) will of course not cancel. Thus, we can measure the system noise while the detectors are under full local oscillator power. This is very important as A.M. noise levels in Gunn oscillators are often so low, as to be right at the system sensitivity.

10.10 THE QUASI-OPTICAL CIRCULATOR

The quasi-optical circulator is based on an original idea and design by Professor Derek Martin at Q.M.C. The circulator used in this set-up was made by Michael Webb using ferrite material kindly supplied by Professor Martin. The circulator consists of a disc of self magnetized ferrite with an appropriate quarter wavelength anti-reflection material (flourosint) bonded to its surface. When a polarised beam is incident on the ferrite the plane of polarisation is rotated as it passes through the ferrite. If the length of the ferrite is chosen correctly, the plane of polarisation can be made to rotate through 45 degrees. If two polarisers are placed at 45 degrees to one another on either side of the ferrite (and appropriate coupling optics) a four port circulator is produced. The success of the isolator is largely dependent on how accurately the ferrite is cut and polished to the correct thickness to produce the necessary 45 degree rotation. The magnetism of the ferrite was found to be strongly affected by cutting and polishing and it was necessary to 'remagnetise' the magnet to bring it back into its saturated state. The first circulator (made by Michael Webb) had the following measured characteristics.

FREQUENCY (GHz)	ISOLATION	ONE WAY INSERTION LOSS INCLUDING REFLECTION
75	14dB	0.9dB
85	>40dB	0.42dB
90	26.5dB	0.18dB
95	27.8dB	0.46dB
100	>34dB	0.39dB
105	>32dB	0.66dB

If we define the ports on one side of the ferrite as INPUT PORTS 1 and 2 and the ports on the other side as OUTPUT ports 3 and 4. Power is sent through INPUT PORT 1.

FIG. 10.3 QUASI-OPTICAL CIRCULATOR

SETUP FOR THE MEASUREMENT OF THE ISOLATION AND LOSS OF THE CIRCULATOR OVER A WIDE FREQUENCY RANGE. POWER MEASUREMENTS ARE MADE AT THE DETECTOR FOR BOTH ORIENTATIONS OF THE CIRCULATOR, AND WITH THE CIRCULATOR REMOVED COMPLETELY

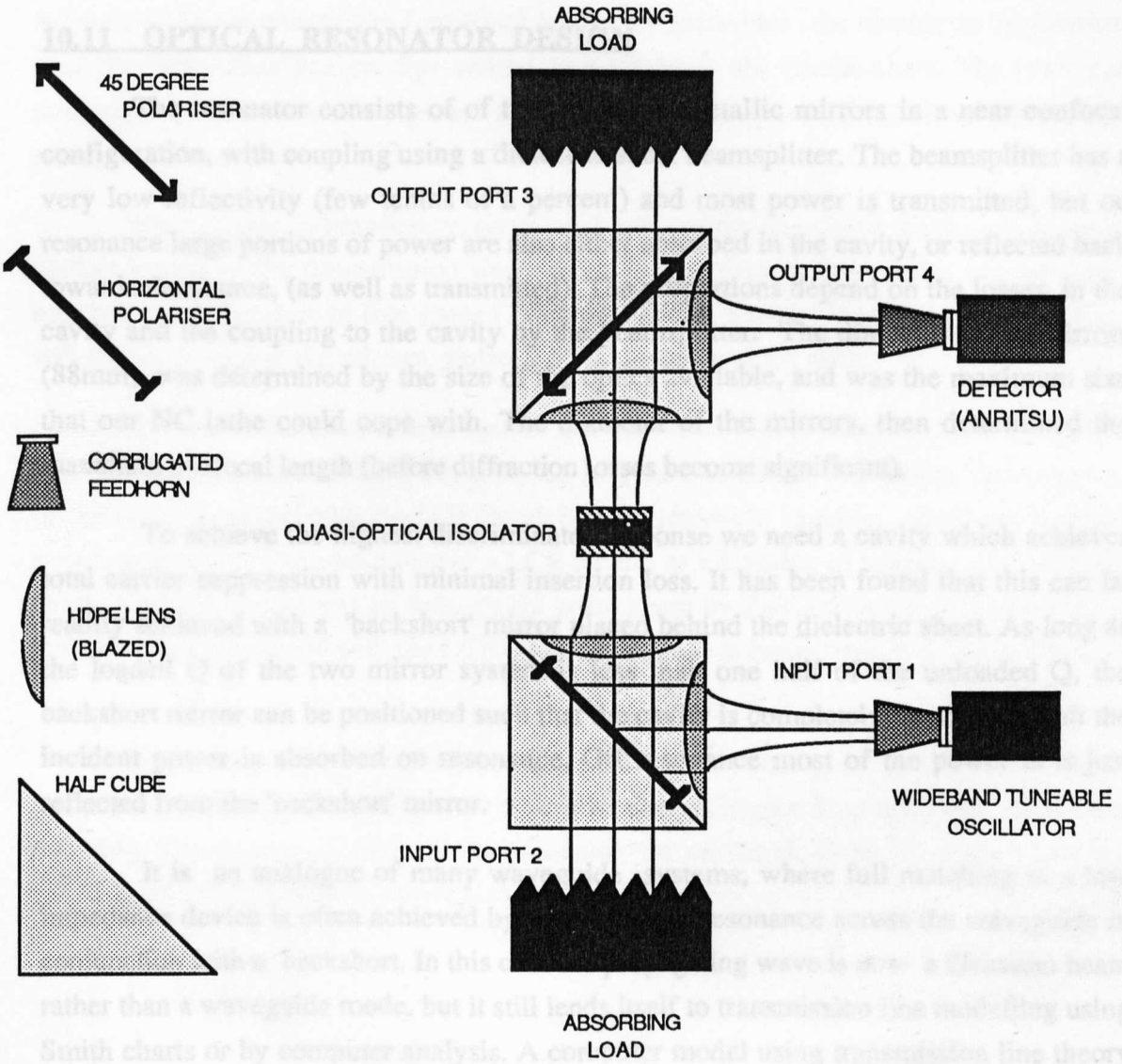

Isolation was defined as the ratio of the powers measured at OUTPUT PORT 4 with the ferrite turned one way and then the other. OUTPUT PORT 3 terminated with a matched load (Eccosorb), or vice-versa.

Insertion loss was defined as the ratio of twice the power at OUTPUT PORT 4 with the ferrite removed completely, to the power received at PORT 4 with the ferrite in place. OUTPUT PORT 3 terminated with a matched load.

10.11 OPTICAL RESONATOR DESIGN

The resonator consists of of two spherical metallic mirrors in a near confocal configuration, with coupling using a dielectric sheet beamsplitter. The beamsplitter has a very low reflectivity (few tenths of a percent) and most power is transmitted, but on resonance large portions of power are also either absorbed in the cavity, or reflected back towards the source, (as well as transmitted). The proportions depend on the losses in the cavity and the coupling to the cavity by the beamsplitter. The diameter of the mirrors (88mm), was determined by the size of the optics available, and was the maximum size that our NC lathe could cope with. The diameter of the mirrors, then determined the maximum confocal length (before diffraction losses become significant).

To achieve the highest discriminator response we need a cavity which achieves total carrier suppression with minimal insertion loss. It has been found that this can be readily achieved with a 'backshort' mirror placed behind the dielectric sheet. As long as the loaded Q of the two mirror system is less than one half of the unloaded Q, the backshort mirror can be positioned such that the cavity is completely matched and all the incident power is absorbed on resonance. Off resonance most of the power is is just reflected from the 'backshort' mirror.

It is an analogue of many waveguide systems, where full matching to a low impedance device is often achieved by using a series resonance across the waveguide in conjunction with a backshort. In this case the propagating wave is now a Gaussian beam rather than a waveguide mode, but it still lends itself to transmission line modelling using Smith charts or by computer analysis. A computer model using transmission line theory has given excellent agreement with experimental results and a good qualitative analysis is given below.

10.12 ANALYSIS OF THREE MIRROR SYSTEM

There are a number of different techniques of analysing the three mirror system, but perhaps the simplest physical model can be seen using Smith charts.

We can think of the resonator as an infinite number of simple tank circuits all coupled to the transmission line via the dielectric beam-splitter. Each of these can be represented as a simple series LCR circuit, which is only appreciably excited near resonance. As we change the frequency across the resonance, the change in impedance near that resonance can be represented as a circle on the Smith chart. The resonant frequency is where the circle passes through the zero reactance line, where the load is purely resistive.

When the circle passes through the mid-point of the chart then we can say there is perfect match to the transmission line, which in this case is free space. i.e. we have matched the impedance of free space (377 ohms) to the resistive loss in the cavity which will mainly be due to the mirrors, and will be of the order of 0.1 ohm.

To analyse the three mirror system it is beneficial to first consider the simple case of a series LCR circuit across a transmission line terminated by a backshort. Because the backshort is in parallel with the LCR circuit it is convenient to consider admittances rather than impedances. The admittance of a LCR circuit, as a function of frequency on a Smith chart, is a circle which passes through the point given by Z_0/R on resonance, where R is the resistance associated with the LCR circuit. This case is considered in detail in Chapter 4.

In the case of the resonator, the LCR circuit analogue is only valid near resonance, where the R is replaced by an effective resistance R_{eff} that depends on the coupling. The resonance point for the resonator on the Smith Chart is given by the so called coupling parameter K which is thus defined by:

$$K = \frac{Z_0}{R_{eff}} \qquad 10.1$$

Now the backshort will have the effect of transforming this admittance, by moving each point on the LCR circle a given distance along a constant admittance circle (which depends on the length of the transmission line to the short). Perfect matching to the waveguide can be achieved at the cross-over points of the LCR circle and the $G/Y_0 = 1$ circle. It can be clearly seen from the diagram that as long as $K = Z_0/R > 1$ then matching

can be achieved at two different frequencies, which will be roughly equally spaced around the resonant frequency of the LCR circuit. For K = 1 it can be seen that matching is only achieved at the resonant frequency when the backshort is one quarter of a wavelength away. For K < 1 then R > Z_0 and there is no cross-over point, and full matching can never be achieved, as has already been discussed in Chapter 4.

As already mentioned with the resonator, the situation is slightly more complicated because the 'tank' circuit is now only coupled to the transmission line via the beam splitter. Thus the circuit now only looks like a series LCR near resonance, where the coupling also effects a resonant impedance transformation. However, the load admittance will still be a circle as a function of frequency, and the same analysis as before can be applied as long as we substitute for an effective resistance for the resonator.

For small coupling and losses, it can be shown that the effective resistance across the transmission line, for the resonator, is very closely approximated by:

$$R_{eff} \approx Z_0 \cdot \frac{\alpha_{resonator}}{R_{dielectric}} \qquad 10.2$$

where Z_0 is the impedance of free space, α is the one way power loss in the resonator, and R is the reflectivity of the dielectric beam-splitter. Substituting in Eq. 10.1, we have the coupling parameter K given by,

$$K \approx \frac{R_{dielectric}}{\alpha_{resonator}} \qquad 10.3$$

The same previous analysis now applies with this new value of coupling parameter. Again matching will only be achieved when K >= 1. It is interesting to note that when K < 1, then the effective resistance placed across the line is actually greater than the impedance of free space! even though α may be very small. Again it is impossible for the backshort to match fully in this case. Matching thus depends critically on the ratio of the reflectivity of the dielectric beam-splitter to the one way power absorption loss. This power absorption loss includes the resistive loss in the mirrors, absorption loss in the dielectric and air, and diffraction loss due to the finite size of the mirrors.

It should be noted however, that in the ideal case K=1, as, although full matching can be achieved with K > 1, the phase and amplitude of the sidebands are distorted with respect to one another as can be seen in the Smith chart shown in Fig 10.5 Indeed, although full matching cannot be achieved, it may be better to have K < 1 for accurate FM noise measurements, as in this case the sidebands are not significantly distorted with respect to one another, when the mirror is placed an odd number of quarter wavelengths away. For

other potential applications, such as the matching of very low impedance quasi-optical detectors, or as a sideband filter it is obviously better to have K > 1.

As an example consider the three cases where the coupling parameter K of the resonator can take the values 0.5, 1 and 3. The impedance of the two mirror resonator, as a function of frequency for the different values of K, lead to the three admittance curves shown in Figure 10.4a. However, we must always include the other port representing transmission through the dielectric. This can be represented as an impedance in parallel with the resonator. It is therefore more useful to consider the admittance of the two mirror system which is represented in Fig. 10.4b.

In the case where there is no third mirror, but the other port is free space, there is an additional effective load impedance Z_0 (free space) in parallel with the resonator. Thus to transform we move one normalised conductance unit along the constant susceptance curves of Fig. 10.4b to get the three admittance curves shown in Fig.10.4c. We can see that off resonance, the cavity appears as a perfectly matched load, which is true as all the power just passes through the low reflectivity dielectric. On resonance, the cavity will look like a resistance placed across a free space transmission line and it will absorb some power and reflect some power. For K=1 half the power will be absorbed in the cavity, one quarter will be reflected and one quarter will be transmitted. For K>>1 (large reflectivity) nearly all the power will be reflected, and for K<<1 (very low reflectivity) nearly all the power will be transmitted.

When the 'backshort' mirror is introduced we now have a variable reactance and a resistance which is approximately zero. As long as the effective path length of the resonator is very large compared to distance of the third mirror from the beam-splitter, the reactance will be effectively constant over the bandwidth of the resonator. Thus the movement of the third backshort mirror can be represented on the Smith chart by a movement along a constant conductance circle. Thus the resonator where the coupling parameter K=3 can be matched by placing the third mirror n/2± wavelengths away from resonator. The resonator with K=1 can be fully matched if the mirror is an odd number of quarter wavelengths away, however the resonator where K=0.5 can never be matched with the 'backshort mirror'. The smallest VSWR is achieved when the the mirror is an odd number of quarter wavelengths away. These admittances are shown in Fig.10.4c.

It can thus be seen that for K < 1 the cavity can never be fully matched. However, for a coupling parameter K>1 although the cavity can be fully matched, it can be seen that it also leads to a distortion of the sidebands. In Figs. 10.5 a,b,c,d the distortion can be seen for values of K=1.1, K=1.4, K=2.0 and K=10 when the the backshort mirror is

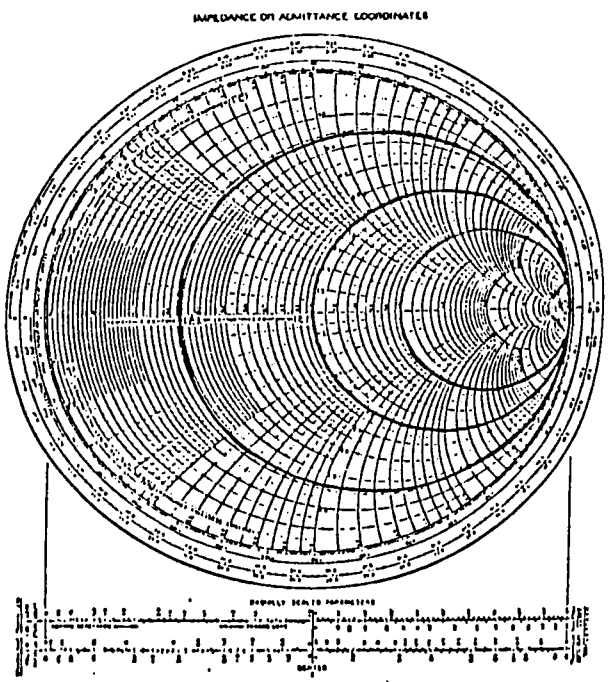

Fig. 10.4a Smith Chart showing Impedance of Two Mirror System for coupling parameters K=0.5, K=1, K=3

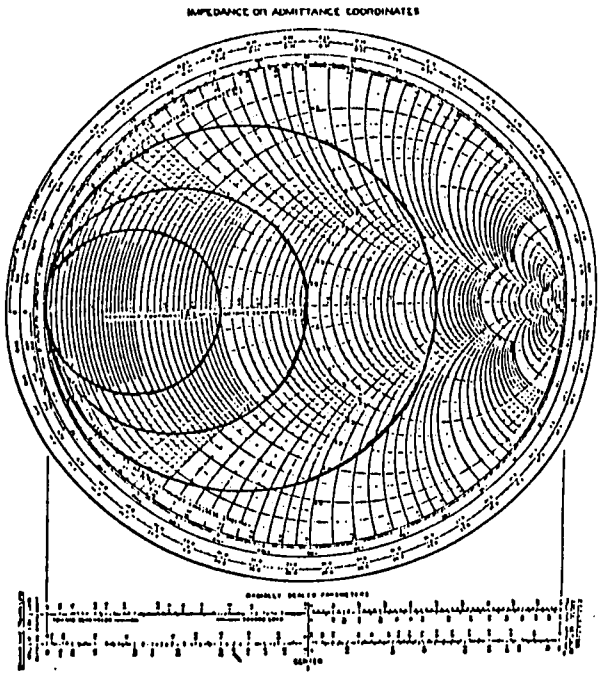

Fig. 10.4b Smith Chart showing Admittance of Two Mirror System Coupling parameters K=0.5, K=1, K=3

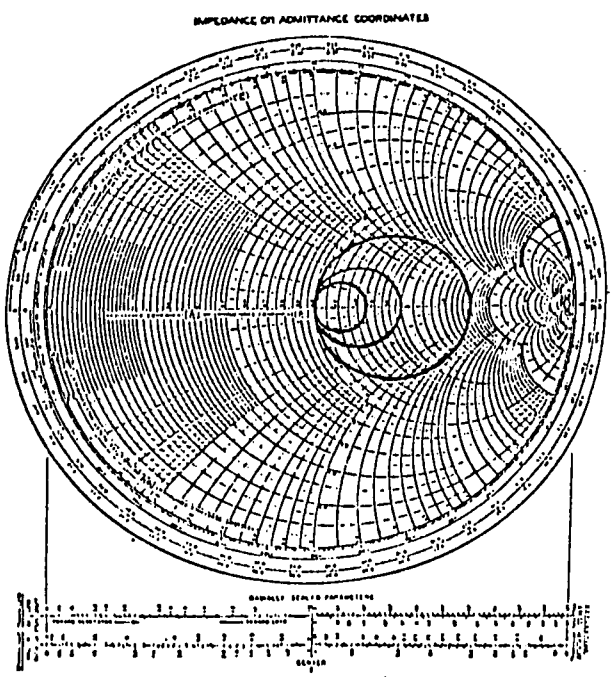

Fig. 10.4c Input Admittance of Cavity System with matched absorbing load placed behind the dielectric sheet. Coupling parameters K=0.5, K=1, K=3

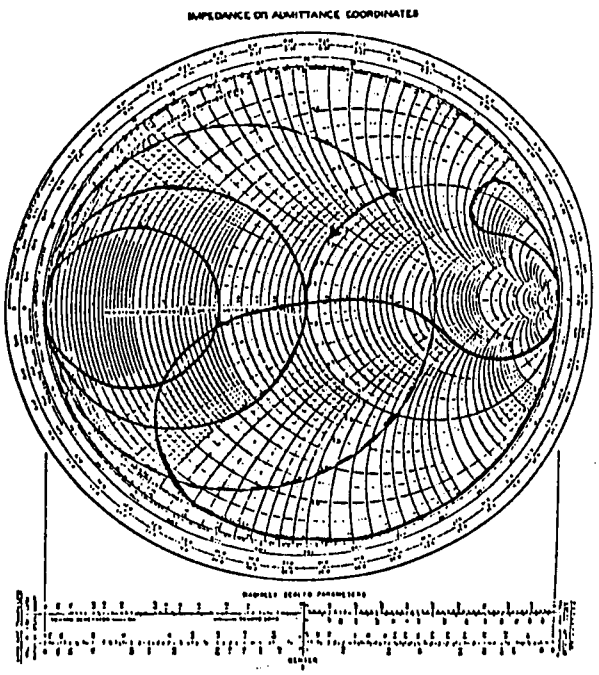

Fig. 10.4d Input Admittance of Cavity System with the third 'Backshort' Mirror positioned for maximum absorption (matching) in the cavity.
Coupling parameters K=0.5, K=1, K=3

Fig. 10.5a K = 1.1

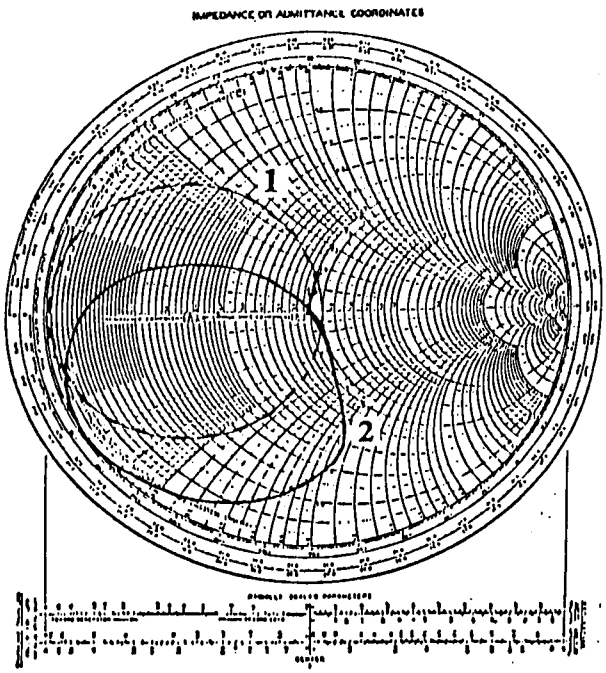

Fig. 10.5b K = 1.4

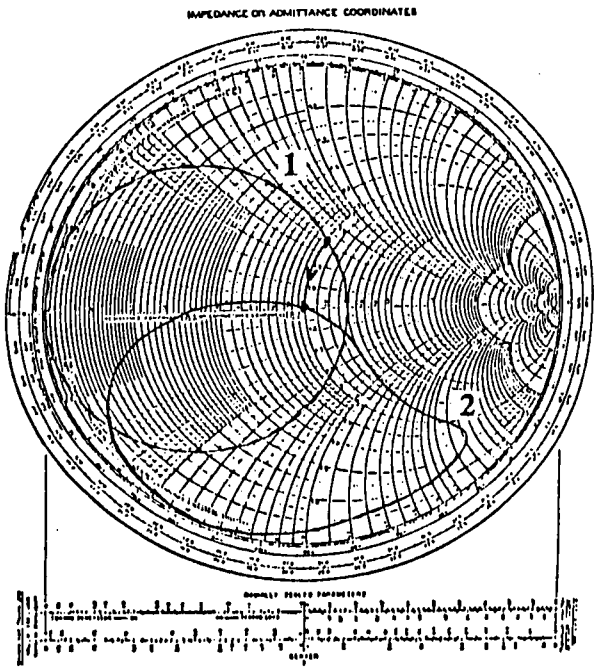

Fig. 10.5c K = 2.0

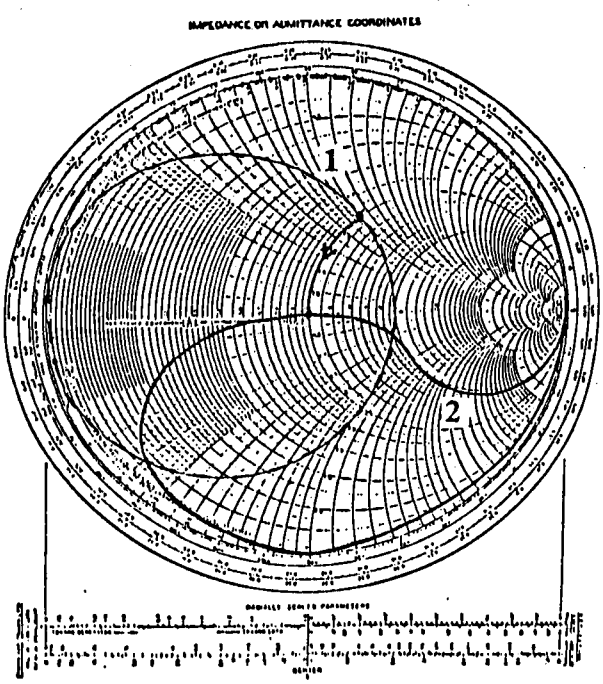

Fig. 10.5d K = 10.0

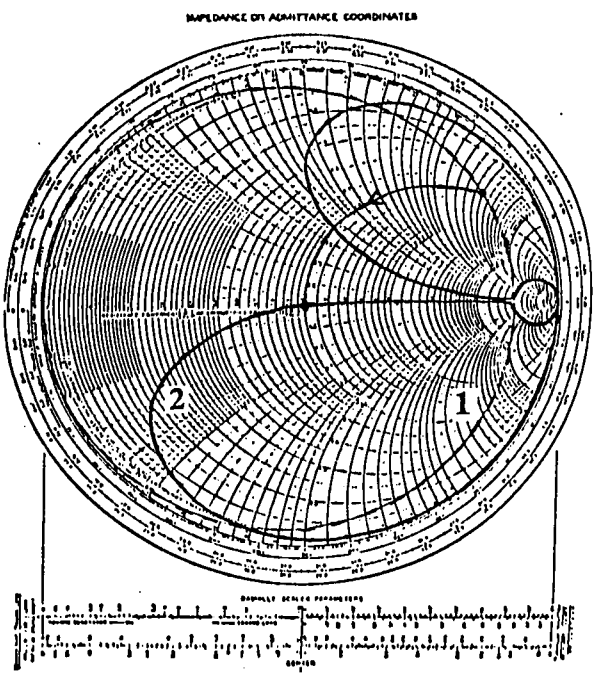

Fig. 10.5 Smith charts showing (1) The Admittance of the Two Mirror Sysrtem and (2) The Input Admittance of the Three Mirror Cavity System with the 'Backshort' Mirror positioned for maximum absorption (matching) in the cavity. These are illustrated for various different values of Coupling Parameter a) K=1.1, b) K=1.4 c) K=2, K=10. This illustrates how the sideband distortion becomes greater as the value of K becomes greater. The coupling parameter K is the ratio of the reflectivity of the dielectric to the one way power loss in the cavity.

adjusted for the full matching condition. It can be seen that the distortion is greatest for large values of K (No sideband distortion and full matching is only achieved for K = 1).

10.13 THE RESONATOR Q

The loaded Q_L of the cavity is given by the number of half wavelengths in the cavity multiplied by the Finesse:

$$Q_L = F.q = \omega/\Delta\omega_{cav} \qquad 10.4$$

where $q = 2L/\lambda$ and F approximates $\pi/(\alpha+R)$ where α is the one way power absorption loss, and R is the reflection from the beam-splitter. Clearly the longer the cavity the larger the Q, although for any given mirror size the Q will eventually be limited by diffraction losses as the mirrors are moved apart. The unloaded Q_u is when $R \approx 0$, when F approximates π/α.

Note that $Q_u/Q_L = 1 + R/\alpha = 1 + K$

Full matching is only possible when $R >= \alpha$, when $K >= 1$ and $Q_L <= Q_u/2$.

(The approximations are excellent for α and R small. Exact expressions can be found or easily derived from Chapter 7).

10.14 MEASUREMENT OF RESONATOR Q

To measure the resonator Q, the set-up illustrated in Fig 10.1 was utilised using two oscillators operating near 83GHz, with the reference arm blocked. This frequency was chosen simply because high power oscillators were available at the time, and the detectors available were badly matched and of a low sensitivity. The frequency of the oscillator was swept over the cavity resonance by changing the bias voltage over one or two hundred millivolts. The voltage tuning of the oscillator was typically about 200MHz/V. The frequency change was noted by taking off some power using a 10dB coupler and mixing with another oscillator operating near the same frequency. The resulting difference frequency was amplified and monitored using a spectrum analyser or a delay line discriminator.

To ensure that there were no noticeable pulling effects on the oscillator from reflections from the resonator, initial experiments used about 15dB of attenuation between

the oscillator and the resoanator. In fact, without this attenuation the apparent cavity response could be distorted by moving the oscillator relative to the cavity. Sometimes there was a small frequency jump (≈ 1MHz) of the second harmonic oscillator, caused by the reflection near resonance. This effect was considerably reduced with the attenuation, and future measurements were considerably eased when a wideband isolator became available.

Initially, one oscillator had its frequency swept by applying a triangular wave to the bias voltage, and a portion of the reflected wave from the cavity was detected using a crystal.The power from the crystal was shown on an oscilloscope as a function of bias sweep, which showed very clearly the linewidth of the cavity. To ensure that the frequency was sweeping linearly across the resonance with bias voltage, the detector output was also monitored with respect to the voltage output of a delay line discriminator, operating at a few hundred MHz. Both measurements gave substantially the same values for the measured Q, (within experimental error), which would indicate that the sweep is effectively linear.

Initial experiments showed that the sweep rate had to be very low to allow accurate measurement of the Q, as the cavity response time is by no means negligible. The bias voltage sweep and detector output was subsequently controlled and monitored by an ARCHIMEDES computer via several A to D and D to A boards. The oscillator was typically swept over 17MHz over a period of almost 30 seconds, and the detector output stored and printed as a function of bias voltage.

10.15 RESONATOR Q RESULTS

The Q was measured for a variety of different beamsplitters, polarisation, and mirror combinations. The coupling/reflection is a function of the polarisation and the beam-splitter optical thickness. The reflection is expected to change roughly by a factor of 8 when the polarisation state is altered. The cavity losses were expected to be dominated by resistive mirror losses, although the loss in several different dielectrics was also shown to be significant.

The resonator consisted of three mirrors with a radius of curvature of 36cm and diameter 8.8cm, which were separated by ≈ 37cm. At a frequency of 83GHz (λ = 3.6mm), this gave a Fresnel number N ≈ 1.5, in an approximately confocal cavity. This means that diffraction losses should be negligible. The mirrors were made of copper, brass and aluminium and produced using an NC lathe. A set of polished and unpolished

aluminium mirrors were also tested to compare results with the polishing being done with a water based paste. (The NPL do not polish their copper mirrors). Beamsplitters made from 28μm KAPTON, 10μm MELINEX, PVC (clingfilm), and assorted thicknesses of polythene and other plastics (made from various foodbags!) were also tested. The foodbags were ALCAN 'freezer bag', ALCAN 'food bag', ALCAN 'microwave bag', and an ALCAN 'multi-purpose bag'. (It has proved very difficult in obtaining simple uncontaminated polythene sheets in small quantities).

Typical results are shown from Fig.10.6 to 10.12 for the different dielectrics tested, with Fig 10.13 indicating the discriminator curve for the two resonances. Roughly speaking, the horizontal polarisation gives an indication of the unloaded Q and the vertical polarisation gives an indication of the loaded Q. In some of the results a piece of ECCOSORB was placed in front of the resonator during the scan to indicate the zero reflection state. This showed that most of the resonators could be matched if the polarisaation was vertical, although there was clear evidence of side-band distortion where the linewidth was above 1MHz.

The results showed that the KAPTON had a very sizeable loss (at least 5 times the published bulk loss), followed by the 'microwave' and 'multi-purpose' bags. The MELINEX and the clingfilm gave better results but were 'thin' compared to the other test sheets and still seemed to have significant loss. Best results were obtained with the ALCAN 'food bag' and the ALCAN 'freezer bag'! This is perhaps not so surprising as these are believed to be made mainly from polythene which has a very low bulk loss ($\approx$0.01 Np cm^{-1}), although the manufacturers of bags also tend to add various plasticisers which may be more lossy. There was evidence to suggest that this may be the dominant loss, as the Q did not change significantly when different brass, aluminium and copper mirrors were used in the resonator. In addition, the plastics may be polarisation sensitive as the bags have a definite grain. The polished aluminium gave better results than the unpolished aluminium, and it is planned to polish the remaining mirrors.

The Q's obtained suggest a resonator loss of around 0.3% per pass. This still compares favourably with many other published results, although the NPL have achieved 0.15%. It is hoped with the polishing of the copper mirrors, and optimisation of the dielectric sheet, that this figure may be approached.

There was some slight variance in some of the results which is believed to be due to oscillator pulling and perhaps some drift during the measurement. Although in general, the oscillators used were extremely stable.

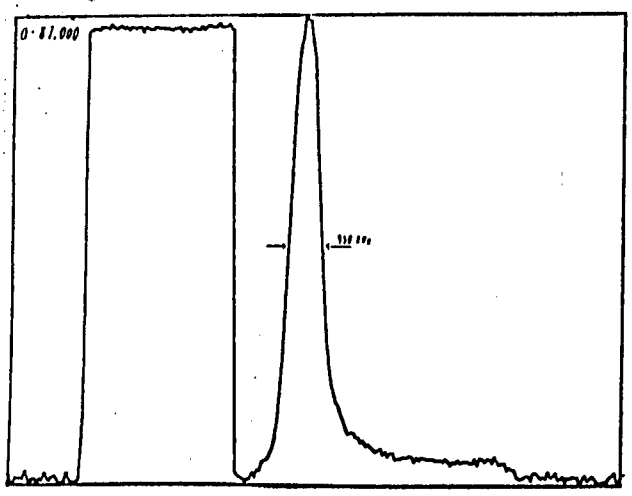

FIGURE 10.6a 10μm MELINEX VERTICAL POLARISATION
Q = 87,000

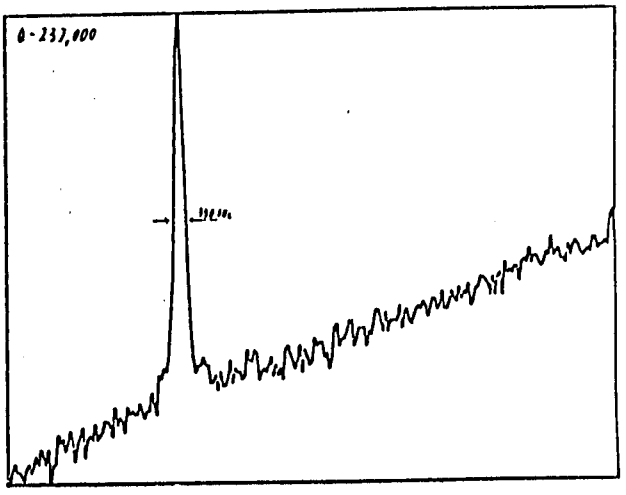

FIGURE 10.6b 10μm MELINEX HORIZONTAL POLARISATION
Q ≈ 237,000

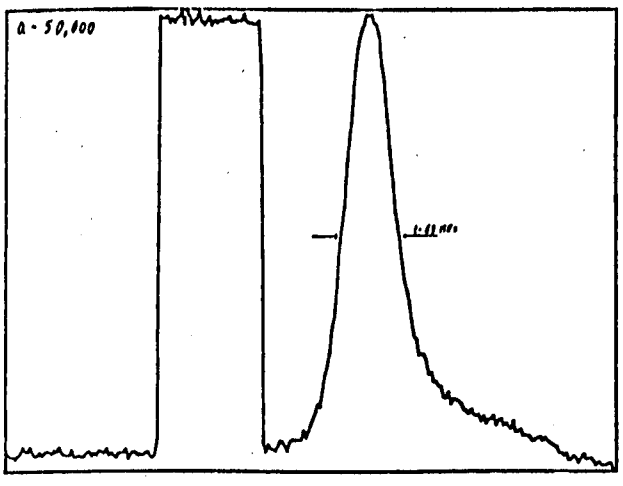

FIGURE 10.7a 28μm KAPTON VERTICAL POLARISATION
Q ≈ 50,000

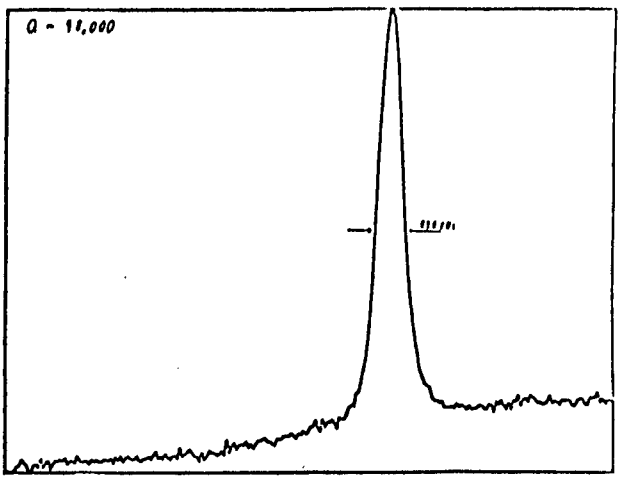

FIGURE 10.7b 28μm KAPTON HORIZONTAL POLARISATION
Q ≈ 98,000

FIGURES INDICATING THE TYPICAL MEASURED Q OF THE THREE MIRROR QUASI-OPTICAL CONFOCAL RESONATOR (R=360mm) USING DIFFERENT DIELECTRIC BEAMSPLITTERS TO COUPLE IN THE POWER

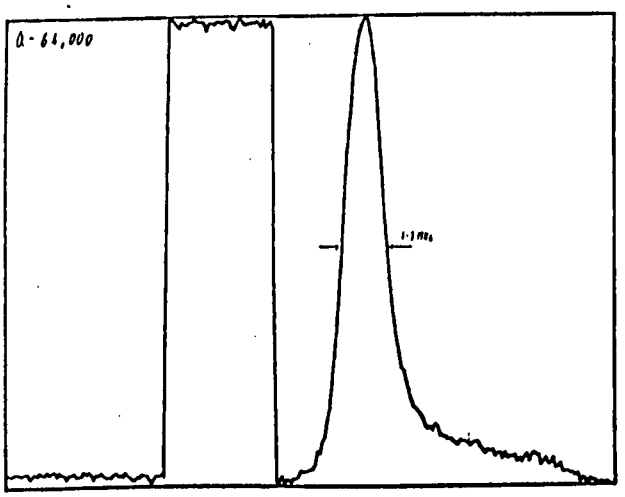

FIGURE 10.8a ALCAN MULTI-P
VERTICAL POLARISATION
Q ≈ 64,000

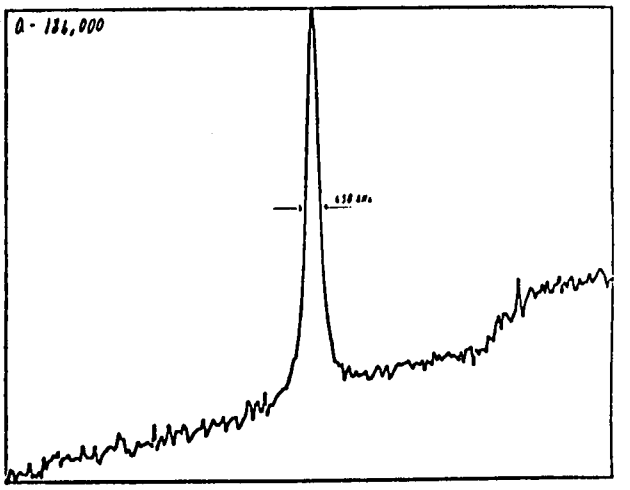

FIGURE 10.8b ALCAN MULTI-P
HORIZONTAL POLARISATION
Q ≈ 184,000

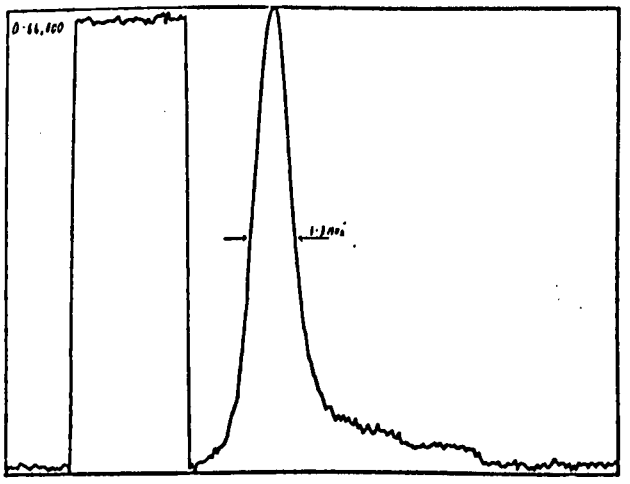

FIGURE 10.9a ALCAN MICROWAVE
VERTICAL POLARISATION
Q ≈ 64,000

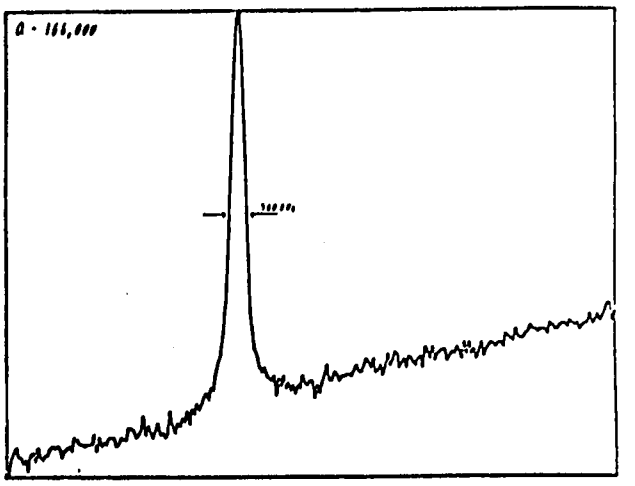

FIGURE 10.9b ALCAN MICROWAV
HORIZONTAL POLARISATION
Q ≈ 166,000

FIGURES INDICATING THE TYPICAL MEASURED Q OF THE THREE MIRROR QUASI-OPTICAL CONFOCAL RESONATOR (R=360mm) USING DIFFERENT DIELECTRIC BEAMSPLITTERS TO COUPLE IN THE POWER

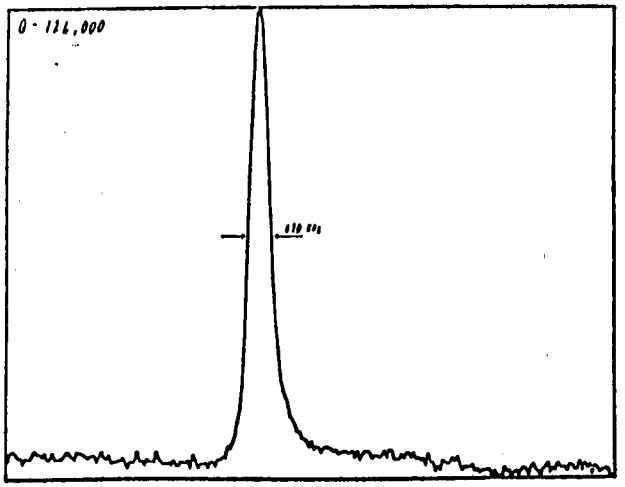

FIGURE 10.10a CLINGFILM
VERTICAL POLARISATION
Q ≈ 124,000

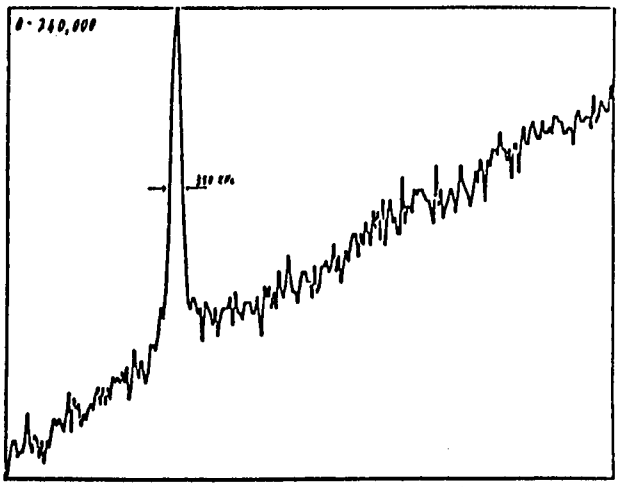

FIGURE 10.10b CLINGFILM
HORIZONTAL POLARISATION
Q ≈ 240,000

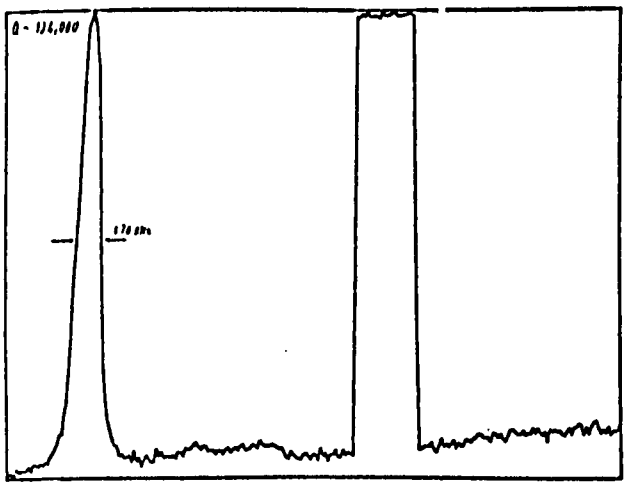

FIGURE 10.11a ALCAN FREEZER
VERTICAL POLARISATION
Q ≈ 124,000

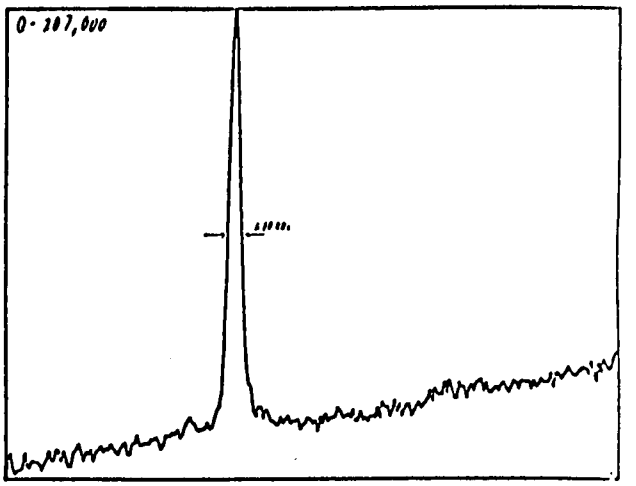

FIGURE 10.11b ALCAN FREEZER
HORIZONTAL POLARISATION
Q ≈ 207,000

FIGURES INDICATING THE TYPICAL MEASURED Q OF THE THREE MIRROR QUASI-OPTICAL CONFOCAL RESONATOR (R=360mm) USING DIFFERENT DIELECTRIC BEAMSPLITTERS TO COUPLE IN THE POWER

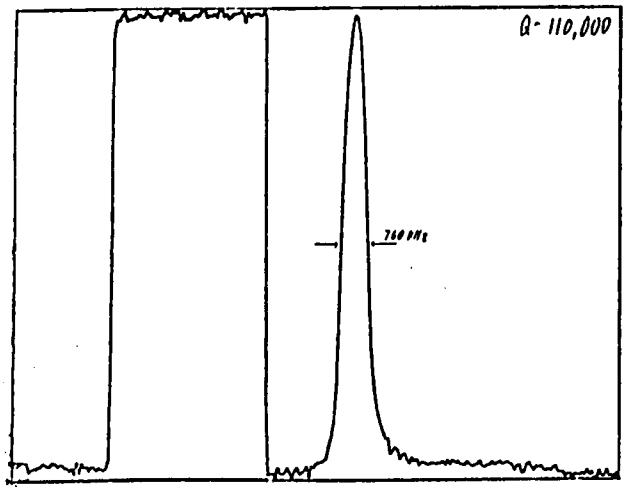

FIGURE 10.12a ALCAN FOOD VERTICAL POLARISATION Q ≈ 110,000

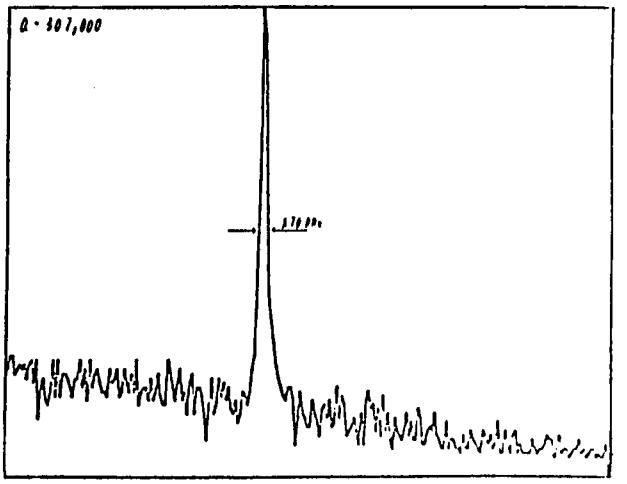

FIGURE 10.12b ALCAN FOOD HORIZONTAL POLARISATION Q ≈ 307,000

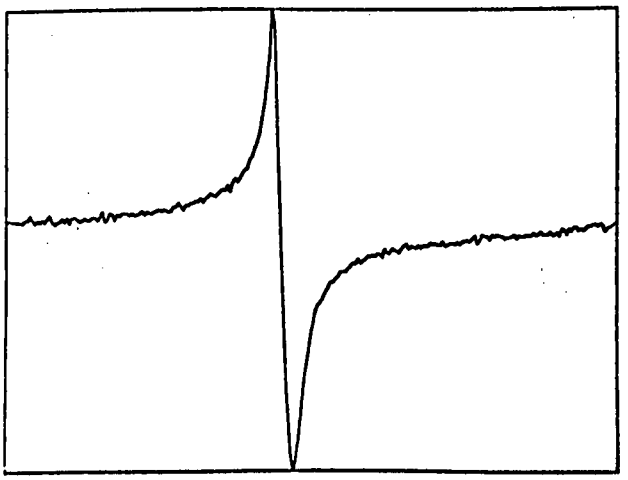

FIGURE 10.12a ALCAN FOOD VERTICAL POLARISATION DISCRIMINANT

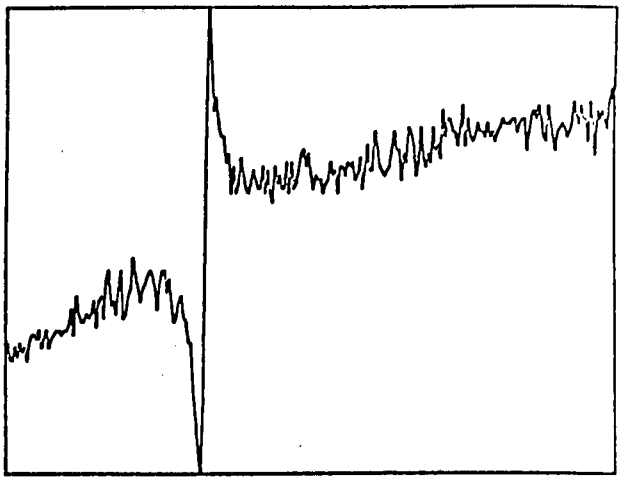

FIGURE 10.12b ALCAN FOOD HORIZONTAL POLARISATION DISCRIMINANT

FIGURES INDICATING THE TYPICAL MEASURED Q OF THE THREE MIRROR QUASI-OPTICAL CONFOCAL RESONATOR (R=360mm) USING A DIELECTRIC BEAMSPLITTER TO COUPLE IN THE POWER (ALCAN FOOD BAG). ALSO SHOWN IS THE TYPICAL FREQUENCY DISCRIMINANT THAT IS PRODUCED BY THE NOISE MEASUREMENT SYSTEM OF FIG.10.1

From published figures for the bulk loss, it was originally thought the loss in almost any thin dielectric sheet would not contribute significantly to the overall cavity loss. However, it is well known that losses can vary greatly depending on the manufacturing process and it would appear that the loss tangent is often greater in sheet form than it is in the bulk. It is also suspected that in some samples the loss may also be a function of polarisation. This has to be tested further. Several samples have been sent to the NPL for accurate calibrated measurements of the loss.

It is expected that the final system will have polished copper mirrors and a polythene beam-splitter, and will operate with a confocal cavity length of 52cm for frequencies above 80GHz.

10.16 CALIBRATION OF RESULTS

There are three methods of calibrating the noise spectrum that is seen on the spectrum analyser. The first is to modulate the source at a frequency with a known modulation index. This can be achieved using the Crosby zero-crossing method as outlined in [2]. The second, and the most appropriate calibration for low noise A.M. noise measurements is to compare the sidebands produced with two different thermal loads. For F.M. noise measurements, where the noise is very much higher than the system noise floor it is possible to calibrate the system with reference to the shape of the discriminator curve.

10.17 F.M. NOISE CALIBRATION USING DISCRIMINATOR CURVE

Noise is usually defined in terms of L(f) which is the ratio of the single sideband noise power in a 1 Hz bandwidth to the total carrier power specified at a given offset f of the carrier. For small phase deviations (small enough to produce negligible higher order sidebands) this is also equal to one half the spectral density of phase fluctuations $S_{\Delta\phi}(f) = \Delta\phi^2_{rms}(f)$ [9].

$$L(f) = \frac{P_{ssb}\ (\text{per 1 Hz})}{P_c}\ [\text{dBc/Hz}] \approx \frac{1}{2}\,\Delta\phi^2_{rms}(f)\ (\text{per 1Hz}) \qquad 10.5$$

In this context it is also worth noting the relation between L(f), $S_{\Delta\phi}(f)$ and the spectral density of frequency fluctuations $S_{\Delta f}(f)$.

$$S_{\Delta f}(f) = \Delta f^2_{rms}(f) = f^2 S_{\Delta\phi}(f) = f^2 \Delta\phi^2_{rms}(f) = 2 f^2 L(f) \qquad 10.6$$

Now for a frequency discriminator using a resonator, it can be shown that inside the resonator bandwidth, the system acts like a frequency discriminator, whereas outside the resonator bandwidth the system acts as a phase detector.

It can be shown that the voltage output V from a frequency discriminator is of the form [11]:

$$V = 2V_B \frac{(\frac{\Delta f.Q}{f_0})}{1 + (\frac{\Delta f.Q}{f_0})^2} \qquad 10.7$$

where V_B is the is the peak voltage fluctuation on the discriminator curve and is a function of the mixer sensitivity and the input power. f_0 is the resonant frequency and Δf is the frequency offset from the carrier. When $\Delta f.Q/f_0$ is small ($\approx<1/2$) then the denominator of 10.7 approximates 1 and there is a near linear relation between ΔV and Δf, similar to the analysis for the delay line system.

In fact, it is easy to show that inside the resonator bandwidth (for $\Delta f < f_0/2Q$) there is an equivalent time delay $\tau = Q/\pi f_0$. For typical experimental values of: Q = 100,000, frequency = 100GHz, the delay approximates 0.32μs which is equivalent to a delay line of length 50m.

Any frequency fluctuation Δf produces a voltage fluctuation ΔV given by,

$$\Delta V = V_B 2\pi\tau \Delta f = V_B \frac{2Q}{f_0} \Delta f \qquad (\text{for } f < \frac{f_0}{2Q}) \qquad 10.8$$

The quantity $K_D = V_B.2Q/f_0$ is the frequency discriminator slope constant, and is the figure of merit for the system.

Typical values for the frequency discriminator constant in this system can be of the order 0.3μV/Hz measured at the output of the mixer for an input power level of 4mW from the oscillator. This compares with a conversion sensitivity of 0.03μV/Hz for an input power of 65mW in the quasi-optical noise measurement system described in [3].

By combining Eqs. 10.6 and 10.8 we have the following equation,

$$L(f) = \frac{1}{2f^2}\frac{\Delta V^2_{rms}(1Hz)}{(V_B.2\pi\tau)^2} = \frac{1}{2}\left(\frac{\Delta V_{rms}(1Hz)}{V_B}\right)^2\left(\frac{f_0}{2Qf}\right)^2 \qquad 10.9$$

If we reference this to the noise spectrum measured on a spectrum analyser in dBm we have,

$L(f) = \Delta V^2_{rms}$ (dBm) Noise spectrum measured on analyser
$- 10 \log_{10}$ (B) where B is the bandwidth of the measurement
$+ 20 \log_{10} (0.22/V_B)$ dB Output referenced to 1mW and 50Ω input
$+ 20 \log_{10} (f_0/2Qf)$ dB Correction for discriminator slope
- 3 dB Accounts for 1/2 - Single sideband measurement

Outside the bandwidth of the resonator, the noise from the resonator arm is in complete phase quadrature with the signal from the reference arm of the system. The system therefore measures $\Delta\phi^2_{rms}$ with a phase detector constant V_B. Therefore, any small phase fluctuation $\Delta\phi$ produces a voltage fluctuation ΔV given by:

$$\Delta V(f) = V_B \Delta\phi(f) \qquad (\text{for } f >> f_0/2Q) \qquad 10.10$$

Therefore, by combining Eqs 10.5 and 10.9 we have,

$$L(f) = \frac{1}{2}.\left(\frac{\Delta V_{rms}(1Hz)}{V_B}\right)^2 \qquad 10.11$$

If we reference this to the noise spectrum measured on the spectrum analyser measured in dBm,

$L(f) = \Delta V^2_{rms}$ (dBm) Noise spectrum measured on analyser
$- 10 \log_{10}$ (B) where B is the bandwidth of the measurement
$+ 20 \log_{10} (0.22/V_B)$ dB Output referenced to 1mW and 50Ω input
- 3 dB Accounts for 1/2 - Single sideband measurement

It should also be noted that there is a transitional region between these regimes where $f \approx > f_0/2Q$. The literature is a little vague as to the appropriate correction for this region, although it has been noted before that there appears to be a smooth transition for the system acting as a frequency discriminator to a phase detector.

10.18 F.M. NOISE MEASUREMENTS

A number of F.M. noise measurements have been made on various diodes at various frequencies, and some of these preliminary results are presented in this section. The noise was measured using a HP8535B Spectrum Analyser and then the results were calibrated using the formulae given in the previous section. It should be noted that the calibration is slightly suspect above 500kHz ($\approx f_0/2Q$), as we move into the transition region between the resonator acting as a frequency discriminator and phase detector. In addition, the effective phase detector constant V_B may be slightly larger than the frequency discriminator constant V_B, which may make the noise figures shown a little too large above 500kHz. Some typical results are shown in Figures 10.14 to 10.18. It should be noted that one of the reasons that the noise level for the Thomson CSF InP diode is rather large, is that this diode was working in fundamental mode in what was probably an unusually low Q cavity.

The results shown however are consistent and repeatable, and it is certainly possible to make comparisons between different types of diodes. It should be noted that most of the measurements were at an input power level of a few mW, and the noise floor was typicaly 20-30dB below this level.

It is hoped to also calibrate the system using thermal loads at a future date and with standard oscillators with known noise characteristics.

F.M. NOISE MEASUREMENT ON GEC DIODE
BATCH DB742, F=94GHz
Vb = 0.24V, Q=100,000, K~400MHz/V

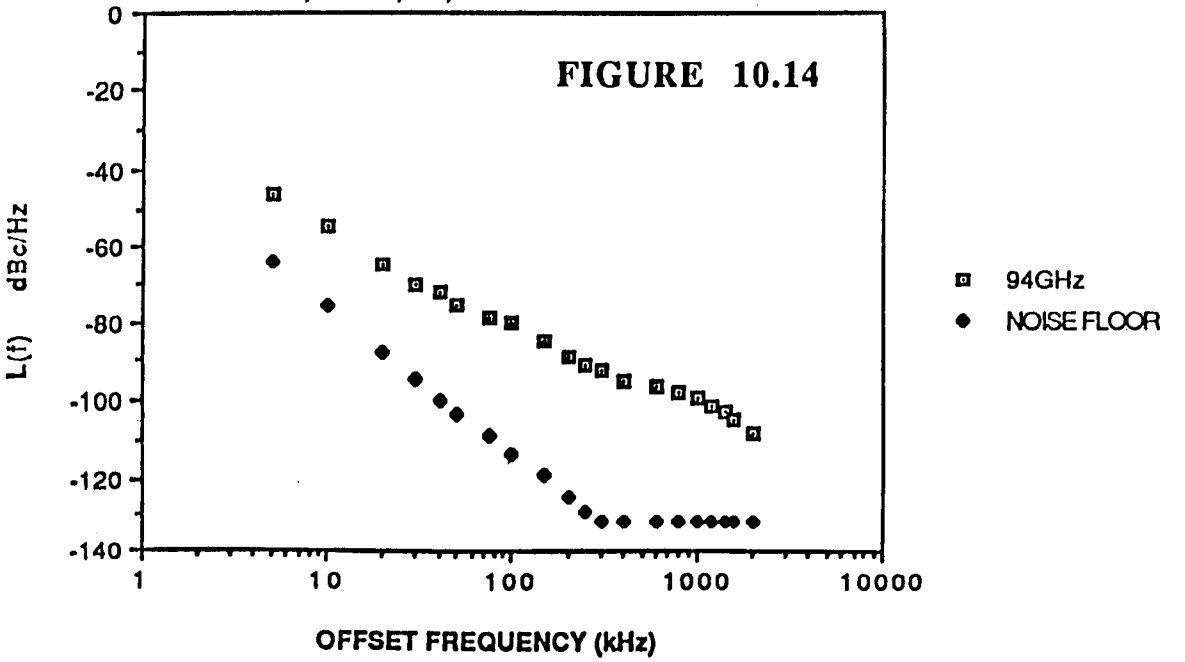

FIGURE 10.14

F.M. NOISE MEASUREMENT ON GEC GUNN
DIODE : BATCH DB736, F=84.75GHz
Vb = 0.48V, Q=85,000, K~400MHz/V

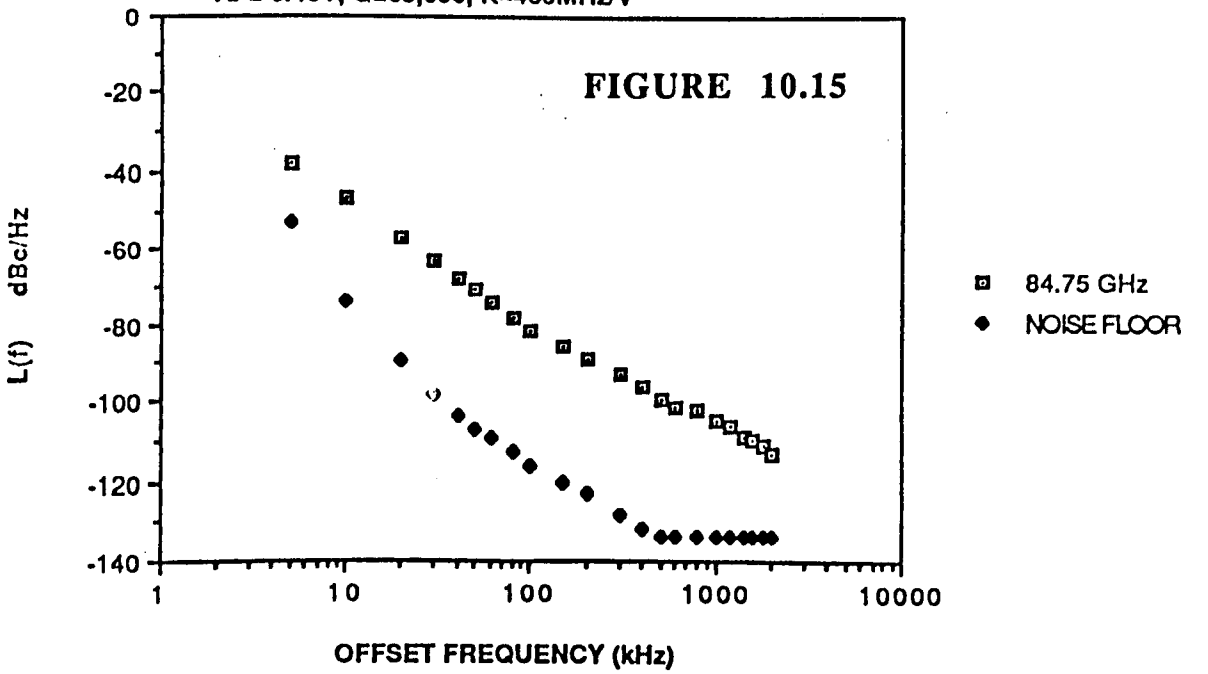

FIGURE 10.15

F.M.NOISE MEASUREMENT OF VARIAN LOW POWER GaAs GUNN DIODE, F= 99.5GHz
Vb =0.075V, Q=92000, K=127MHz/V

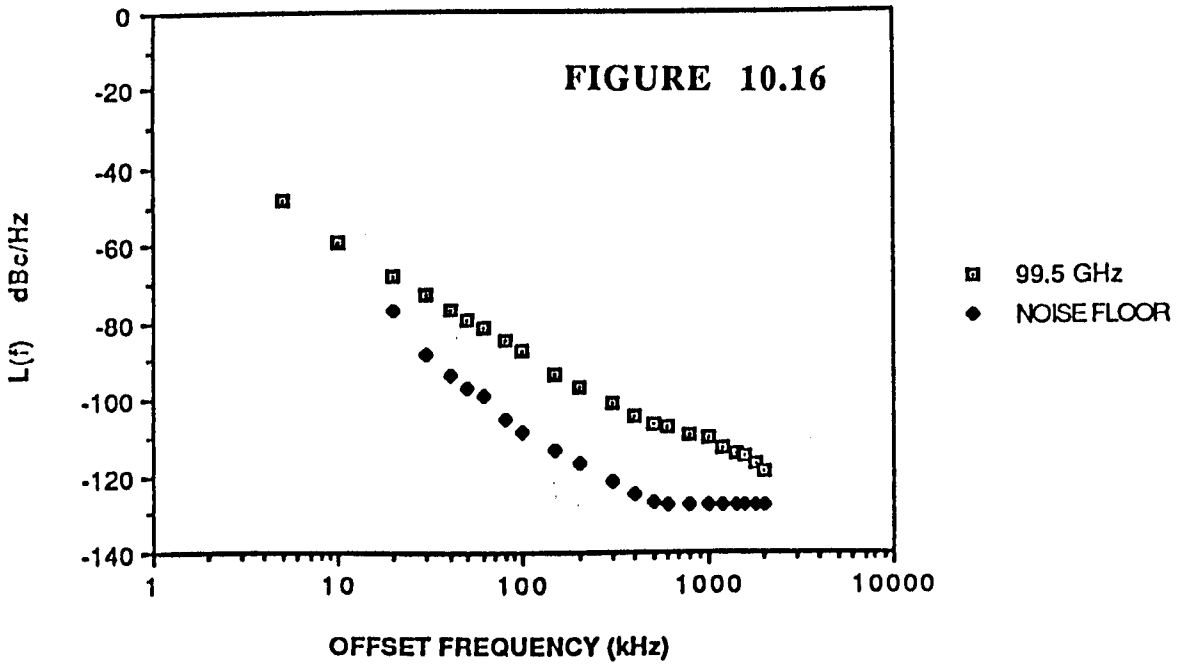

FIGURE 10.16

F.M. NOISE MEASUREMENT ON VARIAN GaAs LOW POWER GUNN DIODE, F = 100GHz
Vb = 0.38V, Q = 120,000

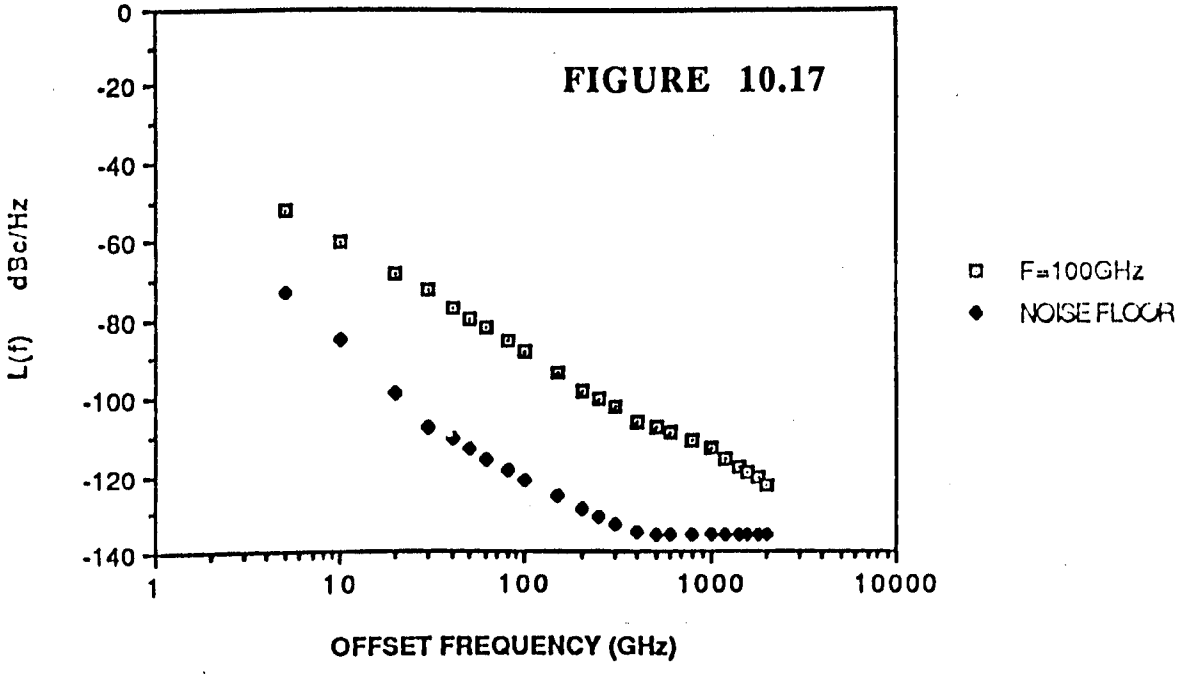

FIGURE 10.17

REFERENCES

1) A.A.Lance, W.D.Seal, F.Labaar, "Phase noise and AM Noise Measurements", Chapter 7, Infrared and Millimetre Waves, Volume 11, 1984

2) J.G.Ondria, "A Microwave System for Measurements of AM and FM Noise Spectra", IEEE Trans. Vol. MTT-16, No.9, Sept. pp.767-781, 1968

3) W.Harth et al. "FM Noise Measurement of W-Band IMPATT diodes with a Quasi-Optical Direct Detection System", Electron. Lett. Vol.18, No.9, pp.355-6, 1982

4) T.J.Simmons, D.C.Smith, "Direct Measurement of FM Noise in 80GHz Solid-State Oscillators", Electron. Lett. Vol.18, No.7, pp. 308-9, 1982

5) N.J.Cronin, "Heterodyne detection using a cooled InSb Mixer for mm-Wave Astronomy", PhD Thesis, London, 1977

6) J.G.Ondria, "Noise Measurements of W-Band (75-110 GHz) CW GaAs Gunn and Silicon IMPATT Oscillators", 1980 IEEE MTT-S International Microwave Symposium Digest, pp.24-26

7) H.Okamoto, "Noise Characteristics of GaAs and Si IMPATT Diodes for 50GHz Range Operation", IEEE Trans. Vol. ED-22 No.8, August pp.558-65 1975

8) P.Z.Peebles, A.H.Green, "A microwave discriminator at 35GHz", Proc.IEEE, 1980, Vol.68, pp.286-88

9) D.Scherer, "The "Art" of Phase Noise Measurement", Hewlett Packard RF & Microwave Measurement Symposium and Exhibition, Oct. 1984

10) T.Decker, B.Temple, "Choosing a Phase Noise Measurement Technique - Concepts and Implementation", Hewlett Packard RF & Microwave Measurement Symposium and Exhibition

11) J.C.G.Lesurf, "A novel optical circuit for use with coherent sources", In Preperation, St.Andrews 1990

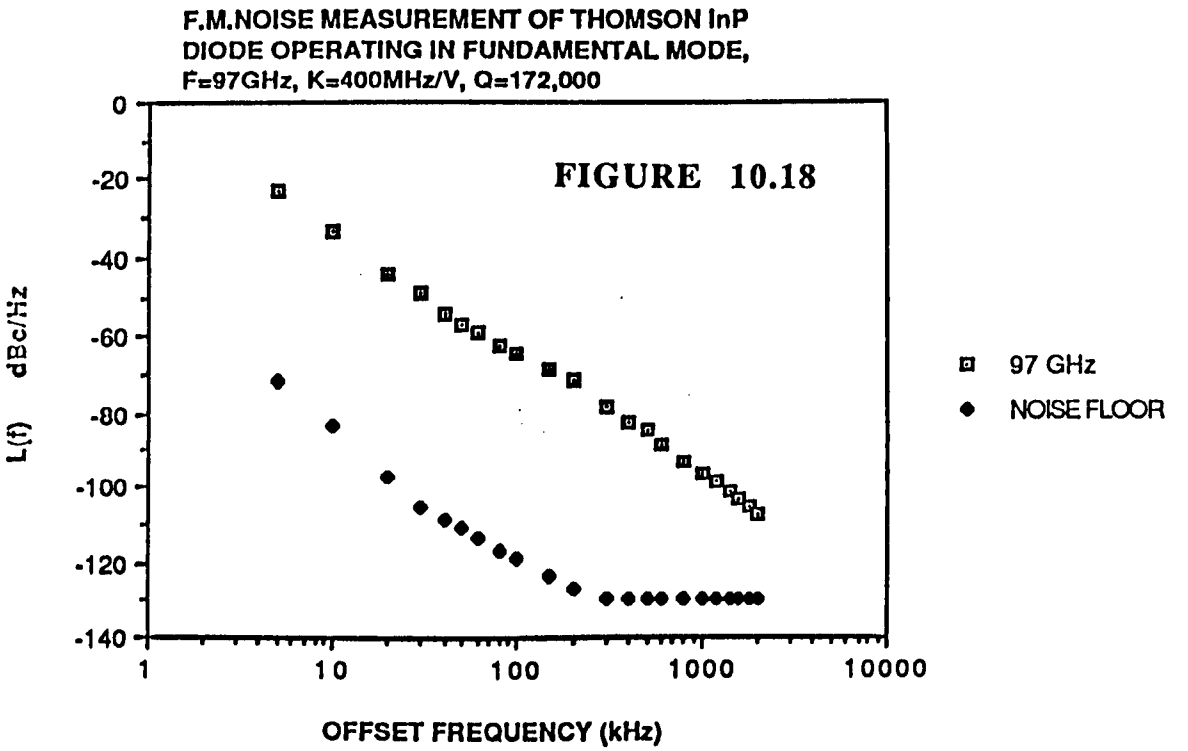
F.M.NOISE MEASUREMENT OF THOMSON InP
DIODE OPERATING IN FUNDAMENTAL MODE,
F=97GHz, K=400MHz/V, Q=172,000
FIGURE 10.18
L(f) dBc/Hz
0
-20
-40
-60
-80
-100
-120
-140
1
10
100
1000
10000
OFFSET FREQUENCY (kHz)
97 GHz
NOISE FLOOR

11.0 SUMMARY AND CONCLUSIONS

This section summarises the work in the thesis and suggests further work for the future.

A highly tuneable Gunn oscillator has been developed which has been shown to be capable of large power outputs over very substantial bandwidths (> 20GHz). It has also been used to characterise a number of different experimental Gunn devices. The tuning characteristics of the oscillator have been examined as a function of the cap circuit, and anomalies such as power dips and frequency jumps have been noted and explained.

There are a number of advancements and improvements that could be made in a number of systems that are used in the characterisation of Gunn diodes and other high frequency oscillators. Probably the most critical parameter is the determination of the impedance seen at the output frequency. With the development of the impedance bridge (which is due to be completed in the next few months), it should be possible to accurately measure the impedance characteristics of the cap circuit, and to measure the impedance of the Gunn devices themselves. One should then be in a position to quantitatively design circuits for maximum power output for various devices. However, a large number of measurements need to be done to determine the optimum impedance over a wide frequency range for a particular device, as well as examining the effect of secondary parameters such as temperature and bias.

The frequency measurement system could also be improved in a number of ways. The movement of the traveling roof mirror could be made more smooth and linear, and it certainly important that standing waves produced by reflections from the detector are minimised. It is difficult to reduce the direct reflection from the Golay detector, but the VSWR could be significantly reduced by the incorporation of a quasi-optical isolator before the detector. The accuracy of the frequency measurement could also be further improved by using a more elaborate analysis of the output. At the moment, the number of zero crossings are measured and the distance traveled by the roof mirror measured. However, if either the starting or final zero crossing is slightly out it can significantly effect the whole answer. A better way would be to use more of the information present in the interferometric signal, by Fourier analysing the signal (N.B. Not a F.F.T.), and iterating to find the largest Fourier component, although of course it would also take substantially more time.

The noise measurement system has shown itself to provide state of the art measurements at millimetre wave frequencies. It also has the advantage over comparable systems of being ultra wide-band, and requiring very substantially less lo power output

than comparable systems. However, the system is not fully optimised and there are a number of improvements or additions that could be envisaged. There also now remains a substantial amount of work to characterise different types of Gunn and other high frequency devices in terms of their noise characteristics, as well as examine them as a function of rf output impedance, temperature and bias. The eventual aim being to identify the main noise mechanisms, and improve on them within the manufacturing process.

One obvious improvement to the noise measurement system would be to lock the cavity (using piezo-electrics) to the oscillator rather than the other way round. This would certainly make it much more user friendly as a noise measurement facility, as it will not always be possible to phase lock the source. There is also still probably room for improving the Q of the system by using lower loss dielectric sheets, although it is of course also possible to make a larger cavity if a larger Q is required. In an ultimate system it may be possible to have an evacuated cavity and superconducting mirrors. The Q of a system like this would possibly have the potential of rivaling temperature stabilised crystal oscillators as a reference frequency, although it would be limited by the temperature and vibrational stability of the cavity.

The noise measurement system as it stands should have the potential of being able to measure the noise characteristics of even the best phase-locked sources. This also raises the possibility that that the high Q cavity could be used to provide a reference to phase lock sources more accurately than frequency multiplication chains, (which also multiply up any noise). It certainly should have a better high frequency performance, although it may be more susceptible to long term thermal drift, and at the moment there is no accurate determination of the absolute resonant frequency. The thermal drift could be substantially improved by lagging the cavity, and using spacers between the mirrors using some of the new composite materials that have close to zero expansion coefficient at room temperature. There probably is also room for improving the cavities sensitivity to vibration.

There are also one or two further improvements that could be effected to improve the ultimate accuracy of a phase locked system using a high Q cavity. At the moment, the noise floor of such a phase locking scheme would be effected by the 1/f noise of the mixer system. However, this could be overcome by frequency modulating the source, and then phase detecting against this modulation. An absolute frequency could be determined by frequency modulating the source at a sufficiently high frequency to lock the oscillator sideband to the next mode in the cavity. By modulating at two separate frequencies it is possible to lock both the oscillator and the cavity to fixed reference frequencies, without direct harmonic multiplication.

Both these passive and modulation stabilisation techniques are extensively and successfully used in stabilisation schemes at optical frequencies where millihertz stability between two optical lasers has been achieved. These ideas have recently come to the fore with the need for highly stable optical oscillators to (hopefully) allow the measurement of gravity waves. However, they were in fact originally proposed by R.Pound for microwave frequencies back in the 1950's.

For a long while optics has been taking and using a wide variety of microwave techniques. It would seem there is now there is a lot of potential for taking good ideas at optical frequencies and transferring them back to millimetre wave frequencies, and it is likely that these techniques will be seen more and more in the future.

APPENDIX A

ELECTROPLATING AND ELECTROFORMING SOLUTIONS

This APPENDIX gives details of the recipes and some details for simple copper plating. Much of what is given is taken from "The Electroplaters Handbook" by Ammen.

1) General Copper Bath

25 ounces (208.75 gms) COPPER SULPHATE
6 ounces (170.1 gms) SULPHURIC ACID
1 gallon (3.78 litres) DISTILLED WATER
Room Temperature - 90 Degrees Fahrenheit
Pure Copper Annode

2) Bright Copper Bath

27 ounces (765.45 gms) COPPER SULPHATE
4 ounces (113.4 gms) SULPHURIC ACID
0.005 ounces (0.142 gms) THIOUREA (Thiocarbamide $(NH_2)_2CS$)
0.1 ounce (2.835 gms) BRER RABBIT MOLLASSES
Room Temperature - 90 degrees Fahranheit
Pure Copper Annode

REMEMBER - always add acid slowly to water and **NEVER** the other way round, as a violent reaction and spitting can take place.

An improvement in the hardness and quality of the plated copper, and in the speed of the process can also be effected by the use of organic copper cyanides, although for optimum results the solution should be pumped and filtered, and the electrodes covered with a "sludge bag". The toxicity of the substance and the need for active removal of the exuded vapour are obvious disadvantages, but excellent results have been obtained with this process.

Generally speaking, the higher the temperature and the better the plating, as you decrease the resistance of the solution to the passage of current. Note that solution lost by evaporation should be replaced by distilled water and not the original solution.

With both these solutions a current of 70mA per square inch will normally give a good clean deposit. Note, the weaker the current, and the more finely grained and the closer knit the deposit, although obviously the plating time becomes longer.

A good rule of thumb is that the must have a surface area roughly four times than the area being plated, and there should be an anode for each vertical plane that is to be plated. The anode should be between 9 and 15cm away from the object to be plated.

Usually, even, symmetrical and faster plating can be more easily achieved if the solution is agitated, and/or if the former is rotated slowly. This is because the bath between the anode and cathode becomes lower in metal content than other parts of the tank. However, for plating corrugations the current will take the shortest path and plate the highest points first. Plating in the corrugations will only preferentially take place when the metal content in this path starts to be exhausted, and the path to the path to the recess appears to be of lower conductivity. Thus, in this case the solution should not be agitated (8).

With all plating it is very important that the solution, the mandril and the anode is as pure and clean as possible. The following steps are advised/possible:

1) In all plating solutions the water should be distilled, and in all cleaning solutions it should at least contain no chlorine. (Normally if water is left in a shallow container with a large surface area for 24 hours, most of the chlorine will have gassed out).

2) The mandril and the anode should be as pure as possible.

3) Animal and vegetable fat (often obtained via skin contact) can be removed with caustic soda (lye/sodium hydroxide) or soap. With lye use rubber gloves and an eye shield. Aluminium, tin and zinc react with a caustic solution, so it is important to work fast and rinse well.

4) Mineral oil/grease can be removed by benzene (highly inflammable) or carbon tetrachloride. A 50/50 mix gives a very good noninflammable cleaning liquid.

5) Electro cleaning can also be used. Use a stainless steel beaker as the anode. For aluminium, zinc and tin use:

4 ounces (113.4 gms) SODIUM BICARBOBATE
4 ounces (113.4 gms) WASHING SODA
1 gallon (3.78 litres) WATER

For Copper and Brass use:

1 ounce (28.35 gms) LYE
5 ounces (141.75 gms) WASHING SODA
2 ounces (56.7 gms) TRISODIUM PHOSPHATE
1 ounce (28.35 gms) LAUNDRY SOAP
1 gallon (3.78 litres) WATER

When a voltage is applied large amounts of hydrogen is given off. The cleaning is done by the mechanical action of the bubbles and the chemical action of the solution. About 5V should be applied for no more than three minutes, and then the current should be reversed for a few seconds to get rid of the hydrogen bubbles.

6) Pickles and Bright Dips - These are processes where by chemical tarnishes (usually oxide films) can and should be removed. This should be done after the object has been cleaned of all grease and oils. Basically what one is doing, is dissolving the unwanted oxide with an acid or base solution. Usually this will also dissolve the metal, so care must be taken, and afterwards one should rinse, and then neutralise the base or acid, and then rinse again. A pickle is generally used for removing tarnishes, a bright dip is used for cleaning up the metal and leaving a bright finish.

For Aluminium:

A suitable etch is:

3 - 9 ounces (85 - 250 gms) LYE
1 gallon (3.78 litres) WATER
200 degrees Fahrenheit

(NOTE when the aluminium starts to react, copious amounts of hydrogen are produced, which is explosive. Therefore use forced ventilation).

A suitable neutralizing bath is:

1 volume NITRIC ACID
1 volume WATER

Dip the item in this solution for a few seconds and the rinse in clean hot water and then clean cold water.

A suitable bright dip for aluminium is:

1 volume HYDROFLOURIC ACID
1volume NITRIC ACID
100 volumes WATER
Room Temperature

Place in dip for about a minute but BEWARE - hydroflouric acid is highly corrosive to skin, and it is also highly toxic by ingestion and inhalation.

For Copper:

A suitable copper etch is:

1 part SULPHURIC ACID
5 parts WATER, boiling or near boiling (preferably in a copper pan)

After pickling one can scale dip. This results in a nice smooth finish after bright dipping. A suitable scale dip is:

1 gallon (3.78 litres) SULPHURIC ACID
1/2 gallon (1.9 litres) NITRIC ACID
3 gallons (11.34 litres) WATER
Add aditional sulphuric if action is too violent.

For a bright finish for copper:

1 gallon (3.78 litres) of SULPHURIC ACID
1/2 gallon (1.9 litres) of NITRIC ACID
1 gallon of water
1 teaspoon salt NaCl (Table Salt)

Remembering to rinse in running hot and then cold water after each process.

For Steel (and Iron):

A good etch/pickle for Steel is:

1 volume HYDROCHLORIC ACID
1 volume WATER
Room Temperature

A very good bright dip for steel is:

15 ounces (425.25 gms) CHROMIC ACID
1 gallon (3.78 litres) WATER
140 degrees Fahrenheit

Or at room temperature:
10 fluid ounces (295.6ml) NITRIC ACID

4 fluid ounces (118.24 ml) SULPHURIC ACID
1 gallon (3.78 litres) WATER

7) Plate Stripping: If the plating has not gone well then one can strip off the plate chemically by the following ways:

a) Copper Plating from Steel (or Iron):

20 ounces (567 gms) SODIUM SULPHIDE
2 ounces (56.7 gms) FLOWERS OF SULPHUR
1 gallon (3.78 litres) WATER

Boil until the flowers of sulphur dissolve, and then soak the copper plated item for five minutes. The copper should be converted to copper sulphide which can simply be brushed away. To remove every last bit of CuS the item can be placed in a saturated solution of Oxone (Potassium Peroxymonosulfate). That is 25gms of Oxone dissolved in 100ml of water.

b) Copper (or Zinc or Silver) from Aluminium:

1 volume NITRIC ACID
1 volume WATER
90 - 100 degrees Fahrenheit

Copper, zinc and silver are all readily soluble in nitric acid, whereas aluminium becomes passive and does not dissolve.

APPENDIX B

TRANSMISSION LINE MODELLING USING ABCD MATRICES

There are a number of different ways that transmission lines can be represented with matrices, but in this thesis the voltage/current representation was consistently used for modelling and designing porposes.

VOLTAGE / CURENT REPRESENTATION

For any linear two port junction we may write:

$$V_1 = \mathcal{A}V_2 + \mathcal{B}I_2$$
$$I_1 = \mathcal{C}V_2 + \mathcal{D}I_2 \qquad \text{A1}$$

where V_1 and I_1 are input quantities, and V_2 and I_2 are the output quantities.

This can be written in matrix form as,

$$\begin{bmatrix} V_1 \\ I_1 \end{bmatrix} = \begin{bmatrix} \mathcal{A} & \mathcal{B} \\ \mathcal{C} & \mathcal{D} \end{bmatrix} \begin{bmatrix} V_2 \\ I_2 \end{bmatrix} \qquad \text{A2}$$

The advantage of this representation is that the ratio of the voltage and current at some given point, directly gives the impedance, or the ratio between the electric and magnetic fields at that point. In addition, it is a simple computational matter to multiply matrices together to work out impedances of more complicated structures. For example, we can put $Z_{load} = V_2/I_2$ where it is easy to transform to the input load Z_{in} (= V_1/I_1), from the relation,

$$Z_{in} = \frac{\mathcal{A}Z_{load} + \mathcal{B}}{\mathcal{C}Z_{load} + \mathcal{D}} \qquad \text{A3}$$

where all the above quantities are complex (for lossless structures they will be pure imaginary).

The $\mathcal{ABCD}$ parameters of a transmission line of characteristic impedance Z_C is given by:

$$\begin{bmatrix} \mathcal{A} & \mathcal{B} \\ \mathcal{C} & \mathcal{D} \end{bmatrix} = \begin{bmatrix} \cos \beta l & i Z_c \sin \beta l \\ i Y_c \sin \beta l & \cos \beta l \end{bmatrix} \quad \text{A4}$$

or in the more general case, if one allows for distributed losses, the $\mathcal{ABCD}$ parameters are given by:

$$\begin{bmatrix} \mathcal{A} & \mathcal{B} \\ \mathcal{C} & \mathcal{D} \end{bmatrix} = \begin{bmatrix} \cosh(\gamma l) & Z_c \sinh(\gamma l) \\ Y_c \sinh(\gamma l) & \cosh(\gamma l) \end{bmatrix} \quad \text{A5}$$

where $\gamma = \alpha + i\beta$

and α is the resistive loss per unit length, and β is the propagation parameter, $\beta = 2\pi / \lambda_g$.

For a lumped circuit impedance in series with a transmission line (distributed impedance), the representation is of the form:

$$\begin{bmatrix} \mathcal{A} & \mathcal{B} \\ \mathcal{C} & \mathcal{D} \end{bmatrix} = \begin{bmatrix} 1 & Z_S \\ 0 & 1 \end{bmatrix} \quad \text{A6}$$

where Z_S is the impedance of the lumped circuit component in series with the transmission line (i.e. R + i wL, -i/wC).

For a lumped circuit impedance in parallel with a transmission line, the representation is of the form:

$$\begin{bmatrix} \mathcal{A} & \mathcal{B} \\ \mathcal{C} & \mathcal{D} \end{bmatrix} = \begin{bmatrix} 1 & 0 \\ Y_P & 1 \end{bmatrix} \quad \text{A7}$$

where Y_P is the admittance of the lumped circuit component in parallel with the transmission line.

The values of many common discontinuity capacitances or inductances (waveguide posts, irises etc.) can typically be looked up in such references as Marcuvitz [1]. These

have been found by matching the evanescent waves across the boundary/discontinuity and then calculating the energy stored in this region.

It therefore becomes a simple method to calculate impedances through any network, by multiplying $\mathcal{ABCD}$ matrices together. The ratio of the voltage and current will give the impedance of the line at that particular point.

LUMPED CIRCUIT REPRESENTATION

It is useful to note that a length l of transmission line can be represented as a series of lumped components in series and in parallel. Either, as two capacitances in parallel connected by a series inductance, or two inductances in series separated by a capacitance in parallel as illustrated below

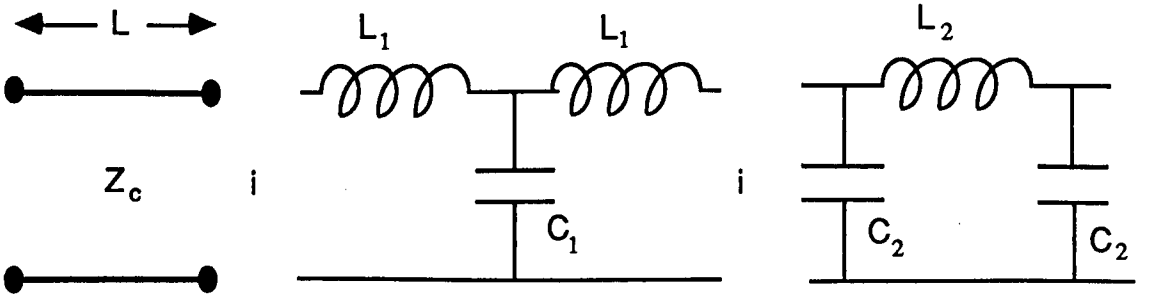

EQUIVALENT CIRCUITS FOR A TRANSMISSION LINE

where $wL_1 = Z_C \tan(\beta l/2)$ and $wC_1 = Y_C \sin(\beta l)$

and $wL_2 = Z_C \sin(\beta l)$ and $wC_2 = Y_C \tan(\beta l/2)$

This is easily proved by multiplying out the respective individual capacitance and inductance matrices.

This representation is very useful when trying to design waveguide or coaxial-circuit filters as standard lumped circuit filter theory can be used.